Ramesh S. Chaughule
Deepak P. Patkar
Raju V. Ramanujan *Editors*

Nanomaterials for Cancer Detection Using Imaging Techniques and Their Clinical Applications

Springer

Nanomaterials for Cancer Detection Using Imaging Techniques and Their Clinical Applications

Ramesh S. Chaughule • Deepak P. Patkar
Raju V. Ramanujan
Editors

Nanomaterials for Cancer Detection Using Imaging Techniques and Their Clinical Applications

Springer

Editors
Ramesh S. Chaughule
Department of Chemistry
Ramnarain Ruia Autonomous College
Mumbai, India

Deepak P. Patkar
Nanavati Max Super Speciality Hospital
Mumbai, India

Raju V. Ramanujan
School of Materials Science and Engineering
Nanyang Technological University
Singapore, Singapore

ISBN 978-3-031-09635-8 ISBN 978-3-031-09636-5 (eBook)
https://doi.org/10.1007/978-3-031-09636-5

This Springer imprint is published by the registered company Springer Nature Switzerland AG
The registered company address is: Gewerbestrasse 11, 6330 Cham, Switzerland

Foreword by Dr. Zaver Bhujwalla

I am delighted to write this foreword for *Nanomaterials for Cancer Detection Using Imaging Techniques and Their Clinical Applications*, expertly edited by Professor Chaughule and colleagues. Professor Chaughule is also a distinguished contributor to this volume.

Targeted and non-targeted nanomaterials decorated with imaging reporters hold significant promise in the personalized treatment of cancers. Imaging becomes especially important within the backdrop of the abnormal vasculature of cancers as it establishes delivery of these nanomaterials and provides visualization of the heterogeneity of delivery. Heterogeneity is a hallmark of cancers. This heterogeneity that occurs at the molecular and functional levels within the cancer cell and within the tumor microenvironment creates a tumor ecosystem unsurpassed in complexity with redundancy of pathways and networks that pose a formidable challenge for cancer detection and treatment. These heterogeneities within the tumor and between tumors create an urgent need for non-invasive imaging-based strategies for detection and treatment to achieve personalized precision medicine in cancer.

This book represents a comprehensive collection of chapters from experts in the field that are presented in five different sections that focus on multiple aspects of nanomaterials for multimodal imaging applications in cancer detection, drug delivery, and theranostics. The chapters cover applications in different types of cancers describing applications of innovative nanomaterials, including hybrid nanoparticles, that provide a range of therapeutic and diagnostic options. Key issues in the applications of nanomaterials in cancer such as biocompatibility and toxicity are addressed, as are the clinical trial process and factors that increase the success rate of translating nanomaterials from discovery to clinical translation.

The collection of articles in this book provides valuable, timely, and much-needed information that will be useful to a range of disciplines. Research scientists in academic centers and industry, students, clinicians, and technologists will benefit from the chapters contributed by leading experts in the exciting field of the use of nanomaterials in cancer detection and theranostics.

Zaver M. Bhujwalla

William R. Brody Professor of Radiology,
Director, Division of Cancer Imaging Research
The Johns Hopkins University School of Medicine
Baltimore, MD, USA

Foreword by Dr. Sachdeva

I am very delighted to write this forward for *Nanomaterials for Cancer Detection Using Imaging techniques and Their Clinical Applications*, which has been ably and deftly edited by Professor Chaughule and his colleagues.

Nanoparticles provide several potential advantages over conventional agents, including the extension of circulating half-life, passive accumulation at tumor sites due to the enhanced permeability and retention effect, reduced toxicity, and integration of multiple diverse functions in a single complex. Nanoparticles have intrinsic properties that offer unique imaging and functionalization utility. This effect increases the chances of nanoparticles to extravasate from tumor blood vessels and into tumor tissues. Many different types of nanomaterials have been developed to provide contrast in medical imaging. The advancement of personalized medicine nano theranostics is expected to be the main goal in biomedical research in the coming years. Currently, nano theranostics have been applied for medical practice on a limited basis because we do not yet have enough knowledge regarding the type and number of biomarkers in individuals during the progression of cancer and other diseases. Our knowledge about the long-term effects of nanomaterials needs to be improved also. Hence, there is an unmet need for more information which needs to be fulfilled by various researchers and publications.

This current book encompasses five exhaustive sections on areas ranging from imaging modalities, magnetic nanoparticles in bioimaging, theranostic nanoparticles with special emphasis on eye cancer, and targeted anticancer drugs on the market. Furthermore, this book gives a good compilation of the current status of the progress in the field of cancer detection and imaging through the presentation of multidisciplinary chapters which are focused on advances in nanotechnologies for diagnostics and therapy. The chapters have been written by experts in the field and have the latest information for readers so that they can appreciate the evolving science of imaging in cancer diagnostics and therapy.

The editors and publishers need to be applauded for bringing forth a magnificent reference book comprising the latest advances in the field of nanomaterials, cancer, and imaging with significant clinical applications. I sincerely hope and wish that this book would be one of the greatest treasures for the researchers in academia, industry, research institutes, and clinicians for times to come.

Mandip Singh Sachdeva
Section Leader and Professor, College of Pharmacy and Pharmaceutical Sciences,
Institute of Public Health
Florida A&M University
Gainesville, FL, USA

Foreword by Dr. Bo Fei

This book covers an emerging multidisciplinary area of nanotechnology, biomedical imaging, and cancer research. I was excited to read the contents of the book that covers many research topics that I have been involved in my own academic career over the past 30 years as an investigator and educator in bioengineering, radiology, and imaging sciences. I have witnessed the evolvement of the fields of molecular imaging, photodynamic therapy, and nanomedicine over the years. The book not only covers the development of the new technologies but also introduces their novel applications in disease detection, diagnosis, and therapy.

The book provides background knowledge and state-of-the-art techniques for graduate students, postdoctoral fellows, medical residents, physicians, and pharmaceutical scientists who are interested in this interdisciplinary field of nanomaterials and imaging for cancer detection and therapy. Readers will be introduced to various imaging technologies including magnetic resonance imaging, positron emission tomography, single-photon emission computed tomography, and optical imaging. The book covers different types of nanomaterials such as liposomes, dendrimers, polymers, polymeric nanocarriers, carbon nanotubes, nanoshells, and magnetic nanodroplets. Example clinical applications of biomedical imaging and nanomaterial technologies are also described in the book, which include cancer detection and diagnosis, photodynamic therapy, photothermal therapy, and image-guided therapy.

The field of nanomedicine and bioimaging is rapidly growing. This is a timely book that would help us catch up with the new developments and the trend in the field. Congratulations to Dr. Chaughule and his colleagues and the publisher.

Baowei Fei

Director, Quantitative Bioimaging Laboratory,
Director, Center for Imaging and Surgical Innovation,
Cecil H. and Ida Green Chair in Systems Biology Science,
Professor of Bioengineering
The University of Texas at Dallas
Richardson, TX, USA

Professor of Radiology
The University of Texas Southwestern Medical Center
Dallas, TX, USA

Preface

The book entitled ***Nanomaterials for Cancer Detection Using Imaging Techniques and Their Clinical Applications*** is addressed to pharmaceutical scientists, clinicians in hospitals, and postgraduate students seeking updated and critically important information on nanomaterials used in theranostics, imaging as contrast agents, diagnostics (cancer detection), and drug delivery.

Nanotechnology is a relatively new, rapidly developing field. It has enormous scope in medical science, pharmacy, biotechnology, and materials. Studies on nanoparticles are currently being carried out in preclinical and clinical development using inorganic, metallic, hybrid, organic including various liposomes, polymeric micelles, dendrimers, quantum dots nanoparticles. Their unique size-dependent properties and convenient surface for molecular assembly make these materials superior in medical, pharmaceutical, and biological research.

Certain advanced treatments are based on nanoparticles using photodynamic and photothermal therapy which can be used to selectively destroy cancer cells upon stimulation by laser and light sources. PDT (photodynamic therapy) is based on the destruction of the cancer cells by laser-generated atomic oxygen (cytotoxic). This dye is taken in by the cancer cells which are destroyed due to its cytotoxic nature. There is a lot of potential in nanomedicine research for drug delivery. Improvement of drug bioavailability is one of the vital nanotechnology applications. Drug bioavailability makes it possible for the drug molecule to reach only the targeted part of the body. Polymer nanoparticles encapsulated in a red blood cell membrane allow them to move freely in the bloodstream while absorbing toxins.

Molecular imaging provides a versatile platform for the novel design of nanoprobes. This has an advantage in enhancing the sensitivity, specificity, and signaling capabilities of various biomarkers in human diseases. Polymeric nanomaterials have improved present chemotherapy delivery methods by reducing side effects when the dosage is increased. This process increases residual time in the body and offers a sustained and tunable release. This method can deliver multiple drugs in one carrier. The nanosystems such as liposomes, dendrimers, polymers, polymeric nanocarriers, carbon nanotubes, and nanoshells are carriers of bioactive molecules. Hybrid nanoparticles are emerging as advanced materials with tunable properties

for enhanced performance; therefore, research groups are now focusing on the development of hybrid nanoparticles. Most of these technologies with clinical applications are discussed in this book in detail.

We are pleased to introduce this book to aspiring and working scientists, medical practitioners and students, biologists, material scientists, and pharmacists. The book is arranged in five parts. Imaging modalities are used for detecting cancer and contrast agents for enhancement of signal detection. The book starts with the presently available imaging modalities and their applications for various cancer detection. For medical imaging and oncology, nanoparticles are used to generate reactive oxygen species and free electrons which disrupt cellular membrane damaging cancerous cells. It also discusses nanoparticles that can provide unique imaging applications to monitor the progress of radiotherapy treatment. The chapters (1 and 2) providing this information are grouped in the first part. The second part includes the chapters on discussion on magnetic nanofluid droplets, magnetic nanomaterials for hyperthermia and bioimaging, and intranasal drug delivery to the central nervous system proposing theory and modeling. These chapters (3–5) are grouped in the second part.

The third part discusses general nanotechnology for cancer detection and treatment including theranostic nanoparticles. Also, it emphasizes the detection of lungs, the use of electrospun nanofibers, biomarkers imprinting leading to the detection of breast cancers (using molecularly imprinted polymer-based electrochemical sensors), nanoparticles with biocompatibility, and toxicity. The use of hybrid (organic and metallic) nanoparticles for multimodal imaging and diagnosis and biomedical applications is also a very important topic of today's research in cancer detection. The fourth part has applications to eye cancer. In this chapter, the application of nanoparticles in diagnostics is discussed, which is able to enhance the existing diagnostic and screening tools for detecting eye diseases precisely while monitoring the disease progression. Different nano theranostics applications for specific ophthalmology applications are also presented.

The fifth part has applications of developed anticancer drugs from the industry. Recent advances in nanotechnology and biotechnology have contributed to the development of drugs with varying desirable characteristics such as targeting specific receptors, long-duration pharmacokinetics, sustained drug release, as well as signal-controlled drug delivery. The approvals of Bexxar®, Verluma®, and ProtaScint® validate the utilization of modalities such as proteins and peptides for tumor imaging and translate to clinical therapies. The chapter 16 "Protein and peptide-based therapeutics for cancer imaging" elucidates the limitations of proteins and peptides as targeting motifs due to heterogeneity observed in target expression as well heterogeneity in the tumor microenvironment. Further, this chapter concludes that these issues can be overcome by developing multifunctional imaging agents which can be tracked and imaged using two independent imaging modalities.

The second group in the fifth part has designed the TheraCour polymer drug (chapter 17). Their application is most advanced in the antiviral field as well as potential applications in the cancer field as targeting therapeutics. The third group (chapter 18) in this fifth part discusses the clinical trial process, market statistics,

and factors to increase the success rate from lab to clinic using nanomaterials for cancer theranostics. Rigorous, long-term toxicity studies, thorough analysis of risk-benefit profile, and cost of theranostics are crucial for their successful use in the clinic. Artificial intelligence computational methods will prove pivotal in driving successful clinical trials by enabling patient selection and enrollment and rapidly processing massive patient data.

The editors wish to thank all the distinguished and expert contributors for their enthusiastic participation in this endeavor and also some contributors who sent their contributions at the last hour. We are confident that the book will serve as a valuable guide for researchers and students of medicine, pharmacy, materials chemistry, and biology. Dr. Chaughule wishes to thank Dr. Suhas Pednekar, Vice-Chancellor, Mumbai University; Dr. Anushree Lokur, Principal, Ramnarain Ruia Autonomous College, Mumbai; and his family members for all the support. Special thanks are due to Ms. Navjeet Kaur for her assistance in arranging all the abstracts, chapters, and tables. Prof. R. V. Ramanujan thanks Dr. Varun Chaudhary for his careful assistance and insightful input on all the chapters. Dr. Patkar wishes to acknowledge the efforts of teachers and dedicated doctors like Dr. Chaughule and his entire team of editors that such endeavors take shape. It has been a privilege for him to be associated with this textbook and he is certain that this book will provide the much-needed guidance on nanotechnology and its usefulness in cancer detection and research.

Last but not least, the editors sincerely thank the Springer Nature staff for their support from time to time.

Mumbai, India — Ramesh S. Chaughule
Mumbai, India — Deepak P. Patkar
Singapore, Singapore — Raju V. Ramanujan

Contents

Imaging Modalities and Their Applications in Cancer Detection Using Nanomaterials

Gauri Rane, Deepak Patkar, and Ramesh Chaughule

1 Introduction

The use of nanotechnology has opened up a new era of diagnosis and treatment of diseases and traumatic injuries. The special nanomaterials, having clinical application properties, have an advantage in showing physiological interactions from the molecular level to the systemic level. Radiology is a diagnostic field that has become imperative in medicine. Now molecular imaging is a field of medical imaging which is based on imaging molecules within living patients and thus enabling us to visualize and assess biological processes in a noninvasive manner [1]. This has the added advantage of diagnosing diseases at an early stage before significant anatomical alterations have already occurred. Most medical imaging modalities make use of contrast agents which could be metal ions, radioactive isotopes, microbubbles, or nanobubbles. These are injected into the patient's bloodstream and then traced using an imaging modality, e.g., ultrasound (USG), magnetic resonance imaging (MRI), computed tomography (CT), positron emission tomography (PET), PET-CT, etc.

Targeted contrast agents have found an important place in imaging including nanoparticles [2], iodinated molecules [3], Gd chelates [4], fluorescent dyes [5], and specific biomarkers which can be imaged using the conventional imaging modalities. Amongst these nanoparticles due to their intrinsic and unique magnetic or optical properties have emerged as powerful tools for molecular imaging especially their long circulation time, which is useful for targeted delivery. The word nanoparticle usually refers to a particle with a size ranging from 1 to 100 nm.

G. Rane (✉) · D. Patkar
Nanavati Max Super Speciality Hospital, Mumbai, India

R. Chaughule
Department of Chemistry, Ramnarain Ruia Autonomous College, Mumbai, India

R. S. Chaughule et al. (eds.), *Nanomaterials for Cancer Detection Using Imaging Techniques and Their Clinical Applications*,
https://doi.org/10.1007/978-3-031-09636-5_1

These nanostructured materials have a long history of use as contrast agents in various imaging modalities and as ideal drug delivery vehicles.

1.1 History of Nanotechnology

Nanoscience and nanotechnology are evolving science and research areas involving the study and making of structures, systems, and agents with unique properties due to the structural composition of their atoms in the range of 1–100 nm scale. These technological advancements have gained significant importance in recent times and are being extensively researched in medicine, especially in oncology. The field is showing growth in every field like chemistry, engineering, and medical science. Richard Feynman envisioned the use of machines to make smaller machines almost down to the molecular level [6]. More details on the basic principles of nanotechnology are reported in subsequent chapters of this book.

1.2 Nanotechnological Applications

Studies are being conducted worldwide to make use of nanotechnological advancements in medical practice both in diagnostics and therapeutic aspects. The target areas of diagnosis and therapy are the same, for example, in cancerous tumors; the unique properties of nanoparticles are being extensively studied. These nanoparticles can be used as superior agents to locate and define the extent of cancerous lesions as well as act as delivery agents to help therapeutic treatments reach the tumors ideally. As a result, these have led to the development of nanotheranostics and nanotechnology for both imaging as well as treatment. Targeted and personalized medicine with tailored, patient-specific treatments is becoming increasingly popular, and nanotechnology is proving to be a boon for this technique (Fig. 1).

Medical imaging in healthcare is crucial and important to diagnose diseases. Radiology as a diagnostic field has become imperative in medicine. It is at the heart of all specialties be it neurology, surgery, medicine, or gynecology and obstetrics. The physicians frequently need diagnostic scans such as X-ray, CT scans, MRIs, PET, or combinations of PET-CT scans to confirm any disease. Imaging helps to know the ongoing progress of the illness and adjust necessary protocols. For example, ultrasonic technology producing sonogram images in women gives details of the parts of the body being formed in the womb to the physician. Ultrasound is also effective in the progress of soft tissues of the neck, breasts, abdomen, pelvis, etc. Early signs of breast cancer can be detected using mammography.

Ultrasound (USG) is a widely used imaging modality in medicine due to its several merits over other modalities like wide availability, adaptability, noninvasiveness, and real-time imaging. For example, ultrasonic technology producing sonogram images in women gives details of the parts of the body being formed in

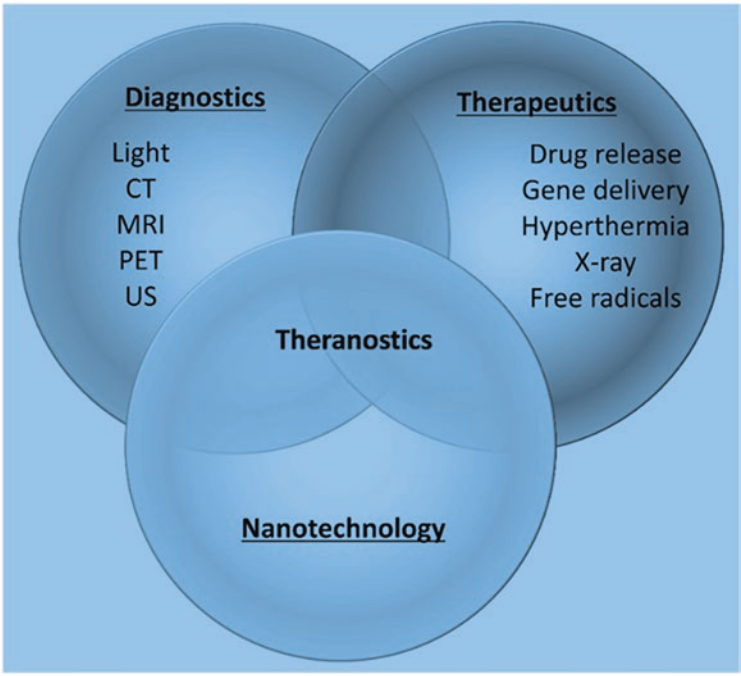

Fig. 1 Paradigm of nanotechnological applications. (Reprinted from Ref. [7])

the womb to the physician. The confirmation of pregnancy, whether intra- or extra-uterine, is done by USG. Fatal medicine is one area where radiology has shown to be of extreme importance, and the value it adds is only increasing day by day. Anomaly scans used to be earlier done around 16–18 weeks of pregnancy, but now the trend has changed. First-trimester anomaly scans have gained much importance. NT scans can pick up severe anomalies like anencephaly early in pregnancy and provide the mother as well as the family with emotional as well as physical trauma. Ultrasound is also effective in the progress of soft tissues of the neck, breasts, abdomen, pelvis, etc. Early signs of breast cancer can be detected using mammography.

CT (computerized tomography) scans (during surgical procedures) allow physicians and radiologists to identify internal structures and, in turn, their shapes, size, density, and texture which is ultimately useful to the practitioners to monitor the exact location of the problem to give the best treatment. In an X-ray, the structures overlap; however, in a CT image overlapping structures are removed. CT scan is an investigation which is based on the use of X-rays in an advanced manner. It is different from a conventional X-ray image as it makes use of multiple X-rays projected from several angles and positions to form a representative image.

Along with ultrasound, fetal MRI has also shown significant promise over the last few years, and it has been extremely useful in detecting anomalies of the brain and spine where ultrasound might be inconclusive. Unlike X-ray, MRI is one of the best scans in the medical field because it does not emit radiation, and therefore it is

safe for the human body. MRI technique combines radio waves with magnets to create a unique image that can be used to view defects such as tumors, injuries, and abnormalities within the body.

2 Imaging Modalities

2.1 Magnetic Resonance Imaging

2.1.1 Principles of MRI

MRI is based on the interaction of atomic nuclei in the presence of a magnetic field externally. The human body consists of about 70% of water molecules. Protons in the water molecules of the body align with the direction of the strong magnetic field when the body is inserted in the magnet and precess about it due to their magnetic moment. The frequency of the precessional motion ω is described by the Larmor relationship

$$\omega = \gamma \mathrm{Bo}$$

where ω is the frequency of precession, γ is the gyromagnetic ratio, and Bo is the external magnetic field strength. To obtain an image, frequency variation across the sample is necessary. Therefore, pulsed linear magnetic field gradients are applied to the main magnetic field. With these magnetic field gradients, the frequency spectrum can be converted into position-dependent signal intensity. By using a two-dimensional Fourier transformation, the spin population at any definite position (PIXEL) is obtained. The imaging unit (VOXEL) consists of x- and y-axis dimensions and the z-axis as a thin slice section that is selectively excited by applying a z-axis magnetic field gradient at the same time as a 90° excitation RF pulse producing an image map using the computer. In the 2D FT spin-echo sequence, the acquisition of the signal occurs at a certain echo time TE after the excitation of the spin system, and then the signal will decay according to the T_2 relaxation process with the relation:

$$\mathrm{M}\left(\mathrm{TE}\right) = \mathrm{Me}^{-\mathrm{TE/T2}}$$

Thus, signal intensity or contrast in images mainly depends on TE. To generate a two-dimensional image of N × N picture elements, the sequence will be repeated N times. From the above explanation, it is clear that the intensity of MR image normally depends on a combination of parameters, viz., spin density, T_1, T_2, and diffusion behavior [8]. The MRI machine that we use in our imaging center is shown in Fig. 2, which is being used for studying pathologies of the nervous system (Figs. 3, 4, and 5).

Fig. 2 3 Tesla GE 750 W discovery with MRgFUS at Nanavati Max Super Speciality Hospital, Mumbai

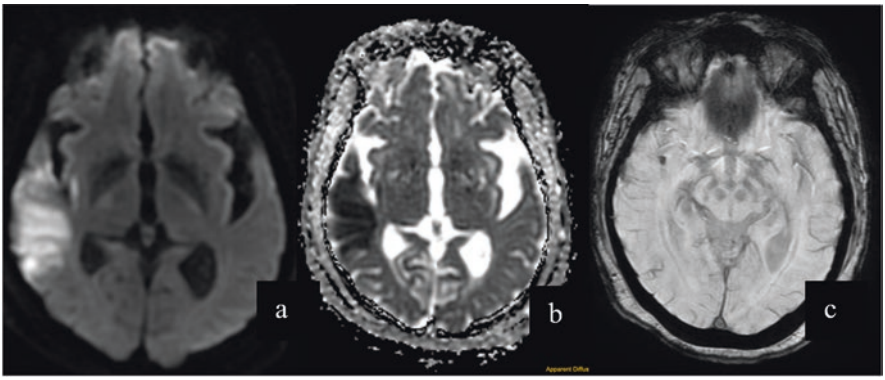

Fig. 3 Axial MRI images of the brain showing an acute infarct in the right middle cerebral artery (MCA) territory secondary to a thrombus in the inferior division of the right middle cerebral artery. Diffusion weighted image (**a**) showing restricted diffusion in the right temporal region with loss of ADC values. (**b**) An area of blooming seen on SWAN images in the inferior division of right MCA (**c**)

2.1.2 Applications of Nanoparticles in MRI

Contrast agents used in MRI are gadolinium based which have relatively low relaxivity, and as high dose of agents is required, they may cause severe side effects such

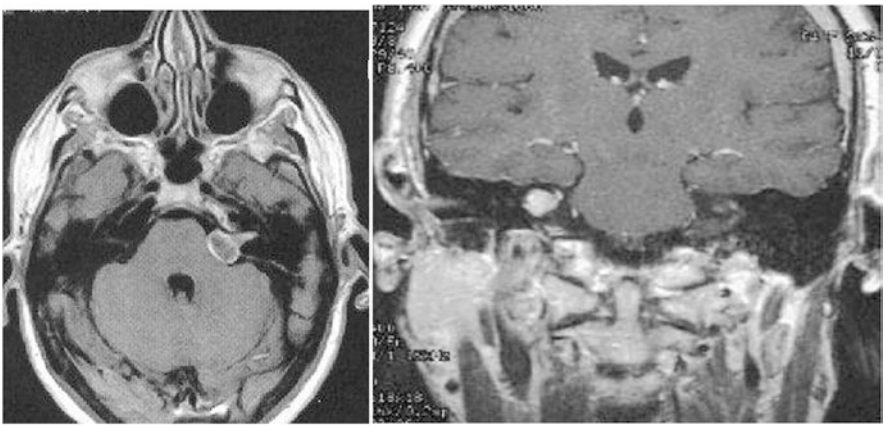

Fig. 4 MRI brain with cerebello-pontine angle showing CP angle lesion-acoustic schwannoma

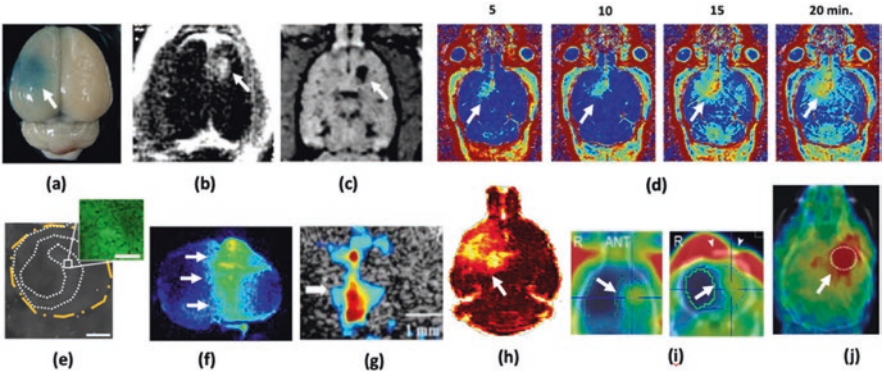

Fig. 5 Representative images demonstrating the use of various modalities to monitor FUS-BBBO: (**a**) staining with Evans blue dye (arrow), (**b**) TI-weighted CE-MRI, (**c**) T2-weighted CE-MRI, (**d**) MRI T1 relaxometry to sequentially follow the distribution of penetrating Gd-DTPA, (**e**) fluorescent-tag dextran penetration using optical microscopy, (**f**) autoradiography, (**g**) dynamic ultrasound imaging, (**h**) DCE-MRI, (**i**) 99mTc-DTPA SPECT, and (**j**) 68Ga PET (*min* minutes, *ANT* anterior) [9]

as nephrogenic systemic fibrosis (NSF) [10]. MR images need to be high resolution in order to provide good soft tissue contrast which is impeded by the intrinsic short circulation time of gadolinium-based agents. To overcome this drawback, gadolinium chelates are conjugated onto a macromolecule, but the non-excreted ions increase the possibility of side effects [11]. Iron oxide-based nanomaterials have been extensively studied as a safe contrast agent in order to overcome these limitations of gadolinium-based contrast agents. The iron oxide nanoparticles are processed and degraded in the body by the reticuloendothelial system. The iron ions which are degraded are then stored in the form of ferritin which is then used in several biological processes like the production of red blood cells. In comparison to

gadolinium-based complexes, iron-based NPs have higher sensitivity and biocompatibility. The US Food and Drug Administration (FDA) has approved many nanoparticles based on iron oxide compounds. For example, Feridex was used as a T_2 contrast agent for imaging liver cancer, and Resovist is also used to characterize focal liver lesions in some countries [12]. Ferumoxytol is clinically approved as an MRI contrast agent and for simultaneous treatment of iron deficiency anemia due to the tendency to be taken up by macrophages [13].

The construction of most nanoparticles is done in such a way that their size is small enough to pass within capillaries and enter cells. These nanoparticles can carry about 100,000 molecules of metal. This helps in increasing the contrast agent density. Polymer nanoparticles and carbon nanotubes are used as vehicles for gadolinium ions or iron oxide nanocrystals. One of the most attractive nanomaterials for various biomedical applications is iron oxide nanoparticles which provide excellent imaging contrast. MRI is high resolution but insensitive to molecular signals. If a sample contains nanoparticles, the sensitivity increases. Ultrasmall paramagnetic iron oxide particles help in the improvement of the nodal staging of patients with bladder cancer. Sensitivity and negative predictive values significantly increase. Manganese (Mn) oxide nanoparticles which are silica-coated can be used to study the dynamics of the nerve cell and its function as Mn enters the neurons through channels reserved for Ca. This can help in measuring the rate of transport down the length of the axon. They can be used in cardiac MRI as cell entry and retention of Mn^{2+}ceases early during ischemia which is resumed in viable cells on reperfusion. Mn^{2+} releasers may therefore be effective MRI markers of viability. These help to detect microthrombi in vulnerable plaques. Fibrin-targeted nanoparticles may help in detecting microthrombi in vulnerable plaques. T1WI image is acquired with targeted fibrin-specific paramagnetic nanoparticles. Nanoparticles can also be used to detect and quantify angiogenesis in tumors by using nanoparticles targeted to αvβ3 integrin. Transplanted labeled stem cells can also be monitored. The future of nanoparticles in MRI is bright. It will combine both detection and treatment into a single process. Nanoparticles coupled to the radio frequency of MRI can convert radio frequency into heat energy that kills the cancer cells. Hybrid contrast agents-PET marker (e.g., Cu^{64}) can be added to an MR marker, creating an MRI/PET contrast agent.

For best MR images, contrast agents play an important role. They are evaluated on the basis of their relaxivities which determine the increase in relaxation rates of water protons. The relaxivities (r_2) of the coated magnetic nanoparticles were measured in our laboratory (RSC), and the results obtained in our clinic (DP) showed that r_2 of the Fe complex was higher than that of MRI contrast agent Gd-DTPA used in general clinics. The drug was conjugated to the Fe_3O_4 nanoparticles which can be used for various applications such as photodynamic therapy, hyperthermia, etc. Fe_3O_4 NPs coated with PEG polymer and photosynthesizer drug show a uniform size distribution. Polymer coating prevents oxidation and allows for conjugation of functional ligands with uniform size distribution. T_2 is mainly influenced by outer-sphere processes. T_2 relaxivity (r_2) increases as the size is higher than that of bare Fe_3O_4 NPs. Figure 6 shows the T_2-weighted MR images. The degree of the T_2

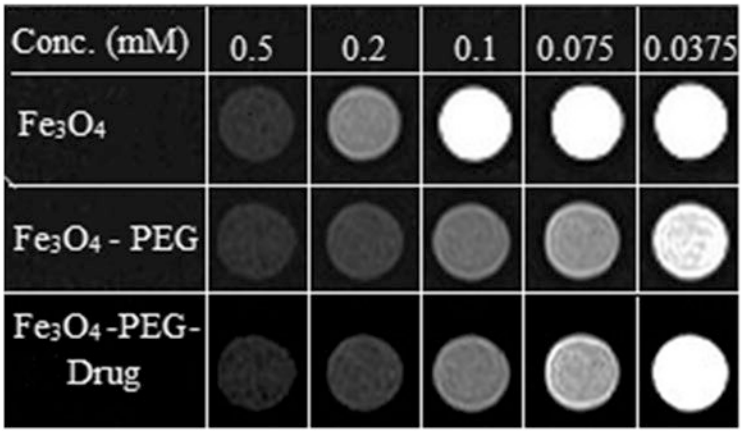

Fig. 6 MRI images of Fe_3O_4, Fe_3O_4-PEG, and Fe_3O_4-PEG-drug for Fe conc. of 0.5, 0.2, 0.1, 0.075, and 0.0375 mM in water [14]

contrast effect is typically represented by the spin-spin relaxivity r_2 ($r_2 = 1/T_2 s^{-1}$), where higher values of r_2 result in a greater contrast effect [14].

2.2 Ultrasonography

2.2.1 Principles

Ultrasound (USG) is a widely used imaging modality in medicine due to its several merits over other modalities like wide availability, adaptability, noninvasiveness, and real-time imaging.

For example, ultrasonic technology producing sonogram images in women gives details of the parts of the body being formed in the womb to the physician. Ultrasonography uses the interaction between sound waves and tissue surfaces to produce an image of the organ/tissue or, in Doppler modes, determine the velocity of moving tissue, primarily blood. The images obtained are real-time and dynamic, which are used to derive functional and structural knowledge about target organs. The confirmation of pregnancy, whether intra- or extrauterine, is done by USG. Fatal medicine is one area where radiology has shown to be of extreme importance, and the value it adds is only increasing day by day. Anomaly scans used to be earlier done around 16–18 weeks of pregnancy, but now the trend has changed. First-trimester anomaly scans have gained much importance. NT scans can pick up severe anomalies like anencephaly early in pregnancy and provide the mother as well as the family with emotional as well as physical trauma.

2.2.2 Applications of Nanotechnology in Ultrasonography

Most imaging modalities use contrast agents for certain studies to provide better results. Contrast agents have been extensively used in diagnostic ultrasound for detecting diseases as these tend to increase the reflected signal received from flowing blood. In clinical ultrasound, the various applications of microbubbles in contrast studies like sono-hysterosalpingography have become extremely important. Microbubbles are small (typically 3 μm in diameter) gas-filled bubbles, which are surrounded by various shell materials like fats, surfactant polymers, etc. that are used as contrast in sonography [15]. They can be injected intravenously like in tumor vascularity assessment or introduced into certain body cavities like uterine instillation for determining fallopian tube patency or for evaluation of vesicoureteric reflux in children where microbubbles are injected into the bladder cavity [16]. According to several published studies, these techniques comparatively show high sensitivity and specificity than the conventional methods of X-ray micturating cystourethrography (MCU) and hysterosalpingography (HSG), also eliminating the use of ionizing radiation in children and women planning a pregnancy [17].

Microbubbles resonate in an ultrasound beam, rapidly contracting and expanding in response to the pressure changes of the sound wave and enhancing both greyscale images and flow-mediated Doppler signals. But these conventional microbubbles have low stability and are larger in size which makes it difficult to exit vasculature. With the development of nanotechnology, nanoparticles seem to be a good tool for precise diagnosis and therapy especially due to their nanoscale properties. Microbubbles are predominantly used as blood pool agents, but they have a drawback due to their size. These are not able to permeate through blood vessels easily and thus may remain limited to certain investigations like those of the cardiac system. Microbubbles are stabilized gas bubbles surrounded by shell materials like lipid, surfactant polymer, or other materials. They also have limited use in tumor-directed imaging due to their comparatively larger size than nanobubbles.

The size of nanobubbles is significantly smaller than microbubbles, in the range of 101–210 nm, thus increasing bioavailability and making it easier to exit vessels and enhance intratumoral distribution during the assessment of tumors. Also, in comparison to microbubbles, the surface area-to-volume ratio of nanoparticles is much higher when compared to that of traditional microbubbles [18–20]. Due to their structural arrangement, blood circulation times can be prolonged, and high accumulation time can be achieved in tumors [21]. Nanoparticles have been used for tumor analysis and therapy as well. Because of neovascularization, several new leaky vessels develop in tumors which can be targeted. These particles accumulate in tumors passively due to the increased permeability of vessels. Another way is to add ligands that can bind to specific target sites, avoiding normal tissue, for example, delivery of drugs to cancer.

High-intensity focussed ultrasound (HIFU) is a noninvasive technique for therapeutic purposes which makes the use of ultrasound waves to ablate tissue by using the thermal and tissue-penetrating characteristics of high-intensity ultrasonic waves

which induce tissue coagulative necrosis. Nanoparticles have been used with HIFU to enhance the efficiency by deposition of thermal energy within deeper tissues.

In the case of chemotherapeutic drug agents, nanoparticles have been used to protect the drug from degradation by encapsulating and releasing it at the required location without compromising the efficacy. NPs are used as drug delivery systems, which can protect the drug from degradation by securely encapsulating it in their structure and releasing it at the tumor site under internal and external stimuli [22]. Figure 7 is the photograph of the USG machine being used in our hospital. Figure 8 represents ultrasound images showing the differences in the contrast in the ultrasound images with and without the use of nanobubbles.

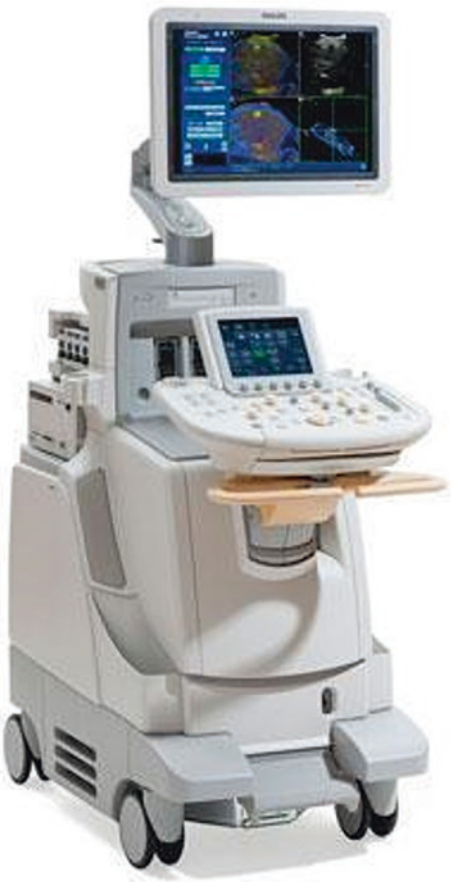

Fig. 7 Philips IU 22 X Matrix USG machine

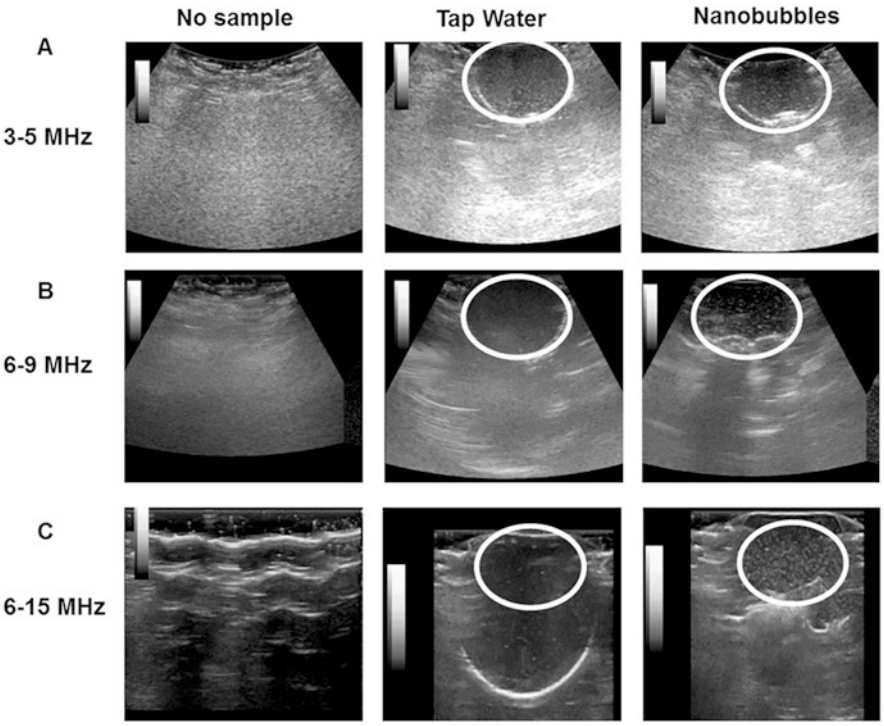

Fig. 8 Ultrasound images of ONBs. No sample, tap water, and nanobubbles were compared. (**a**) Images with a 3–5 MHz transducer. (**b**) Images for a 6–9 MHz transducer. (**c**) Images with a 6–15 MHz transducer [23]

2.3 CT Scan

2.3.1 Principles

Roentgen discovered X-rays in 1895. Immediately after his discovery, X-ray imaging was invented. X-rays are emitted by scanners from various angles. In this technique, X-rays propagate through space as electromagnetic energy. During this process, while interacting with atoms, they either absorb or scatter. The difference between the X-rays absorbed by the body and X-rays transmitted through the body is measured by the detectors in the scanner and is termed attenuation. The amount of attenuation is determined by the density of the imaged tissue. For example, bone is high-density tissue, and hence, it absorbs maximum radiation, and the remaining reduced amount is detected by the scanner. On the contrary, low-density tissue such as the liver absorbs minimum radiation, and the bigger signal is detected by the scanner. Physicians see that radiation exposure from an X-ray is low to save damage to the radiated tissue. X-rays are commonly used to image bones and teeth and chests, dislocations, bone decay, etc.

CT (computed tomography) scan is an advanced form of X-ray radiation. This technique uses multiple X-rays from various angles and positions and then forms a detailed image. Normal X-ray is a traditional 2D image, while the CT technique gives a 3D picture of diseased tissue. This helps to view images from different angles to diagnose the tumor clearly. A 3D image of the human body is generated by the use of advanced mathematical algorithms on a monitor as stacked images. CT scans (during surgical procedures) allow physicians and radiologists to identify internal structures and in turn, their shapes, size, density, and texture which is ultimately useful to the practitioners to monitor the exact location of the problem to give the best treatment. In an X-ray, the structures overlap; however, in a CT image, overlapping structures are removed. It differs from traditional X-rays.

Image of almost the entire body, from the neck to the thighs, can be created in a very short time. Hence, CTs are incredibly useful for diagnosing and staging cancer. Location of spread of cancer can be seen very effectively in the lungs, liver, or bone and is considered as the first choice to stage cancer. It is very effective for surveying the entire body to look for places where cancer has spread, such as the lungs, liver, or bone (Figs. 9, 10, 11, and 12). Many a time, CT is the first choice to stage cancer. But due to radiation problems, it is not advisable to have multiple CT scans.

Fig. 9 Siemens Biograph 64 SLICE PET-CT scanner PET-CT machine at Nanavati Max Super Speciality Hospital (previously known as Dr. Balabhai Nanavati Hospital). India's first whole-body CT in the country

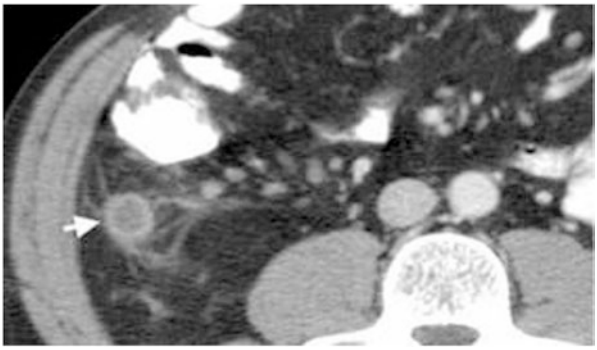

Fig. 10 CT scan of the abdomen and pelvis showing an inflamed appendix with wall thickening and surrounding fat stranding

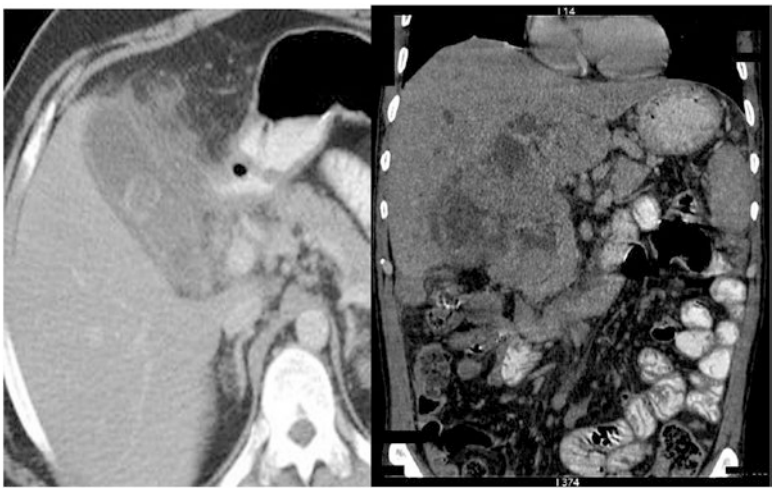

Fig. 11 CT scan of the abdomen showing features of cholecystitis

2.4 PET Scan

2.4.1 Principles

Positron emission tomography (PET) is an excellent molecular imaging modality (nuclear imaging technique) and a minimally invasive imaging procedure with a wide range of clinical and research applications. PET enables the study of biological function in both health and disease, in contrast to MRI and CT, which are more suited to study a body's morphologic changes (functional MRI is an exception which is used to study certain brain functions by measuring blood flow changes). A defined quantity of radioactive dye is injected into a peripheral vein. The emitted radioactivity is detected when these radioactive particles are spread through the

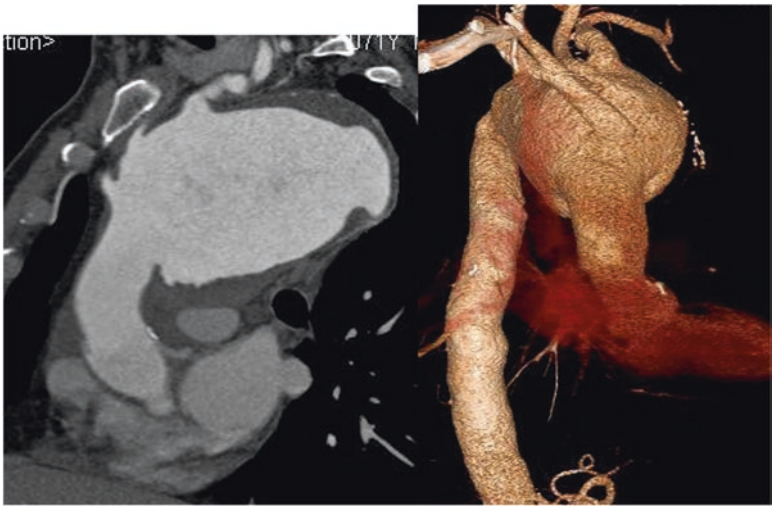

Fig. 12 CT chest showing a large aortic aneurysm

body, and this information is used to see how the organs and tissue are functioning. The scanner picks up the particles in the affected organs and sends the images it captures to a computer that creates usable images for further studies. PET scans can help identify changes that occur at the cellular level. They can detect diseases before they are apparent on other imaging tests. The routine radiotracer used for clinical PET imaging is fluorine-18-fluoro-2-deoxy-D-glucose (F-18-FDG) which is a glucose molecule with one oxygen substituted with radioactive F-18 (positron-emitting radioisotope). PET scans are generally used for illnesses related to the blood, organs, and brain to diagnose epilepsy and Alzheimer's disease.

Generally, PET scan images are not well informative compared to images created by MRIs or CT scans. A new hybrid PET-CT scan is available that combines the two techniques and creates a very detailed, accurate image to detect cancer.

2.5 PET-CT

2.5.1 Principles

A combination of PET scanner with CT scanner is a new nuclear medicine technique. PET-CT is a unique combination for cancer tumor detection. PET and CT provide qualitative and quantitative metabolic information of the tumor. PET provides metabolic information, while CT provides anatomic information. Thus, PET-CT has the ability to accurately localize increased radiotracer activity to specific normal or abnormal anatomic locations (REF1). PET-CT scans are widely used for evaluating the extent of disease and provide more accurate staging. Usually, this

combination is very useful for detecting and localizing lung cancers. The benefit of PET-CT is that it helps clinicians to assess structural as well as functional activity of organs and pathologies. A substance called a "tracer" contains glucose with a little bit of radioactive material attached before the test. This tracer acts like a dye for imaging (bright spot) and is safe for the patients. PET-CT scans are useful for the detection of brain diseases and heart problems.

2.6 Mammography

Mammography is a specialized breast imaging technique that uses low-dose X-rays. It is used for breast cancer screening as well as for diagnostic purposes when patients present with symptoms like a lump in the breast, nipple discharge, etc.

Mammography plays an important role in breast cancer screening and has been used in combination with ultrasound mammography for better detection. The breast tissue is compressed between two surfaces to evenly spread out the tissue. Mammography is one of the investigations used worldwide for breast cancer screening, and several guidelines have been laid down. They can help detect cancers of the breast even before they cause signs and symptoms. Mammograms have been shown to reduce the risk of death due to breast cancer.

A. **FFDM**

FFDM (full-field digital mammography) is a technique that uses solid-state detectors which convert X-rays into electronic signals which are used to produce images of the breasts. These images can be printed on films or viewed on the computer screen. Computer-aided detection (CAD) systems are especially useful for lesion pick-up. This helps by searching mammography images for the presence of abnormal areas of increased density, microcalcifications, or mass that may be suspicious. It helps radiologists by bringing attention to an area that might have been overlooked.

Breast tomosynthesis is a technique similar to a CT scan where a series of slices are used to reconstruct a three-dimensional image of the breast. It is also known as three-dimensional mammography or digital breast tomosynthesis (DBT). This technique may be particularly helpful in small early breast cancers which may not be seen on conventional images or in dense breasts. Detection of multiple breast tumors, as well as better delineation of size, shape, and location of the mass, is better with tomosynthesis.

B. **Diagnostic Mammography**

Diagnostic mammography is used to assess a patient with symptoms/abnormal clinical findings, such as a breast lump or nipple discharge. Diagnostic mammography is usually done after the initial screening mammogram, which is abnormal, for evaluating the area of abnormality in detail.

3 Nanoparticles for Computed Tomography (CT)

CT scan is a widely used imaging mainly due to its low cost, easy availability, high spatial resolution, and less time. The basic principle of CT scan is attenuation of X-rays by different tissues and contrast agents. Since differential attenuation of X-rays is dependent on the mass density and the atomic number of various tissues, slight changes in the soft tissues might be difficult to detect, so we acquire good quality images. Barium sulfate suspensions and iodinated contrast agents are used as standard CT contrast agents mainly due to their high atomic numbers. Barium sulfate suspensions are used primarily for imaging the gastrointestinal system due to the toxic nature of barium ions. Iodinated agents, like iopamidol and iodixanol, are used as injectable CT contrast agents administered intravenously.

Nano-sized iodinated contrast agents have been introduced to overcome the limitations of current CT contrast agents. These include micellar, polymeric, and liposomal contrast agents. Nanoparticles due to their size prevent getting filtrated by the kidneys and thus have a longer circulation time. As the K-edge energy level of iodine is significantly lower than the energy of X-ray photons in CT, contrast agents based on heavy metals are used for more sensitive imaging.

The various nanoparticles being studied are gold-, tantalum-, tungsten-, and bismuth-based contrast agents. Gold nanoparticles have a K-edge energy level of 80.7 keV and thus have a better contrast effect than iodine-based agents as well. Gold nanomaterials in various shapes such as spheres, rods, cages, and shells have been studied because of their excellent biocompatibility and facile synthesis [24, 25]. Gold nanoparticles, 1.9 nm in size, produced by Nanoprobes Inc. were studied as an X-ray imaging contrast agent [26].

Gold particles have been used in the imaging of tumors and blood vessels less than 100 μm in diameter. Polyethylene glycol (PEG)-coated gold has also been developed. The gold nanoparticles accumulate in organs with rich RES like the liver and help in the diagnosis of hepatomas amongst normal liver tissue (Fig. 13). Gold nanoparticles have a drawback in that they are expensive to be used routinely. Work is being done towards finding cheaper alternatives. For instance, lanthanides have been used as CT contrast agents because gadolinium complexes have been used as MRI contrast agents in clinics. Other particles being studied are bismuth- and tungsten-based nanoparticles.

.

4 A Comparison of CT and MRI

Both CT and MRI devices have their own strengths in detecting and monitoring cancer and its stages. The radiologist uses the particular machine depending on which images of the parts of the body are to be imaged. The CT scan uses ionizing radiation using X-rays to capture 360-degree images of bones, organs, and tissues.

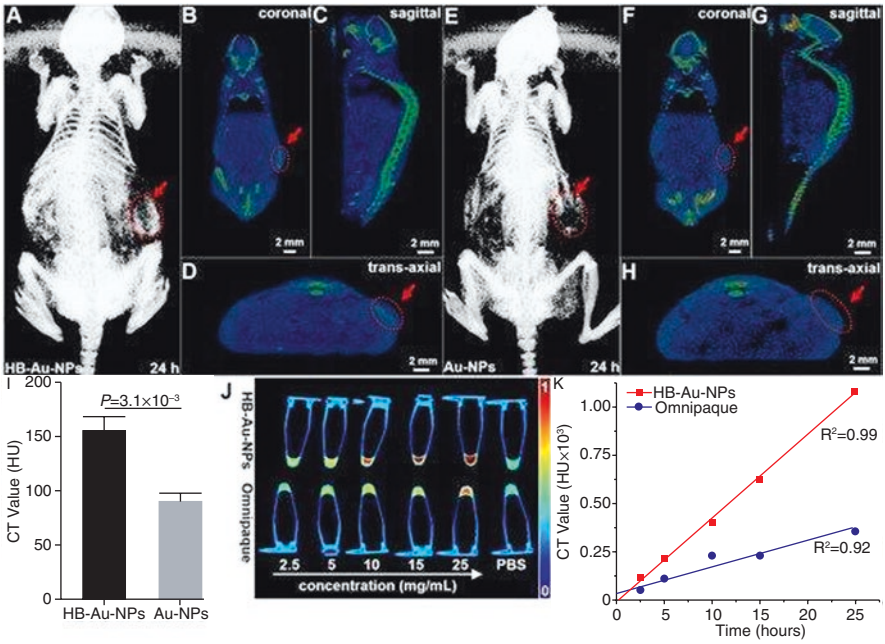

Fig. 13 CT images. Representative 3D-reconstructed whole-body CT images at 24 h following intravenous injection of (**a–d**) HB-Au-NPs and (**e–h**) Au-NPs are shown. The locations (arrows) of implanted human OE33 xenograft tumors are shown in the axial, sagittal, and coronal views. (**i**) Quantified results showed a mean value of 155.08 ± 14.94 HU for HB-Au-NPs and 90.47 ± 9.05 HU for Au-NPs from $n = 3$ animals, $p = 3.1 \times 10^{-3}$ by unpaired t-test. (**j**) CT image of HB-Au-NPs and Omnipaque in vials at different concentrations, including 0 (PBS), 2.5, 5, 10, 15, and 25 mg/mL). (**k**) Intensities increase linearly with the concentration of HB-Au-NPs, $R^2 = 0.99$, and Omnipaque, $R^2 = 0.92$ [27]

It is very much helpful to diagnose severe injuries of the chest, head, spine, fractures, etc. since the creation of images takes a few minutes. Also, it is possible to pinpoint the location and size of the tumor. CT scans use ionizing radiation, and this might be some damage to DNA and, in turn, may cause a mild increase in the risk of cancer.

An MRI, however, often does a better job at diagnosing problems in the joints, soft tissues, ligaments, and tendons. It is an excellent tool for evaluating spinal ligaments. Unlike CT, an MRI scan, however, uses powerful magnets and radio waves to create the images. So, the patient is not exposed to ionizing radiation. The MRI applies a magnetic field to align protons of the body and radio waves in the form of short pulses to the protons in the body. 3D images of the infected organs are created by processing the signal with the help of a computer. The processing of the signal usually takes more than 30 min. Some cancers, such as liver, prostate, and uterine, which cannot be detected by CT, are detected by MRI scans.

Contrast dyes are commonly used in both CT scan and MRI before or during the procedure. This helps the radiologist see organs and pathologies with more clarity.

5 Conclusion and Outlook

Molecular imaging is widely being used for quantitative noninvasive diagnosis of several clinical conditions, cancer staging, and quantification of biological processes. Rather than using a single modality, a combination of different modalities always yields more information. Nanotechnology has provided hope of providing more useful molecular information, but the clinical applications are yet to be done. New and promising nanoparticles are being developed as new treatment options soon as carriers for drugs, therapeutic agents, or imaging agents provided all characterizations including toxicity and efficacy studies are done on these newly developed nanomaterials so that human trials can be performed.

References

1. https://en.wikipedia.org/wiki/Molecularimaging
2. Kircher MF, et al. A brain tumor molecular imaging strategy using a new triple-modality MRI-photoacoustic-Raman nanoparticle. Nat Med. 2012;18:829–34. https://doi.org/10.1038/nm.2721.
3. Hyafil F, Cornily JC, Feig J, et al. Noninvasive detection of macrophages using a nanoparticulate contrast agent for computed tomography. Nat Med. 2007;13:636–41. https://doi.org/10.1038/nm1571.
4. Ye D, Shuhendler AJ, Pandit P, Brewer KD, Tee SS, Cui L, Tikhomirov G, Rutt B, Rao J. Caspase-responsive smart gadolinium-based contrast agent for magnetic resonance imaging of drug-induced apoptosis. Chem Sci. 2014;5:3845–52. https://doi.org/10.1039/C4SC01392A. Crossref, ISI, Google Scholar
5. Zhu S, et al. Molecular imaging of biological systems with a clickable dye in the broad 800- to 1,700-nm near-infrared window. Proc Natl Acad Sci U S A. 2017;114:962–7. https://doi.org/10.1073/pnas.1617990114.
6. Bayda S, Adeel M, Tuccinardi T, Cordani M, Rizzolio F, et al. Molecules. 2020;25:112. https://doi.org/10.3390/molecules25010112.
7. Endo-Takahashi Y, Negishi Y. Microbubbles and nanobubbles with ultrasound for systemic gene delivery. Pharmaceutics. 2020;12:964.
8. Chaughule RS, Desai SB. Clinical applications using new MR sequences. In: Chaughule RS, Ranade SS, editors. Looking into living things through MRI. Mumbai: Prism Publications; 2006. p. 153–61.
9. Chen K-T, Wei K-C, Liu H-L. Focused ultrasound combined with microbubbles in central nervous system applications. Pharmaceutics. 2021;13:1084. https://doi.org/10.3390/pharmaceutics13071084).
10. Perazella MA. Current status of gadolinium toxicity in patients with kidney disease. Clin J Am Soc Nephrol. 2009;4:461–9. https://doi.org/10.2215/CJN.06011108.
11. Boros E, Gale EM, Caravan P. MR imaging probes: design and applications. Dalton Trans. 2015;44:4804–18. https://doi.org/10.1039/c4dt02958e. Crossref, PubMed, ISI, Google Scholar
12. Achilefu S. Introduction to concepts and strategies for molecular imaging. Chem Rev. 2010;110:2575–8. https://doi.org/10.1021/cr1001113. Crossref, PubMed, ISI, Google Scholar
13. Lu M, Cohen MH, Rieves D, Pazdur R. FDA report: ferumoxytol for intravenous iron therapy in adult patients with chronic kidney disease. Am J Hematol. 2010;85:315–9. https://doi.org/10.1002/ajh.21656. PubMed, ISI, Google Scholar

14. Chavan P, Pednekar S, Chaughule R, Patkar D. Microwave assisted synthesis of magnetic nanoparticles with higher relaxivities as contrast agents for MRI. Int J Recent Sci Res. 2017;8(4):16687–91.
15. Li L, Guan Y, Xiong H, et al. Fundamentals and applications of nanoparticles for ultrasound-based imaging and therapy. Nano Select. 2020;1:263–84. https://doi.org/10.1002/nano.202000035.
16. Blomley MJK, Cooke JC, Unger EC, Monaghan MJ, Cosgrove DO. Microbubble contrast agents: a new era in ultrasound. BMJ. 2001;322:1222. https://doi.org/10.1136/bmj.322.7296.122.
17. Darge K, Troeger J, Duetting T, Zieger B, Rohrschneider W, Moehring K, Weber C, Toenshoff B. Reflux in young patients: comparison of voiding US of the bladder and retrovesical space with echo enhancement versus voiding cystourethrography for diagnosis. Radiology. 1999;210(1):201–7. https://doi.org/10.1148/radiology.210.1.r99ja40201. PMID: 9885609
18. Rabinow B. Nanosuspensions in drug delivery. Nat Rev Drug Discov. 2004;3:785–96. https://doi.org/10.1038/nrd1494.
19. Yang W, Peters JI, Williams RO. Inhaled nanoparticles—A current review. Int J Pharm. 2008;356(1–2):239–47. ISSN 0378-5173. https://doi.org/10.1016/j.ijpharm.2008.02.011.
20. Palmberger TF, Albrecht K, Loretz B, Bernkop-Schnürch A. Thiolated polymers: evaluation of the influence of the amount of covalently attached L-cysteine to poly (acrylic acid). Eur J Pharm Biopharm. 2007;66(3):405–12. https://doi.org/10.1016/j.ejpb.2006.11.017. Epub 2006 Dec 1. PMID: 17267191
21. Petros RA, DeSimone JM. Strategies in the design of nanoparticles for therapeutic applications. Nat Rev Drug Discov. 2010;9(8):615–27. https://doi.org/10.1038/nrd2591. Epub 2010 Jul 9. PMID: 20616808
22. Lim E-K, Jang E, Lee K, Haam S, Huh Y-M. Delivery of cancer therapeutics using nanotechnology. Pharmaceutics. 2013;5:294–317. https://doi.org/10.3390/pharmaceutics5020294.
23. Khan MS, Hwang J, Lee K, Choi Y, Jang J, Kwon Y, Hong JW, Choi J. Surface composition and preparation method for oxygen nanobubbles for drug delivery and ultrasound imaging applications. Nanomaterials. 2019;9:48. https://doi.org/10.3390/nano9010048.
24. Dreaden EC, Alkilany AM, Huang X, Murphy CJ, El-Sayed MA. The golden age: gold nanoparticles for biomedicine. Chem Soc Rev. 2012;41:2740–79. https://doi.org/10.1039/c1cs15237h.
25. Xi D, Dong S, Meng X, Lu Q, Meng L, Ye J. Gold nanoparticles as computerized tomography (CT) contrast agents. RSC Adv. 2012;2:12515–24. https://doi.org/10.1039/C2RA21263C.
26. Hainfeld JF, Slatkin DN, Focella TM, Smilowitz HM. Gold nanoparticles: a new X-ray contrast agent. Br J Radiol. 2006;79:248–53. https://doi.org/10.1259/bjr/13169882.
27. Chen J, Nguyen VP, Jaiswal S, Kang X, Lee M, Paulus YM, Wang TD. Thin layer-protected gold nanoparticles for targeted multimodal imaging with photoacoustic and CT. Pharmaceuticals. 2021;14:1075. https://doi.org/10.3390/ph14111075.

Nanoparticles for Enhanced Radiotherapy and Imaging Applications

Danny Jian Hang Tng, Li Ming Chong, Melvin Lee Kiang Chua, Yong Zhang, and Ken-Tye Yong

1 Introduction

Cancer is one of the leading causes of death globally; it is estimated that almost ten million deaths per year are attributed to cancer [1]. It is an increasingly difficult to treat disease, requiring a coordinated approach of multiple treatment modalities to achieve favourable outcomes. Radiotherapy (RT) is one of the key methods by which cancer is treated. In radiotherapy, energy is applied in a targeted fashion to neoplastic cells, causing genetic material and organelle damage, thereby causing cellular death [2]. This energy may arise from an external source, such as a linear accelerator, which produces high-energy X-rays that achieves targeted delivery using computer control to ensure maximal dosage at the tumour. Alternatively, the

Danny Jian Hang Tng and Li Ming Chong are co-first authors.

D. J. H. Tng
Department of Infectious Diseases, Singapore General Hospital, Singapore, Singapore

Program in Emerging Infectious Diseases, Duke-NUS Medical School, Singapore, Singapore

Division of Radiation Oncology, National Cancer Centre Singapore, Singapore, Singapore

L. M. Chong
Department of Biomedical Engineering, Faculty of Engineering, National University of Singapore, Singapore, Singapore

M. L. K. Chua
Division of Radiation Oncology, National Cancer Centre Singapore, Singapore, Singapore

Division of Medical Sciences, National Cancer Centre Singapore, Singapore, Singapore

Oncology Academic Program, Duke-NUS Medical School, Singapore, Singapore

R. S. Chaughule et al. (eds.), *Nanomaterials for Cancer Detection Using Imaging Techniques and Their Clinical Applications*,
https://doi.org/10.1007/978-3-031-09636-5_2

energy can also arise from an internal source, such as in molecular radiotherapy (radionuclide therapy), where intravenously administered radionuclides, such as radium-223, undergo radioactive decay to produce short-range, energetic alpha particles at the site of the neoplasm. To achieve maximal damage to the tumour and concurrently limit side effects from radiotherapy treatment, radiotherapy is often administered using conformal therapy. This is where the internal or external energy is administered in such a manner to maximize the energy dosage at the sites of disease, [3] while at the same time, minimizing energy dosage to the neighbouring healthy tissues. Radiotherapy achieves its therapeutic effects by leveraging the difference in cellular repair when cancerous and healthy cells are exposed to radiation. As defective DNA repair mechanisms are present in many cancerous cells, the repeated radiation energy exposure would damage the cellular genetic material, leading to cellular dysfunction and death, thereby eradicating the tumour [4]. On the other hand, healthy cells are less affected by radiation energy, as the DNA repair mechanisms are intact, allowing recovery if in between radiation dose sub-sessions or dose 'fractions'. As a result, radiotherapy is often administered using fractionated dosing, where the complete dose is administered over days to weeks. This allows healthy tissues to repair whilst still damaging the tumour cells. A balance often has to be derived during treatment. If the fractional dosage is too high, or if the fractions are too close to one another, higher tumour cell kill would be achieved, but this is at the expense of radiotoxicity in the healthy tissues. This is due to the cellular repair mechanisms within these healthy tissues not being able to keep up with the damage caused during treatment sessions [5].

In external beam radiotherapy, conformal therapy is achieved by shaping the delivered beam energy using a series of heavy metal collimators to absorb the outgoing beam in a manner whereby the healthy tissues are minimally exposed to the beam, whilst still maintaining the needed dose at tumour sites for therapy. Additionally, the beam can also be delivered from multiple angles, and its energy can be adjusted such that critical structures, known as the organs at risk (OAR), such as the heart, brain, or liver, are minimally dosed, whilst maintaining the required dosage for tumour treatment in the diseased tissue. This technique is known as modulated therapy, and many variations are available, such as volumetric modulated arc therapy (VMAT), intensity-modulated radiation therapy (IMRT), and stereotactic body radiation therapy (SBRT) [6, 7]. When applied optimally, this has allowed radiotherapy to even achieve similar long-term outcomes as surgical

Y. Zhang
Department of Biomedical Engineering, Faculty of Engineering, National University of Singapore, Singapore, Singapore

NUS Graduate School for Integrative Sciences and Engineering, National University of Singapore, Singapore, Singapore

K.-T. Yong (✉)
Faculty of Engineering, School of Biomedical Engineering, The University of Sydney, Camperdown, NSW, Australia
e-mail: ken.yong@sydney.edu.au

excision in the treatment of some cancers [8]. Besides controlling the direction of the beam, the dosage can also be adjusted based on the different penetration and dosing physics of the different particles used to deliver energy. For example, these particles can take the form of X-rays, protons, electrons, and heavy metal ions. Each particle exhibits different tissue interactions, resulting in different dose distributions within tissues. The application of these different dose distributions allows the dosage to be adjusted for maximal tumour cell death [9]. The combined use of these techniques has allowed radiotherapy to be the choice of treatment for many different malignancies [10–12]. However, dosage to healthy tissue cannot be completely avoided, resulting in side effects after treatment of the adjacent tumour [13]. Similarly, in molecular radiotherapies, where the radioactive drugs are delivered systemically, damage to healthy tissues cannot be completely avoided and side effects are similarly experienced by patients.

Nanoparticles and nanomaterials are an emerging technology which has significant potential to address the challenges encountered in radiotherapy. This is in part, due to the discovery that nanoparticles made of high atomic mass elements, have been observed to exhibit unique physical phenomena when excited by an energy source. Some examples include scintillating or upconversion nanoparticles which can absorb the energy received from X-rays, protons, heavy ions, etc. and convert it into other forms of energies, allowing these materials to generate effects such as reactive oxygen species (ROS), which would result in tumour cytotoxicity. Alternatively, these materials can produce photons which can, in turn, activate conjugated photosensitizers to produce ROS to illicit the same antineoplastic effect [14–17]. This concept is known as radiodynamic therapy (RDT). This can be viewed as an extension to traditional photodynamic therapy (PDT), which makes use of external photonic energy to transfer energy to photosensitizers, which would cause increased oxidative damage to cancer cells. However, PDT is currently primarily used to treat surface cancers such as skin tumours [18, 19] as its effect is limited to surface sites due to the penetration of visible range photonic energy being limited to several millimetres of tissue depth [20]. The application of nanoparticles pushes this concept to the next level, resulting in the creation of RDT, where these ROS producing nanoparticles can be activated using more deeply penetrating energies used in radiotherapies, such as X-ray and proton beam energies, which have greater penetration than visible range photons. Early studies in animal models show that the combined tumour cytotoxic effects from these radioactivated ROS producing nanomaterials and external beam energy have the potential to achieve more favourable treatment outcomes than when used separately [21]. This would potentially allow greater treatment effects while not escalating the radiation dose. To further improve RDT, targeted delivery of photosensitizers into tumours is of paramount importance. This ensures the maximum antineoplastic effect when energy is delivered to the tumour. Nanoparticles have further enabled this in their role as targeted carriers for photosensitizers. This can be achieved through passive targeting, whereby the various physical properties such as the shape or charge of the nanoparticles can be adjusted to increase accumulation in tumours [22, 23].

Alternatively, the flexible surface chemistry of nanoparticles also allows active targeting, whereby the nanoparticle surface is functionalized with tumour-seeking ligands which would exhibit increased uptake due to an overexpression of the receptors for these ligands in neoplastic cells [24]. These strategies have been demonstrated with great effect in many animal models which show increased concentrations of photosensitizers in tumour sites, leading to an increase in cytotoxic activity after activation using external energy [25]. In terms of molecular radiotherapy, nanoparticles have functioned as carriers for increased delivery of radionuclides to tumour sites and also retention structures for the still radioactive daughter nuclei. Retention enables the radionuclide effects to be prolonged and also enables multimodal therapies with other antineoplastic agents such as chemotherapeutic drugs [26]. Importantly, the application of these nanoparticles in radiotherapies has enabled the concurrent imaging of these tumours during treatment with the use of techniques such as bioluminescence, fluorescence, single-photon emission computed tomography (SPECT), etc. In this chapter, the various methods by which nanoparticles are employed to improve therapeutics in radiotherapy using RDT, enhancing radionuclide therapies and also imaging applications for monitoring treatment response, are discussed (Fig. 1).

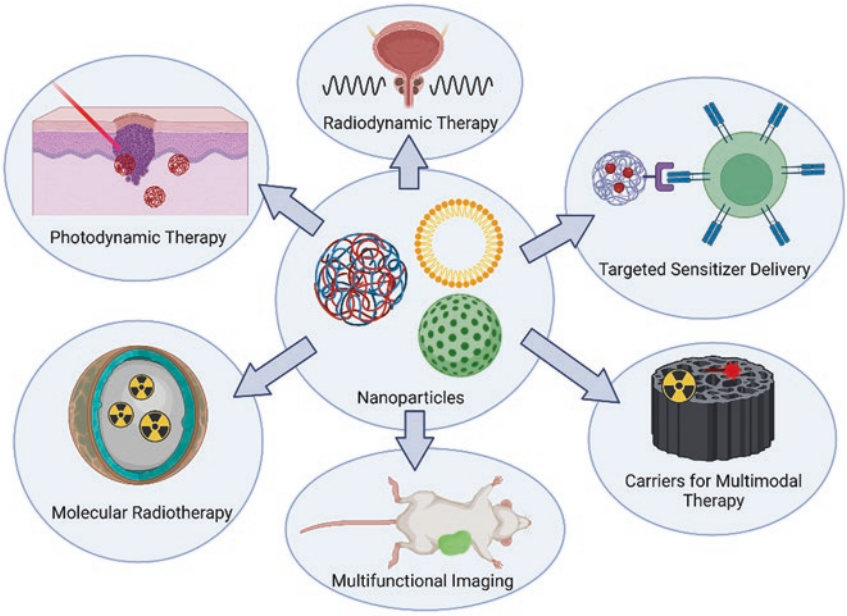

Fig. 1 Applications of nanoparticles in radiotherapy (Created in BioRender)

2 Radiotherapy Concepts

2.1 X-Ray Beam Radiotherapy

Radiotherapy is one of the pillars of oncologic treatment since it was first introduced two centuries ago [27]. Together with surgery and chemotherapy, many combination treatment regimens have been devised using radiotherapy. Combination therapy regimens have demonstrated improved clinical outcomes by minimizing single treatment modality associated toxicities [28]. Radiotherapy can be used either for tumour eradication or as an adjuvant therapy to lower the risk of recurrence [29]. The most common form of radiotherapy today is external beam therapy, whereby an external beam is delivered to tumour cells to induce DNA damage, resulting in tumour cell death [30]. The most common form of beam energy used today are X-ray beams, but other beams such as protons, electrons, and heavy metal ions have also been used. In X-ray radiotherapy, a linear accelerator (LINAC) (Fig. 2a) is used to produce these X-rays by way of electromagnetic conversion, using internal collisions of electrons against a heavy metal target [31]. The energy and depth of penetration of these X-rays can be adjusted through the adjustment of various parameters of the LINAC, and the resultant beam can be shaped by using a heavy metal collimator (Fig. 2b) at the exit of the LINAC gantry to block the dose to unwanted areas of the patient's body.

Though the collimator would shield much of the healthy tissues from unneeded exposure, there would still be many healthy tissues in the path toward the tumour. To further reduce radiotoxicity in healthy tissues, the beam is commonly delivered across multiple directions or 'fields' by rotating the gantry along its axis. During

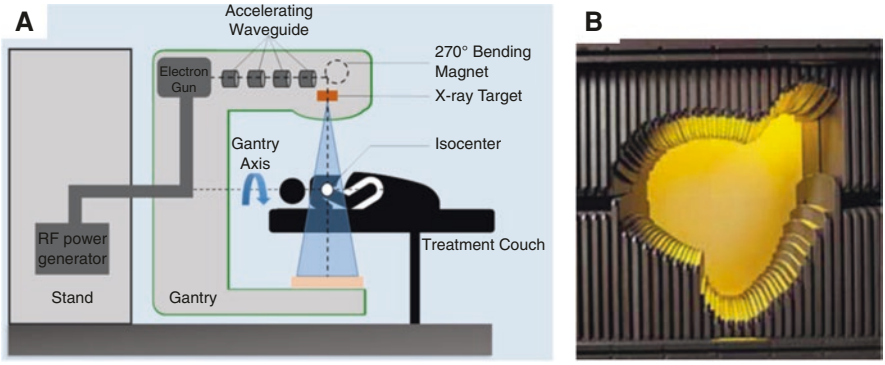

Fig. 2 Schema for external beam therapy: (**a**) Diagram of a linear accelerator (LINAC) used in radiotherapy [32]. Jumeau R, Ozsahin M, Schwitter J, et al. Stereotactic radiotherapy for the management of refractory ventricular tachycardia: promise and future directions. Frontiers in cardiovascular medicine. 2020;7:108; licensed under a Creative Commons Attribution (CC BY) license. (**b**) Multileaf collimator located at the exit of the LINAC that is used to shape the outgoing X-ray beam [33]. Jeraj M, Robar V. Multileaf collimator in radiotherapy. Radiology and Oncology. 2004;38(3)

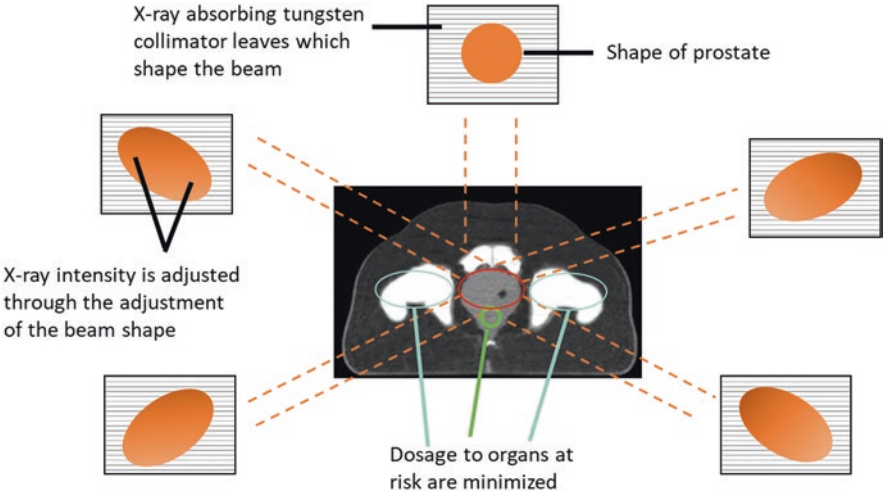

Fig. 3 Rotational gantry used in intensity-modulated radiation therapy (IMRT) for the treatment of prostate cancer using X-ray beams. A schematic depicting the cross-section of a pelvis with a prostate tumour marked in red. The summation of multiple beams results in a radiocytotoxic dose at the site of the tumour whilst avoiding dosage to organs at risk marked in green and cyan

this rotation, the dose can be further adjusted by changing the intensity of the X-ray beam accordingly. This would be in addition to dynamically changing the shape of the collimator. An example would be intensity-modulated radiotherapy (IMRT) as depicted in Fig. 3, where prostate cancer is the target. It can be seen that the X-rays are delivered from different directions intersecting at the tumor. This allows the tumour to be exposed to a high dose whilst enabling a steep dose gradient from the tumour to the normal tissue interphase, thus reducing the damage to normal tissues. IMRT is achieved using advanced computer simulations, automation, and planning, and there are several techniques for delivery [34]. There are several other similar approaches, such as helical techniques like volumetric arc therapy (VMAT), tomotherapy, and stereotactic body radiotherapy (SBRT), which leverages on image guidance and optimal dose modulation to allow delivery of very large doses per treatment [35–38].

2.2 Proton Beam Therapy

Protons are the second most common beam energy used in radiotherapy. The allure of proton radiotherapy lies in its unique energy delivery distribution. Unlike X-rays, proton beams do not deliver energy past their peak dose, leaving all the tissues past the dose peak of the beam to be unaffected. This region of peak dose is called the Bragg peak [39]. Through the adjustment of the beam parameters, the placement of the Bragg peak can be placed strategically to maximally deliver energies to the

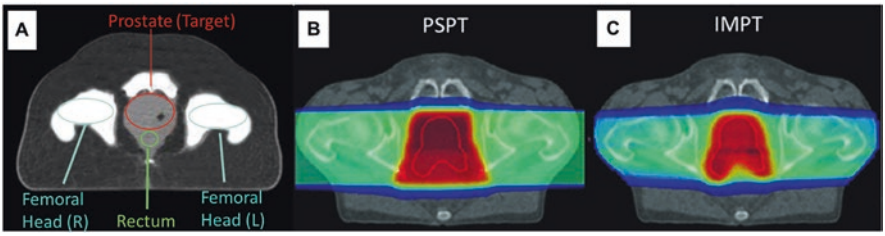

Fig. 4 Dosage distributions using different types of modulated proton beam therapies. (**a**) Schematic diagram of a pelvic cross-section showing a prostate tumour to be treated and the surrounding organs at risk in the pelvis. (**b**) Passive-scattering proton therapy (PSPT) [42] and (**c**) intensity-modulated proton therapy (IMPT) [42]. Vanneste et al., BioMed research international, 2016; licensed under a Creative Commons Attribution (CC BY) license

tumour whilst avoiding vital organs located past the Bragg peak. The energy distributions can be appreciated in Fig. 4, which shows the different dosage patterns within the pelvis of a patient being treated for prostate cancer [40–42]. Figure 4a shows the prostate tumour to be treated with the femoral heads and rectum outlined as the organs at risk. Similar to X-ray therapy, proton beam therapy can be modulated in various ways resulting in different dosage patterns, such as passive-scattering proton therapy (PSPT) (Fig. 4b) or intensity-modulated proton therapy (IMPT) (Fig. 4c). With these unique treatment profiles, proton therapies can sometimes produce better treatment outcomes than X-rays [43], especially in circumstances where the tumour to be treated is in very close proximity to an organ at risk [44].

2.3 Heavy Ion Beam Radiotherapy

Heavy ion beams have also been gaining attention for their utility to eradicate tumours. The field is very wide, and there are many different candidate heavy ions. Of these, carbon ion radiotherapy (CIRT) is one of the most widely studied. Heavy ions have a similar dosage profile exhibited by protons, having a Bragg peak-like distribution, with no dose past the peak. In addition, since carbon ions have a higher atomic number, these ions have higher momentum compared to protons, leading to reduced scattering and deflections during dosing. The result is a focused beam that does not deviate along the intended track, coupled with a higher linear energy transfer (LET) compared with protons [45]. This allows CIRT to be potentially more biologically effective than protons for the same physical absorbed dose, and thus CIRT can confer a more pronounced tumour killing, even for radioresistant tumours [46–48].

2.4 *Molecular Radiotherapy (Radioisotope/ Radionuclide Therapy)*

External beams are not the only avenue by which energy can be delivered to tumours to induce cytotoxicity. Another method involves the delivery of energy from within the body through the use of radioactive compounds which produce energetic alpha, beta, or gamma radiation on decay. One method by which this can be achieved is through the implantation of a sealed radiation source. This is known as brachytherapy and is used today for the treatment of many prostates and gynaecological cancers [49]. Radiation can also be administered intravenously; this is known as molecular radiotherapy or radioisotope therapy. The radioisotopes accumulate in the target tumours, undergo decay, and emit radiation causing cytotoxic damage [50]. Radium-223 is an example of a radionuclide used to treat cancer. It is a calcium mimetic that is readily incorporated into bone tissue, making it ideal for the treatment of bone metastasis [51]. Radium-223 also has radionuclide properties, releasing short-range alpha particles which travel approximately 100 μm distances upon radioactive decay. These alpha particles are highly energetic, causing localized double-stranded DNA breaks, thereby causing cancer cell death (Fig. 5).

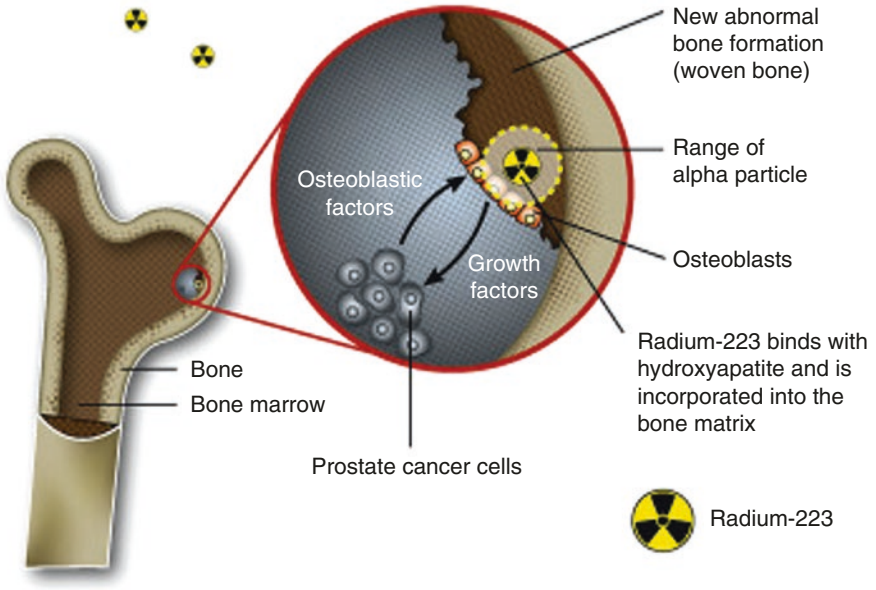

Fig. 5 Schematic working principle of molecular radiotherapy/radionuclide therapy in the treatment of metastatic bone disease. Radium-223, a radionuclide, undergoes radioactive decay, resulting in short-range alpha particles that cause damage to metastatic cells [53]. (This article was published in Journal of the Formosan Medical Association, 116(11), Cha T-L, Wu TT-L, Vogelzang NJ, et al., Optimal usage of radium-223 in metastatic castration-resistant prostate cancer, 825–836, Copyright Elsevier 2017)

Phase-III trials have already been employed using molecular radiotherapy such as in the ALSYMPCA trial, which studied the efficacy and safety of radium-233. It showed that there was a survival benefit of 14.9 months versus 11.3 months when comparing treatment and placebo groups. Furthermore, radium-223 treatment groups showed patients had low myelosuppression rates and lower occurrences of adverse events [52].

2.5 Enhancement of Radiotherapy Using Nanoparticles

In the proceeding sections, it will be discussed in further detail how nanoparticles can help overcome the challenges faced in different aspects of radiotherapy. The physical properties of nanoparticles will be discussed in how the antineoplastic effects in each radiotherapy modality can be enhanced, resulting in improved targeted therapies.

3 Photodynamic Therapy (PDT)

Photodynamic therapy is a treatment modality by which photosensitive compounds absorb energy from oncoming photons and create reactive oxidative species (ROS). The photonic energy causes the electrons within the photosensitizers to enter an excited state and subsequently return to their ground state via phosphorescence or oxidative pathways. In particular, these oxidative pathways would cause the generation of ROS in the form of superoxide anions [54] and triplet oxygen molecules [55]. These reactive species would cause free radical damage, resulting in tumour cell death [56]. The main mechanism of cellular destruction is through the disruption of cellular membranes, resulting in the dysfunction of many key structures such as mitochondria, lysosomes, and nuclear membranes [57–60]. In a sense, PDT is a form of photon beam therapy, where photons in the visible light range are used to activate photosensitizers and achieve tumour cell death.

The photosensitive compounds used in PDT contain naturally occurring compounds such as chlorophyll, bacteriochlorophyll, and haem [61], which have excitation wavelength ranging from 380 to 750 nm. This poses a major challenge, as photons in these wavelengths do not penetrate well into deep tissue [62]. Thus, treatment with compounds excitable in these ranges has limited ROS production capabilities at deeper ranges, as these wavelengths are strongly attenuated by the skin, resulting in reduced activation [20]. One of the ways which have been explored to overcome this limitation is through the use of more deep tissue penetrating photons, such as those in the near-infrared (NIR) region. Having a wavelength in the range of 700–1000 nm, NIR photons can penetrate up to a few centimetres within tissue to activate NIR photosensitizers using targeted photonic sources, providing highly conformal treatment to the intended site [63, 64]. From a practical

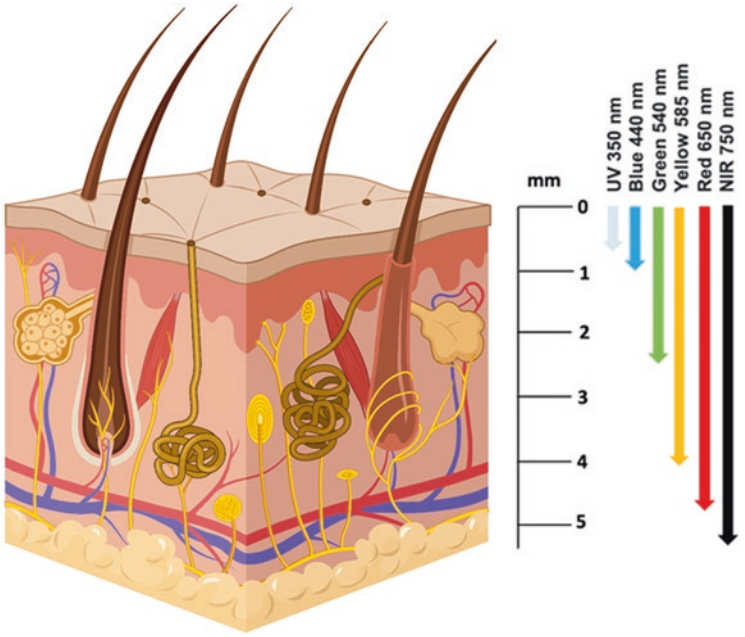

Fig. 6 Photons at different wavelengths and the corresponding penetration depths within the skin layers (Created with BioRender)

standpoint, this means that using NIR, lesions can be treated past the subcutaneous layer of the skin as opposed to only the epidermal region when using visible light as seen in Fig. 6.

4 Evolution of Photodynamic Therapy (PDT) to Deep PDT and Radiodynamic Therapy (RDT)

Nanoparticles provide an avenue of which to overcome one of PDT's major limitations, treatment depth. This is due to the fact that PDT uses photosensitizers which are activated by photons in the 380 to 750 nm wavelengths and are unable to penetrate deeper than 1 cm of the skin [20]. Thus, the application of PDT for deeper tumours is difficult. Unlike the usual photosensitizers used in PDT, nanoparticles in the form of upconversion or scintillating nanoparticles interact with more deeply penetrating photons such as X-rays, which are typically used in radiotherapy. The application of such nanoparticles in radiotherapy has resulted in new treatment techniques such as deep PDT and radiodynamic therapy (RDT). In the proceeding sections, it will be discussed how nanoparticles gradually extended the range of treatment of PDT, from the invention of deep/near-infrared (NIR) PDT to that of RDT, which can potentially treat up to any depth of the body.

4.1 Deep/Near-Infrared (NIR) PDT

Upconversion nanoparticles (UCNPs) are made of elements that can absorb lower energy photons and subsequently emit photons with higher energy after enough energy has been delivered to the nanoparticles. UCNPs can be doped with rare-earth lanthanides, which allow the absorption of deeper penetrating NIR photons and the subsequent emission of photons in the ultraviolet-visible (UV-vis) range. This is particularly attractive for deep PDT applications, as NIR photons, which have a wavelength of 700–1000 nm, can achieve a penetration depth of several centimetres into tissues, significantly extending the range of PDT into deep tissue [63, 64]. This mechanism occurs via three main pathways: excited-state absorption (ESA), energy transfer upconversion (ETU), and photon avalanche (PA). In both ESA and ETU, NIR photons will be absorbed by the UCNP which would enter an excited intermediate state, followed by emission of UV-vis photons in situ [65]. PA can be viewed as a combination pathway, where the absorbed NIR photons undergo ESA followed by a cross-relaxation process to neighbouring ions which also eventually results in the emission of UV-vis photons [66]. The efficiency of these UCNPs is determined by the type of lanthanide used, for instance, erbium, thulium, etc., where each lanthanide enters differing transition states with emissions of photons with different wavelengths [67–71]. These higher energy photons then subsequently activate photosensitizers within the nanoparticles such as zinc-phthalocyanine and chlorin e6, which would, in turn, produce ROS, similar to the classical PDT mechanism and thus confer cytotoxicity to tumour cells [72–75]. This is schematically illustrated in Fig. 7.

The potential of UCNPs for cancer treatment has been demonstrated by Zhang et al. A superball nanostructure was fabricated, which consisted of two types of UCNPs that were activated by different wavelengths of NIR photons (Fig. 8a) [74]. The first set of UCNPs was activated by NIR photons at 980 nm wavelength which subsequently produced a red fluorescence. This in turn activated zinc-phthalocyanine photosensitizers which were conjugated to the nanoparticles to produce ROS to

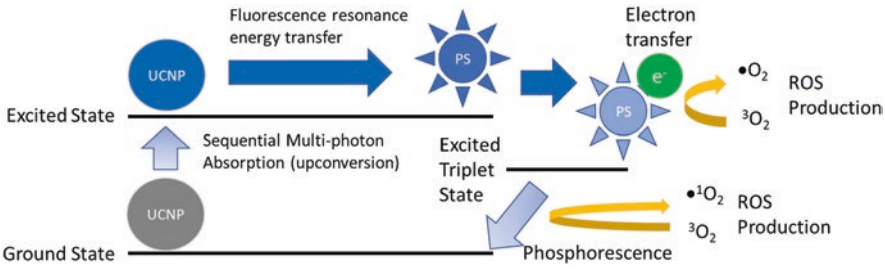

Fig. 7 Upconversion nanoparticles (UCNPs) and the mechanism of reactive oxygen species (ROS) generation after absorption of near-infrared photons. The UCNP electrons enter an excited state, and energy is transferred via fluorescence resonance energy transfer biosensor (FRET), resulting in the generation of photons that in turn activate conjugated photosensitizers (PS) for ROS generation

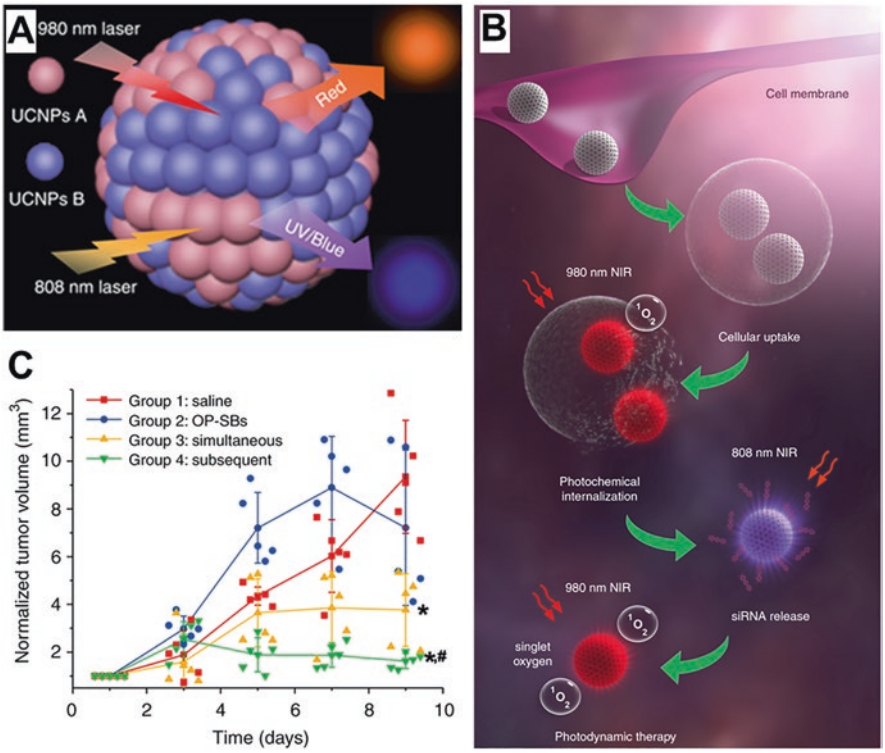

Fig. 8 Multifunctional superball upconversion nanoparticles for deep PDT: (**a**) Schematic diagram, (**b**) sequential activation showing the activation of siRNA release for knockdown of reactive oxidation species resistance followed by activation of photosensitizers for the production of reactive oxidation species, (**c**) in vivo tumour volume following treatment in simultaneous activation and subsequent activation of the different UCNPs [74]. Zhang et al., Nature communications, 10, 1, 2019; licensed under a Creative Commons Attribution (CC BY) license

induce tumour cell death. The second set of UCNPs were loaded with short interfering RNA (siRNA) and was used to knock out genes associated with protection against ROS damage, thus enabling such UCNPs to be even more effective for deep PDT. This was postulated to be due to overcoming possible acquired resistances by cancer cells against free radical damage [76, 77]. The release of these siRNAs was triggered by irradiating the nanoparticles with NIR photons at 808 nm wavelength, prior to activating them for deep PDT, thus first sensitizing them to ROS damage before the initiation of deep PDT (Fig. 8b). This stepwise/subsequent activation of the superball nanostructure UCNPs resulted in a higher proportion of tumour cell death than simultaneous activation in as quick as 5 days after treatment in mouse models (Fig. 8c). It can be seen that in addition to the multimodal treatment functions endowed by nanoparticles as in the earlier studies using porphysomes, this study further demonstrates multimodal treatment using nanoparticles to perform PDT and siRNA therapeutics. Furthermore, these UCNPs have also shown how the

depth of treatment of PDT was increased through the use of NIR photons, achieving a tissue penetration depth of up to twice that of visible range photons.

4.2 Nanoparticles for X-Ray Radiodynamic Therapy

The treatment of cancers up to several millimetres through the use of NIR PDT was a significant advancement, however there are many cancers within the body cavity that are located in regions NIR photons cannot penetrate. To enable deeper PDT applications, materials which are able to interact with more deeply penetrating energies such as x-rays are required. Lanthanide-doped nanoparticles are one such example, being able to capture and convert X-rays to other wavelengths, further extending PDT depth. The absorbed X-rays are converted into optically visible photons through luminescence, which would, in turn, activate conjugated photosensitizers to produce ROS and thereby induce tumour cellular damage, enabling PDT at deeper depths [15]. This mechanism is known as X-ray excited optical luminescence (XEOL), and it is the foundation of X-ray RDT. High atomic number elements such as lanthanides are key to this approach, as these materials have higher X-ray absorption [78, 79]. Together with the current state-of-the-art X-ray radiotherapy and advanced conformal dosing techniques, X-ray RDT has the potential to revolutionize the treatment of cancer by providing highly targeted dosing whilst achieving tumour cytotoxicity multimodally by both ROS- and X-ray-induced cellular damage.

To produce XEOL, X-ray RDT commonly utilizes scintillating nanoparticles (ScNP). Europium-doped sodium gadolinium fluoride ($NaGdF_4$:Eu) nanoparticles are one such example [80]. The engineering of these scintillating nanoparticles is complex as there are many steps involved in converting the oncoming X-ray energy for luminescence. The absorbed X-ray energy within the nanoparticles can be further scintillated to optical photons for luminescence imaging or drug activation. Briefly, scintillating mechanism can be split into three stages: conversion, tunnelling, and emission. In the conversion stage, the absorbed X-ray energy gradually dissipates through excitation and ionization. Upon reaching a threshold, interband transitions occur, electron-hole pairs are created and thermalized in the respective conduction and valence band. In the tunnelling stage, these electron-hole pairs known as excitons, tunnel through the lattice structure of the nanoparticle. In the emission stage, these excitons are trapped in luminescence centres and undergo recombination to release optical photons. In the presence of fluoride anions, the highly energetic X-rays are able to displace them to create traps. The depth of these traps is dependent upon the anion's displaced distance and the host crystal dopant [81, 82]. As the excitons get trapped and released gradually into the luminescence centre, the emission lifetime increases. This is known as persistent luminescence or the XEOL afterglow effect (Fig. 9).

A major hurdle in the early development of developing X-ray RDT is the efficiency of the XEOL process. In $NaGdF_4$:Eu nanoparticles, europium and

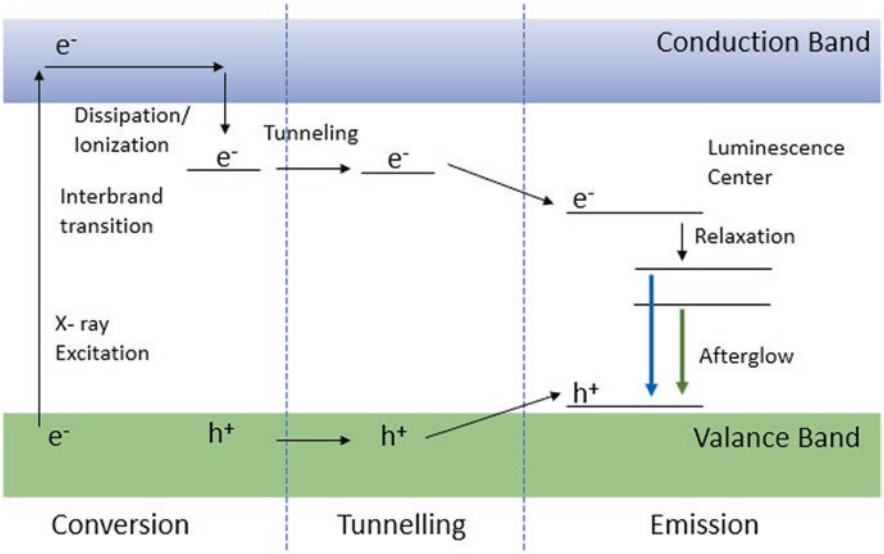

Fig. 9 Mechanism of X-ray excited optical luminescence (XEOL) afterglow showing the three stages of conversion, tunnelling, and emission

gadolinium work in concert as energy acceptors and stabilizers for the energy transmission from the oncoming X-rays to eventual optical luminescence [83]. The combination of these two materials in a nanocrystal is important as it improves the overall X-ray scintillation yield from the lanthanide europium ion [84]. The addition of sodium yttrium fluorine into the host crystal further enhances yield as it suppresses direct relaxation of excited electron states [85] and allows europium for partial f-orbital transitions to increase yield [80]. More recent approaches have even demonstrated that encapsulation of ScNP within fluorine-based shells such as sodium lutetium fluoride can further enhance XEOL [81, 86]. By the control of these shell parameters, the yield of these ScNPs could be further enhanced through the reduction of energy losses during the scintillating energy transfer process [87–89].

Beyond simply minimizing energy losses from the X-ray scintillation process, the field of ScNPs have progressed to provide sustained luminescence, thereby providing sustained ROS production over time, even when the X-ray photon source has been switched off. This is termed the XEOL afterglow effect and it is dependent on the nanocrystal defect depths. As such, radiotherapy regimes could be modified to take advantage of this effect for potentially better clinical outcomes. The combination of radiotherapy and X-ray photon RDT in mouse models have been shown to produce synergistic effects compared to radiotherapy alone or RDT alone [90]. Figure 10a shows the bioluminescence images (BLI) of the mice models with H1299 tumours implanted into the lungs of the mice. The H1299 cells were luciferase-expressing, and a higher bioluminescence signal indicated the presence

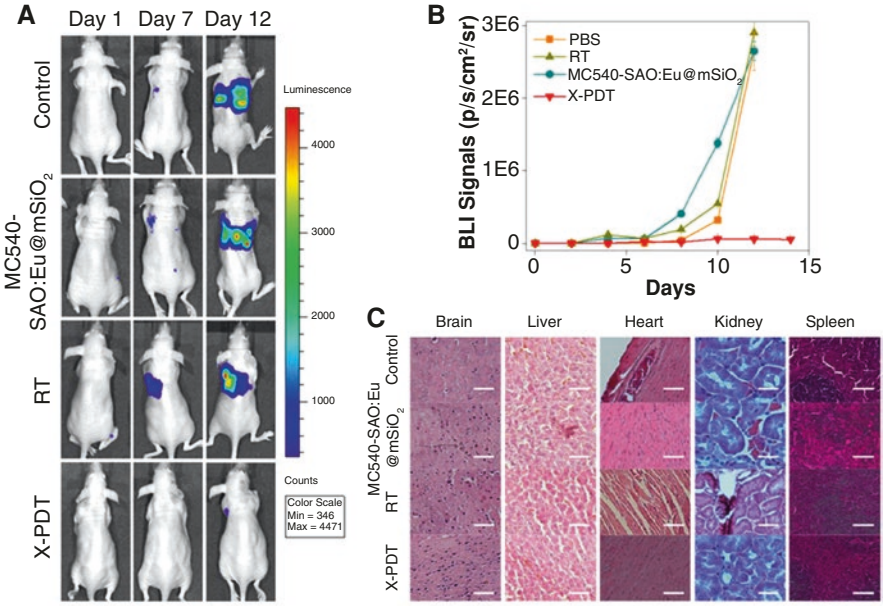

Fig. 10 Photon RDT in mice models: (**a**) Bioluminescence images (BLI) of mice treated with X-ray photon RDT (X-PDT), radiotherapy (RT), MC540-SAO:Eu@mSiO2 nanoparticles, and control (PBS) on days 1, 7, and 12. (**b**) In vivo bioluminescent imaging showing tumour size at different time points. (**c**) H&E staining of organ tissues taken from the four groups; scale bars denote 100 μm [90]. Wang GD, Nguyen HT, Chen H, et al. X-ray induced photodynamic therapy: a combination of radiotherapy and photodynamic therapy. Theranostics. 2016;6(13):2295

of the tumour cells. In all treatment groups, the tumour's growth was suppressed. On day 12, X-ray photon RDT (denoted as X-PDT in this study) induced much greater tumour suppression as compared to radiotherapy (RT) alone. This is further illustrated in Fig. 10b, which demonstrates the BLI intensities of the mouse models per day, showing complete tumour suppression in the X-ray RDT (X-PDT) group. The mice were also sacrificed at the end of treatment monitoring and assessed for systemic toxicities in their various organs as shown in the H&E staining as depicted in Fig. 10c. There was no histological evidence of organ injury as compared to the control group from X-ray RDT (X-PDT). These results demonstrated the potential of X-ray photon RDT to greatly suppress tumour growth whilst at the same time reducing systemic side effects.

Besides the generation of ROS using conjugated photosensitizers, there are several types of nanoparticles that are capable of converting X-rays directly to ROS for cancer therapy. One such example are copper-based copper-cysteamine (Cu-Cy) scintillating nanoparticles which can absorb energy from X-rays and enter an excited state. Subsequently, relaxation of these excited states via multiple mechanisms can occur within these nanoparticles back to its ground state without the need to pass energy to other ions within the nanoparticle. The final mechanism before the

electrons return to the ground state involves intersystem crossing with surrounding oxygen, thereby producing ROS directly in the process, without the need for a conjugated photosensitizer. Similar to lanthanide-based ScNP, when used in concert with RT, greater tumour suppression was achieved, with an observed time to tumour progression being three times longer as compared to with RT alone (30 days vs 10 days) when tested in in vivo mouse models [21]. Using 2′-7'dichlorofluorescin diacetate (DCFH-DA) imaging to detect ROS, B16 cell cultures were incubated with Cu-Cy nanoparticles and irradiated with X-rays (Fig. 11a). In the cultures which were incubated with Cu-Cy nanoparticles, a green fluorescence signal was detectable where none was detected in the control which was incubated in PBS. This indicates that Cu-Cy nanoparticles were able to induce ROS formation without any conjugated photosensitizer. Similar to lanthanide-based ScNPs, Cu-Cy nanoparticles were also able to produce ROS when conjugated with photosensitizers as seen in the bottom row of Fig. 11a. Photocatalytic ScNPs is another class of ScNPs which form ROS without the use of photosensitizers. Examples of these would be $NaCeF_4$:Gd, Tb, and BiOI@$Bi2S_3$ nanoparticles. The mechanism of these ScNPs differ from Cu-Cy ScNPs in that the energy from the incoming X-ray is passed directly to water molecules and this energy breaks the molecules down into ROS and also hydroxyl-free radicals using the ScNP photocatalytic property, through hole and electron interactions [91, 92]. These nanoparticles have shown similar tumour suppression capabilities as other ScNPs [91]. Another example would be Nanoscale metal-organic frameworks (MOFs) are also nanostructured scintillators that are activated by X-rays. To absorb X-rays, these MOFs utilize heavy

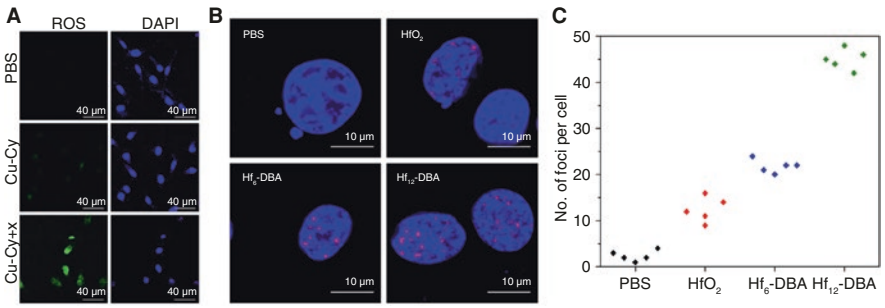

Fig. 11 Other forms of scintillating nanoparticles in vitro. (**a**) 2′-7'dichlorofluorescin diacetate (DCFH-DA) imaging of X-ray photon-induced cell apoptosis using copper-cysteamine (Cu-Cy) scintillating nanoparticles and Cu-Cy conjugated with photosensitizers (Cu-Cy + X), with green fluorescence indicating the presence of ROS generation [21]. Zhang et al., Signal transduction and targeted therapy, 5, 1, 2020; licensed under a Creative Commons Attribution (CC BY) license. (**b**) γ-H2AX assay illustrating double-strand breaks in CT26 cells treated with metal-organic layer scintillating nanoparticles after X-ray photon irradiation, blue fluorescence denoting DAPI-stained nucleus and red fluorescence denoting antibody-labelled γ-H2AX indicating double-strand breaks in the cells. (**c**) The number of double-strand breaks per nucleus following treatment with metal-organic layer scintillating nanoparticles [97], Ni et al., Nature communications, 9, 1, 2019; licensed under a Creative Commons Attribution (CC BY) license

transition metals which have a high atomic number, as was the approach used in lanthanide-doped ScNPs to induce X-ray photon scintillation [93–95]. When X-rays interact with these heavy transition metals, the metals act as electron pumps to trigger conjugated photosensitizers in order to produce ROS for tumour killing activity. Additionally, through electron scattering effects, these MOFs are also able to directly generate reactive hydroxyl-free radicals without the assistance of conjugated photosensitizers. Therefore, MOFs are able to leverage on multiple mechanisms by which ROS can be generated to induce tumour cytotoxicity. To enhance the yield of these ROS, the surface-area-to-volume ratio of these MOFs can be adjusted into ultra-thin two-dimensional sheets known as metal-organic layers (MOL) [95, 96]. In vitro imaging using γ-H2AX assays shows Hafnium (Hf)-based 2,5-di(p-benzoate)aniline (DBA) MOLs causing double-strand breaks in HfO_2-, Hf_6-DBA-, and Hf_{12}-DBA-incubated cultures denoted in red fluorescence after X-ray irradiation (Fig. 11b) [97]. It can be seen that with increased Hf or organic mass in these ScNPs, more double-strand breaks were induced, highlighting the potential for MOLs for X-ray activated cancer treatment (Fig. 11c).

Studies with nanoparticle facilitated X-ray RDT highlight the vast potential of these therapies for cancer treatment. One important limitation though is that, most of the current work on these approaches utilizes X-ray with kilovoltage energies [16, 98, 99], rather than megavoltage energies, of which the latter is more generally used in today's radiotherapy regimes. It is not yet clear how megavoltage-energized X-ray will interact with ScNPs and if similar efficiencies for RDT can be achieved. In the effort to clinically translate these therapies, there have already been a few initial studies in this area, such as works done by Dou et al.[15] and S Clement et al., who have demonstrated X-ray absorption is still possible using megavoltage photons, though more research is needed in these areas to determine their clinical translatability [100].

4.3 Nanoparticles for Proton Radiodynamic Therapy (Proton RDT)

Energetic protons are also another modality by which cancer is treated in radiotherapy. Similar to X-ray RDT, nanomaterials can be triggered to generate ROS using energetic protons for tumour killing as well. This is known as proton RDT, and using the unique dosage characteristics of protons in tissues, this can be used to strategically activate these nanomaterials at tumour sites for highly conformal therapies. Protons have been observed to interact with some nanomaterials to produce optical fluorescence, X-rays, gamma photons, and even secondary electrons [101–105]. The mechanism by which this occurs is via energy transfer from the irradiated protons to electrons within these nanomaterials. When energy is absorbed, the electrons move to an excited state and in so doing, causes a synchronous ionization event whereby secondary energetic electrons are produced. These energetic

electrons and/or secondary electrons would then undergo further ionization, collision, and phonon-coupling interactions within the nanomaterial. At some point, the remaining energy will match the luminescence centre's energy level, whereby these centres relax and emit photons within the optical range [101]. Similar to X-ray RDT, the photons would then activate conjugated photosensitizers to produce ROS for tumour cytotoxic effects. To increase the probability of such interactions and subsequent luminescence, high atomic number elements are again preferred for the fabrication of nanoparticles for proton RDT, as these elements would have a higher secondary electron yield [105, 106].

Proton RDT is relatively new, and there are only a few studies on this topic at the moment. This effect was recently demonstrated by Grigalavicius et al. in which protons were used to activate different photosensitizers to produce ROS and fluorescence [107]. Figure 12a–c shows the proton-induced fluorescence in meta-tetra(hydroxyphenyl)chlorin (mTHPC), protoporphyrin IX (PpIX), and erythrosin B photosensitizers after exposure to a proton beam, respectively. It can be appreciated that these fluorescence signals approximately follow a Bragg peak distribution, similar to that of proton dosing within tissues. The dosage and subsequent fluorescence were confined to the proximal region, and no distal signal was observed. Thus, in practice, this profile can be tuned in such a manner whereby the proton dosage is only at the tumour, causing maximal fluorescence generation at that region, whilst sparing the distal regions from any dosage and subsequent toxicities. Additionally, it was observed that different photosensitizers resulted in different fluorescence patterns. For instance, mTHPC displayed a tight and shallow distribution, whilst erythrosin B exhibited a wider and deeper distribution. This suggested that the adjustment of different photosensitizers in proton RDT could be used to shape the dosage according to the tumour size. Singlet oxygen generation was detected via the fluorescence measurement of photoprotoporphyrin, the photoproduct of PplX, after proton beam exposure. Upon addition of an oxygen scavenger, 1,4-diazabicyclo [2.2.2] octane (DABCO), a drop in the spectral intensity was observed, indicating no photoproduct being produced (Fig. 12d). To illustrate the tumour-killing potential of this approach, M059K glioblastoma cells were treated in vitro using cercosporin photosensitizer and proton irradiation. Compared to the cultures using proton irradiation alone, it was noted that the effect of the ROS generated from the photosensitizers resulted in up to 40% increased tumour toxicity, thus highlighting the potential of proton RDT for cancer therapies. The advantage of using protons in such an approach over the more popular X-ray is to leverage upon the Bragg peak property seen with proton dosing and synergize the activation of photosensitizers in these areas. Nanoparticle approaches for proton PDT can incorporate high atomic number elements.

Nanoparticle approaches which incorporate high atomic number elements such as gold have also been investigated for radiosensitization for proton therapy [108]. Charnay et al. have demonstrated this approach using large 50 nm gold nanoparticles and the administration of a proton beam at 200 MeV to CHO-K1 cells. Upon incubation, these nanoparticles were confirmed to be internalized into CHO-K1 cells using transmission electron micrographs. The gold nanoparticles were

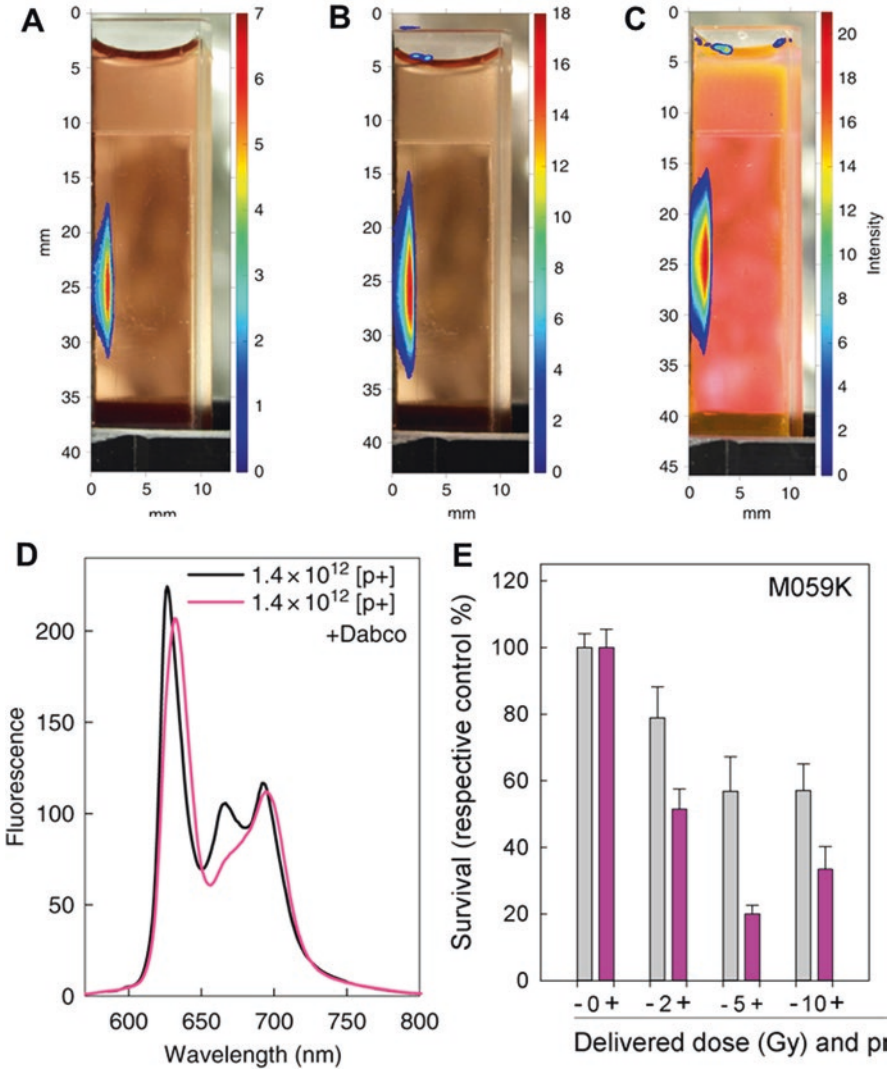

Fig. 12 Proof of concept of proton-induced fluorescence. (**a**–**c**) Fluorescence images captured during proton irradiation superimposed with yield heat map representations of the fluorescence emission from different photosensitizers. (**a**) Meta-tetra(hydroxyphenyl)chlorin (mTHPC). (**b**) Protoporphyrin IX (PpIX). (**c**) Erythrosin B. (**d**) Fluorescence spectra at 405 nm excitation showing protoporphyrin IX (PpIX) photoproduct (photoprotoporphyrin) production after proton irradiation with and without singlet oxygen-specific scavenger 1,4-diazabicyclo[2.2.2]octane (DABCO). (**e**) Cell death in glioblastoma M059K cell lines using cercosporin photosensitizer and proton irradiation (pink) versus proton irradiation alone (grey) [107]. Grigalavicius et al., Nature communications, 10, 1, 2019; licensed under a Creative Commons Attribution (CC BY) license

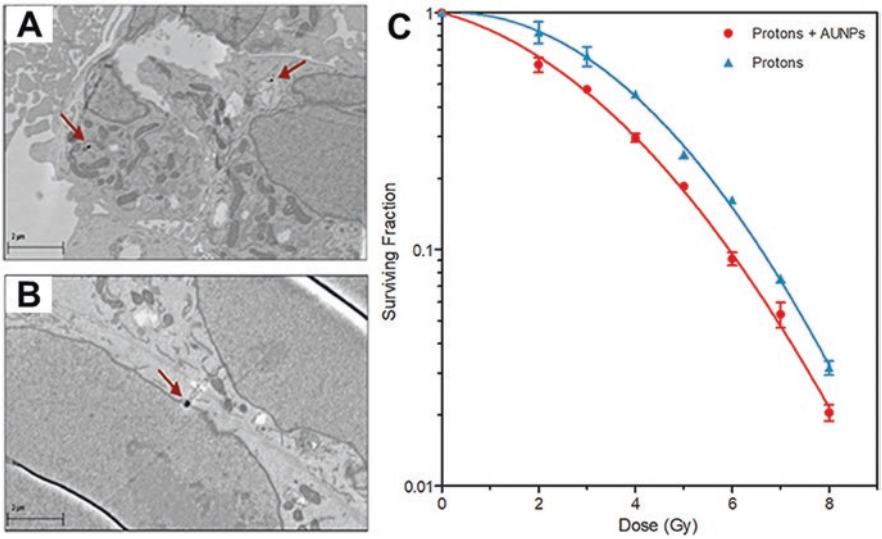

Fig. 13 Uptake of AuNPs into CHO-K1 cells and subsequent irradiation with protons. (**a**) Transmission electron micrograph (TEM) of AuNP showing random localization within vacuoles of the cells and (**b**) TEM showing AuNP incorporated into the nuclear membrane and (**c**) surviving fractions of CHO-K1 cell cultures after treatment using both protons versus protons with AuNPs [108]. Cunningham C, De Kock M, Engelbrecht M, Miles X, Slabbert J, Vandevoorde C. Radiosensitization Effect of Gold Nanoparticles in Proton Therapy. Frontiers in public health. 2021;9; licensed under a Creative Commons Attribution (CC BY) license

observed to be randomly distributed in the cell vacuoles (Fig. 13a) with a number of particles being located close to critical structures in the cell such as the nuclear membrane (Fig. 13b). To examine the effect of such nanoparticles in the context of proton therapy, CHO-K1 cell cultures were incubated with these AuNPs and given varying doses of proton beams from 2 Gy to 8 Gy. This was compared to cultures irradiated to proton beam alone, and it was seen that in the cultures which were incubated with AuNPs, an increased proportion of tumour cells were killed at all dosages. These results show the radiosensitizing effect of AuNPs.

4.4 Ion Beam Radiodynamic Therapy (Ion Beam RDT)

With the gaining popularity of ion beam therapy for treatment and as facilities are increasingly being built across the globe in recent years, researchers have also begun to incorporate nanoparticle technologies into ion beamlines [108, 109]. The physical mechanism underlying ion-activated luminescence (ionoluminescence) differs from X-ray-excited optical luminescence (XEOL). These positively charged ions interact with the target nanoparticle's ionic/atomic electronic structure via inelastic Coulomb scattering. The targeted ions/atoms get ionized and eject

secondary electrons, which in turn serve as electron pumps to either excite simple sensitizer-emitter pairs or produce excitons. This is similar to the conversion process in X-ray scintillation, for luminescent emission. This effect was demonstrated by Mi et al., where nanodiamonds were irradiated with helium ions to produce luminescence (Fig. 14a) versus that of standard 543 nm photons (Fig. 14b). It could be seen that the ionoluminescence imaging had increased resolution compared to photons [109]. Next, the nanodiamond's (ND) capability in radiosensitization of the cancer cells was also demonstrated through incubating hepatoblastoma cell cultures with NDs and irradiation with different dosages of protons compared to cultures without NDs. 3D microscopy confocal images were taken and analysed for their foci counts of γH2AX (Fig. 14c) and 53BP1 (Fig. 14d). Comparing the cultures which were treated with radiation only (denoted by "-") with the cultures which were treated with both radiation and NDs (denoted by "+"), it was observed that the inclusion of NDs did not provide any additional radio-enhancement. NDs thus were not able to provide any additional cytotoxic effect but did improve imaging

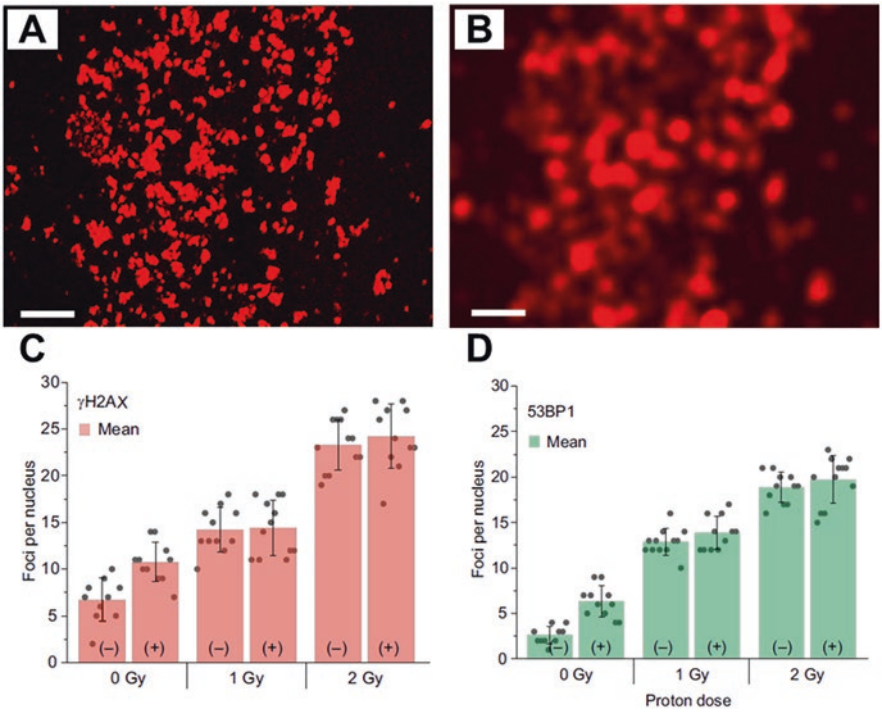

Fig. 14 Luminescence imaging of nanodiamond (ND) clusters and radiosensitization effects in cancer cells. (**a**) Ionoluminescence using MeV helium ion beam, (**b**) photoluminescence using 543 nm confocal laser, (**c**, **d**) fluorescence microscopy of hepatoblastoma cells with foci counts per nucleus of (**c**) γH2AX and (**d**) indicating DNA damage after exposure to different doses of protons with (+) and without (−) nanodiamonds [109]. Mi Z, Chen C-B, Tan HQ, et al. Quantifying nanodiamonds biodistribution in whole cells with correlative iono-nanoscopy. Nature Communications. 2021;12(1):1–9.; licensed under a Creative Commons Attribution (CC BY) license

capabilities significantly, which demonstrated one of the imaging capabilities of such nanoparticles. Nanoparticle-enhanced ion beam therapy is still emerging, and more research in this area are expected to improve these effects.

5 Nanoparticle-Enhanced Molecular Radiotherapies

Molecular radiotherapies involve the use of intravenously administered radionuclides. These therapies work by leveraging on the radioactive elements' decay, producing high-energy by-products such as alpha, beta, or gamma radiation. These high energy particles induce damage to the genetic material in cancer cells, thereby causing cellular death. Furthermore, during decay, daughter nuclei are also produced which are also radioactive and are able to similarly emit high energy particles. These daughter products may exit the sites of treatment, subsequently causing radiotoxicity to the surrounding healthy tissues. Nanoparticles can significantly enhance molecular radiotherapies by not only functioning as delivery carriers of these radionuclides to tumour sites, but also function as retainment structures for the daughter products formed from initial decay. This allows the high energy particles produced from radioactive decay of these daughter nuclei to continue to cause cytotoxic damage to tumour cells and also simultaneously limits toxicity to the adjacent healthy tissues. One recently investigated approach involves the use of lanthanide phosphate nanoparticles to carry radioisotopes such as radium-223 for the treatment of bone metastasis. The nanoparticles consisted of a lanthanide phosphate core with two outer lanthanide shells. The nanoparticle core alone was observed to be able to retain up to 88% of radium-223 over 35 days. With the addition of the outer lanthanide shells, this was improved to >99% over 27 days, potentially significantly limiting the damage to surrounding healthy tissues. In addition, the daughter nuclei, lead 211, was also shown to be retained at similar rates, allow for further radioactive decay products to act at the tumour site [110]. Like calcium, lanthanides are bone seekers and intrinsically accumulated at bone sites [111]. These have been used widely in many applications for imaging and oncologic therapy such as for the treatment of bone metastasis [112]. There have also been similar methods using an additional gold shell (Fig. 15), which also show the capability to retain their radioisotope cargo and the daughter by-product francium 221 [113].

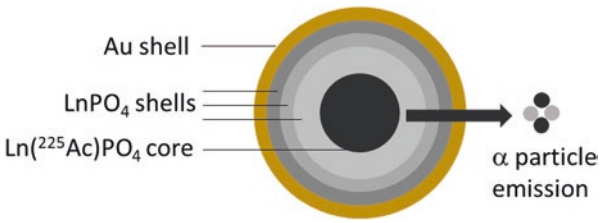

Fig. 15 An idealized schematic of a four-shell LnPO4 NP containing 225Ac in the core

Nanoparticles have also shown enhancement of radionuclide therapy through the concurrent delivery of other chemotherapeutic agents for increased tumour cytotoxicity. Chen et al. have demonstrated this concept using bone-seeking albumin-gadolinium oxide nanoparticles loaded with both radioactive iodine and doxorubicin, a chemotherapeutic agent (Fig. 16a) [26]. These nanoparticles were surface-functionalized with bisphosphonates which endowed these particles with bone-seeking properties. Once internalized by the metastatic cancer cells in the bone, cytotoxicity is achieved via two mechanisms: radiotoxicity from the beta particles produced by iodine-131 (^{131}I) radionuclide decay and chemocytotoxicity from doxorubicin (DOX). This allowed the tumours to be treated multimodally, which produced enhanced cytotoxic effects. Metastatic bone animal rat models were

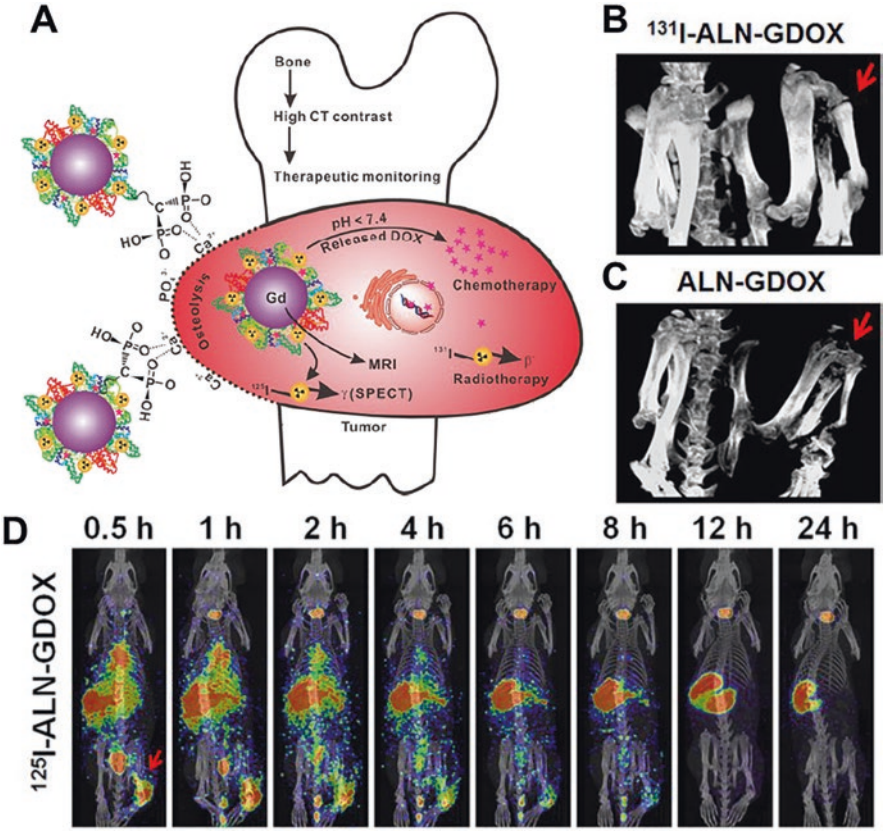

Fig. 16 (**a**) Schematic diagram and working principle of nanoparticle system for co-delivery of radionuclides and chemotherapeutic agents. (**b**, **c**) Micro-CT image of rat tibias receiving different nanoparticles, (**b**) ^{131}I-ALN-GDOX, (**c**) ALN-GDOX, and (**d**) in vivo single-photon emission computed tomography (SPECT) [26]. (Reprinted (adapted) with permission from Chen Z, Yu H, Lu W, Shen J, Wang Y, Wang Y. Bone-seeking albumin-nanomedicine for in vivo imaging and therapeutic monitoring. ACS Biomaterials Science & Engineering. 2019;6(1):647–653. Copyright © 2020, American Chemical Society)

treated with these nanoparticles and evaluated for their effects after 15 days of treatment. Micro-computed tomography images were taken of the femurs of the mice to visualize the extent of bone lysis from the metastatic bone deposits. Rats treated with DOX-loaded nanoparticles alone showed increased osteolysis and decreased bone density as compared to rats who were treated with nanoparticles with both iodine-131 and DOX (Fig. 16b, c). Lastly, the inclusion of iodine-125 enables these particles to be multifunctional, allowing single-photon emission computed tomography (SPECT) to be performed (Fig. 16d).

6 Tumour-Seeking Nanoparticles for Tumour Monitoring, Diagnostics, and Radiotherapy

It has been extensively discussed in this review how existing radiotherapy techniques can be enhanced with nanoparticle technology. Through the synergy of external beam radiotherapy and photosensitizers to produce cytotoxic ROS, enhanced tumour damage is possible. However, this was predicated that the photosensitizer would have been present in sufficient concentrations at the tumour site. To this end, the delivery of these photosensitizers is essential for the success of PDT and RDT. Furthermore, imaging techniques enabled by these nanoparticles are also crucial to this effort to confirm the delivery of these photosensitizers prior to the initiation of therapy. Ideally, these nanoparticles should be tumour-seeking and achieve selective delivery to tumours, thereby allowing for the concurrent diagnosis of the tumour and treatment using nanoparticle-enhanced radiotherapies as discussed in the previous sections. The classic approach of achieving this was through the conjugation of these photosensitizers to biomolecular carriers to improve uptake to tumour sites; however, this afforded no diagnostic advantage, and it would be challenging to confirm the delivery of the photosensitizers to the tumours.

More recently, the usage of nanoparticles as nanocarriers of these photosensitizers has gained increased traction as they have shown to have several advantages over simple conjugation-based approaches [114]. These nanocarriers have been shown to increase the concentration of the required photosensitizers at the intended sites [20]. This would translate to greater effects when the external beam energy has been applied. Furthermore, these nanoparticles can be loaded with specialized imaging components such as fluorescent agents, gadolinium contrast compounds, etc. for imaging purposes. Nanoparticle-enhanced delivery can result from two main mechanisms. The first of which would be targeting of the tumour via active targeting with tumour-specific ligand/receptor-mediated uptake mechanisms or via passive targeting with the enhanced permeability retention effect. The second method is via prolonging the circulation time or the half-life of these photosensitizers through nanoparticle encapsulation, thereby increasing chances of uptake in tumour sites, thereby conferring increased radio-cytotoxicity effects upon photon or proton beam irradiation. Therefore, nanoparticles are a powerful tool by functioning as a targeted

photosensitizer delivery vehicle and also to perform tumour-specific imaging, both for diagnosis of the tumour and also the confirmation of the uptake of photosensitizers prior to the commencement of radiotherapy.

6.1 Passive Targeting: Preferential Accumulation

Cancerous tissues behave very differently from healthy cells. Chief amongst these differences is that most cancers have disordered proliferation, ignoring regular patterns of growth, multiplying rapidly, and also ignoring tissue boundaries. Thus, cancerous tissues tend to possess aberrant angiogenesis and disordered growth, resulting in disordered vasculature and drainage. This would result in the preferential retention and penetration of certain small molecules and particles. This effect is known as the enhanced permeability and retention effect (EPR) [115]. By tuning the various physical properties of these nanoparticles, such as their shape, size, surface charge, etc., it is possible to enhance the accumulation of these nanocarriers within tumours. The subsequent imaging of these nanocarriers and also allowing the localization of these nanocarriers into tumours for irradiation to trigger the aforementioned cytotoxic effects for tumour treatment.

One of the most prominent nanoparticle-based carriers today are lipid nanoparticles (LNP), which have gained in popularity in the past 3 years due to the global COVID-19 pandemic. LNPs have been used as a delivery vehicle for mRNA therapeutics to great effect in the form of mRNA vaccines [116]. These are vaccines against the Severe Acute Respiratory Syndrome Coronavirus 2 (SARS-CoV-2), the etiological pathogen of COVID-19 [117]. LNPs are well studied for their ability to deliver small molecules, with various clinical trials reporting their efficacy and safety [118]. There is huge interest in appropriating these findings and technology for use in other areas such as in oncology, where there has been a slow push for making therapeutic vaccines against specific cancers to improve clinical outcomes [119]. The area of LNPs is highly diverse, consisting broadly of crystalline and non-crystalline LNPs, each with its own advantages and disadvantages. One potential candidate which can fulfil the needs for targeted delivery and bioavailability are polymeric LNPs. These are nanoparticles that consist of a polymer core and a phospholipid exterior [120]. The synthesis of these polymeric nanoparticles can be highly controlled using a microfluidic technique, allowing their physical properties such as shape and size to be tightly regulated [121]. When produced in specific sizes, polymeric LNPs have been shown to have preferential uptake in tumour tissues, allowing for passive targeting of disease sites [22, 23]. These LNPs can also be further modified with surface functionalization of its phospholipid exterior with cell-specific antibodies/proteins, allowing them to be more targeted to cancer cells. Furthermore, polymeric LNPs have been shown to have longer circulation times, lasting several days within systemic circulation before degradation, allowing the successful delivery of its payload to required sites. Lastly, the safety of these polymeric LNPs has also been well studied; all their structural components have received

approval from several government bodies such as the United States Food and Drug Administration (US FDA) for use in medical therapies [122]. These lipid polymeric nanoparticles are also prime vehicles by which radiosensitizers can be loaded and thus be delivered to specific sites within the body. As demonstrated by Tng et al. [23], these lipid polymeric nanocarriers can be easily synthesized into different sizes, which exhibit differential uptake rates in different 3-dimensional tumours spheroids in vitro. This was further demonstrated by Homan et al. [123]; in vivo, where the injection of polymeric nanoparticles of different molecular weights resulted in different rates of retention as illustrated in Fig. 17. It was observed that the 10kDa nanoparticles produced the most tumour selective accumulation as compared to no accumulation seen in the 1kDa nanoparticles and the non-specific accumulation in the larger 60 kDa nanoparticles after 24 h. These studies highlight the ability of nanoparticle systems to passively target tumours for concurrent imaging and therapeutic applications. The imaging capabilities would allow for diagnostic visualization of the tumour prior to radiotherapy administration or for interval imaging to monitor the progress of treatment.

Besides specific imaging of the tumour for diagnosis and monitoring, the selective delivery characteristics of nanoparticles can be used for concurrent targeted nanoparticle enhanced therapeutics as well. Thierry et al. have demonstrated the use of lipid nanoparticles to deliver verteporfin photosensitizers for PDT in ovarian cancer animal models [124]. These nanoparticles were approximately 50 nm in diameter, and using a lipid fluorescent marker tagged to these lipid nanoparticles for

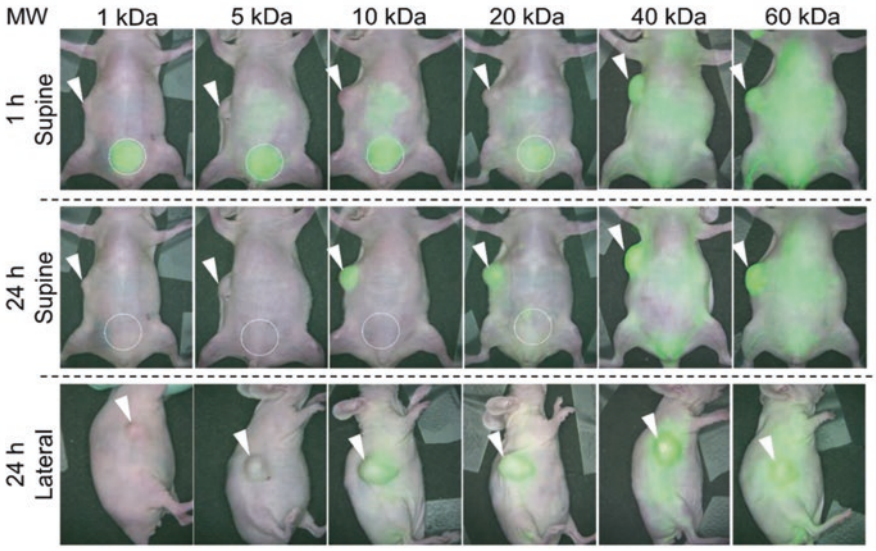

Fig. 17 Tumour targeting efficiency of PEG-ZW800s nanoparticles after intravenous injection of different sized nanoparticles showing the near-infrared imaging of tumour-bearing mice models at different timepoints [123]

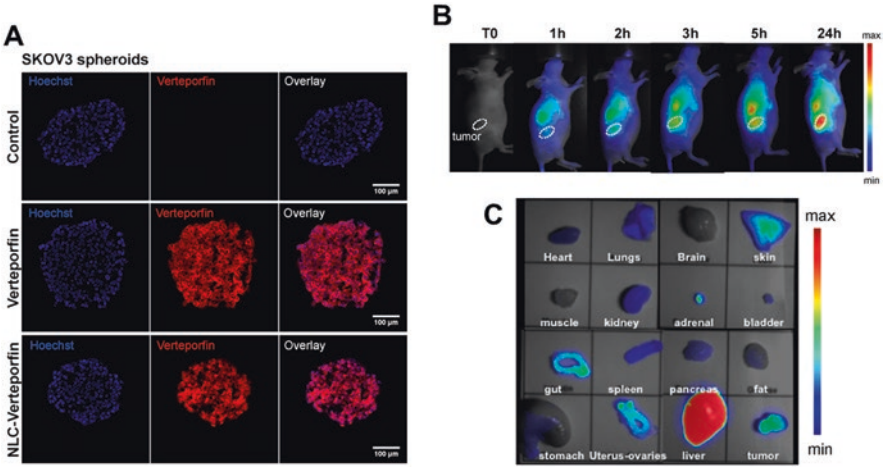

Fig. 18 (**a**) Verteporfin-loaded lipid nanoparticles in SKOV3 spheroids, (**b**) mice with SKOV3 tumour implants injected intravenously with NLC LipImage, fluorescence imaging showing the distribution of LNPs and (**c**) fluorescence imaging on isolated organs after 24 h of intravenous injection of NLC LipImage [124]. Michy T, Massias T, Bernard C, et al. Verteporfin-loaded lipid nanoparticles improve ovarian cancer photodynamic therapy in vitro and in vivo. Cancers. 2019;11(11):1760; licensed under a Creative Commons Attribution (CC BY) license

imaging of the tumour, they were first shown to exhibit uptake in vitro by tumour spheroids (Fig. 18a). Thereafter, these nanoparticles were administered into tumour-bearing mice for concurrent imaging and treatment using PDT. Figure 18b depicts the preferential uptake of the nanoparticles into the site of the tumour and also the liver, 24 h after administration. *Ex vivo* fluorescence imaging of the animal organs (Fig. 18c) showed significant uptake of the LNPs and the co-encapsulated veteporfin photosensitizers into the tumour, whilst the majority of the other visceral organs demonstrated significantly lower uptake of LNPs. Of note, though the liver showed the highest relative uptake in this study, in PDT, treatment sites can be controlled by the targeted photonic exposure of the tumor site only, thereby reducing radiotoxicity to the liver, making nanoparticle enhanced PDT a highly conformal treatment.

6.2 Active Targeting via Ligand/Receptor Interactions

Neoplastic cells also exhibit distinct cell surface biology compared to healthy cells. For example, neoplastic breast cells have been known to upregulate several surface receptors such as HER2, BRACA, and ER. These upregulated receptors have been used to selectively target these cancer cells using various chemotherapeutic drugs [125]. In the same vein, the binding ligands to these receptors can be functionalized onto the nanocarrier surfaces, which would, in turn, cause preferential uptake into these cancerous cells, which would subsequently release photosensitizers for

PDT. This approach has been demonstrated by Kathrin et al., who used spermine and acetal-modified dextran (SpAcDex) nanoparticles to deliver photosensitizers to tumour sites [126]. SpAcDex nanoparticles have high encapsulation efficiencies of photosensitizers and can even transport hydrophobic photosensitizers such as 5,10,15,20-tetraphenyl-21H,23H-porphyrin (TPP). These hydrophobic sensitizers would otherwise have poor uptake at tumour sites due to their poor water solubility [127]. Kathrin et al. have shown that through the use of folate-functionalized SpAcDex nanoparticles, uptake of TPP into human KB cells was enhanced. These cells are of cervical cancer origin and have upregulated folate receptors [24]. This resulted in an increase in uptake of folate-functionalized SpAcDex nanoparticles and the subsequent internalization of TPP, thus achieving targeted delivery to these cancerous cells [126]. The incorporation of folate groups increased delivery of these nanoparticles after 6 hrs and 24 h, seen on fluorescence imaging of KB cells as illustrated in Fig. 19. Further irradiation with a light source after delivery showed that photocytotoxic effects were achieved, showing the effectiveness of these nanoparticles as targeted delivery systems for PDT.

This concept was further demonstrated in vivo using animal mouse models. Hyaluronic acid (HA) was used as a ligand to target cancers which overexpress CD44 and hyaluronic acid-mediated motility receptors (RAHMM) [128, 129]. These receptors are commonly overexpressed in many solid organ tumours [72]. This property can be exploited for nanoparticle ligand-mediated targeted delivery of photosensitizers. HA has been shown to have increased uptake in these cells, making HA-based nanoparticles a good candidate for targeted therapies [130]. HA-coated nanoliposomes loaded with doxorubicin have been shown to have increased uptake in human xenograft mouse models and minimal uptake in control models without the disease. Using this approach, HA-functionalized nanoparticles have been used to deliver photosensitizers for PDT. Gao et al. have shown how photosensitizer-loaded manganese dioxide nanoparticles modified with HA (ICG-HANP/MnO2 (IHM) nanocomplexes) were able to have preferential accumulation

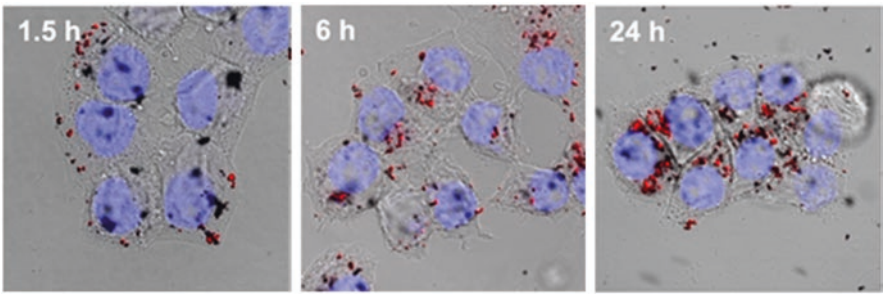

Fig. 19 Confocal imaging of human KB cells incubated at different time points with SpAcDex nanoparticles loaded with 5,10,15,20-tetraphenyl-21H,23H-porphyrin (TPP) photosensitizers [126]. Butzbach K, Konhäuser M, Fach M, et al. Receptor-mediated uptake of folic acid-functionalized dextran nanoparticles for applications in photodynamic therapy. Polymers. 2019;11(5):896; licensed under a Creative Commons Attribution (CC BY) license

within tumour-bearing mouse models whilst having minimal accumulation in other sites other than the liver (Fig. 20a) [25]. Thereafter, ultrasound imaging noted an increased generation of ROS in these tumours after photoactivation, conferring significant photocytotoxic activity to the tumour compared to the control tumours (Fig. 20b), thus illustrating how nanoparticle facilitated active targeting can be used to enhance the PDT effects in tumours while limiting systemic toxicity.

6.3 Crossing Physiological Barriers

In several sites within the body, drug delivery is severely limited due to physiological barriers restricting the free passage of substances. One such example is that of the blood-brain barrier, which restricts the delivery of photosensitizers via simple intravenous administration [131]. Nanoparticle systems such as mesoporous silica (MSN) have great potential to function as such delivery vehicles to these privileged sites as they can be surface modified with molecules such as polyethylene glycol and poly(ethylenimine), which not only allows it to cross the blood-brain barrier but also reduces non-specific protein binding sequestering by the RES system [132–134]. The loading efficiency of these nanoparticles is important, as a larger amount would more easily reach the therapeutic concentration after crossing the physiological barrier. Silica-based nanoparticles are widely known for their biocompatibility and drug loading efficiency [135, 136]. In particular, MSNs are able to accommodate drug weights of up to 60% of the nanoparticle weight [137]. This is due to the

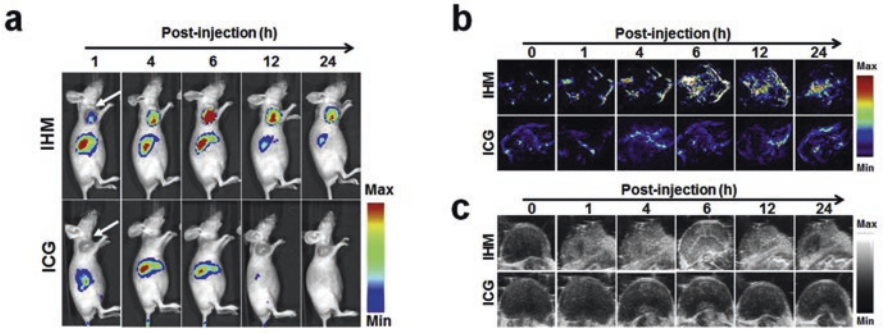

Fig. 20 Noninvasive in vivo imaging monitoring the tumour accumulations of ICG-HANP/MnO2 (IHM) nanocomplex. (**a**) NIR fluorescent imaging of intravenously injected IHM accumulation in SCC7 tumour-bearing mice at different times. Arrows indicate the location of the tumour. (**b**) Photoacoustic imaging of intravenously injected IHM accumulation in SCC7 tumour-bearing mice at different times. (**c**) Ultrasound imaging monitoring the generation of oxygen in tumours after intravenously injected IHM [25]. This article was published in Biomaterials, 112, Gao S, Wang G, Qin Z, et al., Oxygen-generating hybrid nanoparticles to enhance fluorescent/photoacoustic/ultrasound imaging-guided tumour photodynamic therapy, 324–335, Copyright Elsevier 2017

sponge-like structure of MSNs allowing the drugs to be loaded within the pores [138]. Being internalized within the MSN, the photosensitizers can be shielded from the host environment, allowing them to maintain their functional capabilities longer, due to reduced photosensitizer degradation [139, 140]. Brezániová et al. have demonstrated that silica-based nanoparticles (Fig. 21a) were able to deliver temoporfin photosensitizers across the blood-brain barrier in mouse models [140], demonstrating their potential for use in the treatment of tumours in such privileged locations through the use of optical fibres, as demonstrated by Teh et al. (Fig. 21b, c) [141].

7 Conclusion

Nanoparticles have unique physical interactions with the energetic X-ray, proton, and heavy ion beams used in radiotherapy. These have opened up many new paradigms of treatment such as RDT, allowing the treatment of deeply located tumours using nanoparticle photosensitizer conjugates. Such therapies were previously impossible due to the inability of traditional photosensitizer compounds to absorb deeply penetrating beams such as X-rays and protons. Furthermore, nanoparticles play a key role, not only in the targeted delivery of photosensitizer compounds to the tumour sites but also as an imaging tool to visualize the tumour sites prior to commencement of therapy. These nanocarriers have also been shown to be versatile enough to cross the blood-brain barrier, showing the capability of these nanoparticles to treat even immune-privileged regions such as the central nervous system. Current studies show the potential of nanoparticles in many pre-clinical studies using animal models, where nanoparticles have been observed to increase tumour

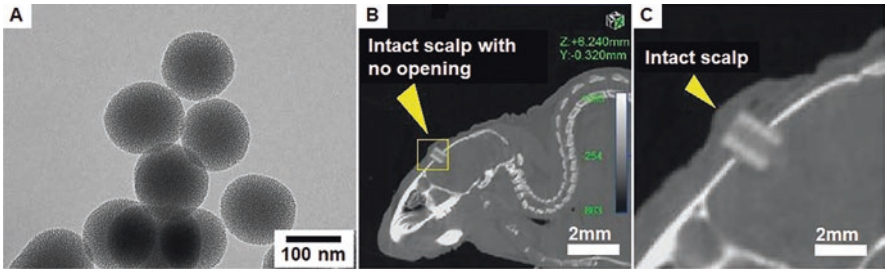

Fig. 21 Mesoporous silica. (**a**) Transmission electron micrograph of photosensitizer-loaded nanoparticles [140]. This article was published in Photodiagnosis and Photodynamic Therapy, 21, Brezániová I, Záruba K, Králová J, et al., Silica-based nanoparticles are efficient delivery systems for temoporfin, 275–284, Copyright Elsevier 2018. (**b**) Optical fibre implant for the treatment of brain tumours and (C) close-up photo showing epithelized implant [141]. Teh DBL, Bansal A, Chai C, et al. A Flexi-PEGDA Upconversion Implant for Wireless Brain Photodynamic Therapy. Advanced Materials. 2020;32(29):2001459. Copyright Wiley-VCH GmbH. Reproduced with permission

cytotoxicity in conjunction with radiotherapies. Indeed, nanomaterials are set to revolutionize the field of radiotherapy, leading to multitudes of applications and improved treatment outcomes.

References

1. Ferlay J, Colombet M, Soerjomataram I, et al. Estimating the global cancer incidence and mortality in 2018: GLOBOCAN sources and methods. Int J Cancer. 2019;144(8):1941–53.
2. Ang KK, Byers RM, Peters LJ, et al. Regional radiotherapy as adjuvant treatment for head and neck malignant melanoma. Preliminary results. Arch Otolaryngol Head Neck Surg. 1990;116(2):169–72.
3. Schulz-Ertner D, Tsujii H. Particle radiation therapy using proton and heavier ion beams. J Clin Oncol. 2007;25(8):953–64.
4. Hellevik T, Martinez-Zubiaurre I. Radiotherapy and the tumor stroma: the importance of dose and fractionation. Front Oncol. 2014;4:1.
5. Kong FM, Ritter T, Quint DJ, et al. Consideration of dose limits for organs at risk of thoracic radiotherapy: atlas for lung, proximal bronchial tree, esophagus, spinal cord, ribs, and brachial plexus. Int J Radiat Oncol Biol Phys. 2011;81(5):1442–57.
6. De Ruysscher D, Niedermann G, Burnet NG, Siva S, Lee AWM, Hegi-Johnson F. Radiotherapy toxicity. Nat Rev Dis Primers. 2019;5(1):13.
7. Bhide SA, Nutting CM. Recent advances in radiotherapy. BMC Med. 2010;8:25.
8. Becker G, Kortmann RD, Skalej M, Bamberg M. The role of radiotherapy in the treatment of craniopharyngioma–indications, results, side effects. Front Radiat Ther Oncol. 1999;33:100–13.
9. Newhauser WD, Zhang R. The physics of proton therapy. Phys Med Biol. 2015;60(8):R155–209.
10. Ribrag V, Ell Hajj M, Janot F, et al. Early locoregional high-dose radiotherapy is associated with long-term disease control in localized primary angiocentric lymphoma of the nose and nasopharynx. Leukemia. 2001;15(7):1123–6.
11. Coates J, Souhami L, El Naqa I. Big data analytics for prostate radiotherapy. Front Oncol. 2016;6:149.
12. Locke J, Karimpour S, Young G, Lockett MA, Perez CA. Radiotherapy for epithelial skin cancer. Int J Radiat Oncol Biol Phys. 2001;51(3):748–55.
13. Chua MLK, Wee JTS, Hui EP, Chan ATC. Nasopharyngeal carcinoma. Lancet. 2016;387(10022):1012–24.
14. Liang L, Lu Y, Zhang R, et al. Deep-penetrating photodynamic therapy with KillerRed mediated by upconversion nanoparticles. Acta Biomater. 2017;51:461–70.
15. Dou Y, Liu Y, Zhao F, et al. Radiation-responsive scintillating nanotheranostics for reduced hypoxic radioresistance under ROS/NO-mediated tumor microenvironment regulation. Theranostics. 2018;8(21):5870–89.
16. Chen H, Wang GD, Chuang YJ, et al. Nanoscintillator-mediated X-ray inducible photodynamic therapy for in vivo cancer treatment. Nano Lett. 2015;15(4):2249–56.
17. Kirakci K, Zelenka J, Rumlova M, et al. Octahedral molybdenum clusters as radiosensitizers for X-ray induced photodynamic therapy. J Mater Chem B. 2018;6(26):4301–7.
18. Tardivo JP, Del Giglio A, de Oliveira CS, et al. Methylene blue in photodynamic therapy: from basic mechanisms to clinical applications. Photodiagn Photodyn Ther. 2005;2(3):175–91.
19. Banerjee SM, MacRobert AJ, Mosse CA, Periera B, Bown SG, Keshtgar MRS. Photodynamic therapy: inception to application in breast cancer. Breast. 2017;31:105–13.
20. Ash C, Dubec M, Donne K, Bashford T. Effect of wavelength and beam width on penetration in light-tissue interaction using computational methods. Lasers Med Sci. 2017;32(8):1909–18.

21. Zhang Q, Guo X, Cheng Y, et al. Use of copper-cysteamine nanoparticles to simultaneously enable radiotherapy, oxidative therapy and immunotherapy for melanoma treatment. Signal Transduct Target Ther. 2020;5(1):58.
22. Maeda H, Greish K, Fang J. The EPR effect and polymeric drugs: a paradigm shift for cancer chemotherapy in the 21st century. J Pt I. 2006;193:103–21.
23. Tng DJH, Song P, Lin G, et al. Synthesis and characterization of multifunctional hybrid-polymeric nanoparticles for drug delivery and multimodal imaging of cancer. Int J Nanomed. 2015;10:5771.
24. Siwowska K, Schmid RM, Cohrs S, Schibli R, Müller C. Folate receptor-positive gynecological cancer cells: in vitro and in vivo characterization. Pharmaceuticals (Basel). 2017;10(3):72.
25. Gao S, Wang G, Qin Z, et al. Oxygen-generating hybrid nanoparticles to enhance fluorescent/photoacoustic/ultrasound imaging guided tumor photodynamic therapy. Biomaterials. 2017;112:324–35.
26. Chen Z, Yu H, Lu W, Shen J, Wang Y, Wang Y. Bone-seeking albumin-nanomedicine for in vivo imaging and therapeutic monitoring. ACS Biomater Sci Eng. 2019;6(1):647–53.
27. Ahmad SS, Duke S, Jena R, Williams MV, Burnet NG. Advances in radiotherapy. BMJ. 2012;345:e7765.
28. Al-Mamgani A, Heemsbergen WD, Peeters ST, Lebesque JV. Role of intensity-modulated radiotherapy in reducing toxicity in dose escalation for localized prostate cancer. Int J Radiat Oncol Biol Phys. 2009;73(3):685–91.
29. Creutzberg CL, van Putten WL, Koper PC, et al. Surgery and postoperative radiotherapy versus surgery alone for patients with stage-1 endometrial carcinoma: multicentre randomised trial. PORTEC study group. Post operative radiation therapy in endometrial carcinoma. Lancet. 2000;355(9213):1404–11.
30. Toulany M. Targeting DNA double-strand break repair pathways to improve radiotherapy response. Genes (Basel). 2019;10(1):25.
31. Faddegon BA, Asai M, Perl J, et al. Benchmarking of Monte Carlo simulation of bremsstrahlung from thick targets at radiotherapy energies. Med Phys. 2008;35(10):4308–17.
32. Jumeau R, Ozsahin M, Schwitter J, et al. Stereotactic radiotherapy for the management of refractory ventricular tachycardia: promise and future directions. Front Cardiovasc Med. 2020;7:108.
33. Jeraj M, Robar V. Multileaf collimator in radiotherapy. Radiol Oncol. 2004;38(3):235–40.
34. Holt A, van Vliet-Vroegindeweij C, Mans A, Belderbos JS, Damen EM. Volumetric-modulated arc therapy for stereotactic body radiotherapy of lung tumors: a comparison with intensity-modulated radiotherapy techniques. Int J Radiat Oncol Biol Phys. 2011;81(5):1560–7.
35. Dell'Oro M, Giles E, Sharkey A, Borg M, Connell C, Bezak E. A retrospective dosimetric study of radiotherapy patients with left-sided breast cancer; Patient selection criteria for deep inspiration breath hold technique. Cancers (Basel). 2019;11(2):259.
36. Fagundes M, Hug EB, Pankuch M, et al. Proton therapy for local-regionally advanced breast cancer maximizes cardiac sparing. Intl J Part Ther. 2015;1(4):827–44.
37. Lischalk JW, Chen H, Repka MC, et al. Definitive hypofractionated radiation therapy for early stage breast cancer: Dosimetric feasibility of stereotactic ablative radiotherapy and proton beam therapy for intact breast tumors. Adv Radiat Oncol. 2018;3(3):447–57.
38. Gerber DE, Chan TA. Recent advances in radiation therapy. Am Fam Physician. 2008;78(11):1254–62.
39. Bortfeld T. An analytical approximation of the Bragg curve for therapeutic proton beams. Med Phys. 1997;24(12):2024–33.
40. Calais J, Cao M, Nickols NG. The utility of PET/CT in the planning of external radiation therapy for prostate cancer. J Nucl Med. 2018;59(4):557–67.
41. Rechner LA, Howell RM, Zhang R, Etzel C, Lee AK, Newhauser WD. Risk of radiogenic second cancers following volumetric modulated arc therapy and proton arc therapy for prostate cancer. Phys Med Biol. 2012;57(21):7117–32.

42. Vanneste BG, Van Limbergen EJ, van Lin EN, van Roermund JG, Lambin P. Prostate cancer radiation therapy: what do clinicians have to know? Biomed Res Int. 2016;2016:6829875.
43. Blanchard P, Garden AS, Gunn GB, et al. Intensity-modulated proton beam therapy (IMPT) versus intensity-modulated photon therapy (IMRT) for patients with oropharynx cancer – a case matched analysis. Radiother Oncol. 2016;120(1):48–55.
44. Gondi V, Yock TI, Mehta MP. Proton therapy for paediatric CNS tumours – improving treatment-related outcomes. Nat Rev Neurol. 2016;12(6):334–45.
45. Tashiro M, Souda H, Yoshida T, Sakurai H. Reconstruction of dose distributions for fine carbon-ion beams using iterative approximation toward carbon-knife. Phys Med Biol. 2020;65(22):225023.
46. Hamad MK. Bragg-curve simulation of carbon-ion beams for particle-therapy applications: a study with the GEANT4 toolkit. Nucl Eng Technol. 2021;53:2767–73.
47. Karger CP, Peschke P. RBE and related modeling in carbon-ion therapy. Phys Med Biol. 2017;63(1):01TR02.
48. Lorat Y, Reindl J, Isermann A, Rube C, Friedl AA, Rube CE. Focused ion microbeam irradiation induces clustering of DNA double-strand breaks in heterochromatin visualized by nanoscale-resolution electron microscopy. Int J Mol Sci. 2021;22(14):7638.
49. Morton G, McGuffin M, Chung HT, et al. Prostate high dose-rate brachytherapy as monotherapy for low and intermediate risk prostate cancer: efficacy results from a randomized phase II clinical trial of one fraction of 19 Gy or two fractions of 13.5 Gy. Radiother Oncol. 2020;146:90–6.
50. Hennrich U, Kopka K. Lutathera®: the first FDA-and EMA-approved radiopharmaceutical for peptide receptor radionuclide therapy. Pharmaceuticals. 2019;12(3):114.
51. Sartor O, Coleman R, Nilsson S, et al. Effect of radium-223 dichloride on symptomatic skeletal events in patients with castration-resistant prostate cancer and bone metastases: results from a phase 3, double-blind, randomised trial. Lancet Oncol. 2014;15(7):738–46.
52. Parker C, Nilsson S, Heinrich D, et al. Alpha emitter radium-223 and survival in metastatic prostate cancer. N Engl J Med. 2013;369(3):213–23.
53. Cha T-L, Wu TT-L, Vogelzang NJ, et al. Optimal usage of radium-223 in metastatic castration-resistant prostate cancer. J Formos Med Assoc. 2017;116(11):825–36.
54. Silva EF, Serpa C, Dąbrowski JM, et al. Mechanisms of singlet-oxygen and superoxide-ion generation by porphyrins and bacteriochlorins and their implications in photodynamic therapy. Chem Eur J. 2010;16(30):9273–86.
55. Wang Z, Zhao J. Bodipy–anthracene dyads as triplet photosensitisers: effect of chromophore orientation on triplet-state formation efficiency and application in triplet–triplet annihilation upconversion. Org Lett. 2017;19(17):4492–5.
56. Schuitmaker J, Baas P, Van Leengoed H, Van der Meulen F, Star W, van Zandwijk N. Photodynamic therapy: a promising new modality for the treatment of cancer. J Photochem Photobiol B Biol. 1996;34(1):3–12.
57. Cai X, Liu Y, Hu Y, et al. ROS-mediated lysosomal membrane permeabilization is involved in bupivacaine-induced death of rabbit intervertebral disc cells. Redox Biol. 2018;18:65–76.
58. Liu Z, Xiong L, Ouyang G, et al. Investigation of copper cysteamine nanoparticles as a new type of radiosensitizers for colorectal carcinoma treatment. Sci Rep. 2017;7(1):1–11.
59. Van der Paal J, Neyts EC, Verlackt CC, Bogaerts A. Effect of lipid peroxidation on membrane permeability of cancer and normal cells subjected to oxidative stress. Chem Sci. 2016;7(1):489–98.
60. De La Haba C, Palacio JR, Martínez P, Morros A. Effect of oxidative stress on plasma membrane fluidity of THP-1 induced macrophages. Biochimica et Biophysica Acta (BBA)-Biomemb. 2013;1828(2):357–64.
61. Abrahamse H, Hamblin MR. New photosensitisers for photodynamic therapy. Biochem J. 2016;473(4):347–64.

62. Mallidi S, Anbil S, Bulin A-L, Obaid G, Ichikawa M, Hasan T. Beyond the barriers of light penetration: strategies, perspectives and possibilities for photodynamic therapy. Theranostics. 2016;6(13):2458.
63. Chen G, Shen J, Ohulchanskyy TY, et al. (α-NaYbF4: Tm3+)/CaF2 core/shell nanoparticles with efficient near-infrared to near-infrared upconversion for high-contrast deep tissue bioimaging. ACS Nano. 2012;6(9):8280–7.
64. Dang X, Bardhan NM, Qi J, et al. Deep-tissue optical imaging of near cellular-sized features. Sci Rep. 2019;9(1):1–12.
65. Qin H, Wu D, Sathian J, Xie X, Ryan M, Xie F. Tuning the upconversion photoluminescence lifetimes of NaYF 4: Yb 3+, Er 3+ through lanthanide Gd 3+ doping. Sci Rep. 2018;8(1):1–8.
66. Lee C, Xu EZ, Liu Y, et al. Giant nonlinear optical responses from photon-avalanching nanoparticles. Nature. 2021;589(7841):230–5.
67. Wang F, Deng R, Wang J, et al. Tuning upconversion through energy migration in core–shell nanoparticles. Nat Mater. 2011;10(12):968–73.
68. Ruan L, Zhang Y. NIR-excitable heterostructured upconversion perovskite nanodots with improved stability. Nat Commun. 2021;12(1):219.
69. Mei Q, Bansal A, Jayakumar MKG, et al. Manipulating energy migration within single lanthanide activator for switchable upconversion emissions towards bidirectional photoactivation. Nat Commun. 2019;10(1):1–11.
70. Zhang Z, Jayakumar MKG, Shikha S, Zhang Y, Zheng X, Zhang Y. Modularly assembled upconversion nanoparticles for orthogonally controlled cell imaging and drug delivery. ACS Appl Mater Interfaces. 2020;12(11):12549–56.
71. Zheng X, Shikha S, Zhang Y. Elimination of concentration dependent luminescence quenching in surface protected upconversion nanoparticles. Nanoscale. 2018;10(35):16447–54.
72. Chen Y-T, Chen Z, Du Y-CN. Immunohistochemical analysis of RHAMM expression in normal and neoplastic human tissues: a cell cycle protein with distinctive expression in mitotic cells and testicular germ cells. Oncotarget. 2018;9(30):20941–52.
73. Xia L, Kong X, Liu X, et al. An upconversion nanoparticle–zinc phthalocyanine based nanophotosensitiser for photodynamic therapy. Biomaterials. 2014;35(13):4146–56.
74. Zhang Z, Jayakumar MKG, Zheng X, et al. Upconversion superballs for programmable photoactivation of therapeutics. Nat Commun. 2019;10(1):4586.
75. Chen X, Zhao Z, Jiang M, Que D, Shi S, Zheng N. Preparation and photodynamic therapy application of NaYF4: Yb, Tm–NaYF4: Yb, Er multifunctional upconverting nanoparticles. New J Chem. 2013;37(6):1782–8.
76. Yang Y, Shao Q, Deng R, et al. In vitro and in vivo uncaging and bioluminescence imaging by using photocaged upconversion nanoparticles. Angew Chem. 2012;124(13):3179–83.
77. Duan X, Li Y. Physicochemical characteristics of nanoparticles affect circulation, biodistribution, cellular internalization, and trafficking. Small. 2013;9(9–10):1521–32.
78. Xing H, Zheng X, Ren Q, et al. Computed tomography imaging-guided radiotherapy by targeting upconversion nanocubes with significant imaging and radiosensitization enhancements. Sci Rep. 2013;3(1):1–9.
79. Liu M, Shi Z, Wang X, et al. Simultaneous enhancement of red upconversion luminescence and CT contrast of NaGdF 4: Yb, Er nanoparticles via Lu 3+ doping. Nanoscale. 2018;10(43):20279–88.
80. Sudheendra L, Das GK, Li C, et al. NaGdF4: Eu3+ nanoparticles for enhanced X-ray excited optical imaging. Chem Mater. 2014;26(5):1881–8.
81. Ou X, Qin X, Huang B, et al. High-resolution X-ray luminescence extension imaging. Nature. 2021;590(7846):410–5.
82. Pei P, Chen Y, Sun C, et al. X-ray-activated persistent luminescence nanomaterials for NIR-II imaging. Nat Nanotechnol. 2021;16(9):1011–8.
83. Pack DW, Manthey WJ, McClure DS. Cê 3+: Nâ+ pairs in CaF 2 and SrF 2: absorption and laser-excitation spectroscopy, and the observation of hole burning. Phys Rev B. 1989;40(14):9930.

84. Wojtowicz A, Glodo J, Wisniewski D, Lempicki A. Scintillation mechanism in RE-activated fluorides. J Lumin. 1997;72:731–3.
85. Nepomnyashchikh A, Radzhabov E, Egranov A, Ivashechkin V. Luminescence of BaF2–LaF3. Radiat Meas. 2001;33(5):759–62.
86. Band I, Kharitonov YI, Trzhaskovskaya M. Photoionization cross sections and photoelectron angular distributions for X-ray line energies in the range 0.132–4.509 keV targets: 1≤ Z≤ 100. At Data Nucl Data Tables. 1979;23(5):443–505.
87. Xu X, Zhou Z, Liu Y, et al. Optimising passivation shell thickness of single upconversion nanoparticles using a time-resolved spectrometer. APL Photonics. 2019;4(2):026104.
88. Zuo J, Li Q, Xue B, et al. Employing shells to eliminate concentration quenching in photonic upconversion nanostructure. Nanoscale. 2017;9(23):7941–6.
89. Johnson NJ, He S, Diao S, Chan EM, Dai H, Almutairi A. Direct evidence for coupled surface and concentration quenching dynamics in lanthanide-doped nanocrystals. J Am Chem Soc. 2017;139(8):3275–82.
90. Wang GD, Nguyen HT, Chen H, et al. X-ray induced photodynamic therapy: a combination of radiotherapy and photodynamic therapy. Theranostics. 2016;6(13):2295.
91. Zhong X, Wang X, Zhan G, et al. NaCeF4:Gd,Tb scintillator as an X-ray responsive photosensitiser for multimodal imaging-guided synchronous radio/radiodynamic therapy. Nano Lett. 2019;19(11):8234–44.
92. Guo Z, Zhu S, Yong Y, et al. Synthesis of BSA-coated BiOI@ Bi2S3 semiconductor heterojunction nanoparticles and their applications for radio/photodynamic/photothermal synergistic therapy of tumor. Adv Mater. 2017;29(44):1704136.
93. Ni K, Lan G, Veroneau SS, Duan X, Song Y, Lin W. Nanoscale metal-organic frameworks for mitochondria-targeted radiotherapy-radiodynamic therapy. Nat Commun. 2018;9(1):1–13.
94. Lu K, He C, Guo N, et al. Low-dose X-ray radiotherapy–radiodynamic therapy via nanoscale metal–organic frameworks enhances checkpoint blockade immunotherapy. Nature Biomed Eng. 2018;2(8):600–10.
95. Lan G, Ni K, Xu R, et al. Nanoscale metal–organic layers for deeply penetrating X-ray-induced photodynamic therapy. Angew Chem. 2017;129(40):12270–4.
96. Ni K, Lan G, Chan C, et al. Ultrathin metal-organic-layer mediated radiotherapy-radiodynamic therapy. Matter. 2019;1(5):1331–53.
97. Ni K, Lan G, Chan C, et al. Nanoscale metal-organic frameworks enhance radiotherapy to potentiate checkpoint blockade immunotherapy. Nat Commun. 2018;9(1):1–12.
98. Sun W, Luo L, Feng Y, et al. Aggregation-induced emission gold clustoluminogens for enhanced low-dose X-ray-induced photodynamic therapy. Angew Chem. 2020;132(25):10000–7.
99. Sun W, Shi T, Luo L, et al. Monodisperse and uniform mesoporous silicate Nanosensitizers achieve low-dose X-ray-induced deep-penetrating photodynamic therapy. Adv Mater. 2019;31(16):1808024.
100. Clement S, Deng W, Camilleri E, Wilson BC, Goldys EM. X-ray induced singlet oxygen generation by nanoparticle-photosensitiser conjugates for photodynamic therapy: determination of singlet oxygen quantum yield. Sci Rep. 2016;6(1):1–9.
101. Mi Z, Zhang Y, Vanga SK, et al. Subwavelength imaging through ion-beam-induced upconversion. Nat Commun. 2015;6(1):1–6.
102. Chen X, Chen C-B, Udalagama CN, et al. High-resolution 3D imaging and quantification of gold nanoparticles in a whole cell using scanning transmission ion microscopy. Biophys J. 2013;104(7):1419–25.
103. Punzón-Quijorna E, Kelemen M, Vavpetič P, Kavalar R, Pelicon P, Fokter SK. Particle induced X-ray emission (PIXE) for elemental tissue imaging in hip modular prosthesis fracture case. Nucl Instrum Methods Phys Res, Sect B. 2020;462:182–6.
104. Martins PM, Dal Bello R, Ackermann B, et al. PIBS: proton and ion beam spectroscopy for in vivo measurements of oxygen, carbon, and calcium concentrations in the human body. Sci Rep. 2020;10(1):1–14.

105. Rashid RA, Abidin SZ, Anuar MAK, et al. Radiosensitization effects and ROS generation by high Z metallic nanoparticles on human colon carcinoma cell (HCT116) irradiated under 150 MeV proton beam. OpenNano. 2019;4:100027.
106. Wälzlein C, Scifoni E, Krämer M, Durante M. Simulations of dose enhancement for heavy atom nanoparticles irradiated by protons. Phys Med Biol. 2014;59(6):1441.
107. Grigalavicius M, Mastrangelopoulou M, Berg K, et al. Proton-dynamic therapy following photosensitiser activation by accelerated protons demonstrated through fluorescence and singlet oxygen production. Nat Commun. 2019;10(1):3986.
108. Cunningham C, De Kock M, Engelbrecht M, Miles X, Slabbert J, Vandevoorde C. Radiosensitization effect of gold nanoparticles in proton therapy. Front Public Health. 2021;9:699822.
109. Mi Z, Chen C-B, Tan HQ, et al. Quantifying nanodiamonds biodistribution in whole cells with correlative iono-nanoscopy. Nat Commun. 2021;12(1):1–9.
110. Rojas JV, Woodward JD, Chen N, Rondinone AJ, Castano CH, Mirzadeh S. Synthesis and characterization of lanthanum phosphate nanoparticles as carriers for 223Ra and 225Ra for targeted alpha therapy. Nucl Med Biol. 2015;42(7):614–20.
111. Vidaud C, Bourgeois D, Meyer D. Bone as target organ for metals: the case of f-elements. Chem Res Toxicol. 2012;25(6):1161–75.
112. Vitha T, Kubíček VC, Hermann P, et al. Lanthanide (III) complexes of bis (phosphonate) monoamide analogues of DOTA: bone-seeking agents for imaging and therapy. J Med Chem. 2008;51(3):677–83.
113. McLaughlin MF, Woodward J, Boll RA, Rondinone AJ, Mirzadeh S, Robertson JD. Gold-coated lanthanide phosphate nanoparticles for an 225Ac in vivo alpha generator. Radiochimca Acta. 2013;101(9):595–600.
114. Moret F, Reddi E. Strategies for optimizing the delivery to tumors of macrocyclic photosensitisers used in photodynamic therapy (PDT). J Porphyrins Phthalocyanines. 2017;21(04–06):239–56.
115. Nakamura Y, Mochida A, Choyke PL, Kobayashi H. Nanodrug delivery: is the enhanced permeability and retention effect sufficient for curing cancer? Bioconjug Chem. 2016;27(10):2225–38.
116. Forni G, Mantovani AJCD. COVID-19 vaccines: where we stand and challenges ahead. Differentiation. 2021;28(2):626–39.
117. Capobianchi MR, Rueca M, Messina F, et al. Molecular characterization of SARS-CoV-2 from the first case of COVID-19 in Italy. Clin Microbiol Infect. 2020;26(7):954.
118. Polack FP, Thomas SJ, Kitchin N, et al. Safety and efficacy of the BNT162b2 mRNA Covid-19 vaccine. New Eng J Med. 2020;384(16):1577.
119. Chakraborty C, Sharma AR, Bhattacharya M, Lee S-S. From COVID-19 to cancer mrna vaccines: moving from bench to clinic in the vaccine landscape. Front Immunol. 2021;12(2648):679344.
120. Tan L, Sun X. Recent advances in mRNA vaccine delivery. J Nano Res. 2018;11(10):5338–54.
121. Lim J-M, Bertrand N, Valencia PM, et al. Parallel microfluidic synthesis of size-tunable polymeric nanoparticles using 3D flow focusing towards in vivo study. Nanomedicine. 2014;10(2):401–9.
122. Ghitman J, Biru EI, Stan R, Iovu H. Review of hybrid PLGA nanoparticles: future of smart drug delivery and theranostics medicine. Mater Des. 2020;193:108805.
123. Kang H, Rho S, Stiles WR, et al. Size-dependent EPR effect of polymeric nanoparticles on tumor targeting. Adv Healthc Mater. 2020;9(1):1901223.
124. Michy T, Massias T, Bernard C, et al. Verteporfin-loaded lipid nanoparticles improve ovarian cancer photodynamic therapy in vitro and in vivo. Cancers. 2019;11(11):1760.
125. Liyanage PY, Hettiarachchi SD, Zhou Y, et al. Nanoparticle-mediated targeted drug delivery for breast cancer treatment. Biochimica et Biophysica Acta (BBA) Rev Cancer. 2019;1871(2):419–33.

126. Butzbach K, Konhäuser M, Fach M, et al. Receptor-mediated uptake of folic acid-functionalized dextran nanoparticles for applications in photodynamic therapy. Polymers. 2019;11(5):896.
127. Malacarne MC, Banfi S, Rugiero M, Caruso EJP. Drug delivery systems for the photodynamic application of two photosensitisers belonging to the porphyrin family. Photochem Photobiol Sci. 2021;20(8):1011–25.
128. Dey A, Koli U, Dandekar P, Jain R. Investigating behaviour of polymers in nanoparticles of chitosan oligosaccharides coated with hyaluronic acid. Polymer. 2016;93:44–52.
129. Wei W-H, Dong X-M, Liu C-G. In vitro investigation of self-assembled nanoparticles based on hyaluronic acid-deoxycholic acid conjugates for controlled release doxorubicin: effect of degree of substitution of deoxycholic acid. Intl J Mol Sci. 2015;16(4):7195–209.
130. Peer D, Margalit R. Tumor-targeted hyaluronan nanoliposomes increase the antitumor activity of liposomal doxorubicin in syngeneic and human xenograft mouse tumor models. Neoplasia (New York, NY). 2004;6(4):343.
131. Goodell TT, Muller PJ. Photodynamic therapy: a novel treatment for primary brain malignancy. J Neurosci Nurs. 2001;33(6):296–301.
132. Glorani G, Marin R, Canton P, et al. Pegylated silica nanoparticles: cytotoxicity and macrophage uptake. J Nanopart Res. 2017;19(8):1–14.
133. Rao L, Xu J-H, Cai B, et al. Synthetic nanoparticles camouflaged with biomimetic erythrocyte membranes for reduced reticuloendothelial system uptake. Nanotechnology. 2016;27(8):085106.
134. Mendiratta S, Hussein M, Nasser HA, Ali AAA. Multidisciplinary role of mesoporous silica nanoparticles in brain regeneration and cancers: from crossing the blood–brain barrier to treatment. Part Part Syst Charact. 2019;36(9):1900195.
135. Janßen HC, Angrisani N, Kalies S, et al. Biodistribution, biocompatibility and targeted accumulation of magnetic nanoporous silica nanoparticles as drug carrier in orthopaedics. J Nanobiotechnol. 2020;18(1):1–18.
136. Zhang B, Wei L, Chu Z. Development of indocyanine green loaded Au@ Silica core-shell nanoparticles for plasmonic enhanced light-triggered therapy. J Photochem Photobiol A Chem. 2019;375:244–51.
137. Zhang Y, Zhi Z, Jiang T, Zhang J, Wang Z, Wang S. Spherical mesoporous silica nanoparticles for loading and release of the poorly water-soluble drug telmisartan. J Control Release. 2010;145(3):257–63.
138. Qian HS, Guo HC, Ho PCL, Mahendran R, Zhang Y. Mesoporous-silica-coated up-conversion fluorescent nanoparticles for photodynamic therapy. Small. 2009;5(20):2285–90.
139. Yao M, Ma M, Zhang H, et al. Mesopore-induced aggregation of cobalt Protoporphyrin for photoacoustic imaging and antioxidant protection of stem cells. Adv Funct Mater. 2018;28(47):1804497.
140. Brezániová I, Záruba K, Králová J, et al. Silica-based nanoparticles are efficient delivery systems for temoporfin. Photodiagn Photodyn Ther. 2018;21:275–84.
141. Teh DBL, Bansal A, Chai C, et al. A flexi-PEGDA Upconversion implant for wireless brain photodynamic therapy. Adv Mater. 2020;32(29):2001459.

Magnetic Droplets for Advanced Theranostics: Cancer Diagnosis, Targeted Delivery, and Therapeutics

V. B. Varma and A. J. Chavan

We cannot solve our problems with the same thinking we used when we created them.

Albert Einstein

Abbreviations (Technical)

A:B:C	Droplet A in droplet B in continuous phase C
AMFC	Alternating magnetic field cycle
CP, DP	Continuous phase, dispersed phase
H_o, H_{no}	Applied uniform, nonuniform magnetic fields
FR	Flow rate [$m^3 \cdot s^{-1}$ or $\mu l \cdot h^{-1}$]
FRR	Flow rate ratio
MNDs	Magnetic nanofluid droplets
MNEs	Magnetic nanoemulsions
MNFs	Magnetic nanofluids
MNPs	Magnetic nanoparticles
PDMS	Polydimethylsiloxane
RT	Room temperature
SMF	Static magnetic field
3D	Three-dimensional

V. B. Varma (✉)
School of Materials Science and Engineering, Nanyang Technological University, Singapore, Singapore

Singapore-HUJ Alliance for Research and Enterprise (SHARE), Nanomaterials for Energy and Energy-Water Nexus (NEW), Campus for Research Excellence and Technological Enterprise (CREATE), Singapore, Singapore
e-mail: vbvarma@ntu.edu.sg

A. J. Chavan
Singapore, Singapore

R. S. Chaughule et al. (eds.), *Nanomaterials for Cancer Detection Using Imaging Techniques and Their Clinical Applications*,
https://doi.org/10.1007/978-3-031-09636-5_3

Notation (Bold Face Denotes Vector Quantities)

$\mathbf{v}$	Fluid velocity [$m \cdot s^{-1}$]
$\nabla \mathbf{p}$	Gradient of pressure p
$\mathbf{H}$	Applied magnetic field strength [$A \cdot m^{-1}$]
$\mathbf{B}$	Magnetic flux density [T]
$\mathscr{V}$	Magnetic scalar potential
$\mathbf{F}$	Volume force [$N \cdot m^{-3}$]
$\mathbf{M}$	Magnetization [A·m or mT]

Material Properties

ρ	Density [$kg \cdot m^{-3}$]
μ	Magnetic permeability [$N \cdot A^{-2}$]
χ	Magnetic susceptibility [−]
$\mathscr{K}$	Thermal conductivity [$W \cdot m^{-1} \cdot K^{-1}$)]
η	Viscosity [cP or mPa·s]
$\mathscr{C}$	Volume concentration (% v/v)
H_c, T_c	Coercivity, Curie temperature of MNPs/MNDs

Subscripts

m	Magnetic
H	At applied magnetic field H
amf	Alternating magnetic field component
o	Uniform magnetic field component
no	Nonuniform magnetic field component

Biomedical Terms/Drugs

ALMS	Alginate-lanthanide microsphere
BHF	Barium-hexaferrite
BIONs	Bacterial iron oxide nanowires
CAPE	Caffeic acid phenethyl ester
C.C.s	Cancer cells
CD-DST	Collagen gel droplet-embedded drug sensitivity test
CaD	Cancer diagnosis
CEA	Carcinoma embryonic antigen

CTN	Cancer theranostics
CaT	Cancer therapeutics
DEMA	2-(N,N-Diethylaminoethyl) methacrylate
DMC	DXR-loaded magnetic coacervates
DXR	Doxorubicin
FOLFIRI	Fluorouracil and leucovorin + irinotecan
FOLFOX	Fluorouracil and leucovorin + oxaliplatin
HCG	Human chorionic gonadotropin
HepC	Hepatitis C
ICG	Indocyanine green
IL-8	Interleukin-8
IONC	Iron oxide nanocube
MTX	Methotrexate
NIPAM	N-isopropylacrylamide
NPL	Nano platelets
PFH	Perfluorohexane
PFOB	Perfluorooctyl bromide
PFP	Perfluoropentane
PSNPs	Porous silicon nanoparticles
PTX	Palictaxel
PUMND	Plasmid-loadable magnetic/ultrasound-responsive nanodroplets
SPIONs	Superparamagnetic iron oxide nanoparticles
TMNCPs	Thermomagnetic nanocomposite particles
VBL	Vinblastine
VEGF	Vascular endothelial growth factor
VNs	Virus-mimetic nanocapsules

1 Introduction

Magnetism and magnetic materials revolutionized technological and scientific advancements in various eras, first by the discovery of the compass, second by electric motors, and third by magnetic storage for the current Internet-computer age. The next revolution of magnetic materials was with their nano form, which opened new applications for biomedical, energy, heat transfer, refrigeration, shielding, and point-of-care devices. These application regimes are determined by the particle size, magnetic-thermal-mechanical properties, and form of use (composites, fluid dispersion, droplets, bulk structure, etc.). This chapter mainly focuses on use cases in the droplet form for biomedical applications using superparamagnetic behavior (Fig. 1).

Magnetic materials in nano form exhibit a different set of properties termed superparamagnetic behavior. This state is characterized by the magnetic properties only in the presence of an applied magnetic field; as soon as the field is removed, this nanomaterial loses its magnetization. When these magnetic nanoparticles are dispersed in a career medium like oil or water, the resulting magnetic nanofluid

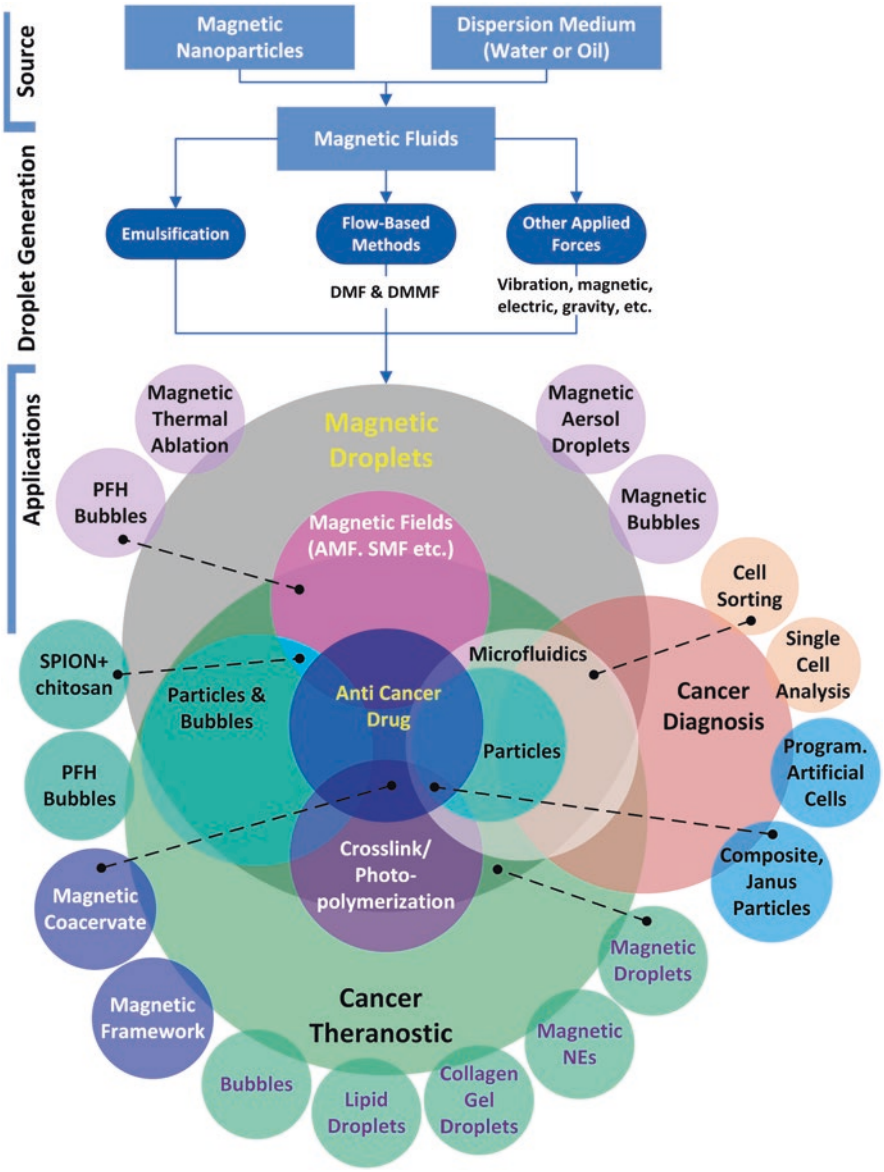

Fig. 1 Schematic of magnetic nanofluid droplets (MNDs) for cancer theranostics (CTN). Magnetic nanofluids can be synthesized by a range of techniques forming the source of MNDs. MNDs can be produced by three methods: (i) Emulsification. (ii) Flow-based methods, mainly consisting of droplet microfluidics (DMF) and droplet micro-magnetofluidics (DMMF); DMF is always preferred due to high precision, high yield droplet generation, and inline control on droplet shape, size, and merging. (iii) Under an applied force, e.g., magnetic, electric, gravitational, and piezoelectric; however, only the vibration-based method is the most popular compared to other applied force techs. Applications of generated MNDs consist of three subsections: (i) MNDs and nanoemulsions (NEs), (ii) particles and bubbles, and (iii) microfluidic techniques for cancer diagnosis (CaD) and single-cell analysis (e.g., CTC sorting, capture, detection), as well as the development of particles for cancer therapy (CaT) and CTN

(MNF) exhibits liquid magnet-like behavior. Under an applied magnetic field, MNF moves towards the direction of the magnetic field. The MNF was invented for rockets to employ fuel motion in the absence of gravity. MNF's interesting properties and specific use cases under different types of magnetic fields were elaborated by Rosenzweig's ferrohydrodynamics approach, established in the 1970s [1], and interesting liquid magnet-like behavior was observed by others [2–4]. Since all magnetic materials exhibit temperature-dependent magnetic properties, magnetic nanofluids follow the suite. Magnetic nanofluids exhibit a specific set of properties under different combinations of magnetic field and temperature [5–9].

Superior biocompatibility of magnetic nanoparticles (MNPs) promoted their use for a range of biomedical applications and, consequently, FDA approval of MNP-based drugs/compositions as the contrast for MRI (Gastromark®, Lumiren®, Feridex®) and imaging of lymph node metastases (Endorem®, Combidex®), as well as to treat iron deficiency anemia (Feraheme®, Ferumoxytol®) and body's elimination of heavy metals or chemicals (Radiogardase®) [10]. On the other hand, MNFs have been extensively used for CTN; specifically, Jordan et al. conducted a phase 2 study of cancer therapeutics for various cancer types [11, 12]. Moreover, MNPs and MNFs are conventional magnetic materials for biomedical applications and cancer theranostics, widely reviewed and also available in book forms [10, 12–15]. Specifically, the review article of Das et al. [16] covered the fundamental physics of MFH and provided a comprehensive table comparing MNP size, synthesis method, surface coating, SAR value, biocompatibility, and applications. They also discussed the effect of MNP shape on MFH performance.

Magnetic nanofluid droplets (MNDs) provide a spectrum of advantages with choice of dispersion-continuous phase, viscosity, surface tension, MNP concentration, magnetic properties, and most importantly nl to pl volume container with an ability to split or merge on command. Furthermore, the MND's control is wireless, programmable, remote, and without direct contact, reducing the risk of contamination and increasing the accuracy and precision of the operation required for the CTN. Hence, MNDs open up an entirely new avenue of CTN applications; this chapter covers the same in detail.

Figure 1 shows the foundation and full spectrum of the magnetic nanofluid droplets (MNDs)-based approach for cancer detection, single-cell analysis, drug delivery, cancer therapeutics, and cancer theranostics. Magnetic nanofluids are the core of the MND-based CTN approach; one can achieve it by different physical, chemical, or other suitable techniques. In addition, these fluids are now commercially available with the choice of dispersion medium and magnetic properties. Once fluids are obtained, droplets (dispersed phase, DP) can be prepared in a continuous phase (CP) by different methods [17]: (i) Emulsion-based techniques provide droplets in high yield, but usually, uniformity and control are less compared to other techniques, very sensitive to the viscosity of the CP and DP. (ii) Flow-based methods, specifically droplet microfluidic (DMF) methods, provide high uniformity, high yield (by multiplexing at high flow rates), and superior inline control of droplet size and shape. For DMF, high-precision flow control is required, which is generally achieved by pressure-driven pumps or syringe pumps. Droplet micro-magnetofluidics

is a combination of DMF platform [17] (driven by syringe or pressure pumps) and magnetic fields providing precise control of the size, the shape, merging, mixing, and sorting of the droplets with wireless, programmable, and remote-controlled capabilities [6, 8, 9, 18]. (iii) Other applied forces can also be utilized for droplet generation, such as electric, gravity, magnetic, piezoelectric, ultrasonic, etc. The vibration-based methods are most popular due to droplet productions at a high yield and uniformity; however, this technology can only produce a simple droplet configuration.

Once magnetic nanofluid droplets are generated, CTN can be achieved via the following approaches (*the scope of this chapter*).

(i) MNDs can be directly utilized for cancer therapeutics, diagnosis, or both, i.e., CTN. These droplets can be in the form of an aerosol and in a suitable dispersion medium for thermal ablation of cancer cells or contain suitable chemicals (PFH) for cavitation bubbles. MFH can be achieved in alternating magnetic field cycles for cancer therapy.

(ii) MNDs generated from the emulsion-based approach can produce particles useful for detection, targeted drug delivery, on-command drug release, and CTN. Nanoemulsions (NEs) need to have a crosslinking material and a trigger to achieve crosslinking either chemically or by physical methods, viz., light, heat, drying, and UV radiation. For emulsion-based methods, though the yield is high, control and drug loading efficiency are inferior to microfluidic-based techniques.

(iii) Droplet micro-magnetofluidics (DMMF) integrates magnetic droplets, magnetic fields, and microfluidics, forming the third category for CTN. Compared to all other techniques, DMMF is a state-of-the-art technique to generate highly uniform droplets, and wireless and programmable control of droplet behavior and can form complex particles in shapes-configurations that are not possible by conventional methods. One can use multiple flow streams, mix them on command, generate droplets, rapid-multiplexed operation, merge-mix them, or bring them close enough to form complex structures without merging. Hence, the DMMF approach provides a broad range of cancer detection techniques, nanoparticle loading to provide controlled release, guided delivery, contrast agents, and multimodal therapy and an efficient, simultaneous loading of hydrophobic and hydrophilic anticancer drugs for multimodal therapeutics.

This chapter, hence, is organized in the above three categories. Section 2 establishes the detailed theoretical foundation via governing equations and control parameters for wireless, programmable, and remote-controlled magnetic droplets and particles, magnetic heating, and magnetic field-based capture and release utilized in cancer diagnosis and therapeutics. Section 3 provides a general overview of experimental techniques and background, in brief. The remaining sections elaborate the state-of-the-art MND-based interesting cancer theranostics approaches reported in the literature. More emphasis was given on direct utilization of magnetic nanofluid droplets for cancer therapeutics. Section 4 will cover particles produced from MNDs

for CTN. Finally, Sect. 5 will explore the DMMF approaches for cancer detection and therapeutics, as well as particles produced by DMMF for CTN.

2 Theoretical Background and Experimental Methodology

The following section elaborates on the theoretical background of magnetism and magnetic materials. This theoretical background is also suitable for developing a numerical simulation model to obtain complex field distributions and greater insight into magnetic field-controlled magnetic droplets for cancer theranostics. One can obtain programmable wireless control by both uniform and nonuniform magnetic fields; however, the mechanism of operation is entirely different for either case.

2.1 Governing Equations for Magnetic Control

The governing equations describing magnetic control of MNDs and magnetic particles are summarized in the following subsections.

2.1.1 Magnetic Field Equations

An externally applied magnetic field of a permanent magnet or an electromagnet acting on a magnetic material of susceptibility χ_{mnf} is described by Maxwell's equations [19]:

$$\nabla \times \mathbf{H} = \mathbf{0}, \tag{1}$$

$$\mathbf{H} = -\nabla \mathrm{V}_{\mathrm{m}}, \tag{2}$$

$$\nabla \cdot \mathbf{B} = \mathbf{0}, \text{and} \tag{3}$$

$$\mathbf{B} = \mu_0 \left(\mathbf{H} + \mathbf{M}\right) = \mu_0 \left(1 + \chi_{mnf}\right) \boldsymbol{H}. \tag{4}$$

where $\mathbf{M} = \chi_{\text{mnf}}\,\mathbf{H}$ is the magnetization of a MNF and B denotes the magnetic flux density. μ_0 and μ_r denote vacuum and relative permeabilities, respectively. MNF permeability and susceptibility are respectively defined by $\mu_{\text{mnf}} = \mu_r \mu_0$ and $\chi_{\text{mnf}} = (\mu_{\text{mnf}}/\mu_0 - 1) = \mu_r - 1$.

2.1.2 Field-Dependent Magnetization and Susceptibility

For an externally applied magnetic field **H**, the magnetization M_H and magnetic volume susceptibilities χ_H are given by [1, 6],

$$M_H = \mathrm{M_s}\,\mathcal{L}(\gamma H) \tag{5}$$

$$\chi_H = \left(\frac{M_s}{H}\right)\mathcal{L}(\gamma H) \tag{6}$$

where $\gamma = 3\chi_0/M_s$. χ_0 is the initial magnetic susceptibility and $\mathrm{M_s}$ is saturation magnetization.

$\mathcal{L}(\gamma H)$ is the Langevin function mathematically stated as

$$\mathcal{L}(\gamma H) = \coth(\gamma H) - \left(\frac{1}{\gamma H}\right) \tag{7}$$

2.1.3 Flow and Energy Equations

The conservation of mass, momentum, and energy governs the mass and energy transport of the MFC device via equations [1–4, 6, 7] of continuity and Navier-Stokes (NS) for ferrofluid velocity **v** and pressure p:

$$\nabla\cdot\mathbf{v} = \mathbf{0} \tag{8}$$

$$\underbrace{\rho\left(\frac{\partial \mathbf{v}}{\partial t}\right)}_{F_a} + \underbrace{\rho(\mathbf{v}\cdot\nabla)\mathbf{v}}_{F_c} = \underbrace{-\nabla p}_{F_p} + \underbrace{\rho\mathbf{g}}_{F_g} + \underbrace{\nabla\cdot\left(\eta\left(\nabla\mathbf{v} + (\nabla\mathbf{v})^{\mathbf{T}}\right)\right)}_{F_\eta} - \underbrace{\gamma\lambda\delta_s\nabla\phi}_{F_s} + \underbrace{\mathbf{F}_{\mathrm{vol}}}_{F_m} \tag{9}$$

he left-hand side of the equation defines the fluid or droplet motion by two-volume force components, viz., due to acceleration ($\mathbf{F_a}$) and convection (F_c). The right-hand side consisted of contributions from the volume forces due to pressure change ($\mathbf{F_p}$), gravity ($\mathbf{F_g}$), and fluid viscosity ($\mathbf{F_\eta}$). Contribution from the gravitational force can be neglected if the droplet size is small (generally, a few hundred μm). External force contributions are included in the force term $\mathbf{F_{vol}}$: in this case, the magnetic volume force ($\mathbf{F_m}$) experienced by MNDs. The MND's properties are defined by the set of physical (η, ρ, κ, C_p) and magnetic (χ_m, M_s, μ_m, T_c, H_c) parameters. F_s denotes the continuum body force due to interfacial tension γ for a droplet with curvature λ. The smoothed delta function (δ_s) is zero everywhere except at the interface, limiting the influence of the surface tension to a narrow region around the interface. ϕ is the level set function [6, 20].

2.1.4 Thermal Energy Equation

We need to consider thermal effects in heat-mass transfer analysis if there are temperature changes during the utilization of MNFs or MNDs. Temperature changes can occur during MFH under an applied AMF. We need to include thermal energy equation in the analysis or simulations as given by [7, 21].

$$\rho C_p \frac{\partial T}{\partial t} + \rho C_p \left(\mathbf{v} \cdot \nabla T\right) = \nabla \cdot \left(\kappa \nabla T\right) \tag{10}$$

2.2 Temperature-Dependent Viscosity

The behavior of both MNFs and MNDs is strongly dependent on viscosity. The viscosity of any fluid changes sharply with temperature, which can be captured with high accuracy by the power-law equation [22] of the form given by,

$$\left(\eta_T\right)^{-0.2661} = \left(\eta_K\right)^{-0.2661} + \left(\frac{\mathrm{T} - \mathrm{K}}{233}\right). \tag{11}$$

where η_K is known viscosity (cP) at the known temperature K °C. η_T is the required unknown viscosity at temperature T °C. Varma et al. [23] modeled eight types of magnetic nanofluids in viscosity range from 1 cP to 120 cP, obtaining good agreement between experiments and simulations using the above equation. One can use the same approach to include viscosity variation of MNDs during MFH to investigate drug release, cancer therapy, or crosslinking of particles for CTN.

2.3 Magnetic Volume Force

There are two components of the magnetic volume force ($\boldsymbol{F_m}$): (i) $\boldsymbol{F_o}$ contributed by the uniform field $\mathbf{H_o}$ and (ii) $\mathbf{F_{no}}$ contributed by nonuniform magnetic field $\mathbf{H_{no}}$, as given by

$$\boldsymbol{F}_o = \mathbf{H}\left(\nabla \cdot \mathbf{B}\right) = -\left(\frac{H^2}{2}\right)\nabla\mu = -\mu_0 \mathcal{C}\left(\frac{\mathrm{H}^2}{2}\right)\nabla\chi_H \tag{12}$$

$$\boldsymbol{F}_{no} = \mathbf{B}\cdot\nabla\mathbf{H} = \mu_0 \boldsymbol{M}\nabla H = \mu_0 \mathcal{C}\chi_H\left(\frac{\nabla \mathrm{H}^2}{2}\right) \tag{13}$$

$\mathcal{C}$ is MNP volume fraction.

2.4 *MNF's and MND's Heating in Alternating Magnetic Field and SAR Calculations*

A magnetic material (MNPs, MNFs, or MNDs) under radio frequency (RF) or alternating magnetic field (AMF) exhibit heating which is a function of system power ($f \times H^2$), MNP particle size, and magnetic properties of the material (M_s, H_c, T_c, SAR, ILP) (Fig. 2). The specific absorption ratio (SAR) and intrinsic loss of power (ILP) are two main performance metrics characterizing the MFH. T_c-tuned MNPs provide an automated cut-off of heating beyond the safe limits for an efficient MFH-based CTN. This section briefly describes the theory and relevant performance metrics of MFH.

2.4.1 Applied Alternating Magnetic Field (H_{ac}), Internal Energy, and Power Dissipation

Change in internal energy for heating by magnetic field obtained from work done $\delta W = \mathbf{H}\delta\mathbf{B}$ under adiabatic condition [26–28] is given by

$$dU = \boldsymbol{H} \cdot d\boldsymbol{B} \tag{14}$$

Here, both **H** and **B** are colinear fields inside the sample; hence, the dot product reduces to $dU = H\,dB$. Since $B = \mu_0 (H + M)$, substitution and integration by parts of the above equation provide an increase in internal energy for a cyclic process, as given by,

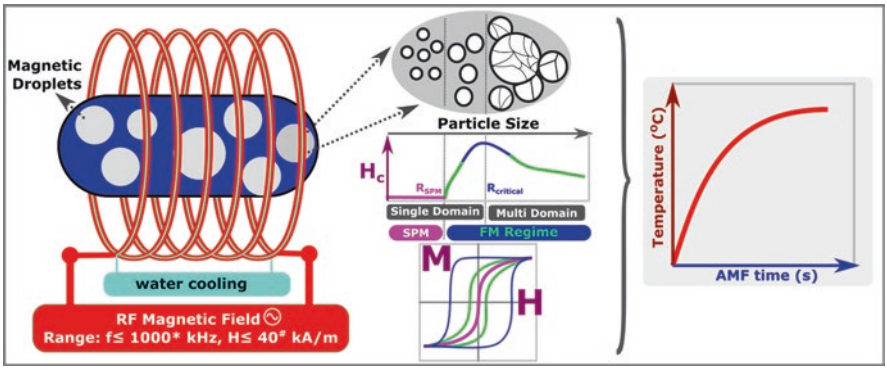

Fig. 2 Schematic of magnetic hyperthermia setup. MNFs and MNDs under radio frequency (RF) or alternating magnetic field (AMF) exhibit MFH which is a function of system power, particle size, and magnetic properties of the material. SAR and ILP are two main performance metrics of MFH. T_c-tuned MNPs provide an automated MFH cut-off required for a safe MFH-based CTN. * [24] reported maximum frequency and # [25] reported maximum field

$$\Delta U = -\mu_0 \oint M \, dH \tag{15}$$

Suppose the frequency of the magnetic field leads to lagging magnetization. In that case, the right-hand side of the above equation will be positive, implying magnetic work's conversion to internal energy increase. Let us assume a complex form of MNF susceptibility $\chi_m = \chi_a - i\,\chi_b$ (with real component χ_a and imaginary component χ_b). The alternating magnetic field and resulting magnetization then take the form,

$$H_{amf}(t) = H_a \cos \omega t = \mathrm{Re}[H_a e^{i\omega t}] \tag{16}$$

$$M(t) = \mathrm{Re}\left[\chi H_a e^{i\omega t}\right] = H_a \left(\chi_a \cos \omega t + \chi_b \sin \omega t\right) \tag{17}$$

where H_a is the field amplitude. Substituting Eqs. (16) and (17) in Eq. (15), we get

$$\Delta U = 2\mu_0 H_a^2 \chi_b \int_0^{\frac{2\pi}{\omega}} \sin^2 \omega t \, dt \tag{18}$$

Here, the real component χ_a vanishes, and the imaginary component, also termed as loss component, χ_b remains. The power dissipation P for $f = 2\pi/\omega$ then takes the form as given by,

$$P = f \Delta U = \mu_0 \pi \chi_b f H_a^2 \tag{19}$$

2.4.2 Practical Approach for the Relationship to Material Properties

The imaginary part of susceptibility can be obtained as the function of magnetic material properties and an applied magnetic field frequency f by the time-dependent magnetization M(t). M(t) equation and equilibrium magnetization M_a for an AMFC amplitude H_a (Eq. (16)) are given by [3, 26],

$$\dot{M}(t) = -\frac{\left(M(t) - M_a\right)}{\tau} \tag{20}$$

$$M_a = \chi_H H_a \cos \omega t = \mathrm{Re}\left[\chi_H H_a e^{i\omega t}\right] \tag{21}$$

Let's use exponential forms of $M(t)$ (Eq. (17)) and M_0 (Eq. (21)) in the differential Eq. (20); we obtain,

$$\chi = \frac{1}{1 + i\omega\tau} \chi_H \tag{22}$$

$$\chi_a = \frac{1}{1+(\omega\tau)^2}\chi_H \tag{23}$$

$$\chi_b = \frac{\omega\tau}{1+(\omega\tau)^2}\chi_H \tag{24}$$

After plugging in the obtained value of χ_b in Eq. (19), the power dissipation density during the MNF or MND heating in an applied AMFC of frequency f takes the form as given by,

$$P = f\,\Delta U = \mu_0 \pi\, f H_a^2\, \chi_H \frac{2\pi f\tau}{1+2\pi f\tau} \tag{25}$$

Here, the magnetic fluid susceptibility χ_H is field-dependent and is derived in the earlier section. The parameter τ is effective relaxation time, which is a function of Brownian (τ_B) and Neel (τ_N) relaxation time expressed as given by,

$$\frac{1}{\tau} = \frac{1}{\tau_B} + \frac{1}{\tau_N} \tag{26}$$

2.4.3 SAR and ILP Calculations

The magnetic fluid hyperthermia (MFH) of magnetic nanofluids and droplets is contributed from Brownian, Neel relaxations, or hysteresis loss, which is quantified by the specific absorption rate (SAR, also termed as the specific loss power, (SLP)) [12, 29]. The SAR can be calculated by different approaches [30], viz., by (i) measuring the initial slope (ΔT/Δt) for a fixed time duration (first 10 s or 100 s, etc.), (ii) correcting the slope by including a loss parameter with reference to the baseline curve, (iii) exponential curve fitting (by Box-Lucas method) of the MFH profile, and (iv) by steady-state temperature measurement. The initial slope increase approach is the most popular method utilized for the SAR [$W \cdot g^{-1}$] measurement [31–33], which is given by,

$$SAR = C\left(\frac{\Delta T}{\Delta t}\right)\frac{M_{MNF}}{M_{MNP}} \tag{27}$$

where C and M_{MNF} are the specific heat capacity and the mass of the MNF in SI units. M_{MNP} is the mass of the MNPs inside the MNF under test. The initial slope $\Delta T/\Delta t$ is determined for the initial sharp increase of the MNF heating profile under an applied AMF power. Hence, the SAR is strongly dependent on the applied AMF power.

For a more generalized comparison of MFH performance independent of AMF power, one can use the intrinsic loss of power (ILP) (nH$m^2 \cdot kg^{-1}$), as given by [31, 34, 35],

$$ILP = \frac{SAR}{AMF\ \text{Power}} = \frac{SAR}{H^2 f} \tag{28}$$

where H [kA·m^{-1}] and f [kHz] are the AMF field strength and frequency, respectively.

3 Experimental Methods

Magnetic fluid and droplets exhibit response to an applied magnetic field. This response depends on the type, magnitude, and direction of the field and the magnetic properties of the materials such as saturation magnetization, coercivity, and toxicity for biomedical applications. There are three main types of magnetic fields, viz., uniform, nonuniform, and time-varying magnetic fields. A superimposition of the main types with each other produces a hybrid magnetic field.

A uniform magnetic field can be generated by an electromagnet, a Helmholtz coil, or a combination of permanent magnets. Generally, for the case of electromagnet feedback loop-based method is utilized, where a Hall probe senses the magnetic field and the system then tunes the current to the set value of the field. Higher field uniformity and magnetic field strength can be achieved by using an electromagnet system. However, the electromagnet system is bulky and utilizes higher power than permanent magnets. Therefore, a permanent magnetic field-based approach is utilized when a stand-alone, portable, and miniaturized system is required. Permanent magnets can directly be integrated with the device to apply a magnetic field; however, this approach does not provide programmable field control. A hybrid magnetic field approach can overcome both challenges by overlapping the electromagnet's field over a permanent magnet, generating the required distribution of H_o and H_{no}.

Two comprehensive review articles describe different magnetic field systems for a range of biomedical applications [36, 37]. Specifically, Yang et al. [36] covered a range of state-of-the-art magnetic actuation systems as well as fundamentals of magnetic actuation and magnetic field generation. They systematically described different actuation systems consisting of single permanent magnet, multiple permanent magnets, paired coils, distributed stationary electromagnets, and movable electromagnets. They also elaborated applications of described magnetic actuation systems to control catheters, capsule endoscope, and motion (crawling, walking, swarming, dragging, swimming, rolling) of magnetic composites, suitable for different biomedical applications (cell manipulation, surgery, therapy, tissue engineering, imaging, biopsy, sensing, and in vitro testing). For MND-based CTN, hybrid magnetic control and MFH systems can be designed and developed by integrating the approaches discussed in this article.

4 Magnetic Nanofluid Droplets (MNDs) for Cancer Detection and Therapeutics

The use of magnetism or magnetic materials for medical applications is not new. Old Indian literature reports the use of magnetism to remove metal needles from the body. However, magnetic materials or magnetism-based methods were not used much until the 1970s due to their complexity, lack of depth, and control tech. In 1971, Lauterbur invented MRI and theorized it in 1973 [38]. It took another 6 years for the first full-body scan by MRI performed by Damadian R. However, the developed method was too slow for practical use. Finally, Lauterbur and Mansfield addressed it, and their strategy was adopted for routine MRI, bagging a Nobel prize for the same. After that, research in MNPs was quiet except for their use as MRI contrast [39, 40].

The next breakthrough came with the use of MNPs and MNFs for theranostics with their capabilities of magnetically guided drug delivery, contrast for continuous monitoring, localization in the area of interest, on command release of drug in the desired amount, and multimodality via MFH. Combining MNPs/MNFs with this approach provided a new direction, gaining much interest and coverage in a range of interdisciplinary fields for biomedical applications (Fig. 3). Following the advancement of the field, MND-based techniques, such as droplet magnetofluidics, droplet micro-magnetofluidics, and resulting nano/micro/bulk particles, emerged as potential, new application regimes. These regimes are systematically elaborated in the following sections and subsections.

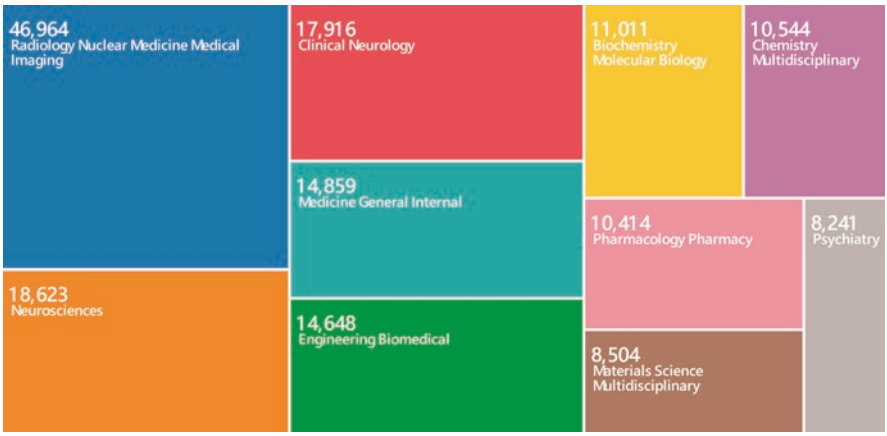

Fig. 3 Tree map chart of biomedical applications of magnetic materials reported for a range of interdisciplinary fields. Magnetic materials are used in extensive regimes due to their versatility for drug delivery, MRI contrast, remote-programmable control, and multimodal therapy. (Source: Web of Science database (dated 23 Jan 2022) was used for the data collection with search string '(mag*) AND (drug or medic*)')

4.1 Droplets for Cancer Diagnosis, Therapy, and Theranostics

In literature, lipid, droplets, and collagen gel droplets are the simplest droplet configurations directly employed for cancer detection and/or therapeutics [41, 42]. Table 1 compares different MND configurations reported for cancer diagnosis, therapy, and theranostics. Tirinato [41] et al. demonstrated the use of lipid droplets as a new functional marker for colorectal cancer detection by activating the PI3K/AKT pathway to increase CD133 and CD44v6 CSC marker expression. They found that glucose increases the number of reactive oxygen species and lipid droplets in colorectal cancer stem cells and the addition of *atorvastatin*, a lipid-reducing drug, successfully kills the cancer stem cells. Curtarello [42] et al. employed VEGF treating ovarian cancer and investigated variation in lipid droplet profile. They found upregulation of pathways leading to lipid droplet accretion in tumors and achieved CaT via liver X receptor *agonist* (LXRA), selectively inhibiting cancer growth. Generally, cytoplasmic lipid droplet buildup implies *apoptosis* and may govern drug resistance. Their drug +LXRA approach amplified cell deaths, providing a potential CTN methodology. Ochiai et al. [43] determined growth inhibition rate of primary colorectal cancer and impact of tumor location in chemotherapy (FOLFOX, FOLFIRI)-treated patients by collagen gel droplet-embedded drug sensitivity test. They found that molecularly targeted agents provide improved clinical outcomes compared to anticancer drugs for colorectal cancer patients with left-sided tumors. Lorton et al. [44] developed oxygen-loaded perfluorooctyl bromide (PFB) droplets (developed size range: 172–3000 nm) for CTN application. They controlled oxygen partial pressure by their special in situ 19F MRI contrast mapping method. This method provides high MRI contrast due to PFB droplets and eliminates hypoxia by oxygen delivery to stop tumor growth.

4.2 MNDs for Cancer Therapy and Theranostics

MNDs-based approach consists of one fixed magnetic functionality with or without other functionalities to diagnose and treat different types of cancer (Table 1). Due to its simplicity, the least complex approach of direct utilization of MNDs without any other functionalities is always preferred. Dames et al. [45] demonstrated lung cancer CTN by MNP-loaded aerosol droplets (nanomagnetosols) by simulations and experimentally in mice under a nonuniform magnetic field gradient, also extendable to other types of lung diseases. They built a conical coil to achieve a high field gradient of 1000 $T \cdot m^{-1}$ required for this method. Under an applied magnetic field, a 5× increase in nanomagnetosols delivery was observed compared to the case without magnetic field in the targeted lung, and a 2× reduction was observed in the untargeted lung compared to the case without magnetic field.

MNDs under an alternating magnetic field exhibit heating which can be utilized to treat cancer. Moreover, due to the additional volume force contributed by the

Table 1 Droplets, emulsions, and bubble-based cancer diagnosis (CaD), therapeutics (CaT), or both (cancer theranostics, CTN)

References	Cancer type/Model/ Cell line	Drug type/Acting agent	Use	Findings. CaT/CaD/synthesis @ *method, drug*	Droplets		Cancer cells, %mortality @ C
					Phases	Size (nm)	
[41]	Cancer stem cells	Atorvastatin to reduce lipid	CaD, CaT	CaD by activating PI3K/AKT pathway. CaT by *atorvastatin*	Lipid droplets		>90%
[42]	Ovarian cancer cells	Exogenous lipids	CaT	Lipid metabolism upregulation increased lipid droplets in tumors reproduced by hypoxic conditions	Lipid droplets		
[43]	Colorectal cancer	FOLFOX, FOLFIRI	CaD, CaT	Molecularly targeted agents ⇒ better clinical therapy compared to anticancer drugs	Collagen gel droplets		
[44]	–	PFB droplets	CaD	In situ ^{19}F MRI contrast mapping of oxygen partial pressure	PFB droplets	1000	–
[45]	Simulations and mice	Nanomagnetosols	CaT	Targeted delivery of magnetic aerosol droplets to the lung	Aerosol droplets+ SPION	80	
[46]	–	Magnetically polarizable NEs	CaT	MNE investigations to enhance SAR value @ *size, dispersity, field*	MNEs + agar	192	–
[47]	–	MNDs	CaT	CaT at low MNP loading by 30% SAR increase @ aligned MNEs	Octane-based MNF+ agar	200	–
[48]	4 T1 xenografted mice tumor	Magnetic-thermal ablation	CTN	CTN injectable, thermosensitive MNE hydrogel. Increased SAR @ *MNP chains, MND's crosslinking*	Silicone oil + PEGDA + Zn ferrite MNPs	55	100% @ 3 mg/ ml + 30d AMFC
[49]	MCF-7 breast cancer cells	PFH NE bubbles	CTN	Imaging by nonlinear ultrasound + laser-activated vaporization into bubbles to kill cancer cells	PFH NE+ silica-coated gold NP	400	93% @ 1.5μg/ ml
[31]	HepG2 liver cancer cell	MFH of droplets and DXR release	CTN	Wireless, programmable, multimodal (thermo-chemotherapy) CTN @ *biomimetic DMCs*	Peptide coacervates + MNPs + drug	550	100% @ 550μg/ ml for 3 MFC

[50]	HCT-116 cells	CAPE	CaT	CAPE-loaded MNDs for long-term storage @ *one-step anti-solvation*	Eugenol + Fe_3O_4 NP	204	≈100% @ 20μg/ml
[51]	Cervical cancer cells HeLa	MNPs with and without surfactants	CaT	MNPs coated on HeLa cells for cancer therapeutics; higher cytotoxicity without surfactants	Cells coated with MNPs	–	–
[52]	Urothelial cancer	–	CaD	Evaluated digital droplet PCR assays for post CaT monitoring	Blood/urine samples	–	Diagnosis
[53]	Breast cancer cells (4 T1)	Magnetic framework	CTN	CTN by assembled magnetic internal framework and release by an external magnetic field	Gallium-based alloys	–	
[54]	Subcutaneous tumor	VNs + MFH + DXR or PTX	CTN	Infect cancer cells by VNs, MFH therapeutics, and drug delivery	SPION + protein shell	160	98% @ 1% wt/wt
[55]	Liver cancer cells injected in nude mice	PUMND	CTN	H_o guided PUMND, plasmids release at tumor cells by ultrasounds cavitation	Lipid+ SPION + plasmid	270	40% @ 6 s exposure

Notation and abbreviations: *C* concentration/drug dose in μg/ml or weight/weight (wt/wt), *CTN* cancer theranostics, *MNFs* magnetic nanofluids, *MNDs* magnetic nanofluid droplets, *MNEs* magnetic nanoemulsions, *AMFC* alternating magnetic field cycle, *CAPE* caffeic acid phenethyl ester, *CDT* collagen gel droplet-embedded drug sensitivity test, *PFH* perfluorohexane, *NEs* nanoemulsions, *FOLFOX* fluorouracil and leucovorin + oxaliplatin or *FOLFIRI* fluorouracil and leucovorin + irinotecan, *DXR* doxorubicin, *DMC* DXR-loaded magnetic coacervates, PTX palictaxel, *VNs* virus-mimetic nanocapsules, *PUMND* plasmid-loadable magnetic/ultrasound-responsive nanodroplets, *PFB* perfluorooctyl bromide

susceptibility change in MNDs at the surface, trapping MNDs at the target site is more efficient compared to the MNF's case. Additional insight into the thermal behavior of MNDs under an AMFC can increase their further use for future CTN. With the same motivation, Philip's research group [46, 47] reported different approaches for magnetic nanoemulsions (MNEs), increasing their SAR values, hence, the MFH efficiency. In [46] they investigated 100–200 nm MNEs and found an increasing trend of SAR values with the square of H_{amf} field.

Furthermore, they found that the field-based droplets heating was mainly due to Neel-Brownian at MNP scale and Brownian relaxation at droplet scale compared to MNF heating which is only due to Neel-Brownian relaxation. They also investigated the effect of droplet size, polydispersity-uniformity, field strength, demagnetization effects, viscosity, and particle concentration, which will be helpful to enhance the performance. In [47], improved SAR of aligned droplets under an applied field demonstrated enhanced MFH in an agar matrix representing a tissue. The enhancement was attributed to a 3× increase in uniaxial anisotropy and relaxation time, resulting in a 30% increase in the SAR. These findings can be utilized to achieve the required MFH performance at a reduced MNP loading.

4.3 Modified MNDs for Cancer Therapy and Theranostics

MNDs can be modified to achieve multimodal therapy by adding one or more functionalities with or without anticancer drugs (Table 1). Without anticancer drugs, cancer treatment is usually performed by inducing heating. The upper portion of Fig. 1 applications summarizes this approach. Wu et al. [48] performed CTN by MNE hydrogel demonstrated via 4 T1 xenografted tumor in mice. The hydrogel droplets were restricted to the tumor site by preventing leakage and diffusion by an applied magnetic field. The magnetic chain formation under an applied field and crosslinking of droplets further enhanced the MFH performance demonstrating 100% mortality of cancer cells; hence, it is a potential approach for localized CaT. Fernandes et al. [49] developed PFH nanoemulsions with silica-coated gold nanoparticles. The nanoemulsion was used for cancer theranostics by nonlinear ultrasound-based imaging and laser-activated vaporization bubbles for cancer therapy. This method achieved 93% mortality of cancer cells at the droplet loading of 1.5μg/ml. In addition, they found that the PFH bubble-based imaging utilized here was more stable than conventional contrast imaging due to reduced tissue-specific signals increasing its S/N ratio.

4.4 Drug-Loaded MNDs for Cancer Therapy and Theranostics

With drug-loaded MNDs, cancer treatment is achieved by the multipronged attack, viz., both heating and drug delivery (Table 1). Wang et al. [50] used rice protein to develop 200 nm-sized droplets exhibiting 4 months of stability for CTN without using any stabilizers synthesized by one-step anti-solvation at a neutral pH. The droplet system demonstrated a 20% improvement in the enclosed drug (CAPE) performance compared to the standard drug delivery. Bhardwaj et al. [51] investigated MNPs with and without surfactants forming a coating of HeLa human cancer cell lines comprising a droplet-like configuration suitable for cancer therapeutics via MFH. They observed higher cytotoxicity for MNPs without surfactants. Pritchard et al. [52] evaluated a digital droplet PCR assay-based CaD platform for post urothelial cancer therapy. They utilized blood and urine samples for the CaD of 2 stage 1 patients and 18 stage 2 patients. They developed a new assay on the same platform to detect telomerase reverse transcriptase promoter mutations and identified a novel mutation of CNTNAP4 G727.

MNDs can also be modified by nonconventional approaches/functionalities to obtain a range of novel CTN methodologies enhancing biocompatibility or MFH efficiency, or both. Lim et al. [31] developed coacervate magnetic droplets by a biomimetic polymer for wireless, remote-controlled, programmable multimodal CTN. They synthesized peptide coacervates with a high loading of DXR for multimodal liver cancer treatment, demonstrating 100% mortality of HepG2 liver cancer cells. The use of biomimetic peptides contributes to the superior biocompatibility of magnetic coacervates compared to other approaches. Li et al. [53] reported gallium-based biomimetic liquid mWl droplets developed by magnetic framework for breast cancer (4 T1) treatment. They demonstrated CTN capabilities under an applied electric and magnetic field-controlled assembly for loading a chemical indicator and anticancer drug and on command release killing breast cancer cells (4 T1). Fang et al. [54] performed multimodal CaT of a subcutaneous tumor by virus-mimetic nanocapsules (VNs) to infect cancer cells, MNPs for MFH, control, and DXR or PTX drugs to kill cancer cells. VNs average size was 160 nm, and this approach killed 98% cancer cells @ 1% wt/wt VN concentration. Dong et al. [55] demonstrated CTN capabilities of plasmid-loaded MNDs treating liver cancer cells injected in nude mice by intracellular delivery of plasmid. A nonuniform magnetic field guided the droplets to the tumor site and 6 s ultrasound cavitation releasing 16–19 plasmids/droplets.

4.5 MNDs for Cancer Diagnosis

MND-based approaches can also be integrated with pre or post-cancer therapy to monitor and quantify treatment efficacy and accelerate drug trial or therapy development processes (Table 1). Pritchard et al. [52] evaluated a digital droplet PCR

assays-based CaD platform for post urothelial cancer therapy. They utilized blood and urine samples for the CaD of 2 stage 1 patients and 18 stage 2 patients. They developed a new assay on the same platform to detect telomerase reverse transcriptase promoter mutations and identified a novel mutation of CNTNAP4 G727.

5 MND-Based Magnetic Particles for Cancer Theranostics

MNDs can also achieve CTN by converting them into particles utilizing a range of methods: (i) addition of a polymer and its crosslinking by photopolymerization, heating, or chemical-based method, (ii) solvent extraction/evaporation method, (iii) chemical reactions, and (iv) catalysis. Out of these methods, the first two are the most popular in the research community due to ease of use, control, and adding more functionalities. Table 2 compares different MND-based magnetic particle approaches reported for cancer diagnosis, therapy, and theranostics.

In addition, MNPs can be added to other droplets to impart magnetic properties to them and remove them after use. However, this approach provides wireless, programable, and remote-controlled capabilities that may not suit every droplet system. Ostrovski et al. [56] developed an inhalation framework using 450 nm-sized aerosols containing SPION for lung cancer treatment localizing it by a permanent magnet, achieving 10× enhanced deposition. Their method traps and deposits aerosols by momentarily halting the ventilator cycle and immediately applying a magnetic field at the target; the deposition is quantified by fluorescent bead solution.

5.1 Emulsion Techniques: Developing Magnetic Particles for Cancer Theranostics

Guo et al. [57] developed PLGA nanoplatforms for multimodal CTN of SKBR-3 breast cancer. The method involved ultrasound imaging-guided (via SPION), near-infrared light-controlled phototherapy executed by perfluorohexane (PFH) bubble burst, and paclitaxel (PTX) drug release. W:O:W double emulsion method synthesized the particles containing PFH and PTX on the PLGA-SPION platform with an average size of 348 nm. Niu et al. [58] achieved CTN by 290 nm-sized PLGA particles containing MNPs, indocyanine green (ICG), and perfluoropentane (PFP) synthesized by a modified double emulsion method. Their phase-shifting fluorescent MNPs enhanced the photothermal therapy employed for cancer therapy, which generates microbubbles and releases the drug on the tumor site.

Najafipour et al. [59] performed CTN of MCF-7 breast cancer cells by multimodal thermomagnetic nanocomposite particles containing MNPs, PNIPAM, DEMA, and loaded with anticancer drug methotrexate (MTX). The ultrasonic-based emulsion copolymerization method produced the required particles with an

Table 2 MNDs and emulsions for cancer detection (CaD), therapeutics (CaT), or both (cancer theranostics, CTN)

Ref	Cancer cell (CC) line/*type*	Drug type/ acting agent	Delivery mechanism/ findings @ synthesis methodology	Particle/*droplet*		Application
				Phase A in B (A:B)	Size (nm)	
[56]	Lung cancer	Magnetic aerosol	SPION-aerosols localized by permanent magnet's field	SPION: Liquid:Air	450	CTN
[57]	SKBR-3 breast CC	PFH bubble burst + PXT drug release	Near-infrared light-controlled, targeted, biocompatible drug delivery on a nanoplatform @ double emulsion	MNP + drug (W:O:W)	348	CTN
[58]	MCF-7 breast CC	Ablation + drug delivery	Phase-shifting fluorescent MNPs for enhanced photothermal therapy @ modified double emulsion	MNP/ICG@ PLGA	290	CTN
[60]	MCF-7 breast CC	MTX	Thermomagnetic nanocomposite particles @ ultrasonic, emulsion copolymerization	NIPAM+ DEMA	50	CTN
[61]	A549 lung CC	PXT	Stimuli-sensitive drug carrier @ hot oil-in-water emulsification	SPION+ lipid	2000	CTN
[63]	HCT116 colon CC	Curcumin	Magnetically controlled drug release, MFH @ Pickering emulsions	MNPs+ cellulose	7500	CTN
[59]	CEA biomarker	Regional hydrophilicity	Magnetic bead-based sandwich immunoassay to detect CEA cancer biomarker @ soft lithography	(W:Air)	1000	CaD

(continued)

Table 2 (continued)

Ref	Cancer cell (CC) line/*type*	Drug type/ acting agent	Delivery mechanism/ findings @ synthesis methodology	Particle/*droplet*		Application
				Phase A in B (A:B)	Size (nm)	
[62]	DU145 prostate	5-fluorouracil	Drug release + photothermal particles @ multiple emulsion solvent evaporations	MNP + Au + PLGA	73	CTN
[64]	MCF-7 breast CC	Melatonin	Targeted CTN by nanocomposite particles @ single emulsion solvent extraction	PLGA + MNPs +	300	CTN
[65]	HepG2 liver CC	DXR	MRI T2 contrast, magneto-mechanical IONC @ emulsion-evaporation method	MNPs+ DXR	100	CTN

Notations/abbreviations: *PFH* Perfluorohexane, *PXT* paclitaxel, *PFOB* perfluorooctyl bromide, *ICG* indocyanine green, *PFP* perfluoropentane, *CEA* carcinoma embryonic antigen, *ALMS* alginate-lanthanide microsphere, *BHF* barium-hexaferrite, W:O (water droplets in oil), O:W:O (oil drops in water drops in oil), W:A (water droplets in air), *NPL* nanoplatelets, *TMNCPs* thermomagnetic nanocomposite particles, *NIPAM* N-isopropylacrylamide, *DEMA* 2-(N,N-diethylaminoethyl) methacrylate, *MTX* methotrexate, *IONC* iron oxide nanocube

average size of 50 nm. The therapy consisted of pH- and temperature-controlled drug release as well as MFH. Maximum release was demonstrated at the pH of 5.5 and temperature of 42 °C. Reczynska et al. [60] produced and showed the efficacy of multifunctional stimuli-sensitive drug carriers against A549 lung cancer cells. The particles consisted of SPION and PXT loading synthesized by hot oil-in-water emulsification. The method produced inhalable 2000 nm-sized particles for the CTN of lung cancers via pulmonary delivery. Low et al. [61] demonstrated the CTN of HCT116 colon cancer by 7500 nm-sized particles via magnetically controlled curcumin drug release and the MFH. They used Pickering emulsions to convert MNPs + cellulose phases to the required particles.

5.2 Crosslinking and Solvent Extraction Techniques: Developing Magnetic Particles for Cancer Theranostics

Hu et al. [62] developed a magnetic bead-based sandwich immunoassay platform by controlling regional hydrophilicity of a PDMS chip for rapid biosensing of carcinoma embryonic antigen (cancer biomarkers). They used soft lithography to

develop the PDMS platform 1000 nm-sized water droplets on the surface on hydrophilic sites. Rad et al. [63] used multiple emulsion solvent evaporation synthesis resulting in 70 nm PLGA particles consisting of gold and magnetic NPs. The synthesized particles demonstrated multimodal CTN of DU145 *prostate* by 5-fluorouracil drug release and photothermal therapy. Xie et al. [64] developed 300 nm-sized composite particles of MNPs and melatonin in the PLGA matrix and demonstrated the CTN of the breast cancer cell line (MCF7). They used the solvent extraction method to produce particles.

Janus particles recently gained interest in developing detection platforms and therapies for a range of cancer and other diseases. The main advantages of using Janus structures in the form of particles are as follows: (i) directly accessible constituent functionalities in contrast to core-shell structures with directional control; (ii) possibility to integrate two or more trigger mechanisms with rapid, wireless, programmable control provided by magnetic phase; and (iii) ability to form any shapes of particles, which is otherwise not possible by conventional techniques, providing complex barcoded nano/micro-structures. For example, Zhang et al. [65] demonstrated CTN of HepG2 liver cancer cells by enhanced DXR loading, MRI T2 contrast, and magneto-mechanical torque to kill cancer cells. An emulsion-evaporation method produced the required Janus nanoparticles with an average size of 100 nm consisting of iron oxide nanocubes and DXR in a porous silica structure.

6 Droplet Micro-Magnetofluidics (DMMF) for Cancer Detection and Therapeutics

The last section's end paragraph described some of the key advantages of Janus particles. It is challenging to produce complex, shape-controlled particles by conventional particle synthesis techniques. Droplet microfluidics is the most preferred technique to fabricate Janus particles. In addition to particle fabrication, droplet microfluidics was extensively used for point-of-care testing to rapidly diagnose different diseases, different lab-on-chip applications (e.g., organ-on-a-chip, skin-on-a-chip, liver-on-a-chip, heart-on-a-chip, etc.), single-cell analysis (e.g., sort circulating tumor cells (CTC) and perform its analysis), and recently AI-integrated enzyme production, gene expression, and cell mutation analysis to increase yield of various biological processes. An excellent review article by Dimitriou et al. [66] elaborated on natural hydrogel-based DMF techniques developing multicellular spheroid configurations. They have described a range of applications of this methodology, including drug testing by constructing artificial tumors as well as cancer theranostics by deploying anticancer drugs and artificial cellular assemblies.

This section will elaborate one regime of droplet microfluidics termed as droplet micro-magnetofluidics (DMMF) obtained by integrating magnetic nanofluids/particles and magnetic fields for droplet control, its utilization for particle fabrication,

and relevant application-specific DMMF approaches for cancer diagnosis, treatment, and cancer theranostics (Table 3).

6.1 DMMF: Basics and Janus Fabrication

Integration of droplet microfluidics with magnetofluidics imparts remote, wireless, and programmable control of static and moving droplets; the resulting field is called droplet micro-magnetofluidics (DMMF). DMMF provides a new capability of controlling phases inside moving droplets. The type of magnetic field and its distribution are the deciding factors for achieving specific nanoparticle distribution. Varma et al. [6, 8, 9, 67] were the first to demonstrate uniform magnetic field-based DMMF technology to perform merging, mixing, and sorting of interior droplet phases during the motion of the droplets. In [6, 9, 67], they pioneered the development of experiments and simulations of uniform field-based DMMF platforms. They investigated the role of flow rate, flow rate ratio, magnetic field strength, field distribution, and MNP loading on droplet behavior and on command droplet's shape change, merging, mixing, and sorting. In [9], their detailed simulation model predicted the merging conditions for uniform magnetic fields, which was experimentally validated categorizing flow rate-dependent regimes in multi-droplet merging, two droplet merging, and no merging. In addition, their studies determined the role of interfacial tension on droplet size, shape, and merging behavior.

The use of nonuniform magnetic fields of permanent magnets offers minimum cost of setup development; however, precise control on magnet position is inevitable due to high sensitivity to the field gradient. One way to address this is by hybrid magnetic field use. Ramanujan's research group [8, 18, 68] used hybrid magnetic fields (combination of uniform and nonuniform magnetic fields) for Janus particle synthesis as well as droplet merging and in situ droplet size change after merging. Their Janus synthesis setup provided a surfactant-free, wash-less synthesis of magnetic Janus particles and demonstrated its use for protein detection. The magnetic control was achieved at a very low magnetic nanofluid content. This platform is useful to include the choice of any polymeric phase and desired functionalities in Janus particles required for cancer detection and cancer theranostics by multiple drug loading (hydrophilic or hydrophobic) and two or more trigger mechanisms (MFH, IR, or ultrasound) for release.

6.2 DMMF-Based Particles for Cancer Theranostics

In literature, different DMF and DMMF approaches have been developed for particle fabrication due to ease of integration of new functionalities as well as excellent control on particle size, shape, and polydispersity. Huang et al. [69] developed SPION- and vinblastine-loaded chitosan particles for cancer theranostics achieved

Table 3 Droplet micro-magnetofluidics (DMMF) for cancer detection (CaD), cancer therapeutics (CaT), cancer theranostics (CTN), or circulating cancer cell (CTC) sorting

Ref.	Droplet/particle				Release mechanism/findings @ methodology/ synthesis method, if any	Application
	Control by	Phases	Size	Shape		
[6, 8]	DMMF, FR, FRR, $H_o + H_{no}$	PGDA+MNPs	150µm	Multifunctional magnetic Janus particles (MJP)	Wash-less, surfactant-free, rapid, & programmable synthesis of MJPs by DMMF technique	CaD, CaT
[69]	FR	SPION+ chitosan	550µm	Multifunctional MBs	Vinblastine-loaded multifunctional MBs for magnetic drug release @ DMF	Drug delivery
[79]	pH + DMMF	PSNPs + BIONs	26.5µm	Multifunctional MBs	Hypromellose acetate succinate-based 5 fluorouracil+ curcumin-loaded MBs @DMF	Synergistic *colorectal* CaT
[70]	3D printed DMF	W:O:Alginate shell	430	Spherical multi-core droplets inside a shell	–	CaD, CaT
[75]	SERS + H_{no}	SPION, Ag NPs	80µm	Spherical droplets	Simultaneous SERS detection of VEGF, IL-8 secreted by single cell	CaD via single cell
[76]	DMMF	MNPs:Si-oil	10µL	–	Early cancer diagnosis POCT via HepC detection	CaD
[72]	DMMF	W (cells):O (MNF)	30µm	Spherical droplets	Label-free sorting by negative magnetophoresis	CTC sorting
[73]	DMMF	PBD:O		Spherical droplets	Superior CTC sorting @ LMP (18/ml) vs commercial Adna test (1.5/ml)	Prostate CTC sorting
[74]	DMMF	W:O (FC-40)	100 nL	Spherical droplets	DMMF mRNA extraction from cDNA, reverse transcription, RNA	mRNA extraction
[77]	Soft magnetic structure	MBs:W:O	100 nL	Spherical droplets	Superior cancer diagnosis by gene expression study, mRNA extraction @ droplet fingering fluidic capacitor	CaD
[78]	Digital DMF + DMMF	MBs:W:Air	100 nL	Spherical droplets	Chemiluminescence to detect 50µg/mL HCG, very important for prognosis of several cancers	CaD:Chorionic gonadotropin

Notation/abbreviations: Phase A in phase B in phase C (A:B:C), *FR* flow rate, *FRR* flow rate ratio, $H_o + H_{no}$ hybrid magnetic field, MBs magnetic microparticles/beads, *C* concentration/drug dose in µg/ml, VBL vinblastine, *SPIONs* superparamagnetic iron oxide nanoparticles, *VEGF* vascular endothelial growth factor, *IL-8* interleukin-8, *HepC* hepatitis C, *HCG* human chorionic gonadotropin, *PSNPs* porous silicon nanoparticles, *BIONs* bacterial iron oxide nanowires, *LMP* lateral magnetophoresis

by magnetic field-assisted guidance and on command release of vinblastine. They adopted the DMF approach to preparing droplets of SPION+ vinblastine+ chitosan phase crosslinked in 20%NaOH solution, achieving vinblastine loading efficiency of ~68%. The developed magnetic beads exhibited ~400μm size and 100% release in 80–130 min under the AMFC. For synergistic colorectal cancer therapy, Maher et al. [68] developed pH-responsive multifunctional curcumin and five fluorouracil-loaded MBs. MB's average size was 26.5μm, and the structure consisted of porous silicon nanoparticles and magnetic nanowires. Li et al. [70] reported an interesting magnetic Janus droplet inside a shell configuration developed by symmetry breaking approach employed via 3D printed microfluidic platform producing artificial chassis of multilayered, functional shells with the desired gradient. The developed process helps to advance artificial cell models and fabricate particles for multimodal drug+ gene delivery by combining organic, inorganic, and biomedical functionalities in the same droplet.

Length scale effects are very critical for DMF and DMMF methodology since with the reduction of droplet size (specifically, less than l μm diameter), surface tension and drag force tend to have very high values. Moreover, due to smaller droplet size, magnetic content and the magnetic response of the droplets will be very small. Hence, working in the sub-micron ($\leq$1μm) droplet size range to produce good quality particles using the DMMF methodology is challenging. However, one can address this challenge by (i) electromagnets to apply high magnetic field strength or (ii) adopting a chemical synthesis approach on the DMF platform to produce nanoparticles [71].

6.3 DMMF for Cancer Cell Sorting and Diagnosis

A range of DMMF-based detection devices used permanent magnet's nonuniform magnetic fields for single-cell sorting [72–74] (e.g., to sort circulating tumor cells) and its analysis to diagnose cancer inside droplets or by fabricating functionalized complex particles. Sun et al. [75] developed a SERS-based DMMF device to simultaneously detect vascular endothelial growth factor (VEGF) and interleukin-8 (IL-8) secreted by a single cell. The single-cell analysis was performed inside spherical droplets by SPION and Ag NPs by two SERS signals, one a turn-on signal due to immune-sandwich and another amplified signal due to collection effect induced by the magnetic field. Shin et al. [76] performed early cancer diagnosis by rapid hepatitis C (HepC) detection on DMMF based on the point-of-care test (POCT) platform. Their disposable real-time PCR performed multiplexed detection via functionalized MNPs, providing accurate detection up to 45 I.U. per 10μL sample volume. Serra et al. [77] developed a soft magnetic structure by water in oil 100 nL-sized droplets. They integrated droplet fingering fluidic capacitor resulting in superior cancer diagnosis demonstrated by gene expression study and mRNA extraction. Piao et al. [78] performed immunoassays on a digital DMMF utilizing 100 nL droplets and successfully detected 50μg/mL human chorionic gonadotropin (HCG) by

chemiluminescence. HCG detection is vital for the early detection of several types of cancers. For the immunoassay, they used magnetic forces to separate and resuspend HCG antibody-coated paramagnetic particles.

7 Conclusions

Magnetic nanofluid droplets (MNDs) are an exciting new avenue for achieving cancer theranostics (CTN). This chapter provided comprehensive coverage of the same, starting from the theoretical foundation of the field and essential fundamental equations. Then, different approaches of MND-based CTN, categorized in three sections, were systematically described from the simplest form of magnetic aerosol to complex droplets and magnetic Janus structures for simultaneous diagnosis and multimodal cancer therapy. Each section of MNDs, MND-based particles, and droplet micro-magnetofluidics consisted of the elaboration of important representative examples as well as a comprehensive comparison of relevant representative approaches.

The MND's can readily integrate a range of functionalities to obtain (i) a versatile platform for cancer theranostics by programmable, remote, and wireless guidance for cargo delivery with live contrast imaging, (ii) flexible nl to pl sized liquid containers to encapsulate desired hydrophobic and hydrophilic drugs, and (iii) CTN by multiple triggering components for multimodal, controlled, on command drug release. Moreover, these MND configurations can be transformed into solid or semisolid particles by including suitable polymers and crosslinking mechanisms. The field of droplet micro-magnetofluidics (DMMF) obtained by integrating MNDs, microfluidics, and suitable magnetic field system can fabricate complex Janus particles/structures for multimodal CTN, and it can perform rapid single-cell analysis, cancer diagnosis, and point-of-care testing for early warning of several types of cancers.

The AI-integrated DMMF platform can accelerate the development time severalfold via a combinatorial chemistry approach. Hence, this direction can provide limitless R and D possibilities of cancer diagnosis, therapy, and cancer theranostics for future research.

References

1. Rosensweig RE. Ferrohydrodynamics. New York: Dover Publications, Inc; 2013.
2. Finlayson B. Convective instability of ferromagnetic fluids. J Fluid Mech. 1970;40:753–67.
3. Shliomis MI. Magnetic fluids. Soviet Phys Uspekhi. 1974;17:153.
4. Odenbach S. Recent progress in magnetic fluid research. J Phys Condens Matter. 2004;16:R1135–R50.
5. Cohn D, Sloutski A, Elyashiv A, Varma VB, Ramanujan R. In situ generated medical devices. Adv Healthc Mater. 2019;8:e1801066.

6. Varma VB, Development of magnetic structures by micro-magnetofluidic techniques. PhD thesis. Singapore: Nanyang Technological University; 2017. Available: https://dr.vbvarma.com/2017phd.
7. Varma VB, Pattanaik MS, Cheekati SK, Ramanujan RV. Superior cooling performance of a single channel hybrid magnetofluidic cooling device. Energ Convers Manage. 2020;223:113465.
8. Varma VB, Wu RG, Wang ZP, Ramanujan RV. Magnetic Janus particles synthesized using droplet micro-magnetofluidic techniques for protein detection. Lab Chip. 2017;17:3514–25.
9. Varma VB, Ray A, Wang ZM, Wang ZP, Ramanujan RV. Droplet merging on a lab-on-a-chip platform by uniform magnetic fields. Sci Rep. 2016;6:37671.
10. Mukherjee S, Liang L, Veiseh O. Recent advancements of magnetic nanomaterials in cancer therapy. Pharmaceutics. 2020;12:147.
11. Maier-Hauff K, Ulrich F, Nestler D, Niehoff H, Wust P, Thiesen B, et al. Efficacy and safety of intratumoral thermotherapy using magnetic iron-oxide nanoparticles combined with external beam radiotherapy on patients with recurrent glioblastoma multiforme. J Neuro-Oncol. 2011;103:317–24.
12. Pankhurst QA, Connolly J, Jones SK, Dobson J. Applications of magnetic nanoparticles in biomedicine. J Phys D Appl Phys. 2003;36:R167–R81.
13. Caizer C. Magnetic nanoparticles in human health and medicine. Wiley; 2021.
14. Sharma SK, Javed Y. Magnetic nanoheterostructures: diagnostic, imaging and treatment. Springer Nature; 2020.
15. Mukherjee S. Recent advances in innovative magnetic nanomaterials for cancer theranostics. Morgan & Claypool Publishers; 2019.
16. Das P, Colombo M, Prosperi D. Recent advances in magnetic fluid hyperthermia for cancer therapy. Colloids Surf B Biointerf. 2019;174:42–55.
17. Han WB, Chen XY. A review on microdroplet generation in microfluidics. J Braz Soc Mech Sci. 2021;43:12.
18. Ray A, Varma VB, Jayaneel PJ, Sudharsan NM, Wang ZP, Ramanujan RV. On demand manipulation of ferrofluid droplets by magnetic fields. Sensor Actuat B-chem. 2017;242:760–8.
19. Griffiths DJ. Introduction to electrodynamics. Upper Saddle River: Prentice Hall; 1962.
20. Ghaffari A, Hashemabadi SH, Bazmi M. CFD simulation of equilibrium shape and coalescence of ferrofluid droplets subjected to uniform magnetic field. Colloid Surf A. 2015;481:186–98.
21. Incropera FP, DeWitt DP, Bergman TL, Lavine AS. Fundamentals of heat and mass transfer. 6th ed. Hoboken: Wiley; 2007.
22. Viswanath DS, Ghosh TK, Prasad DH, Dutt NV, Rani KY. Viscosity of liquids: theory, estimation, experiment, and data. Dordrecht: Springer; 2007.
23. Varma VB, Cheekati SK, Pattanaik MS, Ramanujan RV. A magnetofluidic device to cool light emitting diodes. Energy Rep. 2022 (accepted).
24. Kandasamy G, Maity D. Multifunctional theranostic nanoparticles for biomedical cancer treatments – a comprehensive review. Mat Sci Eng C-Mater. 2021;127:22.
25. Alphandery E, Faure S, Seksek O, Guyot F, Chebbi I. Chains of magnetosomes extracted from AMB-1 magnetotactic bacteria for application in alternative magnetic field cancer therapy. ACS Nano. 2011;5:6279–96.
26. Rosensweig RE. Heating magnetic fluid with alternating magnetic field. J Magn Magn Mater. 2002;252:370–4.
27. Stratton JA. Electromagnetic theory. New York/London: Mcgrow-Hill Book Company Inc; 1941.
28. Griffiths DJ. Introduction to electrodynamics. 4th ed. Upper Saddle River: Pearson Education, Inc; 2013.
29. Ortega D, Pankhurst QA. Magnetic hyperthermia. Nanoscience. 2013;1:e88.
30. Raouf I, Khalid S, Khan A, Lee J, Kim HS, Kim MH. A review on numerical modeling for magnetic nanoparticle hyperthermia: progress and challenges. J Therm Biol. 2020;91:12.
31. Lim ZW, Varma VB, Ramanujan RV, Miserez A. Magnetically responsive peptide coacervates for dual hyperthermia and chemotherapy treatments of liver cancer. Acta Biomater. 2020;110:221–30.

32. Purushotham S, Ramanujan RV. Thermoresponsive magnetic composite nanomaterials for multimodal cancer therapy. Acta Biomater. 2010;6:502–10.
33. Purushotham S, Ramanujan RV. Modeling the performance of magnetic nanoparticles in multimodal cancer therapy. J Appl Phys. 2010;107
34. Kallumadil M, Tada M, Nakagawa T, Abe M, Southern P, Pankhurst QA. Suitability of commercial colloids for magnetic hyperthermia. J Magn Magn Mater. 2009;321:1509–13.
35. Kossatz S, Ludwig R, Dähring H, Ettelt V, Rimkus G, Marciello M, et al. High therapeutic efficiency of magnetic hyperthermia in xenograft models achieved with moderate temperature dosages in the tumor area. Pharm Res. 2014;31:3274–88.
36. Yang ZX, Li Z. Magnetic actuation systems for miniature robots: a review. Adv Intelligent Syst. 2020;2:18.
37. Liu YL, Chen D, Shang P, Yin DC. A review of magnet systems for targeted drug delivery. J Control Release. 2019;302:90–104.
38. Lauterbur PC. Image formation by induced local interactions: examples employing nuclear magnetic resonance. Nature. 1973;242:190–1.
39. Paul C. Lauterbur – biographical. NobelPrize.org. Nobel Prize Outreach AB 2022. Available at https://www.nobelprize.org/prizes/medicine/2003/lauterbur/biographical/. Accessed 21 Jan 2022.
40. Sir Peter Mansfield – Biographical. NobelPrize.org. Nobel Prize Outreach AB 2022. Available at https://www.nobelprize.org/prizes/medicine/2003/mansfield/biographical/. Accessed Fri. 21 Jan 2022.
41. Tirinato L, Pagliari F, Di Franco S, Sogne E, Marafioti MG, Jansen J, et al. ROS and lipid droplet accumulation induced by high glucose exposure in healthy colon and colorectal cancer stem cells. Genes Dis. 2020;7:620–35.
42. Curtarello M, Tognon M, Venturoli C, Silic-Benussi M, Grassi A, Verza M, et al. Rewiring of lipid metabolism and storage in ovarian cancer cells after anti-VEGF therapy. Cell. 2019;8
43. Ochiai T, Nishimura K, Watanabe T, Kitajima M, Nakatani A, Nagayasu K, et al. Impact of primary tumor location as a predictive factor in patients suffering from colorectal cancer treated with cytotoxic anticancer agents based on the collagen gel droplet-embedded drug sensitivity test. Oncol Lett. 2019;17:1842–50.
44. Lorton O, Hyacinthe JN, Desgranges S, Gui L, Klauser A, Celicanin Z, et al. Molecular oxygen loading in candidate theranostic droplets stabilized with biocompatible fluorinated surfactants: particle size effect and application to in situ(19)F MRI mapping of oxygen partial pressure. J Magn Reson. 2018;295:27–37.
45. Dames P, Gleich B, Flemmer A, Hajek K, Seidl N, Wiekhorst F, et al. Targeted delivery of magnetic aerosol droplets to the lung. Nat Nanotechnol. 2007;2:495–9.
46. Lahiri BB, Ranoo S, Zaibudeen AW, Philip J. Magnetic hyperthermia in magnetic nanoemulsions: effects of polydispersity, particle concentration and medium viscosity. J Magn Magn Mater. 2017;441:310–27.
47. Lahiri BB, Ranoo S, Philip J. Effect of orientational ordering of magnetic nanoemulsions immobilized in agar gel on magnetic hyperthermia. J Magn Magn Mater. 2018;451:254–68.
48. Wu H, Song L, Chen L, Huang Y, Wu Y, Zang F, et al. Injectable thermosensitive magnetic nanoemulsion hydrogel for multimodal-imaging-guided accurate thermoablative cancer therapy. Nanoscale. 2017;9:16175–82.
49. Fernandes DA, Appak-Baskoy S, Berndl E, Kolios MC. Laser activatable perfluorocarbon bubbles for imaging and therapy through enhanced absorption from coupled silica coated gold nanoparticles. RSC Adv. 2021;11:4906–20.
50. Wang T, Wang R, Chen Z, Zhong Q. Magnetization of eugenol to fabricate magnetic-responsive emulsions for targeted delivery of caffeic acid phenethyl ester. RSC Adv. 2017;7:43455–63.
51. Bhardwaj A, Jain N, Parekh K. Investigating the effect of outer layer of magnetic particles on cervical cancer cells HeLa by magnetic fluid hyperthermia. Cancer Nanotechnol. 2021;12
52. Pritchard JJG, Hamilton G, Hurst CD, Fraser S, Orange C, Knowles MA, et al. Monitoring of urothelial cancer disease status after treatment by digital droplet PCR liquid biopsy assays. Urol Oncol. 2020;38:737 e1- e10.

53. Li F, Shu J, Zhang L, Yang N, Xie J, Li X, et al. Liquid metal droplet robot. Appl Mater Today. 2020;19
54. Fang JH, Lee YT, Chiang WH, Hu SH. Magnetoresponsive virus-mimetic nanocapsules with dual heat-triggered sequential-infected multiple drug-delivery approach for combinatorial tumor therapy. Small. 2015;11:2417–28.
55. Dong W, Huang A, Huang J, Wu P, Guo S, Liu H, et al. Plasmid-loadable magnetic/ultrasound-responsive nanodroplets with a SPIO-NP dispersed perfluoropentane core and lipid shell for tumor-targeted intracellular plasmid delivery. Biomater Sci. 2020;8:5329–45.
56. Ostrovski Y, Dorfman S, Poh W, Chye Joachim Loo S, Sznitman J. Focused targeting of inhaled magnetic aerosols in reconstructed in vitro airway models. J Biomech 2021;118:110279.
57. Guo Y, Wang XY, Chen YL, Liu FQ, Tan MX, Ao M, et al. A light-controllable specific drug delivery nanoplatform for targeted bimodal imaging-guided photothermal/chemo synergistic cancer therapy. Acta Biomater. 2018;80:308–26.
58. Niu C, Xu Y, An S, Zhang M, Hu Y, Wang L, et al. Near-infrared induced phase-shifted ICG/Fe3O4 loaded PLGA nanoparticles for photothermal tumor ablation. Sci Rep. 2017;7:5490.
59. Hu SW, Xu BY, Ye WK, Xia XH, Chen HY, Xu JJ. Versatile microfluidic droplets array for bioanalysis. ACS Appl Mater Interfaces. 2015;7:935–40.
60. Najafipour A, Gharieh A, Fassihi A, Sadeghi-Aliabadi H, Mahdavian AR. MTX-loaded dual Thermoresponsive and pH-responsive magnetic hydrogel nanocomposite particles for combined controlled drug delivery and hyperthermia therapy of cancer. Mol Pharm. 2021;18:275–84.
61. Reczynska K, Marchwica P, Khanal D, Borowik T, Langner M, Pamula E, et al. Stimuli-sensitive fatty acid-based microparticles for the treatment of lung cancer. Mat Sci Eng C-Mater. 2020;111:12.
62. Rad JK, Alinejad Z, Khoei S, Mahdavian AR. Controlled release and photothermal behavior of multipurpose nanocomposite particles containing encapsulated gold-decorated magnetite and 5-FU in poly(lactide-co-glycolide). ACS Biomater Sci Eng. 2019;5:4425–34.
63. Low LE, Tan LT, Goh BH, Tey BT, Ong BH, Tang SY. Magnetic cellulose nanocrystal stabilized Pickering emulsions for enhanced bioactive release and human colon cancer therapy. Int J Biol Macromol. 2019;127:76–84.
64. Xie WS, Gao Q, Wang D, Wang W, Yuan J, Guo ZH, et al. Melatonin potentiates "inside-out" nano-thermotherapy in human breast cancer cells: a potential cancer target multimodality treatment based on melatonin-loaded nanocomposite particles. Int J Nanomedicine. 2017;12:7351–63.
65. Zhang W, Choi H, Yu B, Kim D-H. Synthesis of iron oxide nanocube patched Janus magnetic nanocarriers for cancer therapeutic applications. Chem Commun. 2020;56:8810–3.
66. Dimitriou P, Li J, Tornillo G, McCloy T, Barrow D. Droplet microfluidics for tumor drug-related studies and programmable artificial cells. Glob Chall. 2021;5:2000123.
67. Varma VB, Ray A, Wang Z, Wang Z, Wu R, Jayaneel PJ, et al. Control of ferrofluid droplets in microchannels by uniform magnetic fields. IEEE Magn Lett. 2016;7:1–5.
68. Ray A, Varma VB, Wang Z, Wang Z, Jayaneel PJ, Sudharsan NM, et al. Magnetic droplet merging by hybrid magnetic fields. IEEE Magn Lett. 2016;7:1–5.
69. Huang KS, Yang CH, Wang YC, Wang WT, Lu YY. Microfluidic synthesis of vinblastine-loaded multifunctional particles for magnetically responsive controlled drug release. Pharmaceutics. 2019;11
70. Li J, Baxani DK, Jamieson WD, Xu W, Rocha VG, Barrow DA, et al. Formation of polarized, functional artificial cells from compartmentalized droplet networks and nanomaterials, using one-step, dual-material 3D-printed microfluidics. Adv Sci. 2020;7:1901719.
71. Baki A, Wiekhorst F, Bleul R. Advances in magnetic nanoparticles engineering for biomedical applications—a review. Bioengineering. 2021;8:134.
72. Buryk-Iggers S, Kieda J, Tsai SSH. Diamagnetic droplet microfluidics applied to single-cell sorting. AIP Adv. 2019;9

73. Cho H, Chung JS, Han KH. A direct comparison between the lateral magnetophoretic microseparator and AdnaTest for isolating prostate circulating tumor cells. Micromachines. 2020;11:13.
74. Ferraro D, Champ J, Teste B, Serra M, Malaquin L, Descroix S, et al. Droplet microfluidic and magnetic particles platform for cancer typing. In: Taly V, Viovy JL, Descroix S, editors. Microchip diagnostics: methods and protocols. 2017. p. 113–121.
75. Sun D, Cao F, Xu W, Chen Q, Shi W, Xu S. Ultrasensitive and simultaneous detection of two cytokines secreted by single cell in Microfluidic droplets via magnetic-field amplified SERS. Anal Chem. 2019;91:2551–8.
76. Shin DJ, Trick AY, Hsieh YH, Thomas DL, Wang TH. Sample-to-answer droplet magnetofluidic platform for point-of-care hepatitis C viral load quantitation. Sci Rep. 2018;8:9793.
77. Serra M, Gontran E, Hajji I, Malaquin L, Viovy JL, Descroix S, et al. Development of a droplet microfluidics device based on integrated soft magnets and fluidic capacitor for passive extraction and Redispersion of functionalized magnetic particles. Adv Mater Technol. 2020;5:10.
78. Piao YH, Wang XB, Xia HM, Wang WQ. Digital microfluidic platform for automated detection of human chorionic gonadotropin. Microfluid Nanofluid. 2019;23:8.
79. Maher S, Santos A, Kumeria T, Kaur G, Lambert M, Forward P, et al. Multifunctional microspherical magnetic and pH responsive carriers for combination anticancer therapy engineered by droplet-based microfluidics. J Mater Chem B. 2017;5:4097–109.

Magnetic Nanomaterials for Hyperthermia and Bioimaging

Richa Chaudhary and Varun Chaudhary

1 Introduction

Cancer is a broad term used for a group of diseases. Cancer is the rapid creation of abnormal cells which grow beyond their natural boundaries and spread to adjacent organs. Cancer is one of the main causes of death worldwide. The World Health Organization (WHO) reported ~10 million deaths in 2020 associated with cancer, and sadly this number is expected to increase in coming years.

The clinical treatments for cancer are chemotherapy, radiotherapy, immunotherapy, gene therapy, hormonotherapy, surgery, and hyperthermia (Fig. 1a). None of these clinical treatments can guarantee a complete recovery from cancer. Hyperthermia is considered a medical procedure that kills malignant cancer cells and can be prescribed as either a primary or adjuvant treatment. The term "hyperthermia" is a combination of two Greek words, hyper and therme, which are associated with rise and heat, respectively. Hyperthermia also known as thermal therapy or thermotherapy means the rise in temperature of selected tissue or complete body. An early report on hyperthermia was published by German surgeon Carl D. W. Bush in 1886 [1, 2]. According to Bush, the sarcoma that developed on the face of a 43-year-old lady was cured because of fever from bacterial skin infection "erysipelas" [1, 2]. In 1898, F. Westermark confirmed the effectiveness of hot water for cancer treatment [3]. Nonetheless, the medical application of hyperthermia was not grown sufficiently with time because of inappropriate heating methods and temperature measuring technology. Hyperthermia and multimode therapy, in which hyperthermia is used along with other therapies, have received high interest recently.

R. Chaudhary · V. Chaudhary (✉)
School of Materials Science and Engineering, Nanyang Technological University, Singapore, Singapore
e-mail: varun004@e.ntu.edu.sg

R. S. Chaughule et al. (eds.), *Nanomaterials for Cancer Detection Using Imaging Techniques and Their Clinical Applications*,
https://doi.org/10.1007/978-3-031-09636-5_4

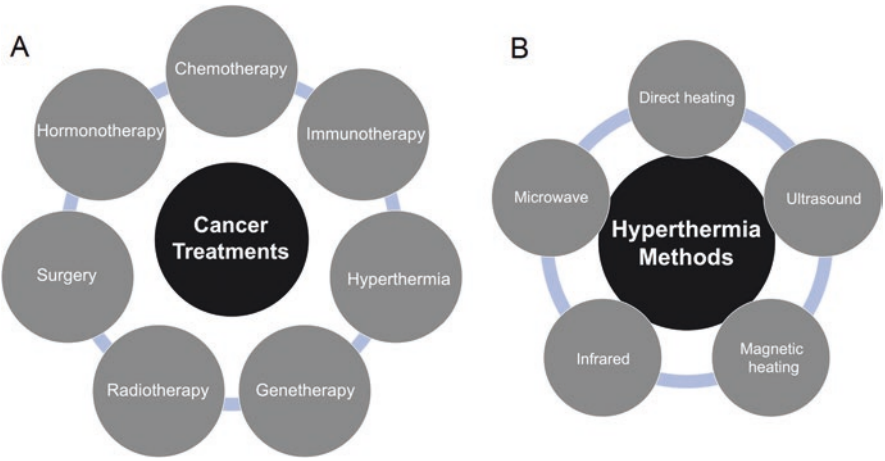

Fig. 1 (**a**) Types of cancer treatments and (**b**) possible heating sources for hyperthermia treatments

In hyperthermia, high temperatures applied to cancer tissue result in the death of cancer tissue with minimal side effects to normal tissues. A treatment only by hyperthermia may not be enough to kill the cancer tissues completely. Hyperthermia is usually used along with other form of cancer treatments, e.g., chemotherapy, radiotherapy, etc. Hyperthermia can damage those cancer cells which were not killed by radiation, or it can enhance the cancer cell sensitivity to radiation. A substantial improvement in survival rates has been witnessed in patients treated with combined hyperthermia and radiotherapy compared with radiotherapy alone [4–6].

Hyperthermia treatment is possible using various sources of heating, e.g., microwave, infrared, ultrasound, direct heating, etc. (Fig. 1b). However, hyperthermia using these methods has many limitations [7], e.g.,

(i) Laser or microwaves can damage superficial tissues, which results in an additional pain to patients.
(ii) Treating deeply located cancer cells is a challenge.

In comparison, magnetic hyperthermia (MH), which relies on local heating of tumors, exhibits various advantages over other therapies. The magnetic response of magnetic nanoparticles (MNP) to an alternating magnetic field can treat deep tumors in a targeted fashion with minimum damage to surrounding healthy tissues.

Diagnosis of cancer at an early stage is the most effective method for the management of cancer treatment. Therefore, a technique to detect the early stages of cancer is always in high demand. Bioimaging can image a disease and aid in the understanding of the relevant biological structure and its functionality. Cancer therapy combined with imaging techniques is an effective way to monitor the efficacy of treatment. Computed tomography (CT), positron emission tomography (PET), single-photon emission computed tomography (SPECT), magnetic resonance imaging (MRI), ultrasound imaging (US), etc. are employed to evaluate the therapeutic

process and clinical diagnosis [8]. MRI exhibits several advantages over the other techniques, e.g., better soft tissue contrast and clearer differentiation between fat, water, muscle, and other soft tissue. The image contrast of MRI can be further enhanced using MNP as a contrast agent. Such MNP can be injected in the blood vessels and targeted to the tumors using external magnetic field gradient. The resulting MRI images can be beneficial in diagnosing a wide variety of diseases.

This chapter discusses magnetic hyperthermia (MH), the use of magnetic nanoparticles in enhancing the contrast of MRI and multimodal MRI. The importance of size, shape, composition, and magnetic properties of magnetic nanoparticles (MNP) for hyperthermia and MRI applications is discussed. Heat generation mechanism of MH, the principle of MRI, biocompatibility of MNP, and current and future trends of MH and MNP coupled bioimaging are elucidated.

2 Magnetic Hyperthermia (MH)

One of the primary targets of hyperthermia is to kill cancer cells, with minimum damage to healthy tissues, by heating the affected region to a clinically defined temperature. In 1957, for the first time, micron size magnetic particles were applied for inductive heating of lymph nodes in dogs [9]. Clinical trials of MH were performed by MagForce Nanotechnologies, Germany, in the early 2000s, and it is currently being used for cancer treatment in several other countries, e.g., Japan and China [10, 11]. Magnetic hyperthermia (MH) is capable of localized and controlled heating of deep tissues. MH is based on the exposure of MNP to an external electromagnetic field in the radiofrequency range (kHz to MHz) [10, 12]. The heat can be delivered locally to the tumor tissue by the MNP using an external alternating magnetic field (AMF). The heat transfer to the tumor can be controlled by optimizing the magnetic properties of MNP, the AMF strength, and the frequency. The ability of heating the MNP through AMF is generally assessed by the specific absorption rate (SAR). Obtaining high SAR at values of magnetic field strength and frequency which are safe for healthy tissues is necessary for the use of MNP for in vivo MH applications [13]. Iron oxide MNP shows high SAR and good biocompatibility. Therefore, several synthesis routes have been developed to obtain high-quality particles with tunable composition, shape, size, surface chemistry, and magnetic properties.

2.1 Heating Process in Magnetic Hyperthermia

Understanding the heating process of MNP in biological conditions is of high interest. Therapies based on MH have been studied in various types of cancer, e.g., brain tumor, prostate cancer, or breast carcinoma [14–18]. The technique comprises

targeting MNP to the tumor tissue, followed by application of an external AMF which produces heat through loss mechanisms of the MNP [11, 19–21].

The magnetic moments of MNP dispersed in a carrier medium are affected by the AMF [22, 23]. The change in magnetic moments may be either physical rotation of the MNP or internal switching of the direction of the magnetic moments, known as Brownian and Neel relaxation, respectively. The magnetic energy is converted to thermal energy by the friction between the MNP and the surroundings (in Brownian relaxation) and/or the interaction of the magnetic moment with the atoms in the MNP (in Neel relaxation) or by hysteresis loss. Nonbiological applications of the heat generated by MNP in AMF include remotely controlled magnetocuring [24, 25] and optical switching [26] (Fig. 2).

The Néel (τ_N) and Brownian (τ_B) relaxation times can be defined as [27].

$$\tau_N = \tau_0 \exp\left(\frac{KV}{k_B T}\right) \tag{1}$$

$$\tau_B = \frac{3\eta V_H}{k_B T} \tag{2}$$

where K is the magnetic anisotropy, V is the volume of MNP, k_B is the Boltzmann constant (1.38×10^{-23} J K^{-1}), η is the viscosity of the medium, V_H is the hydrodynamic volume of the particle, and T is the absolute temperature (K).

Usually, the particle size distribution is broad, and Brownian and Neel processes occur simultaneously [27]. The effective relaxation time can be defined as.

$$\frac{1}{\tau} = \frac{1}{\tau_B} + \frac{1}{\tau_N} \tag{3}$$

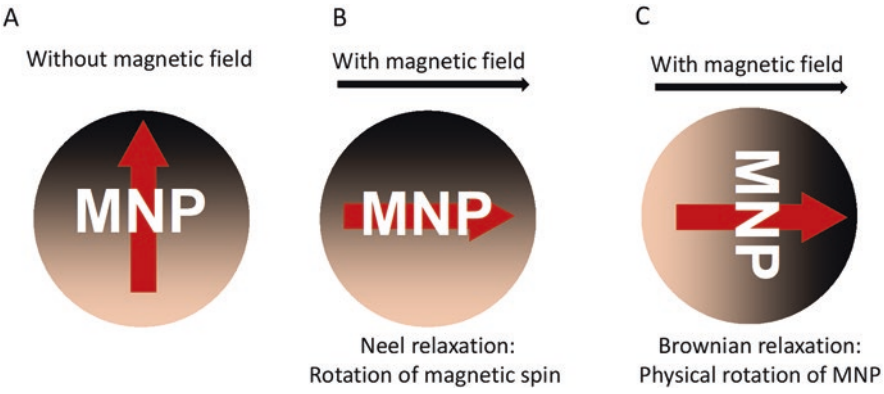

Fig. 2 Schematic of heating mechanism of MNP under AMF: (**a**) without field, (**b**) Brownian relaxation, and (**c**) Neel relaxation

The heating power of MNP is calculated by the power loss (P) and is given by [28].

$$P = \mu_0 \pi \chi_0 f H_{ac}^2 \frac{2\pi f \tau}{1+\left(2\pi f \tau\right)^2} \tag{4}$$

Thus, the heat generation process depends on the frequency, the amplitude of the applied AMF, and the effective relaxation time of MNP.

Specific absorption rate (SAR) or specific loss power (SLP) represents the heating efficiency of a material. SAR can be expressed as the ratio of the power loss and the mass of the MNP (m_{MNP}) [18].

$$\boldsymbol{SAR} = \frac{\boldsymbol{P}}{\boldsymbol{m}_{\boldsymbol{MNP}}} \tag{5}$$

SAR can be measured using calorimetric and magnetometric methods. In the calorimetric method, AMF of a specific amplitude and frequency applied on MNP results in a rise in the temperature of MNP. Samples should be covered by thermal insulators to avoid heat loss to the surroundings during the experiment. SAR is calculated from the change in the temperature of the sample with time under AMF and frequency, defined by the equation below [25, 28, 29].

$$SAR = c_{\text{solvent}} \frac{m_{\text{sample}}}{m_{MNP}} \left(\frac{dT}{dt}\right) \tag{6}$$

where C_{solvent} is the specific heat capacity of the solvent, m_{sample} is the mass of the sample, m_{MNP} is the mass of the MNP, and dT/dt is the slope of the temperature versus time curve. Another approach to calculate the SAR is by AC magnetometry measurements. The SAR can be determined from the area of the hysteresis curve using [30].

$$\text{SAR} = A_{\text{hys}} \times f \tag{7}$$

where A_{hys} is the area enclosed by the hysteresis curve and f is the frequency. A large SAR is necessary for therapeutics, while the AC field and frequency are constrained by biological constraints. A direct comparison of reported SAR for different materials measured under varying conditions is not straightforward since it depends on the applied AMF strength and frequency (Eqs. 4 and 5). This issue can be resolved by normalizing the SAR to the amplitude of AMF and frequency which is known as intrinsic loss power (ILP) [31, 32].

$$ILP = \frac{\text{SAR}}{H_{ac}^2 f} \tag{8}$$

ILP is a system-independent parameter and permits direct comparison between the measurements performed using distinct experimental conditions and instruments by various investigators. However, this equation is not valid for large MNP and SAR measured at high frequency and high AMF [33].

2.2 *Effect of MNP Size, Shape, and Composition on Magnetic Hyperthermia*

For biomedical applications, MNP which exhibit superparamagnetic behavior at room temperature are preferred [34–36]. These MNP should be stable in a physiological environment for biological applications. MNP such as cube-shaped iron oxide [37], hybrid core–shell materials [38, 39], iron oxide multigrain structures [40], hollow nanostructures [41], magnetite nanocrystals [42, 43], etc. have been studied. MNP of Fe_3O_4 and related spinels containing cobalt, nickel, manganese, or other substitutions have been evaluated [44–59].

The SAR is quite sensitive to the MNP characteristics. Hence, there is a strong need for the optimization of MNP for MH applications. In MH, Néel relaxation, Brownian relaxation, and hysteresis loss are responsible for MNP heating [60]. Their relative impact is highly dependent on size, shape, crystal anisotropy, agglomeration of the MNP, and the nature of the surroundings [28, 60, 61]. Octahedral iron oxide MNP can exhibit higher SAR than their spherical counterparts because of their superior magnetic properties. SAR values of octahedra examined at a frequency of 358 kHz and a field strength of 800 Oe increase from 1220 to 2629 W-g^{-1} with a change in the particle size from 22 to 98 nm [62]. Table 1 and Fig. 3 show the change in SAR of iron oxide MNP with particle morphology, size, applied field, and frequency.

3 Magnetic Imaging

Bioimaging techniques can aid in the detection of certain diseases as well as to understand the structure and the function of the relevant entity being studied. Magnetic resonance imaging (MRI), based on the principle of nuclear magnetic resonance (NMR), is a widely used technique in the imaging of soft tissues. Compared to other imaging techniques, MRI has numerous benefits including enhanced soft tissue contrast, high spatial resolution, and no radiation risk [71]. The penetration depth of MRI is sufficient to image organs within the human body. However, the poor sensitivity of MRI is a limitation for the detection of small biological targets, such as small tumors. The use of MNP as MRI contrast agents can help to address the low sensitivity issue.

Table 1 Effect of size and shape of MNP on MH performance

Morphology	Particle size (nm)	Magnetic field (Oe)	Frequency (kHz)	SAR ($W\text{-}g^{-1}$)	References
Cubes	20	300	700	2277	[63]
	30	125	410	960	[42]
	35	300	320	1391	[64]
	40	250	325	960	[65]
	60	8	1000	2614	[66]
Octahedra	6	310	247	163	[67]
	8	310	247	184	[67]
	12	310	358	275	[67]
	22	800	358	1220	[62]
	43	800	358	2483	[62]
	98	800	358	2629	[62]
Nanoplates	12 × 3	800	310	125	[68]
	225 × 26	580	488	4400	[69]
Rods	45 × 10	415	390	1072	[70]
	41 × 7	800	310	540	[30]
	65 × 5.7	800	310	1300	[30]

Hydrogen atoms in living organisms, primarily in the form of water or hydrocarbon, are used to produce a signal. The magnetic resonance signal is obtained by placing a patient in a strong magnetic field (B_0). The hydrogen nuclear spins align either in the same or opposite direction to the magnetic field, corresponding to the lower-energy state or higher-energy state, respectively [72]. When radiofrequency (RF) pulses are applied, the nucleus absorbs the energy, and the number of the spins in a higher-energy state (i.e., antiparallel with B_0) increases. Upon removal of RF, the nuclei relax to the equilibrium state (i.e., parallel with B_0) by emitting the energy gained during the application of RF. This process involves two types of relaxation, known as T_1 (longitudinal) and T_2 (transverse), associated with longitudinal magnetization recovery and transverse magnetization decay, respectively. These relaxation processes can be recorded and then reconstructed into images by MRI. These images are commonly classified into T_1-weighted and T_2-weighted MRI images. The contrast of these MRI images can be tuned. In the case of T_1-weighted images, faster T_1 relaxation rate (R_1) results in brighter contrast. A faster T_2 relaxation rate (R_2) yields darker contrast in T_2-weighted images. However, the contrast difference between the target and surrounding tissues is sometimes insufficient.

The relaxation rate and therefore the image contrast can be enhanced using MNP as a contrast agent. Such MNP can be injected in blood vessels and targeted to the tumors using an external magnetic field gradient. The optimal properties of MNP, such as size and composition of the core, thickness, and type of shell, are important to enhance signal quality. The T_2 relaxation rate (R_2) of superparamagnetic nanoparticles dispersed in a solution can be defined by quantum mechanical outer-sphere theory [73–75].

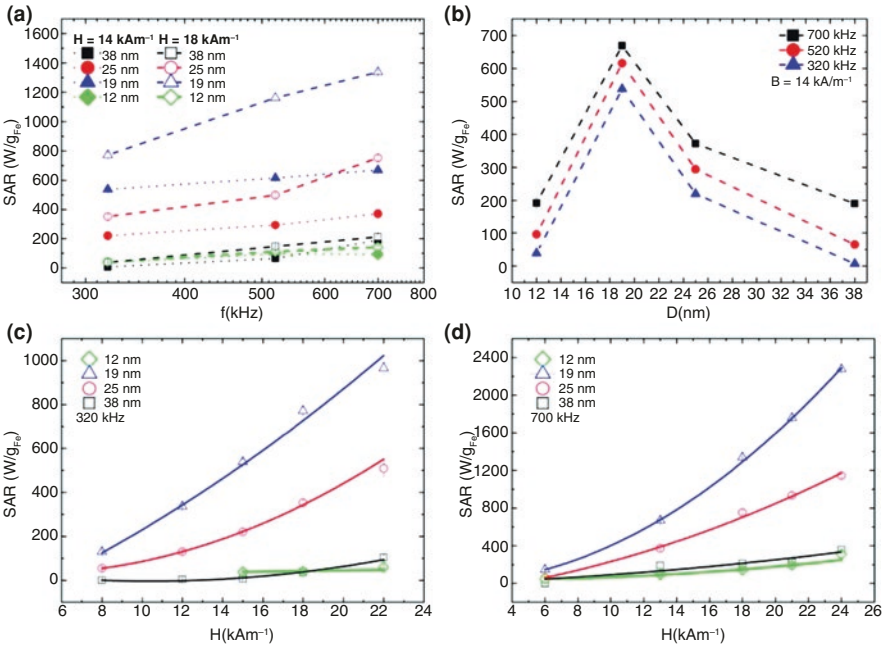

Fig. 3 SAR values as a function of (**a**) frequency, (**b**) particle size, (**c**) alternating magnetic field strength at a frequency of 320 kHz, and (**d**) alternating magnetic field frequency of 700 kHz. (Reprinted with permission from [63] P. Guardia et al., ACS Nano 2012; 6:3080-91 Copyright © 2012, American Chemical Society)

$$R_2 = \frac{1}{T_2} = \frac{256\pi^2\gamma^2}{405} M_s{}^2 v \times \frac{r^2}{D\left(1+\frac{L}{r}\right)} \tag{9}$$

where γ, M_s, v, r, D, and L are the proton gyromagnetic ratio, saturation magnetization, the volume fraction, the radius of MNP (core), the diffusion coefficient of water molecules, and the thickness of the surface coating, respectively. It is clear from Eq. 9 that MNP with large M_s is necessary to attain efficient T_2 contrast. Saturation magnetization is usually an intrinsic property of bulk materials; however, for MNP, it strongly depends on particle size, shape, and surface properties. The saturation magnetization of MNP (M_s) can be calculated using the following equation:

$$M_s = M_s^{\text{Bulk}} \frac{(r-d)^3}{r^3} \tag{10}$$

where M_s^{Bulk} is the saturation magnetization of the material in bulk form, r is the radius of MNP, and d is the thickness of the spin disordered surface layer. Usually,

the larger spherical nanoparticles approach the bulk saturation magnetization (M_s^{Bulk}) values and exhibit high T_2 relaxation rates (R_2). However, particles with large size exhibit ferri- or ferromagnetic properties, which results in interparticle agglomeration [76].

3.1 *Effect of MNP Composition, Shape, and Size on T_2 Relaxation Rate (R_2)*

Superparamagnetic iron oxide MNP are T_2 contrast agents for MRI because of their good biocompatibility and physiological stability [77, 78]. T_2 relaxation rate (R_2) can be tuned by the composition and effective magnetic radius of MNP (which depends on the morphology) [75, 79–83]. The mass magnetization of $MnFe_2O_4$, Fe_3O_4, $CoFe_2O_4$, and $NiFe_2O_4$ was found to be 110, 101, 99, and 85 emu/g of magnetic atoms, respectively. The corresponding effective spin magnetic moment was 5, 4, 3, and 2 μ_B, respectively [79]. Figure 3a shows the relaxivity (R_2) with changing MNP composition for a fixed particle size of MNP. $MnFe_2O_4$ exhibits better contrast and higher relaxation rate (R_2) compared to Fe_3O_4, $CoFe_2O_4$, and $NiFe_2O_4$ MNP. The R_2 decreases monotonically for lower effective magnetic moment of MNP. The R_2 increases with larger particle size for both $MnFe_2O_4$ and Fe_3O_4 (Fig. 4b). The signal intensity of T_2-weighted images decreases substantially with increasing Fe concentration (Fig. 4c). The dipolar interactions of the magnetic moments of MNP and protons of water make the images darker [84]. The T_2 relaxivities of polyvinylpyrrolidone iron oxides (PVP-IOs) increase with the size of the MNP and the Fe concentration (Fig. 4d).

Additionally, octopod iron oxide MNP are found to be very effective as T_2 contrast agents for in vivo MRI, confirming the importance of morphology for T_2 relaxivity [75]. The octopod shape iron oxide MNP with an edge length of 30 nm exhibited M_s of ~71 emu/g yet a high R_2 of ~679 mM^{-1} s^{-1} [75]. The shape anisotropy in such octopod nanoparticles and a substantial increase in the effective radii of the magnetic cores are the possible reason for high T_2 relaxivities. Such magnetic structures are projected as potential T_2 contrast agents for in vivo MRI. However, the size of these MNP is beyond the lower size limit for kidney clearance [85].

4 Multimodal Imaging

Two or more imaging techniques can provide accurate information compared to an individual method [86]. The limitations of a particular modality can be removed by grouping multiple techniques with complementary strengths [87]. For example, information about the tumor can be obtained by PET images, while anatomical data can be gathered by CT and MRI images. Multimodal imaging probes or

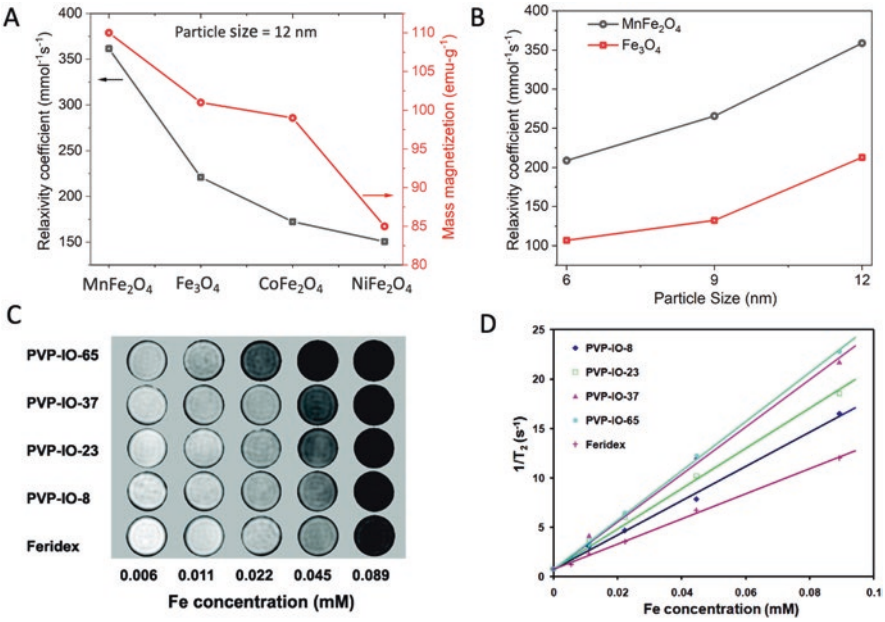

Fig. 4 (**a**) Relaxivity (R_2) of $MnFe_2O_4$, Fe_3O_4, $CoFe_2O_4$, and $NiFe_2O_4$. Particle size of all the MNP was the same, i.e., 12 nm. $MnFe_2O_4$ MNP exhibited the strongest MR contrast effect and the highest R_2 coefficient, (**b**) change in relaxivity (R_2) with particle size of Fe_3O_4 and $MnFe_2O_4$ MNP, (**c**) T_2-weighted MR images of polyvinylpyrrolidone iron oxides (PVP-IOs) in aqueous solution with various concentrations, (**d**) $1/T_2$ versus the Fe concentration for PVP-IOs and Feridex. ("**c**" and "**d**" are reprinted with permission from [84], J. Huang et al., ACS Nano. 2010; 4:7151–60, Copyright © 2012, American Chemical Society)

nanoparticles have the capability to cross the borders of a single imaging modality. Different modalities can be combined in, e.g., iron oxide-based multifunctional magnetic nanoparticles which can carry more than two imaging agents. Multimodal imaging such as trimodal PET/CT/optical and bimodal MRI/ PET agents based on iron oxide MNP have been examined [87–89]. Magnetic nanoparticles (MNP) have capability to be considered as superior and predominant multimodal imaging agents [90]. The iron oxide-based magnetic nanoparticles have drawn significant attention for the diagnosis/treatment of cancers because of their high magnetization, magnetic susceptibility, and low cohesivity as compared to common paramagnetic contrast agent (Gd-DTPA) [91, 92]. For cancer therapies, MNP can focus on the exact desirable spot and efficiently treat the tumor by raising the tumor temperatures to therapeutic levels. On the other hand, MNP work as thermal seeds in the targeted tumor, which can be imaged using MRI. In this way, the therapy and diagnostics are combined in a single platform. Furthermore, the imaging contract using nanoparticles can be far increased by doping the manganese with Fe_2O_3, due to the high sensitivity of ^{55}Mn for MRI. However, the efficiency of multimodal and multifunctional applications primarily depends on the quality of magnetic nanoparticles.

MRI/PET multimodal imaging offers significant advantages over single imaging modality. MRI/PET contrast probes that combine a magnetic core with the radionuclide and ^{64}Cu or ^{124}I labelled on the polymeric surfaces of the particles have been developed [93–96]. This multimodal approach allows MRI linked with PET images with greater sensitivity of contrast than MRI alone [96, 97]. The human serum albumin-covered MNP were labelled with ^{64}Cu-DOTA and Cy5.5 and examined in a subcutaneous U87MG xenograft mouse model with PET/MRI/NIRF imaging [94].

MNP with controlled size, shape, and composition are necessary for MH, MRI, and multimodal systems. Therefore, synthesis, functionalization, and biocompatibility of MNP are briefly discussed in following section.

5 Synthesis of Magnetic Nanoparticles

Choosing a synthesis method to control the size, shape, and composition of MNP is useful to fine-tune the magnetic properties [98]. The reaction temperature, time, gas flow, type of precursors, precursors to solvent ratio, and number of stabilizing ligands can affect the characteristics of the MNP. Optimization of reaction parameters is necessary to get high-quality MNP. Nanoparticles exhibit very high surface energy especially if particle size is <10 nm. Chemical modification of the surface of these particles can affect the nanomaterial properties significantly. The modified surface can possess different magnetic characteristics compared to the particle core [99].

There are a number of methods to synthesize the MNP including micro-emulsion, co-precipitation, micelles, polyols, mechanochemical, etc. [100–136]. All methods have their own advantages and limitations. Chemical methods allow the formation of nanoparticles with a narrower particle size distribution. In the chemical methods, usually, we start from metal precursors and dissolve them in a solvent. Magnetic nanoparticles of the oxides can be easily synthesized using different chemical methods. Some of the chemical methods and corresponding pros and cons are listed in Table 2.

As can be seen from Table 2, hydrothermal and thermal decomposition methods result in a narrow size distribution, good control of shape, and high yield. However, these chemical reactions occur at high temperature/pressure and take a long time to complete.

Iron oxide nanoparticles with particle sizes in the range 4–28 nm were synthesized by thermal decomposition of an iron precursor in high boiling solvents [141]. The M_s was found to be increased for larger size of the MNP [141, 142]. Monodisperse Fe_3O_4 MNP were prepared using the high-temperature chemical reduction of $Fe(acac)_3$ in phenyl ether, oleic acid, and oleylamine [143]. Seed-mediated growth was used to control particle size, in a size range from 3 to 20 nm.

Table 2 Summary comparison of synthesis methods for magnetic nanoparticles [137–140]

Method	Biosynthesis	Electrochemical	Sonochemical method	Micro-emulsion	Aerogel vapour	Co-precipitation	Polyol and sol-gel	Hydro- and solvothermal	Thermal decomposition
Reaction atmosphere	Ambient	Ambient	Ambient	Ambient	Insert atmosphere	Ambient	Ambient	high pressure	Insert atmosphere
Reaction temperature (°C)	Room Temperature	Room Temperature	20-50	20-80	>100	20-150	20-200	150-220	100-350
Reaction time	Hours to days	Hours to days	Minutes	Hours	Minutes to hours	Minutes	Hours	Hours to days	Hours to days
Size distribution	Broad	Medium	Narrow	Narrow	Medium	Medium	Narrow	Very narrow	Very narrow
Shape control	Not good	Medium good	Not good	Good	Medium good	Not good	Good	Very good	Very good
Yield	Low	Medium	Medium	Low	High	High	Medium	High	High

Desired and undesired items are highlighted by green and orange color

5.1 Particle Size and Shape Effect on the Magnetic Properties

Magnetic properties can be altered if at least one dimension of the specimen is in the nanometer range [139, 144]. A change in several magnetic properties, e.g., superparamagnetism, remanence enhancement, and exchange averaging of anisotropy, may be observed at small sizes. The transition from superparamagnetic to single domain to multi-domain for MNP depends on size and/or geometry of the particles.

The influence of particle radius (r) on the magnetic properties can be expressedby $r = \sqrt[3]{\frac{6k_BT}{K_U}}$, where k_B, T, and K_U are Boltzmann constant, temperature, andanisotropy constant, respectively. Saturation magnetization increases for larger particle size until a threshold size that exhibits a M_s close to the bulk value [145–147].

MFe_2O_4 (M = Mn, Fe, Co, Ni, and Zn) MNP were synthesized using a technique in which an amine was utilized as a reducing and surface coating agent [148]. The particle sizes were tuned by controlling the amine-to-precursor ratio and by seed-mediated growth. The M_s of the MNP was changed by changing the composition and size from 27 emu/g ($ZnFe_2O_4$ with particle size of 4 nm) to 86 emu/g ($MnFe_2O_4$ with particle size of 16 nm). The M_s of MFe_2O_4 MNPs was maximum for M = Mn, while it was a minimum for M = Zn. Higher M_s was observed for increasing particle size.

The influence of the surfactant and reducing agent on the shape, size, and magnetic properties of iron oxide nanoparticles was studied [149]. Pseudospherical/faceted particles with size in the range of 4–20 nm and M_s of 80 to 85 emu/g at a temperature of 5 K were achieved when using oleic acid as a surfactant. Moreover, decanoic acid results in larger pseudocubic particles of 45 nm and a larger M_s of 92 emu/g, which is close to the bulk M_s of magnetite. The size and shape of MNP

can be changed by introducing a different reducing agent, e.g., 1,2-hexadecanediol, hydrazine, decanoic acid, etc. [149, 150]. Particles with a cube shape have a higher M_s than spheres [151]. Cubic iron oxide MNP exhibited higher crystallinity than their spherical counterparts [152]. A summary of the dependence of M_s and H_c on the size, shape, and composition of the MNP is shown in Table 3 and Fig. 5.

The surface and interface effects are significant when particle size decreases, e.g., cobalt nanoparticle with a diameter of ~1.6 nm exhibits more than half of the total spins on the surface [138, 161]. Therefore, surface spins play a key role in the magnetic characteristics of magnetic nanoparticles. The broken symmetry on the surface can alter the lattice constant and atom coordination. Therefore, surface

Table 3 The dependence of magnetic properties at room temperature on size, shape, and composition of MNP

MNP	Particle size (nm)	Shape	Magnetic properties		References
			M_s (emu/g)	H_c (Oe)	
$Zn_{0.4}Fe_{2.6}O_4$	22	Sphere	145	–	[151]
	18	Cubes	165	60	
Fe_3O_4	8.5	Spheres	31	0	[152]
	8	Cubes	40	0	
Fe_3O_4	12	Spheres	80	0	[153]
	12 (side)	Cubes	40	0	
	12 (width)	Rods	18	~55	
	12 (width)	Octahedron	80	0	
Fe_3O_4	8		80.1	153	[154]
$Ni_{0.04}Fe_{2.96}O_4$	8		84.2	180	
$Ni_{0.06}Fe_{2.94}O_4$	10		80.5	250	
$Ni_{0.11}Fe_{2.89}O_4$	8		82.8	190	
$Ni_{0.8}Zn_{0.2}Fe_2O_4$	36	Spheres	43.1	65.8	[155]
$Ni_{0.6}Zn_{0.2}Mg_{0.2}Fe_2O_4$	41	Spheres	41.7	57.0	
$Ni_{0.4}Zn_{0.2}Mg_{0.4}Fe_2O_4$	45	Spheres	41.0	35.0	
$Ni_{0.2}Zn_{0.2}Mg_{0.6}Fe_2O_4$	35	Spheres	30.4	17.4	
$Zn_{0.2}Mg_{0.8}Fe_2O_4$	59	Spheres	36.1	11.9	
Fe_3O_4	12	Spheres	101		[79]
$MnFe_2O_4$	12	Spheres	110		
$CoFe_2O_4$	12	Spheres	99		
$NiFe_2O_4$	12	Spheres	85		
Fe_3O_4	7	Spheres	58.4	0	[156]
	13.2	Spheres	61.1	~0	
	25.6	Spheres	68.3	~0	
	32.9	Spheres	64.2	32.3	
	51.6	Spheres	71.2	62	
	97.3	Spheres	85.9	87.4	
	19	Cubes	76.1	~0	
	30	Cubes	67.5	33.7	
	36	Cubes	67.5	86.2	
	42	Cubes	92.1	277.2	
	106	Cubes	87.4	327.2	

MNP	Particle size (nm)	Shape	Magnetic properties		References
			M_s (emu/g)	H_c (Oe)	
Fe_3O_4	16.6	Octopods	50.6	~0	[157]
	20.1	Octopods	68.4	25	
	26.4	Octopods	66.7	72	
	35.5	Octopods	65.3	100	
	40.2	Octopods	65.5	151	
	47.4	Octopods	81.7	103	
Fe_3O_4	10.5	~ Spheres	53.4		[158]
$Mn_{0.2}Fe_{0.8}Fe_2O_4$	10.6	~ Spheres	56.3		
$Mn_{0.4}Fe_{0.6}Fe_2O_4$	12.3	~ Spheres	63.3		
$Mn_{0.6}Fe_{0.4}Fe_2O_4$	13.6	~ Spheres	68.2		
$Mn_{0.8}Fe_{0.2}Fe_2O_4$	17.4	~ Spheres	68.7		
$MnFe_2O_4$	19.0	~ Spheres	68.8		

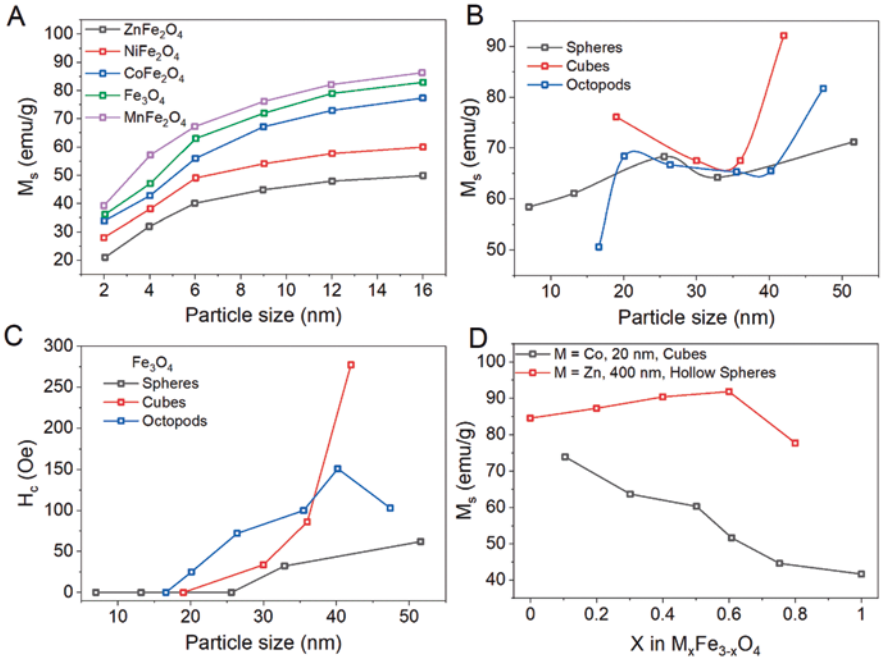

Fig. 5 Magnetic properties (**a**) M_s versus size for various oxide MNP, (**b**) M_s versus size for various shapes of iron oxide MNP, (**c**) H_c versus size for different shapes of iron oxide MNP, and (**d**) M_s versus composition for cubes ($CoFe_2O_4$) and hollow spheres ($ZnFe_2O_4$). (Data are taken from Refs. [148, 157, 159, 160])

atoms experience large anisotropy, and core to surface exchange anisotropy is also possible. Large anisotropy on the surface resulting from the broken symmetry of their surroundings is known as Neel surface anisotropy [101, 162].

With decreasing particle size, the magnetic anisotropy (K_{eff}) may surpass the value obtained from crystalline and shape anisotropy, due to the change in surface anisotropy. The anisotropy energy of a spherical particle (K_{eff}) is defined as the sum of the contribution from the bulk (core) and from the surface: $K_{\text{eff}} = K_V + {}^{6}\!/_{d} K_S$, where K_V, K_S, and d, are bulk anisotropy, surface anisotropy, and particle diameter, respectively. Hence, the K_{eff} can be changed by altering the surface of the MNP [163].

6 Surface Modification and Biocompatibility of Magnetic Nanoparticles

The surface modification of MNP is vital for applications in MH and MRI. Without surface coatings, iron oxide MNP are hydrophobic in nature [139, 164]. The hydrophobic interactions between the nanoparticles result in agglomeration. These agglomerated particles act as clusters. Magnetic dipole–dipole attractions among clusters result in ferromagnetic interactions. This results in increased aggregation of particles.

Surface coating of MNP is mandatory to reduce agglomeration of the nanoparticles and to have functional groups, e.g., drugs, targeting ligands, proteins, etc. [137, 165–169]. For these coatings, a large group of materials have been explored including inorganic materials (e.g., gold, silica, etc.) and organic materials (e.g., dextran, chitosan, polyethylene glycol, etc.) [170–172]. The functionalization and surface coating of MNP results in a change in magnetic properties. A nonmagnetic coating on the surface will reduce the effective value of M_s. If the coating is magnetic, interface coupling between the two types of magnetic order can result in a change in anisotropy and a shift in the hysteresis loop known as "exchange bias."

For multimodal imaging and multifunctional applications, maintaining good biocompatibility and low toxicity is required. Surface modification of the MNP has been used to improve the biocompatibility for in vivo applications [173–176]. CdSe/Fe_3O_4 nanoparticles can be used for bioimaging and anticancer therapy. In addition, co-encapsulation of CdSe/Fe_3O_4 has shown better biocompatibility than only Fe_3O_4 MNP (Fig. 6) [175].

7 Challenges and Outlook

In the last few decades, there is a significant growth in understanding the mechanism and role of MNP in MH, MRI, and multimodal imaging. Future research can examine (i) the factors which result in a major change in properties under in vivo condition, (ii) level of toxicity, and (iii) more clinical trials. Tight particle size distribution, the efficient surface functionalization of MNP, and more homogeneous distribution of these functionalized MNP within the targeted area are challenges. The clinical applications of MNP in therapy and imaging are compelling; however, acceleration in development and validation is needed.

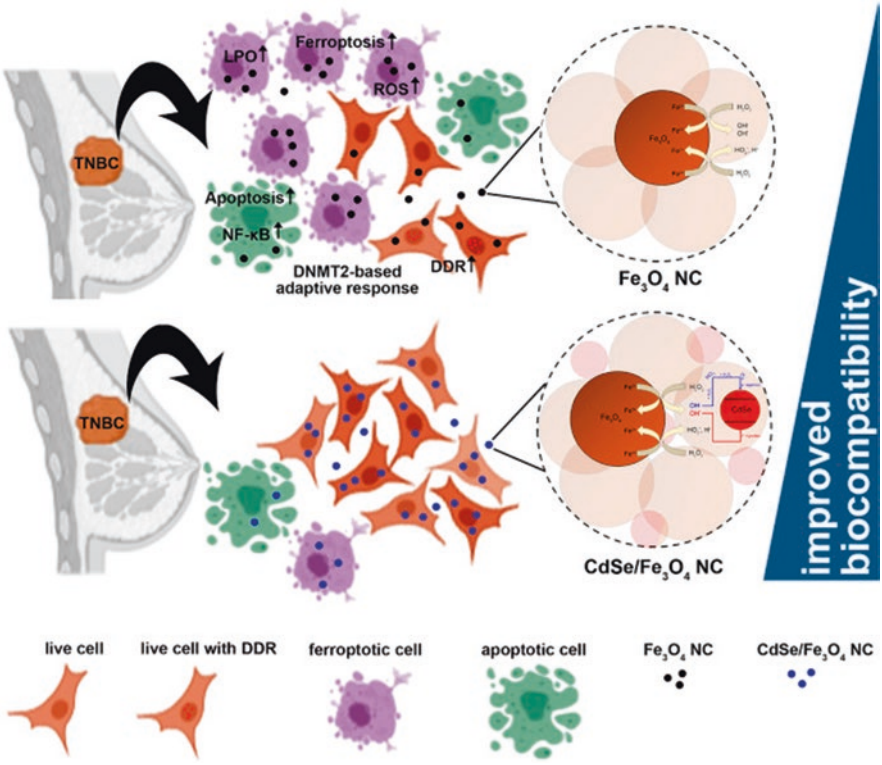

Fig. 6 Biocompatibility of Fe_3O_4 MNP and CdSe/Fe_3O_4 nanoparticles using triple-negative breast cancer cells (TNBC) as a cellular model. (Reprinted from [175], MA Antoniak et al. Materials Science and Engineering: C. 2021:112224.© 2021, Elsevier)

References

1. Bush W. Uber den Finfluss wetchen heftigere Eryspelen zuweilen auf organlsierte Neubildungen dusuben. Verh Natruch Preuss Rhein Westphal. 1886;23:28–30.
2. Vander Vorst A, Rosen A, Kotsuka Y. RF/microwave interaction with biological tissues: New York Wiley; 2006.
3. Westermark F. Uber die Behandlung des ulcerirenden Cervix carcinoma mittels Knonstanter Warme. Zentralbl Gynakol. 1898;22:1335–7.
4. Hildebrandt B, Wust P, Ahlers O, Dieing A, Sreenivasa G, Kerner T, et al. The cellular and molecular basis of hyperthermia. Crit Rev Oncol Hematol. 2002;43:33–56.
5. Wust P, Hildebrandt B, Sreenivasa G, Rau B, Gellermann J, Riess H, et al. Hyperthermia in combined treatment of cancer. Lancet Oncol. 2002;3:487–97.
6. Wang Y, Zou L, Qiang Z, Jiang J, Zhu Z, Ren J. Enhancing targeted cancer treatment by combining hyperthermia and radiotherapy using Mn–Zn ferrite magnetic nanoparticles. ACS Biomater Sci Eng. 2020;6:3550–62.
7. Attar MM, Haghpanahi M, Amanpour S, Mohaqeq M. Analysis of bioheat transfer equation for hyperthermia cancer treatment. J Mech Sci Technol. 2014;28:763–71.
8. Mallidi S, Luke GP, Emelianov S. Photoacoustic imaging in cancer detection, diagnosis, and treatment guidance. Trends Biotechnol. 2011;29:213–21.

9. Gilchrist RK, Medal R, Shorey WD, Hanselman RC, Parrott JC, Taylor CB. Selective inductive heating of lymph nodes. Ann Surg. 1957;146:596–606.
10. Thiesen B, Jordan A. Clinical applications of magnetic nanoparticles for hyperthermia. Int J Hyperth. 2008;24:467–74.
11. Kobayashi T. Cancer hyperthermia using magnetic nanoparticles. Biotechnol J. 2011;6: 1342–7.
12. Pankhurst QA, Connolly J, Jones SK, Dobson J. Applications of magnetic nanoparticles in biomedicine. J Phys D Appl Phys. 2003;36:R167.
13. Bordet A, Landis RF, Lee Y, Tonga GY, Asensio JM, Li C-H, et al. Water-dispersible and biocompatible iron carbide nanoparticles with high specific absorption rate. ACS Nano. 2019;13:2870–8.
14. Jordan A, Scholz R, Maier-Hauff K, van Landeghem FKH, Waldoefner N, Teichgraeber U, et al. The effect of thermotherapy using magnetic nanoparticles on rat malignant glioma. J Neuro-Oncol. 2006;78:7–14.
15. Johannsen M, Gneveckow U, Eckelt L, Feussner A, WaldÖFner N, Scholz R, et al. Clinical hyperthermia of prostate cancer using magnetic nanoparticles: presentation of a new interstitial technique. Int J Hyperth. 2005;21:637–47.
16. Alphandéry E, Faure S, Seksek O, Guyot F, Chebbi I. Chains of magnetosomes extracted from AMB-1 magnetotactic bacteria for application in alternative magnetic field cancer therapy. ACS Nano. 2011;5:6279–96.
17. Mirza S, Ahmad MS, Shah MIA, Ateeq M. Magnetic nanoparticles: drug delivery and bioimaging applications (Chapter 11). In: Shah MR, Imran M, Ullah S Metal nanoparticles for drug delivery and diagnostic applications: Elsevier Amsterdam; 2020. p. 189–213.
18. Abenojar EC, Wickramasinghe S, Bas-Concepcion J, Samia ACS. Structural effects on the magnetic hyperthermia properties of iron oxide nanoparticles. Progr Nat Sci Mat Intl. 2016;26:440–8.
19. Tishin AM, Spichkin YI, Zverev VI, Egolf PW. A review and new perspectives for the magnetocaloric effect: new materials and local heating and cooling inside the human body. Int J Refrig. 2016;68:177–86.
20. Purushotham S, Ramanujan RV. Modeling the performance of magnetic nanoparticles in multimodal cancer therapy. J Appl Phys. 2010;107:114701.
21. Gopalakrishnan S, Vaidyanathan K. Magnetic nanoparticles for hyperthermia a new revolution in cancer treatment. In: Joshy KS, Sabu T, Thakur VK, editors. Magnetic nanoparticles: a new platform for drug delivery. Singapore: Springer Singapore; 2021. p. 119–32.
22. Rosenweig RE. Ferrohydrodynamics. New York: Cambridge University Press; 1985.
23. Périgo EA, Hemery G, Sandre O, Ortega D, Garaio E, Plazaola F, et al. Fundamentals and advances in magnetic hyperthermia. Appl Phys Rev. 2015;2:041302.
24. Chaudhary R, Chaudhary V, Suda Y, Ramanujan RV, Steele TWJ. Optimizing the magnetocuring of epoxy resins via electromagnetic additives. Adv Mater Interf. 2021;17:2100881.
25. Chaudhary R, Chaudhary V, Ramanujan RV, Steele TWJ. Magnetocuring of temperature failsafe epoxy adhesives. Appl Mater Today. 2020;21:100824.
26. Owuor PS, Chaudhary V, Woellner CF, Sharma V, Ramanujan RV, Stender AS, et al. High stiffness polymer composite with tunable transparency. Mater Today. 2018;21:475–82.
27. Rosensweig RE. Heating magnetic fluid with alternating magnetic field. J Magn Magn Mater. 2002;252:370–4.
28. Gonzales-Weimuller M, Zeisberger M, Krishnan KM. Size-dependant heating rates of iron oxide nanoparticles for magnetic fluid hyperthermia. J Magn Magn Mater. 2009;321:1947–50.
29. Chaudhary V, Zhong Y, Parmar H, Sharma V, Tan X, Ramanujan RV. Mechanochemical synthesis of iron and cobalt magnetic metal nanoparticles and iron/calcium oxide and cobalt/calcium oxide nanocomposites. ChemistryOpen. 2018;7:590–8.
30. Das R, Alonso J, Nemati Porshokouh Z, Kalappattil V, Torres D, Phan M-H, et al. Tunable high aspect ratio iron oxide nanorods for enhanced hyperthermia. J Phys Chem C. 2016;120:10086–93.

31. Kallumadil M, Tada M, Nakagawa T, Abe M, Southern P, Pankhurst QA. Suitability of commercial colloids for magnetic hyperthermia. J Magn Magn Mater. 2009;321:1509–13.
32. Sandler SE, Fellows B, Mefford OT. Best practices for characterization of magnetic nanoparticles for biomedical applications. ACS Publications; 2019.
33. Ortega D, Pankhurst QA. Magnetic hyperthermia. Nanoscience: volume 1: nanostructures through chemistry: the Royal Society of. Chemistry. 2013:60–88.
34. Akbarzadeh A, Samiei M, Davaran S. Magnetic nanoparticles: preparation, physical properties, and applications in biomedicine. Nanoscale Res Lett. 2012;7:144.
35. Morcos SK. Nephrogenic systemic fibrosis following the administration of extracellular gadolinium based contrast agents: is the stability of the contrast agent molecule an important factor in the pathogenesis of this condition? Br J Radiol. 2007;80
36. Ersoy H, Rybicki FJ. Biochemical safety profiles of gadolinium-based extracellular contrast agents and nephrogenic systemic fibrosis. J Magn Reson Imaging. 2007;26:1190.
37. Kolosnjaj-Tabi J, Di Corato R, Lartigue L, Marangon I, Guardia P, Silva AKA, et al. Heat-generating iron oxide nanocubes: subtle "Destructurators" of the tumoral microenvironment. ACS Nano. 2014;8:4268–83.
38. Parchur AK, Ansari AA, Singh BP, Hasan TN, Syed NA, Rai SB, et al. Enhanced luminescence of $CaMoO_4$:Eu by core@shell formation and its hyperthermia study after hybrid formation with Fe_3O_4: cytotoxicity assessment on human liver cancer cells and mesenchymal stem cells. Integr Biol. 2014;6:53–64.
39. Prasad AI, Parchur AK, Juluri RR, Jadhav N, Pandey BN, Ningthoujam RS, et al. Bi-functional properties of Fe_3O_4@YPO_4: Eu hybrid nanoparticles: hyperthermia application. Dalton Trans. 2013;42:4885–96.
40. Hugounenq P, Levy M, Alloyeau D, Lartigue L, Dubois E, Cabuil V, et al. Iron oxide monocrystalline nanoflowers for highly efficient magnetic hyperthermia. J Phys Chem C. 2012;116:15702–12.
41. Niraula G, Garcia F, Longo JP, Coaquira JA, Menezes ASD, Zoppellaro G, et al. Engineering shape anisotropy of Fe_3O_4-γ-Fe_2O_3 hollow nanoparticles for magnetic hyperthermia. ACS Appl Nano Mater. 2021;4(3):3148–3158.
42. Hergt R, Hiergeist R, Zeisberger M, Schüler D, Heyen U, Hilger I, et al. Magnetic properties of bacterial magnetosomes as potential diagnostic and therapeutic tools. J Magn Magn Mater. 2005;293:80–6.
43. Alphandéry E, Carvallo C, Menguy N, Chebbi I. Chains of cobalt doped magnetosomes extracted from AMB-1 magnetotactic bacteria for application in alternative magnetic field cancer therapy. J Phys Chem C. 2011;115:11920–4.
44. Sharifi I, Shokrollahi H, Amiri S. Ferrite-based magnetic nanofluids used in hyperthermia applications. J Magn Magn Mater. 2012;324:903–15.
45. Mazario E, Menéndez N, Herrasti P, Cañete M, Connord V, Carrey J. Magnetic hyperthermia properties of electrosynthesized cobalt ferrite nanoparticles. J Phys Chem C. 2013;117:11405–11.
46. Cespedes E, Byrne JM, Farrow N, Moise S, Coker VS, Bencsik M, et al. Bacterially synthesized ferrite nanoparticles for magnetic hyperthermia applications. Nanoscale. 2014;6:12958–70.
47. Adam A, Parkhomenko K, Duenas-Ramirez P, Nadal C, Cotin G, Zorn PE, et al. Orienting the pore morphology of core-shell magnetic mesoporous silica with the sol-gel temperature. Influence on MRI and magnetic hyperthermia properties. Molecules. 2021;26:971.
48. Cardona JEM, Louaguef D, Gaffet E, Ashammakhi N, Alem H. Review of core/shell nanostructures presenting good hyperthermia properties for cancer therapy. Mater Chem Front. 2021;5:6429–43.
49. Das R, Kim NP, Attanayake SB, Phan MH, Srikanth H. Role of magnetic anisotropy on the hyperthermia efficiency in spherical Fe_3−x$CoxO_4$ (X = 0–1) nanoparticles. Appl Sci (Switzerland). 2021;11:1–10.
50. Jamir M, Islam R, Pandey LM, Borah JP. Effect of surface functionalization on the heating efficiency of magnetite nanoclusters for hyperthermia application. J Alloys Compd. 2021;854
51. Lavorato GC, Das R, Alonso Masa J, Phan MH, Srikanth H. Hybrid magnetic nanoparticles as efficient nanoheaters in biomedical applications. Nanoscale Adv. 2021;3:867–88.

52. Liu W, Chen L, Chen M, Wang W, Li X, Yang H, et al. Self-amplified apoptosis targeting Nanoplatform for synergistic magnetic–thermal/chemo therapy in vivo. Adv Healthc Mater. 2020;9:2000202.
53. Ma X, Wang Y, Liu XL, Ma H, Li G, Li Y, et al. Fe_3O_4-Pd Janus nanoparticles with amplified dual-mode hyperthermia and enhanced ROS generation for breast cancer treatment. Nanoscale Horizons. 2019;4:1450–9.
54. Marchianò V, Salvador M, Moyano A, Gutiérrez G, Matos M, Yáñez-Vilar S, et al. Electrodecoration and characterization of superparamagnetic iron oxide nanoparticles with bioactive synergistic nanocopper: magnetic hyperthermia-induced ionic release for antibiofilm action. Antibiotics. 2021;10:1–15.
55. Niraula G, Coaquira JAH, Aragon FH, Bakuzis AF, Villar BMG, Garcia F, et al. Stoichiometry and orientation- and shape-mediated switching field enhancement of the heating properties of Fe_3O_4 circular Nanodiscs. Phys Rev Appl. 2021;15
56. Niraula G, Coaquira JAH, Zoppellaro G, Villar BMG, Garcia F, Bakuzis AF, et al. Engineering shape anisotropy of Fe_3O_4-γ-Fe_2O_3 hollow nanoparticles for magnetic hyperthermia. ACS Appl Nano Mater. 2021;4:3148–58.
57. Saghatchi F, Mohseni-Dargah M, Akbari-Birgani S, Saghatchi S, Kaboudin B. Cancer therapy and imaging through functionalized carbon nanotubes decorated with magnetite and gold nanoparticles as a multimodal tool. Appl Biochem Biotechnol. 2020;191:1280–93.
58. Wang HY, Zhang Y, Ren XH, He XW, Li WY, Zhang YK. HA targeted-biodegradable nanocomposites responsive to endogenous and exogenous stimulation for multimodal imaging and chemo-/photothermal therapy. Nanoscale. 2021;13:886–900.
59. Gavilán H, Avugadda SK, Fernández-Cabada T, Soni N, Cassani M, Mai BT, et al. Magnetic nanoparticles and clusters for magnetic hyperthermia: optimizing their heat performance and developing combinatorial therapies to tackle cancer. Chem Soc Rev. 2021;50:11614–67.
60. Deatsch AE, Evans BA. Heating efficiency in magnetic nanoparticle hyperthermia. J Magn Magn Mater. 2014;354:163–72.
61. Guibert C, Dupuis V, Peyre V, Fresnais J. Hyperthermia of magnetic nanoparticles: experimental study of the role of aggregation. J Phys Chem C. 2015;119:28148–54.
62. Lv Y, Yang Y, Fang J, Zhang H, Peng E, Liu X, et al. Size dependent magnetic hyperthermia of octahedral Fe_3O_4 nanoparticles. RSC Adv. 2015;5:76764–71.
63. Guardia P, Di Corato R, Lartigue L, Wilhelm C, Espinosa A, Garcia-Hernandez M, et al. Water-soluble iron oxide nanocubes with high values of specific absorption rate for cancer cell hyperthermia treatment. ACS Nano. 2012;6:3080–91.
64. Guardia P, Riedinger A, Nitti S, Pugliese G, Marras S, Genovese A, et al. One pot synthesis of monodisperse water soluble iron oxide nanocrystals with high values of the specific absorption rate. J Mater Chem B. 2014;2:4426–34.
65. Tong S, Quinto CA, Zhang L, Mohindra P, Bao G. Size-dependent heating of magnetic iron oxide nanoparticles. ACS Nano. 2017;11:6808–16.
66. Bae KH, Park M, Do MJ, Lee N, Ryu JH, Kim GW, et al. Chitosan oligosaccharide-stabilized ferrimagnetic iron oxide nanocubes for magnetically modulated cancer hyperthermia. ACS Nano. 2012;6:5266–73.
67. Mohapatra J, Mitra A, Aslam M, Bahadur D. Octahedral-shaped Fe_3O_4 nanoparticles with enhanced specific absorption rate and ${R}_{2}$ relaxivity. IEEE Trans Magn. 2015;51:1–3.
68. Nemati Z, Salili S, Alonso J, Ataie A, Das R, Phan M, et al. Superparamagnetic iron oxide nanodiscs for hyperthermia therapy: does size matter? J Alloys Compd. 2017;714:709–14.
69. Yang Y, Liu X, Lv Y, Herng TS, Xu X, Xia W, et al. Orientation mediated enhancement on magnetic hyperthermia of Fe_3O_4 nanodisc. Adv Funct Mater. 2015;25:812–20.
70. Geng S, Yang H, Ren X, Liu Y, He S, Zhou J, et al. Anisotropic magnetite nanorods for enhanced magnetic hyperthermia. Chemistry Asian J. 2016;11:2996–3000.
71. Slichter CP. Principles of magnetic resonance. Springer; 2013.
72. Lee N, Yoo D, Ling D, Cho MH, Hyeon T, Cheon J. Iron oxide based nanoparticles for multimodal imaging and Magnetoresponsive therapy. Chem Rev. 2015;115:10637–89.

73. Tong S, Hou S, Zheng Z, Zhou J, Bao G. Coating optimization of superparamagnetic iron oxide nanoparticles for high T2 relaxivity. Nano Lett. 2010;10:4607–13.
74. Gillis P, Moiny F, Brooks RA. On T2-shortening by strongly magnetized spheres: a partial refocusing model. Magn Reson Med. 2002;47:257–63.
75. Zhao Z, Zhou Z, Bao J, Wang Z, Hu J, Chi X, et al. Octapod iron oxide nanoparticles as high-performance T2 contrast agents for magnetic resonance imaging. Nat Commun. 2013;4:2266.
76. Lee N, Kim H, Choi SH, Park M, Kim D, Kim H-C, et al. Magnetosome-like ferrimagnetic iron oxide nanocubes for highly sensitive MRI of single cells and transplanted pancreatic islets. Proc Natl Acad Sci. 2011;108:2662–7.
77. Dadfar SM, Roemhild K, Drude NI, von Stillfried S, Knüchel R, Kiessling F, et al. Iron oxide nanoparticles: diagnostic, therapeutic and theranostic applications. Adv Drug Deliv Rev. 2019;138:302–25.
78. Roca AG, Gutiérrez L, Gavilán H, Fortes Brollo ME, Veintemillas-Verdaguer S, Morales MP. Design strategies for shape-controlled magnetic iron oxide nanoparticles. Adv Drug Deliv Rev. 2019;138:68–104.
79. Lee J-H, Huh Y-M, Jun Y-W, Seo J-W, Jang J-T, Song H-T, et al. Artificially engineered magnetic nanoparticles for ultra-sensitive molecular imaging. Nat Med. 2007;13:95–9.
80. Sun T, Liu Y, Zhou C, Zhang L, Kang X, Xiao S, et al. Fluorine-mediated synthesis of anisotropic iron oxide nanostructures for efficient T2-weighted magnetic resonance imaging. Nanoscale. 2021;13:7638–47.
81. Caspani S, Magalhães R, Araújo JP, Sousa CT. Magnetic nanomaterials as contrast agents for MRI. Materials. 2020;13:2586.
82. Zhang S, Sun S. Iron oxide-based magnetic nanoparticles synthesized from the organic solution phase for advanced biological imaging. Nanotechnol Biomed Imaging Diagnos. 2014:25–48.
83. Anderson D, Anderson T, Fahmi F. Advances in applications of metal oxide nanomaterials as imaging contrast agents. Physica Status Solidi (a). 2019;216:1801008.
84. Huang J, Bu L, Xie J, Chen K, Cheng Z, Li X, et al. Effects of nanoparticle size on cellular uptake and liver MRI with Polyvinylpyrrolidone-coated iron oxide nanoparticles. ACS Nano. 2010;4:7151–60.
85. Li X, Li W, Wang M, Liao Z. Magnetic nanoparticles for cancer theranostics: advances and prospects. J Control Release. 2021;335:437–48.
86. Luengo Morato Y, Marciello M, Lozano Chamizo L, Ovejero Paredes K, Filice M. 14 – hybrid magnetic nanoparticles for multimodal molecular imaging of cancer. In: Ehrmann A, Nguyen TA, Ahmadi M, Farmani A, Nguyen-Tri P, editors. Magnetic nanoparticle-based hybrid materials. Woodhead Publishing; 2021. p. 343–86.
87. Nahrendorf M, Zhang H, Hembrador S, Panizzi P, Sosnovik DE, Aikawa E, et al. Nanoparticle PET-CT imaging of macrophages in inflammatory atherosclerosis. Circulation. 2008;117:379–87.
88. Jarrett BR, Gustafsson B, Kukis DL, Louie AY. Synthesis of 64Cu-labeled magnetic nanoparticles for multimodal imaging. Bioconjug Chem. 2008;19:1496–504.
89. Liu D, Li J, Wang C, An L, Lin J, Tian Q, et al. Ultrasmall Fe@Fe_3O_4 nanoparticles as T1–T2 dual-mode MRI contrast agents for targeted tumor imaging. Nanomedicine. 2021;32:102335.
90. Tian X, Zhang L, Yang M, Bai L, Dai Y, Yu Z, et al. Functional magnetic hybrid nanomaterials for biomedical diagnosis and treatment. Wiley Interdisciplinary Reviews: Nanomedicine and Nanobiotechnology. 2018, p. 10.
91. Xie J, Yan C, Yan Y, Chen L, Song L, Zang F, et al. Multi-modal Mn–Zn ferrite nanocrystals for magnetically-induced cancer targeted hyperthermia: a comparison of passive and active targeting effects. Nanoscale. 2016;8:16902–15.
92. Gao X, Fraulob M, Haïat G. Biomechanical behaviours of the bone–implant interface: a review. J R Soc Interface. 2019;16:20190259.
93. Bartlett DW, Su H, Hildebrandt IJ, Weber WA, Davis ME. Impact of tumor-specific targeting on the biodistribution and efficacy of siRNA nanoparticles measured by multimodality in vivo imaging. Proc Natl Acad Sci. 2007;104:15549–54.

94. Xie J, Chen K, Huang J, Lee S, Wang J, Gao J, et al. PET/NIRF/MRI triple functional iron oxide nanoparticles. Biomaterials. 2010;31:3016–22.
95. Choi JS, Park JC, Nah H, Woo S, Oh J, Kim KM, et al. A hybrid nanoparticle probe for dual-modality positron emission tomography and magnetic resonance imaging. Angew Chem. 2008;120:6355–8.
96. Lee H-Y, Li Z, Chen K, Hsu AR, Xu C, Xie J, et al. PET/MRI dual-modality tumor imaging using arginine-glycine-aspartic (RGD)–conjugated radiolabeled iron oxide nanoparticles. J Nucl Med. 2008;49:1371–9.
97. Stephen ZR, Kievit FM, Zhang M. Magnetite nanoparticles for medical MR imaging. Mater Today. 2011;14:330–8.
98. Issa B, Obaidat I, Albiss B, Haik Y. Magnetic nanoparticles: surface effects and properties related to biomedicine applications. Int J Mol Sci. 2013;14:21266.
99. Gubin SP. Introduction. In: Magnetic nanoparticles. Weinheim: Wiley-VCH Verlag GmbH & Co. KGaA; 2009. p. 1–23.
100. Chaudhary V, Chaturvedi A, Sridhar I, Ramanujan RV. Fe-Ni-Mn nanoparticles for near room temperature magnetic cooling. IEEE Magn Lett. 2014;5:6800104–8.
101. Chaudhary V, Maheswar Repaka DV, Chaturvedi A, Sridhar I, Ramanujan RV. Magnetocaloric properties and critical behavior of high relative cooling power FeNiB nanoparticles. J Appl Phys. 2014;116:163918–26.
102. Chaudhary V, Ramanujan RV. Iron oxide-based magnetic nanoparticles for high temperature span magnetocaloric applications. MRS Online Proc Library. 2014;1708:vv10-08.
103. Chaudhary V, Ramanujan RV. Magnetic and structural properties of high relative cooling power (Fe 70 Ni 30) 92 Mn 8 magnetocaloric nanoparticles. J Phys D Appl Phys. 2015;48:305003.
104. Suresh G, Rajan BD. A simple wet-chemical approach to synthesize shape controlled high magnetic moment Fe71–Co29 nanocrystals. J Alloys Compd. 2011;509:10145–9.
105. Lee B-H, Lee YJ, Min KH, Kim D-G, Kim YD. Synthesis of nano-sized Fe–Co alloy powders by chemical solution mixing of metal salts and hydrogen reduction (CSM-HR). Mater Lett. 2005;59:3156–9.
106. Wu H-Q, Yuan P-S, Xu H-Y, Xu D-M, Geng B-Y, Wei X-W. Controllable synthesis and magnetic properties of Fe–Co alloy nanoparticles attached on carbon nanotubes. J Mater Sci. 2006;41:6889–94.
107. Wang ZH, Choi CJ, Kim BK, Kim JC, Zhang ZD. Microstructure and magnetic property of Fe–Co nanoparticles prepared by chemical vapor condensation process. J Alloys Compd. 2003;351:319–23.
108. Li Q, Li H, Pol VG, Bruckental I, Koltypin Y, Calderon-Moreno J, et al. Sonochemical synthesis, structural and magnetic properties of air-stable Fe/Co alloy nanoparticles. New J Chem. 2003;27:1194–9.
109. Wang Q, Wu A, Yu L, Liu Z, Xu W, Yang H. Nanocomposites of iron−cobalt alloy and magnetite: controllable Solvothermal synthesis and their magnetic properties. J Phys Chem C. 2009;113:19875–82.
110. Raúl P, Manuel O, Morales MP, Pedro T, Nuria ON, Carlos JS. Synthesis of acicular Fe–Co nanoparticles and the effect of Al addition on their magnetic properties. Nanotechnology. 2004;15:S190.
111. Huh SH, Jeong JW, Jeon YT, Moon JY, Lee GH, Park J. FeCo and FeCr binary nanocluster wire (NCW) arrays. Intl J Modern Phys B. 2006;20:4413–21.
112. Tzitzios V, Basina G, Niarchos D, Li W, Hadjipanayis G. Synthesis of air stable FeCo nanoparticles. J Appl Phys. 2011;109:07A313.
113. Kodama D, Shinoda K, Sato K, Sato Y, Jeyadevan B, Tohji K. Synthesis of size-controlled Fe–Co alloy nanoparticles by modified polyol process. J Magn Magn Mater. 2007;310:2396–8.
114. Cho UR, Lee YM, Kumar S, Lee CG, Koo BH. Effect of cu seed on the synthesis and characterization of FeCo alloy nano-particles by using polyol method. Science China-Technol Sci. 2009;52:19–22.

115. Hütten A, Sudfeld D, Ennen I, Reiss G, Wojczykowski K, Jutzi P. Ferromagnetic FeCo nanoparticles for biotechnology. J Magn Magn Mater. 2005;293:93–101.
116. Frey NA, Peng S, Cheng K, Sun S. Magnetic nanoparticles: synthesis, functionalization, and applications in bioimaging and magnetic energy storage. Chem Soc Rev. 2009;38
117. Gao J, Gu H, Xu B. Multifunctional magnetic nanoparticles: design, synthesis, and biomedical applications. Acc Chem Res. 2009;42:1097–107.
118. Hao R, Xing R, Xu Z, Hou Y, Gao S, Sun S. Synthesis, functionalization, and biomedical applications of multifunctional magnetic nanoparticles. Adv Mater. 2010;22:2729–42.
119. Kodama D, Shinoda K, Sato K, Sato Y, Tohji K, Jeyadevan B. Morphology control of FeCo alloy particles synthesized by polyol process. AIP Conf Proc. 2007;898:126–9.
120. Kodama D, Shinoda K, Sato K, Sato Y, Jeyadevan B, Tohji K. Synthesis of Fe-Co alloy particles by modified polyol process. IEEE Trans Magn. 2006;42:2796–8.
121. Turgut Z, Huang M-Q, Gallagher K, McHenry ME, Majetich SA. Magnetic evidence for structural-phase transformations in Fe-Co alloy nanocrystals produced by a carbon arc. J Appl Phys. 1997;81:4039–41.
122. Jeyadevan B, Shinoda K, Justin RJ, Matsumoto T, Sato K, Takahashi H, et al. Polyol process for Fe-based hard(fct-FePt) and soft(FeCo) magnetic nanoparticles. IEEE Trans Magn. 2006;42:3030–5.
123. Desvaux C, Lecante P, Respaud M, Chaudret B. Structural and magnetic study of the annealing of Fe-Co nanoparticles. J Mater Chem. 2010;20:103–9.
124. Joseyphus RJ, Shinoda K, Kodama D, Jeyadevan B. Size controlled Fe nanoparticles through polyol process and their magnetic properties. Mater Chem Phys. 2010;123:487–93.
125. Wu H-Q, Cao Y-J, Yuan P-S, Xu H-Y, Wei X-W. Controlled synthesis, structure and magnetic properties of Fe1 − xNix alloy nanoparticles attached on carbon nanotubes. Chem Phys Lett. 2005;406:148–53.
126. Lima E Jr, Drago V, Cardoso de Lima J, Papaleo Fichtner PF. Nanocrystalline FexNi1−x ($x \leq 0.65$) alloys formed by chemical synthesis. J Alloys Compd. 2005;396:10–7.
127. Wu H-Q, Xu D-M, Wang Q, Wang Q-Y, Su G-Q, Wei X-W. Composition-controlled synthesis, structure and magnetic properties of ternary FexCoyNi100−x−y alloys attached on carbon nanotubes. J Alloys Compd. 2008;463:78–83.
128. Gurmen S, Ebin B, Stopić S, Friedrich B. Nanocrystalline spherical iron–nickel (Fe–Ni) alloy particles prepared by ultrasonic spray pyrolysis and hydrogen reduction (USP-HR). J Alloys Compd. 2009;480:529–33.
129. Yang H, Li X, Zhou H, Zhuang Y, Hu H, Wu H, et al. Monodisperse water-soluble Fe–Ni nanoparticles for magnetic resonance imaging. J Alloys Compd. 2011;509:1217–21.
130. Ban I, Drofenik M, Makovec D. The synthesis of iron–nickel alloy nanoparticles using a reverse micelle technique. J Magn Magn Mater. 2006;307:250–6.
131. Wei X-W, Zhu G-X, Zhou J-H, Sun H-Q. Solution phase reduction to Fe–Ni alloy nanostructures with tunable shape and size. Mater Chem Phys. 2006;100:481–5.
132. Chen Y, Luo X, Yue G-H, Luo X, Peng D-L. Synthesis of iron–nickel nanoparticles via a nonaqueous organometallic route. Mater Chem Phys. 2009;113:412–6.
133. Chaubey GS, Barcena C, Poudyal N, Rong C, Gao J, Sun S, et al. Synthesis and stabilization of FeCo nanoparticles. J Am Chem Soc. 2007;129:7214–5.
134. Kodama D, Shinoda K, Kasuya R, Tohji K, Doi M, Balachandran J. Synthesis of submicron sized Fe20Ni80 particles and their magnetic properties. J Appl Phys. 2010;107:09A320.
135. Seyedi M, Haratian S, Khaki JV. Mechanochemical synthesis of Fe_2O_3 nanoparticles. Procedia Mater Sci. 2015;11:309–13.
136. Iwasaki T, Kosaka K, Mizutani N, Watano S, Yanagida T, Tanaka H, et al. Mechanochemical preparation of magnetite nanoparticles by coprecipitation. Mater Lett. 2008;62:4155–7.
137. Wu W, Wu Z, Yu T, Jiang C, Kim W-S. Recent progress on magnetic iron oxide nanoparticles: synthesis, surface functional strategies and biomedical applications. Sci Technol Adv Mater. 2015;16:023501.
138. Lu AH, Salabas EL, Schüth F. Magnetic nanoparticles: synthesis, protection, functionalization, and application. Angew Chem Int Ed. 2007;46:1222–44.

139. Chaudhary V, Chaudhary R. Magnetic nanoparticles: synthesis, functionalization, and applications. In: Nalwa HS, editor. Encyclopedia of nanoscience and nanotechnology. Stevenson Ranch: American Scientific Publishers; 2018. p. 153–83.
140. Cotin G, Perton F, Blanco-Andujar C, Pichon B, Mertz D, Bégin-Colin S. Design of anisotropic iron-oxide-based nanoparticles for magnetic hyperthermia. Nanomaterials for Magnetic and Optical Hyperthermia Applications: Elsevier; 2019. p. 41–60.
141. Baaziz W, Pichon BP, Fleutot S, Liu Y, Lefevre C, Greneche J-M, et al. Magnetic iron oxide nanoparticles: reproducible tuning of the size and nanosized-dependent composition, defects, and spin canting. J Phys Chem C. 2014;118:3795–810.
142. Park J, Lee E, Hwang N-M, Kang M, Kim SC, Hwang Y, et al. One-nanometer-scale size-controlled synthesis of monodisperse magnetic iron oxide nanoparticles. Angew Chem Int Ed. 2005;44:2872–7.
143. Sun S, Zeng H. Size-controlled synthesis of magnetite nanoparticles. J Am Chem Soc. 2002;124:8204–5.
144. Coey JMD. Magnetism and magnetic materials. Cambridge: Cambridge University Press; 2001.
145. Gu S, Jin Y, Chen P, Yan C, Della Torre E, Bennett LH. Modeling of magnetic material displaying magnetic aftereffect with slow decay rates. Phys B Condens Matter. 2012;407:1372–6.
146. Demokritov SO, Demidov VE, Dzyapko O, Melkov GA, Serga AA, Hillebrands B, et al. Bose-Einstein condensation of quasi-equilibrium magnons at room temperature under pumping. Nature. 2006;443:430–3.
147. Bennett LH, Della Torre E, Johnson PR, Watson RE. A phase diagram for the Bose-Einstein condensation of magnons. J Appl Phys. 2007;101:09G103.
148. Mohapatra J, Mitra A, Bahadur D, Aslam M. Surface controlled synthesis of MFe_2O_4 (M = Mn, Fe, Co, Ni and Zn) nanoparticles and their magnetic characteristics. CrystEngComm. 2013;15:524–32.
149. Guardia P, Labarta A, Batlle X. Tuning the size, the shape, and the magnetic properties of iron oxide nanoparticles. J Phys Chem C. 2011;115:390–6.
150. Sun S, Zeng H, Robinson DB, Raoux S, Rice PM, Wang SX, et al. Monodisperse MFe_2O_4 (M = Fe, Co, Mn) nanoparticles. J Am Chem Soc. 2004;126:273–9.
151. Noh S-h, Na W, Jang J-t, Lee J-H, Lee EJ, Moon SH, et al. Nanoscale magnetism control via surface and exchange anisotropy for optimized Ferrimagnetic hysteresis. Nano Lett. 2012;12:3716–21.
152. Zhen G, Muir BW, Moffat BA, Harbour P, Murray KS, Moubaraki B, et al. Comparative study of the magnetic behavior of spherical and cubic superparamagnetic iron oxide nanoparticles. J Phys Chem C. 2011;115:327–34.
153. de Montferrand C, Hu L, Milosevic I, Russier V, Bonnin D, Motte L, et al. Iron oxide nanoparticles with sizes, shapes and compositions resulting in different magnetization signatures as potential labels for multiparametric detection. Acta Biomater. 2013;9:6150–7.
154. Larumbe S, Gomez-Polo C, Pérez-Landazábal JI, García-Prieto A, Alonso J, Fdez-Gubieda ML, et al. Ni doped Fe_3O_4 magnetic nanoparticles. J Nanosci Nanotechnol. 2012;12:2652–60.
155. Gabal MA, Bayoumy WA. Effect of composition on structural and magnetic properties of nanocrystalline Ni0.8−xZn0.2MgxFe$_2$O$_4$ ferrite. Polyhedron. 2010;29:2569–73.
156. Nemati Z, Alonso J, Rodrigo I, Das R, Garaio E, García JÁ, et al. Improving the heating efficiency of iron oxide nanoparticles by tuning their shape and size. J Phys Chem C. 2018;122:2367–81.
157. Nemati Z, Alonso J, Martinez LM, Khurshid H, Garaio E, Garcia JA, et al. Enhanced magnetic hyperthermia in iron oxide nano-octopods: size and anisotropy effects. J Phys Chem C. 2016;120:8370–9.
158. Doaga A, Cojocariu A, Amin W, Heib F, Bender P, Hempelmann R, et al. Synthesis and characterizations of manganese ferrites for hyperthermia applications. Mater Chem Phys. 2013;143:305–10.

159. Sathya A, Guardia P, Brescia R, Silvestri N, Pugliese G, Nitti S, et al. $CoxFe_3–xO_4$ Nanocubes for Theranostic applications: effect of cobalt content and particle size. Chem Mater. 2016;28:1769–80.
160. Yang Z, Li Z, Yang Y, Xu ZJ. Optimization of $ZnxFe_3–xO_4$ hollow spheres for enhanced microwave attenuation. ACS Appl Mater Interfaces. 2014;6:21911–5.
161. Xavier B, Amílcar L. Finite-size effects in fine particles: magnetic and transport properties. J Phys D Appl Phys. 2002;35:R15.
162. Garanin DA, Kachkachi H. Surface contribution to the anisotropy of magnetic nanoparticles. Phys Rev Lett. 2003;90:065504.
163. Bødker F, Mørup S, Linderoth S. Surface effects in metallic iron nanoparticles. Phys Rev Lett. 1994;72:282–5.
164. Zhang Y, Li X, Zhang Y, Wei J, Wang W, Dong C, et al. Engineered Fe_3O_4-based nanomaterials for diagnosis and therapy of cancer. New J Chem. 2021;45:7918–41.
165. Nguyen DT, Kim K-S. Functionalization of magnetic nanoparticles for biomedical applications. Korean J Chem Eng. 2014;31:1289–305.
166. Bagheri S, Julkapli NM. Modified iron oxide nanomaterials: functionalization and application. J Magn Magn Mater. 2016;416:117–33.
167. Ramanujan RV. Magnetic particles for biomedical applications. In: Narayan R, editor. Biomedical materials. Boston: Springer US; 2009. p. 477–91.
168. Kayal S, Ramanujan RV. Doxorubicin loaded PVA coated iron oxide nanoparticles for targeted drug delivery. Mater Sci Eng C. 2010;30:484–90.
169. Purushotham S, Ramanujan R. Thermoresponsive magnetic composite nanomaterials for multimodal cancer therapy. Acta Biomater. 2010;6:502–10.
170. Gupta AK, Gupta M. Synthesis and surface engineering of iron oxide nanoparticles for biomedical applications. Biomaterials. 2005;26:3995–4021.
171. Chaurasia AK, Thorat ND, Tandon A, Kim J-H, Park SH, Kim KK. Coupling of radiofrequency with magnetic nanoparticles treatment as an alternative physical antibacterial strategy against multiple drug resistant bacteria. Sci Rep. 2016;6:33662.
172. Yang J, Wang J, Li X, Wang D, Song H. Synthesis of urchin-like Fe_3O_4@SiO_2@ZnO/CdS core-shell microspheres for the repeated photocatalytic degradation of rhodamine B under visible light. Cat Sci Technol. 2016;6:4525–34.
173. Ankamwar B, Lai T, Huang J, Liu R, Hsiao M, Chen C, et al. Biocompatibility of Fe_3O_4 nanoparticles evaluated by in vitro cytotoxicity assays using normal, glia and breast cancer cells. Nanotechnology. 2010;21:075102.
174. Li Y, Liu J, Zhong Y, Zhang J, Wang Z, Wang L, et al. Biocompatibility of Fe_3O_4@ Au composite magnetic nanoparticles in vitro and in vivo. Int J Nanomedicine. 2011;6:2805.
175. Antoniak MA, Pązik R, Bazylińska U, Wiwatowski K, Tomaszewska A, Kulpa-Greszta M, et al. Multimodal polymer encapsulated CdSe/Fe_3O_4 nanoplatform with improved biocompatibility for two-photon and temperature stimulated bioapplications. Mater Sci Eng C. 2021;112224
176. Zare M, Sarkati MN. Chitosan-functionalized Fe_3O_4 nanoparticles as an excellent biocompatible nanocarrier for silymarin delivery. Polym Adv Technol. 2021;32:4094–100.

An Up-to-Date Look at In Vitro Models of Nose-to-Brain Drug Delivery

Cansel Kose Ozkan, Ozgur Esim, and Ayhan Savaser

1 Introduction

The nose is the initial segment of the respiratory framework that permits air to enter the body. Simple application and high surface region make it a significant option for nasal medication applications. The nasal route has received a lot of attention for the last 20 years as it offers many advantages such as rapid absorption and onset of pharmacological action, avoidance of liver first-pass effects and high systemic effect, and practicality of the route of administration [1–3]. There is intense interest in using the nasal passages to transport drugs to the brain. The use of many different techniques, like nanosystems, for drug delivery to the brain provides a significant advantage over conventional methods [4]. For example, the most important advantage of drug delivery technology with nanoparticles is that these particles increase the blood-brain barrier penetration of the therapeutic drug molecule [5]. For a long time, the use of nanoparticle drug delivery systems has been studied for increasing the absorption and cellular uptake of p-glycoprotein substrates [6, 7].

In this chapter, the blood-brain barrier, which is a major barrier to drug targeting to the brain, and the main prognostic factors affecting transport across the barrier and the mechanisms used to increase drug concentration in the central nervous system will be explained. In addition, information will be provided on the characteristics of the most commonly preferred nasal route, targeting drugs to the central nervous system in nasal administration, and the evaluation of both conventional and nanoparticular drugs, which are planned to be used experimentally as intranasal applications, in models simulating the blood-brain barrier. Also, a literature review of the recent studies on this subject will be presented in this chapter.

C. Kose Ozkan (✉) · O. Esim · A. Savaser
Gulhane Faculty of Pharmacy, Department of Pharmaceutical Technology, University of Health Sciences, Ankara, Turkey

R. S. Chaughule et al. (eds.), *Nanomaterials for Cancer Detection Using Imaging Techniques and Their Clinical Applications*,
https://doi.org/10.1007/978-3-031-09636-5_5

2 Central Nervous System Diseases Treated by Peripheral Route

The central nervous system is one of the two main parts of the body's nervous system. The nervous system functions as the communication network and control center of the body [8]. And the central nervous system (CNS), which consists of the brain and spinal cord, is the control center of the entire nervous system. All the senses of the body are transmitted to the central nervous system [9]. All the nerve impulses that cause the contraction of the muscles and the secretion of the glands are controlled by the central nervous system. Most central nervous system (CNS) diseases cause disability or mortality. There is no certain cure for many diseases of this vital system [10]. One of the barriers in the treatment of these diseases is not the lack of effective drugs but the inability of active substances to reach the diseased area [11]. Modern drug development efforts are based on the evaluation of the effectiveness of the active substances by injecting them directly into the brain. However, when these developed drugs are applied to the organism by various administration routes, most of them cannot cross the blood-brain barrier (BBB) [12]. It is the BBB that limits the penetration of water-soluble substances from the blood to the central nervous system (CNS) and their penetration into the cerebral parenchyma. Therefore, the active substances used in the treatment of most diseases cannot reach the target brain area, even if they have a low molecular weight [13]. Statistically, only 1% of the known active substances can affect their target area arriving through the BBB; the others fail to cross this barrier [14]. As a result of the low penetration of the active substances into the membranes, the expected therapeutic efficacy cannot be achieved [15, 16].

One of the alternative methods used to reach the diseased area is peripheral routes.

2.1 Multiple Sclerosis

Multiple sclerosis (MS) is a typical human neuroinflammatory CNS disease characterized by diffuse focal and diffuse infiltration of mononuclear cells for white matter and gray matter [17]. For a long period of time, it was thought that MS only affects white matter. However, imaging and histopathological analysis have shown that the cerebral cortex also plays a role in early MS. The rat model for MS disease shows the binding of T cells and diapedesis (blood leakage) from the blood-brain barrier and leptomeningeal vessels [18]. Thus, meningeal vessels provide clues for immune cells to reach the leptomeningeal space and from there to the parenchyma [19]. Clinical specimens associate "subpial demyelinating lesions" topographically with meningeal infiltrates [20]. The presence of MS lesions in the optic nerves and spinal cord and pre-ventricular white matter strengthens the concept of immune cell invasion not only through the blood-brain barrier but also through the leptomeningeal space and blood-CSF barrier [19, 20]. The ratio of the restrictive nature of the

permeability barrier in leptomeningeal vessels is not uniform, and the tendencies for restriction and prevention are concentrated in different CNS areas [21, 22].

2.2 Alzheimer's Disease and Parkinson's Disease

Cerebral vascular EC dysfunction and migration of leukocytes across the blood-brain barrier can be seen in the early stages of the development of neurodegenerative diseases such as Alzheimer's disease (AD) and Parkinson's disease (PD) [21, 23]. However, it is difficult to describe whether such cases constitute the cause or the result of other cases. AD and PD phenotypes are age-dependent and begin years before pathology symptoms [24]. The drug resistance function of the blood-brain barrier decreases with aging, leading to decreased clearance of neurotoxic products and increased oxidative stress in the brain. Thus, the risk of neurodegenerative pathology increases as well [25].

One of the most important factors in AD is amyloid β accumulation. In many studies, it has been shown with CSF measurement or imaging of the brain with positron emission tomography (PET) that amyloid β increases threefold during Alzheimer's disease [26]. The results of the studies on reducing the amyloid load, which is accepted as one of the main approaches for the treatment of the disease, are not promising [26, 27]. One of the current approaches for the treatment of AD is γ-secretase inhibition to reduce amyloid β production [28]. Tarenflurbil and semagacestat made it to phase III, but both were halted for various reasons [29].

2.3 Human Immunodeficiency Virus (HIV)

According to anecdotal reports, HIV can cross the blood-brain barrier during acute infection, but due to the lack of data collected in the pre-seroconversion period, the precise timing for human subjects, the type of CNS infection, and the degree of CNS inflammation are unlikely to be understood [30–32]. The early immunological response of the host and the degree of reservoir load may clarify the early CNS damage and the long-term neuropathogenesis of HIV [33].

2.4 Cancer

Primary and metastatic brain tumors are heterogeneous tumor groups with varying outcomes and management strategies. Primary brain tumors can range from the rare "pilocytic astrocytomas" that are noninvasive and curable without surgery to the multiform glioblastomas, adult intraparenchymal brain tumors, that are invasive and incurable [33, 34].

Common CNS cancer types are malignant glioma, CNS lymphoma, ependymoma, medulloblastoma, and trigeminal neuralgia. Guidelines containing information on treatment approaches and diseases are updated annually when applicable. Since this field is constantly evolving and developing, the most appropriate approach should be considered for each patient [34, 35].

2.5 Infections

2.5.1 Bacterial Meningitis

Bacterial meningitis is a common disease caused by *Streptococcus pneumoniae* and *Neisseria meningitidis* [36]. The rate of incidence of meningococcal meningitis caused by *Neisseria meningitides* for newborns and children is as high as in adults, but there are differences between age groups [37]. Bacteria are encapsulated in the three groups with the highest incidence rate, thus invading the upper airway and entering the bloodstream into the subarachnoid space [38, 39]. The infectious organism first colonizes the nasopharynx. When it enters the blood circulation, the capsule structure prevents the organism from being recognized and destroyed by the body [40]. The organism then crosses the blood-brain barrier and proliferates in the CNS, causing inflammation. Inflammation increases the permeability of the blood-brain barrier and creates vasogenic edema. Cerebral edema increases intracranial pressure, resulting in decreased cerebral perfusion and secondary injuries due to ischemia [41].

2.5.2 Viral Encephalitis

Viral encephalitis is an infection that causes inflammation in the brain parenchyma. Viruses that cause encephalitis are arboviruses, HSV, herpes zoster virus (HZV), Epstein-Barr virus (EBV), cytomegalovirus (CMV), and rabies [42, 43].

2.6 Traumatic Brain Injury (TBI)

TBI is the most common cause of death for children and young adults in developed countries. The pathology of TBI presents high heterogeneity because of immediate and delayed mechanisms [44, 45]. Immediate primary injuries are impact-related and cannot be cured but are considered preventable. In cases of delayed second-phase damage, there is time for intervention, and therefore, they are important. One of the treatment approaches is to increase the blood-brain barrier permeability. VEGF provides promising results in this regard [46]. Other prominent blood-brain barrier damage-inducing candidates are histamine and hydroxytryptamine, which

are used to prevent edema [47]. Reducing MMP activity after head trauma may maintain the blood-brain barrier. Activated protein C (APC), which is an endogenous anticoagulant and provides neuroprotection for strokes, is accepted as a fine approach for the treatment of TBI [48].

2.7 Gilles de la Tourette Syndrome (GTS)

For a long time, GTS was thought to be of psychological origin. But studies have shown that GTS is based on genetic, autoimmune, neuroanatomical, and neurochemical disorders. Neuroimaging shows abnormal activities in the cortical and subcortical areas. The role of dopamine in the neurobiology of GTS has been proven by pharmacological studies, and dopamine antagonism is used in studies on the treatment [49].

2.8 Neurodegenerative Diseases

Spinocerebellar neurodegeneration can lead to different diseases. Neurodegeneration can cause symptoms of incoordination (ataxia), muscle weakness, and sensory loss. Huntington's disease and Friedreich's ataxia are two of the diseases that can be observed under such conditions. Treatment strategies for neurodegenerative disorders use histone deacetylase (HDAC) inhibitors, which act by modifying gene expression. The use of HDAC inhibitors is especially important for Huntington's disease, which is caused by the expansion of the CAG repetitive region of the HTT gene [50].

2.9 Epilepsy

Epilepsy is a chronic neurological disease that affects quite a lot of people around the world. Current treatment approaches fail to treat 30% of patients, and of the patients, 20% experience treatment-resistant seizures. For this purpose, ongoing research focuses on active substances that can be used effectively in different types of seizures. Some broad-spectrum anticonvulsants used for epilepsy cases are useful in the treatment of other CNS diseases. In addition, this type of drug is also used for neuropathic pain, bipolar disorder, migraine, and substance abuse cases [51].

2.10 Migraine

Migraine is a recurrent neurological disorder that causes workforce loss. According to 2017 data, the prevalence of migraine for the 15–55 age group is 21.8% for females and 10.9% for males in Turkey [52]. Migraine is characterized by intermittent severe throbbing unilateral headaches and pain along with nausea, vomiting, and sensitivity to light, sound, or movement. Attacks can last for 4–72 h, and visual disturbances called aura occur in 10–20% of patients. The monthly average of migraine attacks is around 2 [53]. The pathophysiology of migraine is still not fully elucidated. However, a neurological disorder in the brainstem is thought to cause migraine. Migraine basically occurs through three mechanisms: cranial arterial vasodilation, extracerebral neurogenic inflammation, and decreased inhibition of central pain transmission, and activation of the trigeminovascular system centrally and peripherally causes the release of vasoactive neuropeptides such as calcitonin gene-related peptide (CGRP), substance P, and neurokinin A, and this causes vasodilation, sterile inflammation of blood vessels, and pain signal transduction [54]. Serotonin mediator has been associated as a mediator of migraine attacks for many years due to its decreased level during migraine attacks and relieving effect of serotonin infusion on migraine attacks [55]. Sumatriptan is the first selective 5-HT 1B/1D serotonin receptor agonist developed for this purpose. When it was first discovered, it was described as a groundbreaking discovery in the treatment of acute migraine, due to the fact that it had fewer adverse effects than ergot alkaloids [56]. However, its limited oral bioavailability, short half-life, high pain recurrence rate, inability to pass through the blood-brain barrier, and cardiovascular side effects limit its use [57].

3 Ultimate Barrier of the Brain: Blood-Brain Barrier

The first studies proving the blood-brain/blood-cerebrospinal fluid barrier were carried out by Paul Ehrlich at the end of the nineteenth century [58]: Between the dura mater and the arachnoid, numerous layers of smooth cells are bound by tight junctions and ligament junctions and are covered by an incomplete basement membrane. In regions of the cerebellum, the capillary endothelium is joined tightly. The morphological relationship of the blood-cerebrospinal fluid barrier is the cylindrical epithelium of the choroid plexus, which is connected by tight junctions [59]. The blood-brain barrier creates a boundary for the movement of substances between the peripheral circulation and the CNS. In this way, possible neurotoxic substances are restricted from entering the brain, but at the same time, the access of therapeutics to the central nervous system for therapeutic purposes is prevented as well. The blood-brain barrier allows low-rate pinocytosis and has tight junctions. It is located at the microvascular level and is important for the homeostasis of the central nervous system. It also significantly limits the paracellular diffusion of solutes from the blood

to the brain [60]. This restriction occurs with three types of barriers: The blood-brain barrier is primarily composed of endothelial cells covering the cerebral microvessels and peripheral perivascular elements [61]. The cerebral blood capillaries of the brain are composed of brain microvessel endothelial cells (BMVEC). The main difference between BMVEC and normal endothelial cells is the tight junctions. Adjacent endothelial cells form complex tight junctions with significant transendothelial electrical resistance (TEER), creating a physical barrier that significantly limits paracellular permeability across the blood-brain barrier. This structure is in complete contrast to the peripheral circulation with decreased TEER and efficient paracellular permeability. Tight junctions prevent the free penetration of water-soluble substances into the cells and the entry of brain cells into the fluid periphery [62]. In addition to the physical barrier created by tight junctions, the blood-brain barrier also includes different metabolic barriers for drug transport. The endothelial cells of the blood-brain barrier enable minimal pinocytosis, thereby substantially eliminating nonselective transcellular permeability. In addition, each cellular component of the blood-brain barrier produces a set of intracellular and extracellular enzymes that inactivate many compounds that will attempt to cross the blood-brain barrier [63]. Many enzymes covering the blood capillaries of the brain break down or inactivate unwanted peptides and other small molecules in the blood. The capillary endothelium contains many efflux transporters [64]. Certain drugs can cross the endothelial barrier by free diffusion and enter the brain from the blood. If the drug is the substrate of one of the active efflux transporters (AET) produced in the brain microvessels, this uptake can be immediately followed by active efflux from the brain into the blood [65]. The main transport routes from the blood-brain barrier can be listed as follows [66]:

1. Through small arterioles and capillaries, gases are among the molecules that diffuse the fastest from the BBB.
2. Simple transmembrane diffusion.
3. Carrier-mediated transporter proteins.
4. Receptor-mediated transcytosis.
5. Paracellular transition mechanism.

Typically, just small, lipophilic particles can cross an ordinary, sound blood-cerebrum hindrance by transcellular detached dispersion; restricted transport of specific peptide and protein analogs has additionally been accounted for. Fundamental supplements, for example, glucose and iron can enter the CNS with explicit carriers, for example, glucose carrier 1 or receptors like the transferrin receptor [67].

3.1 Prognostic Factors Affecting Transport Across the Blood-Brain Barrier

Molecule size: Although the amount of penetration of large hydrophilic substances into the cerebrospinal fluid is small, there is no definite limit. Molecules with a molecular weight of 500 Da (400–600 Da) can cross the blood-brain barrier in pharmacologically significant amounts. Although there are many examples of small-molecular-weight drugs that can cross the blood-brain barrier, almost all large-molecular-weight drugs have limited permeability of the blood-brain barrier under normal conditions [14].

Liposolubility The entire CNS can be thought of as surrounded by lipid layers since the central nervous system elements are surrounded by at least one cell layer, that is, two lipid membranes per cell that are predominantly tightly connected. The lipophilicity of a compound increases its ability to penetrate these membranes. For diffusion from plasma to CSF, the ideal octanol/water partition coefficient at pH 7.4 is between 1 and 10 and log P between 0 and 1. In addition, drugs with a polar surface area (>80 Å) can cross the blood-brain barrier with pharmacologically significant amounts [68].

Binding to plasma proteins: It significantly affects the entry of drugs into the elements of the central nervous system. Since binding proteins (especially albumin and globulins) are able to cross the blood-brain/blood-cerebrospinal fluid barrier to a small extent, it is believed that in the presence of an intact barrier, the portion of unbound plasma can pass [69].

Physiology of Drugs The intracranial space and the vertebral canal cannot be evaluated as a single physiological area. The CSF area is divided into extracellular and intracellular areas of the brain and spinal cord. Concentrations within different parts of the same region are often different from each other. Following the intravenous injection, most drugs are found in higher concentrations in the lumbar CSF than in the ventricular part. In general, injection of drugs into the lumbar cerebrospinal fluid does not produce an effective concentration in the cisternal and ventricular cerebrospinal fluid [70]. There is no diffusional barrier between the interstitial spaces of nervous tissue and cerebrospinal fluid. Indeed, even enormous molecules can enter the interstitial space of nervous tissue by diffusion from the cerebrospinal fluid space. About two-thirds of the cerebrospinal fluid is produced by the choroid plexus. One-third of the cerebrospinal fluid originates from the extracellular space of the brain and spinal cord, that is, there is a continuous flow between the extracellular space of the brain/spinal cord and the cerebrospinal fluid space, which prevents the formation of equal drug concentration by diffusion in the cerebrospinal fluid space and the extracellular fluid of the nervous tissue [71].

3.2 Mechanisms Increasing Drug Concentration in the Central Nervous System

About 100% of the macromolecules and about 98% of the small molecules applied to the body cannot cross the blood-brain barrier and cannot reach the cerebrospinal fluid or brain extracellular space. Transcranial and intranasal administration and blood-brain barrier carriers are used, or the blood-brain barrier is disrupted in order to transport this type of drug to the brain [72]. Detailed examination of the methods presented in Table 1 is necessary if a method is to have a major impact on the discovery of CNS drugs in the future. In addition, the use of P-gp inhibitors to increase entry into the blood-brain barrier is an accepted approach. As an idea, it has been accepted that P-gp-inhibiting compounds reverse P-gp-mediated multidrug resistance or increase blood-brain barrier permeability of CNS drugs that would otherwise fail treatment due to efflux. However, in such an approach, P-gp dysfunction can both increase the level of accumulation of toxins, as for PD, and weaken the ability of the brain efflux for proteins, as for AD, so it should be monitored throughout treatment [73].

The most straightforward method for expanding drug concentration in CNS is to increase the systemic dose. Drug entry into brain tissue and cerebrospinal fluid can be achieved by temporary artificial disruption of diffusional barriers among the blood, cerebrospinal fluid, and brain tissue. An effective but invasive way to achieve

Table 1 Pharmacological strategies for drug transport from blood-brain barrier to CNS

Strategy	Rationale/opinion
Preparation of prodrugs	It increases the transport of small hydrophilic molecules from the BBB and transporter-mediated prodrug transport by chemical modifications to lipophilic derivatives.
Preparation of lipophilic analogs	There is a relationship between drug lipid solubility and in vivo BBB permeability.
Chemical drug delivery systems	This strategy is a rational drug design approach to not only transporting drugs but also targeting them.
Carrier intermittent drug delivery	Transport systems such as glucose and natural amino acids It provides an increase in capacity and BBB transition.
Receptor−/vector-mediated drug delivery	Connecting the active substance to a vector and ensuring its passage through a catalyzed carrier mechanism ensures its passage from the BBB with a Trojan horse-like deception.
Inhibit drug transport or inhibition of pulse transporters	In addition to the use of inhibitors, it is also an approach to develop drugs that are not substrates of these transporters.
Use of polymeric carriers such as nanoparticles and liposomes	The primary superiority of nanoparticle delivery technology masks the BBB-limited properties of the therapeutic drug molecule of nanoparticles and can slow drug release in the brain and increase peripheral toxicity.
Neuroimmune films (small molecule neurotrophic factors)	It can be administered orally and can pass BBB.

high drug concentration in CNS is an intraventricular injection in addition to intravenous administration [21].

4 Nasal Passages

Although various studies are carried out to overcome BBB, it is statistically known that more than 98% of the dose amount cannot reach the brain after systemic administration of the active substances that are known today for the treatment of CNS diseases. It has become prominent to use intranasal (IN) transport as an alternative to interventional methods, bypassing the blood-brain barrier by taking advantage of the "trigeminal" and olfactory pathways that connect the olfactory and nasal passage to the nervous system, and rapidly target therapeutics such as peptides, proteins, oligonucleotides, viral vectors, and even stem cells to the CNS to achieve results [74]. The innovation in using this noninvasive method is to minimize systemic exposure by rapidly transporting drugs directly from the nasal mucosa to the brain and spinal cord for CNS disorders [75]. It is proven that peptides and proteins administered intranasally have beneficial effects in humans. The intranasal route has long been known for its many advantages such as the rapid onset of effects and being used for non-injection application methods. In addition to the difficulty of reproducibility, limited absorption from the nasal epithelium, which is the most important danger of the intranasal route, limits the application, especially for potent substances. It has been explained by various studies that this situation can be corrected by using permeability enhancers [76].

4.1 Critical Factors for Drug Targeting to the Central Nervous System During Nasal Administration

Due to the different anatomical and physiological structures of the nasal cavity, drug accumulation and accumulation areas depend on the administration device. Drug accumulation is affected by the type of application, formulation particle size, velocities of applied particles, spray angle, and width. The applied system can be selected based on the therapeutic efficacy of the active substance used, the patient population, and market needs. Pharmacokinetic properties and, therefore, bioavailability vary according to the dosage form [77]. The factors that affect intranasal drug administration are summarized in Fig. 1.

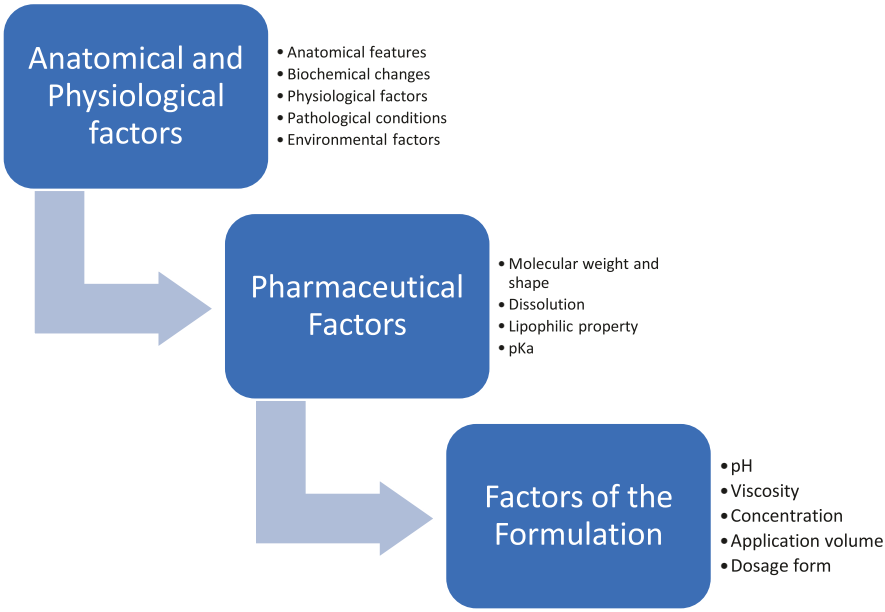

Fig. 1 Factors that affect intranasal drug administration

5 Role of Nanoparticular Transporter Systems in Treatment of Central Nervous System Diseases

At physiological pH, non-ionized and low molecular weight lipophilic active substances can penetrate the CNS. However, various transport strategies have been developed for the transport of small molecules with poor liposolubility and hydrogen bonding functional groups as well as water-soluble active substances such as peptides and proteins to the CNS [78]. One way to overcome BBB is to use NPs as active substance transporters. The average particle sizes of such NPs to be used should be 1–100 nm. The active substance is lined in the polymer or adsorbed on the surface [7, 78–80]. Additionally, the NP/active agent formulation is lined with a surfactant. Like liposomes, NPs are rapidly removed from the blood (more than 90% in 5 minutes) following IV administration [78–84]. Although liposomes with 40–80 nm particle size cannot cross the BBB, NPs with larger particle sizes can pass the BBB. This pharmacological effect of NPs is related to their formulation. Because at this point, the penetration of an active substance in the nanoparticle transporter system through the BBB is no longer determined by the physicochemical properties of the active substance but by the physicochemical and biomimetic properties of the NPs [13, 14]. This eliminates the need for any modification to the active substance. NPs are more commonly preferred due to their properties such as providing high chemical and biological resistance, transporting both hydrophilic and lipophilic active substances, and enabling the administration to the body in different ways. In

addition, targeting can be done with surface modification. The mechanism of NPs to penetrate the BBB has not been fully elucidated. However, it is thought that NPs leave the systemic circulation after administration and cross the BBB through adsorption-mediated transport and receptor-mediated transport [85]. For NPs to be transported by endogenous transporters, they must be surface coated or modified with antigens, antibodies, and receptor ligands and/or have appropriate physicochemical properties. The first methods developed to overcome BBB are aimed at designing NPs with optimum physicochemical properties. In addition, it has been proven that positively charged NPs can pass through the BBB due to their ability to adsorb to tissues. NPs do not have an optimum shape requirement to pass the BBB [86].

Other methods developed to enable penetration through BBB are based on coating the surface of NP with surfactants or polymers such as PEG. Studies have shown that NPs coated with polysorbate 80 or PEG can reach neuronal tissues bypassing the BBB [87]. The most popular strategy in recent years is reaching the CNS with NPs, which can make their way to the brain through known pathways and interact molecularly with the BBB, without disturbing the normal function of the barrier. Examples of nanoparticle drug delivery systems to the brain according to the application methods are shown in Fig. 2.

6 In Vitro Models Used in Drug Penetration to the Brain

There are different approaches to analyzing whether active substances can pass through the brain barrier. All methods differ from each other in terms of the quality of data obtained, as well as cost and difficulty. Various models are used for drug penetration to the brain [88].

6.1 Artificial Membranes

Lipophilicity (Log P or P octanol/water) is thought to be the most important parameter in the central nervous system activity and drug penetration to the brain. Due to its lipophilic properties, n-octanol is the most widely used method in pharmacokinetics. The small polar head and hydrophobic carbon chain of n-octanol make it similar to phospholipid membranes. However, the Log P value alone is not sufficient on its own to explain drug penetration to the central nervous system [89]. In addition, artificial membranes are used as an alternative to the Log P method. Modified high-performance liquid chromatography columns prepared with phospholipids covalently bonded to silica are used for this purpose. In the studies, a linear relationship was found between the delay duration and the distribution between the water phase and liposomes. However, the behavior and stability of

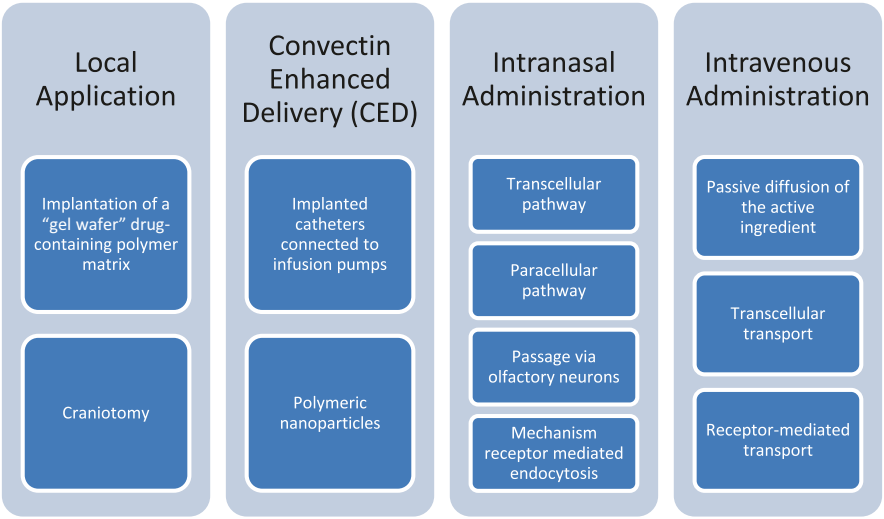

Fig. 2 Nanoparticular drug delivery systems to the brain according to the application methods

lipophilic substances in the selected mobile phase create limitations for this method [90].

6.2 PAMPA Model

Parallel artificial membrane permeability assay (PAMPA) is a method developed by Kanay in 1998 for high-accuracy prediction of the gastrointestinal penetration of drugs. In this method, the donor and acceptor compartments are separated by a liquid artificial membrane. The drug to be tested is placed in the donor compartment. Then, the amounts of this substance in the acceptor and donor phases are examined. Because of its high accuracy, 96-well cell culture plates are generally used. Organic solvents and solvent mixtures prepared with phospholipids can also be used as artificial membranes [91]. With the PAMPA method, it is possible to quickly predict the penetration capacity of many drugs. However, the PAMPA model only provides information about drug penetration by passive diffusion. It is known that many transport pathways and enzymes are effective in drug penetration to the brain. PAMPA only provides information about passive transcellular permeability. For example, the penetration of P-gp substrates through the PAMPA model is higher than in the in vivo and in vitro cell models [92].

6.3 Cell Culture

Cell models are widely used to predict the rate of drug penetration to the brain during drug development. There are various cell types obtained from different sources with different transporter and tight junction structures. These factors influence the reproducibility of permeability studies and the prediction of in vivo penetration to the brain. Therefore, all cell models are different from each other and uniquely model drug penetration to the brain [93]. However, no cell study can fully simulate in vivo penetration to the brain. The biggest advantage of the cell model is the processing speed, as many products can be analyzed simultaneously. In addition, cell models are used to elucidate the transport mechanism dependent on the effective transporters for substance permeability. Furthermore, cell culture studies can also give an idea about metabolism and cellular toxicity. However, reproducibility in cell culture studies is limited, and it is difficult to work in a standard protocol [94].

6.4 Primary Cultures

Studies on the biology of cells for in vitro modeling of the blood-brain barrier were initiated with cattle and pigs due to their large brain areas. Rat, mouse, and human cell culture systems have also been developed over time. None of these cells are the same. They also present intraindividual and interindividual differences. Therefore, it is very difficult to make repeated measurements. Although human brain cells are the gold standard in blood-brain barrier studies, their use is limited for ethical reasons. Primary cell cultures provide interesting results for the penetration of drugs into the brain. However, this model result is not guaranteed, as not all cells in the brain are the same. In addition, it has been shown that the blood-brain barrier properties such as tight junction and transporter properties of brain endothelial cells rapidly lose their effect after culturing [95].

6.5 Immortal Cells

Cattle, human, mouse, and rat endothelial cells have been developed and tested to generate immortalized cells. The cell type with the best blood-brain barrier features is human brain endothelial cells. However, sucrose permeability was not observed in the study, and it was determined that inulin performed low paracellular permeability. In hCEMC/D3 cells developed by Weksler, sucrose permeability and the presence of many pathways were also detected [96].

6.6 Co-cultures

After the development of cell culture models and the determination of brain endothelial cells, it was discovered that these cells alone could not model drug penetration to the brain. For this reason, co-cultures have been developed. In the human brain, there is no permanent connection between brain endothelial cells and cells such as astrocytes, pericytes, and neurons. Studies have shown that the co-culture of astrocytes and brain endothelial cells has a negative effect on the blood-brain barrier properties [97]. The model with the best barrier properties is the BBCEC model developed by Dehouck. When the blood-brain barrier data were correlated, it was observed that the penetration to the brain could be modeled based on molecular weight. Considering all cell cultures, the co-culture models provide the closest results to in vivo values [98].

6.7 Cells Not Originating from the Central Nervous System

Mostly MDCK (Madin-Darby canine kidney) and CaCo-2 (Caucasian colon adenocarcinoma) cell lines are used. MDCK cells are used for easy production and elucidation of MDR1 gene properties, which are similar to P-gp properties. However, it presents a low correlation with the blood-brain barrier. CaCo-2 cells originate from human colon carcinoma and are epithelial cells used in intestinal permeability modeling. These cells are also used to model blood-brain barrier permeability [99]. However, CaCo-2 cells are used as an effective method, especially for studies on P-gp suppression.

7 Studies with Different Perspectives on Models Simulating the Blood-Brain Barrier

In vitro studies on BBB show that low permeability and high TEER results in BBB can be achieved not only by TJs and AJs between cells but also by the structure of the membrane used. It is claimed that the permeability of the BBB models produced is quite realistic since the commonly selected hydrophobic membrane structure limits the permeability of hydrophilic molecules [100].

7.1 In Silico Models

In addition to in vitro models, high-speed and low-cost computer-based in silico models have been started to be used in pharmaceutical and biotechnological studies. It is stated that these models are suitable models that can be used in future studies to determine drug effect and bioavailability; however, in order to obtain reliable results, it is necessary to collect more data about the BBB transport system and its regulation. Because these models could provide successful results only if the parameters uploaded on the computer represent reality [101].

7.2 Static Models

These are usually performed on inserts; the upper surface simulates the luminal, and the lower surface simulates the abluminal part. Different static models such as mono-culture, co-culture, and triple culture systems are created to simulate BBB. There are some important reasons why static models are frequently used today [102]. For example, they are low-cost, require low technical infrastructure, can reach stable TEER values in a short time (3–4 days), and allow imaging of cells. However, despite these and similar other advantages, it has been determined that static models cannot simulate in vivo conditions realistically because they cannot create shear stress that stimulates blood flow, and TEER values obtained from this model type are quite low compared to dynamic models.

In 2D static BBB models, polytetrafluoroethylene (PTFE), polyester, polycarbonate, polyethylene terephthalate (PET), polypropylene, and cellulose esters or collagen type 1-coated PTFE/PET polymers are used as tissue scaffolds. These polymeric membrane surfaces allow nutrient exchange and the penetration of exogenous compounds secreted from cells, but do not allow cell permeability between the two compartments. In addition, the membranes are used to allow cells to absorb and reproduce. Membrane selection constitutes a very important part of the studies because the substrates used in BBB models should act as an extracellular matrix for cells but should not eliminate intercellular interaction. With this interaction, the impact of TJ and AJ proteins in endothelial cells increases, and the permeability of the model decreases, and an increase in TEER can be observed [103].

With inserts, static 3D BBB models can also be created. In one of these models, after the BMEHs were implanted into the matrigel to form a vascular structure, pericytes and astrocytes were added to the medium to ensure that the vascular structures were surrounded by these cells. In these models, better structures can be created compared to inserts due to the fact that the cells are 3D structured to eliminate the lack of in vivo organization of 2D models, the cell-ECM interaction can be examined, and the cell-to-cell interaction is high [102, 103]. However, the system has also disadvantages such as being quite expensive, requiring expertise to set up, limited control, and inability to apply shear stress. Spheroid models, which are

another 3D static BBB model, allow cells to self-arrange without scaffolding to form spherical structures. The outmost layer of the spherical models contains BMEHs, the lower layer is lined with pericytes, and astrocytes are found in the middle of the sphere. Although these models have the advantages of 3D structures, they are models that do not have an ECM-cell correlation and cannot be mechanically stimulated because the ECM is not simulated [104].

7.3 Dynamic Models

An increase in TEER values was observed by modeling the shear stress caused by blood flow in dynamic in vitro BBB models, and it was observed that with the increase in the impact of TJ proteins, the decrease in permeability could better simulate in vivo conditions. It can be said that dynamic 3D models in which shear stress is applied in BBB models created under in vitro conditions are more realistic than static models. Especially in drug development and targeting studies, their use is more effective. For the cone-plate assembly, which is one of the simplest examples of dynamic in vitro models, a conical apparatus is rotated in the nutrient medium in the cell culture reservoir, creating certain shear stress in the liquid and thus modeling the blood flow. In the dynamic hollow-fiber model, endothelial cells are implanted in the inner part (luminal surface) of the microporous hollow fibers and astrocyte and/or pericyte cells in the outer part (abluminal surface). Afterward, the nutrient medium is passed through the fibers continuously, and shear stress between 3 and 20 dyn/cm^2 values caused by in vivo blood flow is modeled [105].

7.4 Microfluidic Systems

These are one type of model on which a lot of research has been done recently. In microfluidic systems, a porous membrane (<10 μm) is placed in the microchannel, and endothelial cells are implanted on the luminal surface and astrocyte and/or pericyte cells on the abluminal surface. This model is advantageous because it uses a small amount of nutrient medium, reaches stability in a short time, and allows shear stress to be applied to the cells, but despite these and similar advantages, it also has some disadvantages. It cannot exactly simulate the 3D vessel model, cannot apply the circular stretching force caused by blood flow to cells, cannot imagine the luminal part, is expensive, and its cell harvesting is problematic [106].

7.5 3D-Printed Microfluidic Technology

This technology provides various advantages compared to traditional production techniques with its features such as the ability to create channels of unmatched shape and complexity, uniform and repeatable production, minimum operating cost and time, product complexity, and reduction of user error. Briefly, in this technique, the 3D designs are created digitally in a 3D medium with CAD software, and then the 3D designs are converted to the stereolithography (SLA) file format (STL) that defines the exterior of a 3D model [80].

7.6 Recent Models

In the model created with bacterial cellulose, which had high hydrophilicity, used in a study, since the barrier was not artificially based on hydrophilic/hydrophobic interaction, it was realized by co-cultivation of cells under optimum conditions and intercellular interactions, and it was observed that the model produced was very realistic [107]. Another study conducted in Germany presents a bioreactor system that provides automated, continuous, and noninvasive online monitoring of cellular barrier integrity during dynamic culture. For this, the bioreactors were fabricated using polydimethylsiloxane (PDMS) casting and 3D printing, and pluggable electrodes based on titanium nitride (TiN)-coated steel pipes were developed to perform EIS measurements. In order to test the monitored bioreactor system, in vitro models of the blood-brain barrier (BBB) derived from human-induced pluripotent stem cells (hiPSC) were cultured for up to 7 days. An equivalent electrical circuit was applied to measure the electrical parameters of the cell layer, and it was observed that TEER value gradually decreased from 2513 $\Omega \cdot cm^2$ to 285 $\Omega \cdot cm^2$ over time, as indicated in the static control culture. This system offers usage options for a variety of dynamic tissue cultures that require a noninvasive monitoring system for barrier integrity [108].

For the last 10–15 years, there have been biotechnological advances that allowed the development of more complex and realistic in vitro BBB models, with a better understanding of the processes that regulate barrier formation and barrier functions. Among these promising new technologies, modulation of stem cell differentiation for the purpose of deriving NVU cell types is an important breakthrough in this context.

Although there is still much to explore for this technology, stem cells could indeed provide a breakthrough in BBB modeling, allowing the in situ development of desired cell cultures on the platform itself.

In terms of platform development, microfluidic systems are developing rapidly, and researchers are more aware of this new technology. The availability of microfluidic platforms is still limited to the labs/research groups developing the system, but the potential for wide adoption among scientists and even industry is increasing.

Further support for the technology could be achieved with the wide use of 3D bioprinting technologies.

8 Conclusion

BBB, which prevents the entry of harmful substances into the bloodstream to the brain, also limits the penetration of drugs planned to be used in treatment to the target area of administration. Efforts to find a solution to this problem are insufficient in the academic and industrial realms. Developing new drugs against CNS diseases such as Alzheimer's disease, Parkinson's disease, Huntington's disease, amyotrophic lateral sclerosis, multiple sclerosis, stroke, brain trauma, spinal cord injury, brain cancer, and AIDS, as well as viral infections in the brain, congenital ataxias, and congenital metabolic diseases, and solving the problems caused by CBE will only be possible with more systematic studies on drug development and targeting these drugs to the brain, which is the target of drugs. Within the progression level in the field of drug targeting to the brain, in order to accelerate the developments and develop new neuropharmaceuticals that can be used clinically, there is a need to fully elucidate the functioning of the endogenous transporter systems in the brain and to reformulate nanoparticle drug transport models based on these systems, supported by molecular biology and genetic approaches.

However, the main objective for the pharmaceutical development of a drug form is to better understand the in vitro and in vivo performance of the drug form. In order to reduce in vivo studies on living organisms during formulation development for the purpose of developing new pharmaceutical drugs, in vitro models with better correlations are needed. There is a great need for models that can simulate the blood-brain barrier for the more efficient use of limited sources due to ethical limitations. However, current in vitro blood-brain barrier (BBB) models, which are frequently used in drug targeting to the central nervous system and drug development studies, cannot yet fully simulate the permeability properties of this special barrier in the brain.

References

1. Djupesland PG. Nasal drug delivery devices: characteristics and performance in a clinical perspective – a review. Drug Deliv Transl Res. 2013;3:42. https://doi.org/10.1007/S13346-012-0108-9.
2. Mygind N, Dahl R. Anatomy, physiology and function of the nasal cavities in health and disease. Adv Drug Deliv Rev. 1998;29:3–12. https://doi.org/10.1016/S0169-409X(97)00058-6.
3. Xu J, Tao J, Wang J. Design and application in delivery system of intranasal antidepressants. Front Bioeng Biotechnol. 2020;8:1450. https://doi.org/10.3389/FBIOE.2020.626882/BIBTEX.

4. Lockman PR, Mumper RJ, Khan MA, Allen DD. Nanoparticle technology for drug delivery across the blood-brain barrier. Drug Dev Ind Pharm. 2002;28:1–13. https://doi.org/10.1081/DDC-120001481.
5. Şahin A, Tonbul H, Çapan Y, Seko I. Brain-targeted nanoparticles to overcome the blood-brain barrier. J Pharmaceut Technol. 2020;1:26–40. https://doi.org/10.37662/jpt.2020.4
6. Peng Y, Chen L, Ye S, et al. Research and development of drug delivery systems based on drug transporter and nano-formulation. Asian J Pharmaceut Sci. 2020;15:220. https://doi.org/10.1016/J.AJPS.2020.02.004.
7. Sezgin-bayindir Z, Ergin AD, Parmaksiz M, et al. Evaluation of various block copolymers for micelle formation and brain drug delivery: in vitro characterization and cellular uptake studies. J Drug Deliv Sci Technol. 2016;36:120–9. https://doi.org/10.1016/J.JDDST.2016.10.003.
8. Browning KN, Travagli RA. Central nervous system control of gastrointestinal motility and secretion and modulation of gastrointestinal functions. Compr Physiol. 2014;4:1339. https://doi.org/10.1002/CPHY.C130055.
9. Herculano-Houzel S. The human brain in numbers: a linearly scaled-up primate brain. Front Hum Neurosci. 2009;3 https://doi.org/10.3389/NEURO.09.031.2009/FULL.
10. Miller AD, Zachary JF. Nervous system. Pathol Basis Veterin Dis. 2017;805 https://doi.org/10.1016/B978-0-323-35775-3.00014-X.
11. Blanco E, Shen H, Ferrari M. Principles of nanoparticle design for overcoming biological barriers to drug delivery. Nat Biotechnol. 2015;33:941. https://doi.org/10.1038/NBT.3330.
12. Patra JK, Das G, Fraceto LF, et al. Nano based drug delivery systems: recent developments and future prospects. J Nanobiotechnol. 2018;16:71. https://doi.org/10.1186/S12951-018-0392-8.
13. Banks WA. Characteristics of compounds that cross the blood-brain barrier. BMC Neurol. 2009;9:1–5. https://doi.org/10.1186/1471-2377-9-S1-S3/FIGURES/1.
14. Pardridge WM. Drug transport across the blood–brain barrier. J Cereb Blood Flow Metab. 2012;32:1959. https://doi.org/10.1038/JCBFM.2012.126.
15. Nau R, Sörgel F, Eiffert H. Penetration of drugs through the blood-cerebrospinal fluid/blood-brain barrier for treatment of central nervous system infections. Clin Microbiol Rev. 2010;23:858. https://doi.org/10.1128/CMR.00007-10.
16. Bozzuto G, Molinari A. Liposomes as nanomedical devices. Int J Nanomedicine. 2015;10:975. https://doi.org/10.2147/IJN.S68861.
17. Lassmann H. Multiple sclerosis pathology. Cold Spring Harb Perspect Med. 2018;8 https://doi.org/10.1101/CSHPERSPECT.A028936.
18. Zenaro E, Piacentino G, Constantin G. The blood-brain barrier in Alzheimer's disease. Neurobiol Dis. 2017;107:41. https://doi.org/10.1016/J.NBD.2016.07.007.
19. Rua R, McGavern DB. Advances in meningeal immunity. Trends Mol Med. 2018;24:542. https://doi.org/10.1016/J.MOLMED.2018.04.003.
20. Muldoon LL, Alvarez JI, Begley DJ, et al. Immunologic privilege in the central nervous system and the blood–brain barrier. J Cereb Blood Flow Metab. 2013;33:13. https://doi.org/10.1038/JCBFM.2012.153.
21. Hersh DS, Wadajkar AS, Roberts N, et al. Evolving drug delivery strategies to overcome the blood brain barrier. Curr Pharm Des. 2016;22:1177. https://doi.org/10.2174/1381612822666151221150733.
22. Diamond B, Honig G, Mader S, et al. Brain-reactive antibodies and disease. Annu Rev Immunol. 2013;31:345. https://doi.org/10.1146/ANNUREV-IMMUNOL-020711-075041.
23. Sweeney MD, Sagare AP, Zlokovic B, v. Blood–brain barrier breakdown in Alzheimer's disease and other neurodegenerative disorders. Nat Rev Neurol. 2018;14:133. https://doi.org/10.1038/NRNEUROL.2017.188.
24. Klein C, Westenberger A. Genetics of Parkinson's disease. Cold Spring Harb Perspect Med. 2012;2 https://doi.org/10.1101/CSHPERSPECT.A008888.
25. Erickson MA, Banks WA. Blood–brain barrier dysfunction as a cause and consequence of Alzheimer's disease. J Cereb Blood Flow Metab. 2013;33:1500. https://doi.org/10.1038/JCBFM.2013.135.

26. Murphy MP, Levine H. Alzheimer's disease and the β-amyloid peptide. J Alzheimer's Dis. 2010;19:311. https://doi.org/10.3233/JAD-2010-1221.
27. Yamazaki Y, Painter MM, Bu G, Kanekiyo T. Apolipoprotein E as a therapeutic target in Alzheimer's disease: a review of basic research and clinical evidence. CNS Drugs. 2016;30:773. https://doi.org/10.1007/S40263-016-0361-4.
28. Wolfe MS. Unlocking truths of γ-secretase in Alzheimer's disease: what is the translational potential? Future Neurol. 2014;9:419. https://doi.org/10.2217/FNL.14.35.
29. Karran E, Hardy J. A critique of the drug discovery and phase 3 clinical programs targeting the amyloid hypothesis for Alzheimer disease. Ann Neurol. 2014;76:185. https://doi.org/10.1002/ANA.24188.
30. Bertrand L, Nair M, Toborek M. Solving the blood-brain barrier challenge for the effective treatment of HIV replication in the central nervous system. Curr Pharm Des. 2016;22:5477. https://doi.org/10.2174/1381612822666160726113001.
31. Cloutier F, Sears-Kraxberger I, Keachie K, Keirstead HS. Immunological demyelination triggers macrophage/microglial cells activation without inducing astrogliosis. Clin Dev Immunol. 2013;2013 https://doi.org/10.1155/2013/812456.
32. Kenyon LC, Biswas K, Shindler KS, et al. Gliopathy of demyelinating and non-demyelinating strains of mouse hepatitis virus. Front Cell Neurosci. 2015;9 https://doi.org/10.3389/FNCEL.2015.00488/FULL.
33. Zayyad Z, Spudich S. Neuropathogenesis of HIV: from initial neuroinvasion to HIV associated neurocognitive disorder (HAND). Curr HIV/AIDS Rep. 2015;12:16. https://doi.org/10.1007/S11904-014-0255-3.
34. Burt Nabors L, Ammirati M, Bierman PJ, et al. Central nervous system cancers: clinical practice guidelines in oncology. J Nat Comprehen Cancer Netw JNCCN. 2013;11:1114. https://doi.org/10.6004/jnccn.2013.0132.
35. Rees JH. Diagnosis and treatment in neuro-oncology: an oncological perspective. Br J Radiol. 2011;84:S082. https://doi.org/10.1259/BJR/18061999.
36. Meningitis. https://www.who.int/news-room/fact-sheets/detail/meningitis. Accessed 27 Feb 2022.
37. Age as a risk factor for meningococcal disease | CDC. https://www.cdc.gov/meningococcal/about/risk-age.html. Accessed 27 Feb 2022.
38. White K, Ostrowski K, Maloney S, Norton R. The utility of cerebrospinal fluid parameters in the early microbiological assessment of meningitis. Diagn Microbiol Infect Dis. 2012;73:27–30. https://doi.org/10.1016/J.DIAGMICROBIO.2012.02.010.
39. Dando SJ, Mackay-Sim A, Norton R, et al. Pathogens penetrating the central nervous system: infection pathways and the cellular and molecular mechanisms of invasion. Clin Microbiol Rev. 2014;27:691. https://doi.org/10.1128/CMR.00118-13.
40. Brooks LRK, Mias GI. Streptococcus pneumoniae's virulence and host immunity: aging, diagnostics, and prevention. Front Immunol. 2018;9:1. https://doi.org/10.3389/FIMMU.2018.01366.
41. Hayman EG, Wessell A, Gerzanich V, et al. Mechanisms of global cerebral edema formation in aneurysmal subarachnoid hemorrhage. Neurocrit Care. 2017;26:301. https://doi.org/10.1007/S12028-016-0354-7.
42. Stringer JL. Models available for infection-induced seizures. Models Seizures Epilepsy. 2006;521–526 https://doi.org/10.1016/B978-012088554-1/50043-8.
43. Said S, Kang M (2021) Viral encephalitis. StatPearls.
44. Scholten AC, Haagsma JA, Panneman MJM, et al. Traumatic brain injury in the Netherlands: incidence, costs and disability-adjusted life years. PLoS One. 2014;9 https://doi.org/10.1371/journal.pone.0110905.
45. Dewan MC, Rattani A, Gupta S, et al. Estimating the global incidence of traumatic brain injury. J Neurosurg. 2019;130:1080–97. https://doi.org/10.3171/2017.10.JNS17352.

46. Hubbard WB, Lashof-Sullivan M, Greenberg S, et al. Hemostatic nanoparticles increase survival, mitigate neuropathology and alleviate anxiety in a rodent blast trauma model. Sci Rep. 2018;8 https://doi.org/10.1038/S41598-018-28848-2.
47. Shlosberg D, Benifla M, Kaufer D, Friedman A. Blood–brain barrier breakdown as a therapeutic target in traumatic brain injury. Nat Rev Neurol. 2010;6:393. https://doi.org/10.1038/NRNEUROL.2010.74.
48. Griffin JH, Fernández JA, Lyden PD, Zlokovic BV. Activated protein C promotes neuroprotection: mechanisms and translation to the clinic. Thromb Res. 2016;141:S62. https://doi.org/10.1016/S0049-3848(16)30368-1.
49. Robertson MM. The Gilles de la Tourette syndrome: the current status. Arch Dis Child Educ Pract Ed. 2012;97:166–75. https://doi.org/10.1136/ARCHDISCHILD-2011-300585.
50. Akbar U, Ashizawa T. Ataxia. Neurol Clin. 2015;33:225. https://doi.org/10.1016/J.NCL.2014.09.004.
51. Löscher W, Potschka H, Sisodiya SM, Vezzani A. Drug resistance in epilepsy: clinical impact, potential mechanisms, and new innovative treatment options. Pharmacol Rev. 2020;72:606. https://doi.org/10.1124/PR.120.019539.
52. Börü ÜT, Koçer A, Lüleci A, et al. Prevalence and characteristics of migraine in women of reproductive age in Istanbul, Turkey: a population based survey. Tohoku J Exp Med. 2005;206:51–9. https://doi.org/10.1620/TJEM.206.51.
53. Migraine – Symptoms and causes – Mayo Clinic. https://www.mayoclinic.org/diseases-conditions/migraine-headache/symptoms-causes/syc-20360201. Accessed 28 Feb 2022.
54. Aggarwal M, Puri V, Puri S. Serotonin and CGRP in migraine. Ann Neurosci. 2012;19:88. https://doi.org/10.5214/ANS.0972.7531.12190210.
55. Gupta S, Nahas SJ, Peterlin BL. Chemical mediators of migraine: preclinical and clinical observations. Headache. 2011;51:1029. https://doi.org/10.1111/J.1526-4610.2011.01929.X.
56. Negro A, Koverech A, Martelletti P. Serotonin receptor agonists in the acute treatment of migraine: a review on their therapeutic potential. J Pain Res. 2018;11:515. https://doi.org/10.2147/JPR.S132833.
57. Senapati S, Mahanta AK, Kumar S, Maiti P. Controlled drug delivery vehicles for cancer treatment and their performance. Signal Transduct Target Ther. 2018;3 https://doi.org/10.1038/S41392-017-0004-3.
58. Saunders NR, Dreifuss JJ, Dziegielewska KM, et al. The rights and wrongs of blood-brain barrier permeability studies: a walk through 100 years of history. Front Neurosci. 2014;8 https://doi.org/10.3389/FNINS.2014.00404.
59. Weller RO, Sharp MM, Christodoulides M, et al. The meninges as barriers and facilitators for the movement of fluid, cells and pathogens related to the rodent and human CNS. Acta Neuropathol. 2018;135:363–85. https://doi.org/10.1007/S00401-018-1809-Z/FIGURES/4.
60. Banks WA. From blood–brain barrier to blood–brain interface: new opportunities for CNS drug delivery. Nature Rev Drug Disc. 2016;15(4):275–92. https://doi.org/10.1038/nrd.2015.21.
61. Correale J, Villa A. Cellular elements of the blood-brain barrier. Neurochem Res. 2009;34:2067–77. https://doi.org/10.1007/S11064-009-0081-Y/FIGURES/3.
62. Persidsky Y, Heilman D, Haorah J, et al. Rho-mediated regulation of tight junctions during monocyte migration across the blood-brain barrier in HIV-1 encephalitis (HIVE). Blood. 2006;107:4770. https://doi.org/10.1182/BLOOD-2005-11-4721.
63. Engelhardt B, Sorokin L. The blood-brain and the blood-cerebrospinal fluid barriers: function and dysfunction. Semin Immunopathol. 2009;31:497–511. https://doi.org/10.1007/S00281-009-0177-0.
64. Upadhyay RK. Drug delivery systems, CNS protection, and the blood brain barrier. Biomed Res Int. 2014;2014 https://doi.org/10.1155/2014/869269.
65. Sharom FJ. The P-glycoprotein multidrug transporter. Essays Biochem. 2011;50:161–78. https://doi.org/10.1042/BSE0500161.

66. Patel T, Zhou J, Piepmeier JM, Saltzman WM. Polymeric nanoparticles for drug delivery to the central nervous system. Adv Drug Deliv Rev. 2012;64:701. https://doi.org/10.1016/J.ADDR.2011.12.006.
67. Lochhead JJ, Thorne RG. Intranasal delivery of biologics to the central nervous system. Adv Drug Deliv Rev. 2012;64:614–28. https://doi.org/10.1016/J.ADDR.2011.11.002.
68. He Q, Liu J, Liang J, et al. Towards improvements for penetrating the blood–brain barrier—recent progress from a material and pharmaceutical perspective. Cell. 2018;7 https://doi.org/10.3390/CELLS7040024.
69. Kadry H, Noorani B, Cucullo L. A blood–brain barrier overview on structure, function, impairment, and biomarkers of integrity. Fluids Barriers CNS. 2020;17(1):1–24. https://doi.org/10.1186/S12987-020-00230-3.
70. Telano LN, Baker S. Physiology, cerebral spinal fluid. StatPearls; 2021.
71. Simon MJ, Iliff JJ. Regulation of cerebrospinal fluid (CSF) flow in neurodegenerative, neurovascular and neuroinflammatory disease. Biochim Biophys Acta. 2016;1862:442. https://doi.org/10.1016/J.BBADIS.2015.10.014.
72. Pardridge WM. The blood-brain barrier: bottleneck in brain drug development. NeuroRx. 2005;2:3. https://doi.org/10.1602/NEURORX.2.1.3.
73. Aryal M, Fischer K, Gentile C, et al. Effects on P-glycoprotein expression after blood-brain barrier disruption using focused ultrasound and microbubbles. PLoS One. 2017;12 https://doi.org/10.1371/JOURNAL.PONE.0166061.
74. Keller LA, Merkel O, Popp A. Intranasal drug delivery: opportunities and toxicologic challenges during drug development. Drug Deliv Transl Res. 2021;2021:1–23. https://doi.org/10.1007/S13346-020-00891-5.
75. Veronesi MC, Alhamami M, Miedema SB, et al. Imaging of intranasal drug delivery to the brain. Am J Nucl Med Mol Imaging. 2020;10:1.
76. Meredith ME, Salameh TS, Banks WA. Intranasal delivery of proteins and peptides in the treatment of neurodegenerative diseases. AAPS J. 2015;17:780. https://doi.org/10.1208/S12248-015-9719-7.
77. Kublik H, Vidgren MT. Nasal delivery systems and their effect on deposition and absorption. Adv Drug Deliv Rev. 1998;29:157–77. https://doi.org/10.1016/S0169-409X(97)00067-7.
78. Bayindir Z, Yuksel N. Provesicles as novel drug delivery systems. Curr Pharm Biotechnol. 2015;16:344–64. https://doi.org/10.2174/1389201016666150206101443.
79. Sezgin-Bayindir Z, Losada-Barreiro S, Bravo-Díaz C, et al. Nanotechnology-based drug delivery to improve the therapeutic benefits of NRF2 modulators in cancer therapy. Antioxidants. 2021;10:685. https://doi.org/10.3390/ANTIOX10050685.
80. Gültekin HE, Tort S, Tuğcu-Demiröz F, Acartürk F. 3D printed extended release tablets for once daily use: an in vitro and in vivo evaluation study for a personalized solid dosage form. Int J Pharm. 2021;596:120222. https://doi.org/10.1016/J.IJPHARM.2021.120222.
81. Amasya G, Ergin AD, Erkan Cakirci O, et al. A study to enhance the oral bioavailability of s-adenosyl-L-methionine (SAMe): SLN and SLN nanocomposite particles. Chem Phys Lipids. 2021;237 https://doi.org/10.1016/J.CHEMPHYSLIP.2021.105086.
82. Esim O, Hascicek C. Lipid-coated nanosized drug delivery systems for an effective cancer therapy. Curr Drug Deliv. 2020;18:147–61. https://doi.org/10.2174/1567201817666200512104441.
83. Derelí N, Gün Ö, Hasçíçek C, et al, Nanosized drug delivery systems for alzheimer disease treatment. Ankara Üniversitesi Eczacılık Fakültesi Dergisi. 2016;40:54–73. https://doi.org/10.1501/ECZFAK_0000000579.
84. Esim O, Hascicek C. Albumin-based nanoparticles as promising drug delivery systems for cancer treatment. Curr Pharm Anal. 2020;17:346–59. https://doi.org/10.2174/1573412916999200421142008.
85. Din FU, Aman W, Ullah I, et al. Effective use of nanocarriers as drug delivery systems for the treatment of selected tumors. Int J Nanomedicine. 2017;12:7291. https://doi.org/10.2147/IJN.S146315.

86. Mitchell MJ, Billingsley MM, Haley RM, et al. Engineering precision nanoparticles for drug delivery. Nature Rev Drug Discov. 2020;20:101–24. https://doi.org/10.1038/s41573-020-0090-8.
87. 293. Chapter 8 Application of surface activity in therapeutics. Stud Interf Sci. 2005;21:233. https://doi.org/10.1016/S1383-7303(05)80047-X.
88. Carpenter TS, Kirshner DA, Lau EY, et al. Article A method to predict blood-brain barrier permeability of drug-like compounds using molecular dynamics simulations. Biophys J. 2014;107(3):630–41. https://doi.org/10.1016/j.bpj.2014.06.024.
89. Pajouhesh H, Lenz GR. Medicinal chemical properties of successful central nervous system drugs. NeuroRx. 2005;2:541. https://doi.org/10.1602/NEURORX.2.4.541.
90. Ong S, Liu H, Pidgeon C. Immobilized-artificial-membrane chromatography: measurements of membrane partition coefficient and predicting drug membrane permeability. J Chromatogr A. 1996;728:113–28. https://doi.org/10.1016/0021-9673(95)00837-3.
91. Yu H, Wang Q, Sun Y, et al. A new PAMPA model proposed on the basis of a synthetic phospholipid membrane. PLoS One. 2015;10 https://doi.org/10.1371/JOURNAL.PONE.0116502.
92. Avdeef A, Bendels S, Di L, et al. PAMPA – critical factors for better predictions of absorption. J Pharm Sci. 2007;96:2893–909. https://doi.org/10.1002/JPS.21068.
93. Fu BM. Experimental methods and transport models for drug delivery across the blood-brain barrier. Curr Pharm Biotechnol. 2012;13:1346. https://doi.org/10.2174/138920112800624409.
94. Erickson MA, Wilson ML, Banks WA. In vitro modeling of blood–brain barrier and interface functions in neuroimmune communication. Fluids Barriers CNS. 2020;17:26. https://doi.org/10.1186/S12987-020-00187-3.
95. Appelt-Menzel A, Cubukova A, Günther K, et al. Establishment of a human blood-brain barrier co-culture model mimicking the neurovascular unit using induced Pluri- and multipotent stem cells. Stem Cell Reports. 2017;8:894–906. https://doi.org/10.1016/J.STEMCR.2017.02.021.
96. Eigenmann DE, Xue G, Kim KS, et al. Comparative study of four immortalized human brain capillary endothelial cell lines, hCMEC/D3, hBMEC, TY10, and BB19, and optimization of culture conditions, for an in vitro blood-brain barrier model for drug permeability studies. Fluids Barriers CNS. 2013;10 https://doi.org/10.1186/2045-8118-10-33.
97. Miranda-Azpiazu P, Panagiotou S, Jose G, Saha S. A novel dynamic multicellular co-culture system for studying individual blood-brain barrier cell types in brain diseases and cytotoxicity testing. Sci Rep. 2018;8 https://doi.org/10.1038/S41598-018-26480-8.
98. Heymans M, Sevin E, Gosselet F, et al. Mimicking brain tissue binding in an in vitro model of the blood-brain barrier illustrates differences between in vitro and in vivo methods for assessing the rate of brain penetration. Eur J Pharmaceut Biopharmaceut Arbeitsgemeinschaft fur Pharmazeutische Verfahrenstechnik eV. 2018;127:453–61. https://doi.org/10.1016/J.EJPB.2018.03.007.
99. Gartzke D, Fricker G. Establishment of optimized MDCK cell lines for reliable efflux transport studies. J Pharm Sci. 2014;103:1298–304. https://doi.org/10.1002/JPS.23901.
100. Prashanth A, Donaghy H, Stoner SP, et al. Are in vitro human blood–brain–tumor-barriers suitable replacements for in vivo models of brain permeability for novel therapeutics? Cancers. 2021;13:1–20. https://doi.org/10.3390/CANCERS13050955.
101. Barh D, Chaitankar V, Yiannakopoulou EC, et al. In silico models: from simple networks to complex diseases. Anim Biotechnol. 2014;385 https://doi.org/10.1016/B978-0-12-416002-6.00021-3.
102. Williams-Medina A, Deblock M, Janigro D. In vitro models of the blood–brain barrier: tools in translational medicine. Front Med Technol. 2021;0:30. https://doi.org/10.3389/FMEDT.2020.623950.
103. Ferro MP, Heilshorn SC, Owens RM. Materials for blood brain barrier modeling in vitro. Mater Sci Eng R Reports Rev J. 2020;140 https://doi.org/10.1016/J.MSER.2019.100522.

104. Urich E, Patsch C, Aigner S, et al. Multicellular self-assembled spheroidal model of the blood brain barrier. Sci Rep. 2013;3 https://doi.org/10.1038/SREP01500.
105. Elbakary B, Badhan RKS. A dynamic perfusion based blood-brain barrier model for cytotoxicity testing and drug permeation. Scientific Rep. 2020;10:1–12. https://doi.org/10.1038/s41598-020-60689-w.
106. Teixeira MI, Amaral MH, Costa PC, et al. Recent developments in microfluidic technologies for central nervous system targeted studies. Pharmaceutics. 2020;12:1–37. https://doi.org/10.3390/PHARMACEUTICS12060542.
107. Liu X, Fang J, Huang S, et al. Tumor-on-a-chip: from bioinspired design to biomedical application. Microsyst Nanoeng. 2021;7:1–23. https://doi.org/10.1038/s41378-021-00277-8.
108. Choi J, Mathew S, Oerter S, et al. Online measurement system for dynamic flow bioreactors to study barrier integrity of hiPSC-based blood–brain barrier in vitro models. Bioengineering. 2022;9:39. https://doi.org/10.3390/BIOENGINEERING9010039.

Theranostic Nanoparticles for Therapy and Imaging in Cancer Detection

Donald A. Fernandes

1 Introduction

Nanoparticles (NPs) have shown to be promising systems for different biomedical applications, with increased interest in bioimaging, drug delivery, and photothermal and photodynamic therapy. Recent developments in nanotechnology have focused on nanoparticles for both imaging and therapy, referred to as theranostic agents. These types of nanoparticles are advantageous due to their ability to monitor tumor size with their drug loading and/or thermal properties used with varying treatment parameters (i.e., treatment time, radiation power). Such nanoparticles also have the capability to release therapeutic agents only when located at the tumor site under specific stimuli (e.g., electromagnetic waves, pH, temperature), leading to significant cancer cell death. The multimodal imaging and synergistic effect provided by nanoparticles are of particular interest over common chemotherapeutic agents, as it provides the ability to specifically distinguish treated tumors while at the same time being able to combine multiple types of treatments (e.g., photothermal/photodynamic therapy, stimuli sensitive drug release) for eliminating or significantly reducing tumor growth. Over the last few decades, there has been tremendous growth in the development of a variety of nanoparticles, where their physical and chemical properties enable for imaging using various modalities (e.g., magnetic resonance, X-ray computed tomography, positron emission tomography, ultrasound, photoacoustic, fluorescence imaging). This chapter provides a review of nanoparticles that have been used for cancer theranostics by going through the different types of particles developed and the different therapeutic and imaging platforms that can be used.

D. A. Fernandes (✉)
Toronto, ON, Canada
e-mail: dfe.anthony@gmail.com

R. S. Chaughule et al. (eds.), *Nanomaterials for Cancer Detection Using Imaging Techniques and Their Clinical Applications*,
https://doi.org/10.1007/978-3-031-09636-5_6

2 Metal-Based Nanomaterials

2.1 Gold Nanoparticles

Metallic nanoparticles such as plasmonic and magnetic nanoparticles are used for theranostics [1] because of their ability to conjugate a variety of therapeutic agents. Their high stability and absorption properties in the electromagnetic spectrum enable them to be used for effective chemotherapy, phototherapy, and imaging. Gold nanoparticles can be synthesized to carry a variety of chemotherapeutic, genetic material and cell membrane targeting agents (i.e., molecules, ligands, proteins) for the treatment of different types of cancer. Gold nanospheres can be surface functionalized with therapeutic and imaging agents where biotin specifically attaches to receptors overexpressed in cancer cells for enhancing internalization (i.e., through endocytosis). Rhodamine B in particles through fluorescence can be used for determining the localization of chemotherapeutic agent paclitaxel in lung and bone cancer cells [2]. Other spherical gold nanoparticles used for theranostics involve the loading of ligands and fluorescent photosensitizers which produce reactive oxygen species (ROS) upon laser excitation for photodynamic therapy [3], aptamers and chemotherapeutic agents (i.e., doxorubicin, DOX) for treatment and imaging of prostate cancer through X-ray computed tomography [4], and cell binding proteins which upon laser excitation enhances pro-apoptotic pathways and thermal energy for cancer cell death while being able to provide acoustic signals for photoacoustic imaging [5].

Recently, in the last few years, there has been a focus on tuning the absorption properties more towards the infrared region by synthesizing different shapes and sizes of gold nanoparticles such as nanostars [6], nanorods [7], nanoshells [8], and nanoclusters [9]. Gold nanoparticles also allow for flexibility in conjugation of different functional groups on their surface enabling a variety of therapeutic agents to be loaded. For example, gold nanostars (RGD-Au DSNS/siRNA polyplexes) have been synthesized and stabilized with dendrimers for conjugation with peptide molecules such as arginine-glycine-aspartate (RGD) and loading of small interfering RNA (siRNA) for gene therapy and silencing of vascular endothelial growth factor protein present in cancer cells. The particles can also be radiated with near-infrared light for photothermal ablation of cancer cells, with the use of thermal emission and X-ray attenuation from gold for thermal and computed tomography imaging, respectively [10]. Zeta (surface) potential values are in the range of 23.2–27.5 mV and decrease under each N/P ratio (i.e., the molar ratio of primary amines of the dendrimers to phosphates in the siRNA backbone) compared to vector alone. The percentage of U87MG cells displaying Cy3-derived red fluorescence signal when RGD-Au DSNS/Cy3-labeled siRNA polyplexes are transfected (i.e., at the N/P ratio of 20:1) was around 87.6%, while only a small portion of cells treated with free Cy3-labeled siRNA displayed the red fluorescence signal (i.e., 3.1%). This is due to better RGD-mediated targeting to cells expressing $\alpha_v\beta_3$ integrin from RGD-Au DSNS/siRNA polyplexes. Cell viability in glioma U87MG cells was ~20% after

incubation with the RGD-Au DSNS/siRNA polyplexes and 5 min near-infrared (NIR) laser irradiation, compared to 46.9% with only RGD-Au DSNS/siRNA polyplexes, ~90% with nanoparticles without siRNA (i.e., RGD-Au DSNSs), and ~ 70% with siRNA treatment only. Treatment with RGD-Au DSNS/siRNA polyplexes can lead to a significant downregulation of vascular endothelial growth factor (VEGF) protein levels for gene therapy. The computed tomography (CT) values (23.3 Hounsfield units (HU) before injection of particles) in tumor regions increase to 665.7 HU at 10 min post-injection showing high accumulation at the tumor region. Under the same NIR irradiation conditions, the RGD-Au DSNS/siRNA polyplexes were better in inhibiting tumor growth, compared to the RGD-Au DSNSs (without siRNA) group of U87MG tumor-bearing mice, especially at 3, 6, and 9 days post-treatment, and significantly better than the RGD-Au DSNS/siRNA and no NIR irradiation group.

Gold nanoshells can be created by first loading chemotherapeutic agents such as doxorubicin in emulsions before adding gold to the surface through the reduction method. Different magnetic molecules such as manganese-porphyrin (Mn-porphyrin, MnP) can be covalently bound to the surface of nanoparticles through a biocompatible polyethylene glycol (PEG) spacer for magnetic resonance imaging through T_1 relaxation of nuclei. The resulting synergistic effect from the nanoparticles (i.e., DOX@PLA@Au-PEG-MnP) by combining drug loading and photothermal ablation from the generation of heat from gold absorption can significantly reduce tumor growth and volume [11]. Combining the DOX@PLA@Au-PEG-MnP nanoparticles (NPs) with NIR laser irradiation enhances the treatment potency compared to DOX@PLA@Au-PEG-MnP particles only, with IC_{50} values of 14.1 μM and 30.8 μM, respectively, after 48 h of incubation in HT-29 colon cancer cells. Compared to DOX only or PLA@Au-PEG-MnP NPs with NIR laser irradiation, tumor volumes were smaller after treatment with DOX@PLA@Au-PEG-MnP particles and NIR laser irradiation (808 nm, 1.5 W cm^{-2}, 10 min), showing the effectiveness of combinational treatment.

The synergistic effect can also be seen using gold nanoclusters (AuNCs@SiO_2–Ce6) with laser excitation, where a silica coating and covalent binding to a photosensitizer such as chlorin e6 (Ce6) can be achieved through 1-(3-Dimethylaminopropyl)-3-ethylcarbodiimide hydrochloride/N-hydroxysuccinimide (EDC/NHS) reaction leading to both photothermal and photodynamic therapy through the generation of heat and reactive singlet oxygen, respectively [12]. Due to the absorption properties of photosensitizers, these nanoparticles can lead to theranostic capabilities through fluorescence imaging. In vivo experiments show that the nanoparticles can accumulate at the tumor for at least 24 h (Fig. 1a) and with greater accumulation compared to in organs (Fig. 1b, c), showing importance of such nanoparticles for cancer treatment. Treatment of tumors from breast cancer cell line using both nanoparticles and laser excitation (10 min of irradiation, 671 nm, 100 mW cm^{-2}) led to significant decrease in tumor volume compared to initial tumor size (i.e., <50% relative tumor volume at day 14) (Fig. 1d) after 2 weeks showing the ability to reduce the rate of tumor growth.

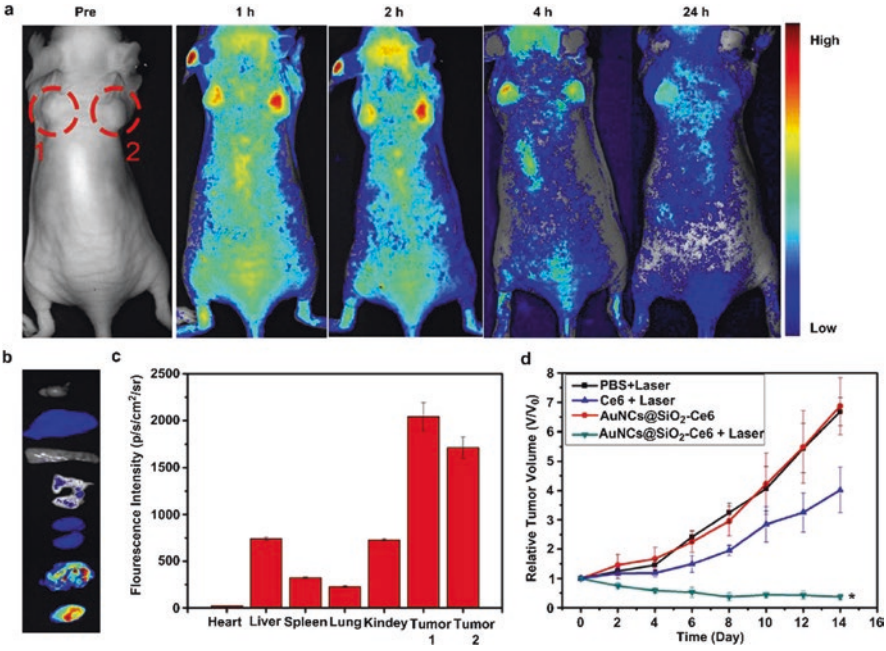

Fig. 1 In vivo photothermal and photodynamic treatment from AuNCs@SiO_2–Ce6. (**a**) Real-time in vivo NIR fluorescence images after intravenous injection of AuNCs@SiO_2–Ce6 in nude mice at different time points, Red circles indicate the location of tumors; (**b**) Ex vivo images of mouse tissues (from top to bottom: heart, liver, spleen, lung, kidneys, tumor 1, tumor 2); (**c**) The fluorescence intensity of organs harvested at 24 h time point from post-injection mice; (**d**) Tumor growth curves of different groups of tumor-bearing mice after treatment. Tumor volumes were normalized to their initial sizes. Error bars represent the standard deviations of 5 mice per group. *, $P < 0.05$. Reprinted from Biomaterials, 34(19), Huang P, Lin J, Wang S, Zhou Z, Li Z, Wang Z, et al., Photosensitizer-conjugated silica-coated gold nanoclusters for fluorescence imaging-guided photodynamic therapy, 4643–54, Copyright (2013), with permission from Elsevier

Different types of nanoparticles can also be combined together for using more than one imaging platform (i.e., multimodal imaging). For example, gold nanorods can be stabilized by a polymer and conjugated to magnetic iron nanoparticles on the surface of each gold nanorod for both magnetic resonance and photoacoustic imaging, with the photothermal effect from both nanoparticles for tumor therapy [13]. One of the most important advantages of multimodal imaging is that the tumors can more precisely be located using contrast from nanoparticles, while at the same time being able to monitor tumors during treatment.

2.2 *Quantum Dots*

Quantum dots are attractive semiconductors for theranostics [14] because of their high quantum yield, size-tunable light emission, and good chemical and photostability. They usually have to be surrounded by a stabilizer such as polymers and silica to reduce their reactivity and improve their biocompatibility. They are mostly composed of elements in groups 12–16 in the periodic Table. A unique property of quantum dots is their broad absorption bands and narrow emission bands and large Stokes shift, enabling multiple nanoparticles to be detected simultaneously (multiplex imaging) that target different regions of biological systems. For example, five different cadmium–selenium or cadmium–tellurium carboxyl quantum dots (Qdots) can be constructed for simultaneous imaging of five different lymphatic basins for predicting the route of cancer metastasis into the lymph nodes [15].

Quantum dots can also be used for dual imaging where tungsten sulfide quantum dots can be used for photoacoustic and computed tomography (CT) with synergistic photothermal therapy and radiotherapy from near-infrared and X-ray excitation, respectively [16]. The nanoparticles can be coated with a lipoic acid conjugated poly(ethylene glycol) (LA-PEG) to improve the biocompatibility of these quantum dots. Fluorescence images of DNA fragmentation and nuclear condensation by staining with Hoechst and γ-H2AX induced by nanoparticles, and/or 808 nm laser lamp (1 W cm^{-2}, 10 min), and/or X-ray radiation (6 Gy) showed significant damage in 4 T1 breast cancer cells. The surviving fraction (% control) from clonogenic assay was <0.05% treated with particles, 808 nm laser lamp radiation (1 W cm^{-2}, 10 min), and X-ray radiation (8 Gy) after 24 h of incubation of cells with particles. Since biocompatibility and rapid clearance due to the immune system are major concerns for theranostics using quantum dots, there are also bioinspired nanoparticles, such as those developed with bovine serum albumin (BSA), to prevent rapid internalization by macrophages and provide greater clinical applicability of such nanoparticles [17].

Molybdenum disulfide (MoS_2) quantum dots with disulfide-doped silica nanoparticles and photosensitizers (i.e., chlorin e6, Ce6) can be designed for tumor targeting (i.e., hyaluronic acid (HA) from particles for attaching to specific cancer cell receptors) and photodynamic therapy and for bioimaging using computed tomography (CT), multispectral optoacoustic tomography (MSOT) and fluorescence (FL) [18]. These nanoparticles allow for trimodal imaging and combination photothermal (PTT) and photodynamic therapy (PDT). Compared to free Ce6, particles with loaded Ce6 and HA (i.e., MoS_2@ss-SiO_2-Ce6/HA) had greater accumulation in tumor sites, with free Ce6 primarily accumulating in the liver. Fluorescence signals from particles were present even after 24 h post-injection, showing good circulation time in blood in 4 T1 tumor-bearing mice.

Copper/carbon quantum dot (or CD)-cross-linked nanosheets (CuCD NSs) can be synthesized (i.e., using hydrothermal treatment) to have high photothermal conversion efficiency and good photothermal stability for multimodal (i.e., photoacoustic, fluorescence) image-guided cancer therapy [19]. The CuCD NSs are internalized by MCF-7 breast cancer cells and captured by lysosomes, before NIR laser

irradiation can release the particles into the cytosol and even the nucleus for increasing the photothermal therapeutic efficiency. Using 3-(4,5-dimethylthiazol-2-yl)-2,5-diphenyl tetrazolium bromide (MTT) assay, MCF-7 cell viability was <20% using CuCD NSs (i.e., at 10–30 μg mL^{-1} Cu) and 808 nm laser irradiation (2 W cm^{-2}) for 10 min, compared to ~70–90% viability with CuCD NSs only and without NIR irradiation. This shows the theranostic capabilities of these particles for breast cancer, with low cytotoxic effects and high biocompatibility from particles alone.

A poly(ethylene glycol) (PEG)-poly-ε-caprolactone (PCL)-polyethylene imine (PEI) triblock copolymer delivery system with entrapped hydrophobic quantum dots can be developed that is capable of delivering nucleic acids and hydrophobic substances (e.g., drugs or dyes) simultaneously. By labeling siRNA with fluorescent AF647 (AF647-siRNA), the nanoparticles can be used as fluorescence resonance energy transfer (FRET)-capable carriers, with confocal microscopy further employed for FRET imaging [20]. FRET can be used for detecting the unpacking of nucleic acid from particles (from FRET efficiency) and for determining effectiveness of carriers, as they have to be designed to release most amount of loaded therapeutic agents once with tumor cells and not during transport.

2.3 Magnetic Nanoparticles

Magnetic nanoparticles have been extensively studied for their theranostic capabilities [21, 22]. Such nanoparticles can exhibit superparamagnetic characteristics enabling significant signal enhancement when located at the tumor region for magnetic resonance imaging (MRI). Different core metals (i.e., cobalt (Co), nickel (Ni), manganese (Mn), iron (Fe)) and their alloys and oxides can be used with coatings of polymers and co-polymers (i.e., polyethylene glycol (PEG), polyethylenimine (PEI), polyvinyl alcohol (PVA), chitosan, dextran, phospholipids), covering nanoparticles through covalent binding and non-covalent (adsorption) interactions for therapeutic loading [23]. Such stabilizers also improve stability, reducing agglomeration, reactivity, and oxidation of particles. Chemotherapeutic agents can be bound to pH-sensitive and biodegradable polymers (i.e., poly(beta-amino ester) (PBAE)) to coat iron oxide nanoparticles, for efficient drug targeting and fast release when in endosomes of cells [24]. Doxorubicin-loaded, iron-containing particles (NP-DOX) showed significant amounts of internalization of iron (Fe) (i.e., 2.24 ± 0.09 pg/cell) after 4 h of incubation with multidrug-resistant glioma cells (i.e., C6-ADR cells) (Fig. 2a) showing that DOX was delivered by cellular internalization, rather than passive diffusion of DOX released by particles from extracellular space. By UV analysis, at 24 h after treatment with NP-DOX, the intracellular concentration of DOX was four-fold higher (i.e., 0.52 ± 0.06 pg/cell) than in cells treated with only DOX (i.e., 0.13 ± 0.01 pg/cell) (Fig. 2b). Such controlled drug release shows the greater effectiveness of NP-DOX in treating drug-resistant cancer cell lines compared to drug alone (Fig. 2c), the latter of which requires higher drug concentrations for treatment due to the presence of multidrug efflux pumps.

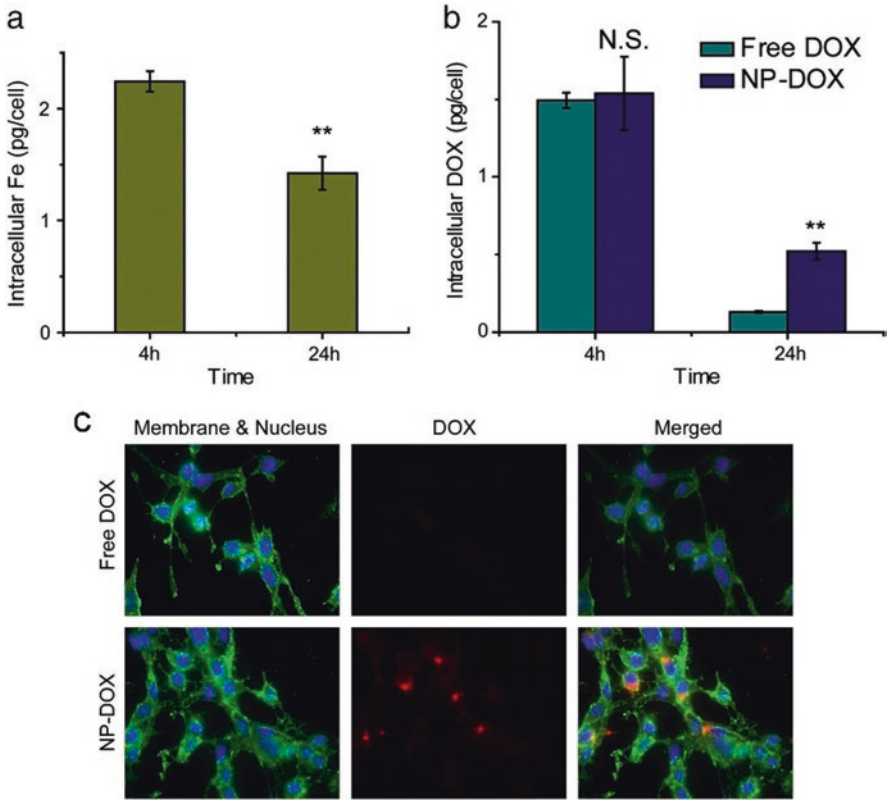

Fig. 2 Cellular internalization studies for free DOX and NP-DOX. (**a**) Intracellular iron quantification of C6-ADR cells at 4 h and 24 h after initial exposure to NP-DOX. (**b**) Intracellular DOX quantification of C6-ADR cells at 4 h and 24 h after initial exposure to NP-DOX or free DOX. N.S. indicates no significance, ** indicates $P < 0.01$, as determined by Student's *t*-test. (**c**) Fluorescence imaging of C6-ADR cells 24 h after the initial incubation with free DOX or NP-DOX, where cell nuclei were shown in blue, the DOX fluorescence in red, and cell membranes in green (WGA-AF488). Reprinted from Journal of Controlled Release, 162(1), Fang C, Kievit FM, Veiseh O, Stephen ZR, Wang T, Lee D, et al., Fabrication of magnetic nanoparticles with controllable drug loading and release through a simple assembly approach, 233–41, Copyright (2012), with permission from Elsevier

The chemical characteristics of nanoparticles can also be changed for internalization in cancer cells. For example, iron oxide nanoparticles can be coated with two polymers, polyacrylic acid (PAA) and polyethylenimine (PEI), through disulfide linkage to increase the positive charge (zeta potential) of particles. Different negatively charged genetic material (i.e., DNA/siRNA) can then be added to the positively charged particle surface through charge interactions, which are released only by the intracellular reducing environment for cancer gene therapy [25]. The superparamagnetic iron oxide (SSPEI60-SPIO) nanoparticles can be used for giving negative contrast in MRI with decrease in T_2 relaxation time with increase in concentration of iron and be used for in vivo tumor therapy and treatment monitoring. From

staining of tissue, the nanoparticles can localize in cancer cells of tumors with some particles also found in organs. Similar to gold nanoparticles, magnetic nanoparticles can also be used for their multiple imaging modality capabilities. For example, molybdenum disulfide/iron oxide (MoS_2/Fe_3O_4) nanoflakes/nanoparticles can be combined and synthesized through hydrothermal route to enhance both the near-infrared (NIR) absorption and photothermal efficiency for use in magnetic resonance and photoacoustic tomography (PAT) imaging [26]. The MoS_2 nanoflakes can be attached to polyethylene glycol (PEG) which can increase the overall biocompatibility of the integrated theranostic agent. Significant cancer cell death can be achieved (i.e., as low as ~5% and ~ 30% viability in HeLa cervical and HepG2 liver cancer cells, respectively) by excitation of nanoparticles using electromagnetic waves, at non-cytotoxic nanoparticle concentrations.

2.4 Upconversion Nanoparticles

Upconversion nanoparticles (UCNPs) are promising theranostic agents [27, 28] because they convert absorbed near-infrared (NIR) light into multi-wavelength, narrow emission bands throughout the ultraviolet-visible-near-infrared (UV-Vis-NIR) spectrum. The NIR excitation to NIR emission conversion from UCNPs is particularly advantageous for in vivo imaging because of deep penetration and reduced absorption and scattering in tissues and organs in the NIR region. Combined with their high photostability and low cytotoxicity, they are effective imaging and therapeutic agents. Nanoparticles of different sizes and with different organic/inorganic shells can be constructed to maximize theranostic capabilities. Benzene-bridged, organosilica-shelled β-$NaLuF_4$:Gd/Yb/Er nanoprobes with a rattle structure can be synthesized for higher luminescence energy transfer efficiency and larger production of singlet oxygen for photodynamic therapy (PDT) [29]. For photodynamic cancer therapy, different photosensitizers which absorb at different wavelengths in the visible-near-infrared region, whether hydrophilic/hydrophobic (i.e., β-carboxyphthalocyanine zinc (ZnPc-COOH), rose Bengal), can be loaded in nanoparticles (UCNP@ROS-ZnPc-COOH). As well, due to the nature of the core of the nanoparticles (i.e., β-$NaLuF_4$), the UCNPs could be used for X-ray computed tomography imaging. In lung cancer cells, excitation of photosensitizer-loaded nanoparticles led to almost complete cell death, at concentrations that are not toxic (without laser excitation). In vitro results for PDT showed that after 4 h of incubation of particles with human H1299 lung cancer cells treated with 980 nm irradiation (0.5 W cm^{-2}, 10 min), viability was about 50% with 0.025 mg mL^{-1} of UCNP@ROS-ZnPc-COOH and less than 12% at concentrations higher than 0.05 mg mL^{-1}. The cell viability with NPs only was higher than 75% showing the high biocompatibility of particles at the same concentrations used for treatment. Different types of metal-based nanoparticles can be synthesized such as cesium [30] and neodymium [31]-based upconversion nanoparticles for drug/peptide loading and imaging, such as X-ray computed tomography and luminescence imaging.

The shell of nanoparticles not only provides particle stability and increased aqueous solubility but also enables loading of different therapeutic agents. Photothermal agents such as dopamine (Dopa) can be transformed into a deprotonated form when incorporated in the mesoporous silica shell with the assistance of polymer polyethylenimine (PEI). Dopa can absorb the blue and green upconversion generated from NIR absorption of UCNPs for photothermal treatment, while the unabsorbed red emission can be used for imaging tumors. The gadolinium (Gd) in the core (i.e., $NaGdF_4$:Yb,Er@$NaGdF_4$:Yb) of particles can be used for T_1-weighted magnetic resonance (MR) (Fig. 3a) and X-ray computed tomography (CT) imaging of tumors (Fig. 3b and c) [32]. Hence loading multiple therapeutic agents in UCNPs and being able to use multiple imaging platforms make such theranostic agents highly effective. The trimodal imaging capability from nanoparticles [33, 34] is especially important as this can enable precise location of tumor regions undergoing treatment as well as be used for monitoring during image-guided therapy.

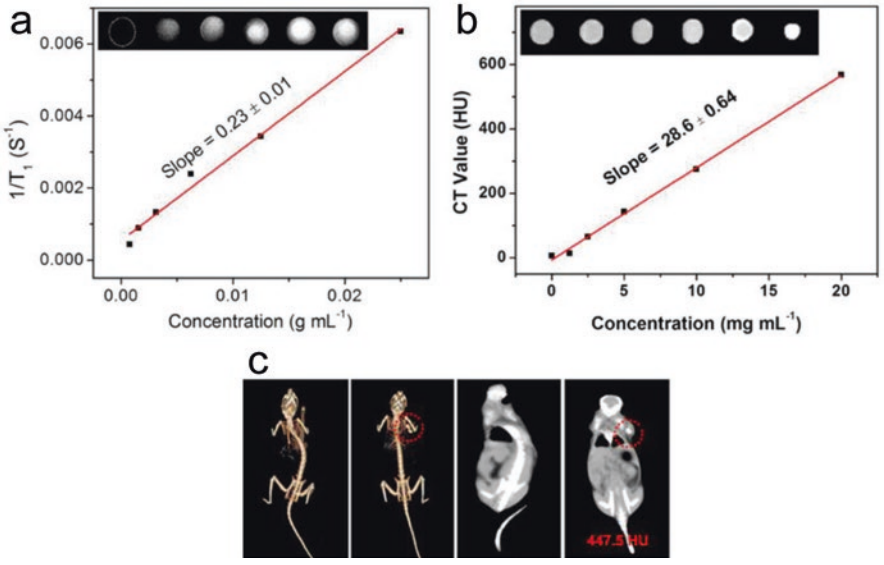

Fig. 3 Magnetic resonance (MR) and X-ray computed tomography (CT) imaging using UCNP@mSiO$_2$-Dopa. The in vitro (**a**) MRI and (**b**) CT images corresponding value as a function of the concentration of UCNP@mSiO$_2$-Dopa. (**c**) In vivo CT images of tumor-bearing Balb/c mouse before and after injection of UCNP@mSiO$_2$-Dopa. Reprinted from Scientific Reports, 7(1), Lv R, Yang P, Chen G, Gai S, Xu J, Prasad PN, Dopamine-mediated photothermal theranostics combined with up-conversion platform under near infrared light, 1–13, Copyright (2017), with permission from Springer Nature under Creative Commons Attribution 4.0 International (CC BY 4.0) License (https://creativecommons.org/licenses/by/4.0/) with no changes

3 Liquid-Based, Aqueous, and Gas-Filled Nanomaterials

3.1 Liposomes

There has been extensive development in liposomes [35] which are characterized by a permeable lipid bilayer with an aqueous internal phase. These vesicle nanoparticles usually contain nontoxic phospholipids and sterols such as cholesterol, which affect the charge, size, stability, and rigidity/fluidity of the bilayer. Multimodal drug-delivering liposomes can be developed for treating different types of cancer [36–38] and can carry different imaging agents for magnetic resonance (e.g., gadolinium, Gd), near-infrared fluorescence (e.g., IRDye 800CW), single-photon emission computed tomography (SPECT), or positron emission tomography (PET) (e.g., using ^{99m}Tc or ^{64}Cu) imaging [39]. For the IRDye-Gd-liposome group, the fluorescence intensities increased till 2 h post-injection, due to retention of particles in tumors with high signals from particles present even after 24 h post infusion. For the free IRDye group, the signals rapidly decreased after injection due to rapid clearance of dye in the circulation system. After 24 h post infusion of IRDye-Gd-liposomes, there is minimal signal in major organs in tumor-bearing rats, showing the ability of particles to accumulate in tumors for theranostics. Signals from images representing gamma radiation emission from isotopes (i.e., ^{99m}Tc) in particles (i.e., ^{99m}Tc-Gd-liposomes) show intratumoral retention and strong signals even at 44 h post infusion.

Liposomes have also been synthesized with photosensitizers [40], which not only generate reactive oxygen species for cancer cell death but also destroy tumor blood vessels. Further incorporating a hypoxia-activated drug (i.e., AQ4N, banoxantrone) can lead to a synergistic effect for further cancer cell death in tumors. Due to the optical properties of the photosensitizer Ce6, such nanoparticles can be used for both fluorescence and photoacoustic imaging, while the addition of ^{64}Cu isotope through chelation can lead to a triple-modal imaging agent [41]. PET imaging shows that the nanoparticles can gradually accumulate over a 24-h period after injection of nanoparticles (Fig. 4a). By quantitative analysis of PET images, the accumulation of liposomes with both AQ4N and Ce6 (i.e., in terms of percentage injected dose per gram, % ID/g) in breast tumors increased linearly till 4 h post-injection and remained relatively constant after 20 h suggesting their high circulation time in the blood required for theranostics (Fig. 4b). The pharmacokinetic and biodistribution profiles were consistent with those from recording the radioactivity (i.e., from ^{64}Cu from particles) from organs/tissues using a gamma counter after 24 h post-injection of particles, which had tumor signals greater than those from many organs/tissues (Fig. 4c). After 24 h injection of AQ4N-*h*Ce6-liposome, photoacoustic (PA) (Fig. 4d) and fluorescence (FL) signals (Fig. 4e) were about ~2.5 and ~1.5 times higher than those without AQ4N-*h*Ce6-liposome injection (Fig. 4f, g), showing the ability of particles to efficiently accumulate in tumors through passive targeting and the enhanced permeability and retention (EPR) effect.

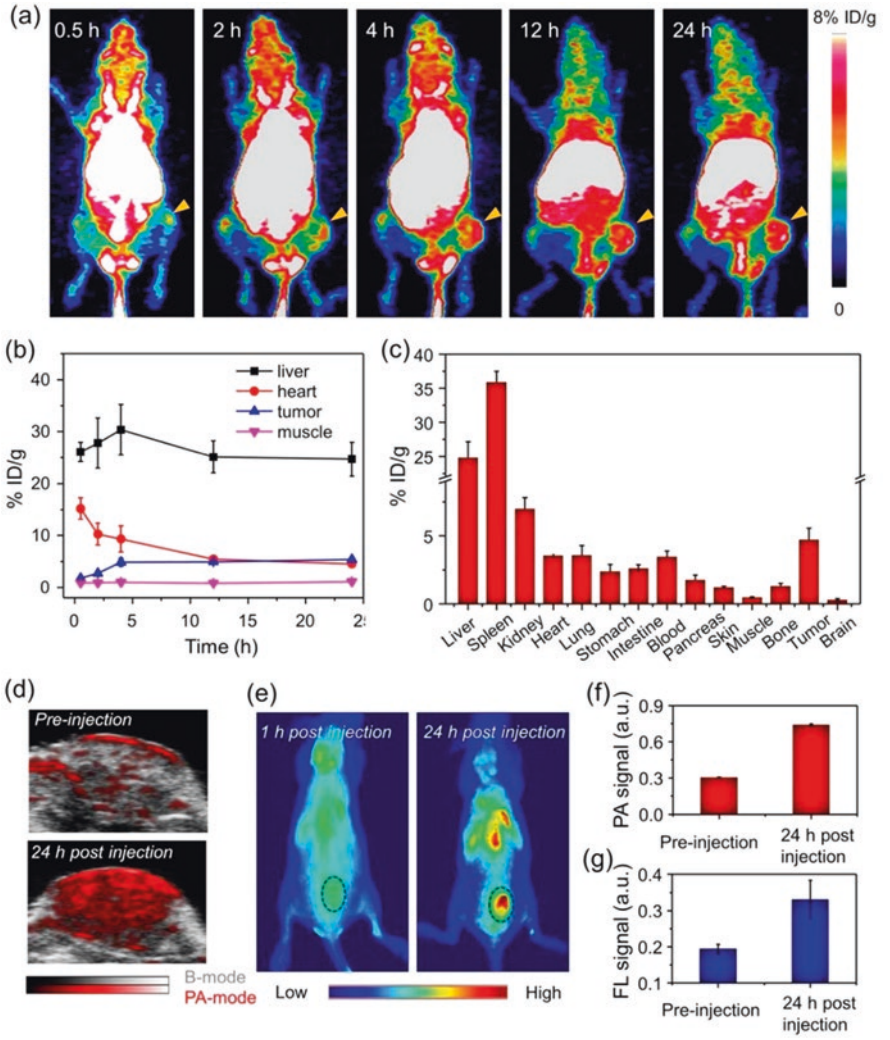

Fig. 4 In vivo multimodal imaging and pharmacokinetic behaviors of AQ4N-*h*Ce6-liposome. (**a**) PET images of 4T1 tumor-bearing mice with intravenous (i.v.) injection of $^{64}Cu^{2+}$-labeled AQ4N-*h*Ce6-liposome recorded at different time intervals post-injection (p.i). The tumors are indicated with yellow arrows. (**b**) Quantification of AQ4N-^{64}Cu-*h*Ce6-liposome levels in the liver, heart, tumor, and muscle of 4T1 tumor bearing mice at various time points p.i. (**c**) Biodistribution of AQ4N-^{64}Cu-*h*Ce6-liposome in various organs and tissues of 4T1 tumor-bearing mice at 24 h p.i. as determined by ^{64}Cu radioactivity measurement by a gamma counter. Error bars were based on the standard errors of the mean of triplicate samples. (**d**) PA imaging of tumor regions recorded before and 24 h post-i.v. injection of AQ4N-*h*Ce6-liposome. (**e**) Fluorescence imaging of 4T1 tumor-bearing mice with i.v. injection of AQ4N-*h*Ce6-liposome at 1 and 24 h p.i. The tumors are indicated with black dashed circles. (**f** and **g**) Semi-quantitatively analyzing the PA (**f**) and fluorescence (FL) signal (**g**) of AQ4N-*h*Ce6-liposome in tumors based on the images shown in (**d** and **e**). Error bars were based on triplicate measurements. Reprinted with permission from Feng L, Cheng L, Dong Z, Tao D, Barnhart TE, Cai W, et al., Theranostic liposomes with hypoxia-activated prodrug to effectively destruct hypoxic tumors post-photodynamic therapy. ACS Nano. 2017;11(1):927–37. Copyright (2017) American Chemical Society

Liposomes can also be controlled to release drugs due to the phase transition (i.e., gel to liquid) of specific lipids (e.g., dipalmitoylphosphatidylcholine (DPPC), 1-tetradecanoyl-2-octadecanoyl-*sn*-glycero-3-phosphocholine (MSPC)) which make liposomes more permeable above physiological temperature (e.g., 40–45 °C). The phase transition can be triggered by localized hyperthermia, releasing the encapsulated near-infrared dyes and drugs from nanoparticles. For example, indocyanine green (ICG) and doxorubicin (DOX) can be co-encapsulated in liposomes, while folate and conjugated gadolinium (Gd) can be used to enhance cancer cell targeting and for magnetic resonance imaging, respectively [42]. Since ICG can act as a photodynamic therapeutic agent upon near-infrared laser excitation, combining both ICG and DOX can lead to significant cancer cell death.

3.2 Nanoemulsions

Nanoemulsions like liposomes are liquid colloids that enable the capability of loading imaging and therapeutic agents both in the core and shell of particles [43–45]. The stability of emulsions depends on amphiphilic emulsifying agents, which reduce the interfacial tension between the two immiscible phases (i.e., aqueous continuous and oil phase inside nanoemulsions). Compared to liposomes, nanoemulsions provide the ability for water-insoluble drugs to be loaded in the hydrophobic core by mixing different amounts of oil for optimizing drug loading/encapsulation and overall size of nanoparticles [46]. Poorly soluble drugs in aqueous environments, such as platinum-based ovarian cancer drugs, cisplatin, and myrisplatin, can be loaded in the core by mixing with an oil (i.e., flax seed oil), prior to emulsification with gadolinium-attached lipids (i.e., for MRI) and endothelial growth factor receptor (EGFR) ligands for enhancing active targeting [47]. The plasma pharmacokinetic profile of the platinum-based drugs can be improved when administered in nanoemulsions as compared to drug only, with no significant changes seen in drug concentration in blood plasma after 24 h in circulation (i.e., after intravenous (IV) and intraperitoneal (IP) administration in nude mice). By analysis of the MRI T_1 signals in tumors, the gadolinium-containing, EGFR-targeted nanoemulsion group showed sustained accumulation over a period of 24 h post-injection of particles, in mice bearing subcutaneous SKOV-3 (ovarian) tumor xenografts. The myrisplatin and C_6-ceramide-loaded, EGFR-targeted theranostic nanoemulsion group of mice could survive much longer compared to mice treated with drug (i.e., cisplatin) only or control mice with no treatment. Loading drugs in emulsions not only increases the amount of such poorly soluble drugs reaching the tumor but also reduces generalized toxicity, including acute nephrotoxicity, chronic neurotoxicity, and adverse gastrointestinal reactions apparent when delivering such drugs without encapsulation in particles.

Important type of theranostic nanoemulsions are optically triggered droplets that can undergo vaporization, due to the incorporation of volatile, phase change perfluorocarbons. This involves the addition of optically absorbing intrinsic

molecules/addition of particles such as gold nanoparticles which can enable such emulsions to undergo a phase transition into bubbles. Different types of fluorescent imaging agents (i.e., 2-(4,4-Difluoro-5-Methyl-4-Bora-3a,4a-Diaza-*s*-Indacene-3-Dodecanoyl)-1-Hexadecanoyl-*sn*-Glycero-3-Phosphocholine, BODIPY 500/510) and drugs (i.e., DOX, PXT, 5-FU) can be loaded, while the conversion process of the nanoemulsions into bubbles provide significant pressure for both cancer cell damage and photoacoustic imaging [48–51]. The resulting bubbles that form can also be used for contrast imaging (i.e., nonlinear ultrasound (NL US) imaging) [52, 53], making these nanoparticles multimodal imaging and therapeutic agents. Such biocompatible theranostic agents can be used at high concentrations without causing significant cytotoxicity while being able to provide significant contrast from tumors loaded with nanoparticles. In addition, other studies have shown that combining both pulsed laser and ultrasound (US) excitation can reduce the overall energy required to convert the nanoemulsions into bubbles, enhancing signal-to-noise ratio and suppressing linear background photoacoustic (PA) and ultrasound (US) signals [54].

The vaporization mechanism for converting droplets into bubbles required for contrast imaging and therapy can also be achieved magnetically (i.e., termed magnetic droplet vaporization, MDV), enabling treatment and imaging of large tumors using a magnetic induction coil. Magnetic nanoparticles such as iron oxide (Fe_3O_4) nanoparticles can be excited using a magnetic field for converting emulsions into bubbles [55]. The heating from iron oxide nanoparticles using alternating current (AC) can lead to vaporization of the perfluorocarbon (perfluorohexane, PFH) core of particles. The resulting bubbles can be used for B-mode and contrast enhanced ultrasound (CEUS) imaging of tumors of nude mice, with signals greater than those in tumors without particles, or particles with no PFH (Fig. 5a). Furthermore, after treatment using nanoparticles with AC magnetic field for 6 min a day for 2 days, the tumors with PFH-PMMs and PMMs were nearly eradicated after 2 weeks compared to tumors with saline only (Fig. 5b). Furthermore, after treatment using nanoparticles with AC magnetic field for 6 min a day for 2 days, the tumors with PFH-PMMs and PMMs were nearly eradicated after 2 weeks compared to tumors with saline (phosphate-buffered saline, PBS) only (Fig. 5b). Staining with hematoxylin and eosin (H.E) of tumor tissue showed clear boundary between untreated and treated cancer cells from vaporization of particles. There was also increased apoptosis after treatment with magnetic droplet vaporization, seen using TUNEL (terminal deoxynucleotidyl transferase dUTP nick end labeling) staining, showing DNA breaks consistent with low levels of expression of cell death regulating protein Bcl-2 (B-cell lymphoma 2) (Fig. 5c).

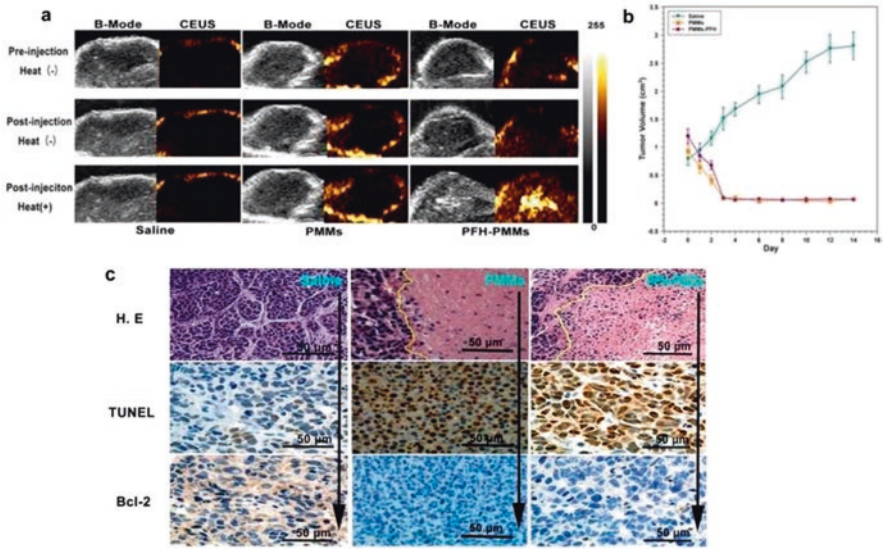

Fig. 5 In vivo ultrasound imaging and treatment using PFH-PMMs. (**a**) Ultrasound images of tumors injected with saline, 40 mg mL^{-1} PMMs or 40 mg mL^{-1} perfluorohexane (PFH)-loaded porous magnetic microspheres (PFH-PMMs) pre- and post-magnetic heating treatment. (**b**) Tumor growth curve of saline (cyan), PMMs (gold) and PFH-PMMs (purple) group after the exposure to the alternating current (A.C.) magnetic field. (**c**) Histopathological sections of tumor tissues from nude mice from the saline (left), PMMs (centre) and PFH-PMMs (right) group. Reprinted with permission from Wang R, Zhou Y, Zhang P, Chen Y, Gao W, Xu J, et al., Phase-transitional Fe_3O_4/perfluorohexane microspheres for magnetic droplet vaporization. Theranostics. 2017;7(4):846. Copyright (2017) Ivyspring International Publisher (distributed under Creative Commons Attribution (CC BY-NC) License at https://creativecommons.org/licenses/by-nc/4.0/ with no changes)

3.3 Nanogels

Nanogels are nanoparticles consisting of cross-linked polymer/biopolymer networks. The ability of nanogels to attach different functional groups and to swell and degrade upon environment stimuli (e.g., temperature, laser excitation, pH) provides versatile opportunities for the storage and controlled release of various therapeutic (e.g., drugs, proteins) and contrast imaging agents [56, 57]. Nanogels with a dense carbohydrate galactose shell can contain clinical drugs and radiosensitizers (e.g., iodoazomycin arabinofuranoside, IAZA) specifically targeting hypoxic tumors for radio-theranostics [58]. Theranostic agents are released due to a temperature-responsive cross-linked core (P(LAEMA)-*b*-P(DEGMA-*st*-MBAm) where LAEMA is 2-lactobionamidoethyl methacrylamide, DEGMA is di(ethylene glycol) methyl ethyl methacrylate, and MBAm is the cross-linker *N,N′*-methylenebis(acrylamide)). The nanogels have good drug loading capacity with the highest encapsulation efficiency of 58.86 ± 4.22% with 1 mM of IAZA. Due to a reversible lower critical solution temperature (LCST) phase transition, controlled drug release is possible due to swelling of nanogels from physiological temperature (i.e., 37 °C) to

25 °C. With the inclusion of radiosensitizers and X-ray radiation, there is significant decrease in survival of cancer cells, with the possibility of photon emission tomography-based imaging of tumors when therapeutic agents are labeled with radionuclides. Results from clonogenic survival assay showed less than 20% surviving fraction for HepG2 HCC liver cancer cells treated with nanogels containing IAZA and 12 Gy radiation dose.

To take advantage of both the temperature-dependent release of therapeutic agents (i.e., temozolomide) and imaging, immobilization of Bi_2O_3 quantum dots (QDs) (Bi_2O_3@PVA) in the interior of poly(vinyl alcohol) (PVA) nanogels can be achieved [59]. The drug release for nanogels through phase transition can be quicker for treatment of cancer cells when the temperature is increased from 37 °C to 40 °C in tumors. At the same time, the quantum dots in nanogels enable for fluorescence imaging for theranostics. Nanogels can be designed for theranostics, by cross-linking the folate-terminated poly(ethylene glycol) (FA-PEG-NH_2) and rhodamine B (RhB)-terminated poly(ethylene glycol) (RhB-PEG-NH_2) modified oxidized alginate (OAL-*g*-PEG-FA/RhB) with cystamine (Cys), with covalent conjugation of therapeutic agents *via* acid-labile Schiff base bond [60]. These nanoparticles are pH/reduction dual responsive due to the multi-functionalities of oxidized alginate (OAL) and acid-labile Schiff base conjugation for drug (i.e., doxorubicin, DOX). The particles can be used for fluorescence imaging, due to the incorporation of rhodamine B. The DOX-COAL-*g*-PEG-FA/RhB theranostic prodrug nanogels show excellent antitumor activity with viability of the HepG2 liver cancer cells decreasing to 46% at the concentration of 100 μg mL^{-1}, compared to >85% viability from nanogels without DOX at the same concentration. Other nanoparticles for theranostics include Fe_3O_4-poly(acrylic acid) nanogels for MRI [61], Gd-/CuS-loaded functional nanogels for MRI and photoacoustic (PA) imaging [62], and polypyrrole nanogels for PA imaging [63].

Nanogels can be synthesized with hyaluronic acid (i.e., through disulfide bonding) [64]. Compared to healthy mice without tumor (Fig. 6a) and tumor-bearing mice (Fig. 6b), increase in fluorescence signals was seen from laser excitation of graphene-doxorubicin-hyaluronic acid (GDH) nanogels in tumor-bearing mice (Fig. 6c). From doxorubicin fluorescence, nanogels were found in all main organs but with lower signals, for reduced systemic toxicity and reduced clearance from the reticuloendothelial system (RES). Compared to graphene with attached doxorubicin, nanoparticles with graphene and doxorubicin had greater accumulation (i.e., ~2 times higher fluorescence signals) in tumors due to less accumulation in other tissues (Fig. 6d). Tumor-bearing mice treated with saline and doxorubicin did not show tumor regression, with volumes of tumors remaining relatively constant over 18 days with treatment with GDH nanogels. With the addition of laser excitation (670 nm for 30 min, 1 W cm^{-2}), the GDH nanogels could reduce tumor volumes from 95 mm^3 to 60 mm^3 (Fig. 6e). The nanoparticles can effectively treat tumors without causing negative biological effects in healthy tissue as seen through histological analysis and little differences in body weight (Fig. 6f).

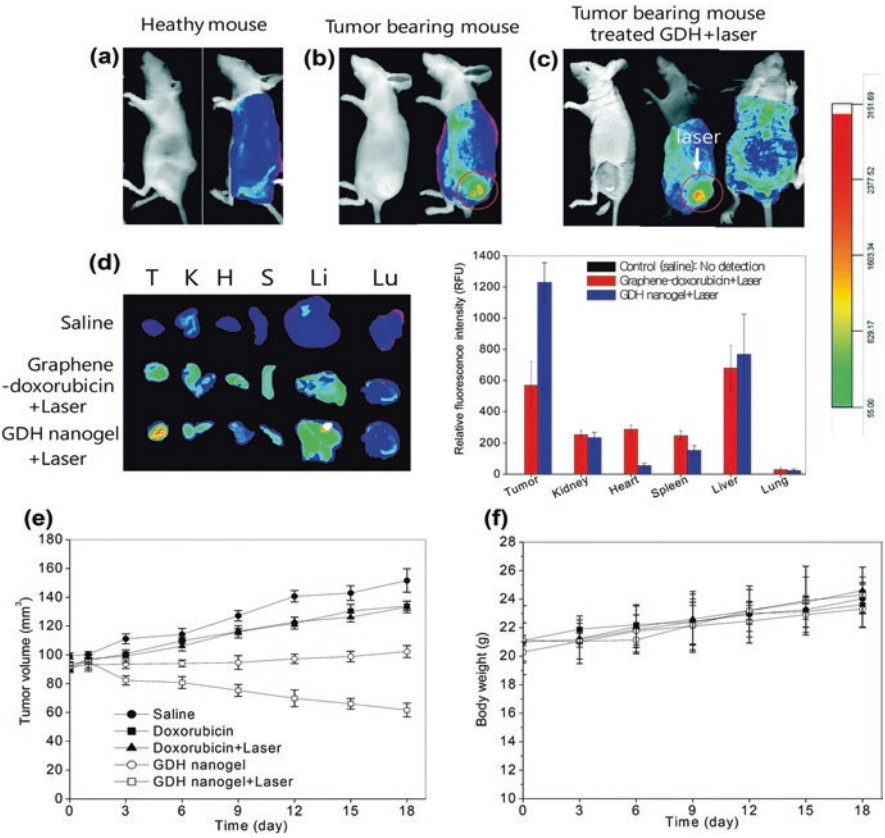

Fig. 6 In vivo optical imaging and thermo-chemotherapy using graphene-doxorubicin-hyaluronic acid (GDH) nanogels. (**a**) and (**b**) are optical imaging of healthy mice and tumor bearing mice, respectively. (**c**) Light responsive imaging. The nanogels were intravenously injected and 670 nm laser was applied to the tumors for 30 minutes. (**d**) Ex vivo imaging and fluorescence intensities of tumors and normal tissues. Organs were arranged in the following order: tumor (T), kidney (K), heart (H), spleen (S), liver (Li), and lung (Lu). (**e**) Thermo-chemotherapy after treating doxorubicin and the nanogels with and without laser irradiation. (**f**) Body weight changes of mice after treatment with the nanogels. The data were plotted as mean ± SEM ($n = 5$). Republished with permission of the Royal Society of Chemistry (Nanoscale) from, A hyaluronic acid nanogel for photo–chemo theranostics of lung cancer with simultaneous light-responsive controlled release of doxorubicin, Khatun Z, Nurunnabi M, Nafiujjaman M, Reeck GR, Khan HA, Cho KJ, et al., 7(24), 2015; permission conveyed through Copyright Clearance Center

3.4 Micro-/Nano-bubbles

Bubbles are gas filled particles that can be used for therapy and imaging, with many already approved for clinical use (e.g., Definity by Lantheus Medical Imaging, SonoVue® by Bracco Diagnostics) [65]. Specifically, ultrasound when used with bubbles can provide noninvasive, image-guided and site-specific treatment.

Scattered ultrasound from oscillating bubbles can be used to detect tumors after accumulation of bubbles while being able to load different drugs in the shell. Compared to conventional microbubbles, perfluoropropane gas core microbubbles (i.e., camptothecin-floxuridine CF MBs) can be engineered with high drug loading capacity (up to 56.7 ± 2.3%) for different therapeutic agents (i.e., camptothecin (CPT), floxuridine (FUDR)) through the use of a mechanical agitation method [66]. Contrast-enhanced ultrasound imaging can be used for imaging treated tumor regions while also being able to convert the bubbles into nanoparticles (CF NPs) for drug release once accumulated. The inertial acoustic cavitation of the MBs can cause sonoporation leading to enhanced cell membrane permeation and cellular drug uptake. Results from in vitro studies showed fluorescence in the CF MBs + ultrasound (US) group of cells increased by 3.48-fold due to the effect of sonoporation, compared to the group without US exposure. Cell viability of 4T1 breast cancer cells was less than 20% after treatment with camptothecin-floxuridine (i.e., CF concentration at 20 μM) MBs + US (1 W cm^{-2}, 1 min) for 4 h and incubation for 72 h. The 4 T1 tumors in mice grew slower and were also seen by immunohistochemical evaluation of Ki67 with camptothecin-floxuridine (CF) MBs + US (1.03 MHz, 50% duty, 1 W cm^{-2}, 3 min) with a final tumor volume of ~500 mm^3 at 14 days after treatment, compared to ~1900 mm^3 with PBS only. Nanoparticles can also be created for specifically targeting cancer cells (i.e., through folate-targeted binding of receptors), followed by triggered drug release and formation of CO_2 bubbles due to heating and decomposition of encapsulated ammonium bicarbonate (NH_4HCO_3) [67]. Upon near-infrared laser irradiation with inclusion of a photothermal agent (IR780), the lipid bilayer of particles (i.e., IR780-BTSL-FA-thermosensitive bubble-generating liposome) becomes more permeable for rapid drug release. With near-IR laser irradiation (780 nm, 1 W cm^{-2}, 15 min) of thermosensitive bubble-generating liposome IR780-BTSL-FA (i.e., at doxorubicin concentration of 100 μg mL^{-1}) after 4 h of incubation of cancer cells, viability was less than 20% for KB human epidermoid carcinoma cells and ~ 40% for A549 human lung cancer cells. In vivo results from tumor-bearing mice treated with both IR780-BTSL-FA and laser irradiation demonstrated the greatest inhibitory effect on tumor growth, showing decrease in tumor volume after treatment, compared to tumors not treated (i.e., saline only injected in mice). After treatment with laser irradiation of nanoparticles, the reduction in body weight of mice was not significant, and no significant organ damage (i.e., necrotic cells) was observed (i.e., through histological evaluation of tissue) suggesting their good biocompatibility and low toxicity.

Nanoparticles can also be synthesized containing bubbles. For example, a doxorubicin-loaded superparamagnetic PLGA-iron oxide multifunctional theranostic agent can be developed for dual-mode US/MR imaging of lymph nodes, which play an important role in the spread of cancer. Ultrasound (US) can be used to release drugs from bubbles for therapy of metastasis in lymph nodes [68]. Immunohistochemical evaluation revealed significantly less proliferating tumor cells, greater apoptotic cells and lower lymphatic microvessel density (LMVD) through proliferating cell nuclear antigen (PCNA), terminal deoxynucleotidyl transferase dUTP nick end labeling (TUNEL) and lymphatic vessel endothelial

hyaluronan receptor (LYVE-1) immunohistochemical staining, respectively. Nanoparticles can also be synthesized consisting of a volatile liquid such as perfluoropentane (PFP), with superparamagnetic iron oxide (SPIO) and light-absorbing dye (i.e., DiR) in the shell [69]. Upon laser irradiation in the near-infrared, the particles convert into bubbles and can be used for magnetic resonance (MR)/photoacoustic (PA)/ultrasound (US)/near-infrared fluorescence (NIRF) multimodal imaging. This optical droplet vaporization (ODV) process can lead to cancer cell death through the generation of significant pressure from the expansion of particles into bubbles.

4 Carbon-Based Nanomaterials

4.1 Fullerene Nanoparticles

Carbon-based nanomaterials have several key advantages over other theranostic agents. Due to their ability to contain a lot of carbon atoms, nanoparticles have high stability in vivo, larger surface area for functionalization, unique electrical and conducting properties, and large space for loading and delivering therapeutic and imaging molecules.

Fullerenes contain carbons that are connected to each other by single or double bonds to form a mesh with fused rings of five to seven atoms, to form different shapes such as hollow spheres (e.g., C_{60}) and ellipsoids (e.g., C_{70}, C_{84}). Fullerenes have various applications in tumor theranostics [70, 71]. For example, a eukaryotic cell-like nanoplatform (EukaCell) can be synthesized to contain a nucleus-like fullerene core, cytoskeleton-like mesoporous silica matrix, and a phospholipid membrane which make the entire nanoparticle more soluble [72]. Both therapeutic and fluorescence imaging agents such as doxorubicin (DOX) and indocyanine green (ICG) can be loaded in nanoparticles through interaction with both silica and fullerene and between DOX and ICG. Both the amount of drug and imaging agent encapsulated in nanoparticles can be controlled by varying the ratio of the amounts of DOX to ICG. The highest encapsulation efficiency and loading content of DOX for

Fig. 7 (continued) intensity of DOX in PC-3 cells treated with LC60S-DI nanoparticles and laser irradiation showing a higher DOX LC results in significantly stronger DOX fluorescence in the cells. DOX (in LC60S-DI nanoparticles) concentration: 10 μg ml^{-1}. Error bars represent ± s.d. ($n > 50$). *$P < 0.05$ (Mann–Whitney *U*-test). (**g**) Release of DOX from LC60S-DI nanoparticles in PBS showing that given the same DOX concentration (0.1 mg ml^{-1}), NIR laser irradiation can induce more drug release from the nanoparticles with a higher drug loading content (LC). The unspecified ratios of DOX to LC60S nanoparticle and DOX to ICG for making the LC60S-DI nanoparticles were 1:20 and 1:1, respectively. The NIR laser irradiation was at 1.5 W cm^{-2} for either 3 (**a**–**c**) or 1 min (**d**–**g**). Reprinted from Nature Communications, 6(1), Wang H, Agarwal P, Zhao S, Yu J, Lu X, He X, A biomimetic hybrid nanoplatform for encapsulation and precisely controlled delivery of theranostic agents, 1–13, Copyright (2015), with permission from Springer Nature (distributed under Creative Commons Attribution 4.0 International (CC BY 4.0) License at https://creativecommons.org/licenses/by/4.0/ with no changes)

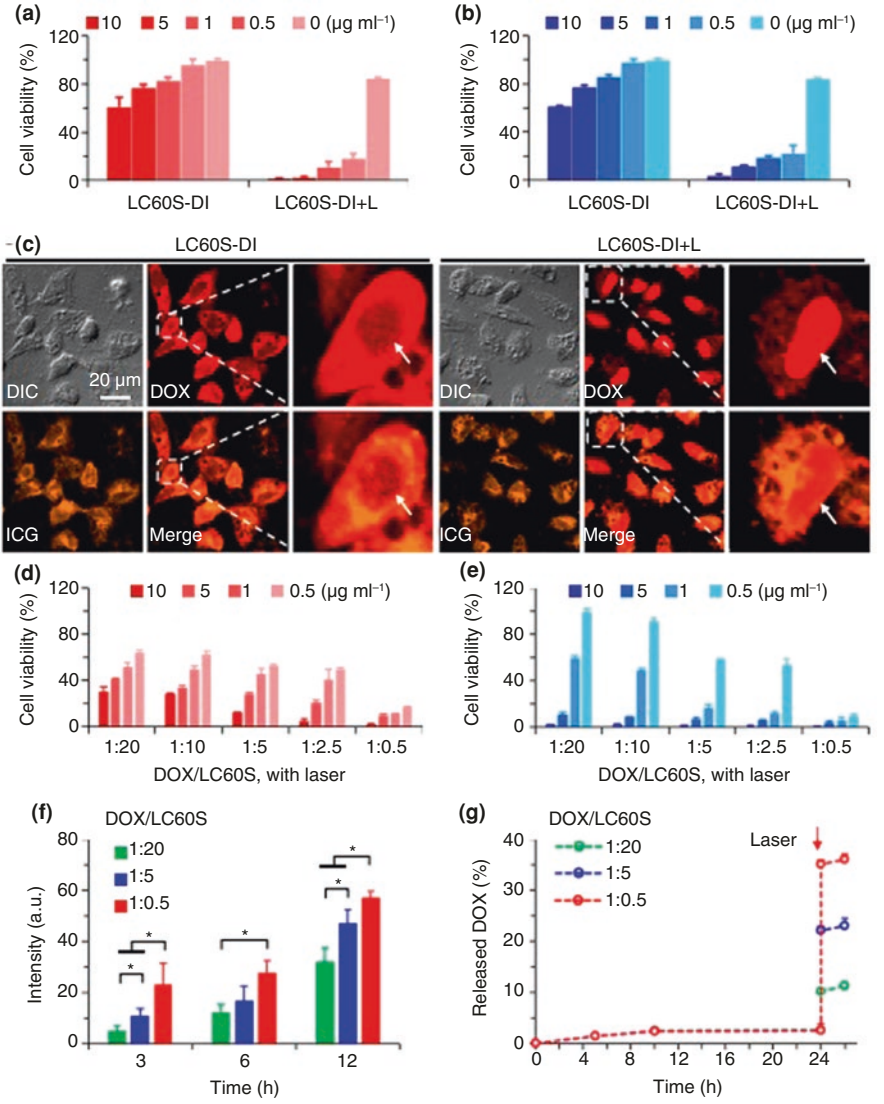

Fig. 7 Cancer cell imaging and treatment with phospholipid bilayer-coated fullerene (LC60S) nanoparticles. Viability of (**a**) PC-3 and (**b**) MDA-MB-231 cancer cells after treated with LC60S-DI (with doxorubicin and indocyanine green) nanoparticles at different concentrations without or with NIR laser (L) irradiation. (**c**) Confocal images showing the DOX and ICG delivered using LC60S-DI nanoparticles are mainly in the cytosol before NIR laser irradiation. With NIR laser irradiation, the enhanced delivery of DOX into the nuclei is evident probably due to the irradiation-induced release of DOX from the nanoparticles. The arrows indicate cell nuclei. Viability of (**d**) PC-3 and (**e**) MDA-MB-231 cancer cells after treated with LC60S-DI nanoparticles made at different drug feeding ratios (i.e., different loading contents, LCs) and NIR irradiation. The data show that the LC60S-DI nanoparticles with higher drug loading content (LC) is more potent against both types of cancer cells at all the four doses. (**f**) The mean fluorescence

(continued)

nanoparticles was seen for feeding ratios of 1:0.5 and 1:0.25 (i.e., DOX/nanoparticle) after mixing for 0.5 and 14 h. At the same time, the amount of theranostic agents that can be released can be controlled by the intensity, duration of laser excitation, and pH of the environment, serving as an important cancer theranostic agent. Encapsulating both DOX and ICG can lead to significant tumor size reduction as ICG is a photosensitizer which results in the generation of reactive oxygen species (ROS) upon near-infrared laser excitation of particles. Results show that phospholipid-coated fullerene particles with DOX and ICG can result in cancer cell viability less than 50% with laser excitation of particles, leading to almost complete death of all cells at highest concentration (i.e., 10 μg mL^{-1}) for both PC-3 prostate (Fig. 7a) and MDA-MB-231 breast cancer cells (Fig. 7b). Compared to without laser irradiation, once internalized in cells, laser irradiation leads to efficient release of therapeutic agents that are able to enter nuclei more, seen by greater fluorescence signals (Fig. 7c). Both the cell viability and amount of drug reaching nuclei for therapy can be optimized by increasing the feeding ratio (i.e., DOX/LC60S nanoparticle) with greatest therapeutic effect seen using 1:0.5 ratio (Fig. 7d–f), with laser irradiation leading to ~35% DOX release (Fig. 7g).

Carboxyl groups containing fluorescent C_{60}–COOH nanoparticles can be prepared via a one-step thiol-ene click reaction for increased water dispersibility, lower cytotoxicity, and outstanding fluorescence properties [73]. Anticancer agents such as cisplatin can be loaded on C_{60}–COOH nanoparticles, with greater drug release in acidic environments (i.e., in tumors and endosomes/lysosomes) at pH 5.5 compared to 7.4. Multifunctional fullerene nanoparticles (^{64}Cu-NOTA-C_{60}-PEG-cRGD) can be conjugated with cyclo (Arg-Gly-Asp) peptides (cRGD) for targeting of integrin $\alpha_v\beta_3$ for cellular internalization. The particles can also contain radiolabels (i.e., ^{64}Cu) for positron emission tomography (PET), with in vivo results showing fast renal clearance profiles making these particles promising and safe theranostic nanoparticles [74]. Fullerene (C_{60})-gold (Au) aggregates can also be created through hydrothermal reaction with a surrounding polyethylene glycol (PEG) layer to increase biological circulation time, particle solubility, and biocompatibility [75]. Gold has been shown to provide contrast through X-ray imaging with excitation by a radiofrequency source, while fullerene can be used for photodynamic therapy upon 532 nm laser excitation. Such nanosystems can serve as important multimodal imaging agents for X-ray and photothermal imaging while at the same time being able to carry different chemotherapeutic agents for synergistic therapeutic effect with photodynamic therapy (PDT) and radiofrequency thermal therapy (RTT). Nanoparticles with trismethylpyridylporphyrin-C_{70} (PC_{70}) dyads in upconversion NPs (UCNPs) can be constructed and decorated on the surface electrostatically by PC_{70} [76]. The UCNP–PEG–FA (folic acid)/PC_{70} nanocomposites can act as theranostic agents for trimodal imaging (fluorescence/upconversion luminescence/magnetic resonance imaging) and photoinduced therapy (i.e., upon NIR irradiation). The UCNPs are used to convert NIR light into ultraviolet-visible light to enable PC_{70} to generate singlet oxygen ($^1O_2$) for photodynamic therapy (PDT). Cell viability results show that UCNP–PEG–FA/PC_{70} show negligible cytotoxicity towards

A549 and HBE lung cells, with greater effect in folate receptor overexpressed Hela-*luc* cells (i.e., luciferase expressing cervical cancer cells).

4.2 Carbon Nanotubes

Carbon nanotubes can provide a variety of imaging and therapy options for theranostics [77]. Single-walled carbon nanotubes (SWCNTs) can be used as Raman imaging probes while at the same time be used for photothermal cancer treatment by attaching gold or silver nanoparticles on their surface [78]. By making SWCNTs positively charged with poly(allylamine hydrochloride) (PAH) by first attaching single-stranded DNA (ssDNA), gold and silver seeds can be attached on nanotubes, which can grow to nanoparticles on the surface by adding a reducing agent such as formaldehyde and ammonium hydroxide. To improve cancer cell receptor targeting, folic acid (FA) can be conjugated on the nanotube surfaces, leading to enhanced Raman scattering signals from molecular bond vibrations, while at the same time being able to lead to effective photothermal ablation of cancer cells.

Similarly, folic acid-containing multi-walled carbon nanotubes (MWCNTs) can simultaneously be decorated with a fluorochrome (i.e., Alexa-fluor, AF488/647) for optical imaging, a radionuclide (i.e., technitium-99 m) for scintigraphic imaging and anticancer agent (i.e., methotrexate, MTX) for cancer therapy [79]. The loading in CNTs can be achieved through covalent conjugation with the surface pendant ester groups, with cleavage and degradation of the ester bond for drug (i.e., MTX) release under acidic pH (i.e., present in tumor environments) and possibly due to the presence of certain serum esterases. The CNT-MTX conjugates could significantly reduce tumor volume and growth compared to treatment with FA-CNTs or MTX alone. To improve biocompatibility and circulation time in the blood and for influencing biodistribution, MWCNTs can be coated or covalently conjugated with natural compounds (i.e., PEGylated vitamin E, D-alpha-tocopheryl polyethylene glycol 1000 succinate (TPGS)) and loaded with docetaxel/coumarin-6 (i.e., DTX-CNTPC) for bioimaging and chemotherapy/photodynamic therapy [80]. The particles with docetaxel showed reduced pulmonary toxicity and mostly lower activity for alkaline phosphatase (ALP) and lactate dehydrogenase (LDH) and lower total protein levels in bronchoalveolar lavage (BAL) fluid of rats after treatment, compared to without drug in nanoparticles and drug only (i.e., Docel™). In addition to reduced toxicity, after 24 h of treatment with A549 lung cancer cells, the TPGS conjugated MWCNTs with drug (i.e., docetaxel DTX) were 80 folds more effective than Docel™, by comparing the IC_{50} (i.e., half-maximal inhibitory concentration) values. Functionalized and oxidized multi-walled carbon nanotubes (ox-MWCNT-NH_3^+) can also provide unique imaging capabilities for theranostics that otherwise would not be possible [81]. For example, due to their echogenicity and acoustic impedance, they can provide significant ultrasound contrast in tissue phantoms and signals comparable to commercial contrast agents (i.e., SonoVue bubbles). The nanoparticles provide

signals within a wide variety of frequencies (i.e., 5.5–10 MHz, megahertz) close to or currently used clinically.

Dual loading with chemotherapeutic agent (i.e., doxorubicin, DOX) and monoclonal antibodies (i.e., for Endoglin/CD105) can be conjugated to SWCNTs for active targeting to 4T1 breast cancer cells using 1-Ethyl-3-[3-dimethylaminopropyl]carbodiimide (EDC)/N-hydroxysulfosuccinimide (NHS) active ester method [82]. Through the use of various assays, the SWCNTs with CD105 antibody and DOX increased cancer cell apoptosis, DNA damage and oxidative stress with concentration. At the same time the SWCNTs can be used for image-guided therapy through bioluminescence and diffusion-weighted (DW) magnetic resonance imaging (MRI). DW-MRI can be used for the assessment of treatment induced changes for breast cancer, after the injection of DOX-conjugated SWCNT complexes. An increase in the apparent diffusion coefficient (ADC) from DW-MRI, due to the liberation of water into the extracellular space is from cell necrosis and is directly related to the number of killed tumor cells. Nanoparticles with iron oxide tagged, CD105 antibody conjugated SWCNTs had lower diffusion coefficients for water compared to with the addition of doxorubicin. In most cases, the biggest values for ADC in tumors were seen for DOX and CD105 antibody conjugated SWCNTs with iron tagged, compared to DOX and CD105 conjugated SWCNTs without iron tagged, SWCNTs with CD105 antibody and SWCNTs with CD105 antibody and iron tagged. The SWCNTs with iron tagged, with DOX and CD105 antibody have great treatment efficacy for cancer therapy and killing most amount of cancer cells.

4.3 Graphene Nanoparticles

Negatively charged graphene oxide (GO) nanoparticles provide high surface area for efficient loading of imaging and therapeutic agents [83]. Particles can electrostatically adsorb onto the surface of other particles such as microcapsules, using the water-in-oil-in-water (W/O/W) double emulsion method followed by layer-by-layer self-assembly technique [84]. The capsules are made positively charged using a polymer called poly(allylamine hydrochloride) (PAH) so that the GO particles can be loaded on the surface of capsules through charge interactions. The addition of both gold (Au) and GO increases the optical absorption in the near-infrared (NIR) region of the capsules, which can be used for photothermal therapy through the heat generated. A unique property of these microcapsules is their ability to contain internal hollow space (i.e., through sublimation), enabling them to be used for contrast-enhanced ultrasound (CEUS), a technique with great sensitivity, with signals from scattering from oscillating particles. The gold from the capsules can also be used for X-ray computed tomography as the high atomic number and electron density of gold can give high X-ray attenuation.

Nanoparticles can form unique nanostructures, such as graphene nanosacks, which can be filled with cargo, with the ability to change the structure for either

rapid or slow cargo release (i.e., through sealing of particles using polymeric fillers) [85]. These unique structures enable graphene/Au/Fe_3O_4 particles to be formed for multimodal imaging for both MRI and X-ray computed tomography. To take advantage of the high quantum yield of quantum dots, graphene oxide quantum dots (GOQDs) can be attached to amine-functionalized Fe_3O_4 nanoparticles through EDC-NHS amide coupling, with the potential for photothermal therapy through heat generated from optical absorption [86]. In addition, the ability to attach anti-GPC3-antibody makes these particles highly sensitive two-photon luminescence probes for selective separation of glypican-3 (GPC3)-expressed circulating tumor Hep G2 liver cancer cells.

Graphene nanosheets can be stabilized by water-soluble chitosan and also can have attached superparamagnetic iron oxide (SPIO) nanoparticles for efficient T_2 magnetic resonance imaging (MRI) and contain fluorescent imaging agents (i.e., Cy5.5) through conjugation [87]. The particles can be used for both gene therapy and chemotherapy by their ability to load both DNA and doxorubicin (DOX), serving as unique theranostic nanoparticles. Along with the capability for MRI, combining other types of iron nanoparticles such as cobalt ferrite ($CoFe_2O_4$) with GO nanosheets can provide unique therapeutic ability, such as pH-sensitive drug release at acidic pH environments, such as those of tumors [88]. The cancer cell viability in HeLa cells decreases with increasing concentration and incubation time when treated with DOX-loaded $CoFe_2O_4$/GO (i.e., with minimal cytotoxicity from the same amount of particles without DOX). The inhibition of cell proliferation is greater for DOX-loaded $CoFe_2O_4$/GO than from DOX alone, indicating higher potency for killing cancer cells using DOX-loaded $CoFe_2O_4$/GO. The cumulative release percent of DOX from loaded $CoFe_2O_4$/GO was 57% after 24 h at pH 4 compared to ~10% at pH 7.4.

4.4 Carbon Nanodiamonds

Carbon nanodiamonds (NDs) are a unique and new type of carbon particles, and due to their shape allow for unique functionalization and conjugation to different types of therapeutic and imaging agents [89, 90]. To improve stability, the NDs can be in a cross-linked nanogel (ND-NG) with different negatively charged (i.e., anionic) therapeutic, photodynamic, and imaging agents added for theranostics through adsorption to the positively charged (i.e., cationic) ND-NG [91]. The NDs can be conjugated with a variety of conventional chemotherapeutic agents or mixed with proteins/peptides/antibodies for dual chemotherapy and targeted cancer cell/gene therapy. NDs can carry specific molecules (i.e., folic acid)/antibodies (i.e., monoclonal antibodies for targeting endothelial growth factor (EGF) receptors) and chemotherapeutic agents (i.e., paclitaxel PTX, doxorubicin DOX) through conjugation, for increased internalization in cancer cells and sustained drug release over several days [92–94]. There also have been development of NDs that can be used to treat cancer through organelle targeting. For example, NDs with doxorubicin, folic acid,

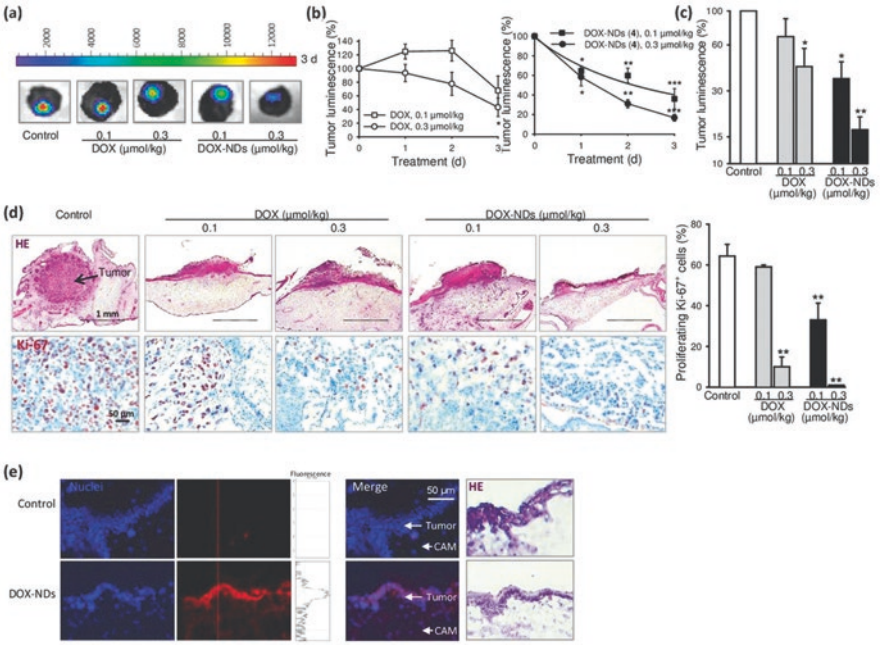

Fig. 8 Antitumor effect of DOX-NDs on breast cancer xenografts in the CAM model. (**a**) DOX-NDs decrease the viability of human cancer xenografts in vivo. Breast cancer cells (0.5×10^6 MDA-MB-231) stably expressing firefly luciferase were grafted onto the chorioallantoic membrane (CAM) of the chick embryo. One day later, xenografts were topically treated with 20 μL of either DOX or the equivalent concentrations of DOX-NDs in 0.9% NaCl. Tumor luminescence was analyzed by IVIS in vivo imaging 1–3 days after treatment and 10 min after addition of D-luciferin with integration time of 1 second. Representative tumors are shown. (**b**) Decrease in tumor growth was monitored by expression of luciferase by MDA-MB-231 cancer xenografts. The data are mean ± SEM (standard error of the mean) of $n = 4–5$. (**c**) Tumor xenograft growth after 3 days treatment as analyzed by luminescence imaging. (**d**) Immunohistochemical analysis of breast cancer xenografts. HE, hematoxylin and eosin staining of whole xenografts grown on CAM; original magnification 50×; Ki-67 antigen staining of tumor xenografts, brown-red nuclei are indicative of proliferating cells, original magnification, 200×. $*P < 0.05$, $**P < 0.01$, Newman–Keuls multigroup comparison. (**e**) Analysis of selective DOX-NDs accumulation in tumor xenografts by using fluorescence microscopy. Frozen sections of tumor xenografts were stained with 4′,6-diamidino-2-phenylindole (DAPI, nuclei, blue) and fluorescent DOX-NDs were visualized with a red filter set (emission wavelength 610 nm). Graphs right to DOX-NDs images demonstrate changes in fluorescence intensity across the image (red line). The corresponding successive cuts were stained with HE to reveal morphology. Original magnifications, 200×. Reprinted from Advanced Functional Materials, 25(42), Wu Y, Ermakova A, Liu W, Pramanik G, Vu TM, Kurz A, et al., Programmable biopolymers for advancing biomedical applications of fluorescent nanodiamonds, 6576–85, Copyright (2015), with permission from John Wiley & Sons

and mitochondrial localizing sequence peptide (MLS-FA-ND-DOX) can be used to increase uptake of DOX in drug-resistant breast cancer (i.e., MCF-7/ADR) cells for circumventing drug resistance [95]. NDs with chemotherapy can treat brain tumor cells through the mediation of dendritic cells (DCs), eliciting an anticancer immune response in glioblastoma [96].

Carbon NDs can be coated with different polymer and biopolymer coatings and therapeutic agents linked to particles, for example, through acid-cleavable linker [97, 98]. These drug-loaded NDs show comparable IC_{50} (i.e., half-maximal inhibitory) concentrations compared to free drug in vitro and significant tumor inhibition in chicken embryo models [98]. The amount of triple negative breast cancer cells (i.e., MDA-MB-231) expressing luminescent firefly luciferase grafted onto chorioallantoic membrane (CAM) of the chick embryo could be detected through luminescence for determining cell death (Fig. 8a). There is a dose- and time-dependent inhibition of breast cancer tumors (Fig. 8b), with superior antitumor effect from DOX-NDs compared to DOX only (Fig. 8c). Immunohistochemical analysis from DOX-ND treatment revealed the number of proliferation antigen Ki-67-positive nuclei was reduced suggesting reduction in tumor growth rate, compared to DOX only and control (i.e., without any treatment) (Fig. 8d). Fluorescence imaging in tumor xenografts confirmed that doxorubicin (DOX) in NDs was localized in nuclei required for treatment through DNA intercalation of cancer cells (Fig. 8e).

Nanodiamonds have also been shown to be able to detect important biological molecules such as ferritin, due to adsorption onto the ND surface through electrostatic interaction and can be implemented for biosensing of important metalloproteins [99]. This is possible due to changes in the electron spin Hahn echo decay rate and T_2 coherence time from NDs and NDs with attached ferritin. Carbon NDs can also be used for other imaging modalities such as photoacoustic (PA) imaging, which is based on the light absorption of particles. In order to create the photoacoustic effect, a focused and pulsed laser is used, where NDs are conjugated with high light absorbing gold nanoparticles for enhancing PA signals [100]. These signals provide potentially a means for temperature imaging deep in tissue [101]. The PA signals correspond to regions in tumors where damage has occurred from significant amount of heat generated from optical absorption. The NDs can also be used for two-photon luminescence imaging [102] and for better contrast and reduced autofluorescence and photodamage compared to other fluorescence imaging techniques (i.e., confocal imaging). Nanodiamonds conjugated with growth hormone (GH) can also be used for specific targeting of membrane receptors in lung cancer cells where specific nanoparticle scattering peaks can be used for confocal Raman mapping [103].

5 Polymer-Based Nanomaterials

5.1 Nanoparticles with Dendrimers

Dendrimers are highly ordered, symmetric molecules used to make nanoparticles [104, 105]. One of the major advantages of using dendrimers is the ability to define and readily tune nanoparticle size and surface functionalities, with the number of exterior functional groups branching out from the core increasing exponentially. A commonly used dendrimer, polyamidoamine (PAMAM), can be used to decorate

superparamagnetic iron oxide nanoparticles (SPION), with the dendrimer containing folic acid (FA) and hydrophobic anticancer drug, 3,4-difluorobenzylidene diferuloylmethane (CDF), for folate-receptor mediated endocytosis, targeting, and therapy of ovarian and cervical cancer cells [106]. Such nanoparticles can be used for magnetic resonance (MR) T_2-weighted imaging, with a significant population of cancer cells undergoing apoptosis due to upregulation of important tumor suppressor phosphatase and tensin homologue (PTEN) and caspase 3 with inhibition of nuclear factor kappa B (NF-κB). PAMAM dendrimer nanoparticles can also be synthesized with a gold core for computed tomography (CT) imaging of colon cancer tumors, with the ability to attach and load stable DNA aptamers (i.e., for transmembrane glycoprotein mucin, MUC-1) and natural therapeutic agent curcumin (inside the cavities of dendrimer), which by itself has poor aqueous solubility and low bioavailability [107].

Dendrimers can also be grafted onto the surface of nanoparticles to improve biocompatibility and conjugation of cancer membrane attaching aptamers such as AS1411 (i.e., using amide condensation reaction). Therapeutic agents can be coupled to PLNPs-PAMAM-AS1411 via an acylhydrazone bond that can be used for persistent luminescence (PL) (i.e., originating from $^2E \rightarrow {}^4A2$ transition of distorted Cr^{3+} ions in gallogermanate) [108]. At acidic pH 5 as in tumors, the hydrazone bond is cleaved due to hydrolysis leading to greater release of therapeutic agents. In vitro results in HeLa cervical cancer cells showed cell viability as low as ~40% when treated with PLNPs-PAMAM-AS1411/DOX. More than 60% tumor inhibition rate was seen with PLNPs-PAMAM-AS1411/DOX in HeLa tumor-bearing mice, which is ~20% more than when mice are treated with PLNPs-PAMAM-DOX (i.e., without AS1411). PAMAM dendrimer/Cu(II) particles can also be developed for radiotherapy-enhanced MRI [109]. The G5.NHAc-Pyr/Cu(II) complexes of particles can induce intracellular reactive oxygen species (ROS) generation and cancer cell apoptosis, with a lower level of protein Bcl-2 (B-cell lymphoma-2) and higher level of proteins PTEN (phosphatase and tensin homologue) and Bax (Bcl-2 associated X protein) and tumor suppressor P53 (i.e., compared to control group). Significant reduction in cancer cell viability is seen using the G5.NHAc-Pyr/Cu(II) complexes in particles in different cell lines (i.e., KB, A549, C6, 4T1) with two times more ROS generated, compared to control group (i.e., normal saline, NS group). The 4T1 breast tumors treated with G5.NHAc-Pyr/Cu(II) complexes had significantly reduced growth rates, with less than 25% of weight of tumors of that of control group (i.e., normal saline, NS group) after radiotherapy.

Nanoparticles with polypropylenimine (PPI) dendrimers can also be created with a single agent (i.e., naphthalocyanine) encapsulated in the hydrophobic interior of dendrimers that provide both therapeutic (i.e., dual photothermal and photodynamic therapy) and imaging (i.e., fluorescence) capabilities [110]. Under continuous near-infrared (NIR) laser excitation, these theranostic agents showed good photostability, preserving their theranostic capability with almost complete cancer cell death and no significant tumor growth after combination treatment. Less than 50% cancer cell viability (i.e., using Calcein AM assay) can be achieved depending on the concentration of the biocompatible particles used, with significant ovarian cancer cell

death seen when using 785 nm laser irradiation for 10 min at 0.3 W cm^{-2} (Fig. 9a). Using combinational therapy (i.e., photothermal and photodynamic) can lead to less than 5% cancer cell viability (Fig. 9b), due to the ability of naphthalocyanine in particles to generate heat (Fig. 9c) and reactive oxygen species (ROS) upon laser excitation (Fig. 9d).

5.2 Micelles

Micelles are nanoscopic aggregates made up of single-chain amphiphilic molecules, which self-assemble in aqueous media above the critical micelle concentration (CMC). The outer corona is hydrophilic, acting as a stabilizer, while the hydrophobic inner core can carry lipophilic/hydrophobic agents for theranostics [111, 112]. Due to their self-assembly above the CMC, they are generally easier to produce compared to other theranostic particles. Micelles are less bulky and have good stability at physiological conditions in blood and low immune response. Lipophilic imaging agents (i.e., IR-780 iodide) can be loaded in the core of micelles with phospholipid mimicking zwitterionic and amphiphilic homopolymer poly(12-(methacryloyloxy)dodecyl phosphorylcholine) (PMDPC) [113]. The developed micelles show good photostability with low leakage of imaging agents upon near-infrared laser excitation. Since micelles contain molecules that are similar to those of lipids of cell membranes, they have improved biocompatibility, with the loaded fluorescent marker used for imaging and photothermal therapy. At a concentration of 50 μg mL^{-1} for theranostic PMDPC-IR-780 micelles (0.9 W cm^{-2}, 808 nm), a temperature rise of ~10 °C was observed after 2 min of irradiation. At a higher concentration of 100 μg mL^{-1}, the temperature further increased by about 16 °C. Cell viability of BxPC-3 pancreatic cancer cells after treatment with micelles (with 5 μg mL^{-1} IR-780) and 5 min of irradiation (0.8 W cm^{-2}, 808 nm) was lower than 20% with strong near-IR fluorescence signals from PMDPC-IR-780 micelles.

ICG-conjugated and ^{125}I-labeled amphiphilic diblock polymer poly(ethylene glycol)–poly(L-tyrosine-^{125}I)–(indocyanine green) (PEG-PTyr(^{125}I)-ICG) can be used to form micelles through simple self-assembly through mixing [114]. These particles can be used for trimodal fluorescence (FL), photoacoustic (PA), and single-photon emission computed tomography (SPECT) imaging and photothermal therapy (PTT) due to the incorporation of indocyanine green (ICG). Dual responsive amphiphilic copolymer poly(ε-caprolactone)-ss-poly(2-(dimethylamino) ethyl methacrylate), PCL-SS-PDMAEMA towards pH/redox can also be synthesized through self-assembly [115]. Acidic pH 5 and addition of glutathione (GSH) leads to reducing conditions mimicking intracellular environment. This leads to swelling of micelles due to increase in electrostatic repulsion between polymer chains, stronger hydrophilicity, and controlled release of loaded therapeutic agents. The additional ability of micelles to carry gold nanoparticles (AuNPs) can lead to imaging capability from X-ray attenuation using computed tomography (CT).

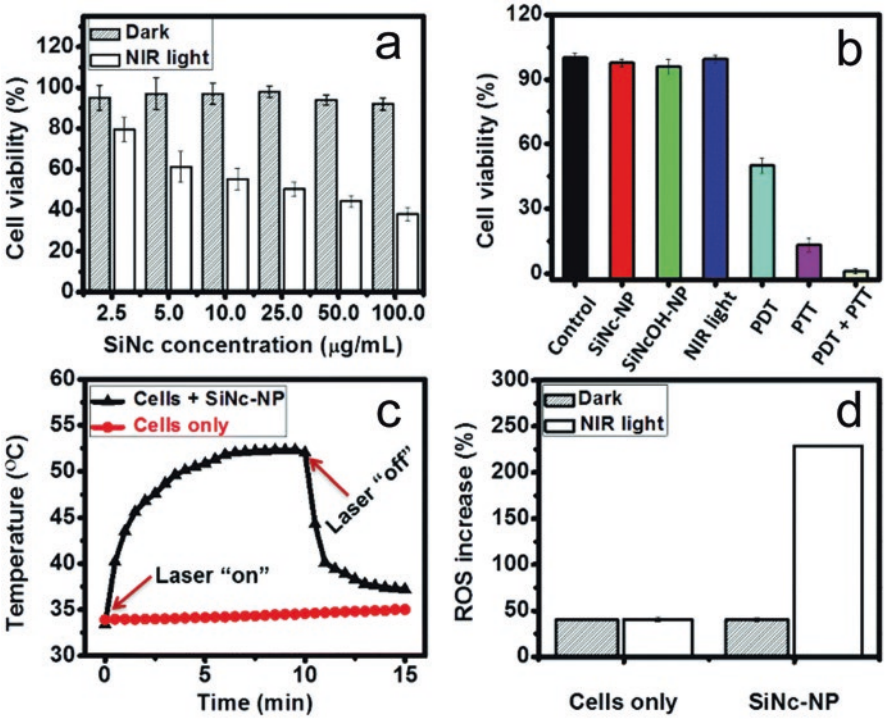

Fig. 9 Dendrimer-encapsulated naphthalocyanine nanoparticles for cancer therapy. (**a**) Dark cytotoxicity and photodynamic (PDT) therapeutic effect of the prepared nanoplatform on A2780/AD ovarian cancer cells incubated with different concentrations of SiNc-NP and irradiated for 10 min using 785 nm laser diode (0.3 W cm^{-2}). (**b**) Combinatorial (PDT + PTT) therapeutic effect of the prepared nanoplatform on A2780/AD ovarian cancer cell pellets incubated with SiNc-NP at a concentration of 25 μg mL^{-1} and irradiated for 10 min using 785 nm laser diode (1.3 W cm^{-2}, yellow bar) compared to the next controls: (1) untreated cells (black bar), (2) cells treated with SiNc-NP and SiNcOH-NP (25 μg mL^{-1}) under dark conditions (red and green bars), (3) untreated cells exposed to the laser diode (785 nm, 1.3 W cm^{-2}, 10 min, blue bar), (4) photodynamic therapy only (SiNc-NP exposed to 0.3 W cm^{-2} light, cyan bar), and (5) photothermal therapy only (SiNcOH-NP exposed to 1.3 W cm^{-2} light, magenta bar). (**c**) Dynamic temperature profile of A2780/AD cells transfected with SiNc-NP (25 μg mL^{-1}) and exposed to the laser diode (785 nm, 1.3 W cm^{-2}). Non-treated cells exposed to the laser diode were used as the control. The arrows indicate when the laser diode was turned on and off, respectively. (**d**) Relative intracellular ROS levels (detected using a 2′,7′-dichlorodihydrofluorescein diacetate (DCFH-DA) assay) in A2780/AD cells incubated with SiNc-NP at a concentration of 25 μg mL^{-1} and irradiated for 10 min using the 785 nm laser diode (1.3 W cm^{-2}). Non-treated cells and cells treated with SiNc-NP under dark conditions were used as the controls. Republished with permission of the Royal Society of Chemistry (Nanoscale) from, Dendrimer-encapsulated naphthalocyanine as a single agent-based theranostic nanoplatform for near-infrared fluorescence imaging and combinatorial anticancer phototherapy, Taratula O, Schumann C, Duong T, Taylor KL, Taratula O, 7(9), 2015; permission conveyed through Copyright Clearance Center

Nanoparticles such as mixed gold and iron oxide micelles (GSMs) can be synthesized as contrast agents for CT and magnetic resonance (MR) imaging [116]. The gold nanoparticles can be used to radiosensitize glioma cell lines where DNA break formation or inhibition of subsequent DNA repair occurs. MRI analysis showed significant uptake of particles in brain tumor tissue. Multi-block polymer, drug loaded micelles can be created where cleavage of PEG segment bearing a pH-sensitive benzoic-imine linkage (BPEG) could act as a switch, capable of activating cell targeting under extracellular conditions of tumors (i.e., lower pH, elevated glutathione concentration compared to normal tissue) [117]. This is followed by triggering the cleavage of disulfide and increasing the rate of drug release in tumors. Superparamagnetic iron oxide nanoparticles (SPION) clustered within the micellar core can be used for MRI contrast from T_2 relaxation. Polymers are important components of micelles which are sensitive to changes in pH, temperature, ultrasound, enzymes, or a combination of any of these factors [118]. This makes these types of particles effective in delivering the majority of therapeutic agents once at tumors while at the same time being able to carry imaging agents for theranostics [119, 120].

5.3 Polyplex Nanoparticles

Polyplexes are complexes formed by nucleic acids and polymers and can be used for effective gene delivery. The polymers used are usually positively charged due to interactions required with negatively charged oligonucleotides. Polyplexes provide better safety profiles compared to viral vectors, not to mention reduced immunogenicity, mutagenesis, and cost. Sodium iodide symporter (NIS)-conjugated nanoparticles with polyethylenimine coupled to synthetic peptide B6 can be used for the treatment of liver cancer [121]. The biodistribution of particles was determined using ^{123}I-scintigraphy with the amount of iodide accumulation in tumors suggesting improved survival from gene delivery and treatment. A composite can be developed for bioimaging with highly fluorescent gold nanoclusters (Au NCs) and biopolymer chitosan, for forming a stable polyplex with suicide gene (pCD−UPRT) for apoptosis of cervical cancer cells after addition of prodrug 5-fluorocytosine (5-FC) [122]. The delivery of the suicide gene produces enzyme, cytosine deaminase-uracil phosphoribosyltransferase (CD−UPRT), converting 5-FC to chemotherapeutic agent 5-FU (5-fluorouracil). Additionally, a pyrimidine salvage enzyme, uracil phosphoribosyltransferase (UPRT), can be used to convert 5-FU to metabolites (e.g., 5-FdUMP and 5-FUTP), inhibiting DNA replication and RNA synthesis in cancer cells.

A redox-sensitive (hyaluronic acid-stabilized redox-sensitive theranostic, HART) polyethylenimine polyplex composed of a doxorubicin (DOX) intercalated Bcl-2 short hairpin RNA (shRNA) encoded plasmid along with a green-synthesized hausmannite (Mn_3O_4) and hematite (Fe_3O_4) nanoparticle (GMF) can be synthesized [123]. The HART nanoassembly leads to intracellular uptake through CD44 mediation, with drug-gene release through hyaluronidase (hylase) and redox-responsive

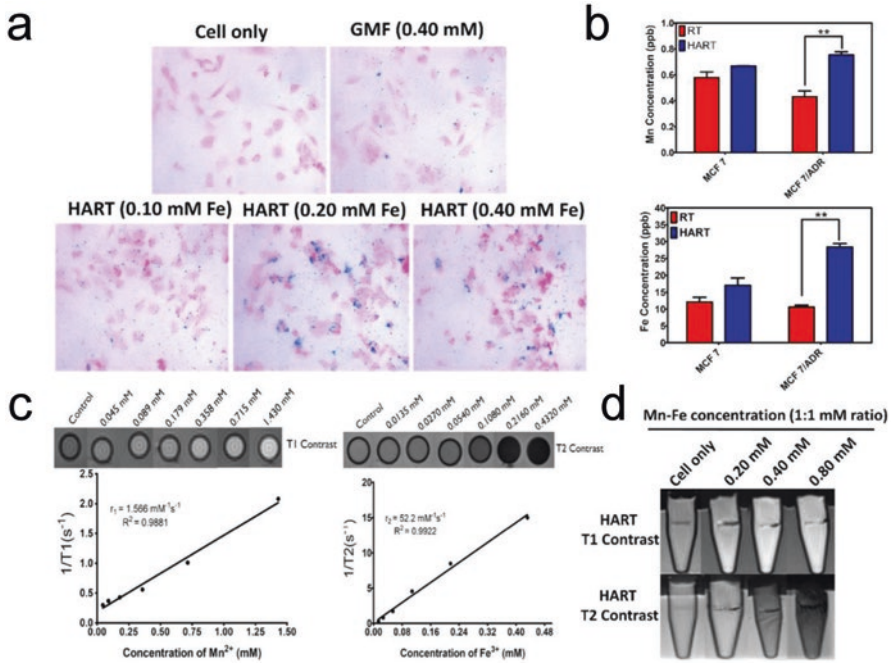

Fig. 10 Dual MRI contrast of HART nanoassembly-treated MCF7/ADR cells. (**a**) Prussian blue staining of HART nanoassembly treated MCF7/ADR cells. (**b**) ICPMS analysis of Mn and Fe in HART nanoassembly treated MCF7/ADR cells. (**c**) T1 and T2 relaxivities of GSP-Mn and GSP-Fe. (**d**) Phantom tube images of T1 and T2 contrast in HART nanoassembly treated MCF7/ADR cells ($n = 4$; SEM; ** indicate $p \leq 0.01$). Reprinted with permission from Rajendrakumar SK, Venu A, Revuri V, George Thomas R, Thirunavukkarasu GK, Zhang J, et al., Hyaluronan-Stabilized Redox-Sensitive Nanoassembly for Chemo-Gene Therapy and Dual T_1/T_2 MR Imaging in Drug-Resistant Breast Cancer Cells. Molecular Pharmaceutics. 2019;16(5):2226–34. Copyright (2019) American Chemical Society

properties. The delivery of HART in multidrug-resistant breast cancer cells, Bcl-2 gene silencing, and DOX delivery lead to cancer apoptosis. In addition, the iron nanoparticles can be used for dual MRI contrast (T_1/T_2) imaging for theranostics. The results from Prussian blue-stained multidrug-resistant MCF-7/ADR breast cancer cells treated with HART nanoassemblies showed increase in iron (Fe) presence with respect to the increase in HART treatment concentration (Fig. 10a). Due to CD44 receptor overexpression in MCF-7/ADR, the manganese (Mn) and iron (Fe) concentrations were significantly increased in the HART nanoassembly treatment compared to the redox-sensitive theranostic (RT) nanoassembly treatment (Fig. 10b). The grape-seed proanthocyanidin (GSP) Fe and Mn nanoparticles in the HART nanoassembly showed enhanced T_1 and T_2 contrast in MCF-7/ADR cells, with linear increase in relaxivities with concentration of nanoparticles (Fig. 10c). This enables the HART nanoassemblies to be used as dual MRI T_1 and T_2 contrast agents at higher concentrations of Mn and Fe in particles (Fig. 10d).

6 Conclusions

Nanoparticles provide tremendous capability for treating cancer, one of the most common group of diseases in the world. Compared to conventional chemotherapy, theranostic nanoparticles provide great potential as they can both passively and actively target cancer cells while at the same time being able to reduce systemic toxicity in healthy tissues. Their physical and chemical properties can be tuned to maximize their ability to locate tumors for diagnosis and treatment, by increasing imaging signals and drug loading (e.g., using chemotherapeutic agents, genetic material) and release after tumor accumulation. As the field of cancer theranostics grows, there is no doubt there will be increased development of nanoparticles that can be used to treat different types of cancer, due to their flexibility for imaging and therapy.

References

1. Gao Q, Zhang J, Gao J, Zhang Z, Zhu H, Wang D. Gold nanoparticles in cancer theranostics. Front Bioeng Biotechnol. 2021;9
2. Heo DN, Yang DH, Moon H-J, Lee JB, Bae MS, Lee SC, et al. Gold nanoparticles surface-functionalized with paclitaxel drug and biotin receptor as theranostic agents for cancer therapy. Biomaterials. 2012;33(3):856–66.
3. Dixit S, Novak T, Miller K, Zhu Y, Kenney ME, Broome A-M. Transferrin receptor-targeted theranostic gold nanoparticles for photosensitizer delivery in brain tumors. Nanoscale. 2015;7(5):1782–90.
4. Kim D, Jeong YY, Jon S. A drug-loaded aptamer– gold nanoparticle bioconjugate for combined CT imaging and therapy of prostate cancer. ACS Nano. 2010;4(7):3689–96.
5. Shao J, Griffin RJ, Galanzha EI, Kim J-W, Koonce N, Webber J, et al. Photothermal nanodrugs: potential of TNF-gold nanospheres for cancer theranostics. Sci Rep. 2013;3(1):1–9.
6. Zhang L, Yang X-Q, Wei J-S, Li X, Wang H, Zhao Y-D. Intelligent gold nanostars for in vivo CT imaging and catalase-enhanced synergistic photodynamic & photothermal tumor therapy. Theranostics. 2019;9(19):5424.
7. Xiong J, Jiang B, Luo Y, Zou J, Gao X, Xu D, et al. Multifunctional nanoparticles encapsulating Astragalus polysaccharide and gold Nanorods in combination with focused ultrasound for the treatment of breast cancer. Int J Nanomedicine. 2020;15:4151.
8. Xu L, Wan C, Du J, Li H, Liu X, Yang H, et al. Synthesis, characterization, and in vitro evaluation of targeted gold nanoshelled poly (d, l-lactide-co-glycolide) nanoparticles carrying anti p53 antibody as a theranostic agent for ultrasound contrast imaging and photothermal therapy. J Biomater Sci Polym Ed. 2017;28(4):415–30.
9. Liu R, Xiao W, Hu C, Xie R, Gao H. Theranostic size-reducible and no donor conjugated gold nanocluster fabricated hyaluronic acid nanoparticle with optimal size for combinational treatment of breast cancer and lung metastasis. J Control Release. 2018;278:127–39.
10. Wei P, Chen J, Hu Y, Li X, Wang H, Shen M, et al. Dendrimer-stabilized gold nanostars as a multifunctional theranostic nanoplatform for CT imaging, photothermal therapy, and gene silencing of tumors. Adv Healthc Mater. 2016;5(24):3203–13.
11. Jing L, Liang X, Li X, Lin L, Yang Y, Yue X, et al. Mn-porphyrin conjugated Au nanoshells encapsulating doxorubicin for potential magnetic resonance imaging and light triggered synergistic therapy of cancer. Theranostics. 2014;4(9):858.

12. Huang P, Lin J, Wang S, Zhou Z, Li Z, Wang Z, et al. Photosensitizer-conjugated silica-coated gold nanoclusters for fluorescence imaging-guided photodynamic therapy. Biomaterials. 2013;34(19):4643–54.
13. Yang H-W, Liu H-L, Li M-L, Hsi I-W, Fan C-T, Huang C-Y, et al. Magnetic gold-nanorod/PNIPAAmMA nanoparticles for dual magnetic resonance and photoacoustic imaging and targeted photothermal therapy. Biomaterials. 2013;34(22):5651–60.
14. Ho Y-P, Leong KW. Quantum dot-based theranostics. Nanoscale. 2010;2(1):60–8.
15. Kobayashi H, Hama Y, Koyama Y, Barrett T, Regino CA, Urano Y, et al. Simultaneous multicolor imaging of five different lymphatic basins using quantum dots. Nano Lett. 2007;7(6):1711–6.
16. Yong Y, Cheng X, Bao T, Zu M, Yan L, Yin W, et al. Tungsten sulfide quantum dots as multifunctional nanotheranostics for in vivo dual-modal image-guided photothermal/radiotherapy synergistic therapy. ACS Nano. 2015;9(12):12451–63.
17. Yang W, Guo W, Le W, Lv G, Zhang F, Shi L, et al. Albumin-bioinspired Gd: CuS nanotheranostic agent for in vivo photoacoustic/magnetic resonance imaging-guided tumor-targeted photothermal therapy. ACS Nano. 2016;10(11):10245–57.
18. Li P, Liu L, Lu Q, Yang S, Yang L, Cheng Y, et al. Ultrasmall MoS2 nanodots-doped biodegradable SiO_2 nanoparticles for clearable FL/CT/MSOT imaging-guided PTT/PDT combination tumor therapy. ACS Appl Mater Interfaces. 2019;11(6):5771–81.
19. Bao Y-W, Hua X-W, Li Y-H, Jia H-R, Wu F-G. Hyperthemia-promoted cytosolic and nuclear delivery of copper/carbon quantum dot-crosslinked nanosheets: multimodal imaging-guided photothermal cancer therapy. ACS Appl Mater Interfaces. 2018;10(2):1544–55.
20. Endres T, Zheng M, Kılıç AE, Turowska A, Beck-Broichsitter M, Renz H, et al. Amphiphilic biodegradable PEG-PCL-PEI triblock copolymers for FRET-capable in vitro and in vivo delivery of siRNA and quantum dots. Mol Pharm. 2014;11(4):1273–81.
21. Yoo D, Lee J-H, Shin T-H, Cheon J. Theranostic magnetic nanoparticles. Acc Chem Res. 2011;44(10):863–74.
22. Xie J, Liu G, Eden HS, Ai H, Chen X. Surface-engineered magnetic nanoparticle platforms for cancer imaging and therapy. Acc Chem Res. 2011;44(10):883–92.
23. Gul S, Khan SB, Rehman IU, Khan MA, Khan M. A comprehensive review of magnetic nanomaterials modern day theranostics. Frontiers in Materials. 2019;6:179.
24. Fang C, Kievit FM, Veiseh O, Stephen ZR, Wang T, Lee D, et al. Fabrication of magnetic nanoparticles with controllable drug loading and release through a simple assembly approach. J Control Release. 2012;162(1):233–41.
25. Li D, Tang X, Pulli B, Lin C, Zhao P, Cheng J, et al. Theranostic nanoparticles based on bioreducible polyethylenimine-coated iron oxide for reduction-responsive gene delivery and magnetic resonance imaging. Int J Nanomed. 2014;9:3347.
26. Yu J, Yin W, Zheng X, Tian G, Zhang X, Bao T, et al. Smart MoS2/Fe3O4 nanotheranostic for magnetically targeted photothermal therapy guided by magnetic resonance/photoacoustic imaging. Theranostics. 2015;5(9):931.
27. Gu Z, Yan L, Tian G, Li S, Chai Z, Zhao Y. Recent advances in design and fabrication of upconversion nanoparticles and their safe theranostic applications. Adv Mater. 2013;25(28):3758–79.
28. Tian G, Zhang X, Gu Z, Zhao Y. Recent advances in upconversion nanoparticles-based multifunctional nanocomposites for combined cancer therapy. Adv Mater. 2015;27(47):7692–712.
29. Lu S, Tu D, Hu P, Xu J, Li R, Wang M, et al. Multifunctional nano-bioprobes based on rattle-structured upconverting luminescent nanoparticles. Angew Chem. 2015;127(27):8026–30.
30. Liu Y, Li L, Guo Q, Wang L, Liu D, Wei Z, et al. Novel Cs-based upconversion nanoparticles as dual-modal CT and UCL imaging agents for chemo-photothermal synergistic therapy. Theranostics. 2016;6(10):1491.
31. Chen Y, Liu B, Deng X, Huang S, Hou Z, Li C, et al. Multifunctional Nd 3+−sensitized upconversion nanomaterials for synchronous tumor diagnosis and treatment. Nanoscale. 2015;7(18):8574–83.

32. Lv R, Yang P, Chen G, Gai S, Xu J, Prasad PN. Dopamine-mediated photothermal theranostics combined with up-conversion platform under near infrared light. Sci Rep. 2017;7(1):1–13.
33. Zhai X, Lei P, Zhang P, Wang Z, Song S, Xu X, et al. Growth of lanthanide-doped LiGdF4 nanoparticles induced by LiLuF4 core as tri-modal imaging bioprobes. Biomaterials. 2015;65:115–23.
34. Kostiv U, Kučka J, Lobaz V, Kotov N, Janoušková O, Šlouf M, et al. Highly colloidally stable trimodal 125 I-radiolabeled PEG-neridronate-coated upconversion/magnetic bioimaging nanoprobes. Sci Rep. 2020;10(1):1–14.
35. Al-Jamal WT, Kostarelos K. Liposomes: from a clinically established drug delivery system to a nanoparticle platform for theranostic nanomedicine. Acc Chem Res. 2011;44(10):1094–104.
36. Shen J, Kim H-C, Wolfram J, Mu C, Zhang W, Liu H, et al. A liposome encapsulated ruthenium polypyridine complex as a theranostic platform for triple-negative breast cancer. Nano Lett. 2017;17(5):2913–20.
37. Lee MH, Kim E-J, Lee H, Kim HM, Chang MJ, Park SY, et al. Liposomal texaphyrin theranostics for metastatic liver cancer. J Am Chem Soc. 2016;138(50):16380–7.
38. Tyler B, Gullotti D, Mangraviti A, Utsuki T, Brem H. Polylactic acid (PLA) controlled delivery carriers for biomedical applications. Adv Drug Deliv Rev. 2016;107:163–75.
39. Li S, Goins B, Zhang L, Bao A. Novel multifunctional theranostic liposome drug delivery system: construction, characterization, and multimodality MR, near-infrared fluorescent, and nuclear imaging. Bioconjug Chem. 2012;23(6):1322–32.
40. Jin CS, Zheng G. Liposomal nanostructures for photosensitizer delivery. Lasers Surg Med. 2011;43(7):734–48.
41. Feng L, Cheng L, Dong Z, Tao D, Barnhart TE, Cai W, et al. Theranostic liposomes with hypoxia-activated prodrug to effectively destruct hypoxic tumors post-photodynamic therapy. ACS Nano. 2017;11(1):927–37.
42. Dai Y, Su J, Wu K, Ma W, Wang B, Li M, et al. Multifunctional thermosensitive liposomes based on natural phase-change material: near-infrared light-triggered drug release and multimodal imaging-guided cancer combination therapy. ACS Appl Mater Interfaces. 2019;11(11):10540–53.
43. Gorain B, Choudhury H, Nair AB, Dubey SK, Kesharwani P Theranostic application of nanoemulsion in chemotherapy. Drug Discov Today. 2020;25(7):1174–88.
44. Tayeb HH, Sainsbury F. Nanoemulsions in drug delivery: formulation to medical application. Nanomedicine. 2018;13(19):2507–25.
45. Sánchez-López E, Guerra M, Dias-Ferreira J, Lopez-Machado A, Ettcheto M, Cano A, et al. Current applications of nanoemulsions in cancer therapeutics. Nanomaterials. 2019;9(6):821.
46. Herneisey M, Liu L, Lambert E, Schmitz N, Loftus S, Janjic JM. Development of theranostic perfluorocarbon nanoemulsions as a model non-opioid pain nanomedicine using a quality by design (QbD) approach. AAPS PharmSciTech. 2019;20(2):1–13.
47. Ganta S, Singh A, Kulkarni P, Keeler AW, Piroyan A, Sawant RR, et al. EGFR targeted theranostic nanoemulsion for image-guided ovarian cancer therapy. Pharm Res. 2015;32(8):2753–63.
48. Fernandes DA, Fernandes DD, Li Y, Wang Y, Zhang Z, Rousseau D, et al. Synthesis of stable multifunctional perfluorocarbon nanoemulsions for cancer therapy and imaging. Langmuir. 2016;32(42):10870–80.
49. Fernandes DA, Kolios MC. Intrinsically absorbing photoacoustic and ultrasound contrast agents for cancer therapy and imaging. Nanotechnology. 2018;29(50):505103.
50. Fernandes DA, Kolios MC. Perfluorocarbon bubbles as photoacoustic signal amplifiers for cancer theranostics. Optical Materials Express. 2019;9(12):4532–44.
51. Fernandes DA, Fernandes DD, Malik A, Gomes G-NW, Appak-Baskoy S, Berndl E, et al. Multifunctional nanoparticles as theranostic agents for therapy and imaging of breast cancer. J Photochem Photobiol B Biol. 2021;218:112110.
52. Fernandes DA, Kolios MC. Near-infrared absorbing nanoemulsions as nonlinear ultrasound contrast agents for cancer theranostics. J Mol Liq. 2019;287:110848.

53. Fernandes DA, Appak-Baskoy S, Berndl E, Kolios MC. Laser activatable perfluorocarbon bubbles for imaging and therapy through enhanced absorption from coupled silica coated gold nanoparticles. RSC Adv. 2021;11(9):4906–20.
54. Arnal B, Wei C-W, Perez C, Nguyen T-M, Lombardo M, Pelivanov I, et al. Sono-photoacoustic imaging of gold nanoemulsions: part II. Real time imaging. Photoacoustics. 2015;3(1):11–9.
55. Wang R, Zhou Y, Zhang P, Chen Y, Gao W, Xu J, et al. Phase-transitional Fe3O4/perfluorohexane microspheres for magnetic droplet vaporization. Theranostics. 2017;7(4):846.
56. Molina M, Asadian-Birjand M, Balach J, Bergueiro J, Miceli E, Calderón M. Stimuli-responsive nanogel composites and their application in nanomedicine. Chem Soc Rev. 2015;44(17):6161–86.
57. Wang H, Chen Q, Zhou S. Carbon-based hybrid nanogels: a synergistic nanoplatform for combined biosensing, bioimaging, and responsive drug delivery. Chem Soc Rev. 2018;47(11):4198–232.
58. Quan S, Wang Y, Zhou A, Kumar P, Narain R. Galactose-based thermosensitive nanogels for targeted drug delivery of iodoazomycin arabinofuranoside (IAZA) for theranostic management of hypoxic hepatocellular carcinoma. Biomacromolecules. 2015;16(7):1978–86.
59. Zhu H, Li Y, Qiu R, Shi L, Wu W, Zhou S. Responsive fluorescent Bi_2O_3@ PVA hybrid nanogels for temperature-sensing, dual-modal imaging, and drug delivery. Biomaterials. 2012;33(10):3058–69.
60. Pei M, Jia X, Zhao X, Li J, Liu P. Alginate-based cancer-associated, stimuli-driven and turn-on theranostic prodrug nanogel for cancer detection and treatment. Carbohydr Polym. 2018;183:131–9.
61. Chen Y, Nan J, Lu Y, Wang C, Chu F, Gu Z. Hybrid Fe_3O_4-poly (acrylic acid) nanogels for theranostic cancer treatment. J Biomed Nanotechnol. 2015;11(5):771–9.
62. Zhang C, Sun W, Wang Y, Xu F, Qu J, Xia J, et al. Gd-/CuS-loaded functional nanogels for MR/PA imaging-guided tumor-targeted photothermal therapy. ACS Appl Mater Interfaces. 2020;12(8):9107–17.
63. Theune LE, Buchmann J, Wedepohl S, Molina M, Laufer J, Calderón M. NIR-and thermo-responsive semi-interpenetrated polypyrrole nanogels for imaging guided combinational photothermal and chemotherapy. J Control Release. 2019;311:147–61.
64. Khatun Z, Nurunnabi M, Nafiujjaman M, Reeck GR, Khan HA, Cho KJ, et al. A hyaluronic acid nanogel for photo–chemo theranostics of lung cancer with simultaneous light-responsive controlled release of doxorubicin. Nanoscale. 2015;7(24):10680–9.
65. Sirsi S, Borden M. Microbubble compositions, properties and biomedical applications. Bubble Sci Eng Technol. 2009;1(1–2):3–17.
66. Liang X, Xu Y, Gao C, Zhou Y, Zhang N, Dai Z. Ultrasound contrast agent microbubbles with ultrahigh loading capacity of camptothecin and floxuridine for enhancing tumor accumulation and combined chemotherapeutic efficacy. NPG Asia Materials. 2018;10(8):761–74.
67. Guo F, Yu M, Wang J, Tan F, Li N. Smart IR780 theranostic nanocarrier for tumor-specific therapy: hyperthermia-mediated bubble-generating and folate-targeted liposomes. ACS Appl Mater Interfaces. 2015;7(37):20556–67.
68. Niu C, Wang Z, Lu G, Krupka TM, Sun Y, You Y, et al. Doxorubicin loaded superparamagnetic PLGA-iron oxide multifunctional microbubbles for dual-mode US/MR imaging and therapy of metastasis in lymph nodes. Biomaterials. 2013;34(9):2307–17.
69. Deng L, Cai X, Sheng D, Yang Y, Strohm EM, Wang Z, et al. A laser-activated biocompatible theranostic nanoagent for targeted multimodal imaging and photothermal therapy. Theranostics. 2017;7(18):4410.
70. Chen Z, Ma L, Liu Y, Chen C. Applications of functionalized fullerenes in tumor theranostics. Theranostics. 2012;2(3):238.
71. Dellinger A, Zhou Z, Connor J, Madhankumar A, Pamujula S, Sayes CM, et al. Application of fullerenes in nanomedicine: an update. Nanomedicine. 2013;8(7):1191–208.
72. Wang H, Agarwal P, Zhao S, Yu J, Lu X, He X. A biomimetic hybrid nanoplatform for encapsulation and precisely controlled delivery of theranostic agents. Nat Commun. 2015;6(1):1–13.

73. Huang H, Liu M, Chen J, Mao L, Zeng G, Wen Y, et al. Facile fabrication of carboxyl groups modified fluorescent C60 through a one-step thiol-ene click reaction and their potential applications for biological imaging and intracellular drug delivery. J Taiwan Inst Chem Eng. 2018;86:192–8.
74. Peng Y, Yang D, Lu W, Hu X, Hong H, Cai T. Positron emission tomography (PET) guided glioblastoma targeting by a fullerene-based nanoplatform with fast renal clearance. Acta Biomater. 2017;61:193–203.
75. Shi J, Chen Z, Wang L, Wang B, Xu L, Hou L, et al. A tumor-specific cleavable nanosystem of PEG-modified C60@ Au hybrid aggregates for radio frequency-controlled release, hyperthermia, photodynamic therapy and X-ray imaging. Acta Biomater. 2016;29:282–97.
76. Guan M, Dong H, Ge J, Chen D, Sun L, Li S, et al. Multifunctional upconversion–nanoparticles–trismethylpyridylporphyrin–fullerene nanocomposite: a near-infrared light-triggered theranostic platform for imaging-guided photodynamic therapy. NPG Asia Mater. 2015;7(7):e205.
77. Venkataraman A, Amadi EV, Chen Y, Papadopoulos C. Carbon nanotube assembly and integration for applications. Nanoscale Res Lett. 2019;14(1):1–47.
78. Wang X, Wang C, Cheng L, Lee S-T, Liu Z. Noble metal coated single-walled carbon nanotubes for applications in surface enhanced Raman scattering imaging and photothermal therapy. J Am Chem Soc. 2012;134(17):7414–22.
79. Das M, Datir SR, Singh RP, Jain S. Augmented anticancer activity of a targeted, intracellularly activatable, theranostic nanomedicine based on fluorescent and radiolabeled, methotrexate-folic acid-multiwalled carbon nanotube conjugate. Mol Pharm. 2013;10(7):2543–57.
80. Singh RP, Sharma G, Singh S, Kumar M, Pandey BL, Koch B, et al. Vitamin E TPGS conjugated carbon nanotubes improved efficacy of docetaxel with safety for lung cancer treatment. Colloids Surf B Biointerf. 2016;141:429–42.
81. Delogu LG, Vidili G, Venturelli E, Ménard-Moyon C, Zoroddu MA, Pilo G, et al. Functionalized multiwalled carbon nanotubes as ultrasound contrast agents. Proc Natl Acad Sci. 2012;109(41):16612–7. https://doi.org/10.1073/pnas.1208312109.
82. Al Faraj A, Shaik AP, Shaik AS. Magnetic single-walled carbon nanotubes as efficient drug delivery nanocarriers in breast cancer murine model: noninvasive monitoring using diffusion-weighted magnetic resonance imaging as sensitive imaging biomarker. Int J Nanomedicine. 2015;10:157–68. https://doi.org/10.2147/ijn.s75074.
83. Yang K, Feng L, Shi X, Liu Z. Nano-graphene in biomedicine: theranostic applications. Chem Soc Rev. 2013;42(2):530–47.
84. Jin Y, Wang J, Ke H, Wang S, Dai Z. Graphene oxide modified PLA microcapsules containing gold nanoparticles for ultrasonic/CT bimodal imaging guided photothermal tumor therapy. Biomaterials. 2013;34(20):4794–802. https://doi.org/10.1016/j.biomaterials.2013.03.027.
85. Chen Y, Guo F, Qiu Y, Hu H, Kulaots I, Walsh E, et al. Encapsulation of particle ensembles in graphene nanosacks as a new route to multifunctional materials. ACS Nano. 2013;7(5):3744–53.
86. Shi Y, Pramanik A, Tchounwou C, Pedraza F, Crouch RA, Chavva SR, et al. Multifunctional biocompatible graphene oxide quantum dots decorated magnetic nanoplatform for efficient capture and two-photon imaging of rare tumor cells. ACS Appl Mater Interfaces. 2015;7(20):10935–43.
87. Wang C, Ravi S, Garapati US, Das M, Howell M, Mallela J, et al. Multifunctional chitosan magnetic-graphene (CMG) nanoparticles: a theranostic platform for tumor-targeted co-delivery of drugs, genes and MRI contrast agents. J Mater Chem B. 2013;1(35):4396–405. https://doi.org/10.1039/C3TB20452A.
88. Wang G, Ma Y, Wei Z, Qi M. Development of multifunctional cobalt ferrite/graphene oxide nanocomposites for magnetic resonance imaging and controlled drug delivery. Chem Eng J. 2016;289:150–60. doi: https://doi.org/10.1016/j.cej.2015.12.072.
89. Chen D, Dougherty CA, Zhu K, Hong H. Theranostic applications of carbon nanomaterials in cancer: focus on imaging and cargo delivery. J Control Release. 2015;210:230–45.

90. Augustine S, Singh J, Srivastava M, Sharma M, Das A, Malhotra BD. Recent advances in carbon based nanosystems for cancer theranostics. Biomater Sci. 2017;5(5):901–52.
91. Wu Y, Alam MNA, Balasubramanian P, Ermakova A, Fischer S, Barth H, et al. Nanodiamond theranostic for light-controlled intracellular heating and nanoscale temperature sensing. Nano Lett. 2021;21(9):3780–8. https://doi.org/10.1021/acs.nanolett.1c00043.
92. Lim DG, Jung JH, Ko HW, Kang E, Jeong SH. Paclitaxel–nanodiamond nanocomplexes enhance aqueous dispersibility and drug retention in cells. ACS Appl Mater Interfaces. 2016;8(36):23558–67.
93. Master AM, Sen Gupta A. EGF receptor-targeted nanocarriers for enhanced cancer treatment. Nanomedicine. 2012;7(12):1895–906.
94. Ryu TK, Baek SW, Lee GJ, Rhee CK, Choi SW. Targeted tumor therapy based on nanodiamonds decorated with doxorubicin and folic acid. Macromol Biosci. 2017;17(2):1600180.
95. Chan MS, Liu LS, Leung HM, Lo PK. Cancer-cell-specific mitochondria-targeted drug delivery by dual-ligand-functionalized nanodiamonds circumvent drug resistance. ACS Appl Mater Interfaces. 2017;9(13):11780–9.
96. Li T-F, Li K, Zhang Q, Wang C, Yue Y, Chen Z, et al. Dendritic cell-mediated delivery of doxorubicin-polyglycerol-nanodiamond composites elicits enhanced anti-cancer immune response in glioblastoma. Biomaterials. 2018;181:35–52.
97. Slegerova J, Hajek M, Rehor I, Sedlak F, Stursa J, Hruby M, et al. Designing the nanobiointerface of fluorescent nanodiamonds: highly selective targeting of glioma cancer cells. Nanoscale. 2015;7(2):415–20.
98. Wu Y, Ermakova A, Liu W, Pramanik G, Vu TM, Kurz A, et al. Programmable biopolymers for advancing biomedical applications of fluorescent nanodiamonds. Adv Funct Mater. 2015;25(42):6576–85.
99. Ermakova A, Pramanik G, Cai JM, Algara-Siller G, Kaiser U, Weil T, et al. Detection of a few metallo-protein molecules using color centers in Nanodiamonds. Nano Lett. 2013;13(7):3305–9. https://doi.org/10.1021/nl4015233.
100. Zhang B, Fang C-Y, Chang C-C, Peterson R, Maswadi S, Glickman RD, et al. Photoacoustic emission from fluorescent nanodiamonds enhanced with gold nanoparticles. Biomed Opt Express. 2012;3(7):1662–9.
101. Wang LV, Hu S. Photoacoustic tomography: in vivo imaging from organelles to organs. Science. 2012;335(6075):1458–62.
102. Hui YY, Zhang B, Chang Y-C, Chang C-C, Chang H-C, Hsu J-H, et al. Two-photon fluorescence correlation spectroscopy of lipid-encapsulated fluorescent nanodiamonds in living cells. Opt Express. 2010;18(6):5896–905.
103. Cheng C-Y, Perevedentseva E, Tu J-S, Chung P-H, Cheng C-L, Liu K-K, et al. Direct and in vitro observation of growth hormone receptor molecules in A549 human lung epithelial cells by nanodiamond labeling. Appl Phys Lett. 2007;90(16):163903.
104. Ma Y, Mou Q, Wang D, Zhu X, Yan D. Dendritic polymers for theranostics. Theranostics. 2016;6(7):930.
105. Saluja V, Mishra Y, Mishra V, Giri N, Nayak P. Dendrimers based cancer nanotheranostics: an overview. Int J Pharm. 2021;600:120485.
106. Luong D, Sau S, Kesharwani P, Iyer AK. Polyvalent folate-dendrimer-coated iron oxide Theranostic nanoparticles for simultaneous magnetic resonance imaging and precise cancer cell targeting. Biomacromolecules. 2017;18(4):1197–209. https://doi.org/10.1021/acs.biomac.6b01885.
107. Alibolandi M, Hoseini F, Mohammadi M, Ramezani P, Einafshar E, Taghdisi SM, et al. Curcumin-entrapped MUC-1 aptamer targeted dendrimer-gold hybrid nanostructure as a theranostic system for colon adenocarcinoma. Intl J Pharmaceut. 2018;549(1):67–75. https://doi.org/10.1016/j.ijpharm.2018.07.052.
108. Zhang H-J, Zhao X, Chen L-J, Yang C-X, Yan X-P. Dendrimer grafted persistent luminescent nanoplatform for aptamer guided tumor imaging and acid-responsive drug delivery. Talanta. 2020;219:121209.

109. Fan Y, Zhang J, Shi M, Li D, Lu C, Cao X, et al. Poly (amidoamine) dendrimer-coordinated copper (II) complexes as a theranostic nanoplatform for the radiotherapy-enhanced magnetic resonance imaging and chemotherapy of tumors and tumor metastasis. Nano Lett. 2019;19(2):1216–26.
110. Taratula O, Schumann C, Duong T, Taylor KL, Taratula O. Dendrimer-encapsulated naphthalocyanine as a single agent-based theranostic nanoplatform for near-infrared fluorescence imaging and combinatorial anticancer phototherapy. Nanoscale. 2015;7(9):3888–902. https://doi.org/10.1039/C4NR06050D.
111. Blanco E, Kessinger CW, Sumer BD, Gao J. Multifunctional micellar nanomedicine for cancer therapy. Exp Biol Med. 2009;234(2):123–31.
112. Wang Z, Niu G, Chen X. Polymeric materials for theranostic applications. Pharm Res. 2014;31(6):1358–76.
113. Chen Y, Li Z, Wang H, Wang Y, Han H, Jin Q, et al. IR-780 loaded phospholipid mimicking Homopolymeric micelles for near-IR imaging and Photothermal therapy of pancreatic cancer. ACS Appl Mater Interface. 2016;8(11):6852–8. https://doi.org/10.1021/acsami.6b00251.
114. Yang L, Zhang C, Liu J, Huang F, Zhang Y, Liang X-J, et al. ICG-Conjugated and 125I-labeled polymeric micelles with high biosafety for multimodality imaging-guided photothermal therapy of tumors. Adv Healthc Mater. 2020;9(5):1901616. https://doi.org/10.1002/adhm.201901616.
115. Xiong D, Zhang X, Peng S, Gu H, Zhang L. Smart pH-sensitive micelles based on redox degradable polymers as DOX/GNPs carriers for controlled drug release and CT imaging. Colloids Surf B Biointerf. 2018;163:29–40. https://doi.org/10.1016/j.colsurfb.2017.12.008.
116. Sun L, Joh DY, Al-Zaki A, Stangl M, Murty S, Davis JJ, et al. Theranostic application of mixed gold and superparamagnetic iron oxide nanoparticle micelles in glioblastoma multiforme. J Biomed Nanotechnol. 2016;12(2):347–56.
117. Wei J, Shuai X, Wang R, He X, Li Y, Ding M, et al. Clickable and imageable multiblock polymer micelles with magnetically guided and PEG-switched targeting and release property for precise tumor theranosis. Biomaterials. 2017;145:138–53.
118. Johnson RP, John JV, Kim I. Poly (l-histidine)-containing polymer bioconjugate hybrid materials as stimuli-responsive theranostic systems. J Appl Polym Sci. 2014;131(18).
119. Augustine R, Kim D-K, Kalva N, Eom KH, Kim JH, Kim I. Multi-stimuli-responsive nanomicelles fabricated using synthetic polymer polylysine conjugates for tumor microenvironment dependent drug delivery. J Mater Chem B. 2020;8(26):5745–55.
120. Johnson RP, Uthaman S, John JV, Lee HR, Lee SJ, Park H, et al. Poly (PEGA)-b-poly (l-lysine)-b-poly (l-histidine) hybrid vesicles for tumoral pH-triggered intracellular delivery of doxorubicin hydrochloride. ACS Appl Mater Interface. 2015;7(39):21770–9.
121. Urnauer S, Klutz K, Grünwald GK, Morys S, Schwenk N, Zach C, et al. Systemic tumor-targeted sodium iodide symporter (NIS) gene therapy of hepatocellular carcinoma mediated by B6 peptide polyplexes. J Gene Med. 2017;19(5):e2957.
122. Sahoo AK, Banerjee S, Ghosh SS, Chattopadhyay A. Simultaneous RGB emitting Au nanoclusters in chitosan nanoparticles for anticancer gene theranostics. ACS Appl Mater Interf. 2014;6(1):712–24.
123. Rajendrakumar SK, Venu A, Revuri V, George Thomas R, Thirunavukkarasu GK, Zhang J, et al. Hyaluronan-stabilized redox-sensitive nanoassembly for chemo-gene therapy and dual T1/T2 MR imaging in drug-resistant breast cancer cells. Mol Pharm. 2019;16(5):2226–34.

Theranostic Nanoparticles in Cancer Diagnosis and Treatment

Dipak Maity, Satya Ranjan Sahoo, Ankur Tiwari, Siddharth Ajith, and Sumit Saha

1 Introduction

Cancer (also known as malignancy) is a term for a group of diseases in which the body's cells multiply uncontrollably. This disease is one of the significant sources of death around the globe [1]. Nanoscience and nanotechnology provide immense potential to stop the spread of cancerous cells in the body. It helps to cure the disease in a specialized way at a nanoscale, thereby efficiently curing the disease. Till now, nanotechnology based cancer theranostics is in its initial stages of application but has a vast potential for research and development in the future. As the name suggests, theranostic is a combination of two words: therapy and diagnostics [2]. On a nanoscale, theranostic improves the diagnosis ability as well as efficiency of therapy [2]. Various theranostic nanomaterials have been evolved for cancer treatment and diagnosis, and it is discussed in a detailed way in this chapter. Due to their small size and high surface energy, nanomaterials react significantly with biomolecules in the cell [3].

D. Maity (✉)
Department of Chemical Engineering, University of Petroleum and Energy Studies, Dehradun, Uttarakhand, India

School of Health Sciences & Technology, University of Petroleum & Energy Studies, Dehradun, Uttarakhand, India

S. R. Sahoo · S. Saha
Materials Chemistry Department, CSIR-Institute of Minerals & Materials Technology, Bhubaneswar, Odisha, India

Academy of Scientific and Innovative Research (AcSIR), Ghaziabad, Uttar Pradesh, India

A. Tiwari · S. Ajith
Department of Chemical Engineering, Institute of Chemical Technology Mumbai-Indian Oil Campus, Bhubaneswar, Odisha, India

R. S. Chaughule et al. (eds.), *Nanomaterials for Cancer Detection Using Imaging Techniques and Their Clinical Applications*,
https://doi.org/10.1007/978-3-031-09636-5_7

The most significant advantage of using nanotechnology is its ability to deliver a targeted agent to the tumor site, which helps in the efficient treatment of the cancer disease. Nanotechnology also provides scientists and researchers with the opportunity to study the development of tumors even during their initial stages. Moreover, it is very essential to detect the tumors in their earlier stages for a proper cure for the cancer disease, which is easily possible using advanced nanotechnology [4]. The level of accuracy and precision that can be obtained by using nanotechnology is much better than the currently employed conventional techniques. Even though there are many advantages, there is also a chance of generating toxicity due to the nanomaterials, which must be researched further [4]. Nevertheless, the advancement of robust theranostic materials is one of the keys to discovering and treating cancer in the twenty-first century [3].

From this chapter, the reader can get a broad picture of the application of nanotechnology in the field of cancer therapy as well as about various theranostic nanomaterials which are investigated in cancer diagnosis and its treatment. Even though this modern technology has shown promising results in cancer theranostics, it has some limitations, which have also been discussed in this chapter. Almost all the aspects of theranostic nanomaterials have been considered, and one can conclude that nanotechnology is the future alternative for cancer treatment.

2 Classification of Theranostic Nanoparticles

Theranostic nanoparticles (TNPs) are multifunctional nanomaterials that are designed for specific and personalized disease management as they possess both diagnostic and therapeutic capabilities in a single biocompatible nanoparticle [5]. TNPs can ideally be those nanomaterials which can effectively accumulate and/or deliver the potential drugs selectively to the target site without affecting any other tissue/organ or the organism itself, are easily eliminated from the organism's body, and must be biodegradable into nontoxic by-products. In cancer treatment, TNPs have proved to be very attractive and promising agents [6]. They have the potential to revolutionize cancer treatment as they possess both the theranostics and drug delivery capability. In the last few decades, with the development of nanotechnology and nanoscience, there has been an increased interest in studies of various kinds of TNPs for simultaneous cancer imaging and therapy. These TNPs have been classified and discussed in detail in this section. A schematic representation of different TNPs used in cancer diagnosis and treatment is shown in Fig. 1.

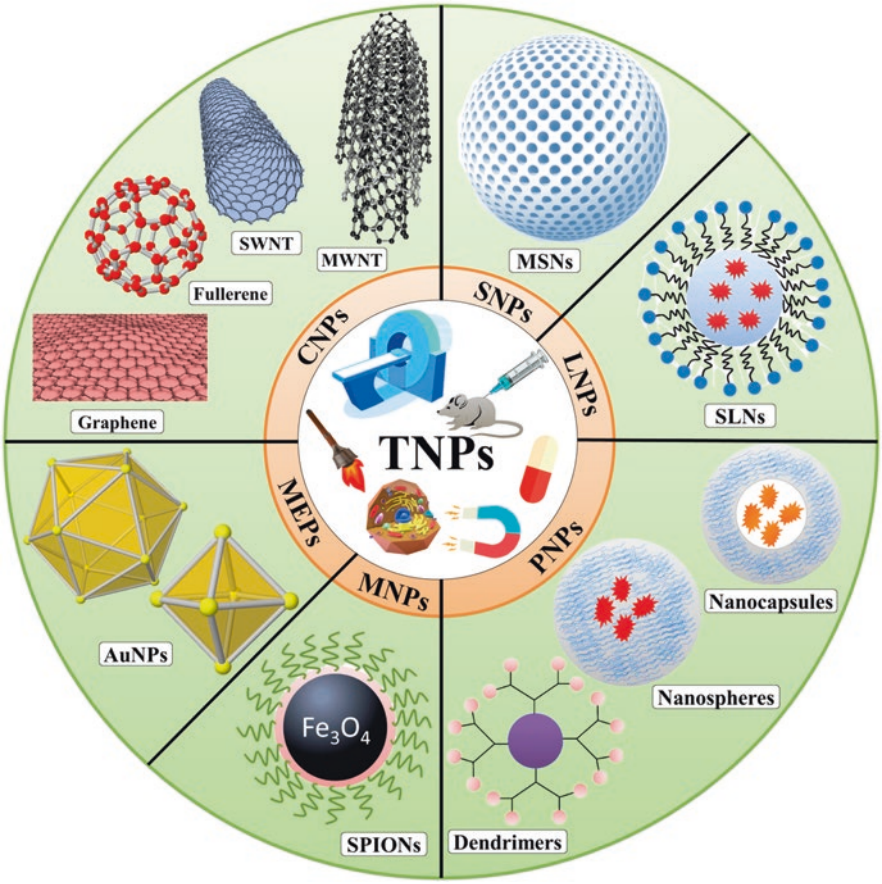

Fig. 1 Schematic representation of different TNPs used in cancer diagnosis and treatment

2.1 Magnetic Nanoparticles

Magnetic nanoparticles (MNPs) are considered one of the essential classes of nanomaterials that are widely studied for their potential application in theranostics and biomedicines. MNPs can be easily manipulated by an externally applied magnetic field, making them one of the important candidates for in vivo applications. MNPs are used in different applications like magnetic biosensing, magnetic imaging, drug delivery/targeting, hyperthermia therapy, etc. MNPs have a large surface-to-volume ratio and unique dissimilar magnetic behavior as compared to their bulk. Different materials like pure metals (Fe, Co, Ni, etc.), alloy (Fe-Pt), and oxides/ferrites (like Fe_3O_4, γ-Fe_2O_3) are commonly used MNPs in nanomedicine. However, pure metals are not suitable for clinical application owing to their toxicity and rapid oxidation tendency. Iron oxide is widely used in the fabrication of MNPs as it is chemically stable, nontoxic, non-immunogenic and biodegradable

[7]. Hence, iron oxide nanoparticles like magnetite (Fe_3O_4) and maghemite (γ-Fe_2O_3) are commonly used MNPs in biomedical applications due to the fact that these MNPs have higher effective areas, improved tissular diffusion, and reduced magnetic dipole-dipole interactions. Additionally, their particle size is smaller enough to circulate through the capillary system of organs and tissues. Nevertheless, their movement can be controlled by magnetic fields as they have high magnetization and can be immobilized close to the target pathogenic tissue [8].

Superparamagnetic iron oxide nanoparticles (SPIONS) are a type of MNPs that display unique superparamagnetic properties as compared to ferro−/ferrimagnetic iron oxide nanoparticles in the presence of an external magnetic field. They have various biomedical applications such as magnetic fluid hyperthermia, MRI, drug delivery, and gene delivery due to their exceptional physicochemical characteristics: magnetic properties, chemical stability, biodegradability, and low toxicity. Generally, the SPIONS have a core-shell structure of magnetite and/or maghemite cores with a surface coating of nonmagnetic organic/inorganic species which prevents the SPIONs from aggregation. These stabilizing coatings play an essential role in determining magnetic and physicochemical properties of the SPION core. Coercivity of the multi-domain MNPs gradually increases with reducing their size and reaches to the maximum at their single-domain size, and subsequently decreases to zero with further reducing their size up to superparamagnetic size. Therefore, SPIONs reveal superparamagnetism behavior (i.e., zero coercivity and remanence) below their superparamagnetic size limit. Moreover, these particles exhibit high saturation magnetization and magnetic susceptibility under the influence of an externally applied magnetic field [9].

2.2 Carbon-Based Nanoparticles

Carbon-based nanoparticles (CNPs) are entirely made up of carbon. Carbon has many allotropic forms like graphite, diamond, and amorphous carbon. CNPs have sp^2-hybridized carbon atoms that have been developed in various dimensions. Different carbon-based nanomaterials can be classified as follows:

1. Fullerene (zero dimensional), a hollow cage-like structure. They are made up of sp^2-hybridized carbon atoms. Its structure is similar to hollow football with pentagonal/hexagonal carbon units organized in a regular pattern. Most of the fullerenes are spheroids in shape (like C_{60}). However, oblong shapes like Rugby balls also exist (like C_{70}). Fullerenes are an allotrope of carbon. They have unique photophysical and photochemical properties, and also good electrical conductivity, and higher strength.
2. Carbon nanotubes (CNTs) (one dimensional), which is structurally one carbon atom thick sheet rolled into hollow elongated tubes having 1 nm of diameter. The carbon atoms are linked in a hexagonal structure. Based on rolling, CNTs can be categorized into single-walled CNTs (SWNTs) and multi-walled CNTs

(MWNTs). In SWNTs, the sheets are single-rolled, whereas MWNTs consist of multiple rolled sheets. Each layer in MWNTs interacts through van der Waals forces. CNTs have high tensile strength, good electrical and thermal conductivity, optical properties, and mechanical properties.

3. Graphene sheets (two dimensional) are allotropic forms of carbon composed of sp^2-bonded carbon atoms that form a hexagonal network of honeycomb lattice in two-dimensional planar surfaces. Generally, the thickness of graphene sheets is 1 nm. The various derivatives of graphene include graphene oxide, reduced graphene oxide, chemically modified graphene oxide, etc. They have unique properties like high electrical conductivity, good chemical stability, large surface area, etc.
4. Graphite and nanodiamonds (three dimensional) are made up of sp^2 carbon atoms arranged in a hexagon sphere, and nanocrystals consisting of tetrahedrally bonded carbon atoms, respectively. Nanodiamonds (NDs) have unique optical properties. Besides, there are also other forms of carbon-based nanomaterials like carbon quantum dots, carbon nanofibers, and carbon black.

CNPs have excellent mechanical, thermal, optical, and chemical properties. With these properties, they also have unique structural dimensions that make them be utilized in widely diverse areas of applications of which biomedical application is very significant. In recent times, CNPs have been utilized in the imaging of cells and tissues and the delivery of therapeutic molecules for different diseases. Moreover, due to the broad one-photon property of CNPs, they have been recently used as imaging agents in tumor diagnosis. The intrinsic two-photon fluorescence property in the long-wavelength region helps in deep tissue optical imaging [10]. Further, CNPs have an internal structure based on graphene sheets assembled to form quasi-spherical nanoparticles, and the external shell can be functionalized with different functional groups. They also show a peculiar optical property, particularly in the UV-Vis spectrum, where it shows a broad range of absorption bands and a tail in the UV and visible regions, respectively. This is due to π-π^* and n-π^* transitions related to C=C and C=O, respectively [11].

2.3 Silica-Based Nanoparticles

Silica-based nanoparticles (SNPs) are colloidal silica (silicon dioxide) nanoparticles that are amorphous and generally spherical. They have different ranges of sizes with different surface chemistry. There are two major types of SNPs, namely, solid silica nanoparticles (SiNPs) and mesoporous silica nanoparticles (MSNs) [12]. Both have different properties. SiNPs have favorable colloidal properties and are photochemically stable. Being biocompatible, the surface of SiNPs can be functionalized (with various functional groups like antibodies, aptamers, and polymers) to be utilized as an optical imaging and drug delivery agents. Further, MSNs have a

high surface area and tunable pores that can be utilized for loading therapeutic or imaging agents.

SNPs are classical types of materials which are largely used in biomedical applications as they are inexpensive and it is very easy to prepare. Their surface characteristics, porosity, and functionalization can be tuned to make them good tools for biomolecule detection and separation (like protein adsorption and separation, nucleic acid detection and purification) and provide a suitable medium for drug delivery, gene delivery, and imaging [13]. Since they are biocompatible, they are typically designed to be used as nanocarriers and/or biomodulators for therapeutic delivery [14]. Moreover, SNPs, especially the porous variant (i.e., MSNs), can be an excellent tool for antimicrobial drug delivery agents due to their high drug loading capacity, tunable pore size and volume, ease of functionalization, and biocompatibility [15]. Besides, SNPs are chemically inert, and their matrix porosity is not susceptible to swelling or change in pH. Therefore, it can be used to encapsulate theranostic agents like photosensitizers, and it can also selectively accumulate in cancer cells for effective cancer treatment (like improving efficacy of photodynamic therapy). Furthermore, SNP surfaces can be easily functionalized or modified with cancer specific biomolecules for tumor cell targeting [16].

2.4 Metallic Nanoparticles

Metallic nanoparticles (MEPs) are generally nanoscale metals whose dimensions lie within a range of 1–100 nm. Faraday, in 1857, was the first to recognize the existence of metallic nanoparticles in solution, and Mie, in 1908, gave the quantitative explanation of their color [17]. In recent years with the development of nanotechnology and nanoscience, MEPs have received enormous attention and increased interest for studies due to which it has been exploited in different application fields, especially in biomedical fields. MEPs have various shapes, tunable surface chemistry/surface functionalization, unique optical properties (like surface plasmon resonance), versatile functionalization, and a good penetration with traceability in the living organism, which makes them be utilized as an excellent theranostics agent in cancer treatment. MEPs generally have a small size of about 50 nm, enabling them to cross or penetrate the capillaries in tissues and cells and thus reach the targeted area. Moreover, they have a high surface/volume ratio with the modified surface, allowing them to carry many potential drugs as a drug carrier and thus help in drug delivery. One of the unique advantages of using MEPs in cancer treatment is that they can efficiently absorb light and convert it to heat. This makes them be used in hyperthermic tumor therapy in which photo stimulation provides thermal energy, which makes this therapy highly specific.

Considering their inherent CCT, PA, fluorescence, surface-enhanced Raman scattering (SERS), and PTT imaging properties, MEPs, particularly Ag and Au have mainly focused on cancer theranostics. In order to improve their biocompatibility and avoid RES uptake, the surfaces of MEPs have been modified with various

molecules (e.g., PEGylated). A significant advantage of MEPs is that they can be functionalized with tumor-specific ligands and stimuli-responsive components and be conjugated with other therapeutic/imaging agents to achieve targeted/triggered delivery and multimodal cancer theranostics [18].

2.4.1 Silver Nanoparticles

Silver has been extensively used in coins and jewelry due to its noble properties like gold since ancient history. Silver is also resistant to bacteria and is thus used as an antibacterial agent with low toxicity. Hippocrates (considered to be the father of modern medicine), known for his outstanding figures in the history of medicines, believed in the healing effect of silver because of its anti-disease properties. Because of this healing effect, it was used to protect water. Silver compounds had been used in curing wound infections instead of antibiotics during World War I. In today's era of nanotechnology and nanoscience, new theranostics approaches have been developed by which silver nanoparticle (AgNPs) is used as medicines. AgNPs are extensively used in industrial and health products, like coating medical devices; biosensors; bioimaging; antibacterial, antifungal, antiparasitic, antiviral, anticancer agents; and drug carriers and therapeutics [19]. The reasons behind its extensive use are its superior physicochemical characteristics, which include high conductivity, better plasmonic properties, and chemical stability, as well as its antibacterial, antiviral, and antifungal properties.

2.4.2 Gold Nanoparticles

Gold is one of the oldest metals, which was discovered several thousand years ago. It is one of the least reactive chemical elements, making it resistant to corrosion and other chemical reactions. The unique bright yellow color of gold made it be used for coinage and jewelry. Thus, gold became the symbol of power and wealth. Ancient Chinese, Arabian, and Indian papers from fifth to fourth centuries BC reported the medicinal application of gold and its complexes which recommended it to treat various diseases. In 1857, Faraday presented the first scientific article on gold nanoparticles, a red colloidal, and described its light scattering features. Like AgNPs, gold nanoparticles (AuNPs) are also extensively used in cancer theranostics due to their unique physicochemical properties like surface plasmon resonance (SPR) and ability to bind with amine and thiol group, which allows surface modification so that it can be used in biomedical applications [20]. Further, AuNPs display tunable physicochemical properties due to their different sizes (2–100 nm) and shapes, including nanospheres, nanorods, nanoshells, nanocages, nanostars, and surface plasmon resonance (SPR) properties, along with tailor-made surface functionalization. As a result, they are extensively used in several single-modal theranostics applications, including optical−/photoacoustic-/CT-imaging of cancer cells, PTT, and anticancer drug delivery [18].

2.5 Polymer Nanoparticles

Polymer nanoparticles (PNPs) are composed of polymers that are prepared by simply converting monomers or bulk polymers to nano-sized polymers. It can be defined as those solid colloidal particles in the range of 10–1000 nm which can be loaded with active compounds on the surface or inside the polymer core. The term "polymer nanoparticles" is collectively used for all types of nano-sized polymer particles, but specifically for polymer nanospheres and nanocapsules [21]. Polymer nanospheres are matrix particles where the entire mass is solid, and molecules are adsorbed at the surface of the sphere or encapsulated within the matrix particles. Whereas nanocapsules are vesicular reservoir systems, which have a liquid core surrounded by a solid material shell that is made up of a continuous polymeric network. Inside the liquid core, usually biologically active molecules (like drugs, genes, nucleic acid, etc.) are dissolved/encapsulated.

In the preparation of PNPs, both natural and synthesized polymers are used. However, natural polymers are more preferred owing to their biodegradability. Thus, natural polymers are used to make polymer nanoparticles for in vivo drug delivery systems. Examples of such natural polymers used for the preparation of PNPs are starch, polypeptides, albumin, polyhydroxyalkanoate (PHAs), gelatin, cellulose, etc. On the other hand, Synthetic polymers used in the preparation of nanoparticles are polyethylene (PE), polyethylene glycol (PEG), poly lactic-co-glycolic acid (PLGA), and polyvinyl alcohol (PVA) [22]. PNPs can be produced by various techniques. Generally, there are two main strategies to prepare PNPs, namely, the dispersion of performed polymer and the direct polymerization of monomers [23].

Further, surfaces of PNPs are often functionalized with different functional groups like surfactant, metal ions, or small molecules for better binding, targeting, and delivery purpose. By converting polymer to PNPs induces unique physicochemical properties. Moreover, due to their small size, high volume to surface area ratio, and tunable pore, polymer nanoparticles are extensively used for various applications like biosensors, drug delivery, stimuli response cargo delivery, and agricultural and environmental applications. The advantage of using PNPs in drug delivery systems includes high drug encapsulation efficiency, high stability, ability to protect drugs, and biocompatibility with tissue and cells. In fact, today, nanotechnology and nanoscience are employed to design such polymer nanoparticles that can effectively and efficiently deliver the drug to the target site and increase the therapeutic effect.

2.6 Lipid Nanoparticles

Structurally, lipids broadly consist of a nonpolar hydrophobic "chain" or "tail" region attached to the polar hydrophilic "head" region. Based on their structure, lipid-based nanoparticles can be classified into liposomes, lipid nano-emulsions (LNEs), solid lipid nanoparticles (SLPs), and nanostructured lipid carriers (NLCs). Liposomes are mainly composed of phospholipids arranged in bilayer structure to form "unilamellar vesicles" in the presence of water due to their amphipathic properties. These vesicles can be used to load drugs and carry them to the target area, thus improving drugs' solubility and stability. They are capable of encapsulating either hydrophobic or hydrophilic drugs. LNEs consist of lipid droplets stabilized by surfactants/phospholipids to prevent them from aggregation and coalescence in an aqueous solution. LNEs are somewhat like liposomes except that the outer phospholipid bilayer structure is absent, and instead, they exhibit a complex micelle-like structure of cationic lipids that encapsulate various oligonucleotides (like RNA and DNA). SLPs are a colloidal system made up of lipids that are solid at room temperature. The solid lipid forms a matrix material that acts as nanocarriers by encapsulating the drug and the matrix is stabilized by a mixture of surfactants or polymer. NLCs are the second generation of lipid-based nanocarriers developed from SLNs due to their limitations, such as lower drug loading efficiency and drug explosion due to its crystallization during storage. NLCs are formed by mixing solid and liquid lipids such as glyceryl tricaprylate, ethyl oleate, isopropyl myristate, and glycerol dioleate. Mixing solid lipids with small amounts of liquid lipids produces NLCs whose matrix is structurally rearranged concerning SLPs, which gives improved properties but at the same time maintains the benefits of SLPs [24].

2.7 Dendrimers

Dendrimers are polymerlike nanoparticles, but structurally they are different from PNPs. The word dendrimer is derived from the Greek word known as "dendron" whose literal meaning is "branching of a tree." Dendrimers are nano-sized polymeric globular branched and symmetrical structures with a size that varies from 1 to 15 nm [25]. Besides, dendrimers have well-defined, homogenous, and mainly monodisperse structures containing treelike branching units growing around a small molecule or polymer core. These branching units can be functionalized with various functional groups (like COOH, COONa, NH_2, or OH) that determine the physicochemical or biological properties of the dendrimers. Dendrimers have unique biological properties such as polyvalency, self-assembly, electronic interactions, chemical stability, low toxicity, and solubility, making them suitable for medical field applications, especially cancer treatment. Dendrimers can carry large amounts of drugs to a specific site and they can be considered as an architectural motif but not as a chemical compound [26]. A variety of dendrimers exists, among which

PAMAM (polyamidoamine) are the most common class of dendrimers and also most employed ones, especially in biotechnological applications, although PPI (polypropylene imines) are the first dendrimers to be reported. Further, they are biocompatible and non-immunogenic, making them a good candidate for drug delivery. PAMAM has the inner core made up of alkyl-diamine with tertiary amine branches surrounding the core.

3 Synthesis of Nanoparticles

With the development of nanotechnology, several synthetic routes have been developed to achieve desired physical and chemical properties in the fabricated nanomaterial. Broadly speaking, there are two synthetic approaches which are identified as (i) top-down approach (ii) bottom-up approach. Both approaches have their own advantages and disadvantages. The top-down approach (destructive approach) begins with a suitable bulk material (as starting material) and then trimming down/breaking down into smaller molecules, and then these smaller molecules are transformed into desired nanoparticles. The bottom-up approach is the reverse of the top-down approach. In the bottom-up approach (constructive approach), nanoparticles are first obtained at the atomic level by miniaturization of material and then by the integrating/self-assembly process, which leads to the formation of nanostructures. During self-assembly, the physical forces operating at nanoscales are used to combine the units: atom by atom, molecule by molecule, and/or cluster by cluster into larger stable nanostructures.

The basic synthetic methods involved in preparing nanomaterials are physical and chemical methods which are basically top-down and bottom-up approaches, respectively. There are also biological methods for synthesizing nanoparticles in which different microorganisms and plant parts are used to prepare nanomaterials. Each method has its own advantages and disadvantages and impacts various properties on the nanomaterial. The procedures used for the synthesis of nanoparticles have been discussed in detail. The methods of synthesis of nanoparticles are summarized in Table 1.

3.1 Physical Methods

3.1.1 Pulse Laser Ablation

Pulse laser ablation is one of the simplest and most common synthetic techniques of nanoparticles from different solvents. The technique consists of a solid disc that rotates with a solution that is placed in a vacuum chamber. The disc is exposed to a high-power pulsed laser beam. The laser beam enters the chamber and hits the targeted disc where the material is placed. The material, when exposed to such

Table 1 Classification, composition, methods of synthesis, and size of nanoparticles with their cancer theranostics applications

Classification	Composition	Method of synthesis	Size	Applications	References
Magnetic nanoparticles	Fe_3O_4, γ-Fe_2O_3	Coprecipitation Microemulsion Hydrothermal Thermal decomposition	1–100 nm	MRI, hyperthermia therapy, MPI	[54–59]
Carbon-based nanoparticles	sp^2-hybridized carbon atoms	Hydrothermal Laser ablation CVD	3–10 nm	Targeted drug delivery, PDT, thermal therapy	[60–65]
Silica-based nanoparticles	Colloidal silica (silicon dioxide)	Microemulsion Stober method	10–500 nm	Fluorescence imaging, targeted drug delivery	[66–70]
Lipid-based nanoparticles	Cholesterol and glycerophospholipid	Microemulsion	50–1000 nm	Functionalization of nanoparticles, targeted drug delivery	[71–73]
Polymer-based nanoparticles	Polymers in nanoscale	Microemulsion Nanoprecipitation Solvent evaporation	10–1000 nm	Multimodal imaging, targeted drug delivery	[74–77]
Metal nanoparticles	Pure metal (e.g., gold, silver, platinum, zinc, iron) or their compounds (e.g., oxides, hydroxides, sulfides, chlorides)	Biological methods Thermal decomposition Coprecipitation Hydrothermal Sputtering	10–100 nm	PDT, thermal therapy, targeted drug delivery, a contrast agent (PA imaging, MRI, fluorescence imaging)	[78–82]

high-power laser radiations, is converted to plasma to produce nanoparticles [27]. Many factors affect the final product, such as type of laser, number of pulses, pulsing time, and type of solvent. Stable nanoparticles are usually synthesized using pulse laser ablation techniques that do not require stabilizing agents or chemicals.

3.1.2 Electron Beam Lithography

Originally lithography has been utilized since the seventeenth century in the application of ink printing. Lithography is the process of transferring a pattern from one media to another. In today's era of nanotechnology and nanosciences, the technique and application of lithography are diversified toward the synthesis/fabrication of nanomaterials. The process of lithography involves patterning on a surface through the exposure of light, ions, and electrons, and subsequently, it etches or deposits the material on the surface to produce the pattern. There are different types of nanolithography techniques such as optical, electron beam, multiphoton, nanoimprint, and

scanning probe lithography [28]. The main advantages of nanolithography are that it can produce a single nanoparticle to a cluster with desired shape and size and the disadvantages that it requires complex equipment which has a high cost with it [29].

Electron beam lithography came into the picture by the late 1960s by modifying the design of SEM. This lithographic technique has the capacity to create patterns at the nanoscale because of its very short wavelength and reasonable electron density characteristics. The process involves electron irradiation of a surface that is covered/coated with an electron-sensitive material (resist) by a focused electron beam. Due to the irradiation, energetic absorption in specific places leads to an intramolecular phenomenon. Electron beam lithography consists mainly of three steps: exposure of the sensitive materials, development of the resists, and pattern transfers. The working principle of electron beam lithography is quite simple. A focused beam of electrons is irradiated on a substrate covered by an electron-sensitive material that changes its solubility properties according to the energy impacted by the electron beam. A typical electron beam lithography system closely resembles an SEM. A typical electron beam lithography setup consists of a chamber, electron gun, and column. Column and chamber are maintained in a high vacuum. The column contains electron-optical elements, which are used to create a beam of electrons and accelerate it, turn it on/off, and focus/deflect [30].

Electron beam resists are generally coated on the substrate to record an image of the pattern to be transferred. These resists are usually high molecular weight polymers that are dissolved in a suitable liquid solvent. When a focused electron beam is irradiated on these polymers, they undergo structural changes. Polymethyl methacrylate (PMMA) is the most commonly used electron resist. It is dissolved in solvents like anisole and chlorobenzene of the desired concentration. This technique synthesizes AuNPs; for instance, Lennox et al. prepared 2D patterned arrays of AuNPs by electron beam lithography [31].

3.1.3 High-Energy Ball Milling

High-energy ball milling is a solid processing technique used to synthesize nanoparticles. It is an inexpensive method to get the nanoparticle from the bulk. The starting bulk material can be of any shape/size. There are many types of milling, such as planetary, vibratory, rod, tumbler, etc. In this process, the powder mixture of the material is placed in a ball mill and subjected to high-energy collisions from the balls by which a vast brute force is applied to the materials. The ball is placed in a container that is closed with tight lids. During the grinding process, it decreases the particle size and produces micro deformation in the crystal lattice of the ground materials. Usually, a ratio of 2:1 by mass of balls to the material is maintained. Sometimes the container is filled with inert gas to prevent it from air contamination [32]. Impurities from the balls may get added—the temperature rises during the collision for which cryo-cooling is used to dissipate the heat generated. During milling, liquids are also used. Sometimes more than one container is used at a time to

prepare large amounts of fine particles. The balls are made up of hardened steel or tungsten carbide.

The mechanical limitation of this process is that ultrafine particles are either difficult to produce or take a long time. However, the simple operation, low cost, and large-scale production of nanoparticles are the main advantages of high-energy ball milling. The final product from this process depends on factors like the type of mill, milling speed, milling time, container, temperature, atmosphere, size and size distribution of the grinding material, process control agent, extent of filling of the container, and ratio by mass of ball to the material.

3.2 Chemical Methods

3.2.1 Coprecipitation Method

Coprecipitation is a very convenient method for synthesizing various nanoparticles such as, iron oxide nanoparticles. The coprecipitation method involves the simultaneous occurrence of conversion of the reactant into solution in their insoluble form followed by nucleation and growth [33]. The precipitation of a crystalline solid occurs in three steps: supersaturation, nucleation, and growth. During supersaturation, the system is unstable, and the precipitation of the product pieces occurs due to any small perturbation. Supersaturation is reached by various physical means like changing temperature or solvent evaporation, etc., and chemical means like the addition of acid, base, etc. These supersaturation conditions are necessary for inducing precipitation. Nucleation is the crucial step that involves the formation of small elementary particles of a new phase that are stable under precipitation conditions. Nucleation is followed by growth or agglomeration of the particle where crystal growth occurs, which affects the size, morphology, purity, and properties of the products. If the rate of nucleation is much higher than the rate of crystal growth, a large number of small particles will be formed, which leads to the formation of an amorphous precipitate. These techniques mostly prepare hydroxide and carbonate due to low solubility [34].

MNPs can be conveniently prepared by the coprecipitation method. Massant in 1981 reported the synthesis of MNP in acid and alkaline media. Since then, it is still used to prepare MNPs like iron oxide. In this technique, an aqueous solution of ferric and ferrous (Fe^{3+} & Fe^{2+}) ions is reduced by a basic solution at a temperature below 100 °C to form a precipitate. The advantages of coprecipitation are high yield, high product purity, organic solvent not used, and low cost [33].

3.2.2 Chemical Vapor Deposition

Chemical vapor deposition (CVD) is a powerful technique for producing high-quality, high-performance solid materials by a chemical reaction in the vapor phase. In a typical CVD method, the heated substrate (wafer) is exposed to one or more volatile precursors, which decompose on it, followed by deposition of a thin film on the substrate. This deposition is carried out in a reaction chamber. The vaporized precursor, along with combining gas, is transported in a CVD reactor where the substrate is kept at a high temperature. The reactant diffuses to the surface of the substrate and undergoes some chemical reaction, nucleates, and grows to form a thin film of the desired material. The by-product formed during the chemical reaction is removed by gas flow through the reactor [35]. It is widely used in the industry for producing thin-film semiconductors. There are many types of CVD like metallo-organic CVD (MOCVD), atomic layer epitaxy (ALE), vapor phase epitaxy (VPE), plasma-enhanced CVD (PECVD), etc. The advantage of CVD is that highly pure potent, and this technique can produce hard nanoparticles. The disadvantages of this technique are that it requires specialized equipment and the gaseous by-products formed are highly toxic and corrosive. A typical CVD system consists of a gas delivery system, a reaction chamber, a vacuum system, an energy system, an exhaust gas treatment system, and an automatic control system [36].

3.2.3 Microemulsion

The emulsion is the liquid-liquid dispersion of two immiscible liquids. They are mixed by mechanical shear and surfactant. The particle grows continuously with time, and hence it gets separated by gravitational forces. Thus, emulsions are thermodynamically unstable. Depending on the size of the droplet, emulsions are categorized as macro-emulsions, mini-emulsions, and microemulsions. Microemulsions (as defined by IUPAC) are dispersions made of water, oil, and surfactant that are isotropic and thermodynamically stable with dispersion droplets of size 1–100 nm (approximately). The microemulsion method is one of the low-temperature routes for the synthesis of nanoparticles. J.H Schulman first coined it in 1959 [37]. The microemulsion synthesis method is widely used for synthesis in inorganic nanoparticles. Nanoparticles can be produced in a controlled manner through the use of microemulsions, which are self-aggregated colloidal systems. Thus, in this method, control over the shape, size, and morphology of metallic nanoparticles is achieved by which we get different shapes and sizes of nanoparticles by just controlling the reaction time, temperature, and other reaction conditions.

When water and oil are mixed, they get separated into two phases due to the interfacial tension between them. This interfacial tension can be avoided by using a surfactant as it has hydrophilic and lipophilic groups that get aligned at the interface of water and oil, thus establishing an interaction between water and oil. There are various categories of microemulsion, like water in oil (W/O) microemulsion where water is dispersed in oil and oil in water (O/W) microemulsion where oil is

dispersed in water. Water in supercritical CO_2 microemulsion is also a kind of microemulsion that was recently developed. Among them, W/O microemulsion is essential as it is used to synthesize inorganic nanoparticles. They are usually called reverse micelles. This reverse micelle acts as nanoreactors. Preparation of metallic nanoparticles in W/O microemulsion usually involves mixing of two microemulsions containing metal salt and a reducing agent, respectively. On mixing the microemulsions, Brownian motion is formed, which results in the collision of reverse micelles. During this collision, an exchange of reaction occurs between two reverse micelles (nanoreactors). After a successful collision, intermicellar exchange of reactant takes place, and thus nucleation starts with a good growth process around the nucleation point [38]. Thus, a good collision is essential for coalescence, mixing of reaction, nucleation, and growth of nanoparticles. Therefore, factors controlling the structure and dynamics of these nanoreactors can be easily manipulated to control the nanoparticles' morphology, size, shape, and composition. Surfactants stabilize these particles and prevent them from growing.

3.2.4 Hydrothermal Method

In the solvothermal process, the chemical reaction occurs in a sealed vessel (known as autoclave) where the temperature is above the boiling point of the solvents used during the chemical reaction. If the solvent used is water, then the process is called the hydrothermal process. In the past, the hydrothermal method was used to study the formation of rocks and minerals. The hydrothermal process was utilized in crystal formation and growth, and in today's era of nanotechnology and nanoscience, it has been used to prepare various NPs. Its simple synthetic process, low cost, effective crystal growth, and convenient operation from solution make it a convenient method for producing nanostructure. Hydrothermal is a subset of solvothermal methods, which has the advantage of being safe and environmentally friendly because it involves water as a solvent for crystal growth instead of organic solvents [39].

Basically, in hydrothermal processes, the species which are poorly or insoluble under normal conditions are dissolved and recrystallized under high temperature and high pressure. The primary step in the hydrothermal process is crystalline growth which can be achieved by the following steps:

1. The reactants are first dissolved in the hydrothermal medium to form ions.
2. Due to the temperature difference in the upper and lower region in an autoclave, the ions are separated. These ions are transported to the low-temperature region, where seed crystals are grown to form a supersaturated solution.
3. Finally, crystal growth occurs, and thus crystallization occurs. The morphology of the crystals grown in this process depends on the growth conditions. This process allows the size, shape, and crystallization control by altering some parameters like growth temperature, reaction time, a precursor used, etc.

Water has a very crucial role in the hydrothermal process. As we know, water's viscosity and surface tension decrease with increases in temperature. Therefore, in a hydrothermal system, the viscosity of water decreases, and the mobility of ions increases, and also, due to an increase in vapor pressure in the hydrothermal system, the mobility of ions increases which accelerates the reaction by the increase in the number of collisions. Therefore, collectively all these phenomena favor the growth of crystals [40].

A wide variety of nanomaterials have been fabricated by this hydrothermal technique using the microwave, mechanical mixing, and electric field to enhance the productivity and efficiency of the process. However, the microwave based hydrothermal mechanism has been gathering more attention by researchers in recent years.

3.2.5 Thermal Decomposition

Thermal decomposition is chemical deposition that is caused by heat. The endothermic reaction breaks the chemical bonds and splits them into smaller ones. Each element has a specific temperature at which it decomposes. The nanoparticles are produced by decomposing the metals at that specific temperature [34]. Thermal decomposition is a unique way to synthesize monodispersed metalic nanoparticles. The size and shape can easily be controlled by manipulating various factors like concentration and type of reactant/precursor, stabilizing/capping agents, temperature, duration of reaction, etc.

Coordinate compounds like organometallic precursors are commonly used in thermal decomposition method as they give high-quality monodispersed metalic nanoparticles. Thermal decomposition of coordinate compounds carried out in presence of stabilizing agents and reducing agents to reduce the metallic ions of the coordination compounds. Generally, surfactants are used as stabilizing agents to stabilize the nanoparticles formed by reducing agents. They are also called capping agents. During thermal decomposition, the reduced species are treated with these capping agents at a particular temperature. Some other examples of capping agents are thiols, carboxylic acids, amines, etc. The suitable temperature at which thermal decomposition will occur is dependent on the nature of metal ions and ligands in the coordination compounds. After thermal decomposition, the product is dissolved in polar/nonpolar solvents like ethanol, hexane, toluene and deionized water. Then, the whole solution is centrifuged to separate the colloidal nanoparticles. It is redispersed in a polar/nonpolar solvents and washed for several times to purify the nanoparticle. Finally, the nanoparticles are dried after washing [41].

3.3 Biological Methods/Green Synthesis Methods

The biological methods for the synthesis of nanoparticles involve plant extracts and microorganisms. Plants, bacteria, fungi, yeast, algae, and viruses have been used to produce low-cost, energy-efficient, nontoxic metallic nanoparticles by various promising biological approaches [42]. Unlike chemical methods, it does not involve toxic chemicals; instead, it is a commonly used green approach for synthesizing nanoparticles as it is cheap, eco-friendly, and can be scaled up to a large scale. It does not involve harsh conditions like high temperatures, high pressure, and very sophisticated and high-cost instruments. Actually, the biological method of synthesis results from the overlap of nanotechnology and biotechnology. Scientists and researchers are increasingly showing interest in this nanoparticle synthesis technique because of its economic viability and ecofriendliness. It is easier to tailor the size, shape, and morphology by just modifying the culture conditions like pH, temperature, and nutrients. Biological species and inorganic materials have a particular interaction from the origin of life. These regular interactions have sustained life on this planet. Researchers have utilized these unique interactions to synthesize nanoparticles from biological entities like plant extracts and microorganisms. They used plant extracts and microorganisms as bio-reductants to reduce metal ions to produce nanoparticles and also as stabilizing agents without using any other additional agents [43].

3.3.1 By Plants

In recent years, phyto-nanotechnology has emerged as a new field to synthesize nanoparticles and apply nanotechnology in the plant system. Due to such increased attention, plants and their extracts have been exploited to synthesize nanoparticles. Different types of plants and their various parts, such as leaf, stem, bark, fruit, etc., have been used to synthesize nanoparticles because of their excellent phytochemical contents it has [44]. Therefore, plants are righteously called chemical factories of nature. These phytocompounds extracted from plants, namely, terpenoids, alkaloids, flavonoids, steroids, phenols, and enzymes, play an essential role in synthesizing nanoparticles as they act as both bio-reductant and stabilizing agents. Biomolecules extracted from plants reduce metal in a single step. This reduction can be easily conducted at room temperature and pressure, which can be easily scaled up [45]. Many nanoparticles like silver gold, palladium, platinum, ZnO, TiO_2, etc. are synthesized by the plat extract-mediated process [46–49].

3.3.2 By Microorganisms

As we all know, microorganisms are used in the bioremediation of toxic metals by reducing them. In recent years microorganisms have been used for the biosynthesis of nanoparticles by reducing metal ions. Microorganisms have the potential to synthesize nanoparticles as it is cost-effective, eco-friendly, and avoids the use of toxic chemical and energy-intensive procedures. Microorganisms are considered nanofactories as they have a variety of enzymes that have the capability to accumulate and detoxify heavy metals. This enzyme also has the capability of reducing metal salts to produce nanoparticles. Various microorganisms such as yeast, bacteria, and fungi have been discovered to synthesize nanoparticles. Various biochemicals from microorganisms like proteins, cofactors, enzymes, etc. play vital roles in the synthesis of nanoparticles as reducing/capping agents. The mechanism of biosynthesis of nanoparticles by microorganisms involves grabbing target ions from the solution and accumulating the reduced metals in their element form by using enzymes produced by the microorganisms [Table 1]. The mechanism can be classified (according to the place of formation of nanoparticles) into intracellular and extracellular types. In intracellular, the ions are transported into the microorganisms to form nanoparticles in the presence of enzymes. The extracellular involves trapping metal ions on the surface of the cell and reducing it in the presence of enzymes [50]. Many microorganisms can produce inorganic nanoparticles. Various nanoparticles like gold, silver, ZnO, and CdS have been produced via biological methods using microorganisms [51–53].

4 Nanoparticles in Cancer Theranostics

4.1 Nanoparticle-Based Cancer Imaging

Early detection of cancer is necessary for its effective treatment. Different imaging techniques have been employed to precisely detect and locate tumors. Nanoparticles have been utilized for tumor imaging in various modalities such as magnetic resonance imaging (MRI), magnetic particle imaging (MPI), fluorescence imaging/optical imaging, photoacoustic imaging, and positron emission tomography (PET). An overview of some of the imaging methods is summarized in Table 2.

4.1.1 Magnetic Resonance Imaging

The human body contains ^{1}H nuclei, which spin about their axis with no net magnetization due to their random orientation. Under being influenced by a strong magnetic field (B), their spins get aligned along the applied external magnetic field, developing a net magnetic moment (M) while still precising about B. The frequency

Table 2 Overview of commonly used clinical imaging techniques

Imaging method	Advantages	Disadvantages	Nanoparticle contrast agents	References
Magnetic resonance imaging (MRI)	(i) High spatial resolution (10–500 micrometers) (ii) unlimited penetration depth	(i) Low sensitivity to contrast agents (ii) high costs Time intensive	(i) Gadolinium-containing probes (ii) superparamagnetic iron oxide nanoparticles (iii) paramagnetic liposomes and polymers	[129–132]
Magnetic particle imaging (MPI)	(i) Enables the scan to be read with ease. (ii) Relative lost imaging method.	(i) Limited ability to target the tumor and control the exposure. (ii) Limited penetration depth.	(i) Gadolinium nanoparticles. (ii) Iron oxide nanoparticles.	[92, 133, 134]
Computed tomography (CT)	(i) High resolution (20–200 micrometers) (ii) Unlimited penetration depth (iii) Fast (iv) Low costs	(i) Low sensitivity to contrasting agents (ii) insufficient soft tissue contrast without injection of contrast agents	(i) Barium-based nanoparticles (ii) Gold-based nanoparticles (iii) Bismuth nanoparticles	[135–137]
Ultrasound	(i) High temporal and spatial resolution (50–100 micrometers) (ii) Rapidly operable (iii) Real-time imaging (iv) Low costs	Not appropriate for whole-body imaging	(i) Nanobubbles (ii) gas-filled microbubbles	[138–140]
Fluorescence imaging (FI)/ optical imaging	(i) High sensitivity for contrast agents (ii) Low costs	Low penetration depths	(i) Quantum dots (ii) Fluorescent nanoparticle probes	[141, 142]
Photoacoustic imaging (PAI)	(i) High sensitivity (ii) real-time imaging (iii) low costs	(i) Limited penetration depth (ii) relatively low specificity to contrast agents	(i) Gold nanoparticles, gold Nanorods (ii) carbon nanotubes (iii) fluorescent/ dye-loaded nanoparticles	[120, 122, 143–145]

(continued)

Table 2 (continued)

Imaging method	Advantages	Disadvantages	Nanoparticle contrast agents	References
Positron emission tomography (PET)	(i) Unlimited tissue bed penetration. (ii) Used for whole-body imaging. (iii) Detailed anatomical information can be obtained when combined with CT or MRI.	(i) Exposure to radiation. (ii) Low spatial resolution. (iii) Expensive.	(i) Carbon-based nanoparticles. (ii) ^{18}F particles (iii) ^{64}Cu particles.	[146–148]

of precession is quantified by the Larmor equation as $\omega = \gamma B$, where γ the proportionality constant is element-specific. On application of radio wave pulse having a frequency (RF) equal to the precession frequency perpendicular to the direction of B, the ^{1}H nuclei (proton) absorb energy (resonance) and spin out of equilibrium, causing it to flip against the direction of the magnetic field [83]. With the removal of the RF pulse, the phase coherence of the exciting spinning proton ceases to exist. The precessing proton releases energy to attain its equilibrium state through decay in magnetization leading to the proton realigning with B. The energy released during the relaxation process of subsequent echo (gradient or spin echo) of the original RF signal is detected by the receiver coils, which are then processed through computation to obtain the final image. The relaxation process for the proton is of particular interest as it affects the contrast of the image produced during magnetic resonance imaging (MRI). This relaxation process proceeds through two concurrently occurring independent ways:

1. T1 (spin-lattice relaxation).
2. T2 (spin-spin relaxation).

T1 relaxation (or spin-lattice relaxation), in simple terms, is the dissipation of energy of the spins with lattice (or the surrounding environment), which may include neighbouring molecules, spins from other ^{1}H atoms, and solvent molecules [84]. It is the time taken to recover magnetization along the longitudinal axis (parallel to the external magnetic field) to 63% of preexcited net magnetization.

T2 (spin-spin) relaxation is when the transverse component of magnetization has 37% of its exciting level magnetization. It may also be expressed as the time required for the axial spin to return to its resting state. Due to factors such as field inhomogeneity and local field distortions due to molecular interactions (after the removal of the RF pulse), not all nuclei precess have the same frequency (Larmor frequency); instead, there are some minor differences (both positive and negative) in their frequency, which leads to nonuniformity in nuclear dipoles that ultimately leads to the energy being distributed through spin-spin interaction.

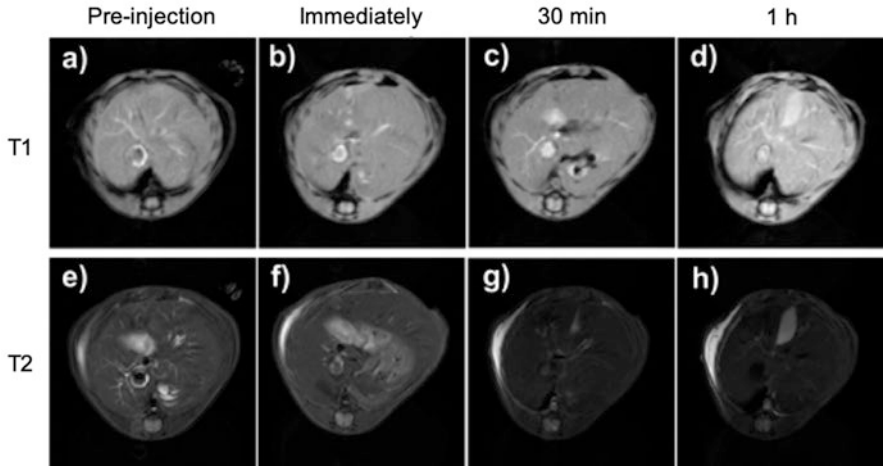

Fig. 2 T1- vs. T2-weighted transverse image of a mice tail vein injected with PEG-stabilized spherical Fe_3O_4/MnO contrast agent [91]. Copyright 2019, American Chemical Society

MRI intensity depends upon local proton density and rate of relaxation; however, the diagnosis that requires better imaging of organs is not possible through intrinsic contrast of MRI (as the signal to noise ratio (SNR) of the images is comparatively low) [85]. Moreover, contrast of the images obtained does not help to identify the stages of the tumor or differentiate between diseased and normal tissues. This is where contrast agents are required due the fact that the local environment affects image quality by exploiting the magnetic behavior of the MNPs. Hence, it is possible to achieve better imaging capabilities by alternating magnetic fields (AMFs) and enhancing the rate of the relaxation process. Further, MRI contrast agents enhance the relaxation process and reduce the relaxation time (T1, T2) for the protons. It is to be noted that though the contrast agents may be labeled as T1 or T2 contrast agents, this nomenclature does not accurately depict its mode of action as T1 agents do impact both T1 and T2 relaxation times. However, their effect on T1 relaxation is greater than on T2 relaxation; likewise, SPIONs (generally considered a T2 contrast agent) impacts T1 relaxation [86].

The characteristic visual difference between the images obtained using T1 and T2 agents is that T1 agents provide positive contrast (bright images), whereas T2 agents result negative contrast in MR images. For example, T1- and T2-weighted transverse images are recorded after injecting PEG-stabilized spherical Fe_3O_4/MnO contrast agent into a BALB/c mice tail vein (Fig. 2). The most extensively utilized T1 agents are Gd^{3+} chelates (e.g., Gd-DTPA) though Mn^{2+} and Fe^{3+} nanoparticles can also be used [87]. Several studies have been reported using ultrasmall superparamagnetic iron oxide nanoparticles as T1 contrast agents [88]. Relaxivity is an important measure to quantify the change in the relaxation time (T1 or T2) that contrast agents can bring to the inherent relaxation times, referred to as longitudinal relaxivity (r1) and transversal relaxivity (r2). The following equation relates the

relaxation time (T) to the concentration of the contrast agent (C), its relaxivity (r), and inherent relaxation time (T0):

$$\frac{1}{T} = \frac{1}{T_0} + r[C]$$

Understanding the factors responsible for impacting relaxation time is instrumental to designing contrast agents that have better sensitivity and significantly that help in selecting the requisite coating materials or conjugates that, besides allowing targeted imaging, aids in enhancing the relaxivity of contrast agents. This interaction between the contrast agents and the surrounding environment is complex. In contrast, the properties of T1 contrast agents (generally paramagnetic cores Gd^{3+}, Mn^{2+}) are impacted by dipole-dipole interaction of core and the H nuclei; for the T2 contrast agent, magnetic inhomogeneity plays the pivotal role, which in turn depends on several factors such as the saturation magnetization of the contrast agent, coating, and the size/radius of MNP [89]. For paramagnetic contrast agents (generally T1), relaxivity also depends on external factors such as temperature and applied magnetic field [90].

4.1.2 Magnetic Particle Imaging

Magnetic particle imaging (MPI) is a tracer imaging modality that can be used to image tissues in vivo based on the spatial distribution of the administered SPIO nanoparticles. A strong magnetic field nonlinearly magnetizes the tracers during imaging against a background of linearly magnetized tissues. In the imaging field of view, SPIONs tracers are saturated by a strong magnetic field gradient, and the unsaturated tracers remain in the vicinity of the field-free region (FFR). On application of an additional time-dependent homogeneous field to the imaging field of view, the particles in the FFR flip induce a signal in the receiver coil. The MPI signal detected is majorly contributed by the tracers at the FFR, allowing MPI spatial encoding [92]. MPI-tailored particles exhibit excellent spatial and temporal resolution, better circulation time, and higher SNR. There is no signal from background tissue in MPI, giving higher contrast. The images obtained using MPI may be used in conjugation with MRI for better diagnosis. SPIONs have been utilized for MPI imaging in vivo, which allows real-time imaging capability. The images obtained had a high spatial resolution, better sensitivity, and specificity [93].

4.1.3 Fluorescence Imaging/Optical Imaging

Optical imaging has been one of the most researched modalities for bioimaging. It allows real-time imaging capabilities. Due to their faster imaging capability, low cost, and non-usage of ionizing radiations, they have been studied as potential

candidates for cancer imaging. Fluorescence imaging quality is mainly dependent on factors such as tissue absorption, scattering, reflection, and autofluorescence [94]. This section will discuss the various types of fluorescence imaging methods that are currently under investigation at different stages of their development and those that are being utilized for in vivo/in vitro imaging applications.

(a) **Up-Conversion and Down-Conversion Nanoparticles.**

The conventional fluorophores suffer from some inherent limitations, such as lower differences in the absorption wavelength and the emission wavelength, making it difficult for the useful signal to be identified; this hinders imaging sensitivity. This causes great difficulty in differentiating the fluorescence signals of the fluorophores. Compared to conventional absorption of multiphoton, the conversion process in up-conversion nanoparticles (UCNPs) and down-conversion nanoparticles (DCNPs) is stepwise, occurring through the real electronic state as adjacent energy levels are very close, so they have better efficiency. These also have better tunability in emission wavelength and can be tuned for the required wavelength to help in imaging deeper tissues [95].

UCNPs are a special class of nanomaterials that can absorb multiple low-energy incident photons (having large wavelength), which causes it to attain an excited state during the transition from the excited state to a stable state; they emit high-energy photons at shorter wavelength, a phenomenon known as the anti-Stokes shift. UCNPs have unique characteristics such as a larger anti-Stokes shift and a larger emission range. These have negligible photobleaching, higher stability, and a longer lifetime [96]. Lanthanide-doped UCNPs have been extensively reported in the literature. It may be composed of a sensitizer part (usually Yb^{3+} is used), an emitter (Tm^{3+}, Ho^{3+} may be used), and a host matrix ($NaYbF_4$, $GdVO_4$, Er^{3+}, Yb^{3+} may be used) [97]. Deep tissue imaging is possible using UCNPs in the NIR range. Cyanine-modified UCNPs have also been reported for use as in vivo molecule monitoring with high sensitivity [98].

On the other hand, DCNP attains an excited state by absorbing high-energy shorter wavelength photons and emitting a long-wavelength photon. Both the conversion processes are nonlinear optical processes. QDs and fluorescent dyes are examples of DCNP. DCNPs have higher quantum yield and SNR. Gold-based nanogapped nanorod DCNP-based fluorescence along with PAI has been used in multimodal imaging to precisely trace drug release and image tumors [99].

(b) **Fluorescence Probe-Based Nanoparticles.**

These nanoparticles may be broadly classified as organic or inorganic molecules. Inorganic molecules mainly are the quantum dots and other fluorescent nanostructures (such as gold nanorods and SWCNTs). The fluorescence probe being used must have the following desirable properties: water solubility, strong fluorescence signal, higher quantum yields, chemical stability in various microenvironment conditions, and high contrast ability [100]. Various types of organic dyes have been studied for use in imaging and image-guided therapy, such as cyanines, methylene blue, squaraine, and porphyrin have been reported [101]. The fluorescence in these dyes is observed as electrons in their molecule transition from the excited state

caused by absorption of incident radiation (UV/visible or infrared range) to a lower energy state during which photons are emitted, leading to fluorescence. Indocyanine green (ICG), an FDA-approved tricarbocyanine dye, has been used to show the efficacy of dyes in tumor imaging [102]. Though dyes such as ICG have been utilized for several decades and have a proven record of their safety, their specificity in imaging cancer is not very encouraging. For example, studies using ICG dye for tumor imaging did allow imaging of the tumors in vivo, but several studies have also pointed out that ICG-based probes nonspecifically accumulate in the liver [103]. This lowers imaging efficiency in such probes. Methylene blue in the NIR has also been utilized to image breast tissue and identify tumors with acceptable sensitivity [104].

Inorganic nanoparticles and nanohybrids have also been researched for application in bioimaging [105]. In the case of metallic nanoparticles, the phenomenon of surface plasmon resonance is observed, which is caused when the light of a certain wavelength is incident on the surface of metallic nanoparticles, causing resonance oscillation of the free conduction electrons imparting it with unique optical properties. The utility of gold nanoparticles (AuNPs) has been studied for passively and actively tumors targeting and their bioimaging in vivo [106, 107]. The excellent chemical stability of AuNPs makes it one of the most suited for bioimaging applications. Novel NIR silica nanoparticle for imaging has also been prepared. It is based on the fluorescence resonance energy transfer principle and has shown to have a significant Stokes shift [108]. Calcium phosphate nanoparticle as an encapsulation of ICG has also been used for in vivo imaging of breast cancer. This has shown to be nontoxic and has better sensitivity to ICG alone [109, 110]. CNTs with surface-modified ligands have also been utilized to image tumors in vivo [111].

Conventionally the fluorescence probes have been irradiated with visible or UV radiation for imaging. However, recently, during the last few decades, studies utilizing the near-infrared (NIR) window for optical imaging applications have been reported and have shown to have significant advantages. Fluorescence in the NIR range has garnered significant interest in optical imaging, the reason being that the radiation's wavelength in range (900–1700 nm) has shown to have minimum absorption by tissues and their constituent organic components, owing to which there is reduced photon scattering and tissue autofluorescence, the background noise is reduced. Imaging properties are significantly enhanced, enabling deeper tissue imaging [112]. Different nanohybrids, QDs, and customized organic dyes have been studied, having peak emission in the NIR range.

(c) **Quantum Dots.**

These are nanocrystalline semiconductors and are engineered to exhibit the required properties. On being exposed to external excitation wavelengths, they emit fluorescence most commonly in the NIR region. The emission of light in quantum dots is due to a phenomenon known as "quantum confinement," which is observed when quantum dots are smaller than their exciton Bohr radius. Compared to organic dyes and other fluorescent probes, QDs have certain advantages such as better, brighter fluorescence emission compared to dyes, better stability, and minimal

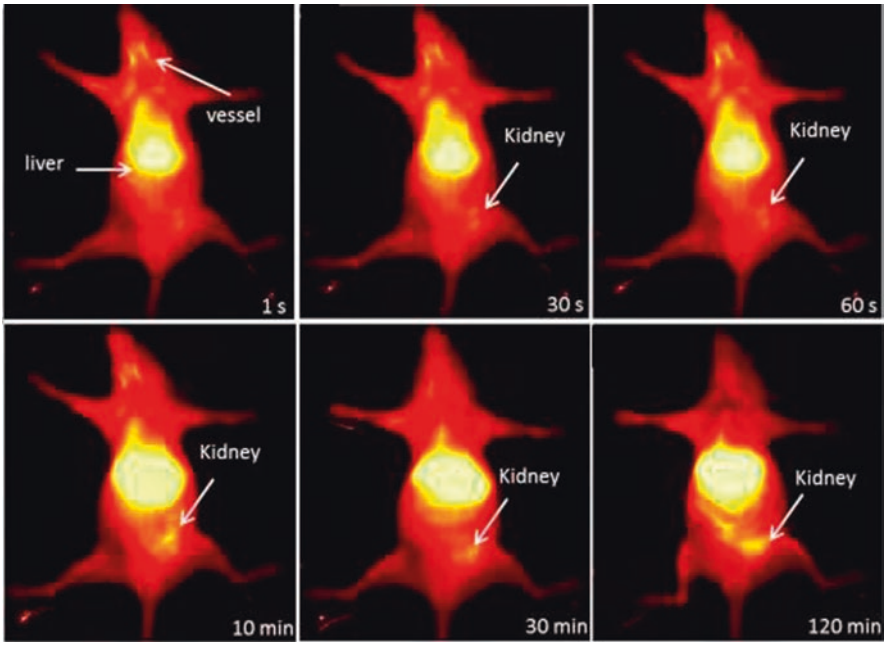

Fig. 3 Fluorescence imaging using graphene quantum dots in mice images at intervals of 1 s, 30 s, 60 s, 10 min, 30 min, and 120 min [119]. Copyright 2019, Elsevier

photobleaching [113]. The fluorescence properties of quantum dots are highly tunable as they depend on their morphology and composition; this provides excellent opportunities in obtaining customized fluorescence based on the specific imaging requirements [114].

The imaging properties of QDs can be further enhanced by improving their efficiency; studies have been conducted using QDs conjugated with antibodies, ligands, and peptides that are sensitive to cancer-related biomarkers. This helps in specifically targeting tumor tissues [115]. CdSe QDs have been extensively studied for in vivo imaging of tumors in mice. While QDs provide excellent imaging and characteristics compared to conventional fluorescence probes such as organic dyes, they have some limitations of their own. Heavy metal-based QDs such as CdSe, when being utilized for imaging, are coated with polymers such as PEG (polyethylene glycol), which makes them quite versatile and nontoxic, but if this external coating is disturbed, then in such scenario, the toxic metallic core may be toxic to cells. The hybrid fluorochrome-QD conjugate may also be used with lower cytotoxicity than Cd [116]. Other metallic QDs such as $AgInS_2$ and ZnS-$AgInS_2$ have lower cytotoxicity and similar imaging capabilities to Cd-based QDs [117]. Graphene quantum dots have also been investigated in bioimaging; they have lower toxicity when compared to Cd-based QDs and have excellent photostability [118]. Fluorescence imaging (FI) using graphene quantum dots dual-doped with both nitrogen and boron in mice images at intervals of 1 s, 30s, 60s, 10 min, 30 min, and 120 min is shown in Fig. 3.

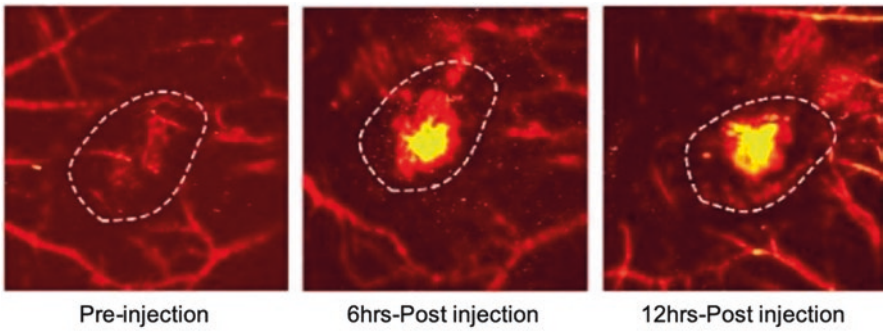

Fig. 4 PAI of tumor in mice 0 h, 6 h, and 12 h after injecting IR783-conjugated chitosan-polypyrrole nanocomposites [126]. Copyright 2021, Springer Nature

4.1.4 Photoacoustic Imaging

Photoacoustic imaging (PAI) is an emerging imaging modality based on converting electromagnetic energy into thermal energy, which generates acoustic pressure waves used to obtain the final image. In this imaging method, tissues that have to be imaged are irradiated with an ultrashort pulsed laser which is absorbed by the tissue, converting light to heat. This results in the generation of an ultrasound wave due to optical absorption and rapid thermal (or thermoelastic) expansion of the tissue. Transducers are used to detect these pressure waves, and an image can be formed based on the contrast due to differences in absorption properties of the tissue components. This hybrid method provides better imaging of deeper tissues while utilizing conventional optical imaging techniques associated with ultrasound [120].

Nanoparticle-based exogenous contrast agents have also been studied in the lab, which has been shown to improve image resolution. AuNPs and SWCNTs are some of the nanomaterials that have already been investigated and have shown promising results [121, 122]. Yamada et al. studied the imaging effectiveness of a conjugate nanoparticle using poly(2-methacryloyloxyethylphosphorylcholine) and 800RS (a hydrophilic, NIR cyanine dye) as a contrast agent in photoacoustic imaging. The 3D images obtained were high quality, better contrast, and high SNR [123]. Gold nanorods coated with silica have also been used for PAI [124]. Methylene blue is also a contrast agent that may be used in PAI, which acts as a hypoxia sensor [125]. Hypoxia is a characteristic of the tumor microenvironment. PA imaging of tumor in mice at 0 hrs, 6 hrs, and 12 hrs after injecting IR783-conjugated chitosan-polypyrrole nanocomposites is determined as shown in Fig. 4.

4.1.5 Positron Emission Tomography (PET)

Positron emission tomography (PET) is a noninvasive, real-time imaging method that utilizes ionizing radiation for bioimaging. It utilizes the nuclear phenomenon of the spontaneous emission of positron emission in radionuclides such as F-18 and carbon-11. Positrons are antimatter to electrons and are similar to electrons, with

the difference being that they carry a positive charge. On being injected into a tissue sample for imaging, the radionuclide undergoes spontaneous decay emitting positron, which encounters an electron in the nearby microenvironment; this leads to the annihilation of the electron and the positron leading to the emission of gamma radiations. The gamma wave detectors receive these gamma radiations, providing signals that are then processed to achieve a detailed image of the tissue sample under consideration [127].

These radionuclides may be doped into nanoparticles which can be made sensitive to the microenvironment and utilize cancer biomarkers to obtain a targeted image of the tumor. PET radiotracers are of different types for imaging tumors as it targets specific cellular events or microenvironments. For example, fluorodeoxyglucose may be utilized to evaluate the cellular glucose metabolism; to evaluate hypoxia microenvironment, 18F-fluoromisonidazole may be used; likewise, to measure cell proliferation, ^{18}F-fluorothymidine may be used [128]. PET provides the ability to evaluate biochemical events in real time with high sensitivity. There is no tissue penetration difficulty and no autofluorescence, but the preparation of the radiotracers is expensive and time-consuming; this makes the PET method unsuitable as a stand-alone method for bioimaging and is therefore generally used after screening is done using cheaper imaging modalities such as MRI, CT, and optical imaging. All the imaging techniques depicted above are shown in Table 2.

4.2 Nanoparticle-Based Cancer Therapy

Nanoparticle-based cancer therapy can be performed by various methods like chemotherapy, magnetic hyperthermia, photothermal therapy, and photodynamic therapy. These different methods of therapy are described in the section below.

4.2.1 Chemotherapy

From the term chemotherapy (CMT) itself, one can decipher that it implies cancer treatment, yet its authentic and historical significance was broader. The term was authored in the early part of the 1900s by Paul Ehrlich [149]. Arsphenamine, the first modern chemotherapeutic agent, used to treat syphilis, is an arsenic compound discovered in the year 1907 [149]. This was subsequently trailed by sulfonamides (sulfa drugs) and penicillin. In today's usage, the sense "any treatment of disease with drugs" is often expressed with the word pharmacotherapy [149]. CMT is an immensely beneficial therapy in the continuous fight against cancer and is regularly utilized related to different medicines. It plays a vital role in bringing down the diseased cells in the body, thereby reducing the probability of spreading cancer and reducing side effect [150]. For instance, in malignant testicular growth, 70% of patients are cured by initial CMT treatment. For patients that experience a recurrence of cancer following CMT treatments, evidence shows that retreating with the

CMT regimen followed by a stem cell transplant is effective on over half of the remaining 30% [150].

From various researches, it is evident that CMT in conjunction with surgery is used in routine to treat colon and rectal cancers [149]. Scientists are creating novel therapeutics with nanomaterials that have novel properties to be utilized in clinical science. Being smaller in size, nanoparticles help to encapsulate drug compounds. The nanoparticles' energy assimilation and reradiation properties permit them to develop further laser and hyperthermia applications, which disturb the diseased tissue [150]. Treatments of cancer are as of now restricted to surgery, radiation, and CMT. Each of the three strategies can harm the tissues, which leads to the incomplete treatment of cancer. Nanotechnology provides the necessary resources to target CMT straightforwardly and specifically to dangerous cells, thereby increasing therapy efficiency [149]. It improves CMT and decreases its unfavorable impacts by directing medications to target malignancy cells specifically. It is highly accurate and, hence, it upgrades the viability of radiotherapies and other current therapy alternatives. Moreover, this has helped to reduce the danger and to upgrade the probabilities for the patients to recover from the disease.

4.2.2 Magnetic Hyperthermia Therapy

MNPs are incredibly fascinating for biomedical applications in the view of their ability to respond to external magnetic fields, which permit their control for targeting in drug delivery. MNPs are very beneficial due to their stable nature in organic conditions and their low toxicity. The MNPs that are widely used in the medical field are mainly made up of iron oxides and ferrites, which are frequently doped with metals like Zn and Ni [151]. Surface coatings/functionalization and encapsulation of the MNPs are carried out to further improve their biocompatibility and bioavailability in targeted drug delivery. Magnetic hyperthermia therapy (MHT) creates the warm environment via a magnetically intervened localized heating of low-recurrence electromagnetic waves through the absorption by MNPs [151]. Thus, if MNPs are delivered inside tumor and the entire patient is exposed to an alternating magnetic field (AMF), the temperature of the tumor will rise. This increase of temperature ideally contracts the size of tumors [151]. MHT is typically applied as an adjuvant to radiotherapy or CMT, to which it fills in as a sensitizer, with an end goal to treat cancer. It utilizes higher temperatures than diathermy and lower temperatures than ablation. Also, when it is combined with radiation treatment, it may be called thermo-radiotherapy.

MHT is a thermal therapy for malignant tumor growth, in view of how MNPs can transform electromagnetic energy into heat by utilizing an AMF at radiofrequency. Many types of research have been explored for MHT-based cancer treatment. MHT was first endeavored in 1957 to treat cancers that had metastasized to the lymph hubs, and it is based upon the standards of limited hyperthermia by utilizing MNPs and consolidating an AMF to generate heat [151]. In MHT, heat is created after neighborhood testimony of MNPs and ensuing utilization of an outer AMF. Generally,

MNPs can produce heat by means of hysteresis losses when exposed to AMFs. The region encased by the hysteresis loop addresses the losses released as heat [152]. The heating capacity relies on the properties of the magnetic material and the AMF boundaries. MHT is widely explored to oppose tumor growth or cancer cell viability by exposure of superparamagnetic nanoparticles to the AMF because of the heat generation via Neel or Brown relaxation mechanism while improving the adequacy of different treatments like radiation and CMT.

For the case of nanostructured magnetic materials, the efficiency of heating hugely relies on a complex relationship between the timescale of the oscillating AMF field vector, magnetic moments, and the intrinsic time-dependent relaxation processes of the nanoparticle. Maier-Hauff et al. effectively showed the decency of superparamagnetic iron oxide nanoparticle-based hyperthermia in human brain growths. They gathered 14 patients with glioblastoma multiforme (GBM), which is a very forceful type of brain cancer. These patients got various medicines consisting of aminosilane-covered superparamagnetic nanoparticles injected straightforwardly into cancer. The nanoparticles were used to raise the temperature in the range of 42–45 °C by exploiting the localized heating by a remotely applied AMF. During the course of the hyperthermia therapy, the patients likewise got fractionated radiation treatment. No critical poison levels were observed [153]. Additionally, Carrouee et al. have created MNPs by combining AgNPs and VNIR color Nile blue (NB) with SPIONs for multimodal imaging dependent on MRI, surface-improved full Raman scattering (SERRS), and NIR-FI [154].

Likewise, Wang et al. have developed MNPs by conjugating fibronectin-focused and endogenous catalyst-activated SPIONs with Cys-Arg-Glu-Lys-Ala (CREKA) peptide and squaraine photosensitizer for MRI-directed FI and PDT of triple-negative breast cancer growths [155]. Very recently, superparamagnetic iron oxide nanoparticles (SPIONs) are widely utilized as highly reliable and efficient MNPs because of their capacity to convey anticancer medications to the cancer site. It helps to instigate magnetic hyperthermia to substitute CMT [18]. In MHT, SPIONs are conveyed (intravenously injected and amassed) at the cancer site, and afterward, the temperature of the growth cells is privately raised to the therapeutic temperature (42–46 °C) on openness to an outer AMF with a radiofrequency [18].

4.2.3 Photodynamic Therapy

Photodynamic therapy (PDT) is a kind of phototherapy involving light and a photosensitizing compound, used in combination with atomic oxygen to evoke cell demise (phototoxicity) [156]. PDT applications mainly include three components: a photosensitizer, a light source, and tissue oxygen [157]. The wavelength of the light source needs to be above the threshold value for exciting the photosensitizer to produce radicals and/or reactive oxygen species. These are free radicals produced through electron abstraction or transfer from a substrate molecule and a highly reactive state of oxygen known as singlet oxygen. Even if one of the components is missing, the desired therapy is not achieved, and the overall efficiency accordingly

requires cautious preparation of both medication and light dosimetry [158]. In general, the medications are given systematically, but since focusing on the process is primarily accomplished through the precise utilization of light, usually, from a laser source, the impact happens to be more localized in action [158]. PDT has a limitation in that it cannot treat advanced diseases because irradiation of the entire body is not possible without the required and adequate number of doses (at least with current technologies). Overall, for cutting-edge diseases, PDT can help improve quality of life and extend survival. PDT can be a specific and remedial therapy for early or localised disease, with numerous expected benefits over available other options.[158].

PDT can be termed as a multistage process: at first, a photosensitizer with negligible dark toxicity is administered, either systemically or topically, without light. Whenever an adequate amount of photosensitizer shows up in the unhealthy/diseased tissue, the photosensitizer is activated by exposure to light for a specified period. The light dose supplies sufficient energy to stimulate the photosensitizer but does not damage neighboring healthy tissue. Target sites are killed by the reactive oxygen [159] and it can be understood that numerous photosensitizers exists for PDT which can be divided into categories that are porphyrins, chlorins, and dyes [160]. Photosensitizers like Allumera, Photofrin, Visudyne, Levulan, Foscan, Metvix, Hexvix, Cysview, and Laserphyrin are commercially available for clinical use, while others being developed, for example, Antrin, Photochlor, Photosens, Photrex, Lumacan, Cevira, Visonac, Amphinex, and Azadipyrromethenes [160–162].

The parts of the cell that photosensitizers target differ significantly. Unlike radiation therapy, where harm is completed by focusing on cell DNA, most photosensitizers target other cell structures. For instance, meta-tetra(hydroxyphenyl)chlorin (mTHPC) restricts the atomic envelope [163], and 5-aminolevulinic acid (ALA) confines in the mitochondria and methylene blue in the lysosomes [164, 165]. PDT is well-known for its use in the treatment of skin inflammation. It is used in clinical settings to treat a wide range of conditions, including wet age-related macular degeneration, psoriasis, and atherosclerosis, and has shown some efficacy in viral medicines, including herpes. It likewise treats threatening cancers including head and neck, lung, bladder, and specific skin [157]. The innovation has also been tried to treat prostate malignancy in a canine model and in human prostate disease patients [166, 167]. It is perceived as a treatment system that is both negligibly intrusive and insignificantly harmful. Other light-based and laser treatments, for example, laser wound recuperating and revival or great beat light hair expulsion, do not need a photosensitizer [159]. Photosensitizers have been used to sanitize blood plasma and water to eliminate blood-borne infections and have been considered for rural utilizations, including herbicides and insecticides. Photodynamic treatment's benefits decrease the requirement for a sensitive medical procedure, extensive recovery, and negligible scar tissue arrangement and distortion. An incidental effect is the related photosensitization of skin tissue [159].

4.2.4 Photothermal Therapy

Photothermal therapy (PTT) refers to using electromagnetic radiation (in infrared frequencies) to treat different ailments, including cancers. This methodology is an expansion of PDT, in which a photosensitizer is energized using a particular band light. The heat released during the activation of the sensitizer to the exciting stage helps to kill the cancer cells. Photodynamic treatment does not harm the surrounding cells because the photosensitizers will generally develop in unusual cells, and the light is centered straight to them, thus not impacting the other cells of the body. Photodynamic treatment does not cause scars, which is helpful for individuals with skin malignancies and precancers. Dissimilar to PDT, PTT does not require the interaction of oxygen with cancer cells. Current investigations additionally show that PTT can utilize longer-frequency light, which is less energetic and, in this way, less damaging to different cells and tissues. Treatment of solid tumors can be efficiently done using such kind of treatment. The current research mainly focuses on nanomaterials for the PTT due to their size and efficacy over other sized particles. The permeability and retention effect are usually high in nanoscale, making it a strong contender for PTT. It has been observed that whenever a tumor is developed, blood vessels are required to improve its growth; these blood vessels located nearer to the tumor have different properties compared to the regular blood vessels. These developments can be prevented by using nanoparticles like gold nanorods (AuNRs), gold nanoshells, etc.

The practicality of utilizing gold nanorods was observed for both cancer cell imaging and photothermal therapy [168]. The authors conjugated antibodies (anti-EGFR monoclonal antibodies) to the outer layer of gold nanorods, permitting the gold nanorods to tie explicitly to certain threatening malignant growth cells (HSC and HOC dangerous cells). After brooding the cells with the gold nanorods, an 800 nm Ti-sapphire laser was utilized to light the cells at different forces. The creators revealed that successful annihilation of the threatening malignant growth cells was observed while nonmalignant cells were safe. When AuNRs are presented to NIR light, the oscillating magnetic field of light makes the free electrons oscillate collectively [169]. It was also experimentally observed that altering the shape and size of AuNRs correspondingly changes the assimilated wavelength. An ideal frequency would be between 700 and 1000 nm because natural tissue is optically transparent at these wavelengths [170]. While all gold nanoparticles (AuNP) are delicate to change in their shape and size, the properties of Au nanorods are susceptible to any adjustment of any of their measurements regarding their length and width or their perspective proportion. At the point when light gleams on a metal nanoparticle, the nanoparticle develops a dipole swaying along with the heading of the electric field. When the oscillation arrives at its maximum value, the corresponding frequency is known as the surface plasmon resonance (SPR) [169]. There are two SPR spectrum bands in AuNRs: one in the NIR region caused by its longitudinal oscillation (with a longer wavelength, it tends to become stronger) and one in the visible region caused by the transverse electronic oscillation (at shorter wavelengths, it becomes weak) [171]. An increase in light absorption for the particle is

characterized by the SPR [169]. It was noticed that the electrons energized by the NIR lose energy very rapidly after absorption due to the collisions between electrons. Whenever the relaxation of the electrons occurs, the energy is released, which is called a phonon that then heats the environment. This heating of the AuNP will help to eliminate the cancerous cells. This interaction is seen when a laser has a constant wave onto the AuNP [169].

Gold nanoshells, are silica nanoparticles that have been coated with a thin layer of gold. PEG linkers were used to associate them to antibodies (anti-HER2 or anti-IgG) [172]. After incubating SKBr3 cancer cells with the gold nanoshells, the cells were irradiated with an 820 nm laser. Then, it was observed that only the cells incubated with gold nanoshells conjugated with the specific antibody were damaged by the laser (anti-HER2). Another type of gold nanoshell is developed on liposomes that act as a soft template to encapsulate drugs inside and/or in a bilayer which is studied for triggered drug release by laser light [173]. PTT alone can wipe out the cancer cells in essential cancer or local lymphatic metastasis in the shallow tissues to reduce their further metastasis in distant organs [174]. However, due to the inhomogeneous distribution of heat within these tissues, PTT alone is insufficient to destroy disease cells and prevent cancer recurrence and metastasis (formation of secondary cancer cells located at a certain distance from a primary site of cancer).

5 Multimodal Theranostics

The various imaging and therapy techniques each have their own set of limitations. It is pretty evident that methods that can provide the combined effect of different imaging and therapeutic modalities which could significantly enhance therapeutic/imaging efficacy for effective cancer theranostics. Multifunctional nanoparticles have been investigated for multimodal treatment and have shown promising results. This section discusses the different multimodal techniques currently under investigation catering to combined imaging and therapy.

5.1 Multimodal Imaging

Cancer detection is highly complex. The survivability of cancer patients depends significantly on its early diagnosis and treatment. The different methods that have been developed for cancer detection are still not perfect, and each of the imaging methods has some of its own shortcomings and advantages. The multimodal imaging method involves utilizing more than one of the bioimaging methods in conjugation. This method helps to negate the shortcomings of the particular imaging methods, thereby providing combined imaging modality having essential imaging features such as real-time imaging capability, high sensitivity, better contrast resolution, and enhanced imaging with high SNR.

Different strategies are being investigated to achieve multimodal imaging. For example, fluorescence/MRI imaging can be used together for molecular imaging. While fluorescence imaging has high sensitivity and planar resolution, it has limitations such as low spatial resolution and lower penetration capability. Utilizing MRI can improve upon the limitations of fluorescence imaging as MRI has better penetration capability and spatial resolution. Gd-doped UCNPs can also be utilized for such types of multimodal imaging [175]. Dual-modal imaging by MRI/PET using radiolabeled SPIO nanoparticles has also been studied, and the resulting image provided excellent resolution [176]. Gd_2O_3:Eu^{3+} nanorods have been studied as a bifunctional nanoparticle with magnetic and luminescence properties enabling high

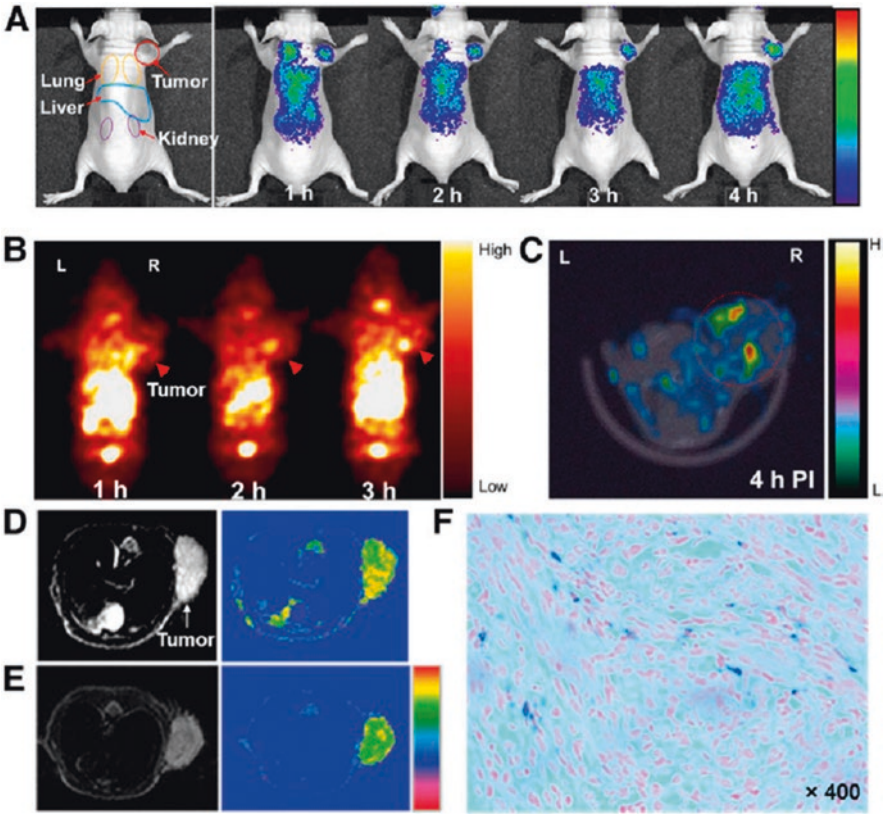

Fig. 5 Representation of multimodality tumor imaging using cMBP-GA-ATP@SPIONs. (**a**) In vivo noninvasive near-infrared fluorescent images of mice with U87MG tumors were taken at 1, 2, 3, and 4 h after injection of CMG-ATP@SPIONs. (**b**) In vivo, static planar g images of mice with U87MG tumors were taken at 1, 2, and 3 h after injection of 125I-cMBP-GA-ATP@SPIONs. (**c**) Transverse SPECT/CT image of the same mouse for 4 hours after injection. In vivo, T2-weighted MR images of mice with U87MG tumors were obtained before (**d**) and at 3 hours after (**e**) injection of cMBP-GA-ATP@SPIONs. (**f**) Staining was done using Prussian blue on tumor sections [182]. Copyright 2013, Society of Nuclear Medicine

contrast cell imaging and low autofluorescence [177]. Fluorescence/PET dual-modal imaging has also been successful in imaging triple-negative breast cancer [178]. Similarly, different combinations such as fluorescence/CT, PAI/MRI, and many other combinations of the different imaging modalities present are also possible to have trimodal imaging combining fluorescence/MRI/CT.

Other strategies such as developing contrast agents that allow multimodal T1-T2 imaging or developing nanocomposites that exhibit diverse properties, say fluorescence and magnetism, are also being investigated. Silica-coated Fe_2O_3 has been reported to exhibit fluorescence besides having magnetic nature [179]. MNP-QD conjugates as imaging nanoprobes have also been reported [180]. Nanoparticles conjugated with fluorescent polymer have been successfully prepared. PET/optical multimodal imaging has been studied using hyperbranched polymers labeled with organic dye and ^{64}Cu, the former is responsible for optical properties, and the latter is responsible for radioactivity that enables PET imaging [181]. Multimodal imaging can solve the limitations to the individual imaging modalities and may serve as a prime tool in detecting cancer in its initial stages for effective treatment. Multimodal imaging based on fluorescence, SPEC/CT, and MRI investigated using the mice model is shown in Fig. 5.

5.2 Multimodal Therapy

As the name suggests, multimodal therapy (MMT) combines two or more therapy to overcome the limitation of monotherapy. By combining various sorts of therapy together, MMTs can enhance cancer therapy. Various multimodal theranostics studies have been performed using different multifunctional nanoparticles combining therapeutic and imaging approaches. Ge et al. have illustrated the image-directed simultaneous PDT/PTT therapeutics and fluorescence imaging through biocompatible and photograph stable CD-based theranostic agents (evident from Fig. 6) [183]. In this work, CDs with various sizes (610 nm) are formulated by utilizing polythiophene benzoic acid (Fig. 6a, b), from which red light was observed on excitation. CDs generated singlet oxygen species and heat all the while under laser illumination (Fig. 6c) showed promising in vitro and in vivo results in the single/combined PDT and PTT cancer therapy as shown in Figure 6 (Fig. 6d, e).

Dai et al. formulated dendrimer-like MSN with hierarchical pores (HPSNs) as pH-responsive MNPs, which can be used in vivo targeted cancer imaging and therapy [184]. Moreover, Sun et al. have prepared DOX-conjugated, Gd-doped, ICG-loaded, and thermosensitive liposome-based MSNs as (MNPs) [185], which have demonstrated outstanding potential in cancer treatment via multimodal imaging (via NIR fluorescence imaging, PAI, and MRI) and also synergetic therapies (via PDT, PTT, and CMT). Recently, Yang et al. have developed perylene diimide-hybridized and ^{64}Cu-chelated photo-theranostic MSNs [186], which displayed a better PET imaging functionality with improved fluorescence and photoacoustic imaging capabilities.

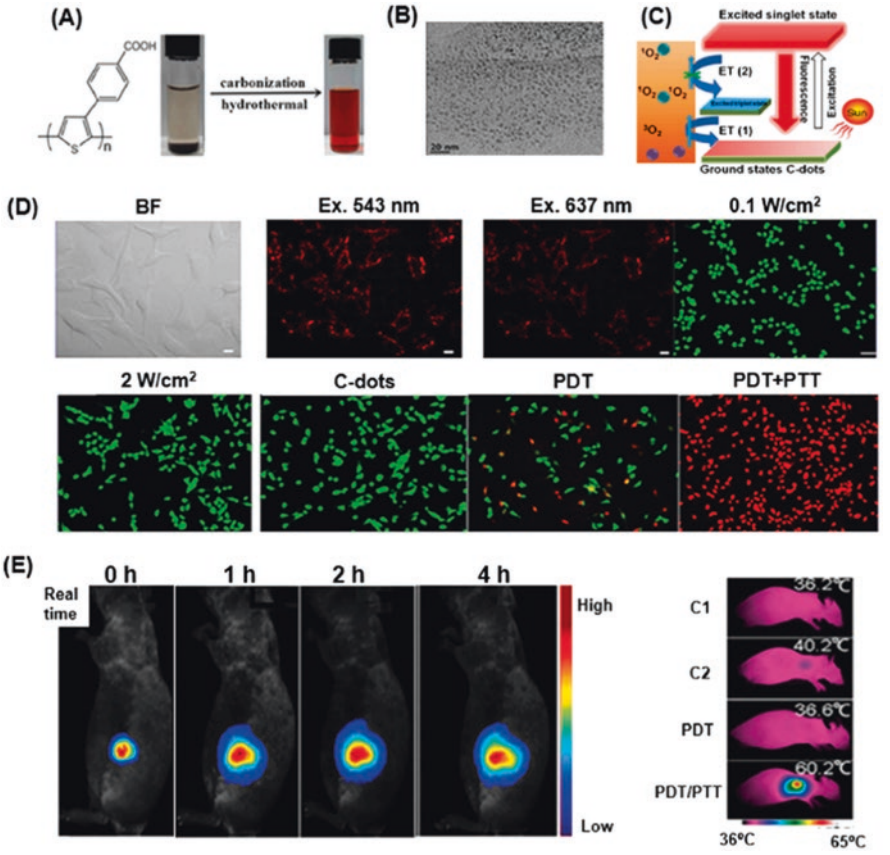

Fig. 6 PDT/PTT combined with C-dot-based bioimaging. (**a**) Fabrication of C-dots. (**b**) TEM image of C-dots. (**c**) The mechanism for the single oxygen $^1O_2$ generation by C-dots. (**d**) In vitro imaging and PDT/PTT with cancer cells. (**e**) Fluorescence images of calcein-AM/PI-stained cancer cells with laser irradiation [18]. Copyright 2021, Elsevier

Considering the results of different studies, it has been observed that multimodal therapy has the best endurance and efficacy compared to other monotherapies. However, further investigations are required to examine and refine the best accessible treatments for the different tumor types using the various possible multimodal treatment modalities.

6 Conclusion and Future Prospects

The biomedical use of nanotechnology is alluded to as nanomedicine, and this is made conceivable by a vast scope of scientific approaches and the advent of clinical techniques. One such methodology is the utilization of nanoparticles in

theranostics. A definitive point for consolidating nanomedicine and theranostics is to improve tumor diagnosis techniques and achieve patient-explicit treatment results. This can be achieved due to their high potential to target explicit organs or tissues. Just as their ability to be controlled with multifunctionality, theranostic nanoparticles have critical benefits that are splendidly appropriate for early cancer diagnosis and targeted therapy. In tumor therapy, nanotechnology can play a pivotal role in bettering conventional CMT besides being useful in other therapies such as MHT, PDT, and PTT. Moreover, different bioimaging modalities which are currently under development utilizing nanoprobes have shown promising results. The advantage of nanoprobes is that they can precisely track molecular activities occurring at the cellular level providing significant insights into the cellular mechanisms. This can be highly beneficial in cancer treatment, where early detection of malignancy directly impacts patient survivability. Furthermore, by introducing explicit modifications on the nanoparticle surfaces, designated controllable medication discharge and atomic imaging identification have been accomplished. Moreover, nanomaterials conjugated with antibodies and peptides have been shown to provide powerful focusing capacities to theranostic nanoparticles [187].

Considering the aspect of multifunctional nanomaterials synthesis, it is necessary to have a repeatable, scalable, and practical assembling strategy to synthesize theranostic nanoparticles. With the current synthesis techniques, it is pretty challenging to have a cost-effective solution for large-scale nanoparticle synthesis which can be used for medical applications. It is also essential to understand the basic pharmacokinetics of the nanoprobes being used to enhance their efficiency and also to reduce their developmental time. The potential toxicity of nanoparticles is also a significant impediment to their in vivo application. Another possible issue regarding the commercial success of nano-based theranostics is the expense of new medication advancements. Contrasted to the continued utilization of existing findings and treatment strategies, new medication improvements require a great deal of labor, material assets, and time. It merits pondering how to persuade manufacturers to put resources into the innovative work of theranostic nanoparticles.

To conclude, nanotechnology can effectively change how conventionally tumors are diagnosed and treated. It may be the necessary tool required for effective cancer treatment through efficient/combined diagnosis, therapy, and monitoring. Multimodal theranostics using multifunctional nanoparticles could be the way forward, given their effectiveness and customizability in cancer treatment, but further investigation on their biocompatibility and bioavailability is necessary.

Acknowledgments Dipak Maity would like to thank the University of Petroleum and Energy Studies (UPES) for getting in-house financial support (SEED Funding: UPES/R&D-HS/2402 2022/08) and all other support. Satya Ranjan Sahoo would like to thank the University Grants Commission of India (UGC) for providing a Junior Research Fellowship (NTA reference number—191620074817). Sumit Saha wishes to thank Prof. Suddhasatwa Basu, Director, CSIR-Institute of Minerals & Materials Technology, Bhubaneswar, India, for in-house financial support (Grant number: CSIR-IMMT-OLP-112) and requisite permissions.

References

1. Ferlay J, Colombet M, Soerjomataram I, Mathers C, Parkin D, Piñeros M, Znaor A, Bray F. Estimating the global cancer incidence and mortality in 2018: GLOBOCAN sources and methods. Int J Cancer. 2019;144(8):1941–53.
2. Raja IS, Kang MS, Kim KS, Jung YJ, Han D-W. Two-dimensional theranostic nanomaterials in cancer treatment: state of the art and perspectives. Cancers. 2020;12(6):1657.
3. Fan Z, Fu PP, Yu H, Ray PC. Theranostic nanomedicine for cancer detection and treatment. Journal of food drug analysis. 2014;22(1):3–17.
4. Jin C, Wang K, Oppong-Gyebi A, Hu J. Application of nanotechnology in cancer diagnosis and therapy – a mini-review. Int J Med Sci. 2020;17(18):2964.
5. Jokerst JV, Gambhir SS. Molecular imaging with theranostic nanoparticles. Acc Chem Res. 2011;44(10):1050–60.
6. Chen F, Ehlerding EB, Cai W. Theranostic nanoparticles. J Nucl Med. 2014;55(12):1919.
7. Wu K, Su D, Liu J, Saha R, Wang J-P. Magnetic nanoparticles in nanomedicine: a review of recent advances. Nanotechnology. 2019;30(50):502003.
8. Akbarzadeh A, Samiei M, Davaran S. Magnetic nanoparticles: preparation, physical properties, and applications in biomedicine. Nanoscale Res Lett. 2012;7(1):144.
9. Maity D, Kandasamy G, Sudame A. Superparamagnetic iron oxide nanoparticles for cancer theranostic applications. In: Rai M, Jamil B, editors. Nanotheranostics: applications and limitations. Cham: Springer; 2019. p. 245–76.
10. Patel KD, Singh RK, Kim H-W. Carbon-based nanomaterials as an emerging platform for theranostics. Materials Horizons. 2019;6(3):434–69.
11. Testa C, Zammataro A, Pappalardo A, Trusso Sfrazzetto G. Catalysis with carbon nanoparticles. RSC Adv. 2019;9(47):27659–64.
12. Kramer SA, Lin W. Silica-based nanoparticles for biomedical imaging and drug delivery applications. In: Handbook of nanobiomedical research. Singapore, World Scientific. p. 403–37.
13. Bitar A, Ahmad NM, Fessi H, Elaissari A. Silica-based nanoparticles for biomedical applications. Drug Discov Today. 2012;17(19):1147–54.
14. Yang Y, Zhang M, Song H, Yu C. Silica-based nanoparticles for biomedical applications: from nanocarriers to biomodulators. Acc Chem Res. 2020;53(8):1545–56.
15. Selvarajan V, Obuobi S, Ee PLR. Silica nanoparticles – a versatile tool for the treatment of bacterial infections. Front Chem. 2020;8(602)
16. Couleaud P, Morosini V, Frochot C, Richeter S, Raehm L, Durand J-O. Silica-based nanoparticles for photodynamic therapy applications. Nanoscale. 2010;2(7):1083–95.
17. Kumar HK, Venkatesh N, Bhowmik H, Kuila A. Metallic nanoparticle: a review, Biomed J Scientific/Tech Res. 2018;4(2):3765–75.
18. Kandasamy G, Maity D. Multifunctional theranostic nanoparticles for biomedical cancer treatments – a comprehensive review. Mater Sci Eng C. 2021;127:112199.
19. Gomes HIO, Martins CSM, Prior JAV. Silver nanoparticles as carriers of anticancer drugs for efficient target treatment of cancer cells. Nanomaterials. 2021;11(4):964.
20. Jain S, Hirst DG, O'Sullivan JM. Gold nanoparticles as novel agents for cancer therapy. Br J Radiol. 2012;85(1010):101–13.
21. Rao JP, Geckeler KE. Polymer nanoparticles: preparation techniques and size-control parameters. Prog Polym Sci. 2011;36(7):887–913.
22. Lu X-Y, Wu D-C, Li Z-J, Chen G-Q. Polymer nanoparticles (Chpater 7). In: Villaverde A, editor. Progress in molecular biology and translational science, vol. 104. Cambridge: Academic; 2011. p. 299–323.
23. Zielińska A, Carreiró F, Oliveira AM, Neves A, Pires B, Venkatesh DN, Durazzo A, Lucarini M, Eder P, Silva AM, Santini A, Souto EB. Polymeric nanoparticles: production, characterization. Toxicol Ecotoxicol. 2020;25(16):3731.

24. García-Pinel B, Porras-Alcalá C, Ortega-Rodríguez A, Sarabia F, Prados J, Melguizo C, López-Romero JM. Lipid-based nanoparticles: application and recent advances in cancer treatment. Nanomaterials. 2019;9(4):638.
25. Mittal P, Saharan A, Verma R, Altalbawy FMA, Alfaidi MA, Batiha GE-S, Akter W, Gautam RK, Uddin MS, Rahman MS. Dendrimers: a new race of pharmaceutical Nanocarriers. Biomed Res Int. 2021;2021:8844030.
26. Abbasi E, Aval SF, Akbarzadeh A, Milani M, Nasrabadi HT, Joo SW, Hanifehpour Y, Nejati-Koshki K, Pashaei-Asl R. Dendrimers: synthesis, applications, and properties. Nanoscale Res Lett. 2014;9(1):247.
27. Amendola V, Meneghetti M. Laser ablation synthesis in solution and size manipulation of noble metal nanoparticles. Phys Chem Chem Phys. 2009;11(20):3805–21.
28. Pimpin A, Srituravanich W. Review on micro-and nanolithography techniques and their applications. Eng J. 2012;16(1):37–56.
29. Hulteen JC, Treichel DA, Smith MT, Duval ML, Jensen TR, Van Duyne RP. Nanosphere lithography: size-tunable silver nanoparticle and surface cluster arrays. J Phys Chem B. 1999;103(19):3854–63.
30. Altissimo M. E-beam lithography for micro-/nanofabrication. Biomicrofluidics. 2010;4(2):026503.
31. Corbierre MK, Beerens J, Lennox RB. Gold nanoparticles generated by electron beam lithography of Gold(I)−thiolate thin films. Chem Mater. 2005;17(23):5774–9.
32. Yadav TP, Yadav RM, Singh DP. Mechanical milling: a top down approach for the synthesis of nanomaterials and nanocomposites. Nanosci Nanotechnol. 2012;2(3):22–48.
33. Rane AV, Kanny K, Abitha VK, Thomas S. Methods for synthesis of nanoparticles and fabrication of nanocomposites (Chapter 5). In: Mohan Bhagyaraj S, Oluwafemi OS, Kalarikkal N, Thomas S, editors. Synthesis of inorganic nanomaterials. Woodhead Publishing; 2018. p. 121–39.
34. Kolahalam LA, Kasi Viswanath IV, Diwakar BS, Govindh B, Reddy V, Murthy YLN. Review on nanomaterials: synthesis and applications. Mater Today Proc. 2019;18:2182–90.
35. Carlsson J-O, Martin PM. Chemical vapor deposition (Chapter 7). In: Martin PM, editor. Handbook of deposition technologies for films and coatings. 3rd ed. Boston: William Andrew Publishing; 2010. p. 314–63.
36. Sun L, Yuan G, Gao L, Yang J, Chhowalla M, Gharahcheshmeh MH, Gleason KK, Choi YS, Hong BH, Liu Z. Chemical vapour deposition. Nature Rev Methods Primers. 2021;1(1):5.
37. Hoar TP, Schulman JH. Transparent water-in-oil dispersions: the Oleopathic hydro-micelle. Nature. 1943;152(3847):102–3.
38. Ganguli AK, Ganguly A, Vaidya S. Microemulsion-based synthesis of nanocrystalline materials. Chem Soc Rev. 2010;39(2):474–85.
39. Djurisic AB, Xi YY, Hsu YF, Chan WK. Hydrothermal synthesis of nanostructures. Recent Pat Nanotechnol. 2007;1(2):121–8.
40. Yang G, Park S-J. Conventional and microwave hydrothermal synthesis and application of functional materials: a review. Materials. 2019; 12(7).
41. Odularu A T. Metal nanoparticles: thermal decomposition, biomedicinal applications to cancer treatment, and future perspectives. Bioinorg Chem Appl. 2018;2018:9354708.
42. Thakkar KN, Mhatre SS, Parikh RY. Biological synthesis of metallic nanoparticles. Nanomedicine. 2010;6(2):257–62.
43. Soni V, Raizada P, Singh P, Cuong H N, S R, Saini A, Saini R V, Le Q V, Nadda A K, Le T-T, Nguyen V-H. Sustainable and green trends in using plant extracts for the synthesis of biogenic metal nanoparticles toward environmental and pharmaceutical advances: a review. Environ Res. 2021; 202: 111622.
44. Iravani S. Green synthesis of metal nanoparticles using plants. Green Chem. 2011;13(10):2638–50.
45. Mittal AK, Chisti Y, Banerjee UC. Synthesis of metallic nanoparticles using plant extracts. Biotechnol Adv. 2013;31(2):346–56.

46. Chandran SP, Chaudhary M, Pasricha R, Ahmad A, Sastry M. Synthesis of gold nanotriangles and silver nanoparticles using Aloevera plant extract. Biotechnol Prog. 2006;22(2):577–83.
47. Song JY, Kim BS. Rapid biological synthesis of silver nanoparticles using plant leaf extracts. Bioprocess Biosyst Eng. 2008;32(1):79.
48. Ahmed S, Ahmad M, Swami BL, Ikram S. A review on plants extract mediated synthesis of silver nanoparticles for antimicrobial applications: a green expertise. J Adv Res. 2016;7(1):17–28.
49. Jadoun S, Arif R, Jangid NK, Meena RK. Green synthesis of nanoparticles using plant extracts: a review. Environ Chem Lett. 2021;19(1):355–74.
50. Zhang X, Yan S, Tyagi RD, Surampalli RY. Synthesis of nanoparticles by microorganisms and their application in enhancing microbiological reaction rates. Chemosphere. 2011;82(4):489–94.
51. Li X, Xu H, Chen Z-S, Chen G. Biosynthesis of nanoparticles by microorganisms and their applications. 2011; 2011: Article 8.
52. Narayanan KB, Sakthivel N. Biological synthesis of metal nanoparticles by microbes. Adv Colloid Interf Sci. 2010;156(1):1–13.
53. Hulkoti NI, Taranath TC. Biosynthesis of nanoparticles using microbes – a review. Colloids Surf B: Biointerfaces. 2014;121:474–83.
54. Avasthi A, Caro C, Pozo-Torres E, Leal M P, García-Martín M L. Magnetic nanoparticles as MRI contrast agents. Surface-Mod Nanobiomater Electrochem Biomed Appl. 2020; 49–91.
55. Paysen H, Loewa N, Stach A, Wells J, Kosch O, Twamley S, Makowski M R, Schaeffter T, Ludwig A, Wiekhorst F. 3D-imaging and quantification of magnetic nanoparticle uptake by living cells. arXiv preprint arXiv:.01259. 2019.
56. Kratz H, Taupitz M, Ariza de Schellenberger A, Kosch O, Eberbeck D, Wagner S, Trahms L, Hamm B, Schnorr J. Novel magnetic multicore nanoparticles designed for MPI and other biomedical applications: from synthesis to first in vivo studies. PloS One. 2018;13(1):e0190214.
57. Giustini A J, Petryk A A, Cassim S M, Tate J A, Baker I, Hoopes P J. Magnetic nanoparticle hyperthermia in cancer treatment. Nano Life. 2010; 1(01n02): 17–32.
58. Jose J, Kumar R, Harilal S, Mathew GE, Parambi DGT, Prabhu A, Uddin M, Aleya L, Kim H, Mathew B. Magnetic nanoparticles for hyperthermia in cancer treatment: an emerging tool. Environ Sci Pollut Res. 2020;27(16):19214–25.
59. Kudr J, Haddad Y, Richtera L, Heger Z, Cernak M, Adam V, Zitka O. Magnetic nanoparticles: from design and synthesis to real world applications. Nano. 2017;7(9):243.
60. Sundaram P, Abrahamse H. Phototherapy combined with carbon nanomaterials (1D and 2D) and their applications in cancer therapy. Materials. 2020;13(21):4830.
61. Casais-Molina M, Cab C, Canto G, Medina J, Tapia A. Carbon nanomaterials for breast cancer treatment. J Nanomater. 2018;2018
62. Shibu ES, Hamada M, Murase N, Biju V. Nanomaterials formulations for photothermal and photodynamic therapy of cancer. J Photochem Photobiol C Photochem Rev. 2013;15:53–72.
63. Rao N, Singh R, Bashambu L. Carbon-based nanomaterials: synthesis and prospective applications. Materials Today: Proceedings. 2021;44:608–14.
64. Ganash EA, Al-Jabarti GA, Altuwirqi RM. The synthesis of carbon-based nanomaterials by pulsed laser ablation in water. Mater Res Express. 2019;7(1):015002.
65. Sajjadi M, Nasrollahzadeh M, Jaleh B, Soufi GJ, Iravani S. Carbon-based nanomaterials for targeted cancer nanotherapy: recent trends and future prospects. J Drug Target. 2021;29(7):716–41.
66. Zheng Z, Jia Z, Qu C, Dai R, Qin Y, Rong S, Liu Y, Cheng Z, Zhang R. Biodegradable silica-based Nanotheranostics for precise MRI/NIR-II fluorescence imaging and self-reinforcing antitumor therapy. Small. 2021;17(10):2006508.
67. Li D, Liu Y, Yu S, Zhang D, Wang X, Zhong H, He K, Wang Y, Wu Y-X. A two-photon fluorescence silica nanoparticle-based FRET nanoprobe platform for effective ratiometric bioimaging of intracellular endogenous adenosine triphosphate. Analyst. 2021;146(15):4945–53.

68. Chen M, Hu J, Wang L, Li Y, Zhu C, Chen C, Shi M, Ju Z, Cao X, Zhang Z. Targeted and redox-responsive drug delivery systems based on carbonic anhydrase IX-decorated mesoporous silica nanoparticles for cancer therapy. Sci Rep. 2020;10(1):1–12.
69. Finnie KS, Bartlett JR, Barbé CJ, Kong L. Formation of silica nanoparticles in microemulsions. Langmuir. 2007;23(6):3017–24.
70. Zhou Y, Quan G, Wu Q, Zhang X, Niu B, Wu B, Huang Y, Pan X, Wu C. Mesoporous silica nanoparticles for drug and gene delivery. Acta Pharm Sin B. 2018;8(2):165–77.
71. Mao K, Zhang W, Yu L, Yu Y, Liu H, Zhang X. Transferrin-decorated protein-lipid hybrid nanoparticle efficiently delivers cisplatin and docetaxel for targeted lung cancer treatment. Drug Design Develop Therapy. 2021;15:3475.
72. Kalaycioglu GD, Aydogan N. Preparation and investigation of solid lipid nanoparticles for drug delivery. Colloids Surf A Physicochem Eng Aspects. 2016;510:77–86.
73. García-Pinel B, Porras-Alcalá C, Ortega-Rodríguez A, Sarabia F, Prados J, Melguizo C, López-Romero JM. Lipid-based nanoparticles: application and recent advances in cancer treatment. Nano. 2019;9(4):638.
74. C-g Q, Y-l C, P-j F, X-z X, Dong M, Yu J-c, Hu Q-y, Shen Q-d GZ. Conjugated polymer nanomaterials for theranostics. Acta Pharmacol Sin. 2017;38(6):764–81.
75. Zielińska A, Carreiró F, Oliveira AM, Neves A, Pires B, Venkatesh DN, Durazzo A, Lucarini M, Eder P, Silva AM. Polymeric nanoparticles: production, characterization, toxicology and ecotoxicology. Molecules. 2020;25(16):3731.
76. Palanikumar L, Al-Hosani S, Kalmouni M, Nguyen VP, Ali L, Pasricha R, Barrera FN, Magzoub M. pH-responsive high stability polymeric nanoparticles for targeted delivery of anticancer therapeutics. Commun Biol. 2020;3(1):1–17.
77. Wong KH, Lu A, Chen X, Yang Z. Natural ingredient-based polymeric nanoparticles for cancer treatment. Molecules. 2020;25(16):3620.
78. Sztandera K, Gorzkiewicz M, Klajnert-Maculewicz B. Gold nanoparticles in cancer treatment. Mol Pharm. 2018;16(1):1–23.
79. Yu Z, Gao L, Chen K, Zhang W, Zhang Q, Li Q, Hu K. Nanoparticles: a new approach to upgrade cancer diagnosis and treatment. Nanoscale Res Lett. 2021;16(1):1–17.
80. Marinescu L, Ficai D, Oprea O, Marin A, Ficai A, Andronescu E, Holban A-M. Optimized synthesis approaches of metal nanoparticles with antimicrobial applications. J Nanomater. 2020;2020
81. Jamkhande PG, Ghule NW, Bamer AH, Kalaskar MG. Metal nanoparticles synthesis: an overview on methods of preparation, advantages and disadvantages, and applications. J Drug Deliv Sci Technol Cancer Res Treat. 2019;53:101174.
82. Sharma A, Goyal AK, Rath G. Recent advances in metal nanoparticles in cancer therapy. J Drug Target. 2018;26(8):617–32.
83. Grover VP, Tognarelli JM, Crossey MM, Cox IJ, Taylor-Robinson SD, McPhail MJ. Magnetic resonance imaging: principles and techniques: lessons for clinicians. J Clin Experim Hepatol. 2015;5(3):246–55.
84. Issa B, Obaidat IM. Magnetic nanoparticles as MRI contrast agents. Magn Reson Imaging. 2019;378:40.
85. Alvares RD, Szulc DA, Cheng H-L. A scale to measure MRI contrast agent sensitivity. Sci Rep. 2017;7(1):1–9.
86. Liu Z, Cai J, Su H, Yang J, Sun W, Ma Y, Liu S, Zhang C. Feasibility of USPIOs for T 1-weighted MR molecular imaging of tumor receptors. RSC Adv. 2017;7(50):31671–81.
87. Huang G, Li H, Chen J, Zhao Z, Yang L, Chi X, Chen Z, Wang X, Gao J. Tunable T 1 and T 2 contrast abilities of manganese-engineered iron oxide nanoparticles through size control. Nanoscale. 2014;6(17):10404–12.
88. Rui Y-P, Liang B, Hu F, Xu J, Peng Y-F, Yin P-H, Duan Y, Zhang C, Gu H. Ultra-large-scale production of ultrasmall superparamagnetic iron oxide nanoparticles for T 1-weighted MRI. RSC Adv. 2016;6(27):22575–85.
89. Zhou Z, Tian R, Wang Z, Yang Z, Liu Y, Liu G, Wang R, Gao J, Song J, Nie L. Artificial local magnetic field inhomogeneity enhances T 2 relaxivity. Nat Commun. 2017;8(1):1–10.

90. Noordin S, Winalski C, Shortkroff S, Mulkern R. Factors affecting paramagnetic contrast enhancement in synovial fluid: effects of electrolytes, protein concentrations, and temperature on water proton relaxivities from Mn ions and Gd chelated contrast agents. Osteoarthr Cartil. 2010;18(7):964–70.
91. Lu C, Dong P, Pi L, Wang Z, Yuan H, Liang H, Ma D, Chai KY. Hydroxyl–PEG–phosphonic acid-stabilized superparamagnetic manganese oxide-doped iron oxide nanoparticles with synergistic effects for dual-mode MR imaging. Langmuir. 2019;35(29):9474–82.
92. Wu L, Zhang Y, Steinberg G, Qu H, Huang S, Cheng M, Bliss T, Du F, Rao J, Song G. A review of magnetic particle imaging and perspectives on neuroimaging. Am J Neuroradiol. 2019;40(2):206–12.
93. Dadfar SM, Camozzi D, Darguzyte M, Roemhild K, Varvarà P, Metselaar J, Banala S, Straub M, Güvener N, Engelmann U. Size-isolation of superparamagnetic iron oxide nanoparticles improves MRI, MPI and hyperthermia performance. J Nanobiotechnol. 2020;18(1):1–13.
94. Lifante J, Shen Y, Ximendes E, Martín Rodríguez E, Ortgies DH. The role of tissue fluorescence in in vivo optical bioimaging. J Appl Phys. 2020;128(17):171101.
95. Loo J F-C, Chien Y-H, Yin F, Kong S-K, Ho H-P, Yong K-T. Upconversion and downconversion nanoparticles for biophotonics and nanomedicine. Coordination Chem Rev. 2019;400:213042.
96. Fan Q, Cui X, Guo H, Xu Y, Zhang G, Peng B. Application of rare earth-doped nanoparticles in biological imaging and tumor treatment. J Biomater Appl. 2020;35(2):237–63.
97. Chen J, Zhao JX. Upconversion nanomaterials: synthesis, mechanism, and applications in sensing. Sensors. 2012;12(3):2414–35.
98. Liang G, Wang H, Shi H, Wang H, Zhu M, Jing A, Li J, Li G. Recent progress in the development of upconversion nanomaterials in bioimaging and disease treatment. J Nanobiotechnol. 2020;18(1):1–22.
99. Chen T, Su L, Ge X, Zhang W, Li Q, Zhang X, Ye J, Lin L, Song J, Yang H. Dual activated NIR-II fluorescence and photoacoustic imaging-guided cancer chemo-radiotherapy using hybrid plasmonic-fluorescent assemblies. Nano Res. 2020;13(12):3268–77.
100. Lo KK-W. Luminescent rhenium (I) and iridium (III) polypyridine complexes as biological probes, imaging reagents, and photocytotoxic agents. Acc Chem Res. 2015;48(12):2985–95.
101. Sheng Z, Cai L. Organic dye-loaded nanoparticles for imaging-guided cancer therapy. Adv Nanotheranost I: Springer; 2016. p. 217–45.
102. Nagahara R, Onda N, Yamashita S, Kojima M, Inohana M, Eguchi A, Nakamura M, Matsumoto S, Yoshida T, Shibutani M. Fluorescence tumor imaging by iv administered indocyanine green in a mouse model of colitis-associated colon cancer. Cancer Sci. 2018;109(5):1638–47.
103. Kaibori M, Matsui K, Ishizaki M, Iida H, Sakaguchi T, Tsuda T, Okumura T, Inoue K, Shimada S, Ohtsubo S. Evaluation of fluorescence imaging with indocyanine green in hepatocellular carcinoma. Cancer Imaging. 2016;16(1):1–7.
104. Zhang C, Jiang D, Huang B, Wang C, Zhao L, Xie X, Zhang Z, Wang K, Tian J, Luo Y. Methylene blue–based near-infrared fluorescence imaging for breast cancer visualization in resected human tissues. Technol Cancer Res Treat. 2019;18:1533033819894331.
105. Choi G, Rejinold NS, Piao H, Choy J-H. Inorganic–inorganic nanohybrids for drug delivery, imaging and photo-therapy: recent developments and future scope. Chem Sci. 2021;
106. Ahmad T, Sarwar R, Iqbal A, Bashir U, Farooq U, Halim SA, Khan A, Al-Harrasi A. Recent advances in combinatorial cancer therapy via multifunctionalized gold nanoparticles. Nanomedicine. 2020;15(12):1221–37.
107. Liu J, Yu M, Zhou C, Yang S, Ning X, Zheng J. Passive tumor targeting of renal-clearable luminescent gold nanoparticles: long tumor retention and fast normal tissue clearance. J Am Chem Soc. 2013;135(13):4978–81.
108. Li D, Liu Y, Yu S, Zhang D, Wang X, Zhong H, He K, Wang Y, Wu Y. Two-photon fluorescence silica nanoparticles-based FRET nanoprobe platform for effectively ratiometric bioimaging of intracellular endogenous adenosine triphosphate. Analyst. 2021.
109. Huang D, He B, Mi P. Calcium phosphate nanocarriers for drug delivery to tumors: imaging, therapy and theranostics. Biomater Sci. 2019;7(10):3942–60.

110. Ashokan A, Gowd GS, Somasundaram VH, Bhupathi A, Peethambaran R, Unni A, Palaniswamy S, Nair SV, Koyakutty M. Multifunctional calcium phosphate nano-contrast agent for combined nuclear, magnetic and near-infrared in vivo imaging. Biomaterials. 2013;34(29):7143–57.
111. Antaris AL, Robinson JT, Yaghi OK, Hong G, Diao S, Luong R, Dai H. Ultra-low doses of chirality sorted (6, 5) carbon nanotubes for simultaneous tumor imaging and photothermal therapy. ACS Nano. 2013;7(4):3644–52.
112. Choi HS, Gibbs SL, Lee JH, Kim SH, Ashitate Y, Liu F, Hyun H, Park G, Xie Y, Bae S. Targeted zwitterionic near-infrared fluorophores for improved optical imaging. Nat Biotechnol. 2013;31(2):148–53.
113. Wang L-W, Peng C-W, Chen C, Li Y. Quantum dots-based tissue and in vivo imaging in breast cancer researches: current status and future perspectives. Breast Cancer Res Treatm. 2015;151(1):7–17.
114. Tholouli E, Sweeney E, Barrow E, Clay V, Hoyland JA, Byers RJ. Quantum dots light up pathology. J Pathol J Pathol Soc Great Br Ireland. 2008;216(3):275–85.
115. Jung S, Chen X. Quantum dot–dye conjugates for biosensing, imaging, and therapy. Adv Healthc Mater. 2018;7(14):1800252.
116. Shen L. Biocompatible polymer/quantum dots hybrid materials: current status and future developments. J Funct Biomater. 2011;2(4):355–72.
117. Kurshanov D, Gromova YA, Cherevkov S, Ushakova E, Kormilina T, Dubavik A, Fedorov A, Baranov A. Non-toxic ternary quantum dots AgInS 2 and AgInS 2/ZnS: synthesis and optical properties. Opt Spectrosc. 2018;125(6):1041–6.
118. Dong J, Wang K, Sun L, Sun B, Yang M, Chen H, Wang Y, Sun J, Dong L. Application of graphene quantum dots for simultaneous fluorescence imaging and tumor-targeted drug delivery. Sensors Actuators B Chem. 2018;256:616–23.
119. Wang H, Mu Q, Wang K, Revia RA, Yen C, Gu X, Tian B, Liu J, Zhang M. Nitrogen and boron dual-doped graphene quantum dots for near-infrared second window imaging and photothermal therapy. Appl Mater Today. 2019;14:108–17.
120. Mehrmohammadi M, Joon Yoon S, Yeager D, Emelianov SY. Photoacoustic imaging for cancer detection and staging. Curr Mol Imaging. 2013;2(1):89–105.
121. De la Zerda A, Zavaleta C, Keren S, Vaithilingam S, Bodapati S, Liu Z, Levi J, Ma T, Oralkan O, Cheng Z. Photoacoustic molecular imaging in living mice utilizing targeted carbon nanotubes. Nature Nanotech. 2008;3:557–62.
122. Han S, Bouchard R, Sokolov KV. Molecular photoacoustic imaging with ultra-small gold nanoparticles. Biomed Opt Express. 2019;10(7):3472–83.
123. Yamada H, Matsumoto N, Komaki T, Konishi H, Kimura Y, Son A, Imai H, Matsuda T, Aoyama Y, Kondo T. Photoacoustic in vivo 3D imaging of tumor using a highly tumor-targeting probe under high-threshold conditions. Sci Rep. 2020;10(1):1–9.
124. Chen Y-S, Frey W, Kim S, Kruizinga P, Homan K, Emelianov S. Silica-coated gold nanorods as photoacoustic signal nanoamplifiers. Nano Lett. 2011;11(2):348–54.
125. Zhang J, Duan F, Liu Y, Nie L. High-resolution photoacoustic tomography for early-stage cancer detection and its clinical translation. Radiol Imaging Cancer. 2020;2(3):e190030.
126. Doan VHM, Nguyen VT, Mondal S, Vo TMT, Ly CD, Vu DD, Ataklti GY, Park S, Choi J, Oh J. Fluorescence/photoacoustic imaging-guided nanomaterials for highly efficient cancer theragnostic agent. Sci Rep. 2021;11(1):1–18.
127. Goel S, England CG, Chen F, Cai W. Positron emission tomography and nanotechnology: a dynamic duo for cancer theranostics. Adv Drug Deliv Rev. 2017;113:157–76.
128. Norregaard K, Jørgensen JT, Simón M, Melander F, Kristensen LK, Bendix PM, Andresen TL, Oddershede LB, Kjaer A. 18F-FDG PET/CT-based early treatment response evaluation of nanoparticle-assisted photothermal cancer therapy. PLoS One. 2017;12(5):e0177997.
129. Narmani A, Farhood B, Haghi-Aminjan H, Mortezazadeh T, Aliasgharzadeh A, Mohseni M, Najafi M, Abbasi H. Gadolinium nanoparticles as diagnostic and therapeutic agents: their

delivery systems in magnetic resonance imaging and neutron capture therapy. J Drug Del Sci Technol Cancer Res Treat. 2018;44:457–66.
130. Maity D, Zoppellaro G, Sedenkova V, Tucek J, Safarova K, Polakova K, Tomankova K, Diwoky C, Stollberger R, Machala L. Surface design of core–shell superparamagnetic iron oxide nanoparticles drives record relaxivity values in functional MRI contrast agents. Chem Commun. 2012;48(93):11398–400.
131. Langereis S, Geelen T, Grüll H, Strijkers GJ, Nicolay K. Paramagnetic liposomes for molecular MRI and MRI-guided drug delivery. NMR Biomed. 2013;26(7):728–44.
132. Kandasamy G, Sudame A, Luthra T, Saini K, Maity D. Functionalized hydrophilic superparamagnetic iron oxide nanoparticles for magnetic fluid hyperthermia application in liver cancer treatment. ACS Omega. 2018;3(4):3991–4005.
133. Kratz H, Eberbeck D, Wagner S, Taupitz M, Schnorr J. Synthetic routes to magnetic nanoparticles for MPI. Biomedizinische Technik/Biomed Eng. 2013;58(6):509–15.
134. Du Y, Lai PT, Leung CH, Pong PW. Design of superparamagnetic nanoparticles for magnetic particle imaging (MPI). Int J Mol Sci. 2013;14(9):18682–710.
135. Mira J G, Potter J L, Fullerton G D, Ezekiel J. Advantages and limitations of computed tomography scans for treatment planning of lung cancer. Intl J Rad Oncol Biol Phys. 1982;8(9):1617–23.
136. Makaju S, Prasad P, Alsadoon A, Singh A, Elchouemi A. Lung cancer detection using CT scan images. Proc Comput Sci. 2018;125:107–14.
137. Jarrett D, Stride E, Vallis K, Gooding MJ. Applications and limitations of machine learning in radiation oncology. Br J Radiol. 2019;92(1100):20190001.
138. Iranmakani S, Mortezazadeh T, Sajadian F, Ghaziani MF, Ghafari A, Khezerloo D, Musa AE. A review of various modalities in breast imaging: technical aspects and clinical outcomes. Egypt J Radiol Nucl Med. 2020;51(1):1–22.
139. Su C, Ren X, Nie F, Li T, Lv W, Li H, Zhang Y. Current advances in ultrasound-combined nanobubbles for cancer-targeted therapy: a review of the current status and future perspectives. RSC Adv. 2021;11(21):12915–28.
140. Guo R, Lu G, Qin B, Fei B. Ultrasound imaging technologies for breast cancer detection and management: a review. Ultrasound Med Biol. 2018;44(1):37–70.
141. Tandale P, Choudhary N, Singh J, Sharma A, Shukla A, Sriram P, Soni U, Singla N, Barnwal R P, Singh G. Fluorescent quantum dots: an insight on synthesis and potential biological application as drug carrier in cancer. Biochem Biophys Rep. 2021;26:100962.
142. Bu L, Shen B, Cheng Z. Fluorescent imaging of cancerous tissues for targeted surgery. Adv Drug Deliv Rev. 2014;76:21–38.
143. Siregar S, Nagoka R, Ishikawa K, Saijo Y. Carbon nanotubes as potential candidate for photoacoustic imaging contrast agent. In: Proceedings of meetings on acoustics 6ICU, Acoustical Society of America. 2017.
144. Zhang R, Wang Z, Xu L, Xu Y, Lin Y, Zhang Y, Sun Y, Yang G. Rational design of a multifunctional molecular dye with single dose and laser for efficiency NIR-II fluorescence/photoacoustic imaging guided photothermal therapy. Anal Chem. 2019;91(19):12476–83.
145. Nyayapathi N, Xia J. Photoacoustic imaging of breast cancer: a mini review of system design and image features. J Biomed Opt. 2019;24(12):121911.
146. Unterrainer M, Eze C, Ilhan H, Marschner S, Roengvoraphoj O, Schmidt-Hegemann N-S, Walter F, Kunz WG, Af Rosenschöld PM, Jeraj R. Recent advances of PET imaging in clinical radiation oncology. Radiat Oncol. 2020;15(1):1–15.
147. Kapoor V, McCook BM, Torok FS. An introduction to PET-CT imaging. Radiographics. 2004;24(2):523–43.
148. Griffeth LK. Use of PET/CT scanning in cancer patients: technical and practical considerations. Taylor & Francis: Baylor University Medical Center Proceedings; 2005.
149. DeVita VT, Chu E. A history of cancer chemotherapy. Cancer Res. 2008;68(21):8643–53.
150. Nichols HJ, Walker JE. Experimental observations on the prophylaxis and treatment of syphilis. J Exp Med. 1923;37(4):525–42.

151. Kumar CS, Mohammad F. Magnetic nanomaterials for hyperthermia-based therapy and controlled drug delivery. Adv Drug Deliv Rev. 2011;63(9):789–808.
152. Périgo EA, Hemery G, Sandre O, Ortega D, Garaio E, Plazaola F, Teran FJ. Fundamentals and advances in magnetic hyperthermia. Appl Phys Rev. 2015;2(4):041302.
153. Maier-Hauff K, Rothe R, Scholz R, Gneveckow U, Wust P, Thiesen B, Feussner A, Von Deimling A, Waldoefner N, Felix R. Intracranial thermotherapy using magnetic nanoparticles combined with external beam radiotherapy: results of a feasibility study on patients with glioblastoma multiforme. J Neuro-Oncol. 2007;81(1):53–60.
154. Carrouée A, Allard-Vannier E, Même S, Szeremeta F, Beloeil J-C, Chourpa I. Sensitive trimodal magnetic resonance imaging-surface-enhanced resonance Raman scattering-fluorescence detection of cancer cells with stable magneto-plasmonic nanoprobes. Anal Chem. 2015;87(22):11233–41.
155. Wang Y, Jiang L, Zhang Y, Lu Y, Li J, Wang H, Yao D, Wang D. Fibronectin-targeting and cathepsin B-activatable theranostic nanoprobe for MR/fluorescence imaging and enhanced photodynamic therapy for triple negative breast cancer. ACS Appl Mater Interf. 2020;12(30):33564–74.
156. Dougherty TJ, Gomer CJ, Henderson BW, Jori G, Kessel D, Korbelik M, Moan J, Peng Q. Photodynamic therapy. JNCI. 1998;90(12):889–905.
157. Chen J, Keltner L, Christophersen J, Zheng F, Krouse M, Singhal A, Wang S-S. New technology for deep light distribution in tissue for phototherapy. Cancer J. 2002;8(2):154–63.
158. Brown SB, Brown EA, Walker I. The present and future role of photodynamic therapy in cancer treatment. Lancet Oncol. 2004;5(8):497–508.
159. Josefsen L B, Boyle R W. Photodynamic therapy and the development of metal-based photosensitisers. Metal-Based Drugs. 2008; 2008.
160. Allison RR, Downie GH, Cuenca R, Hu X-H, Childs CJ, Sibata C. Photosensitizers in clinical PDT. Photodiag Photodyn Ther. 2004;1(1):27–42.
161. Huang Z. A review of progress in clinical photodynamic therapy. Technol Cancer Res Treat. 2005;4(3):283–93.
162. O'Connor AE, Gallagher WM, Byrne AT. Porphyrin and nonporphyrin photosensitizers in oncology: preclinical and clinical advances in photodynamic therapy. Photochem Photobiol. 2009;85(5):1053–74.
163. Foster TH, Pearson BD, Mitra S, Bigelow CE. Fluorescence anisotropy imaging reveals localization of meso-tetrahydroxyphenyl chlorin in the nuclear envelope. Photochem Photobiol. 2005;81(6):1544–7.
164. Wilson JD, Bigelow CE, Calkins DJ, Foster TH. Light scattering from intact cells reports oxidative-stress-induced mitochondrial swelling. Biophys J. 2005;88(4):2929–38.
165. Mellish KJ, Cox RD, Vernon DI, Griffiths J, Brown SB. In vitro photodynamic activity of a series of methylene blue analogues. Photochem Photobiol. 2002;75(4):392–7.
166. Swartling J, Höglund OV, Hansson K, Södersten F, Axelsson J, Lagerstedt A-S. Online dosimetry for temoporfin-mediated interstitial photodynamic therapy using the canine prostate as model. J Biomed Opt. 2016;21(2):028002.
167. Swartling J, Axelsson J, Ahlgren G, Kälkner KM, Nilsson S, Svanberg S, Svanberg K, Andersson-Engels S. System for interstitial photodynamic therapy with online dosimetry: first clinical experiences of prostate cancer. J Biomed Opt. 2010;15(5):058003.
168. Huang X, El-Sayed IH, Qian W, El-Sayed MA. Cancer cell imaging and photothermal therapy in the near-infrared region by using gold nanorods. J Am Chem Soc. 2006;128(6):2115–20.
169. Huang X, El-Sayed MA. Gold nanoparticles: optical properties and implementations in cancer diagnosis and photothermal therapy. J Adv Res. 2010;1(1):13–28.
170. Hauck TS, Jennings TL, Yatsenko T, Kumaradas JC, Chan WC. Enhancing the toxicity of cancer chemotherapeutics with gold nanorod hyperthermia. Adv Mater. 2008;20(20):3832–8.
171. Huang X, Jain PK, El-Sayed IH, El-Sayed MA. Plasmonic photothermal therapy (PPTT) using gold nanoparticles. Lasers Med Sci. 2008;23(3):217–28.
172. Loo C, Lowery A, Halas N, West J, Drezek R. Immunotargeted nanoshells for integrated cancer imaging and therapy. Nano Lett. 2005;5(4):709–11.

173. Abbasi A, Park K, Bose A, Bothun G. Near-infrared responsive gold–layersome nanoshells. Langmuir. 2017;33(21):5321–7.
174. Zou L, Wang H, He B, Zeng L, Tan T, Cao H, He X, Zhang Z, Guo S, Li Y. Current approaches of photothermal therapy in treating cancer metastasis with nanotherapeutics. Theranostics. 2016;6(6):762.
175. Thorat ND, Bohara RA, Yadav HM, Tofail SA. Multi-modal MR imaging and magnetic hyperthermia study of Gd doped Fe_3O_4 nanoparticles for integrative cancer therapy. RSC Adv. 2016;6(97):94967–75.
176. Torigian DA, Zaidi H, Kwee TC, Saboury B, Udupa JK, Cho Z-H, Alavi A. PET/MR imaging: technical aspects and potential clinical applications. Radiology. 2013;267(1):26–44.
177. Yanli W, Xianzhu X, Qianlan L, Ruchun Y, Haixin D, Qiang X. Synthesis of bifunctional Gd2O3: Eu3+ nanocrystals and their applications in biomedical imaging. J Rare Earths. 2015;33(5):529–34.
178. Li M, Fang H, Liu Q, Gai Y, Yuan L, Wang S, Li H, Hou Y, Gao M, Lan X. Red blood cell membrane-coated upconversion nanoparticles for pretargeted multimodality imaging of triple-negative breast cancer. Biomater Sci. 2020;8(7):1802–14.
179. Tang H, Wang M, Meng C, Tao W, Wang C, Yu H. Research on design, fabrication, and properties of Fe_2O_3@ SiO_2/CDs/PEG@ $nSiO_2$ nanocomposites. Materials Letters. 2019; 235:39–41.
180. Lee J, Hwang G, Hong YS, Sim T. One step synthesis of quantum dot–magnetic nanoparticle heterodimers for dual modal imaging applications. Analyst. 2015;140(8):2864–8.
181. Boase NR, Blakey I, Rolfe BE, Mardon K, Thurecht K. Synthesis of a multimodal molecular imaging probe based on a hyperbranched polymer architecture. Polym Chem. 2014;5(15):4450–8.
182. Lee C-M, Cheong S-J, Kim E-M, Lim ST, Jeong YY, Sohn M-H, Jeong H-J. Nonpolymeric surface–coated iron oxide nanoparticles for in vivo molecular imaging: biodegradation, biocompatibility, and multiplatform. J Nucl Med. 2013;54(11):1974–80.
183. Ge J, Jia Q, Liu W, Lan M, Zhou B, Guo L, Zhou H, Zhang H, Wang Y, Gu Y. Carbon dots with intrinsic theranostic properties for bioimaging, red-light-triggered photodynamic/photothermal simultaneous therapy in vitro and in vivo. Adv Healthc Mater. 2016;5(6):665–75.
184. Dai L, Zhang Q, Li J, Shen X, Mu C, Cai K. Dendrimerlike mesoporous silica nanoparticles as pH-responsive nanocontainers for targeted drug delivery and bioimaging. ACS Appl Mater Interf. 2015;7(13):7357–72.
185. Sun Q, You Q, Wang J, Liu L, Wang Y, Song Y, Cheng Y, Wang S, Tan F, Li N. Theranostic nanoplatform: triple-modal imaging-guided synergistic cancer therapy based on liposome-conjugated mesoporous silica nanoparticles. ACS Appl Mater Interf. 2018;10(2):1963–75.
186. Yang Z, Fan W, Zou J, Tang W, Li L, He L, Shen Z, Wang Z, Jacobson O, Aronova MA. Precision cancer theranostic platform by in situ polymerization in perylene diimide-hybridized hollow mesoporous organosilica nanoparticles. J Am Chem Soc. 2019;141(37):14687–98.
187. Langbein T, Weber WA, Eiber M. Future of theranostics: an outlook on precision oncology in nuclear medicine. J Nucl Med. 2019;60(Suppl 2):13S–9S.

Nanomaterials Mediated Diagnosis of Lung Cancer

Arun K. Kotha, Rama Kashikar, Paras Famta, Saurabh Shah, Saurabh Srivastava, and Mahavir Bhupal Chougule

Abbreviations

NPs	Nanoparticles
CT	Computerized tomography
PET	Positron emission tomography
IHC	Immunohistochemistry
NSCLC	Non-small cell lung cancer
SCLC	Small cell lung cancer
LCC	Large-cell carcinoma
ADC	Adenocarcinoma
EGFR	Epidermal growth factor receptor
SCC	Squamous-cell carcinoma
MPM	Malignant pleural mesothelioma
kDa	Kilodalton
WHO	World Health Organization
FDA	Food and Drug Administration
PEI	Poly (ethylenimine)
MRI	Magnetic resonance imaging
EPR	Enhanced permeation and retention
NIRF	Near-infrared fluorescence
ICG	Indocyanine green
Cy5	Cyanine 5.5
PEG	Polyethylene glycol

A. K. Kotha · R. Kashikar · M. B. Chougule (✉)
Department of Pharmaceutical Sciences, Mercer University College of Pharmacy, Atlanta, GA, USA
e-mail: chougule_mb@mercer.edu

P. Famta · S. Shah · S. Srivastava
Department of Pharmaceutics, National Institute of Pharmaceutical Education and Research (NIPER), Hyderabad, India
e-mail: saurabh@niperhyd.ac.in

R. S. Chaughule et al. (eds.), *Nanomaterials for Cancer Detection Using Imaging Techniques and Their Clinical Applications*,
https://doi.org/10.1007/978-3-031-09636-5_8

RES	Reticuloendothelial system
GNP	Gold nanoparticles
SPR	Surface plasmon resonance
AgNPs	Silver nanoparticles
SPION	Superparamagnetic iron oxide
SLN	Solid lipid nanoparticles
VLPs	Viruslike particles
VNPs	Viral nanoparticles
HA	Hyaluronic acid
siRNA	Small interfering RNA
PLGA	Poly lactic-co-glycolic acid
HU	Hounsfield units
PAMAM	Polyamidoamine
CNPs	Chitosan nanoparticles
FA	Folic acid
ACPP	Activatable cell-penetrating peptide
DOX	Doxorubicin
APRIL	Proliferation-inducing ligand

1 Introduction

Cancer is one of the fatal diseases worldwide, with more than 18 million newly diagnosed cases and 9.6 million deaths per year [1]. The International Agency for Research on Cancer estimated that by 2030, due to cancer there will be 22.2 million new cases and 13.2 million deaths [2]. It can result in a huge economic and emotional burden on patients. Among all types of cancer, lung cancer has the highest mortality rate. It comprises 3% of all deaths globally, and it has a poor survival rate of 5 years. It has a poor prognosis and is detected at a very late stage [3], which shows the necessity of developing effective diagnostic strategies to identify and curbing lung cancer. Nanotechnology shows promising results in the diagnosis and treatment of cancer, including lung cancer [4]. By utilizing the inherent properties of nanomaterials, novel nanoparticles (NPs) can be developed to fill the unmet gaps in the diagnosis of lung cancer. In this chapter, information on the use of nanomaterials for the diagnosis of lung cancer is provided.

1.1 Lung Cancer

Lung cancer is the leading cause of cancer deaths worldwide, causing 18.4% of all cancer deaths [1], with 1.76 million deaths worldwide in 2018 and the number of cases expected to grow to 3 million by 2035 [5]. In men, lung cancer is the most widespread cancer, and in women, it is the third most prevalent cancer [6]. The main

risk factors in the development of lung cancer include tobacco smoking; environmental carcinogen exposure via passive smoking, air pollution, and radiation; workplace exposures such as asbestos and arsenic; and epigenetic changes [7].

1.2 Types of Lung Cancer

Based on histopathological and clinical characteristics, lung cancer is categorized into three main categories non-small cell lung cancer (NSCLC), small cell lung cancer (SCLC), and malignant pleural mesothelioma (MPM) [4].

1.2.1 Non-small Cell Lung Cancer

The non-small cell lung cancer (NSCLC) is the most prominent form of lung cancer, and 85% of lung cancers fall into this type. Among these cases, 65% are either metastatic or advanced diseases locally [8]. One of the most common risk factors is cigarette smoking, and other risk factors include air pollutants, alcohol, secondhand cigarette smoke, deep-fried consumables, barbecued meats, a sedentary lifestyle, and genetic predisposition [9]; mutations occur in epidermal growth factor receptors (EGFR). NSCLC is diagnosed only in advanced stages, and the most prevalent symptom is cough, which can be observed in 50–75% of patients, followed by chest pain, hemoptysis, and dyspnea [10]. At present, NSCLC is diagnosed using immunohistochemical (IHC) staining, histological observations, imaging techniques, and mutational and molecular genetics analysis to determine the subtype of NSCLC, and stage of the disease [11, 12].

NSCLC is subdivided into squamous-cell carcinoma (SCC), adenocarcinoma (ADC), and large-cell carcinoma (LCC) [11, 12], and each has specific cellular, genetic, and epigenetic heterogeneity.

1.2.1.1 Adenocarcinoma

Adenocarcinoma (ADC) is the most widespread worldwide [13], and in women, the cases of ADC are increasing at an alarming rate [14]. ADC was responsible for more than 40% of lung cancers and 60% of the NSCLC. ADC is a malignant epithelial neoplasm and shows glandular differentiation or production of mucin. In ADC, exclusive mutations occur in genes such as EGFR, anaplastic lymphoma kinase gene (ALK), and B-Raf proto-oncogene, serine/threonine kinase (BRAF) [15], which in addition to histological analysis are used in tracking the disease progression.

1.2.1.2 Squamous-Cell Carcinoma

Squamous-cell carcinoma (SCC) is the second most common subtype of NSCLC, and it is the reason for up to 20–30% of all NSCLC cases. Interestingly, SCC is the most commonly occurring in men [16]. Cigarette smoking is one of the main causes of SCC. Other factors such as polymorphisms and predisposition in specific genes play a role in DNA repair, such as mutL homolog 1 (MLH1), and detoxification such as cytochrome P450 family 2 subfamilies A member 6 (CYP2A6) and cytochrome P450 family 1 subfamily A member 2 (CYP1A2) [14]. SCC originates in the central portion of the lung, along major airways. They can form cavities when they grow bigger. Histologically, tumor cells typically show keratinization and formation of pearl with dense cytoplasm and hyperchromatic nuclei [16, 17]. Even though there are no SCC-specific markers available, positive expression of p40, p63, cytokeratin-5, and desmocollin-3 serves to differentiate SCC from other types of NSCLC, along with miRNA profiles [18].

1.2.1.3 Large-Cell Carcinoma

Large-cell carcinoma (LCC) is the third most common, represents a minority NSCLC subtype, and is responsible for approximately 3–9% of NSCLC cases. LCC is generally located peripherally and appears necrotic and bulky. LCC encompasses malignancies that do not come into the category of SCC, ADC, or neuroendocrine carcinoma and the ones which do not have any other specific clinical traits and differentiating morphology [18]. It is useful to apply ancillary tests such as immunohistochemistry (IHC) to avoid adding poorly differentiated NSCLC.

1.2.2 Small Cell Lung Cancer

Small cell lung cancer (SCLC) is responsible for 14% of all lung cancer cases. It is a highly aggressive form and centrally located in the major airway. Each year, around 180,000 cases were diagnosed across the world. SCLC is considered either a geriatric or a smoker's disease, due to over 90% of patients coming into at least one of these groups. The possibility of developing SCLC increases with the intensity and duration of smoking [19]. Currently, the WHO categorizes SCLC as a neuroendocrine malignancy with histological attributes of crush artifacts, necrosis, nuclear molding, and a high number of mitoses. For the confirmation of SCLC, biomarkers such as CD56 and thyroid transcription factor-1 are used. In SCLC, thyroid transcription factor-1 (TTF-1) is expressed up to 90% [20]. The hallmark of SCLC is that they have high Ki67 (MIB-1) labeling index (70–100%), which helps to differentiate it from low- and intermediate-grade neuroendocrine tumors (NET) [21].

1.2.3 Malignant Pleural Mesothelioma

Malignant pleural mesothelioma (MPM) is a rarely occurring thoracic malignancy. The incidence of MPM was approximately 2000–3000 cases per year. Over five decades, the cases of MPM have increased and continued to rise due to asbestos, which is the main etiological agent linked with MPM. It was also observed that ionizing radiation and simian virus 40 infection were also have been reasons for developing MPM [22]. Asbestos has a latency period between 20 and 60 years. Exposure to diagnosis has a huge latency period, the reason for an increase in cases of MPM worldwide. Symptoms of MPM are dyspnea and chest pain, and on average, 2–3 months before diagnosis they occur. In the late stages of MPM, they show hyperhidrosis, malaise, weight loss, and fatigue. The diagnosis was performed utilizing computerized tomography (CT) scans and chest X-rays. For the estimation of metastatic disease, positron emission tomography (PET) scans are used. For the complete differentiation to confirm the correct type of MPM, tissue biopsy is used for histological, cytological, and immunohistochemistry analysis which will help in determining the suitable treatment [23]. It is difficult to acquire a ubiquitous genetic fingerprint because of the intrinsic heterogeneity of MPM. Up to 60% of MPM tumors show mutations in the BRCA1-associated protein (BAP1), and it may even incline an individual to MPM [24].

1.3 Diagnosis of Lung Cancer

Early diagnosis of lung cancer is very crucial as it can help in improving survival rates. Generally, a lung cancer diagnosis was performed by using a histological examination of extracted tumors, which will help in choosing the right therapeutic approach to dealing with the tumors. Existing methods such as CT and bronchial biopsy depend on tumor size and need specific medical equipment, which is often not available in all hospitals and involves high costs. Iodine- and barium-based compounds are used as contrasting agents in CT to enhance visibility. Image-guided, needle, and transbronchial biopsies were used to collect lung samples. Also, administering nontargeted contrast agents during diagnosis has limitations such as low specificity and sensitivity which can affect finding the accurate location of the tumor.

While detecting cancer biomarkers such as specific proteins, cells, nucleic acids, and volatile organic compounds in tissues, sputum, urine, blood, and exhaled breath, there were a few problems involved such as less absorptivity of gaseous molecules on solid substrates, low specificity, and detection sensitivity, and involves difficult operations [25, 26].

NP can be used to overcome such problems by conjugating NPs with markers, and receptors which will help in reaching and identifying their morphologies [27, 28]. Innovative diagnostic methods such as array-based sensing and microfluidic arrays use NPs which have huge scope as they require a low sample, require less

time for assays, show ultralow detection thresholds, and have high-throughput capacities [29, 30]. Precise diagnosis is highly important as the information collected determines the type of treatment. For example, in radiotherapy, the exact tumor location and extent of spread must determine for effective therapy. NPs are widely used in cancer diagnosis and treatment as they offer unique properties such as configurable shapes and sizes, excellent plasticity, and adaptable optical, thermal, and magnetic properties [4, 31]. Due to the inherent properties, such as the superparamagnetic ability of Fe_3O_4 NPs [32], and the photoacoustic characteristics of melanin nanoparticles [33], they can be used as direct diagnostic agents. Nanomaterials also help in decreasing toxicity [34].

2 Application of Nanoparticles as a Diagnostic Agent for Lung Cancer

The International Union of Pure and Applied Chemistry defines NPs as microscopic particles with 1–100 nm in dimension [35, 36]. NPs possess unique physicochemical properties due to their size and composition, which allow them to be modified for use in biological and medical applications [4]. "Nanoparticle" is a broad term used for nanocarrier systems with different shapes and sizes (Fig. 1), and these NPs have tremendous potential to revolutionize the diagnosis and treatment of cancers. NPs are obtained such properties due to their high surface area-to-volume ratio, adjustable thermal, electrical magnetic, and optical properties. Also, NPs can be made in a variety of sizes, shapes, hollow or solid, with the required chemical composition. The exogenous and endogenous stimuli can be introduced into NPs by using surface chemistry [32]. Due to their versatile characteristics, NPs have the potential to cross the chemical and biological barriers to exert effective diagnostic and therapeutic activity [4]. By introducing modifications, NPs can be made to decrease invasiveness, improve detection sensitivity, and enhance biocompatibility, to improve the treatment of patients [37].

2.1 Nanomaterial Strategies and Challenges Used in Diagnostics of Lung Cancer

Different types of NP strategies for diagnostic and therapeutic of lung cancer are summarized in the following sections. Understanding the endocytic pathway of nanomaterials in the lung cancer cells is crucial in analyzing the identification of lung cancer, particularly in vivo. Physicochemical properties, i.e., size, shape, surface charge, hydrophilia/hydrophobicity of nanomaterials, and presence of ligand on their surface, affect cellular uptake of nanomaterials [38, 39]. Depending on the NP size [40], shape, and charge, different cellular pathways such as

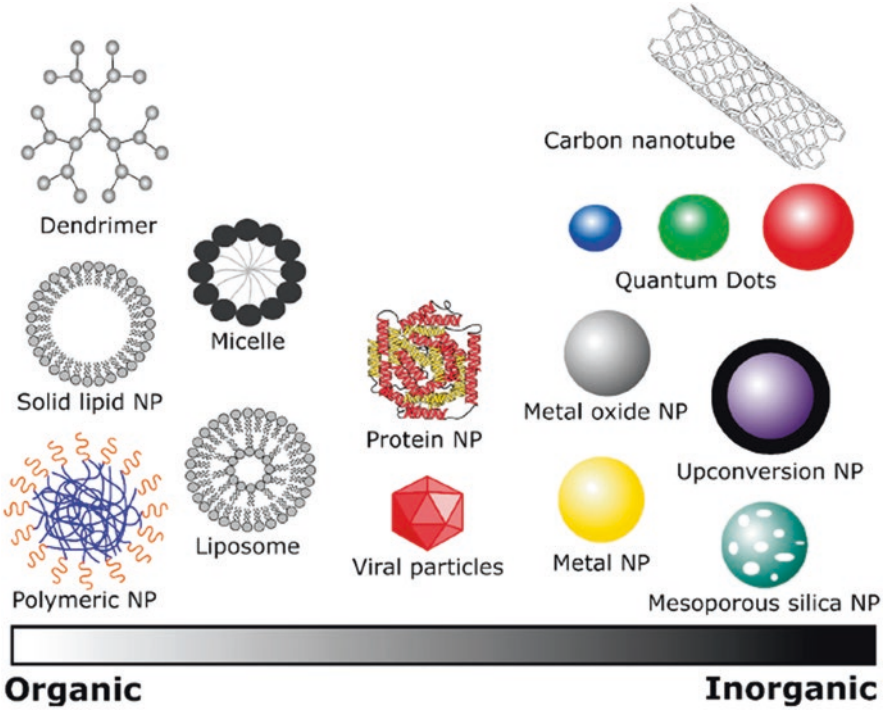

Fig. 1 Types of NPs used in diagnosis and treatment of cancer. Depending on NP composition, NPs are generally categorized as organic (lipids, dendrimers, polymers, and proteins) or inorganic (rare earth elements, metals, and carbonaceous) [4]. (Reprinted from *Pharmacol Ther.* 198, Cryer AM, Thorley AJ., Nanotechnology in the diagnosis and treatment of lung cancer, 189–205., Copyright © 2019, with permission from Elsevier)

clathrin-mediated, receptor-mediated, caveolae-dependent endocytosis and phagocytosis were utilized. For successful diagnostics and therapy, it is crucial to analyze and establish the endocytic pathway of NPs. Other crucial challenges involved in NPs are large-scale manufacturing and reproducibility. Also, there are potential toxicological and safety hazards which might not be completely assessed or considered for analysis. Multiwall carbon nanotubes (MWCNTs) activate the TGF-β/Smad signaling pathway and play a key role in inducing pulmonary fibrosis, and it was observed that tube length plays a role in MWCNT-initiated macrophage activation and following TGF-β1 secretion [41]. The carbon nanotube's needlelike fiber shape has been compared to asbestos. When exposed, long multiwalled carbon nanotubes, length-dependent, exerted asbestos-like scarring of the lung [42]. NPs can show adverse effects on different organs/tissues in the body. They can initiate the development of lung (cancer, asthma, and bronchitis), neurological (e.g., Parkinson's disease and Alzheimer's), and cardiovascular diseases (thrombosis, atherosclerosis, arrhythmia, and hypertension) [43]. Such adverse effects of nanomaterials stress the importance of long-term safety analysis of the materials used in NP formulation.

2.1.1 Polymeric Nanoparticles

2.1.1.1 PLGA Nanoparticles

PLGA has been extensively explored for theragnostic applications in cancer management [44]. PLGA is composed of a copolymeric mixture of poly(lactic acid) and poly(glycolic acid) in different ratios. It has been approved by the US FDA for medical applications owing to its safety and biocompatibility [45]. Numerous factors influence drug delivery *via* PLGA NPs; however, of all factors, the ratio of lactic acid to glycolic acid plays a major role in controlling the solid-state characteristics and release of the drug from the prepared nanoparticles [46]. Li et al. prepared PLGA-based diagnostic nanoprobes for fluorescent and magnetic resonance imaging of lung cancer cells. Nile red, a fluorescent dye, was loaded into the core of the PLGA NPs. For chelation of gadolinium ions onto the surface, the PLGA NPs were first functionalized with the poly(ethylenimine) (PEI) to functionalize the NPs with the surface amine groups. Diethylenetriamine penta-acetic dianhydride was immobilized on the top of the functionalized PLGA NPs using NHS-EDC chemistry. Diethylenetriamine penta-acetic dianhydride was able to chelate the MR contrast imparted by gadolinium ions on the surface of the NPs. The loaded NPs exhibited a particle size of approximately 200 nm. The NPs were nontoxic toward A549 cells and displayed high T1 relaxivity (28.36 mM^{-1} S^{-1}). These PLGA-based formulations exhibit the potential to be used as a contrast agent for both fluorescent and MR imaging for lung cancers [47]. Gao et al. prepared superparamagnetic iron oxide NPs (SPIONs) and doxorubicin (DOX)-loaded PLGA-based theragnostic agents for the active drug delivery and diagnosis of lung cancer cells. The NPs were dual functionalized with folic acid (FA) and activatable cell-penetrating peptide (ACPP) for the active uptake by the lung cancer cells. PLGA NP size was 85 nm, PDI 0.261, and zeta potential of −19.0 mV. After encapsulation of DOX, SPIO, and surface modification with FA and ACPP, the size of F/A-PLGA@DOX/SPIO was 260 nm, PDI of 0.254, and zeta potential of +28.7 mV. Also, NPs show stability in PBS and serum for up to 72 h. When incubated with red blood cells, NPs did not show any hemolytic activity. Both properties show their suitability for biological applications (Fig. 2).

The NPs served as an excellent T2-negative contrast agent for MR imaging. From Fig. 2a, it was observed that the transverse relaxation rate (r^2) of SPIO was 86.258 $mM^{-1}s^{-1}$ and F/A-PLGA@DOX/SPIO showed a high r2 of 156.63 $mM^{-1}s^{-1}$ which is the sign that NPs wrapped a large amount of SPIO into the center of the nanocarrier system. Intracellular trafficking studies were performed in A549 cells, using LysoTracker (green) and Hoechst 33342 (blue) to label lysosomes and nucleus, respectively. Cellular transport and absorption of F/A-PLGA@DOX/SPIO were observed in real time. From Fig. 2b, it was noticed that after 2 h, green and red fluorescent signals overlapped in the lysosomes. After 4 h, red signals in lysosomes appear stronger, and after 6 h, the red fluorescent signal expands in the cytoplasm. These observations confirm that NPs enter the cell and are mainly located in lysosomes before entering the cytoplasm. In vivo MR R_2* imaging of A549

tumor-bearing mice was performed. It was known that there is a correlation between Fe amount in the tissue and the R_2* value. From Fig. 2c, it can be noticed that F/A--PLGA@DOX/SPIO NPs showed the presence of a high orange-red region in the tumor which is the indication of a high R_2* value. When compared to SPIO, F/A--PLGA@SPIO and F/A-PLGA@DOX/SPIO NPs reached maximum R_2* value at 12 h, 24 h, and 24 h respectively, and both values were higher than SPIO-treated group (Fig. 2d, e). Along with better diagnostic potential, the NPs also demonstrated in vivo stability, biocompatibility, and lung cancer cell uptake in vivo [48].

2.1.1.2 Chitosan Nanoparticles

Chitosan is a carbohydrate-based polymer obtained from chitin. Chemically it is N-acetyl glucosamine with extensive applications in drug delivery. It is used for topical as well as parenteral administration of the therapeutic agent [49]. Chitosan is insoluble in aqueous water at the neutral and basic pH, whereas it dissolves in the dilute acidic aqueous solutions due to the protonation of its amine groups [50]. Various properties such as enhanced cell uptake, mucoadhesion, gene transfection, etc. motivate its extensive use in cancer nanotechnology [51]. On et al. prepared indocyanine green (ICG)-conjugated glycol chitosan NPs (CNPs), and Cy5.5-CNPs

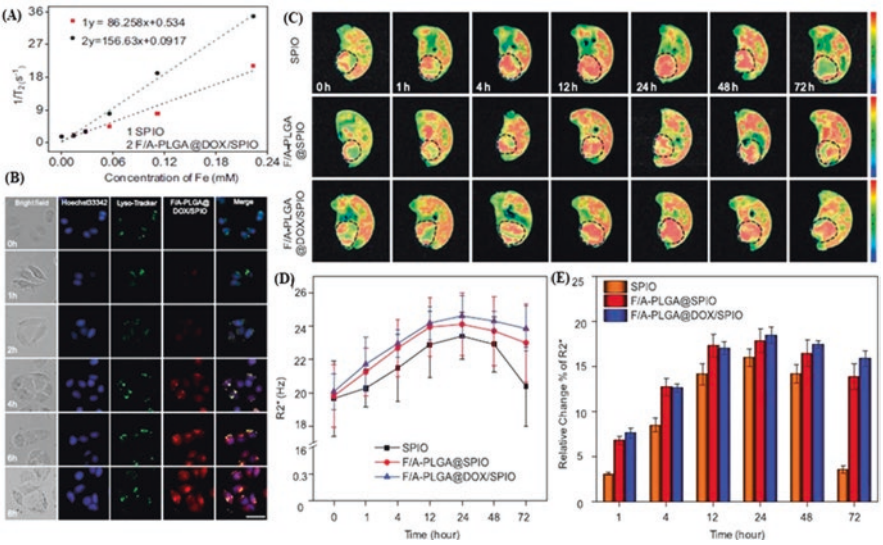

Fig. 2 Characterization and intracellular trafficking of F/A-PLGA@DOX/SPIO NPs. (**a**) T2 relaxation rate (r2) of SPIO and F/A-PLGA@DOX/SPIO NPs. (**b**) Intracellular trafficking of F/A--PLGA@DOX/SPIO in A549 cells and cells stained with LysoTracker (lysosome) and DAPI (nucleus) were treated with NPs at different time points. (**c**) MR R2* maps of A549-bearing mice after being treated with SPIO, and F/A-PLGA@SPIO, F/A-PLGA@DOX/SPIO NPs at different times. (**d**) Tumor R2* values for each treated group. (**e**) % of the relative change of tumor R2* value for each group at different time points. Values are expressed as ± SD of triplicate [48]

for image-guided surgical ablation of VX2 lung cancer tissues from the orthotopic mice and rabbit tumor models. As shown in Fig. 3a, the sizes of ICG-CNPs and Cy5.5-CNPs were 264 ± 3 nm and 261.8 ± 2.69 nm, respectively. Both NPs maintained stability for up to 8 days under physiological conditions. Nanosized spherical structures of ICG-CNP and Cy5.5-CNPs were observed using TEM (Fig. 3a), and the NIRF signals increased proportionally with increasing NP concentration which infers that fluorescent dyes were firmly conjugated to CNPs (Fig. 3b). Owing to the enhanced permeation and retention (EPR) effect, the Cy5.5-CNPs demonstrated higher accumulation in the cytoplasm of VX2 tumor tissue of the rabbit at 24, which was evident from confocal microscope images of VX2 tumor cells. A cell viability test was performed using cell counting kit-8 (CCK-8), and both ICG-CNP and Cy5.5-CNPs showed no cytotoxicity up to 200 μg/ml at 24 h (Fig. 3c). In pharmacokinetic analysis, near-infrared fluorescent (NIRF) signals in mice and rabbit serum were decreased gradually over time. The plasma half-life of NIRF signals in blood was reported to be 4.73 h and 3.25 h in rabbits and mice, respectively (n = 3, mean ±SD) (Fig. 3f). It was observed that in in vivo tumor accumulation studies, the

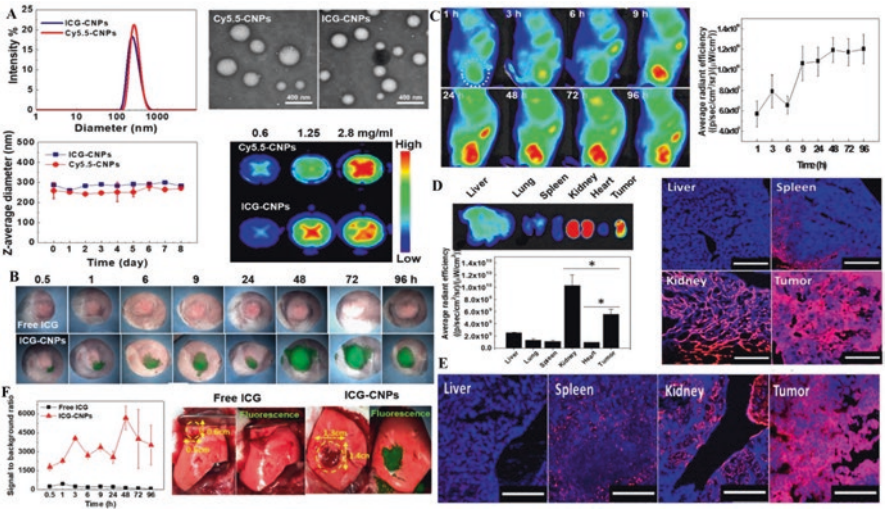

Fig. 3 (**a**) Particle size of Cy5.5 and ICG chitosan nanoparticles by dynamic light scattering and transmission electron microscopy along with interday stability. (**b**) Near-infrared fluorescence signals (0.6–2.8 mg/mL) of Cy5.5 and ICG-loaded nanoparticles. (**c**) Quantitative cell uptake on VX-2 tumor cells and cell viability. (**d**) In vivo biodistribution of Cy5.5-loaded chitosan nanoparticles in the VX2 tumor-bearing mouse with quantified NIRF signals from tumor and other organs with tissue fluorescence imaging. (**e**) Tumor localization of free ICG and ICG-loaded chitosan nanoparticles in rabbit VX2 lung tumor models. (**a**) Noninvasive NIRF imaging of VX2 tumors, ex vivo NIRF images, and tissue fluorescence of the liver, spleen, kidney, and tumor from orthotopic VX2 lung cancer model post 96 h of injection. (**f**) Pharmacokinetic analysis of ICG-CNPs in rabbit and mouse serum. NIRF signals in (**a**) mouse (**b**) rabbit blood. (Reprinted from On et al. [52] licensed under CC BY 4.0 (https://creativecommons.org/licenses/by/4.0/legalcode). Copyright © 2020 Kyeong Cheol On, Jiyun Rho, Hong Yeol Yoon, Hyeyoun Chang, Ji Young Yhee, Jun Sik Yoon, Seo Young Jeong, Hyun Koo Kim, and Kwangmeyung Kim. Published by MDPI)

buildup of fluorescent NPs was increased over time and showed high signal intensities between 48 h and 72 h. In ex vivo NIRF imaging, it was observed that Cy5.5-CNP showed high accumulation in kidneys and tumors when compared to other organs (Fig. 3d). Accumulation of ICG-CNPs was observed clearly when compared to only ICG alone. Real-time NIRF signal due to accumulation of ICG-CNPs could distinguish tumor from normal tissue which helped in image-guided surgical removal of tumor tissue from the lung (Fig. 3e). This successful study warrants clinical trials of these NPs [52]. MicroRNAs play an important role in cancer progression. Their expression in the cancerous tissues and blood is commonly used to diagnose lung cancer. Zhu et al. used chitosan NPs to detect miR-155 in the lung cancer cells. They loaded the mIR-155 molecular beacon into the core of chitosan NPs. The chitosan NPs demonstrated better transfection of miR-155 molecular beacon inside the lung cancer in comparison with the lipid-based nanocarrier. The developed chitosan NPs were biocompatible, were stable, and demonstrated high cell uptake potential [53]. Hence, chitosan demonstrates huge potential as a nucleic acid transfecting carrier for lung cancer detection.

2.1.1.3 Dendrimers

Polyamidoamine (PAMAM) is the commonly used dendrimer in cancer nanotechnology. These architecture polymers can be used to load the cargo on the surface by chemical functionalization as well as intra-structural voids. Hence, these structures can be used to deliver more than one cargo. This ability makes them an ideal carrier for the targeted theragnostic applications [54]. Liu and colleagues prepared gadolinium-modified PAMAM dendrimer-entrapped GNPs as a multimodal contrast for both magnetic resonance imaging and computed tomography. The research group functionalized the dendrimer with various agents; however, the dendrimer functionalized with 1,3-propane sultone showed the best plasma half-life (37.07 h) and antifouling properties. The loaded GNPs exhibited particle size and zeta potential of 2.7 nm and 7.6 mV, respectively. Further, peptide-conjugated GNP-loaded dendrimers demonstrated r1 relaxivity of 13.17 mM S^{-1}, excellent biocompatibility, good X-ray attenuation, and lung cancer-specific cellular uptake by binding to the $\alpha_v\beta_3$ integrin. The dendrimer-based multimodal probe shows potential to be brought into the clinical setup [55]. Wang and co-workers reported folic acid-immobilized GNP-loaded fifth-generation PAMAM dendrimers to be used for CT imaging of the lung's adenocarcinoma. The folic acid functionalization was performed using the EDC-NHS linking. After exposure or administration of particles in vitro and in vivo respectively, the imaging could be done using X-rays to detect SPC-A1 cells in vitro and in a xenograft model in vivo. The prepared dendrimer-based nanostructure was concluded to have biocompatibility after a battery of investigations such as cell viability using MTT assay, cell cycle, and apoptosis analysis using flow cytometry and tissue histology [56].

2.1.1.4 PEGylation-Based Particles

PEG is mainly used to form the hydrophilic part of nanoscale drug delivery systems [57]. PEG is commonly used to functionalize the nanoscale formulation in an attempt to increase biological biocompatibility and circumvent the reticuloendothelial system-mediated removal of the nano-formulations from the body [58]. PEG is used to develop self-assembled NPs in the particle range below 100 nm [59]. Sui and colleagues reported PEGylated gadolinium oxide NPs for better biocompatibility with the physiological system. The NPs were surface-functionalized with PEG and l-cysteine. PEGylated NPs were found to be water-dispersible, stable at RT, and biocompatible with the red blood cells. The relativity indexes of PEGylated NPs and PEGylated-L-cysteine NPs were found to be 3.35 and 3.59 mM/s. However, the PEGylated NPs demonstrated T1-weighted MR imaging both in the presence and absence of L-cysteine. The PEGylation of gadolinium NPs also increased its half-life to 6.2 h [60]. Wang and co-workers PEGylated SPIONs to improve their biocompatibility and improve the imaging sensitivity for MR-guided therapy. The PEGylated NPs were actively targeted using the anti-epidermal growth factor receptor (EGFR) antibodies which bind to the overexpressed EGFR receptors on the lung cancer cells. The actively targeted PEGylated SPIONs demonstrated better accumulation in H460 lung cancer cells with better MRI contrast in the H460 cells both in vitro and in vivo. The MR imaging confirmed a greater accumulation of actively targeted PEGylated SPIONs in comparison with the untargeted SPIONs with an enhanced T2 signal-to-noise ratio [61]. Hou et al. used chlorin e6-conjugated PEG self-assembled NPs for the NIR-based imaging of the A549 lung cancer cells. Chlorin e6 was conjugated to the PEG the REDOX-sensitive disulfide linkage. The nano-formulation showed photodynamic based cytotoxicity; hence, this self-assembled particle demonstrates excellent theragnostic ability. The signals of chlorin 6 dimmed after 10 h of tail vein injection in vivo, whereas PEG NPs maintained strong fluorescent signals even after 36 h of administration [62].

2.1.2 Metal-Based Nanoparticles

2.1.2.1 Gold Nanoparticles

Gold nanoparticles (GNPs) exhibit tremendous physicochemical properties such as surface plasmon resonance (SPR), high surface-to-volume ratio, and the ability to be functionalized with a wide range of molecules and polymers [63]. Mentioned properties make GNPs an ideal carrier for theragnostic applications. Lung cancer is characterized by an elevation in the concentration of volatile compounds excreted during exhalation [64]. Currently employed techniques including GC-MS, ion flow tube MS, etc. require pretreatment and pre-concentration of the sample prior to investigations [65]. However, the following discussed GNP-based sensors gave rapid results subsequently circumventing the need to concentrate the samples before investigations. Barash and co-workers developed molecularly modified GNPs for

the detection of volatile compounds emitted from non-small cell lung cancer. The molecules selected to modify the GNPs demonstrate the same functional groups as the emitted volatile compounds; hence, the synthesized GNPs exhibited high selectivity toward the emitted compounds. The nanosensors were able to identify and separate 55 volatile compounds appearing in NSCLC cell lines. The proposed nanosensor displayed significant potential for clinical translation to detect the lung cancer-specific volatile compounds in the air exhaled by the patient. Such technology can also prove successful in the instantaneous detection of cancerous tissues during surgical operations [66]. Peng and co-workers functionalized GNPs (particle size = 5 nm) with thiols including 1-butanethiol, decanethiol, dodecanol, hexanediol, 2-ethylhexanethiol, and 4-methoxytoluenethiol. The functionalized GNPs were dropped cast over gold electrodes and arranged to form detectors. The studies performed on 56 healthy and 40 patients were able to distinguish and identify volatile biomarkers [67]. Gao et al. prepared GNP-based probes for the detection of lung cancer-selective biomarkers, viz., neuron-specific enolase, cytokeratin 19 fragment antigen, and carcinoembryonic antigen. The detection antibodies were functionalized on the GNPs. The detection of the antigens was carried out by sandwiching the antigens between the capture antibodies (present on the microarrays) and GNP-functionalized detection antibodies. The probe was able to detect the antigens even at the lowest concentrations of 1 ng/mL. The co-detection of four antigens improved the diagnostic accuracy to 87.74%. This rapid and precise GNP-based probe shows excellent potential for clinical applications [68].

2.1.2.2 Silver Nanoparticles

Silver nanoparticles (AgNPs) have been used in the various platforms employed for the imaging and diagnosis of cancer tissues as well as cancer-associated biomarkers. As witnessed in the case of GNPs, AgNPs also demonstrate tremendous physicochemical properties including SPR, high surface-to-volume ratio, and heavy surface functionalization capabilities [69]. Zhang and colleagues utilized AgNPs to augment the Raman signals obtained from the lung cancer tissue slices. Surface-enhanced Raman spectroscopy is commonly used in the area of lung cancer tissue detection, owing to its high sensitivity. The addition of AgNPs to the surface of lung cancer tissues improved the Raman scattering signals of the biomarkers. Improved sensitivity and selectivity of 95.7% each are reported in the study [70]. The same research group also reported the use of AgNPs to augment the signals of subsurface-enhanced spectroscopy obtained from the serum samples. For this study, they employed pyramidal silicon and AgNPs. The PCA-LDA method demonstrated a sensitivity and selectivity of 100% and 90%, respectively [71]. Yang et al. reported biocompatible glutathione-capped silver nanoclusters for the imaging of the live lung cancer cells. The nanoclusters demonstrated lower cytotoxicity in comparison with the silver salts and AgNPs. The nanoclusters demonstrate solvent-dependent fluorescent quantum yield in the live A549 cells in vitro [72]. Recently, Lee and

co-workers grafted AgNPs on the surface of the oxidized porous silica microparticles (Fig. 4).

The prepared structures demonstrated CT contrast intensity of more than 1000 HU. Figure 4a explains the hybrid composite formulation. In the first step, pSiMPs were made by utilizing a constant anodization current of high boron-doped p-type single-crystal silicon wafers in ethanolic hydrofluoric acid (HF) electrolytes resulting in pSiMPs surface being oxidized in aqueous media which contains sodium tetraborate. This step is crucial to increase the hydrophilicity of microparticles and initiate the NP formation of silver ions on its surface. In the next step, metallic silver is deposited onto the Oxi-pSiMPs in the presence of $AgNO_3$ and ammonia (NH_3) using an established protocol [74]. SEM images of the materials pSiMPs (plate-shaped particles), Oxi-pSiMPs (open-pore structure), and AgNPs-pSiMPs (collapsed pore structure) were shown in Fig. 4b. Energy-dispersive X-ray spectroscopy (EDS) element imaging shows the presence of silica, oxygen, and silver (Fig. 4c). CT signals were analyzed; PBS and lipiodol were used as negative (no CT signal) and positive controls (3070 Hounsfield units (HU)), respectively. AgNPs-pSiMPs exerted high CT signal intensity in solid state (1050 HU), dispersed solution in DI H_2O (1050 HU), and in the mixture of DI H_2O and glycerol (1300 HU) (Fig. 4d). AgNPs-pSiMPs were applied in vivo CT imaging of rabbit's lungs for lung marking and treatment (Fig. 4e). Rabbit's chest micro-CT image shows lungs as the dark and vertebral column, ribs, and sternum as white. AgNPs-pSiMPs were injected into the superior lobe of the right lung (yellow circle) (Fig. 4f). Even after 60 min, there was no decrease in CT signal intensity at the injection site. When compared to lipiodol, Ag-NPs-pSiMPs showed a higher localized CT-responsive area (Figure 4h). The NPs demonstrated very low toxicity and were able to maintain a strong CT signal at the site of injection of the lungs. These microparticles show huge potential to be translated as an imaging agent for lung CT scans for the surgical ablation of lung cancers [75].

2.1.2.3 Iron Oxide Nanoparticles

Ferrimagnetic iron oxide NPs have been employed for various theragnostic applications in cancer research. These iron oxide NPs are frequently surface-functionalized to result in superparamagnetic iron oxide NPs (SPIONs). SPIONs are readily used for stimulus-responsive drug delivery as a functionalized theragnostic carrier, a contrast agent for magnetic resonance imaging as well as magnetic particle imaging [76]. SPIONs can be readily synthesized into various particle sizes and can be functionalized using various small-molecule polymers, antibodies, small molecules, and ligands. However, rapid blood clearance and low stability in the physiological matrixes pose a challenge for their theragnostic applications. Yoo et al. formulated folic acid-conjugated SPIONs to be used as an imaging agent in lung cancer diagnosis. The folic acid was functionalized using the PEG-linking technique. The prepared SPIONs demonstrated low blood clearance and high physiological stability. The folic acid-targeted SPIONs demonstrated good uptake by the lung cancer cells

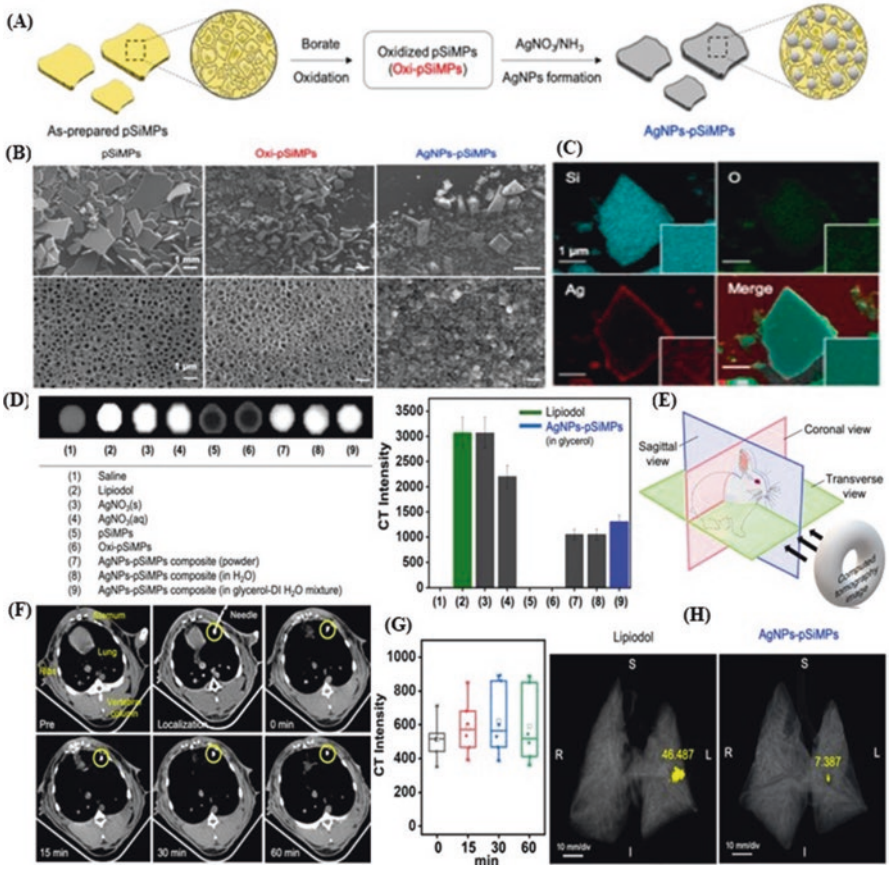

Fig. 4 (**a**) Schematic representation of the preparation of the hybrid composite of AgNPs and pSiMPs. (**b**) SEM images of pSiMPs, oxidized pSiMPs, and AgNPs-pSiMPs. (**c**) EDS element mapping images of Si, Ag, and oxygen. (**d**) In vitro CT images (left) and CT intensity (HU) (right) of prepared formulations. (**e**) Rabbit anatomical sketch to explain CT images in panel F and H. (**f**) Rabbit chest in vivo micro-CT images in the conical view, before and after administration of the hybrid composite. (**g**) HU scale obtained from CT images (yellow circle) in panel F, observed as a function of time postinjections. (**h**) In vivo CT images of the rabbit lungs (3D view) [73]. (Reprinted (adapted) with permission from Lee EM, Lee J, Kim Y, et al. Hybrid Composite of Silver Nanoparticle-Porous Silicon Microparticles as an Image-Guided Localization Agent for Computed Tomography Scan of the Lungs. *ACS Biomater Sci Eng*. 2020;6(8):4390–4396. Copyright © 2020 American Chemical Society)

in vitro and in vivo [77]. Park et al. synthesized radioactive folic acid-functionalized SPIONs labeled with ^{64}Cu, to be used as a diagnostic agent in positron emission tomography as well as MRI. The particle size of citrate and hydrazine-stabilized SPIONs is reported to be 50 nm. The functionalized SPIONs retained ~90% of the radioactivity in pH 7.4 buffer and serum after 24 h. The functionalized NPs showed good cell internalization capabilities in the lung cancer A549 cell lines in vitro [78].

Shahbazi-Gahrouei et al. functionalized SPIONs with anti-epidermal growth factor monoclonal antibody. The prepared nanoprobe showed good biocompatibility toward the Lewis lung carcinoma cells in vivo. The prepared nanoprobe demonstrated good cell uptake and image signal intensity in vivo. This probe displayed a high potential to be translated to the media setup [79]. Wan et al. reported anti-CD-44V6 antibody-conjugated SPIONs for magnetic resonance immune imaging of lung cancer cells. The SPIONs were surface function surface-functionalized and carboxymethyl improved their aqueous dispersibility and saturation magnetization. The functionalization improved the magnetic resonance imaging and cell uptake capabilities of SPIONs into the A549 cell lines in vitro [80].

2.1.2.4 Magnetic Nanoparticles

Cobalt, iron, and nickel are commonly used for the synthesis of magnetic NPs dedicated to biomedical applications [81]. They are used for the development of stimulus-responsive drug delivery systems and thermal ablation of the tumor [82], as a contrast for the MRI [83], and as a probe for biosensing [84]. The surface functionalization capabilities and the ability to release the cargo at controlled rates make them an important carrier for cancer research [85]. The ability to be manipulated by the external magnetic field can be smartly used for the site-specific accumulation for theragnostic biomedical applications [85]. Zhou et al. developed Cy5.5 dye-loaded SPIONs which were functionalized to detect the HCBP-1 overexpressed lung cancer stem cells in the lung cancer xenografts. The SPIONs were stabilized by cationic polyethylenimine and were further functionalized with the HCBP-1 peptide using the EDC linker. The prepared nanocomposite demonstrated high biocompatibility with the red blood cells and lung cells. The nanocomposite demonstrated specific uptake by the lung cancer stem cells from the H-460 lung tumor xenografts. These NPs worked efficiently as the contrast and fluorescent probe for the MRI and fluorescent imaging in vivo. Using this nanocomposite, the lung cancer stem cells were diagnosed in the lung cancer xenografts to detect early metastasis [86]. Wang et al. developed magnetic NPs using microemulsion polymerization and Stober coating techniques. Briefly, SPIONs were formulated by co-precipitation of $FeCl_2$/$FeCl_3$ and stabilization by oleic acid. The surface of the NPs was functionalized with pan-cytokeratin antibody for cancer cell-specific uptake. The magnetic NPs were added to the cell suspension consisting of lung cancer A549 cells. The NPs were able to separate the cancer cells from the mixture under the influence of the magnetic field [87].

2.1.2.5 Silica Nanoparticles

Silica-based NPs are one of the major players in cancer cell detection and imaging. Silica has versatile chemistry, which along with surface negative charge offers huge potential for the functionalization of different fluorescent molecules. Additionally,

silica NPs also offer properties such as biocompatibility, enhanced dye stability present in the pores, and optical transparency [88]. Chen et al. reported ^{19}F-loaded GNP-capped mesoporous NPs for the site-specific release of ^{19}F for the diagnosis of lung cancer cell lines. The release of ^{19}F to the tumor tissues is limited by capping the GNPs on the mesoporous silica NPs by hydrazone linkers. The hydrazone bonds remain intact at the physiological pH of 7.4 and break at the acidic pH below pH 6. The removal of GNPs led to the release of ^{19}F at the tumor site. The delivery of the imaging agent to the lung cancer cells was assured by functionalizing them with folate receptors. Hence, the research group was able to specifically image the A549 cells, while normal cells stayed dark [89]. Lee et al. synthesized gadolinium ion-conjugated silica NPs for contrast enhancement applications in MR imaging. The research group chemically functionalized the surface of silica NPs with amine and carboxylic acid functional groups for easy gadolinium conjugation. The authors reported a higher relaxivity of 9.41 $mM^{-1}s^{-1}$ in comparison with the relaxivity of free gadolinium ions (3 $mM^{-1}s^{-1}$). The study concluded that the hydrophilic nature of amine and carboxylic acid functionalization around the silica NPs allows the water to interact and proton relaxes the gadolinium ions [90].

2.1.2.6 Quantum Dots

Kalkal and colleagues employed quantum dots to develop a non-radiative energy transfer-based fluorescent nanoprobe for the diagnosis of small cell lung cancer. These kinds of sensors are known to be highly sensitive and rapid [91]. The design of the nanoprobe included graphene quantum dots as an energy donor and GNPs as an energy acceptor. The quantum dot used here is nitrogen-doped and surface-functionalized with an amine. The amine functional group was used to functionalize the quantum dots with neuron-specific enolase antibodies. The developed probe detected enolase in the lung cancer cells rapidly (within 16 min), with a low detection limit of 0.9 pg/mL and a broad linear detection range (0.1 pg/mL–1000 ng/mL) [92]. Shivaji et al. prepared quantum dots with particle size of 2–5 nm using tea leaf extract as the stabilizing agent. The extract used was completely nontoxic and hence increased the biocompatibility of the quantum dots. The quantum dots were able to produce high contrast fluorescent images of the A549 lung cancer cells. Concentration-dependent fluorescence emission centered at 670 nm was achieved. The prepared probe also arrested the cell of A549 cells at the S phase, thus promising huge potential as a theragnostic agent for lung cancer management [93]. Nafiujjaman et al. developed graphene quantum and SPION-based supramolecular assembly for the targeted imaging of lung cancer cells. The nanostructure was targeted to αV integrins by functionalizing with iRGD tumor-penetrating protein. The structure was able to retain its fluorescence and targeting capabilities. The co-engineered SPIONs enabled the particles to be used as a contrast for the MRI studies. This two-in-one targeted nanostructure holds tremendous potential to be used as an imaging agent for both fluorescent imaging and MRI in the clinical setup [94].

2.1.3 Biomaterial-Based Nanoparticles

Biomaterial-based NPs can be derived from proteins, viruses, and endogenous lipids, and they can be used for bioimaging and biosensing applications for lung cancer. They offer several advantages when compared to inorganic-based vectors such as biocompatibility, ease of production, and conjugation of ligands for site-specific delivery. Biomaterial-based NPs were successfully developed and used for lung cancer diagnosis. Few biomaterial-based NPs are outlined below.

2.1.3.1 Viral Nanoparticles

Viruses are infectious pathogens, ranging in size from 20 to 400 nm. Viruses are considered naturally present nucleic acid carriers as they transfer and protect their cargo, and this characteristic is used for drug and imaging agent delivery [95]. Viruses offer numerous applications in medicine such as bioimaging, biosensing, drug and gene delivery, theranostics, and vaccine development. Viruses are mainly categorized into three different types, i.e., bacteriophages, plant, and mammalian viruses, which have shown tremendous potential in drug delivery due to their ability to transport genetic material within their capsid and high cell permeability [95]. In viruses, there are two subgroups: viruslike particles (VLPs) and viral nanoparticles (VNPs) [96]. VLPs are considered noninfectious, and they are devoid of genome and counterparts of VNPs. They may also show different immunostimulatory profiles depending on the presence or absence of a viral genome [97]. VNP has self-assembled unique architectures which occur in a wide range of shapes and sizes and offer several distinctive advantages due to their unique properties such as water solubility, stability in aqueous buffer, biocompatibility, uniformity in their morphology, large surface area, inexpensive to produce in large quantity, easy purification, high cellular uptake, and facile, efficient functionalization. Such properties are helpful in biological and imaging applications, and they are difficult to attain with polymers [98, 99]. Another useful advantage is, on the virion surface, at specific, designated positions, it is possible to link fluorescent molecules where the spatial separation of the dye molecules will help in preventing a phenomenon called fluorescence quenching, which results in appearing “super bright” viral particles for imaging [98].

By utilizing mammalian viruses, i.e., adenovirus, lentivirus, and herpesvirus, successful therapeutic agents against multiple diseases were developed [100]. But there have been reports of these viral-based therapies showing severe adverse effects, and, in some cases, fatal outcomes were observed [101]. On the overhand, plant viruses and bacteriophage do cause infections in mammals, and they are considered nontoxic to humans and safer to use imaging and drug delivery applications.

One of the biggest advantages of plant viruses is that they do not show tissue tropisms. This quality can be utilized in nanoparticle formulation to add properties such as membrane crossing, nuclear penetration, binding, and targeting abilities [102]. Currently, several nanotechnology-based systems are under development

based on plant VLP and VNPs such as cowpea mosaic virus (CPMV), tobacco mosaic virus (TMV), physalis mottle virus (PhMV), and potato virus X (PVX) [96].

When compared to synthetic NPs, VLPs offer several advantages in delivering imaging agents due to their short circulation and retention time which dramatically decreases adverse effects [103]. VLPs can be modified to transfer different types of fluorescent labels, and contrast agents also by introducing antibodies, aptamers, and peptides for enhanced targeting of specific cells and tissues. Another interesting method of modification of viral particles was done by utilizing genetic techniques to create mutations that express novel reactive residues on the surface of the virus particle with high specificity and region control.

Among plant viruses, CPMV is used often for optical imaging applications. It has an icosahedral shape and is about 30 nm in size. A distinctive feature of CPMV is that it has the inherent ability to interact with the mammalian protein surface vimentin which helps in imaging endothelium [104], especially tumor endothelium [105]. To enhance the specificity, CPMV was modified with a peptide ligand E7p72, and these E7p72-CPMV particles displayed high specificity to epidermal growth factor-like domain 7 (EGFL7) [106]. Within 90 min, they can be seen through real-time intravital imaging due to the binding of particles to tumor neovasculature. By utilizing genetic engineering techniques, CPMV can be modified to introduce cysteine residues, which are not accessible in wild CPMV. It resulted in the symmetrical display of 60 thiol groups on virus capsid [107]. In the same way, to control and enhance selectivity, viral coat proteins can be replaced by nonreactive groups [108].

A recent study conducted by Gassensmith et al. showed a TMV-metal-organic framework (MOF) hybrid nanoparticle-enhanced TMV VNP retention when given via s.c. into Balb/c mice [109]. Zeolitic imidazolate framework-8 was coated to Cy5-encapsulated TMV (Cy5-TMV@ZIF), and NPs retained fluorescence ~2.5x the time (288 h vs. 120 h) when compared to native Cy5-TMV. The TMV@ZIF NPs were stable even when heated at 100 °C for 20 min or overnight kept in 6 M guanidinium chloride or methanol. Wild-type TMV was not stable [109]. Robertson et al. linked fluorescent dyes to the icosahedral head of the T4 bacteriophage which allowed the identification of A549 lung cancer cells line [110]. They also showed its cellular imaging and flow cytometric applications, by bioconjugation Cy3 and Alexa Fluor 546 with the head of the T4 bacteriophage, which gave a high surface area for the accumulation of approximately 19,000 dyes/viral NPs which resulted in an increase in fluorescence of about 90% with Cy3 dye [110].

2.1.3.2 Protein-Based Delivery

The preparation of protein NPs is predicated on balancing the attractive and repulsive forces within the protein. This is usually accepted that increasing protein uncoiling and decreasing hydrophobic interactions are crucial to the formation of protein NPs [111]. During the process of NP formation, protein undergoes conformational changes counting on its composition, concentration, crosslinking, and preparation conditions like pH, ionic strength, and solvent type. Generally,

surfactants are needed to stabilize the NPs of water-insoluble proteins like gliadin [112]. Uncoiling of proteins throughout the preparation method exposes interactive groups like disulfides and thiols. Following the thermal or chemical crosslinking results in the formation of cross-linked NPs with entrapped drug molecules. Coacervation/desolvation and emulsion-based ways are most ordinarily used for the preparation of protein NPs (Fig. 5).

Small peptides like growth factors and neurotransmitters are involved in several physiological functions within the body. These present amide molecules comprising about 30 amino acids don't seem to be typically used clinically because of their poor chemical and physical stability and short half-life in circulation due to capillary filtration and serum protein degradation [114, 115]. However, small peptides have several advantages as therapeutic agents since they can simply penetrate cells and deliver medication in response to tissue hydrogen ion concentration. As an example, amide-conjugated liposomes have effectively internalized into mitochondria by reversing their surface charge (negative to positive) within the tumor's external environment (pH ~ 6.8) [116]. Hence, peptide-based NPs have gained attention as gene and drug transporters to the targeted tissues [114].

Since the lung mucosal surface is wealthy in antiprotease enzymes, it's naturally porous to small-molecule peptides and proteins following their inhalation. Therefore, lung delivery of peptide-based NPs might lead to quicker absorption and higher local and systemic bioavailability as compared to subcutaneous and intravenous injections. Several studies examined the presence and/or expression of tumor-related proteins in the sputum of lung cancer patients and control subjects. Sun et al. (2009) reported a significantly increased expression of a proliferation-inducing ligand (APRIL) in the sputum of lung cancer patients compared to controls (82% vs. 3%) [117]. Pio et al. in 2010 showed elevated levels of complement factor H in sputum in lung cancer patients, suggesting that large plasma proteins such as factor H reflect increased permeability of the tumor circulation. Quantification of factor H may help improve the sensitivity of sputum cytology for lung cancer diagnosis, but it is not evidence of malignant tumors such as hemoptysis [118]. The aim of the study conducted by Sun et al. was to identify the expression profile of proliferation-inducing ligand (APRIL) in tumor tissue and lung cancer sputum and to evaluate the

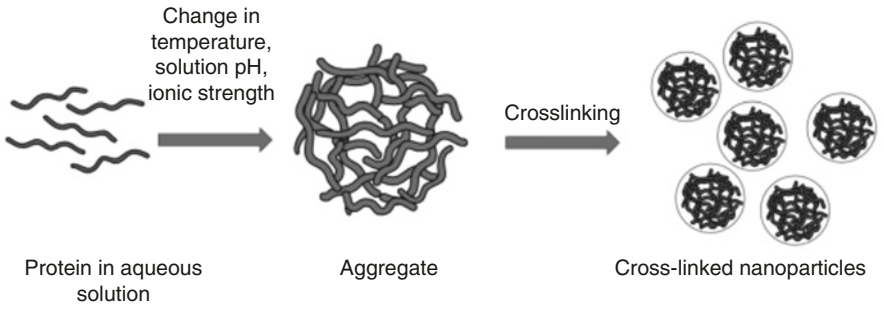

Fig. 5 Preparation of protein nanoparticles in aqueous solution [113]

potential for co-diagnosis of lung cancer by real-time quantitative polymerase chain reaction (RTQ-PCR). The authors used RTQ-PCR to analyze the expression of APRIL mRNA in 75 tissue samples and 71 corresponding lung cancer sputum samples and established their correlation. Expression of the APRIL protein was also observed in tumor tissue by Western blot and immunohistochemistry [117]. Expression analysis revealed increased expression of APRIL in non-small cell lung cancer (NSCLC), and immunohistochemical staining revealed that APRIL protein expression was localized to the membrane and cytoplasm of tumor cells. Expression of APRIL mRNA was increased in lung cancer sputum compared to benign lung disease and healthy subjects. These results support the potential role of the APRIL protein in lung cancer, especially NSCLC. Increased expression levels of APRIL mRNA in NSCLC sputum suggested that APRIL mRNA may serve as an effective and useful diagnostic biomarker for NSCLC [117].

NPs are increasingly used in a variety of applications, especially in the delivery of therapeutic and diagnostic agents. Natural biomolecules such as proteins are attractive alternatives to synthetic polymers that are widely used in pharmaceuticals for safety reasons [113]. In general, protein NPs offer many benefits, including biocompatibility and biodegradability. They can be made under mild conditions without the use of toxic chemicals or organic solvents. NPs derived from intrinsically disordered proteins are biodegradable, metabolic, susceptible to surface modification, and allow the attachment of drugs and target ligands. They have been successfully synthesized from a variety of proteins, including water-soluble proteins (e.g., bovine and human serum albumin) and insoluble proteins (e.g., zein and gliadin) [113].

Zein is a prolamine-rich protein that contains high levels of hydrophobic amino acids, proline, and glutamine. This is the protein found in the proteinaceous form from the endosperm of corn kernels. This hydrophobic protein is widely used in films and coatings. Zein is an FDA-approved GRAS polymer for human use. It is used in the manufacture of particulate systems for drug delivery and food applications [119]. Some studies have used zein to make edible capsules and films. Zein protein NPs are designed to encapsulate several drugs and bioactive compounds such as ivermectin, coumarin, and 5-fluorouracil (5FU). A 9-day in vitro release of coumarin from zein nanoparticles has been reported. These studies have demonstrated the usefulness of zein as a viable drug delivery material. Zein nanoparticles are also a promising delivery system for anticancer and diagnostic agents. There are reports of the use of zein nanoparticles with 5FU and quantum dot (QD) fluorophores to enhance drug delivery and imaging of breast cancer. These multifunctional QD nanoparticles are effective against breast cancer cells while providing high-quality imaging of cancer [119].

2.1.3.3 Apoferritin

Apoferritin is a ubiquitous intracellular protein. It is composed of 24 subunits and self-assembled into a hollow nanocage with an inner diameter of 8 mm and an outer diameter of 12 nm [120]. The very interesting characteristics of apoferritin are assembly and disassembly which can be modified by changing pH conditions. At pH 2.0, the protein cage is dissociated into subunits, and they are reassembled at neutral pH [121, 122]. This phenomenon can be utilized to formulate different NPs for loading therapeutic and imaging agents.

Different types of apoferritin are isolated from bacteria, fungi, plants, mice, and humans. Mammalian apoferritin is made up of heavy (H) subunits (21 kDa) which play a key role in iron oxidation and light (L) subunit (19 kDa) which plays role in the nucleation and mineralization of iron. The subunits (H and L) are homologous and can form a spherical cage-like apoferritin in any proportion [123]. Apoferritin has different affinities for receptors. H-apoferritin binds with transferrin receptor-1 (TfR1), and L-apoferritin binds with scavenger receptor class A member 5 (SCARA5). Apoferritin-encapsulated nanoparticles enter cancer cells via different mechanisms such as micropinocytosis and clathrin-mediated [124] and receptor-mediated endocytosis [125]. Apoferritin is considered biocompatible, biodegradable, and physiologically stable [126]. It possesses innate cancer cell targeting ability as it was proved to recognize TfR1, SCARA5, and chemokine (C-X-C motif) receptor 4 (CXCR4) which is copiously overexpressed on the surface of cancer cells [127, 128]. Also, the small size of the apoferritin is useful not only in overcoming physiological barriers but also in escaping rapid renal clearance [129].

Li et al. in 2012 developed a multifunctional nanostructure based on ferritin, which was used in fluorescence and MR imaging for the diagnosis of human lung adenocarcinoma A549 cells [130]. Apoferritin can also be used to deliver therapeutics. It was shown that daunomycin (DN) was encapsulated into the interior of hyaluronic acid (HA)-conjugated apoferritin nanocages for intracellular, pH-responsive controlled prodrug release. HA binds to the CD44 receptor and helps in targeting cancer cells specifically for DNA delivery [131]. Liang et al. used HFn nanocarrier for the target-specific delivery of doxorubicin (DOX) to HT-29 tumor cells which resulted in a substantial decrease in tumor growth in subcutaneous murine cancer models [132]. Crich SG et al. developed manganese-apoferritin complexes as very effective MRI contrast agents for the identification of hepatocellular carcinoma. Complexes were taken up by liver SCARA5 [133]. Similar strategies can also be applied to the diagnosis of lung cancer. In another study, Makino et al. successfully encapsulated gadolinium into the apoferritin cavity. When compared to the commercially available contrast agent gadolinium-DOTA, it increased the T1 relaxivity to tenfold [134]. By conjugating the apoferritin surface with dextran, they enhanced in vivo blood clearance time of apoferritin, and the formulation didn't show any toxicity. Recently, the bioluminescence imaging concept was developed. Luciferase was attached to the surface of H-ferritin (Hfn) using disulfide-containing linker (Luc-linker@HFn) which undergoes an intramolecular cyclization reaction in the presence of glutathione, a reducing agent in the cytosol, which releases luciferin.

This method overcomes the problems involved in regular fluorescence imaging such as no background signal, no photobleaching, and phototoxicity. It offers extended and efficient imaging [135].

2.1.3.4 Liposomes

A liposome is one of the most successful nano-based drug delivery systems on the market to date, with several FDA-approved liposome formulations [136]. Liposomes are self-assembled carriers with an outer hydrophobic lipid layer and a hydrophilic core. Liposomes can be produced in a variety of sizes from 50 nm to over 1000 nm, depending on the composition of the phospholipids and cholesterol molecules used. Liposomal formulations deliver the drug using specific targeting strategies, including passive targeting, active targeting, stimuli-responsive targeting, heat-responsive targeting, magnetic responsive targeting, and pH-responsive targeting [137]. This target specificity can improve pharmacokinetic and pharmacodynamic profiles, sustained and controlled release of the drug, diagnostic agents, reduced side effects, and reduced toxicity compared to free drug solutions [138]. In the future, it will increase the bioavailability of anticancer drugs, especially at the target site, reduce toxicity, and provide an overall improved therapeutic response [139, 140].

Traditional liposomes, also known as C-liposomes, are composed of cholesterol and lipids (negatively charged or neutral). These liposomes are taken up by the reticuloendothelial system (RES) and serum protein (opsonin). "Intelligent liposomes" can overcome these problems and can be gradually used as an active ingredient delivery system for the treatment of lung cancer. These liposomes contain a phospholipid bilayer, and surface modifications are covered with other molecules [141]. Intelligent liposomes not only have the potential to attack cancer cells but also reduce multidrug resistance (MDR). An advanced liposome formulation that combines pH-sensitive targeting and mitochondrial targeting strategies to prevent the supply of energy and trigger the apoptotic effect of resistant cancer cells has been developed [116]. Long-term circulating liposomes, also called stealth liposomes, are becoming more important in the treatment of lung cancer. Stealth liposomes have longer circulation and drug retention times, thereby increasing the drug concentration at the target site and its interaction with the receptor molecule [142].

Prasad et al. (2021) prepared liposomal nanotheranostics in which gold nanoparticles (AuNP) and luminescent graphene quantum dots (GQD) were encapsulated with a chemotherapeutic agent [143]. The surface of the liposome was functionalized with folic acid for targeted delivery. The prepared targeted liposome theranostics showed site-specific tumor diagnosis and photo-induced tumor resection. The study results confirmed significant contrasting and therapeutic effects of nanotheranostics liposomes with specific and enhanced cell uptake, long-term internalization in tumors, and dual imaging probes [143]. The synergistic and photothermal effects of anticancer drugs showed superior tumor impedance as opposed to treatment alone. In addition, these multi-component-loaded liposomes exhibit good colloidal stability, biocompatibility, and biodegradability, as shown by in vivo imaging.

Therefore, the developed nanohybrid liposome nanotheranostics served as a safe and highly potential platform for multifunctional tumor diagnosis and targeted therapy.

Another interesting study addressed two major challenges in the treatment of NSCLC: the very serious problem of resistance to brain metastases (BM) and tyrosine kinase inhibitors (TKIs). Yin et al. have developed a dual-targeting liposome system for coadministration of gefitinib and simvastatin for the treatment of BM in NSCLC [144]. In this study, fluorescent imaging was used to confirm that dual-targeted liposomes have the powerful ability to efficiently cross the blood-brain barrier and reverse drug resistance. Therefore, the developed liposome product represents a potential strategy for treating patients with advanced NSCLC in BM.

2.1.3.5 Solid Lipid Nanoparticles

Solid lipid nanoparticles (SLNs) improve the bioavailability of the drug and provide a large surface area with more drug load and protection of the drug from the environment. Therefore, one can realize two obvious benefits. It improves encapsulation efficiency [145] and releases the targeted active ingredient [146], resulting in lower active ingredient consumption during the pharmaceutical process [147]. Of all NP delivery systems, SLN has the properties of polymer NPs, liposomes, and fatty emulsions, making SLN the vehicle of choice for drug and diagnostic agents' delivery. Disadvantages associated with SLNs are the growth of lipid particles, polymorphic transitions, propensity for gelation, and essentially low uptake due to the crystal structure of solid lipids [148, 149]. Lipid NPs are usually composed of biocompatible lipids and natural surfactants. Common solid lipids used in the production of SLNs include triglycerides (Compritol 888 ATO and Dynasan, beeswax, carnauba wax, cetyl alcohol, emulsified wax, cholesterol, cholesterol butyrate, etc.). The surface of these lipid NPs can be easily modified by ligands to increase the targeting efficiency of this delivery system. This makes this system useful for active targeting [150, 151].

SLN has spherical morphology with a particle size range of 50–1000 nm. It is shown that SLNs are composed of approximately 0.1–30 (% w/w) solid lipids dispersed in the aqueous phase. Surfactants are used at concentrations of approximately 0.5–5% to increase stability [148, 149]. Solid lipid nanoparticles (SLNs) belong to the class of NP systems. It is composed of lipids that remain solid at body temperature and room temperature [152]. SLN has several advantages over other colloidal carriers, such as biotoxicity and avoidance of first-pass effects**.**

NP-based delivery vehicles hold great promise for intracellular targeting applications by modifying cell signaling and gene expression. Currently, the focus is on the synthesis of ultra-SLN that targets tumors. SLN has been used to improve the bioavailability of anticancer drugs such as etoposide, idarubicin, and doxorubicin [151].

SLN has been studied for the integration of many contrast agents, especially superparamagnetic iron oxide, technetium-99 (99 mTc), ^{64}Cu, and quantum dots. Recently, a study of SLN cancer treatment in which SLN was encapsulated in QD

as a contrast medium was published. The chemotherapeutic drug was a combination of paclitaxel and siRNA. The solid lipid matrix was interspersed with paclitaxel and QD, and the anionic siRNA was electrostatically bound to the cationic outer surface [153]. The combination of the double therapeutic drug paclitaxel loaded into SLN and siRNA was efficiently accumulated in lung cancer and showed synergistic anticancer activity. Importantly, the QD fluorescence of SLN has made it possible to track higher cellular uptake of SLN in vivo onsite and reduce offsite uptake into cancer cells. This study confirms the potential therapeutic potential of SLN as a nanocarrier [153]. Another research study conducted by Andreozzi and his colleagues is clear evidence of SLN's multifunctional therapeutic potential. The radioactively labeled SLN with ^{64}Cu and evaluated its biodistribution by in vivo quantitative assessment, PET imaging, and ex vivo gamma counting [154]. The results of the study confirmed the possibility of in vivo imaging of SLN theranostic and tumor resection at the same time. It is safe, biocompatible, and also biodegradable. The number of research studies conducted to date is very limited, and some other important aspects of SLN also need to be thoroughly investigated from a cancer theranostic perspective, including stimulation of lymphatic absorption by SLN. Any literature we discuss confirms efficient in vivo imaging and drug delivery using SLN, along with safe theranostic applications, biocompatibility, and biodegradability of the developed nanomedicines. The results showed that the theranostic nanoform developed by SLN is optimistic for making an outstanding contribution in the field of cancer treatment with simultaneous diagnosis [154].

Lung tumors are of particular interest because they can be treated with SLN, which is administered directly to the lungs by inhalation. However, this form of treatment is associated with certain restrictions, such as short residence times and poor tolerability, as a result of the uncontrolled release of the active ingredient [155]. In this regard, paclitaxel loaded into SLN has been used to reverse some of these limitations, which is a manufactured SLN coated with a polymer formed from polyfolate (ethylene glycol) and chitosan [156]. SLN was previously developed for the treatment and diagnosis of cancer. It has many technical advantages, including rapid cellular uptake, protection from chemical degradation of compounds, and potential for large-scale production [157, 158].

3 Conclusion

Lung cancer remained one of the most noxious among all cancer types due to heterogenicity, late-stage diagnosis, and challenges in diagnosis such as lack of accurate screening methods. The pharmaceutical and biomedical researcher's work is focused on developing an effective diagnostic product to treat lung cancer patients. Other limiting factors include nonspecificity and side effects of the diagnostic agent. Nanotechnology offers solutions to overcome the challenges associated with a diagnosis of lung cancer due to its unique properties such as physiochemical, biological, and mechanical properties. Nanomaterials from inorganic, organic, and protein

sources can be used to deliver the diagnostic agent to the lung cancer tissue for diagnosis. Polymeric and lipid-based materials are widely used as nanocarriers for the delivery of diagnostic as well as therapeutic agents. They can be conjugated with targeting ligands, functional groups, and load imaging agents, therapeutic agents with extended release. Biocompatible and biodegradable excipient used needs to be considered in the formulation of NP-based diagnostic agents. Metal NPs are broadly used in theranostic applications. The toxicity associated with metals is a primary concern in their use. Protein-based NPs and viral particles recently gained a lot of interest and applications in biomedical sciences. These NPs are biocompatible, are stable, and can reach tissue or cellular targets. Protein-based NPs and viral particles have a few critical challenges to address such as immunogenicity and difficulties in purification. Despite many advantages offered by NPs, the risk factors and toxic effects associated with their long-term use, increasing dose, and the time of exposure risks need to be thoroughly analyzed. By optimizing NP properties such as size, shape, surface type, and charge, the toxicity can be circumvented. Also, NPs' cellular uptake mechanisms and subcellular localization properties can be utilized in designing effective NPs. Genetic engineering can be utilized to create viral particles with various functional groups for diagnosis and drug delivery applications. Further interdisciplinary in vitro and in vivo studies should be performed with NP-based diagnostic products. The understanding of the pathophysiology of lung cancer diseases and the properties of NPs will assist in the development of new diagnostic products.

Acknowledgements This work was partially supported by the National Heart, Lung, and Blood Institute of the National Institutes of Health award, R15HL138718 to Dr. Chougule's lab.

Conflict of Interest The authors declare that there is no conflict of interest.

References

1. Bray F, Ferlay J, Soerjomataram I, Siegel RL, Torre LA, Jemal A. Global cancer statistics 2018: GLOBOCAN estimates of incidence and mortality worldwide for 36 cancers in 185 countries. CA Cancer J Clin. 2018;68(6):394–424. https://doi.org/10.3322/CAAC.21492.
2. Bray F, Jemal A, Grey N, Ferlay J, Forman D. Global cancer transitions according to the Human Development Index (2008–2030): a population-based study. Lancet Oncol. 2012;13(8):790–801. https://doi.org/10.1016/S1470-2045(12)70211-5.
3. Siegel RL, Miller KD, Jemal A. Cancer statistics, 2019. CA Cancer J Clin. 2019;69(1):7–34. https://doi.org/10.3322/CAAC.21551.
4. Cryer AM, Thorley AJ. Nanotechnology in the diagnosis and treatment of lung cancer. Pharmacol Ther. 2019;198:189–205. https://doi.org/10.1016/J.PHARMTHERA.2019.02.010.
5. Ferlay J, et al. Estimating the global cancer incidence and mortality in 2018: GLOBOCAN sources and methods. Int J Cancer. 2019;144(8):1941–53. https://doi.org/10.1002/IJC.31937.
6. Keikha M, Esfahani B. The relationship between tuberculosis and lung cancer. Adv Biomed Res. 2018;7(1):58. https://doi.org/10.4103/ABR.ABR_182_17.

7. Woodman C, Vundu G, George A, Wilson CM. Applications and strategies in nanodiagnosis and nanotherapy in lung cancer. Semin Cancer Biol. 2021;69:349–64. https://doi.org/10.1016/J.SEMCANCER.2020.02.009.
8. Reck M, Heigener DF, Mok T, Soria JC, Rabe KF. Management of non-small-cell lung cancer: recent developments. Lancet (London, England). 2013;382(9893):709–19. https://doi.org/10.1016/S0140-6736(13)61502-0.
9. Molina JR, Yang P, Cassivi SD, Schild SE, Adjei AA. Non-small cell lung cancer: epidemiology, risk factors, treatment, and survivorship. Mayo Clin Proc. 2008;83(5):584–94. https://doi.org/10.4065/83.5.584.
10. Kocher F, et al. Longitudinal analysis of 2293 NSCLC patients: a comprehensive study from the TYROL registry. Lung Cancer (Amsterdam, Netherlands). 2015;87(2):193–200. https://doi.org/10.1016/J.LUNGCAN.2014.12.006.
11. Ettinger DS, et al. Non-small cell lung cancer. J Natl Compr Cancer Netw. 2012;10(10):1236–71. https://doi.org/10.6004/JNCCN.2012.0130.
12. Travis WD, et al. The 2015 World Health Organization classification of lung tumors: impact of genetic, clinical and radiologic advances since the 2004 classification. J Thorac Oncol Off Publ Int Assoc Study Lung Cancer. 2015;10(9):1243–60. https://doi.org/10.1097/JTO.0000000000000630.
13. Tang ER, Schreiner AM, Pua BB. Advances in lung adenocarcinoma classification: a summary of the new international multidisciplinary classification system (IASLC/ATS/ERS). J Thorac Dis. 2014;6(Suppl 5):S489–501. https://doi.org/10.3978/J.ISSN.2072-1439.2014.09.12.
14. Sereno M, et al. Squamous-cell carcinoma of the lungs: is it really so different? Crit Rev Oncol Hematol. 2012;84(3):327–39. https://doi.org/10.1016/J.CRITREVONC.2012.06.009.
15. Bittner N, Ostoros G, Géczi L. New treatment options for lung adenocarcinoma–in view of molecular background. Pathol Oncol Res. 2014;20(1):11–25. https://doi.org/10.1007/S12253-013-9719-9.
16. Drilon A, Rekhtman N, Ladanyi M, Paik P. Squamous-cell carcinomas of the lung: emerging biology, controversies, and the promise of targeted therapy. Lancet Oncol. 2012;13(10) https://doi.org/10.1016/S1470-2045(12)70291-7.
17. Stinchcombe TE. Unmet needs in squamous cell carcinoma of the lung: potential role for immunotherapy. Med Oncol (Northwood, London, England). 2014;31(5):1–9. https://doi.org/10.1007/S12032-014-0960-1.
18. Barbareschi M, et al. Heterogeneity of large cell carcinoma of the lung: an immunophenotypic and miRNA-based analysis. Am J Clin Pathol. 2011;136(5):773–82. https://doi.org/10.1309/AJCPYY79XAGRAYCJ.
19. Van Meerbeeck JP, Fennell DA, De Ruysscher DKM. Small-cell lung cancer. Lancet (London, England). 2011;378(9804):1741–55. https://doi.org/10.1016/S0140-6736(11)60165-7.
20. Nakamura N, Miyagi E, Murata SI, Kawaoi A, Katoh R. Expression of thyroid transcription factor-1 in normal and neoplastic lung tissues. Mod Pathol Off J U S Can Acad Pathol. 2002;15(10):1058–67. https://doi.org/10.1097/01.MP.0000028572.44247.CF.
21. Green I, Lin O, Olgac S, Zakowski MF, Klimstra DS. Immunohistochemical staining of cytologic smears with MIB-1 helps distinguish low-grade from high-grade neuroendocrine neoplasms. Am J Clin Pathol. 2003;120(2):209–16. https://doi.org/10.1309/TGCD-66L3-1DHY-X5HK.
22. Raja S, Murthy SC, Mason DP. Malignant pleural mesothelioma. Curr Oncol Rep. 2011;13(4):259–64. https://doi.org/10.1007/S11912-011-0177-9.
23. van Zandwijk N, et al. Guidelines for the diagnosis and treatment of malignant pleural mesothelioma. J Thorac Dis. 2013;5(6) https://doi.org/10.3978/J.ISSN.2072-1439.2013.11.28.
24. Testa JR, et al. Germline BAP1 mutations predispose to malignant mesothelioma. Nat Genet. 2011;43(10):1022–6. https://doi.org/10.1038/NG.912.
25. Capuano R, Catini A, Paolesse R, Di Natale C. Sensors for lung cancer diagnosis. J Clin Med. 2019;8(2) https://doi.org/10.3390/JCM8020235.

26. Nakhleh MK, et al. Diagnosis and classification of 17 diseases from 1404 subjects via pattern analysis of exhaled molecules. ACS Nano. 2017;11(1):112–25. https://doi.org/10.1021/ACSNANO.6B04930/SUPPL_FILE/NN6B04930_SI_001.PDF.
27. Lux J, Sherry AD. Advances in gadolinium-based MRI contrast agent designs for monitoring biological processes in vivo. Curr Opin Chem Biol. 2018;45:121–30. https://doi.org/10.1016/J.CBPA.2018.04.006.
28. Sun I-C, Ahn C-H, Kim K, Emelianov S. Photoacoustic imaging of cancer cells with glycol-chitosan-coated gold nanoparticles as contrast agents. J Biomed Opt. 2019;24(12):1. https://doi.org/10.1117/1.JBO.24.12.121903.
29. Tang CK, Vaze A, Shen M, Rusling JF. High-throughput electrochemical microfluidic immunoarray for multiplexed detection of cancer biomarker proteins. ACS Sens. 2016;1(8):1036–43. https://doi.org/10.1021/ACSSENSORS.6B00256.
30. Munge BS, Stracensky T, Gamez K, DiBiase D, Rusling JF. Multiplex immunosensor arrays for electrochemical detection of cancer biomarker proteins. Electroanalysis. 2016;28(11):2644–58. https://doi.org/10.1002/ELAN.201600183.
31. Yang C, et al. Surface-engineered vanadium nitride nanosheets for an imaging-guided photothermal/photodynamic platform of cancer treatment. Nanoscale. 2019;11(4):1968–77. https://doi.org/10.1039/C8NR08269C.
32. Huang X, et al. pH-responsive theranostic nanocomposites as synergistically enhancing positive and negative magnetic resonance imaging contrast agents. J Nanobiotechnol. 2018;16(1) https://doi.org/10.1186/S12951-018-0350-5.
33. Xia L, et al. Multimodality imaging of naturally active melanin nanoparticles targeting somatostatin receptor subtype 2 in human small-cell lung cancer. Nanoscale. 2019;11(30):14400–9. https://doi.org/10.1039/C9NR04371C.
34. Toy R, Bauer L, Hoimes C, Ghaghada KB, Karathanasis E. Targeted nanotechnology for cancer imaging. Adv Drug Deliv Rev. 2014;76(1):79–97. https://doi.org/10.1016/J.ADDR.2014.08.002.
35. Batista CAS, Larson RG, Kotov NA. Nonadditivity of nanoparticle interactions. Science (New York, NY). 2015;350(6257) https://doi.org/10.1126/SCIENCE.1242477.
36. Shi J, Kantoff PW, Wooster R, Farokhzad OC. Cancer nanomedicine: progress, challenges and opportunities. Nat Rev Cancer. 2017;17(1):20–37. https://doi.org/10.1038/NRC.2016.108.
37. Mir TA, Yoon JH, Gurudatt NG, Won MS, Shim YB. Ultrasensitive cytosensing based on an aptamer modified nanobiosensor with a bioconjugate: detection of human non-small-cell lung cancer cells. Biosens Bioelectron. 2015;74:594–600. https://doi.org/10.1016/J.BIOS.2015.07.012.
38. Matczuk M, Ruzik L, Aleksenko SS, Keppler BK, Jarosz M, Timerbaev AR. Analytical methodology for studying cellular uptake, processing and localization of gold nanoparticles. Anal Chim Acta. 2019;1052:1–9. https://doi.org/10.1016/J.ACA.2018.10.027.
39. Donahue ND, Acar H, Wilhelm S. Concepts of nanoparticle cellular uptake, intracellular trafficking, and kinetics in nanomedicine. Adv Drug Deliv Rev. 2019;143:68–96. https://doi.org/10.1016/J.ADDR.2019.04.008.
40. Huang Q, Yu H, Ru Q. Bioavailability and delivery of nutraceuticals using nanotechnology. J Food Sci. 2010;75(1) https://doi.org/10.1111/J.1750-3841.2009.01457.X.
41. Wang P, et al. Multiwall carbon nanotubes mediate macrophage activation and promote pulmonary fibrosis through TGF-β/Smad signaling pathway. Small (Weinheim an der Bergstrasse, Germany). 2013;9(22):3799–811. https://doi.org/10.1002/SMLL.201300607.
42. Poland CA, et al. Carbon nanotubes introduced into the abdominal cavity of mice show asbestos-like pathogenicity in a pilot study. Nat Nanotechnol. 2008;3(7):423–8. https://doi.org/10.1038/NNANO.2008.111.
43. Harish V, et al. Review on nanoparticles and nanostructured materials: bioimaging, biosensing, drug delivery, tissue engineering, antimicrobial, and agro-food applications. Nanomaterials (Basel, Switzerland). 2022;12(3) https://doi.org/10.3390/NANO12030457.

44. Berthet M, Gauthier Y, Lacroix C, Verrier B, Monge C. Nanoparticle-based dressing: the future of wound treatment? Trends Biotechnol. 2017;35(8):770–84. https://doi.org/10.1016/J.TIBTECH.2017.05.005.
45. Lai P, Daear W, Löbenberg R, Prenner EJ. Overview of the preparation of organic polymeric nanoparticles for drug delivery based on gelatine, chitosan, poly(d,l-lactide-co-glycolic acid) and polyalkylcyanoacrylate. Colloids Surf B: Biointerfaces. 2014;118:154–63. https://doi.org/10.1016/J.COLSURFB.2014.03.017.
46. Rezvantalab S, et al. PLGA-based nanoparticles in cancer treatment. Front Pharmacol. 2018;0:1260. https://doi.org/10.3389/FPHAR.2018.01260.
47. Li Q, Li C, Tong W. Nile red loaded PLGA nanoparticles surface modified with Gd-DTPA for potential dual-modal imaging. J Nanosci Nanotechnol. 2016;16(6):5569–76. https://doi.org/10.1166/JNN.2016.11735.
48. Gao P, et al. Designing multifunctional cancer-targeted nanosystem for magnetic resonance molecular imaging-guided theranostics of lung cancer. Drug Deliv. 2018;25(1):1811–25. https://doi.org/10.1080/10717544.2018.1494224.
49. Kas HS. Chitosan: properties, preparations and application to microparticulate systems. J Microencapsul. 2009;14(6):689–711. https://doi.org/10.3109/02652049709006820.
50. Ravi Kumar MNV. A review of chitin and chitosan applications. React Funct Polym. 2000;46(1):1–27. https://doi.org/10.1016/S1381-5148(00)00038-9.
51. Ali A, Ahmed S. A review on chitosan and its nanocomposites in drug delivery. Int J Biol Macromol. 2018;109:273–86. https://doi.org/10.1016/J.IJBIOMAC.2017.12.078.
52. On KC, et al. Tumor-targeting Glycol Chitosan nanoparticles for image-guided surgery of Rabbit Orthotopic VX2 lung cancer. Pharmaceutics. 2020;12(7):621. https://doi.org/10.3390/PHARMACEUTICS12070621.
53. Zhu H-Z, et al. Chitosan combined with molecular Beacon for Mir-155 detection and imaging in lung cancer. Molecules. 2014;19(9):14710–22. https://doi.org/10.3390/MOLECULES190914710.
54. Abedi-Gaballu F, et al. PAMAM dendrimers as efficient drug and gene delivery nanosystems for cancer therapy. Appl Mater Today. 2018;12:177–90. https://doi.org/10.1016/J.APMT.2018.05.002.
55. Liu J, et al. Zwitterionic Gadolinium (III)-complexed dendrimer-entrapped gold nanoparticles for enhanced computed tomography/magnetic resonance imaging of lung cancer metastasis. ACS Appl Mater Interfaces. 2019;11(17):15212–21. https://doi.org/10.1021/ACSAMI.8B21679.
56. Wang H, Zheng L, Peng C, Shen M, Shi X, Zhang G. Folic acid-modified dendrimer-entrapped gold nanoparticles as nanoprobes for targeted CT imaging of human lung adenocarcinoma. Biomaterials. 2013;34(2):470–80. https://doi.org/10.1016/J.BIOMATERIALS.2012.09.054.
57. Chen S, et al. Targeting tumor microenvironment with PEG-based amphiphilic nanoparticles to overcome chemoresistance. Nanomedicine. 2016;12(2):269–86. https://doi.org/10.1016/j.nano.2015.10.020.
58. Sun T, Zhang YS, Pang B, Hyun DC, Yang M, Xia Y. Engineered nanoparticles for drug delivery in cancer therapy. Angew Chem Int Ed. 2014;53(46):12320–64. https://doi.org/10.1002/ANIE.201403036.
59. Duhem N, Danhier F, Préat V. Vitamin E-based nanomedicines for anti-cancer drug delivery. J Controll Release Off J Controll Release Soc. 2014;182(1):33–44. https://doi.org/10.1016/J.JCONREL.2014.03.009.
60. Sui Y, et al. Tumor-specific design of PEGylated gadolinium-based nanoscale particles: facile synthesis, characterization, and improved magnetic resonance imaging of metastasis lung cancer. J Photochem Photobiol B Biol. 2020;202:111669. https://doi.org/10.1016/J.JPHOTOBIOL.2019.111669.
61. Wang Z, et al. Active targeting theranostic iron oxide nanoparticles for MRI and magnetic resonance-guided focused ultrasound ablation of lung cancer. Biomaterials. 2017;127:25–35. https://doi.org/10.1016/J.BIOMATERIALS.2017.02.037.

62. Hou W, Xia F, Alves CS, Qian X, Yang Y, Cui D. MMP2-targeting and Redox-Responsive PEGylated Chlorin e6 nanoparticles for cancer near-infrared imaging and photodynamic therapy. ACS Appl Mater Interfaces. 2016;8(2):1447–57. https://doi.org/10.1021/ACSAMI.5B10772.
63. Yeh Y-C, Creran B, Rotello VM. Gold nanoparticles: preparation, properties, and applications in bionanotechnology. Nanoscale. 2012;4(6):1871. https://doi.org/10.1039/C1NR11188D.
64. Filipiak W, et al. Release of volatile organic compounds (VOCs) from the lung cancer cell line CALU-1 in vitro. Cancer Cell Int. 2008;8(1):1–11. https://doi.org/10.1186/1475-2867-8-17.
65. Hakim M, et al. Volatile organic compounds of lung cancer and possible biochemical pathways. Chem Rev. 2012;112(11):5949–66. https://doi.org/10.1021/CR300174A.
66. Barash O, Peled N, Hirsch FR, Haick H. Sniffing the unique 'Odor Print' of non-small-cell lung cancer with gold nanoparticles. Small. 2009;5(22):2618–24. https://doi.org/10.1002/SMLL.200900937.
67. Peng G, et al. Diagnosing lung cancer in exhaled breath using gold nanoparticles. Nat Nanotechnol. 2009;4(10):669–73. https://doi.org/10.1038/nnano.2009.235.
68. Gao W, et al. Highly sensitive detection of multiple tumor markers for lung cancer using gold nanoparticle probes and microarrays. Anal Chim Acta. 2017;958:77–84. https://doi.org/10.1016/J.ACA.2016.12.016.
69. Li Y, et al. Silver nanoparticles for enhanced cancer theranostics: in vitro and in vivo perspectives. J Biomed Nanotechnol. 2018;14(9):1515–42. https://doi.org/10.1166/JBN.2018.2614.
70. Zhang K, et al. Label-free diagnosis of lung cancer with tissue-slice surface-enhanced Raman spectroscopy and statistical analysis. Lasers Med Sci. 2019;34(9):1849–55. https://doi.org/10.1007/S10103-019-02781-W.
71. Zhang K, et al. Label-free and stable serum analysis based on Ag-NPs/PSi surface-enhanced Raman scattering for noninvasive lung cancer detection. Biomed Opt Express. 2018;9(9):4345. https://doi.org/10.1364/BOE.9.004345.
72. Yang J, et al. One-pot one-cluster synthesis of fluorescent and bio-compatible Ag14 nanoclusters for cancer cell imaging. Nanoscale. 2015;7(44):18464–70. https://doi.org/10.1039/C5NR06421J.
73. Lee EM, et al. Hybrid composite of silver nanoparticle-porous silicon microparticles as an image-guided localization agent for computed tomography scan of the lungs. ACS Biomater Sci Eng. 2020;6(8):4390–6. https://doi.org/10.1021/ACSBIOMATERIALS.0C00611.
74. Kim T, Braun GB, She ZG, Hussain S, Ruoslahti E, Sailor MJ. Composite porous silicon-silver nanoparticles as theranostic antibacterial agents. ACS Appl Mater Interfaces. 2016;8(44):30449–57. https://doi.org/10.1021/ACSAMI.6B09518.
75. Eun Mi L, et al. Hybrid composite of silver nanoparticle-porous silicon microparticles as an image-guided localization agent for computed tomography scan of the lungs. ACS Biomater Sci Eng. 2020;6(8):4390–6. https://doi.org/10.1021/ACSBIOMATERIALS.0C00611.
76. Seyed Mohammadali D, et al. Iron oxide nanoparticles: diagnostic, therapeutic and theranostic applications. Adv Drug Deliv Rev. 2019;138:302–25. https://doi.org/10.1016/J.ADDR.2019.01.005.
77. Mi-Kyong Y, et al. Folate-PEG-superparamagnetic iron oxide nanoparticles for lung cancer imaging. Acta Biomater. 2012;8(8):3005–13. https://doi.org/10.1016/J.ACTBIO.2012.04.029.
78. Seungil P, et al. Synthesis of 64 Cu-radiolabeled folate-conjugated iron oxide nanoparticles for cancer diagnosis. J Nanosci Nanotechnol. 2020;20(4):2040–4. https://doi.org/10.1166/JNN.2020.17205.
79. Shahbazi-Gahrouei D, Negar A, Shahbazi-Gahrouei S, Seyed Hossein H, Zeinab S. In vivo study of anti-epidermal growth factor receptor antibody-based iron oxide nanoparticles (anti-EGFR-SPIONs) as a novel MR imaging contrast agent for lung cancer (LLC1) cells detection. IET Nanobiotechnol. 2020;14(5):369–74. https://doi.org/10.1049/IET-NBT.2019.0385.

80. Xinyuan W, et al. The preliminary study of immune superparamagnetic iron oxide nanoparticles for the detection of lung cancer in magnetic resonance imaging. Carbohydr Res. 2016;419:33–40. https://doi.org/10.1016/J.CARRES.2015.11.003.
81. Alagiri M, Muthamizhchelvan C, Ponnusamy S. Structural and magnetic properties of iron, cobalt and nickel nanoparticles. Synth Met. 2011;161(15–16):1776–80. https://doi.org/10.1016/J.SYNTHMET.2011.05.030.
82. Kallumadil M, Tada M, Nakagawa T, Abe M, Southern P, Pankhurst QA. Suitability of commercial colloids for magnetic hyperthermia. J Magn Magn Mater. 2009;321(10):1509–13. https://doi.org/10.1016/J.JMMM.2009.02.075.
83. Lee N, Hyeon T. Designed synthesis of uniformly sized iron oxide nanoparticles for efficient magnetic resonance imaging contrast agents. Chem Soc Rev. 2012;41(7):2575–89. https://doi.org/10.1039/C1CS15248C.
84. Shao H, Yoon TJ, Liong M, Weissleder R, Lee H. Magnetic nanoparticles for biomedical NMR-based diagnostics. Beilstein J Nanotechnol. 2010;1(1):142. https://doi.org/10.3762/BJNANO.1.17.
85. Pankhurst QA, Connolly J, Jones SK, Dobson J. Applications of magnetic nanoparticles in biomedicine. J Phys D Appl Phys. 2003;36(13):R167. https://doi.org/10.1088/0022-3727/36/13/201.
86. Zhou X, Chen L, Wang A, Ma Y, Zhang H, Zhu Y. Multifunctional fluorescent magnetic nanoparticles for lung cancer stem cells research. Colloids Surf B: Biointerfaces. 2015;134:431–9. https://doi.org/10.1016/J.COLSURFB.2015.07.030.
87. Wang Y, Zhang Y, Du Z, Wu M, Zhang G. Detection of micrometastases in lung cancer with magnetic nanoparticles and quantum dots. Int J Nanomedicine. 2012;7:2315. https://doi.org/10.2147/IJN.S30593.
88. Korzeniowska B, Nooney R, Wencel D, McDonagh C. Silica nanoparticles for cell imaging and intracellular sensing. Nanotechnology. 2013;24(44):442002. https://doi.org/10.1088/0957-4484/24/44/442002.
89. Chen S, Yang Y, Li H, Zhou X, Liu M. pH-triggered Au-fluorescent mesoporous silica nanoparticles for 19F MR/fluorescent multimodal cancer cellular imaging. Chem Commun. 2013;50(3):283–5. https://doi.org/10.1039/C3CC47324D.
90. Lee H, et al. Silica nanoparticle-based dual imaging colloidal hybrids: cancer cell imaging and biodistribution. Int J Nanomedicine. 2015;10(Spec Iss):215. https://doi.org/10.2147/IJN.S88311.
91. Das P, Sedighi A, Krull UJ. Cancer biomarker determination by resonance energy transfer using functional fluorescent nanoprobes. Anal Chim Acta. 2018;1041:1–24. https://doi.org/10.1016/J.ACA.2018.07.060.
92. Kalkal A, Pradhan R, Kadian S, Manik G, Packirisamy G. Biofunctionalized graphene quantum dots based fluorescent biosensor toward efficient detection of small cell lung cancer. ACS Appl Bio Mater. 2020;3(8):4922–32. https://doi.org/10.1021/ACSABM.0C00427.
93. Shivaji K, et al. Green-synthesis-derived CdS quantum dots using tea leaf extract: antimicrobial, bioimaging, and therapeutic applications in lung cancer cells. ACS Appl Nano Mater. 2018;1(4):1683–93. https://doi.org/10.1021/ACSANM.8B00147.
94. Nafiujjaman M, Khan HA, Lee YK. Peptide-influenced graphene quantum dots on iron oxide nanoparticles for dual imaging of lung cancer cells. J Nanosci Nanotechnol. 2017;17(3):1704–11. https://doi.org/10.1166/JNN.2017.12825.
95. Elzoghby AO, Samy WM, Elgindy NA. Protein-based nanocarriers as promising drug and gene delivery systems. J Controll Release Off J Controll Release Soc. 2012;161(1):38–49. https://doi.org/10.1016/J.JCONREL.2012.04.036.
96. Chung YH, Cai H, Steinmetz NF. Viral nanoparticles for drug delivery, imaging, immunotherapy, and theranostic applications. Adv Drug Deliv Rev. 2020;156:214–35. https://doi.org/10.1016/J.ADDR.2020.06.024.

97. Wang C, Beiss V, Steinmetz NF. Cowpea mosaic virus nanoparticles and empty virus-like particles show distinct but overlapping immunostimulatory properties. J Virol. 2019;93(21) https://doi.org/10.1128/JVI.00129-19.
98. Li K, Nguyen HG, Lu X, Wang Q. Viruses and their potential in bioimaging and biosensing applications. Analyst. 2010;135(1):21–7. https://doi.org/10.1039/B911883G.
99. Ma Y, Nolte RJM, Cornelissen JJLM. Virus-based nanocarriers for drug delivery. Adv Drug Deliv Rev. 2012;64(9):811–25. https://doi.org/10.1016/J.ADDR.2012.01.005.
100. Lee CS, et al. Adenovirus-mediated gene delivery: potential applications for gene and cell-based therapies in the new era of personalized medicine. Genes Dis. 2017;4(2):43–63. https://doi.org/10.1016/J.GENDIS.2017.04.001.
101. Lehrman S. Virus treatment questioned after gene therapy death. Nature. 1999;401(6753):517–8. https://doi.org/10.1038/43977.
102. Ferrer-Miralles N, Rodríguez-Carmona E, Corchero JL, García-Fruitós E, Vázquez E, Villaverde A. Engineering protein self-assembling in protein-based nanomedicines for drug delivery and gene therapy. Crit Rev Biotechnol. 2015;35(2):209–21. https://doi.org/10.3109/07388551.2013.833163.
103. Steinmetz NF. Viral nanoparticles as platforms for next-generation therapeutics and imaging devices. Nanomedicine. 2010;6(5):634–41. https://doi.org/10.1016/J.NANO.2010.04.005.
104. Leong HS, et al. Intravital imaging of embryonic and tumor neovasculature using viral nanoparticles. Nat Protoc. 2010;5(8):1406–17. https://doi.org/10.1038/nprot.2010.103.
105. Beatty PH, Lewis JD. Cowpea mosaic virus nanoparticles for cancer imaging and therapy. Adv Drug Deliv Rev. 2019;145:130–44. https://doi.org/10.1016/J.ADDR.2019.04.005.
106. Cho CF, et al. Viral nanoparticles decorated with novel EGFL7 ligands enable intravital imaging of tumor neovasculature. Nanoscale. 2017;9(33):12096–109. https://doi.org/10.1039/C7NR02558K.
107. Wang Q, Kaltgrad E, Lin T, Johnson JE, Finn MG. Natural supramolecular building blocks. Wild-type cowpea mosaic virus. Chem Biol. 2002;9(7):805–11. https://doi.org/10.1016/S1074-5521(02)00165-5.
108. Chatterji A, Ochoa WF, Paine M, Ratna BR, Johnson JE, Lin T. New addresses on an addressable virus nanoblock; uniquely reactive Lys residues on cowpea mosaic virus. Chem Biol. 2004;11(6):855–63. https://doi.org/10.1016/J.CHEMBIOL.2004.04.011.
109. Luzuriaga MA, et al. Enhanced stability and controlled delivery of MOF-encapsulated vaccines and their immunogenic response in vivo. ACS Appl Mater Interfaces. 2019;11(10):9740–6. https://doi.org/10.1021/ACSAMI.8B20504.
110. Robertson KL, Soto CM, Archer MJ, Odoemene O, Liu JL. Engineered T4 viral nanoparticles for cellular imaging and flow cytometry. Bioconjug Chem. 2011;22(4):595–604. https://doi.org/10.1021/BC100365J.
111. Ko S, Gunasekaran S. Preparation of sub-100-nm β-lactoglobulin (BLG) nanoparticles. J Microencapsul. Dec. 2008;23(8):887–98. https://doi.org/10.1080/02652040601035143.
112. Duclairoir C, Orecchioni AM, Depraetere P, Nakache E. α-Tocopherol encapsulation and in vitro release from wheat gliadin nanoparticles. J Microencapsul. 2008;19(1):53–60. https://doi.org/10.1080/02652040110055207.
113. Lohcharoenkal W, Wang L, Chen YC, Rojanasakul Y. Protein nanoparticles as drug delivery carriers for cancer therapy. Biomed Res Int. 2014;2014 https://doi.org/10.1155/2014/180549.
114. Fosgerau K, Hoffmann T. Peptide therapeutics: current status and future directions. Drug Discov Today. 2015;20(1):122–8. https://doi.org/10.1016/J.DRUDIS.2014.10.003.
115. Penchala SC, et al. A biomimetic approach for enhancing the in vivo half-life of peptides. Nat Chem Biol. 2015;11(10):793. https://doi.org/10.1038/NCHEMBIO.1907.
116. Jiang L, et al. Overcoming drug-resistant lung cancer by paclitaxel loaded dual-functional liposomes with mitochondria targeting and pH-response. Biomaterials. 2015;52(1):126–39. https://doi.org/10.1016/J.BIOMATERIALS.2015.02.004.
117. Sun B, et al. A proliferation-inducing ligand: a new biomarker for non-small cell lung cancer. Exp Lung Res. 2009;35(6):486–500. https://doi.org/10.1080/01902140902759274.

118. Pio R, et al. Complement factor H is elevated in bronchoalveolar lavage fluid and sputum from patients with lung cancer. Cancer Epidemiol Biomark Prev. 2010;19(10):2665–72. https://doi.org/10.1158/1055-9965.EPI-10-0467/66966/AM/COMPLEMENT-FACTOR-H-IS-ELEVATED-IN-BRONCHOALVEOLAR.
119. Hurtado-López P, Murdan S. Zein microspheres as drug/antigen carriers: a study of their degradation and erosion, in the presence and absence of enzymes. J Microencapsul. 2006;23(3):303–14. https://doi.org/10.1080/02652040500444149.
120. Theil EC. Ferritin: structure, gene regulation, and cellular function in animals, plants, and microorganisms. Annu Rev Biochem. 1987;56:289–315. https://doi.org/10.1146/ANNUREV.BI.56.070187.001445.
121. Harrison PM, Gregory DW. Reassembly of apoferritin molecules from subunits. Nature. 1968;220(5167):578–80. https://doi.org/10.1038/220578A0.
122. Ma-Ham A, Wu H, Wang J, Kang X, Zhang Y, Lin Y. Apoferritin-based nanomedicine platform for drug delivery: equilibrium binding study of daunomycin with DNA. J Mater Chem. 2011;21(24):8700–8. https://doi.org/10.1039/C0JM04321D.
123. Li L, et al. Binding and uptake of H-ferritin are mediated by human transferrin receptor-1. Proc Natl Acad Sci U S A. 2010;107(8):3505–10. https://doi.org/10.1073/PNAS.0913192107.
124. Liu X, et al. Apoferritin-CeO_2 nano-truffle that has excellent artificial redox enzyme activity. Chem Commun (Camb). 2012;48(26):3155–7. https://doi.org/10.1039/C1CC15815E.
125. Liu X, et al. Apoferritin-camouflaged Pt nanoparticles: surface effects on cellular uptake and cytotoxicity. J Mater Chem. 2011;21(20):7105–10. https://doi.org/10.1039/C1JM10575B.
126. Veroniaina H, Pan X, Wu Z, Qi X. Apoferritin: a potential nanocarrier for cancer imaging and drug delivery. Expert Rev Anticancer Ther. 2021;21(8):901–13. https://doi.org/10.1080/14737140.2021.1910027.
127. Alkhateeb AA, Connor JR. The significance of ferritin in cancer: anti-oxidation, inflammation and tumorigenesis. Biochim Biophys Acta. 2013;1836(2):245–54. https://doi.org/10.1016/J.BBCAN.2013.07.002.
128. Wang W, Knovich MA, Coffman LG, Torti FM, Torti SV. Serum ferritin: past, present and future. Biochim Biophys Acta. 2010;1800(8):760–9. https://doi.org/10.1016/J.BBAGEN.2010.03.011.
129. Davis ME, Chen Z, Shin DM. Nanoparticle therapeutics: an emerging treatment modality for cancer. Nat Rev Drug Discov. 2008;7(9):771–82. https://doi.org/10.1038/NRD2614.
130. Li K, et al. Multifunctional ferritin cage nanostructures for fluorescence and MR imaging of tumor cells. Nanoscale. 2012;4(1):188–93. https://doi.org/10.1039/C1NR11132A.
131. Luo Y, Wang X, Du D, Lin Y. Hyaluronic acid-conjugated apoferritin nanocages for lung cancer targeted drug delivery. Biomater Sci. 2015;3(10):1386–94. https://doi.org/10.1039/C5BM00067J.
132. Liang M, et al. H-ferritin-nanocaged doxorubicin nanoparticles specifically target and kill tumors with a single-dose injection. Proc Natl Acad Sci U S A. 2014;111(41):14900–5. https://doi.org/10.1073/PNAS.1407808111.
133. Geninatti Crich S, et al. Mn-loaded apoferritin: a highly sensitive MRI imaging probe for the detection and characterization of hepatocarcinoma lesions in a transgenic mouse model. Contrast Media Mol Imaging. 2012;7(3):281–8. https://doi.org/10.1002/CMMI.492.
134. Makino A, et al. Effective encapsulation of a new cationic gadolinium chelate into apoferritin and its evaluation as an MRI contrast agent. Nanomedicine. Oct. 2011;7(5):638–46. https://doi.org/10.1016/J.NANO.2011.01.015.
135. Bellini M, et al. Engineered ferritin nanoparticles for the bioluminescence tracking of nanodrug delivery in cancer. Small (Weinheim an der Bergstrasse, Germany). 2020;16(39) https://doi.org/10.1002/SMLL.202001450.
136. Lee WH, Loo CY, Traini D, Young PM. Nano- and micro-based inhaled drug delivery systems for targeting alveolar macrophages. Expert Opin Drug Deliv. 2015;12(6):1009–26. https://doi.org/10.1517/17425247.2015.1039509.

137. Li R, et al. Intelligently targeted drug delivery and enhanced antitumor effect by gelatinase-responsive nanoparticles. PLoS One. 2013;8(7) https://doi.org/10.1371/JOURNAL.PONE.0069643.
138. Deshpande PP, Biswas S, Torchilin VP. Current trends in the use of liposomes for tumor targeting. Nanomedicine (London, England). 2013;8(9):1509–28. https://doi.org/10.2217/NNM.13.118.
139. Drummond DC, Noble CO, Hayes ME, Park JW, Kirpotin DB. Pharmacokinetics and in vivo drug release rates in liposomal nanocarrier development. J Pharm Sci. 2008;97(11):4696–740. https://doi.org/10.1002/JPS.21358.
140. Zhang H, Wang ZY, Gong W, Li ZP, Mei XG, Lv WL. Development and characteristics of temperature-sensitive liposomes for vinorelbine bitartrate. Int J Pharm. 2011;414(1–2):56–62. https://doi.org/10.1016/J.IJPHARM.2011.05.013.
141. Voinea M, Simionescu M. Designing of 'intelligent' liposomes for efficient delivery of drugs. J Cell Mol Med. 2002;6(4):465–74. https://doi.org/10.1111/J.1582-4934.2002.TB00450.X.
142. Torchilin VP. Targeted pharmaceutical nanocarriers for cancer therapy and imaging. AAPS J. 2007;9(2) https://doi.org/10.1208/AAPSJ0902015.
143. Prasad R, et al. Liposomal nanotheranostics for multimode targeted in vivo bioimaging and near-infrared light mediated cancer therapy. Commun Biol. 2020;3(1) https://doi.org/10.1038/S42003-020-1016-Z.
144. Yin W, et al. BBB-penetrating codelivery liposomes treat brain metastasis of non-small cell lung cancer with EGFR T790M mutation. Theranostics. 2020;10(14):6122–35. https://doi.org/10.7150/THNO.42234.
145. Dela Cruz CS, Tanoue LT, Matthay RA. Lung cancer: epidemiology, etiology, and prevention. Clin Chest Med. 2011;32(4):605–44. https://doi.org/10.1016/J.CCM.2011.09.001.
146. Dolatabadi JEN, Valizadeh H, Hamishehkar H. Solid lipid nanoparticles as efficient drug and gene delivery systems: recent breakthroughs. Adv Pharm Bull. 2015;5(2):151. https://doi.org/10.15171/APB.2015.022.
147. Lee HY, Mohammed KA, Nasreen N. Nanoparticle-based targeted gene therapy for lung cancer. Am J Cancer Res. 2016;6(5):1118.
148. Scioli Montoto S, Muraca G, Ruiz ME. Solid lipid nanoparticles for drug delivery: pharmacological and biopharmaceutical aspects. Front Mol Biosci. 2020;7 https://doi.org/10.3389/FMOLB.2020.587997.
149. Naseri N, Valizadeh H, Zakeri-Milani P. Solid lipid nanoparticles and nanostructured lipid carriers: structure, preparation and application. Adv Pharm Bull. 2015;5(3):305. https://doi.org/10.15171/APB.2015.043.
150. Singh I, Swami R, Jeengar MK, Khan W, Sistla R. p-Aminophenyl-α-D-mannopyranoside engineered lipidic nanoparticles for effective delivery of docetaxel to brain. Chem Phys Lipids. 2015;188:1–9. https://doi.org/10.1016/J.CHEMPHYSLIP.2015.03.003.
151. Sukumar UK, Bhushan B, Dubey P, Matai I, Sachdev A, Packirisamy G. Emerging applications of nanoparticles for lung cancer diagnosis and therapy. Int Nano Lett. 2013;3(1):1–17. https://doi.org/10.1186/2228-5326-3-45.
152. Makwana V, Jain R, Patel K, Nivsarkar M, Joshi A. Solid lipid nanoparticles (SLN) of Efavirenz as lymph targeting drug delivery system: elucidation of mechanism of uptake using chylomicron flow blocking approach. Int J Pharm. 2015;495(1):439–46. https://doi.org/10.1016/J.IJPHARM.2015.09.014.
153. Mussi SV, Torchilin VP. Recent trends in the use of lipidic nanoparticles as pharmaceutical carriers for cancer therapy and diagnostics. J Mater Chem B. 2013;1(39):5201–9. https://doi.org/10.1039/C3TB20990C.
154. Andreozzi E, Seo JW, Ferrara K, Louie A. Novel method to label solid lipid nanoparticles with 64cu for positron emission tomography imaging. Bioconjug Chem. 2011;22(4):808–18. https://doi.org/10.1021/BC100478K.

155. Bayón-Cordero L, Alkorta I, Arana L. Application of solid lipid nanoparticles to improve the efficiency of anticancer drugs. Nanomaterials. 2019;9(3):474. https://doi.org/10.3390/NANO9030474.
156. Rosière R, et al. New folate-grafted chitosan derivative to improve delivery of Paclitaxel-loaded solid lipid nanoparticles for lung tumor therapy by inhalation. Mol Pharm. 2018;15(3):899–910. https://doi.org/10.1021/ACS.MOLPHARMACEUT.7B00846.
157. He SN, et al. Ternary nanoparticles composed of cationic solid lipid nanoparticles, protamine, and DNA for gene delivery. Int J Nanomedicine. 2013;8:2859. https://doi.org/10.2147/IJN.S47967.
158. Mehnert W, Mäder K. Solid lipid nanoparticles: production, characterization and applications. Adv Drug Deliv Rev. 2001;47(2–3):165–96. https://doi.org/10.1016/S0169-409X(01)00105-3.

Role of Electrospun Nanofibers in Cancer Detection and Treatment

Lohitha Kalluri and Yuanyuan Duan

1 Introduction

Cancer is an extensively prevalent disease worldwide. It results from the DNA mutations within a cell or a group of cells, instigating abnormal proliferation of cells with an ability to invade other normal tissues or organs. Epidemiological studies showed that certain risk factors would lead to DNA mutations within a cell, causing cancer. National cancer institute delineated several suspected cancer risk factors that include aging, alcohol, chronic inflammation, obesity, radiation, sunlight, tobacco, etc. [1, 2]. Understanding the risk factors and cancer etiology is crucial in devising the cancer-preventive and treatment protocols. In the United States, in 2014, evaluated risk factors were found to be attributed to around 42.0% of all cancer incidence cases (659,640 of 1,570,975 cancers, excluding nonmelanoma skin cancers) and 45.1% of cancer deaths (265,150 of 587,521 deaths) [3]. Theoretically, lowering the risk factor exposure to zero would prevent cancer. However, that's practically impossible with the current lifestyle and environmental conditions. Also, exposure to certain risk factors such as aging, sunlight, etc. is inevitable. Cancer risk is the sum of a blend of genetic and environmental factors, such as behavioral, lifestyle, and environmental exposures. It is difficult to quantify the effect of the magnitude of a single risk factor. However, cancers require substantial time to develop after exposure to risk factors [4]. Thus, additional strategies such as early identification, prevention, and treatment protocols need to be developed to intervene in the disease progression and combat this deadly disease.

L. Kalluri · Y. Duan (✉)
Department of Biomedical Materials Science, University of Mississippi Medical Center, Jackson, MS, USA
e-mail: yduan@umc.edu

R. S. Chaughule et al. (eds.), *Nanomaterials for Cancer Detection Using Imaging Techniques and Their Clinical Applications*,
https://doi.org/10.1007/978-3-031-09636-5_9

Metastasis or the spread of cancer cells to other organs is the primary reason for death in cancer patients. The GLOBOCAN estimates reported 19.3 million new cases of cancer and nearly ten million deaths from cancer in 2020. Also, they projected a 47% increase in incidence rates by 2040 due to growth and population aging along with an increased prevalence of risk factors [5]. The past two decades had witnessed rapid progress in cancer research. Despite the favorable progress in in vitro and clinical cancer research relating to its molecular and genetic mechanisms as well as the diagnostic, preventive, and treatment techniques, the disease reduction rates and mortality rates remained the same as what was observed 50 years ago. This might be attributed to the complex nature of the disease affecting nearly every tissue lineage in our bodies, and arising from normal cells as a consequence of diverse mutations affecting numerous genes. Owing to such complexity, conquering cancer poses quite a challenge to modern science [6]. Thus, there is an ongoing quest for novel screening, preventive, diagnostic, and treatment techniques to stop this widely prevalent deadly disease.

For the past two decades, electrospinning technology was adopted to construct tissue-engineered nanofibrous structures due to its ability to closely mimic the mechanical and functional properties of the extracellular matrix of natural tissues [7, 8]. Also, electrospraying technology was widely investigated to generate micro−/nanoparticles for drug delivery applications, with controlled particle agglomeration and high yields [9]. Electrospinning and electrospraying technologies are based on an electrohydrodynamic process, wherein a droplet of polymer solution or polymer melt is charged to create a jet, which is later stretched and elongated under external electrostatic force to generate fibers or particles, respectively. The chain entanglement density of polymer liquid used in these techniques dictates the formation of fibers or particles and thus distinct electrospinning and electrospraying technologies [10]. Lately, these technologies are being explored for producing nanofibers/nanoparticles in cancer research. The electrospun nanofibers have been investigated as ultrasensitive biosensors in cancer research due to their higher surface-area-to-volume ratio, controllable surface conformation, flexible surface modifications, and high biocompatibility. Furthermore, electrospun fiber matrices served as 3D scaffolds for the fabrication of in vitro tumor models and to study drug delivery approaches. Additionally, the production of drug-loaded coaxial nanofibers using coaxial electrospinning technology aided in theranostic applications, wherein the one-step loading of a combination of drugs within fibers facilitated the use of one radioactive drug to identify cancerous cells, and a second radioactive drug to deliver therapy to treat the main tumor and any metastatic tumors [7, 11–21].

In this chapter, the role and importance of electrospun micro−/nanofibers in various aspects of cancer disease research including sensing and diagnosis of cancerous cells, applications in theranostics, 3D in vitro tumor models fabrication, and delivery of chemotherapeutic agents will be discussed. Furthermore, current challenges and probable future applications of these nanofibers in cancer diagnosis and treatment will be discussed.

2 Role of Electrospun Fibers in Cancer Detection

In cancer conditions, it is essential to diagnose the disease as early as possible to favor treatment and prognosis and to avoid metastasis. Currently, biosensors and imaging modalities are the common modalities used to detect cancer onset at early stages. With the advances in nanotechnology, nanoscale transducers were introduced to improve the sensitivity and accuracy of biosensors. Nanoscale fibrous membranes as small as 10 nm in diameter can be fabricated by the electrospinning process. As a consequence, there has been plenty of recent progress in the development of biosensors for cancer detection involving electrospinning [22, 23].

2.1 Electrospun Fiber-Based Biosensors

Biomarkers are measurable molecules present in a person's blood, saliva, or other body fluids, and might include genetic mutations, other changes in DNA, and abnormalities in proteins or other biological molecules that indicate the presence of an anomaly. Certain biomarkers are present in higher quantities in persons with cancer compared to healthy people, thus aiding in the diagnosis, treatment planning, and prognosis for a patient [24, 25]. For instance, BRCA1- and BRCA2-inherited gene mutations can be detected in blood samples, and they indicate high risks of breast and ovarian cancers [26]. Also, biomarkers could allow differentiation between cancers, premalignant lesions that need to be treated, and other benign lesions. Additionally, detection of specific biomarkers that are crucial in cancer developing and progressing mechanisms would aid in devising the preventive and treatment protocols by impeding those biological mechanisms causing cancer [22]. Thus, it is important to accurately identify or sense the minor quantities of these biomarkers that are present in a patient's body fluids for early diagnosis of cancer.

Circulating Tumor Cell (CTC) Biomarkers
Usually, in the early disease process, several cancerous tumors shed either the intracellular molecules, cellular fragments, or whole cells, into the surrounding environment. Quite often, these substances can be detected in the blood, feces, or other body fluids, thus presenting the possibility for easier and less-invasive cancer detection methods. A specific biomarker, "tumor cell DNA" circulating in the blood, has been the focus of interest lately. It is also termed as "circulating tumor DNA," or "ctDNA." This DNA is quite evident by key mutations or certain other abnormalities found in the DNA of intact tumor cells [27–31]. Although these findings are promising, several technical challenges, including increasing the sensitivity of ctDNA/biomarker detection, still need to be improved.

In addition to ctDNA, hypoxia sensing is also crucial in detecting solid tumors. The tumor microenvironment will be hypoxic due to disparity between increased O_2 demand by uncontrolled proliferation of cells and reduced O_2 supply by disorganized vasculature structure, causing areas with reduced pO_2. Tumor cells utilize a

cellular response driven by oxygen sensors that alters a variety of gene expression networks, allowing cells to alter their metabolism, evade natural defenses, and invade the surrounding tissue [32]. Thus, various research groups are investigating the underlying mechanism of how oxygen sensors facilitate adaptation to hypoxic conditions and how these mechanisms could be targeted to improve disease outcomes across various cancer types [32–34]. Furthermore, other biomolecules such as microRNAs, proteins, serum microvesicles, etc. could be monitored for cancer diagnosis and prognosis.

The biosensor consists of a bioreceptor and a transducer. A bioreceptor is a device that interacts with the specific biomarker of interest to produce an effect that can be measured by the transducer. The bioreceptor should have high selectivity and sensitivity for the analyte among various other chemical or biological components [35]. The unique characteristics of electrospun fibers as one-dimensional confinement, large interconnected and tailored pore geometries, nanoscale fibers with high specific surface area, and the ability to functionalize as well as customize the fibers with desired composite materials, etc. make them an effective bioreceptor for biosensing applications. Also, the ability to highly align these fibers in a uniaxial direction by using rotating electrospinning collectors controls the electrical diffusion, and further aids in enhancing their specificity and sensitivity [36, 37].

Electrospinning is a simple inexpensive technique that can be carried out using minimal equipment setup. The setup comprises a syringe pump, a spinneret, a high-voltage power supply, and a collector (Fig. 1) [8]. In summary, a polymer solution will be loaded into the syringe attached to the spinneret and will be ejected at a constant flow rate using a syringe pump. The polymer droplet that is ejected at the tip of the spinneret will be charged due to the application of a high voltage on the spinneret. The charged polymer droplet will produce nanofibers due to the columbic repulsive forces within a charged droplet. These nanofibers will fly toward the grounded collector plate and are deposited on the collector plate due to the potential difference created between high-voltage spinneret and grounded collector. The

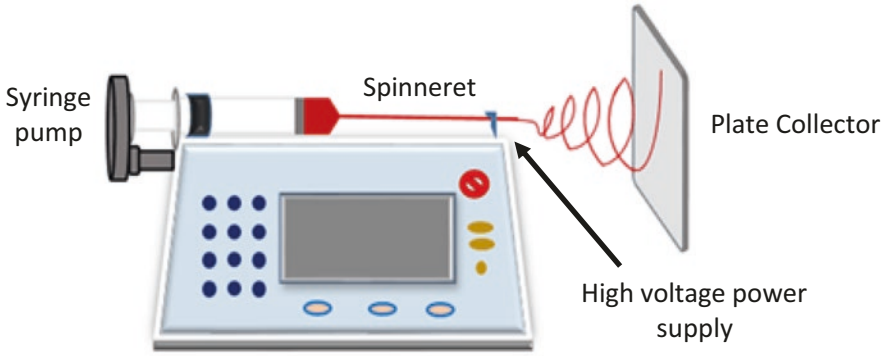

Fig. 1 Schematic of electrospinning equipment setup. (Reproduced with permission [8])

nanofibers with tunable diameters and properties can be prepared by altering the solution properties and various electrospinning parameters.

Additionally, these electrospun nanofibers present with a large surface area and are readily modifiable with desired functional groups and various biorecognition molecules. Several approaches could be used to incorporate the functional entities within the electrospun fibers, including the utilization of inherent properties of the natural polymer, by blending bioactive additives into the electrospinning solution, and post-modification of electrospun fibrous mats. These approaches could also be used to achieve multiple functional entities within a single nanofiber [36, 38].

Also, the electrospinning process produces three-dimensional porous nanofibrous mats that are relatively easier to handle than other unidimensional structures, yet retain the advantages and properties of those unidimensional structures. On incorporation into microchannels, these nanofibrous structures can spread throughout the entire microchannel volume, and provide multiple numerous reaction sites within a small enclosed space. Besides, unlike unidimensional and two-dimensional nanomaterials, these nanofiber mats will retain the functional entities in position and will facilitate the uniform distribution of these entities by preventing agglomeration under varying experimental conditions. Consequently, they are quite useful as biosensors in cancer diagnosis and provide effective cell capturing and ultrasensitive detection of biomarkers within a broad range of quantities. Also, they assist in minimizing the response times and provide faster results [39].

Lastly, the morphology and functional properties of electrospun nanofibers can be easily regulated by controlling the polymer solution properties and electrospinning conditions. As an instance, narrow-diameter fibers can be produced by using low polymer concentrations, low molecular weight polymers, lower flow rates, and high applied voltages. Moreover, electrospun micro-fibrous mats contain greater pore sizes when compared to nanofibrous mats, which provides the flexibility to incorporate electrospun nanofibers as functional elements within the microfluidic chip for cancer diagnostic systems. For example, an electrospun fibrous mat having a greater pore diameter than the tumor cells would be appropriate for affinity-based capturing, while a smaller pore size fibrous mat would be appropriate for detecting or capturing cancer biomarkers such as proteins [36, 40].

Owing to the abovementioned advantages of electrospun nanofibers, several research groups investigated and developed biosensors based on electrospun nanofibers as listed in Table 1. Though the performance of electrospun nanofiber-based biosensors is quite impressive, there are several limitations as low throughput and poor mechanical properties observed over time.

2.2 Microfluidic Techniques

The limitations of nanofiber-based biosensors as low throughput and poor mechanical properties could be addressed by the integration of these nanofibers with microfluidic systems. Within the microfluidic systems, electrospun nanofibers could be

Table 1 Electrospun fiber-based biosensors for identification of a specific biomarker

Electrospun nanofiber materials	Sensing biomarker	Sensitivity	References
Coaxial fibers – Polycaprolactone shell with tris (4,7-diphenyl-1,10-phenanthroline) ruthenium (II) and platinum octaethyl porphyrin dissolved in polydimethylsiloxane core	Real-time oxygen sensors	< 0.5 s response	[20]
Anti-epidermal growth factor receptor-conjugated mesoporous zinc oxide nanofibers	Breast cancer biomarkers – ErbB2; EGFR2	7.76 kΩ/μM; 1 fM (4.34×10^{-5} ng/mL); response within 128 sec for 1.0 fM–0.5 μM test range	[11]
Anti-ErbB2 immobilized porous hierarchical graphene foam modified with electrospun carbon-doped titanium dioxide nanofibers	Breast cancer biomarker – ErbB2	0.585 μA/μM/cm^2 and 43.7 kΩ/μM/cm^2 as quantified by differential pulse voltammetry and electrochemical impedance spectroscopy, respectively	[41]
Carbon nanotubes embedded in zinc oxide nanowires	Carcinoma antigen-125	Sensitivity -(90.14 μA/(U/mL)/cm^2) with a detection limit of 0.00113UmL^{-1} concentration as quantified by differential voltammetry technique	[16]
Poly(3,4-ethylene dioxythiophene): Poly(4-styrene sulfonate)/polyvinyl alcohol nanofiber decorated conducting paper	Carcinoembryonic antigen	Linear detection range, 0.2–25 ng/ml; Sensitivity, 14.2 μA.Ml/ng.cm^2	[42]
FITC-labeled MMP-9-specific peptides were covalently immobilized on a polystyrene/poly(styrene-alt-maleic anhydride) electrospun nanofibrous mat	Matrix metalloproteinase (MMP)-9	Faster response time (30 min) and lower detection limit (10 pM)	[43]
Polyvinyl alcohol/polyacrylic acid nanofibers	pH changes	74 mV/pH	[44]

used as a substrate to increase the available surface for immobilization and thereby increase their sensitivity [45]. On the foundation of the integration of electrospun fibers with microfluidics, second-generation Nano Velcro CTC chips were developed to capture CTCs with high efficiency and enable highly specific isolation of single CTCs immobilized on the nanosubstrates without contamination. The second-generation Nano Velcro CTC chips comprise transparent PLGA-nanofiber-embedded substrate that was prepared by electrospinning PLGA nanofibers onto a commercial laser microdissection slide. These Nano Velcro chips are useful in capturing CTCs from several types of solid tumors like melanoma, breast, lung,

prostate, and pancreatic cancers [46–48]. Since microfluidics in conjunction with electrospun fibers showed high accuracy and sensitivity in detecting cancer biomarkers at low concentrations, the focus of interest lately is the quantification of these detected cancer biomarkers for assessment of cancer prognosis [11, 41].

3 Role of Electrospun Fibers in the Construction of 3D In Vitro Tumor Models

It is quite challenging to mimic the 3D microenvironment of tumor cells to explore the complexity of the in vivo system. Traditional in vitro tumor models have long suffered from oversimplification, predominantly by the use of a nonphysiological substrate with conditions that do not match the disease. It is quite evident that a monolayer of cancer cells on polystyrene culture plates does not replicate the in vivo environment of the whole tumor. Substituting animal models with traditional in vitro tumor models also presents their limitations, either stemming from the disparity in the underlying biology of the animal subject or the lack of control over certain desired experimental conditions [49]. Thus, it is really important to construct the closest 3D in vitro system to the native extracellular matrix and tumor microenvironment.

A variety of 3D scaffolds as nanoparticles, hydrogel-based 3D scaffolds, microspheres, and electrospun fibers have been investigated for in vitro tumor model applications. Most of the investigated in vitro 3D tumor model systems have undesirable functionalities and unfavorable micro−/macrostructures [50, 51]. Within these in vitro systems, electrospun nanofibrous systems containing nanometer to a sub-micrometer range of nanofiber diameters are deemed to promote greater cell-cell and cell-matrix interactions as they resemble the collagen fibrils present within the microenvironment of a cancerous tumor [52]. Further surface modification of these micro−/nanoscale electrospun fibers with peptides or extracellular matrix proteins offers a closer resemblance to the tumor extracellular matrix. The feasibility of encapsulating a wide range and combination of anticancer drugs, modification of surfaces with desired functionalities, tunable fiber alignment, and ability to electrospun 3D fibrous scaffolds aids in the fabrication of rationale 3D in vitro cancer models that could better simulate the in vivo tumor microenvironment [53, 54].

4 Role of Electrospun Fibers in Cancer Therapeutics

The chemotherapeutic agents administered for cancer treatment are cytotoxic and often require high systemic dose administration to maintain the required local concentration during the treatment period. The need for higher dosages increases the risk of adverse side effects and toxicity to nontumorigenic healthy cells. Additionally, owing to the limited extravasation of drugs from the bloodstream, it is difficult for

drugs that are administered systemically to reach the desired target tissue. Thus, to prevent such adverse effects, and to reduce the risk of cytotoxicity, local delivery of chemotherapeutic agents to the location of cancerous tumor is desirable [6].

The local administration or implantation of chemotherapeutic agent-loaded fibrous meshes can be achieved by the following methods. One technique is the implantation of chemotherapeutic agent-loaded fibrous mats within the tumor bed after localization of tumor using magnetic resonance imaging. Another technique is the implantation of chemotherapeutic agent-loaded electrospun fibrous mats into the postoperative tumor cavity immediately following resection of tumors, to eradicate residual cancerous cells and prevent cancer recurrence. The final technique is the intra-tumoral injection of drug-loaded fragmented nanofibers (obtained by cryogenic sectioning or fragmentation of aligned electrospun fibers) [17].

Various electrospinning techniques such as blend electrospinning, coaxial electrospinning, triaxial electrospinning, etc. were investigated for the incorporation of chemotherapeutic agents within nanofibrous meshes. In the blend electrospinning process, bioactive reagents are blended with aqueous polymer solutions prior to the electrospinning process, resulting in the concentration of these bioactive molecules on or near the surface of the nanofibers. This results in a reduction of bioactivity as well as a burst release profile of the blended bioactive agents. Further investigations on sustained drug release mechanisms using blend electrospinning process reported that the reduction in burst release of encapsulated drugs could be achieved by mixing hydrophilic and hydrophobic biopolymers in various ratios [55].

Apart from blend electrospinning, coaxial fibers prepared via coaxial electrospinning enable more sustained drug release profiles and reduce the burst release of encapsulated drugs. By utilizing the coaxial electrospinning process, two or more materials can be electrospun simultaneously. In the coaxial electrospinning process, various polymer solutions were introduced into their respective individual tubes to fabricate core-shell-structured fibers via a coaxial spinneret. The presence of the shell layer surrounding the core layer in core-shell fibers will limit the burst release and facilitate the sustained release of encapsulated biomolecules from the core layer. Additionally, multiple drugs can be encapsulated concurrently into core-shell nanofibers with one drug in the core region, and the other in the shell region. Another advantage of the core-shell nanofibrous scaffold is that it can temporarily protect a certain unstable bioactive agent from a destructive microenvironment of a tumor [56].

Usually, sustained release of bioactive agents/drugs loaded in the core region of coaxial nanofibers occurs only when the outer shell material is hydrophobic. If the shell material is hydrophilic, there will be a relatively rapid release of encapsulated bioactive agents, resembling the burst release profile. This has limited the in vivo application potential of coaxial nanofiber-mediated drug delivery systems as the majority of natural degradable polymeric biomaterials including collagen, gelatin, albumin, peptides, etc. that are preferred for the shell layer are hydrophilic [57]. Though synthetic polymers such as PCL and PLGA were used lately as shell materials, natural biopolymers are preferred and more biocompatible than synthetic polymers. Furthermore, the acidic microenvironment created in vivo by the degradation products of synthetic polymers is reported to decrease the bioactivity of

released bioactive agents that are encapsulated within the core region. To resolve this issue, triaxial structured electrospun nanofibrous mats were introduced for the controlled dual release of biomolecules. In triaxial structured coaxial fibers, the core area comprises one chemotherapeutic drug, the middle layer is made of a hydrophobic biodegradable polymer such as PCL, PLGA, etc., and the outer shell layer consists of a hydrophilic polymer loaded with a second bioactive agent. Owing to the presence of a hydrophobic buffer region in the middle region of a triaxial structure, around 24-fold slower drug release profile was reported in comparison with the coaxial fibers. Furthermore, an initial desired burst release of about 80% could be achieved by loading the desired bioactive agent in the outer hydrophilic region. Thus, the desired drug release profiles could be tailored to meet the specific requirements by the use of triaxial structured nanofibers [58].

Furthermore, incorporating nanospheres/micelles into the core-sheath-structured electrospun nanofibrous mats will improve the micelle stability and can promote an extended release in comparison with micellar formulations [59–61]. Yang et al. developed and reported an implantable localized drug delivery device for cancer. This device is prepared using coaxial electrospinning technique using cross-linked gelatin fibers to encapsulate drug-loaded micelles (mixture of PVA- and DOX-loaded active-targeting micelles assembled from a folate-conjugated PCL/PEG copolymer). The degradation of the gelatin nanofibrous matrix enables the sustained release of the micelles into implanted tumors, and the released micelles will concentrate around the cancer cells and will enter the cells through folate receptor-mediated endocytosis mechanism [59, 60].

Lately, multilayered electrospun nanofiber-based drug delivery devices were developed to meet the clinical application demands. These 3D nanofiber-based drug delivery devices facilitate good control over the sustained release of encapsulated agents. Within these multilayered structures, the nanofibrous layer that does not contain any biomolecules or hydrophilic components will serve as a barrier to impede water diffusion, and subsequently delay the release of drugs from the other drug-loaded nanofibrous layers [6, 24, 62].

Several research groups developed and investigated the chemotherapeutic agents within nanofibrous devices for controlled and sustained release at implanted locations, and they are tabulated in Table 2. However, all these local devices were either at developmental, in vitro/in vivo research stages, or preclinical trials and are not yet available for use in clinical practice.

5 Role of Nanofibers in Theranostic Applications

Cancer theranostics is a novel concept of blending the diagnostic and therapeutic features within a single device or a system. Magnetic nanoparticles are a vital part of these systems due to their ability to respond to an external magnetic field. These magnetic nanoparticles will generate heat on application/exposure to an alternating magnetic field, and thus enhance image contrast in magnetic resonance imaging.

Table 2 Chemotherapeutic agent-loaded electrospun nanofibrous local drug delivery devices developed and investigated by several research groups for cancer treatment

Anticancer drug	Electrospun fibers	Type of cancer cells	References
Paclitaxel	PLGA; chitosan/PEO	C6 glioma cell line; prostate cancer	[18]
Ibuprofen outside mesoporous silica nanoparticles (MSN) and doxorubicin and sodium bicarbonate-loaded MSNs	PLLA	Human hepatocellular carcinoma HuH-7 cell line	[63]
1,3-Bis(2-chloroethyl)-1-nitrosourea	PEG-PLLA	Glioma C6 cells	[64]
Doxorubicin and doxorubicin-loaded mesoporous silica nanoparticles	PLLA	Triple-negative human breast cancer cell line (MDA-MB-231)	[65]
Daunorubicin	Poly(N-isopropyl acrylamide)-co-polystyrene	Leukemia	[66]
Daunorubicin and Fe_3O_4 nanoparticles	PLA	Leukemia cancer cells	[67]
Paclitaxel and doxorubicin	PEG-PLA	Glioma C6 cells	[19]
Titanocene dichloride	PLLA	Human lung tumor SPCA-1 cells	[12]
CPT11, SN-38	PCL/PGC-C18	Human colorectal cell line (HT-29)	[68]
5-Aminolevulinic acid	PVA	HuCC-T1 cholangiocarcinoma cells	[21]
Hydroxycamptothecin	PEG-PDLA	HepG-2 hepatoma cells	[14]
Fe_3O_4 nanoparticles	Chitosan	Colon adenocarcinoma	[69]
MMP-2 RNAi plasmid and paclitaxel	Polyethylenimine/DNA nanoparticles/PLGA	Brain tumor	[70]
Doxorubicin and camptothecin	PLGA/gelatin/ZnO nanospheres	HepG-2 liver cancer cells	[62]
Hydroxycamptothecin loaded into hydroxyapatite nanoparticles and doxorubicin loaded into mesoporous silica nanoparticles (DOX@MSNs)	PLGA	HeLa human cervical cancer cells	[71]
Cyclophosphamide and oxaliplatin	PLA	Human hepatocellular carcinoma (HCC) cells	[72]
Sodium dichloroacetate and diisopropylamine dichloroacetate	PLA	C26 colon carcinoma cells	[73]
Combretastatin A-4 and hydroxycamptothecin	PEG-PLA	Breast cancer	[15]
5-fluorouracil and oxaliplatin	PLA	HCT-8 human colorectal cancer cells and C26 colon carcinoma cells	[74]

(continued)

Table 2 (continued)

Anticancer drug	Electrospun fibers	Type of cancer cells	References
Cisplatin	PEO/PLA; PCL/PGC-C18	Murine cervical cancer U14 cells; Lewis lung carcinoma murine cell line	[75] [13]
Pt(IV) prodrug-backboned micelle and dichloroacetate	PVA	HeLa human cervical cancer cells	[76]
Temozolomide	PLGA/PLA/PCL	Recurrent glioblastoma	[17]

Abbreviations: *MMP-2* matrix metalloproteinase-2, *PCL* poly(ε-caprolactone), *PEO* poly(ethylene oxide), *PEG* poly(ethylene glycol), *PGC-C18* poly(glycerol monostearate-co-ε-caprolactone), *PLA* poly(lactic acid), *PLLA* poly(L-lactic acid), *PLGA* poly(lactic-co-glycolic acid), *PVA* poly(vinyl alcohol)

The direct administration of these magnetic nanoparticles into the tumor or by intravenous administration can lead to undesired side effects due to leakage to adjacent healthy tissues. However, retaining these particles in a polymeric nanofibrous mesh prevents the leakage or loss of these particles. Also, implanting these magnetic nanoparticle-loaded nanofibers in the tumor site ensures high magnetic nanoparticle loading, and enhances magnetic response. In addition, loading these magnetic nanoparticle-loaded polymeric nanofibers with chemotherapeutic agents via emulsion or coaxial electrospinning enables sustained drug release in the tumor site. Therefore, a magnetic polymeric drug-loaded nanofiber produced by electrospinning is an ideal nanosystem for cancer theranostic application [77, 78].

6 Conclusion

Despite rapid progress in cancer research, many electrospun fiber-based devices are still in preclinical research. Cancer research is an ongoing advancing field and will require much more testing before its clinical use in full potential. However, with increasing global incidence and prevalence rates of cancer, there is an urgent need for developing a viable strategy to rapidly translate the utilization of electrospun nanofiber-based devices from lab research to clinical trials for declining the cancer incidence and prevalence rates.

Despite the favorable progress on the production of electrospun nanofibrous 3D scaffolds, engineering 3D in vitro cancer models is still a challenge to simulate the exact physiology and microenvironment of solid tumors owing to the variation in their genotypic and phenotypic characteristics. In the future, an amalgamation of electrospinning with a 3D bioprinting technique might provide a valuable tool to engineer and develop an elaborated 3D in vitro cancer model for the complete and accurate understanding of cancer initiation mechanisms, biomarkers, and drug delivery systems.

References

1. Danaei G, Ding EL, Mozaffarian D, Taylor B, Rehm J, Murray CJ, et al. The preventable causes of death in the United States: comparative risk assessment of dietary, lifestyle, and metabolic risk factors. PLoS Med. 2009;6(4):e1000058.
2. Anand P, Kunnumakkara AB, Sundaram C, Harikumar KB, Tharakan ST, Lai OS, et al. Cancer is a preventable disease that requires major lifestyle changes. Pharm Res. 2008;25(9):2097–116.
3. Islami F, Goding Sauer A, Miller KD, Siegel RL, Fedewa SA, Jacobs EJ, et al. Proportion and number of cancer cases and deaths attributable to potentially modifiable risk factors in the United States. CA Cancer J Clin. 2018;68(1):31–54.
4. Loomans-Kropp HA, Umar A. Cancer prevention and screening: the next step in the era of precision medicine. NPJ Precis Oncol. 2019;3:3.
5. Sung H, Ferlay J, Siegel RL, Laversanne M, Soerjomataram I, Jemal A, et al. Global cancer statistics 2020: GLOBOCAN estimates of incidence and mortality worldwide for 36 cancers in 185 countries. CA Cancer J Clin. 2021;71(3):209–49.
6. Cheng Z, Li M, Dey R, Chen Y. Nanomaterials for cancer therapy: current progress and perspectives. J Hematol Oncol. 2021;14(1):85.
7. Liu Z, Ramakrishna S, Liu X. Electrospinning and emerging healthcare and medicine possibilities. APL Bioeng. 2020;4(3):030901.
8. Duan Y, Kalluri L, Satpathy M. Effect of electrospinning parameters on the fiber diameter and morphology of PLGA nanofibers. Dental Oral Biol Craniof Res. 2021:1–7.
9. Wang J, Jansen JA, Yang F. Electrospraying: possibilities and challenges of engineering carriers for biomedical applications—a mini review. Front Chem. 2019;7
10. Lim L-T, Mendes AC, Chronakis IS. Chapter five – electrospinning and electrospraying technologies for food applications. In: Lim L-T, Rogers M, editors. Advances in food and nutrition research, vol. 88. Academic; 2019. p. 167–234.
11. Ali MA, Mondal K, Singh C, Malhotra BD, Sharma A. Anti-epidermal growth factor receptor conjugated mesoporous zinc oxide nanofibers for breast cancer diagnostics. Nanoscale. 2015;7(16):7234–45.
12. Chen P, Wu QS, Ding YP, Chu M, Huang ZM, Hu W. A controlled release system of titanocene dichloride by electrospun fiber and its antitumor activity in vitro. Eur J Pharm Biopharm. 2010;76(3):413–20.
13. Kaplan JA, Liu R, Freedman JD, Padera R, Schwartz J, Colson YL, et al. Prevention of lung cancer recurrence using cisplatin-loaded superhydrophobic nanofiber meshes. Biomaterials. 2016;76:273–81.
14. Luo X, Xie C, Wang H, Liu C, Yan S, Li X. Antitumor activities of emulsion electrospun fibers with core loading of hydroxycamptothecin via intratumoral implantation. Int J Pharm. 2012;425(1–2):19–28.
15. Luo X, Zhang H, Chen M, Wei J, Zhang Y, Li X. Antimetastasis and antitumor efficacy promoted by sequential release of vascular disrupting and chemotherapeutic agents from electrospun fibers. Int J Pharm. 2014;475(1–2):438–49.
16. Paul KB, Singh V, Vanjari SRK, Singh SG. One step biofunctionalized electrospun multiwalled carbon nanotubes embedded zinc oxide nanowire interface for highly sensitive detection of carcinoma antigen-125. Biosens Bioelectron. 2017;88:144–52.
17. Ramachandran R, Junnuthula VR, Gowd GS, Ashokan A, Thomas J, Peethambaran R, et al. Theranostic 3-dimensional nano brain-implant for prolonged and localized treatment of recurrent glioma. Sci Rep. 2017;7:43271.
18. Xie J, Wang CH. Electrospun micro- and nanofibers for sustained delivery of paclitaxel to treat C6 glioma in vitro. Pharm Res. 2006;23(8):1817–26.
19. Xu X, Chen X, Wang Z, Jing X. Ultrafine PEG-PLA fibers loaded with both paclitaxel and doxorubicin hydrochloride and their in vitro cytotoxicity. Eur J Pharm Biopharm. 2009;72(1):18–25.

20. Xue R, Behera P, Xu J, Viapiano MS, Lannutti JJ. Polydimethylsiloxane core-polycaprolactone shell nanofibers as biocompatible, real-time oxygen sensors. Sens Actuators B Chem. 2014;192:697–707.
21. Yoo JJ, Kim C, Chung CW, Jeong YI, Kang DH. 5-aminolevulinic acid-incorporated poly(vinyl alcohol) nanofiber-coated metal stent for application in photodynamic therapy. Int J Nanomed. 2012;7:1997–2005.
22. Bohunicky B, Mousa SA. Biosensors: the new wave in cancer diagnosis. Nanotechnol Sci Appl. 2010;4:1–10.
23. Sobiepanek A, Kobiela T. Application of biosensors in cancer research. Rev Res Cancer Treat. 2018;4:4–12.
24. Cleeton C, Keirouz A, Chen X, Radacsi N. Electrospun nanofibers for drug delivery and biosensing. ACS Biomater Sci Eng. 2019;5(9):4183–205.
25. Xiong H, Yan J, Cai S, He Q, Peng D, Liu Z, et al. Cancer protein biomarker discovery based on nucleic acid aptamers. Int J Biol Macromol. 2019;132:190–202.
26. Kuchenbaecker KB, Hopper JL, Barnes DR, Phillips KA, Mooij TM, Roos-Blom MJ, et al. Risks of breast, ovarian, and contralateral breast cancer for BRCA1 and BRCA2 mutation carriers. JAMA. 2017;317(23):2402–16.
27. Bettegowda C, Sausen M, Leary RJ, Kinde I, Wang Y, Agrawal N, et al. Detection of circulating tumor DNA in early- and late-stage human malignancies. Sci Transl Med 2014; 6(224):224ra24.
28. Gray ES, Rizos H, Reid AL, Boyd SC, Pereira MR, Lo J, et al. Circulating tumor DNA to monitor treatment response and detect acquired resistance in patients with metastatic melanoma. Oncotarget. 2015;6(39):42008–18.
29. Pessoa LS, Heringer M, Ferrer VP. ctDNA as a cancer biomarker: A broad overview. Crit Rev Oncol Hematol. 2020;155:103109.
30. Cheng F, Su L, Qian C. Circulating tumor DNA: a promising biomarker in the liquid biopsy of cancer. Oncotarget. 2016;7(30):48832–41.
31. Plaks V, Koopman CD, Werb Z. Cancer. Circulating tumor cells. Science. 2013;341(6151):1186–8.
32. Muz B, de la Puente P, Azab F, Azab AK. The role of hypoxia in cancer progression, angiogenesis, metastasis, and resistance to therapy. Hypoxia (Auckl). 2015;3:83–92.
33. Deep G, Panigrahi GK. Hypoxia-induced signaling promotes prostate cancer progression: exosomes role as messenger of hypoxic response in tumor microenvironment. Crit Rev Oncog. 2015;20(5–6):419–34.
34. Feng J, Byrne NM, Al Jamal W, Coulter JA. Exploiting current understanding of hypoxia mediated tumour progression for nanotherapeutic development. Cancers (Basel) 2019; 11(12).
35. Bhalla N, Jolly P, Formisano N, Estrela P. Introduction to biosensors. Essays Biochem. 2016;60(1):1–8.
36. Wongkaew N. Nanofiber-integrated miniaturized systems: an intelligent platform for cancer diagnosis. Anal Bioanal Chem. 2019;411(19):4251–64.
37. Mane PP, Ambekar RS, Kandasubramanian B. Electrospun nanofiber-based cancer sensors: a review. Int J Pharm. 2020;583:119364.
38. Reddy VS, Tian Y, Zhang C, Ye Z, Roy K, Chinnappan A, et al. A review on electrospun nanofibers based advanced applications: from health care to energy devices. Polymers. 2021;13(21):3746.
39. Giannitelli SM, Costantini M, Basoli F, Trombetta M, Rainer A. Electrospinning and microfluidics: an integrated approach for tissue engineering and cancer. Electrofluidodyn Technol (EFDTs) Biomater Med Dev. 2018:139–55.
40. Matlock-Colangelo L, Baeumner AJ. Recent progress in the design of nanofiber-based biosensing devices. Lab Chip. 2012;12(15):2612–20.
41. Ali MA, Mondal K, Jiao Y, Oren S, Xu Z, Sharma A, et al. Microfluidic immuno-biochip for detection of breast cancer biomarkers using hierarchical composite of porous graphene and titanium dioxide nanofibers. ACS Appl Mater Interf. 2016;8(32):20570–82.

42. Kumar S, Rai P, Sharma J, Sharma Iitk A, Malhotra B. PEDOT:PSS nanofibers decorated conducting paper for cancer diagnostics. Adv Mater Technol. 2016;1
43. Han SW, Koh WG. Hydrogel-framed nanofiber matrix integrated with a microfluidic device for fluorescence detection of matrix metalloproteinases-9. Anal Chem. 2016;88(12):6247–53.
44. Shaibani PM, Etayash H, Naicker S, Kaur K, Thundat T. Metabolic study of cancer cells using a pH-sensitive hydrogel nanofiber light addressable potentiometric sensor. ACS Sens. 2017;2(1):151–6.
45. Rezaei Z, Mahmoudifard M. Pivotal role of electrospun nanofibers in microfluidic diagnostic systems – a review. J Mater Chem B. 2019;7(30):4602–19.
46. Zhao L, Lu Y-T, Li F, Wu K, Hou S, Yu J, et al. High-purity prostate circulating tumor cell isolation by a polymer nanofiber-embedded microchip for whole exome sequencing. Adv Mater. 2013;25(21):2897–902.
47. Chen JF, Zhu Y, Lu YT, Hodara E, Hou S, Agopian VG, et al. Clinical applications of NanoVelcro rare-cell assays for detection and characterization of circulating tumor cells. Theranostics. 2016;6(9):1425–39.
48. Jiang R, Lu YT, Ho H, Li B, Chen JF, Lin M, et al. A comparison of isolated circulating tumor cells and tissue biopsies using whole-genome sequencing in prostate cancer. Oncotarget. 2015;6(42):44781–93.
49. Pape J, Emberton M, Cheema U. 3D cancer models: the need for a complex stroma, compartmentalization and stiffness. Front Bioeng Biotechnol. 2021;9
50. Szot CS, Buchanan CF, Freeman JW, Rylander MN. 3D in vitro bioengineered tumors based on collagen I hydrogels. Biomaterials. 2011;32(31):7905–12.
51. Zhang X, Wang W, Yu W, Xie Y, Zhang X, Zhang Y, et al. Development of an in vitro multicellular tumor spheroid model using microencapsulation and its application in anticancer drug screening and testing. Biotechnol Prog. 2005;21(4):1289–96.
52. Chen S, Liu B, Carlson MA, Gombart AF, Reilly DA, Xie J. Recent advances in electrospun nanofibers for wound healing. Nanomedicine (Lond). 2017;12(11):1335–52.
53. Zervantonakis IK, Hughes-Alford SK, Charest JL, Condeelis JS, Gertler FB, Kamm RD. Three-dimensional microfluidic model for tumor cell intravasation and endothelial barrier function. Proc Natl Acad Sci U S A. 2012;109(34):13515–20.
54. Hartman O, Zhang C, Adams EL, Farach-Carson MC, Petrelli NJ, Chase BD, et al. Biofunctionalization of electrospun PCL-based scaffolds with perlecan domain IV peptide to create a 3-D pharmacokinetic cancer model. Biomaterials. 2010;31(21):5700–18.
55. Zamani M, Prabhakaran MP, Ramakrishna S. Advances in drug delivery via electrospun and electrosprayed nanomaterials. Int J Nanomed. 2013;8:2997–3017.
56. Minden-Birkenmaier BA, Selders GS, Fetz AE, Gehrmann CJ, Bowlin GL. Electrospun systems for drug delivery (Chapter 7). In: Uyar T, Kny E, editors. Electrospun materials for tissue engineering and biomedical applications. Woodhead Publishing; 2017. p. 117–45.
57. Altan A, Aytac Z, Uyar T. Carvacrol loaded electrospun fibrous films from zein and poly(lactic acid) for active food packaging. Food Hydrocoll. 2018;
58. Han D, Steckl A. Triaxial electrospun nanofiber membranes for controlled dual release of functional molecules. ACS Appl Mater Interfaces. 2013;5
59. Yang G, Wang J, Li L, Ding S, Zhou S. Electrospun micelles/drug-loaded nanofibers for time-programmed multi-agent release. Macromol Biosci. 2014;14(7):965–76.
60. Yang G, Wang J, Wang Y, Li L, Guo X, Zhou S. An implantable active-targeting micelle-in-nanofiber device for efficient and safe cancer therapy. ACS Nano. 2015;9(2):1161–74.
61. Mehnath S, Chitra K, Karthikeyan K, Jeyaraj M. Localized delivery of active targeting micelles from nanofibers patch for effective breast cancer therapy. Int J Pharm. 2020;584:119412.
62. Wei J, Hu J, Li M, Chen Y, Chen Y. Multiple drug-loaded electrospun PLGA/gelatin composite nanofibers encapsulated with mesoporous ZnO nanospheres for potential postsurgical cancer treatment. RSC Adv. 2014;4(53):28011–9.

63. Yuan Z, Zhao X, Zhao J, Pan G, Qiu W, Wang X, et al. Synergistic mediation of tumor signaling pathways in hepatocellular carcinoma therapy via dual-drug-loaded pH-responsive electrospun fibrous scaffolds. J Mater Chem B. 2015;3(17):3436–46.
64. Xu X, Chen X, Xu X, Lu T, Wang X, Yang L, et al. BCNU-loaded PEG-PLLA ultrafine fibers and their in vitro antitumor activity against Glioma C6 cells. J Control Release. 2006;114(3):307–16.
65. Yuan Z, Pan Y, Cheng R, Sheng L, Wu W, Pan G, et al. Doxorubicin-loaded mesoporous silica nanoparticle composite nanofibers for long-term adjustments of tumor apoptosis. Nanotechnology. 2016;27(24):245101.
66. Song M, Guo D, Pan C, Jiang H, Chen C, Zhang R, et al. The application of poly (N-isopropylacrylamide)-co-polystyrene nanofibers as an additive agent to facilitate the cellular uptake of an anticancer drug. Nanotechnology. 2008;19(16):165102.
67. Lv G, He F, Wang X, Gao F, Zhang G, Wang T, et al. Novel nanocomposite of nano fe(3)o(4) and polylactide nanofibers for application in drug uptake and induction of cell death of leukemia cancer cells. Langmuir. 2008;24(5):2151–6.
68. Yohe ST, Herrera VL, Colson YL, Grinstaff MW. 3D superhydrophobic electrospun meshes as reinforcement materials for sustained local drug delivery against colorectal cancer cells. J Contr Rel. 2012;162(1):92–101.
69. Lin TC, Lin FH, Lin JC. In vitro feasibility study of the use of a magnetic electrospun chitosan nanofiber composite for hyperthermia treatment of tumor cells. Acta Biomater. 2012;8(7):2704–11.
70. Lei C, Cui Y, Zheng L, Chow PK, Wang CH. Development of a gene/drug dual delivery system for brain tumor therapy: potent inhibition via RNA interference and synergistic effects. Biomaterials. 2013;34(30):7483–94.
71. Chen M, Feng W, Lin S, He C, Gao Y, Wang H. Antitumor efficacy of a PLGA composite nanofiber embedded with doxorubicin@MSNs and hydroxycamptothecin@HANPs. RSC Adv. 2014;4(95):53344–51.
72. Liu S, Wang X, Zhang Z, Zhang Y, Zhou G, Huang Y, et al. Use of asymmetric multilayer polylactide nanofiber mats in controlled release of drugs and prevention of liver cancer recurrence after surgery in mice. Nanomedicine. 2015;11(5):1047–56.
73. Liu D, Wang F, Yue J, Jing X, Huang Y. Metabolism targeting therapy of dichloroacetate-loaded electrospun mats on colorectal cancer. Drug Deliv. 2015;22(1):136–43.
74. Zhang J, Wang X, Liu T, Liu S, Jing X. Antitumor activity of electrospun polylactide nanofibers loaded with 5-fluorouracil and oxaliplatin against colorectal cancer. Drug Deliv. 2016;23(3):794–800.
75. Zong S, Wang X, Yang Y, Wu W, Li H, Ma Y, et al. The use of cisplatin-loaded mucoadhesive nanofibers for local chemotherapy of cervical cancers in mice. Eur J Pharm Biopharm. 2015;93:127–35.
76. Zhang Z, Wu Y, Kuang G, Liu S, Zhou D, Chen X, et al. Pt(iv) prodrug-backboned micelle and DCA loaded nanofibers for enhanced local cancer treatment. J Mater Chem B. 2017;5(11):2115–25.
77. Liu M, Liu H, Sun S, Li X, Zhou Y, Hou Z, et al. Multifunctional hydroxyapatite/Na(Y/Gd) F4:Yb3+,Er3+ composite fibers for drug delivery and dual modal imaging. Langmuir 2014; 30(4): 1176–1182.
78. Huang P, Li Z, Lin J, Yang D, Gao G, Xu C, et al. Photosensitizer-conjugated magnetic nanoparticles for in vivo simultaneous magnetofluorescent imaging and targeting therapy. Biomaterials. 2011;32(13):3447–58.

Biocompatibility and Toxicity Perspective for the Development of Nanomaterials for Cancer Detection and Treatment

Hatice Gamze Sogukomerogullari and Tugba Taskin-Tok

1 Introduction

When common critical diseases are evaluated throughout the world, cancer is at the beginning of these diseases. Cancer is a type of disease that reduces the quality of life of patients, requires painful and long treatment, uses many drugs and side effects of these drugs, and sometimes even causes death [1]. Early diagnosis and correct treatment are very important in cancer cases [2]. Since it is such a common type of disease, new studies on this subject are brought to the literature every day. Moreover, the diagnosis and treatment of cancer, as well as the biocompatibility and toxicity of the compounds used in the treatment, are included in these studies.

Chemotherapy is the most widely used method in the treatment of cancer cases [3]. However, as it is known, some anticancer drugs used in chemotherapy can not only destroy cancer cells but also damage normal cells [4]. Patients also experience various adverse side effects such as poor specificity and limited accumulation of such drugs, myelosuppression (depression of the immune system), organ damage, alopecia (hair loss), and gastrointestinal distress. For this reason, there are many studies that are predicted to be used in the treatment of cancer diseases every day. Many different areas stand out among these studies. There are many organic-based,

H. G. Sogukomerogullari
Medical Services and Techniques Department, Health Services Vocational School, Gaziantep University, Gaziantep, Turkey

T. Taskin-Tok (✉)
Faculty of Arts and Sciences, Department of Chemistry, Gaziantep University, Gaziantep, Turkey

Department of Bioinformatics and Computational Biology, Institute of Health Sciences, Gaziantep University, Gaziantep, Turkey
e-mail: ttaskin@gantep.edu.tr

R. S. Chaughule et al. (eds.), *Nanomaterials for Cancer Detection Using Imaging Techniques and Their Clinical Applications*,
https://doi.org/10.1007/978-3-031-09636-5_10

inorganic-based, DNA-based, RNA-based, polymer-based nanomaterials and anticancer studies in the literature.

In this study, the biocompatibility and toxicity of anticancer studies involving organic- and inorganic-based nanomaterials will be determined, and the effects of organic- and inorganic-based nanomaterial-containing structures on anticancer studies will be revealed.

1.1 Nanotechnology

Nanotechnology is a phrase that has been around for a long time. Although nanotechnology has existed from the beginning of time, the discovery of nanotechnology is commonly credited to Dr. Richard Phillips Feynman, an American physicist and Nobel Laureate [5]. Taniguchi is credited as being the first to adopt the term "nanotechnology" in 1974. In his book *Engines of Creation*, Eric Drexler popularized the term "nanotechnology" in 1986 [6].

The most generally cited definition of nanotechnology comes from the US government's National Nanotechnology Initiative (NNI). Nanotechnology is defined as "research and technology development at the atomic, molecular, and macromolecular levels in the length scale of approximately 1–100 nanometer range, to provide a fundamental understanding of phenomena and materials at the nanoscale, and to create and use structures, devices, and systems that have novel properties and functions because of their small and/or intermediate size," according to the National Nanotechnology Initiative [6].

The development of useful materials and structures in the nanoscale range of 0.1–100 nanometers by different physical or chemical processes is known as nanotechnology or molecular engineering [7]. The word "nano" comes from the Greek word *nanos*, which means "dwarf." A nanometer is one billionth of a meter (10^{-9}) [5]. To put it another way, it's atomic and molecular engineering. It's an interdisciplinary field that encompasses chemistry, colloidal science, biology, and applied physics among others.

The methods of obtaining nanoscale materials can be evaluated in two ways. These are top-down, and bottom-up approaches as given in Scheme 1.

There are many nanoscale studies in the literature. The usage areas of nanomaterials are increasing daily. Especially in medicine and medicinal chemistry branches, interest in this field has intensified as the remarkable effects of nanoscale materials have been observed. Nanoscale anticancer studies can be classified as organic-based, inorganic-based, DNA-based, RNA-based, polymer-based nanomaterials as shown in Scheme 2.

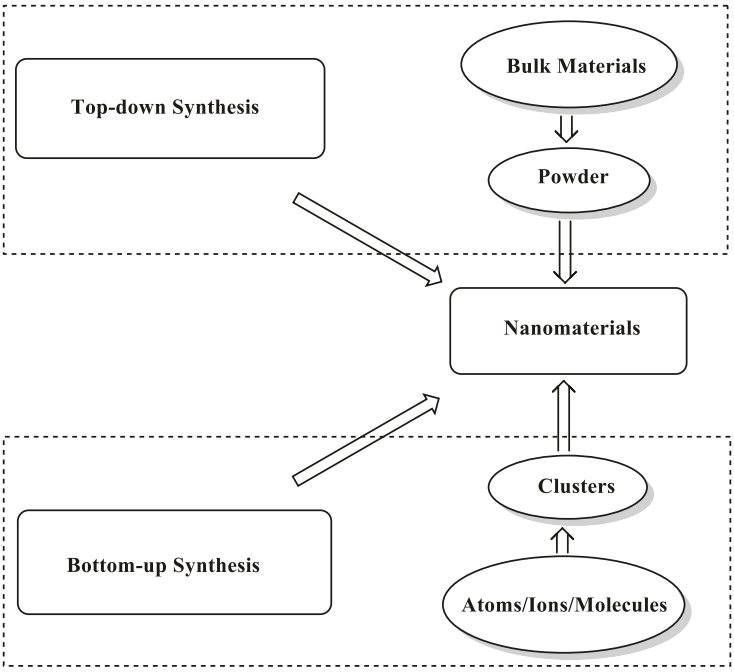

Scheme 1 Top-down and bottom-up approaches for nanomaterials' synthesis

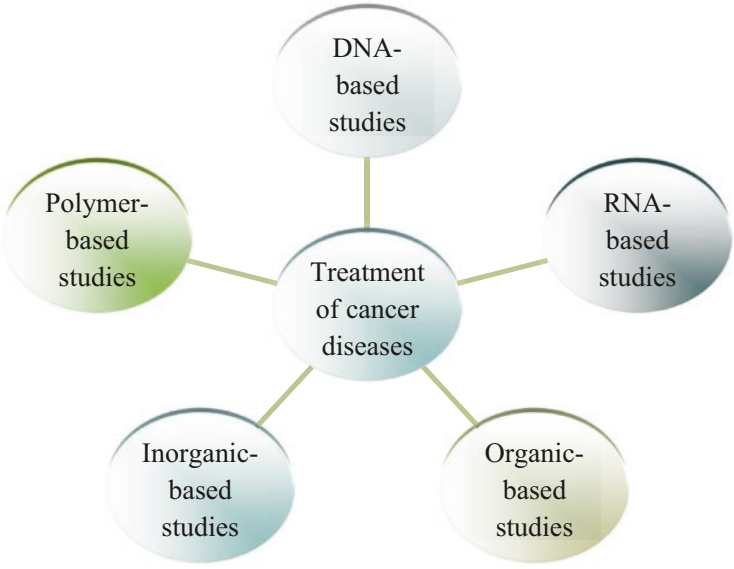

Scheme 2 Different-based studies for the treatment of cancer diseases

1.2 Nanomaterials in Treatment of Cancer Diseases

1.2.1 Organic-Based Nanomaterial Studies

Organic nanomaterials are used in anticancer applications [8]. Because of its intriguing pharmacological features and therapeutic potential, the stream of heterocycles has sparked a lot of curiosity. Its relevance as a building block for critical intermediates in the synthesis of numerous natural products with a wide spectrum of pharmacological and biological actions, such as anticancer medicines and antitumor chemicals, has increased [9].

1.2.2 Inorganic-Based Nanomaterial Studies

Several commonly used inorganic nanomaterials have been employed as nanomedicine to deliver medicinal and/or in vivo imaging ingredients selectively for cancer therapy and diagnostic purposes [10, 11]. Carbon nanostructures (e.g., graphene, nanotubes, nanodiamonds), metallic NPs (e.g., titanium, silver, iron, gold), and inorganic NPs such as mesoporous silica NPs are all examples of inorganic nanomaterials [10–12]. In cellular models of breast cancer, studies have revealed that GO-doxorubicin has stronger anticancer activity [13].

1.2.3 DNA-Based Nanomaterial Studies

DNAzymes are single-stranded DNA molecules that catalyze a variety of processes, including RNA or DNA cleavage and ligation [14–16]. DNAzymes have been widely exploited as effective signal transducers for enhanced biosensing due to their unique cofactor-dependent and sequence-specific catalytic properties [17–20] and even as potent gene silencing therapeutic agents [21–23]. The medicinal RNA-hydrolytic DNAzyme has recently been identified as a potent anticancer medication capable of blocking several tumorigenic pathways by effective intracellular biocatalytic cleavage of oncogene substrates [24–29]. In comparison with ribozymes, siRNA, and antisense oligonucleotides, DNAzyme has a high biostability and does not hijack the endogenous RNA-induced silencing complex [28, 29].

DNA nanoparticles outperform other nanomaterials in terms of properties. DNA molecules serve as both construction materials (self-assembly) and medicinal agents (gene therapy), allowing for the integration of complex structures and functions. Because of its programmability, DNA is an excellent building block for nanostructures of diverse dimensions and shapes. The nanostructures created can be employed as carriers to deliver a range of medications efficiently [30]. Further, the addition of functional DNA sequences [31–33] (G-quadruplex, ribozyme, aptamer, i-motif sequence, and among others) endows DNA nanostructures with functions such as stimulus responsiveness, targeting, and life activity regulation, promoting DNA nanostructures' great potential in the cure of major diseases (Table 1) [34–37].

Table 1 List of nanomedicines for cancer therapy approved by the FDA [34–37]

Tradename	Material	Drug	Company	Indicatiın	Year(s) Approved
Doxi ®	Liposome-PEG	Doxorubicin	Janssen	MBC, metastatic ovarian cancer	1995
Eligard ®	PLGA	Leuprolide acetate	Tolmar	Prostate cancer	2002
Abraxane ®	Albumin	Paclitaxel	Celgene	Metastatic breast cancer	2005
Genexol PM ®	mPEG-PLA	Paclitaxel	Samyang corporation	Metastatic breast cancer	2007
Onivyde ®	Liposome	Irinotecan	Merrimack	Pancreatic cancer	2015

1.2.4 RNA-Based Nanomaterial Studies

RNA interference (RNAi) might be used to treat cancer [38, 39]. MicroRNA (miRNA) is a noncoding short RNA with a length of 20–24 base pairs that may efficaciously control gene expression in the intracellular area and is one of the critical constituents for the induction of RNAi [40]. Closely positioned mature miRNA interacts to supplementary target messenger RNA in the cytoplasm (mRNA). By limiting ribosome binding and mRNA translation, the condition may impede gene expression. Furthermore, the development of a microribonucleoprotein complex (miRISC) including abscisate beta-glucosyltransferase (AOG) and glycine-tryptophan proteins causes RNAi to degrade mRNA (thus downregulating the oncogene and suppressing cancer). Short interference RNA (siRNA) is a noncoding small RNA that can be used in RNA interference-mediated cancer treatment [41].

1.2.5 Polymer-Based Nanomaterial Studies

Polymersomes, hydrogels, nanofibers, micelles, NPs, nanogels, and dendrimers are examples of polymeric nanomaterials [8, 11, 42]. PVP has recently been effectively introduced as a substitute for the PEG moiety, combining the benefits of PVP with the micellar morphology [43–45]. PVP was coupled to hydrophobic polymer blocks such as poly(D, L-lactide) [43], poly(-caprolactone) [44], and poly(vinylacetate) [45] in these investigations, and the resultant NPs had minimal toxicity and improved the efficacy of numerous anticancer medicines.

1.3 Benefits of Nanomaterials in the Therapy of Cancer Diseases

With the use of nanotechnology in the diagnosis, therapy, and management of cancer, the fight against the disease has begun to be addressed in a much larger dimension. NPs, by active or passive targeting, increase the intracellular concentration of

medicines to cancerous tissue while showing as little toxicity as possible to healthful tissue. Prepared NPs can be designed to be sent to the target region. Drug release can be provided and regulated with temperature-sensitive or pH-sensitive nanoparticles. Prepared NPs can be designed to be sent to the target region. Drug release can be provided and regulated with temperature-sensitive or pH-sensitive nanoparticles. Such that, in the drug distribution of pH-sensitive nanoparticles, drugs can be administered in an acidic TME, or the drug is released in the target region by temperature-sensitive nanoparticles sent by the temperature given by sources such as ultrasound waves and magnetic fields. Moreover, by adjusting the physicochemical features of the NPs such as dimension, form, molecular mass, and surface chemistry, nanoparticles can be sent to the targeted region [46].

1.4 Current Research

In this section, examples from recent nanoscale anticancer studies in the literature will be given. Moreover, inferences will be made by making evaluations on the biocompatibility and toxicity of these studies.

In 2018, Dehkhodaei used a sonochemical approach to synthesize a novel Schiff base Pd (II) complex in bulk and nanoscales. In the study, Schiff base derived from isopropylamine and 2-hydroxybenzaldehyde and its Pd (II) complex (**N1**) were synthesized (Scheme 3). Afterward, it was stirred in an ultrasonic bath at 180 W for 30 min and then centrifuged at 5000 rpm for 15 min to obtain a nanoscale Pd (II) Schiff base complex. The MTT assay was then utilized to define the fraction of HeLa carcinoma cells that were viable. The findings confirmed that shrinking the size has a significant impact on cancer cell annihilation. In addition, nanoscale complexes attained IC_{50} at a concentration of 10 μM. Using a mix of experimental and computational approaches, the binding capacity of the nano- and bulk-scale Pd(II) Schiff base complex with calf thymus DNA and human serum albumin was examined. The predicted binding constants for the complex at both the bulk and nanoscales revealed that the nanoscale complex binds to DNA more strongly than the bulk-scale complex. This finding is consistent with the results of the MTT experiment. The ONIOM findings revealed that the compound's structural characteristics altered in tandem with its binding to DNA and HSA, demonstrating a strong interplay between the compound and the current biomolecules [47].

In 2017, Dehkhodaei obtained Schiff base from the reaction of 3-amino-prop-1-ene with 2-hydroxybenzaldehyde. Then, by immersing the ultrasonic probe in the reaction medium and giving high-intensity ultrasonic waves, the Schiff base ligand was metalized in nanosize with Ni $(OAc)_2$ (**N2**) (Scheme 4). The anticancer activity of the chemical is modified by its size, according to the MTT assay. The binding constants for the DNA complex and the HSA complex were calculated to be about $10^4\ M^{-1}$ [48].

In 2016, Abdel-Rahman synthesized and characterized the Schiff base ligand derived from 3-methoxysalicylaldehyde and 2-amino-3-hydroxypyridine and its

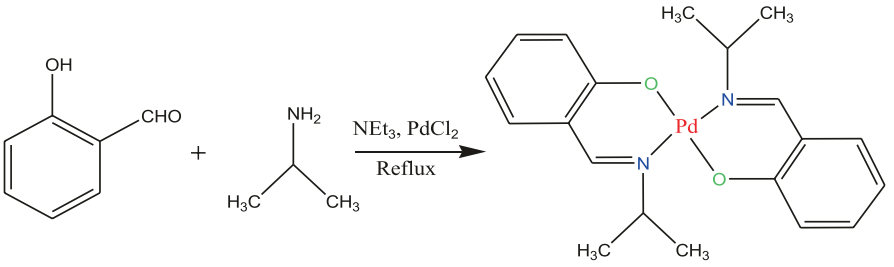

N1

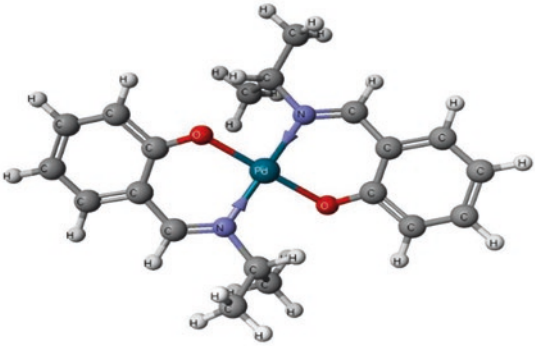

Scheme 3 Synthetic paths for preparation of PdL_2 and optimized structure of PdL_2 (**N1**) [47]

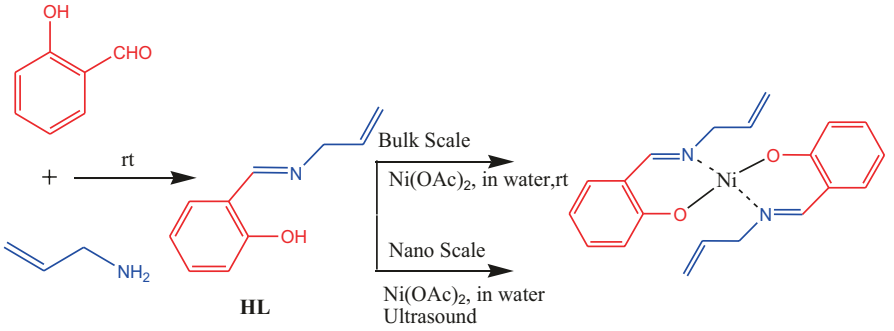

N2

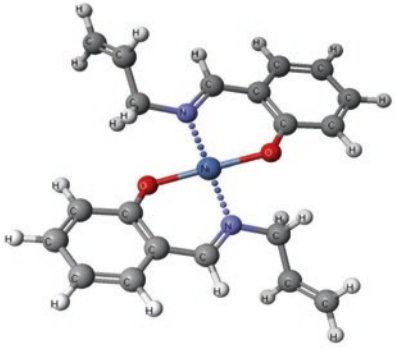

Scheme 4 Synthetic paths for the preparation of NiL_2 in its bulk and nanoscale forms and optimized structure of NiL_2 (**N2**) [48]

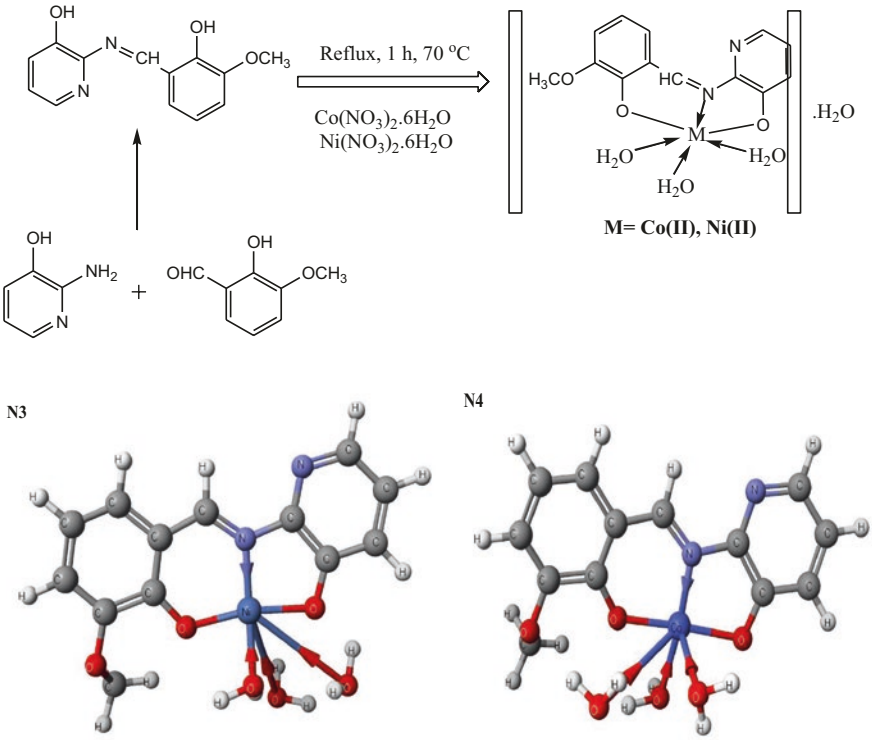

Scheme 5 Synthetic paths for the preparation of Ni(II) (**N3**), Co(II) (**N4**) complexes and optimized structure of Ni(II) and Co(II) complexes [49]

nanoscale Ni(II) (**N3**) and Co(II) (**N4**) complexes (Scheme 5). The nanoscale of the complexes was achieved by the sonochemistry method. Afterward, metal oxide nanoparticles were prepared by calcination of the related complex at 500 °C. When controlled with the clinically utilized vinblastine standard, the cytotoxicity of the Schiff base complexes on human breast carcinoma cells (MCF-7 cell line) and colon cancer cells (HCT-116 cell line) exhibited substantial cytotoxicity against carcinoma cell proliferation [49].

In 2022, Adwin Jose synthesized and characterized Schiff base ligand (DPMN) from the reaction of 2-amino-4,6-dimethoxypyrimidine and 2-hydroxy-5-nitrobenzaldehyde. Air stable copper nanoparticles (DPMN-CuNPs) (**N5**) were synthesized by the modified Brust-Schiffrin method using Schiff base and $CuCl_2$ (Scheme 6). In the study, antioxidant, antibacterial, and anticancer studies were conducted. When the anticancer results of the prepared DPMN-CuNPs were evaluated, it was stated that they had important anticancer activity toward distinct cancer cells and at the same time showed the least toxic effect against normal cells. Moreover, this material (DPMN-CuNPs) has been reported to have catalytic activity in nitrophenol reduction, methylene blue degradation, and methyl orange reduction [50].

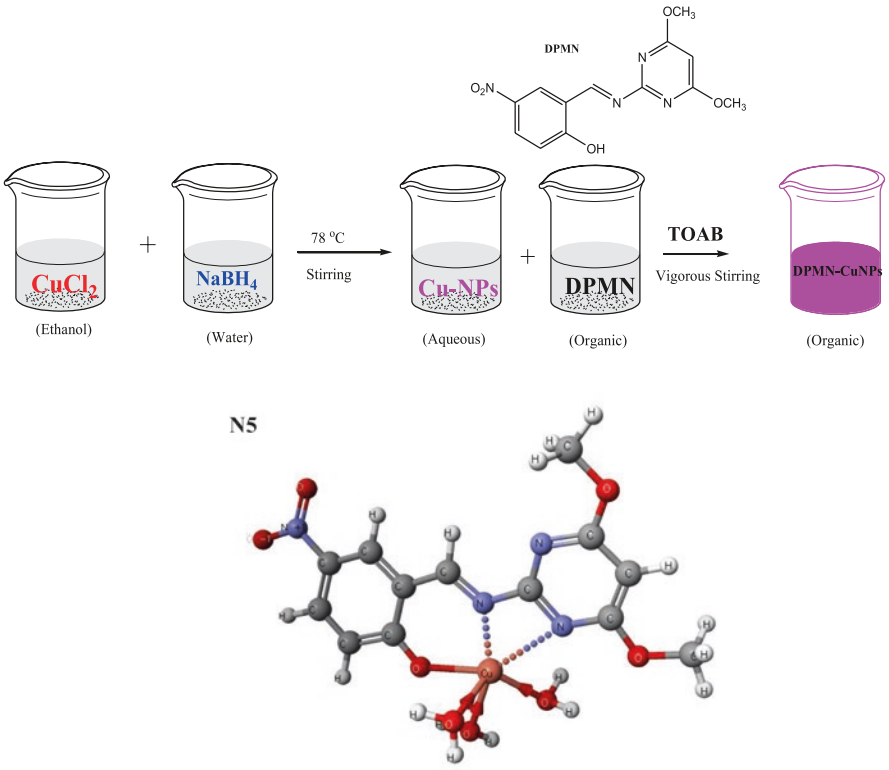

Scheme 6 Synthetic paths for the suggested structure of DPMN-CuNPs (**N5**) in its nanoscale forms and optimized structure of DPMN-CuNPs [50]

In 2016, Abdel-Rahman synthesized and characterized Schiff base ligand and its Cd(II) (**N6**), Fe(II) (**N7**), and Zn(II) (**N8**) complexes derived from 3-methoxysalicylaldehyde and 2-amino-3-hydroxypyridine (Scheme 7). The synthesized complexes prepared metal oxide nanoparticles by thermal decomposition. Antimicrobial and anticancer studies of the complexes have been carried out. Furthermore, when checked with the clinically utilized vinblastine standard, the cytotoxic activity of the produced Schiff base complexes on human hepatic cellular carcinoma cells (HepG-2) and colon cancer cells (HCT-116 cell line) demonstrated substantial cytotoxicity impact against carcinoma cell proliferation [51].

Yaghabi synthesized and characterized both bulk and nano forms of Zn(II) (**N9**), Cd(II) (**N10**), and Hg(II) (**N11**) complexes derived from 2,4,6-tri(2-pyridyl)-1,3,5-triazine (tptz) in 2019 (Fig. 1). The MTT technique was used to assess the cytotoxic activity of the complexes in bulk and nano forms against the MCF-7 cell line in vitro. The IC_{50} values vary from 2.2 ± 0.1 to 28.6 ± 0.6 μM. These findings showed that the produced complexes might be used as anticancer drugs in both nano and bulk forms [52].

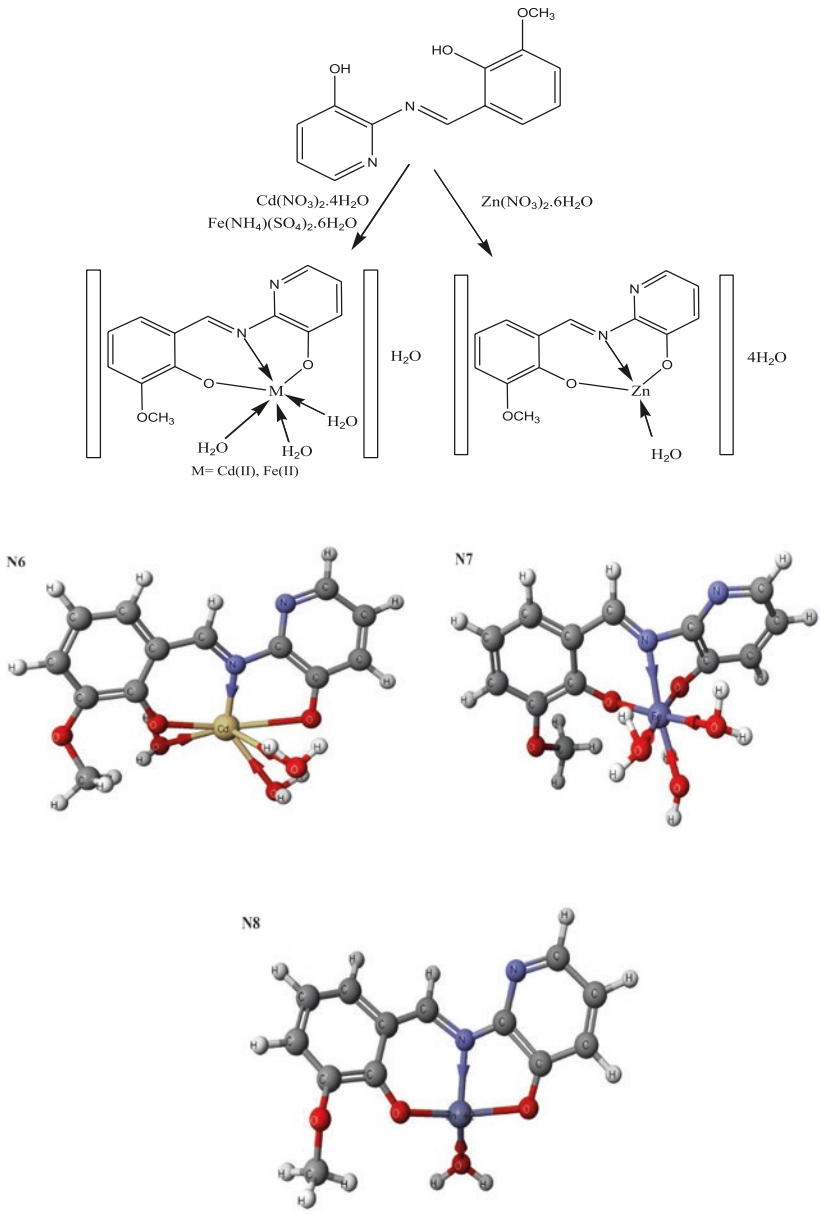

Scheme 7 Suggested structures of ligand and its Cd(II) (**N6**), Fe(II) (**N7**), Zn(II) (**N8**) metal complexes [51]

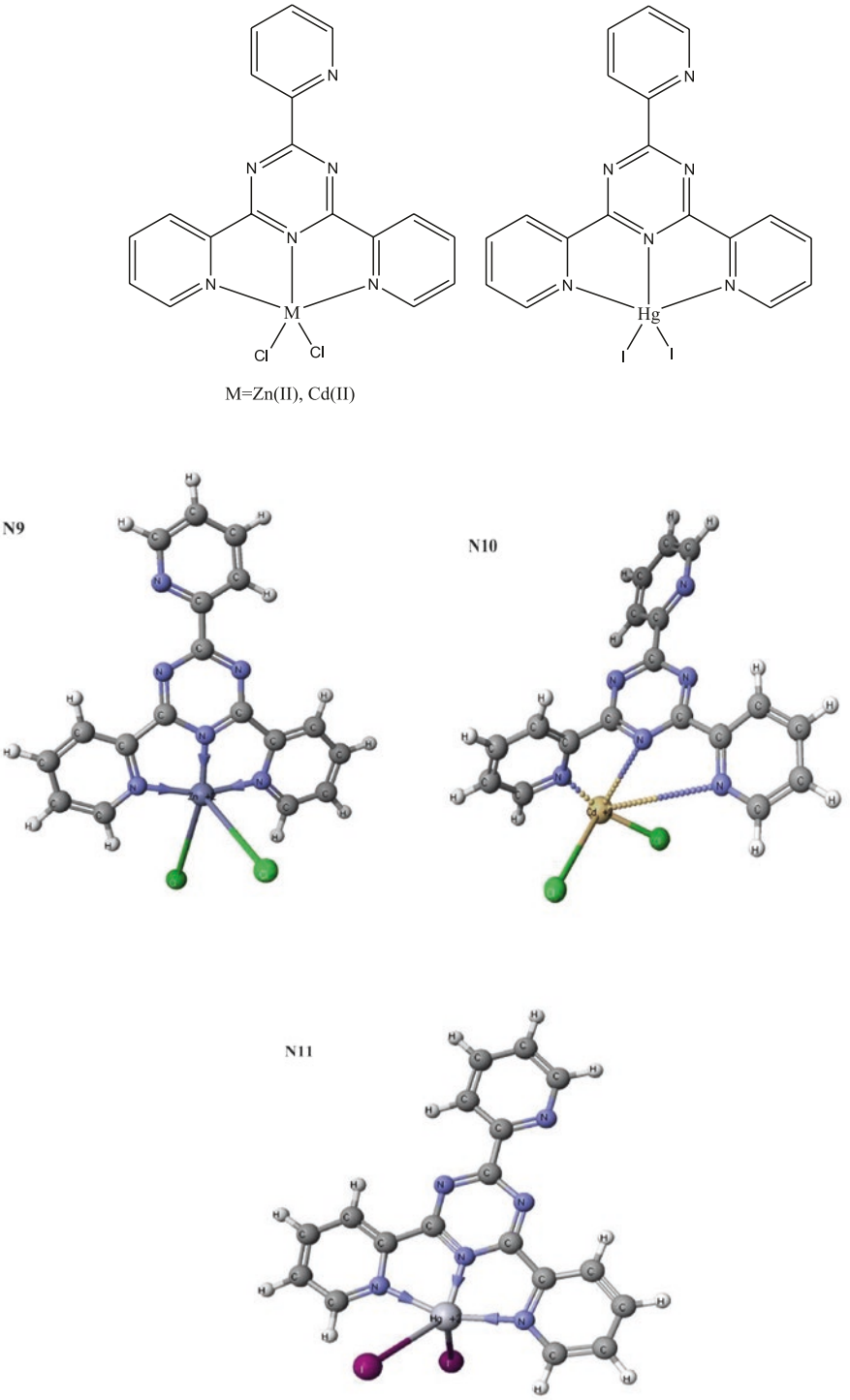

Fig. 1 Suggested and optimized structures of Zn (II) (**N9**), Cd(II) (**N10**), and Hg(II) (**N11**) metal complexes [52]

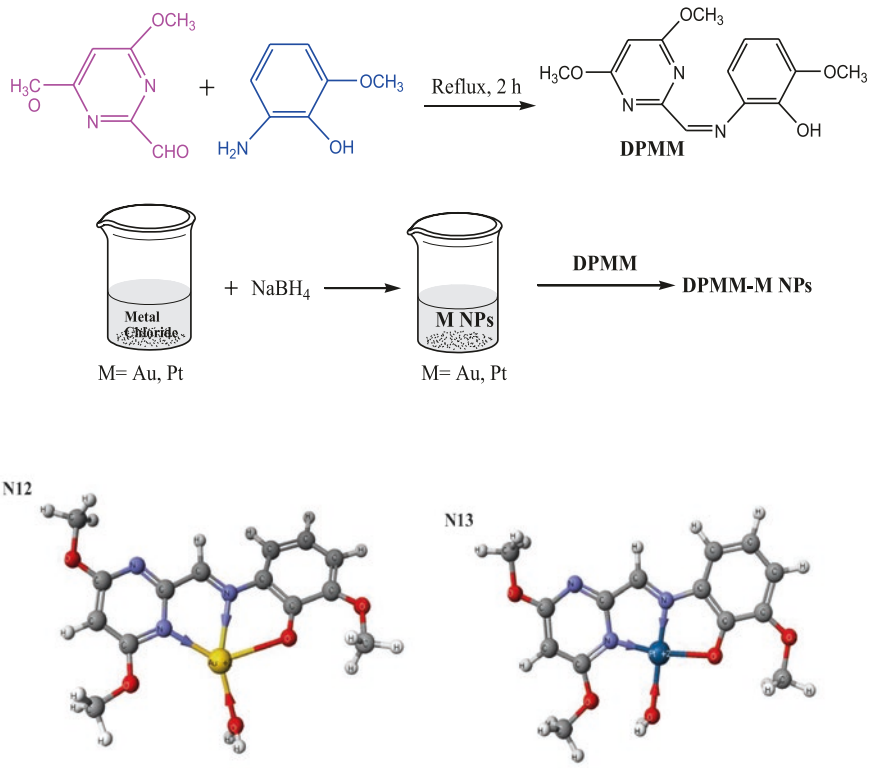

Scheme 8 Synthetic routes for the preparation of DPMM. Generation of DPMM capped Au (**N12**) and Pt NPs (**N13**) and optimized structures of metal complexes [53]

In 2017, Sankarganesh reported [They prepared pyrimidine-based Schiff base ligand 2-(4,6-dimethoxypyrimidine-2-yl)methyleneenamino)-6-methoxyphenol (DPMM) and gold (Au) (**N12**) and platinum (Pt) (**N13**) nanoparticles prepared by the modified Brust-Schiffrin method], given in Scheme 8. In addition to the anticancer study, antioxidant and antimicrobial studies were conducted. Furthermore, the MTT assay was used to test the anticancer activity of DPMM, DPMM-Au NPs, and DPMM-Pt NPs in vitro against cancer (MCF-7, HeLa, and HEp2) and normal (NHDF) cell lines. In comparison with the conventional medication cisplatin, these findings show that DPMM-Au NPs and DPMM-Pt NPs have high cytotoxic action against cancer cell lines and have the least damaging effect on normal cell lines [53].

In 2022, El-ghamry synthesized the tridentate hydrazone ligand and its Co (II), Ni(II), and Cu(II) complexes (Figs. 2 and 3). Moreover, it has been reported to synthesize and characterize hydrazone ligand and 8-hydroxyquinoline (8-HQ) and mixed ligand Co(II), Ni(II), and Cu(II) complexes. Besides these, the nano Cu (II) complex was also prepared. The antitumor activity investigation demonstrated that the ligand HL inhibited HepG-2 cell growth, with activity increasing with complexation, the Cu (II) complex 1 displayed the maximum cytotoxic activity [54].

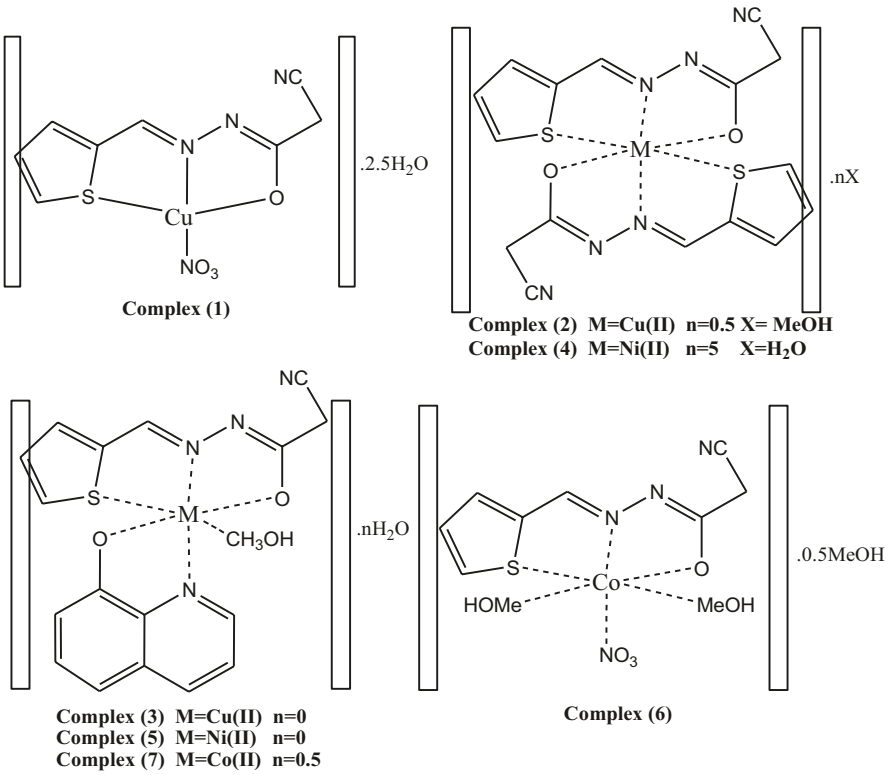

Fig. 2 Suggested structures of 1 (**N14**), 2 (**N15**), 3 (**N16**), 4 (**N17**), 5 (**N18**), 6 (**N19**), 7 (**N20**) metal complexes [54]

1.5 The Related Nanomaterials Under Perspective of In Silico Methods

In recent times, nanomaterials have progressively found applications in different areas such as technology, industry, and medicine. Their small particle size and their chemical and physical features are useful for diverse biomedical activities. Due to their physical resemblance with proteins, nanomaterials can improve medical imaging, diagnostics, and therapy.

In recent years, the development of in silico techniques such as combinatorial chemistry and high-throughput screening, absorption, and dispersal remarkably enhanced the number of compounds for which early information on absorption, distribution, metabolism, and excretion (ADME) and toxicity (T) were required, which in turn drove development. The absorption, distribution, metabolism, excretion, and toxicity (ADMET) features of chemicals act as vital roles at each step of drug exploration and advancement. So, it is essential to find effective molecules with better ADMET features.

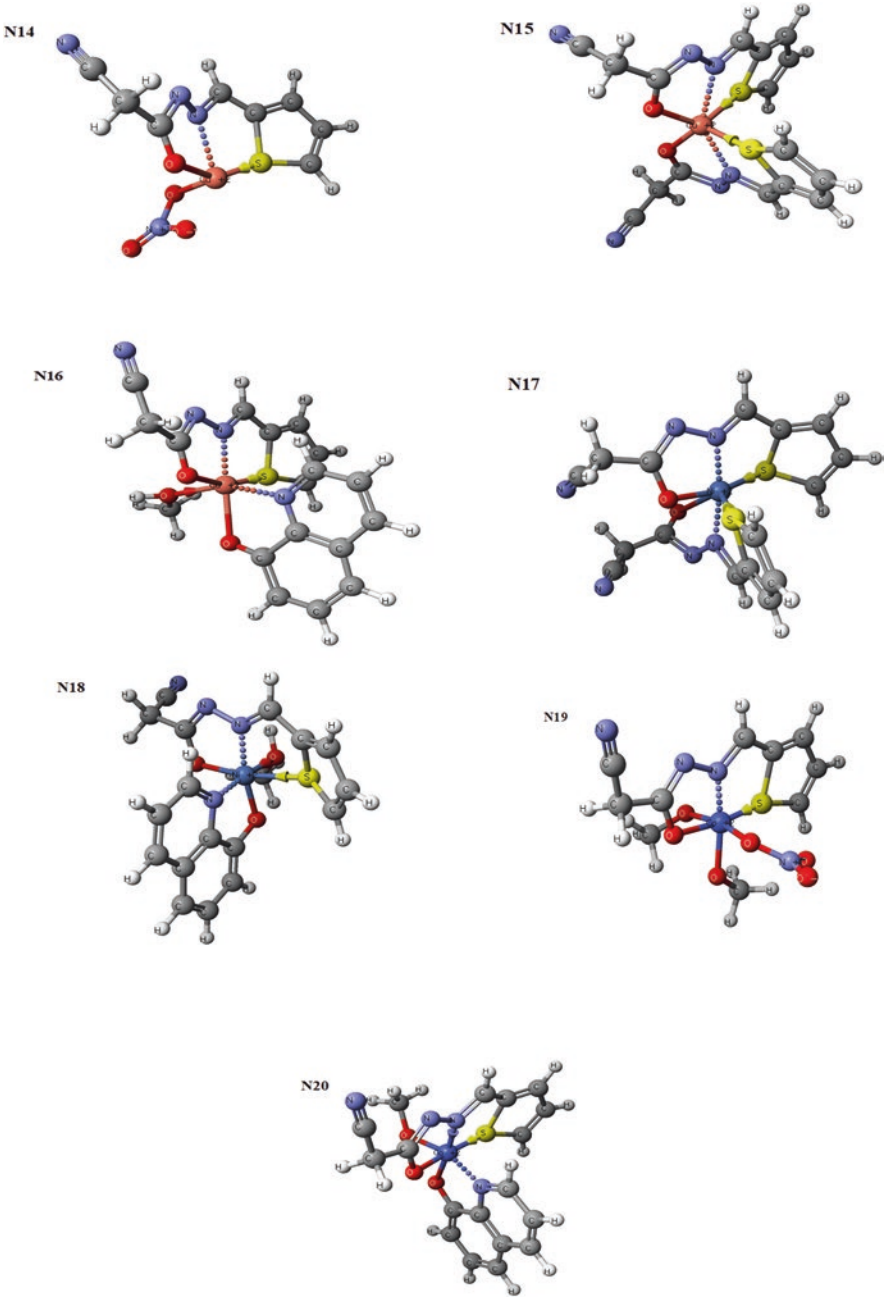

Fig. 3 Suggested optimized structures of 1 (**N14**), 2 (**N15**), 3 (**N16**), 4 (**N17**), 5 (**N18**), 6 (**N19**), 7 (**N20**) metal complexes [54]

The structure of the selected inorganic nanomaterials (**N1–N20**) was drawn (Table 2) and optimized accurately in MO-G using PM6 parameters in a vacuum using SCIGRESS [55]. *Drug-like properties* including solubility, permeability, metabolic stability, and transporter impacts are of critical importance. These factors affect oral bioavailability, metabolism, clearance, toxicity, as well as in vitro pharmacology. The drug-likeness prediction is performed to define pharmacokinetic properties of the selected nanomaterials. It includes studies (Lipinski et al. [56] and Veber et al. [57]) performed using Discovery Studio (DS) 3.5 [58] for the nanomaterials. The *in silico absorption*, *distribution*, *metabolism*, *excretion*, *and toxicity* (ADMET) properties that are very significant in the medicine process for the selection of a probable agent were generated with the help of the sub-protocol of DS 3.5. Afterward, *molecular docking* was conducted using AutoDock 4.2 [59] program to learn more about the interaction mechanisms of the current nanomaterial-DNA. A 3D structure model Protein Data Bank (PDB) code, 1BNA of DNA as the target, was obtained from PDB [60]. The nucleotides in the crystal structure did not mutate. Crystal structure resolution was <2.0 Å. The conformational views occurred for each nanomaterial docking with DNA based on the Lamarckian genetic algorithm. The best modes for the nanomaterials (**N1–N20**) with the lowest binding free energy complex in the biomolecules as targets were investigated for docking results including the docking energy, interplay types, and RMSD values.

1.5.1 Computational Results

ADMET analysis is a significant technique to control whether in vivo agents can reach the acceptable ranges. These rules are molecular weight no more than 500, no more than 5 hydrogen bond donors, no more than 10 hydrogen bond acceptors, and LogP (the log value of octanol-water partition coefficient) no more than 5, according to the "Rule of Five" [56, 57]. The other second rule by Veber et al. suggests no more than 10 rotatable bonds, polar surface area no more than 140 A^2, or no more than 12 hydrogen bond donors and acceptors. These ranges are employed to filter drug-like compounds in DS 3.5 [58]. All the nanomaterials except **N5**, **N6**, and **N7** revealed zero violations of Lipinski and Veber rules as given in Table 3. In addition, aqueous solubility, human intestinal absorption (HIA), blood-brain barrier penetration (BBB), Cytochrome P450 (CYP450) 2D6 inhibition, hepatotoxicity, and plasma protein binding were used and analyzed as ADME descriptors for the nanomaterials, (**N1–N20** in Table 4).

The ADME results of nanomaterial compounds, which are thought to exhibit potential drug candidates, except for **N5**, **N14**, and **N19** compounds, are given in Table 4. If attention is paid, all of them show hepatotoxic properties. Toxicity estimation analysis was also performed to determine whether the respective nanomaterials were toxic. Expected results are listed in Table 5. Nearly all compounds were found to exhibit acceptable toxicity for drug development in the treatment of cancer diseases.

Table 2 The simplified molecular-input line-entry system (SMILES) of the 20 nanomaterial compounds (**N1–N20**)

Compound	SMILES
N1	CC(C)[N+]1=Cc2ccccc2O[Pd]13Oc4ccccc4C=[N+]3C(C)C
N2	C=CC[N+]1=Cc2ccccc2O[Ni]13Oc4ccccc4C=[N+]3CC=C
N3	COc1cccc2C=[N+]3c4ncccc4O[Ni]3(Oc12)([OH2])([OH2])[OH2]
N4	COc1cccc2C=[N+]3c4ncccc4O[Co]3(Oc12)([OH2])([OH2])[OH2]
N5	O.O.O.COc1cc(OC)nc(\N=C\c2cc(ccc2O[Cu])[N+](=O)[O−])n1
N6	O.O.O.[Cd].COc1cccc(\C=N\c2ncccc2O)c1O
N7	O.O.O.[Fe].COc1cccc(\C=N\c2ncccc2O)c1O
N8	O.[Zn+2].COc1cccc(\C=N\c2ncccc2O)c1O
N9	[Cl−][Zn+2][Cl−].c1ccc(nc1)c2nc(nc(n2)c3ccccn3)c4ccccn4
N10	Cl[Cd]Cl.c1ccc(nc1)c2nc(nc(n2)c3ccccn3)c4ccccn4
N11	[I−][Hg+2][I−].c1ccc(nc1)c2nc(nc(n2)c3ccccn3)c4ccccn4
N12	O.[Au].COc1cc(OC)nc(\C=N\c2cccc(OC)c2O)n1
N13	O.[Pt].COc1cc(OC)nc(\C=N\c2cccc(OC)c2O)n1
N14	[O−][N+](=O)O[Cu+2]12OC(=N[N+]1=CC3=CC=[CH2]S23)CC#N
N15	N#CCC1=N[N+]2=CC3=CC=CS3[Cu+2]245(OC(=N[N+]4=CC6=CC=CS56)CC#N)O1
N16	CO[Cu+2]123(OC(=N[N+]1=CC4=CC=CS24)CC#N)Oc5cccc6ccc[n+]3c56
N17	N#CCC1=N[N]2=CC3=CC=CS3[N+2]245(OC(=N[N]4=CC6=CC=CS56)CC#N)O1
N18	CO[N+2]123(OC(=N[N]1=CC4=CC=CS24)CC#N)Oc5cccc6C=CC=[N]3c56
N19	CO[Co+2]12(OC)(O[N+](=O)[O−])OC(=N[N+]1=CC3=CC=CS23)CC#N
N20	CO[Co+2]123(OC(=N[N+]1=CC4=CC=CS24)CC#N)Oc5cccc6ccc[n+]3c56

We executed molecular docking studies regardless of the results of drug-likeness and ADMET analyses in the previous parts. A total of 20 compounds were selected for the analysis on affinity, which is shown by the docking binding energy (a low docking binding energy indicates a high binding affinity) (Table 6). Three-dimensional (3D) representation of the binding pose, interactions, H bond donor and acceptor surface of the five compounds (**N3, N10, N11, N9, and N2**) with the highest binding energies in the **N1–N20** compounds towards DNA complex are presented in (Fig. 4).

The binding energies of 20 nanomaterials, which react with DNA targets in molecular docking calculations, are between −9.35 and −5.30 kcal/mol. Compound **N3** (Ni(II)L) is the structure that exhibits the best binding and interplay with DNA, with a binding energy value of −9.35 kcal/mol. When we examine the interaction types of compound 3, it makes hydrogen bonds with the B, DT20; A, DA6; A, DT7; and A, DT8 nucleotides of DNA; electrostatic interactions with A, DT8, and B, DC21; and also hydrophobic interaction with B: DT19 (Fig. 4). Then, **N10**, **N7**, **N11**, **N5**, **N9**, and **N2** are followed by their binding energy values in Table 5. The molecule with the lowest binding tendency with DNA is the nanomaterial structure formed by **N19** which is Co (II) metal, with an organic molecule.

Table 3 Drug-likeness properties of the 20 nanomaterial compounds based on the Lipinski and Veber rules

Name	MW (≤500 g/mol)	AlogP (≤5)	MPSA (≤140 A^2)	NRB(≤10)	HA_ Lipinski (≤10)	HD_ Lipinski (≤5)	HA_ Veber (≤12)	HD_ Veber (≤12)
N1	432.853	4.707	33.26	2	4	2	2	2
N2	381.094	4.488	33.26	4	4	2	2	2
N3	355.977	1.836	116.68	1	8	7	7	4
N4	356.217	1.836	116.68	1	8	7	7	4
N5	420.842	2.368	206.15	6	12	6	11	3
N6	410.703	1.693	169.44	3	8	8	8	5
N7	354.137	1.693	169.44	3	8	8	8	5
N8	327.67	2.107	123.05	3	6	4	6	3
N9	450.659	−2.916	163.07	3	6	0	6	0
N10	495.645	3.61	77.34	3	6	0	6	0
N11	768.743	−3.792	212.67	3	6	0	6	0
N12	504.268	2.329	117.56	5	8	3	8	2
N13	502.38	2.329	117.56	5	8	3	8	2
N14	322.808	1.839	115.51	3	8	3	6	4
N15	452.013	0.89	113.96	2	8	2	6	4
N16	433.972	2.281	82.84	2	7	2	5	3
N17	403.482	0.478	113.96	2	9	3	6	5
N18	385.44	1.87	82.84	2	8	3	5	4
N19	379.255	1.507	129.7	5	10	3	8	4
N20	429.359	2.281	83.03	2	7	2	5	3

MW molecular weight, *ALogP* octanol/water partition coefficient, a measure for lipophilicity, *MPSA* molecular polar surface area, *nRB* number of rotatable bonds, *Num_H_Acceptors_Lipinski* number of hydrogen bond acceptors, *Num_H_Donors_Lipinski* number of hydrogen bond donors, *Num_H_Acceptors* number of hydrogen bond acceptors based on Veber, *Num_H_Donors* number of hydrogen bond donors based on Veber

Overall, as a result of all computational applications on the 20 compounds discussed, **N3**, **N10**, **N11**, **N9**, and **N2** nanomaterial structures should be considered as potential agents in cancer treatment and diagnostic studies.

2 Conclusion

Cancer is one of the diseases which is a major problem for all countries of the world today. The prediction of the International Agency for Research on Cancer (IARC) affiliated to the World Health Organization (WHO) for 2030 is that cancer will rank first among the causes of death. Various disadvantages of traditional methods used in cancer diagnosis and treatment reduce the effectiveness of these methods. However, although there have been many attempts to combine new technologies

Table 4 ADMET analysis of the 20 nanomaterial compounds

Comp.	PSA_2D (<140 Å^2)	AlogP98 (<5)	HIA	Solubility	BBB	CYP2D6	Hepa-totoxic	PPB
N1	17.86	4.645	0	1	0	I	T	True
N2	17.86	4.426	0	2	0	I	T	True
N3	38.051	1.804	0	2	2	NI	T	False
N4	38.051	1.804	0	2	2	NI	T	False
N5	103.458	2.989	0	3	4 (undefined)	NI	T	False
N6	73.145	2.314	0	3	3	NI	T	False
N7	73.145	2.314	0	3	3	NI	T	False
N8	73.145	2.314	0	3	3	NI	T	True
N9	67.566	2.639	0	2	2	NI	T	False
N10	67.566	2.639	0	2	2	NI	T	True
N11	67.566	2.639	0	2	2	NI	T	False
N12	81.451	2.536	0	3	3	NI	T	True
N13	81.451	2.536	0	3	3	NI	T	True
N14	93.438	−1.458	1	4	4 (undefined)	NI	T	False
N15	86.376	1.396	0	3	3	NI	T	False
N16	66.397	2.543	0	2	2	NI	T	True
N17	86.376	−0.152	0	3	3	NI	T	False
N18	66.397	0.996	0	2	3	NI	T	True
N19	111.299	−2.159	3	4	4 (undefined)	NI	T	False
N20	66.397	2.543	0	2	2	NI	T	True

PSA_2D 2D polar surface area, *AlogP98* the logarithm of the partition coefficient between n-octanol and water, *HIA* human intestinal absorption, *BBB* blood-brain barrier, *CYP2D6* cytochrome P450 2D6 binding, *NI* non-inhibitor; for CYP2D6, non-inhibitor, *NT* nontoxic for hepatotoxic, *PPB* plasma protein binding; more than 90% for PPB value is true, chemicals strongly bound. Less than 90% for PPB value is false, chemicals weakly bound

with traditional approaches to fight cancer, nanotechnology has shown wide applications in both treatment and diagnosis [61].

Nanotechnology has also been widely used in the remedy of several carcinomas lately. Because nanomaterials provide the opportunity to diagnose tumors at an early stage, in other words, nanostructures can enter a single tumor cell and increase the limits of imaging techniques. Chemotherapy drugs used in cancer treatment directly target tumors and have limited effects on healthy tissues, and the side effects of chemotherapy drugs are eliminated. Thus, the necessary doses are delivered to the cancerous tissues, shortening the recovery period and increasing the success of the treatment. In summary, nanomaterials have contributed to the improvement of cancer diagnosis and therapy with their improved pharmacokinetics and pharmacodynamics features.

Many nanomaterials, especially inorganic and organic nanomaterials, can be used as a potential nanocarrier for the early detection of cancer and loading of chemotherapeutic drugs. Particularly relevant nanomaterials, due to their small size and surface modifications, can remain in the circulation for a long time and be effective

Table 5 Toxicity prediction of the 20 nanomaterial compounds

Comp.	Mouse female NTP prediction	Mouse male NTP prediction	Rat female NTP prediction	Rat male NTP prediction	Ames prediction	Skin irritancy	Ocular irritancy	Aerobic biodegradability prediction
N1	Carcinogen	Carcinogen	Carcinogen	Carcinogen	Non-mutagen	None	None	Non-degradable
N2	Carcinogen	Non-carcinogen	Non-carcinogen	Carcinogen	Non-mutagen	None	None	Non-degradable
N3	Non-carcinogen	Non-carcinogen	Non-carcinogen	Non-carcinogen	Non-mutagen	None	Mild	Non-degradable
N4	Non-carcinogen	Non-carcinogen	Non-carcinogen	Non-carcinogen	Non-mutagen	None	Mild	Non-degradable
N5	Non-carcinogen	Non-carcinogen	Carcinogen	Carcinogen	Mutagen	Mild	Mild	Non-degradable
N6	Non-carcinogen	Non-carcinogen	Non-carcinogen	Non-carcinogen	Mutagen	None	Moderate	Non-degradable
N7	Non-carcinogen	Non-carcinogen	Non-carcinogen	Non-carcinogen	Mutagen	None	Moderate	Non-degradable
N8	Non-carcinogen	Non-carcinogen	Non-carcinogen	Non-carcinogen	Mutagen	None	Moderate	Non-degradable
N9	Non-carcinogen	Carcinogen	Non-carcinogen	Non-carcinogen	Non-mutagen	None	Mild	Non-degradable
N10	Non-carcinogen	Carcinogen	Non-carcinogen	Non-carcinogen	Non-mutagen	None	Severe	Non-degradable
N11	Non-carcinogen	Non-carcinogen	Non-carcinogen	Non-carcinogen	Mutagen	None	Mild	Non-degradable
N12	Non-carcinogen	Non-carcinogen	Carcinogen	Carcinogen	Mutagen	None	Moderate	Non-degradable
N13	Non-carcinogen	Non-carcinogen	Carcinogen	Carcinogen	Mutagen	None	Moderate	Non-degradable
N14	Non-carcinogen	Non-carcinogen	Non-carcinogen	Non-carcinogen	Non-mutagen	Mild	Moderate	Non-degradable
N15	Non-carcinogen	Non-carcinogen	Non-carcinogen	Non-carcinogen	Non-mutagen	Mild	Moderate	Non-degradable
N16	Carcinogen	Carcinogen	Non-carcinogen	Carcinogen	Non-mutagen	Mild	None	Non-degradable
N17	Non-carcinogen	Non-carcinogen	Non-carcinogen	Non-carcinogen	Non-mutagen	Mild	Moderate	Non-degradable
N18	Non-carcinogen	Non-carcinogen	Non-carcinogen	Non-carcinogen	Non-mutagen	Mild	None	Non-degradable
N19	Non-carcinogen	Non-carcinogen	Non-carcinogen	Non-carcinogen	Non-mutagen	Mild	Moderate	Non-degradable
N20	Carcinogen	Carcinogen	Non-carcinogen	Carcinogen	Non-mutagen	Mild	None	Non-degradable

NTP National Toxicology Program, *comp* compound

Table 6 Binding energy values of the compounds **N1–N20** against DNA

Compound	Free energy of binding (kcal/mol)
N1	−7.99
N2	*−8.48*
N3	*−9.35*
N4	−7.91
N5	−8.74
N6	−7.12
N7	−9.07
N8	−8.12
N9	*−8.55*
N10	*−9.22*
N11	*−8.94*
N12	−6.51
N13	−6.50
N14	−7.33
N15	−7.05
N16	−8.34
N17	−7.59
N18	−7.19
N19	−5.30
N20	−6.80

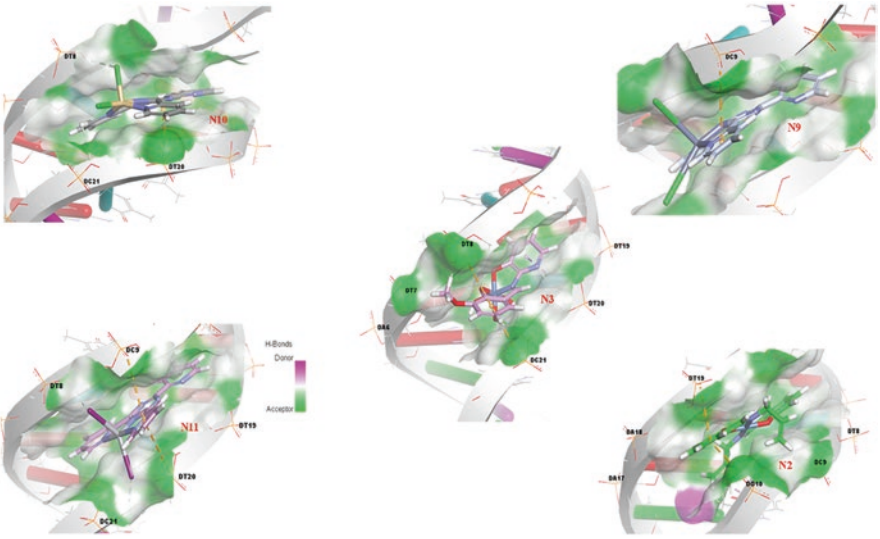

Fig. 4 3 D orientations of the compounds **N3, N10, N11, N9 and N2** against DNA based on the calculated binding energy values of the compounds **N1–N20**

by targeting primarily tumor sites. Among metallic nanomaterials, especially Ni, Cd, Fe, Hg, Cu, Zn, Pd, Co, Au, and Pt, nanomaterials are widely used in drug delivery systems. Despite their extremely advantageous properties, nanomaterials to be used on living organisms must have various properties such as being physiologically compatible (biocompatible), degradable in a physiological environment, and the ability to be excreted through the kidneys or bile. However, the studies reveal that some nanomaterials cause irreversible damage to cells in various ways depending on their composition and size [62–65].

Given the limitations associated with nanotechnology, further studies are needed to develop medicine releases, maximizing their effectiveness while keeping damages to a minimum. By improving the interplay between the physicochemical features of the nanomaterials used, safer and more effective derivatives can be provided for diagnosis and therapy in cancer management. In many studies, the toxicity of nanomaterials is attributed to their physicochemical features, namely, their small size and surface area. Therefore, unlike traditional toxicology, the safety/toxicity evaluation of a particular nanomaterial is based not only based on its chemical content but also on its size, surface structure, form, etc. [65–67]. For these reasons, nanomaterials in this chapter were investigated using in silico methods, which are more economical in terms of labor, time, and cost, to investigate the biocompatibility and toxic effects of nanomaterials very carefully.

As a result of in silico methods including drug-likeness, ADME, toxicological analyzes, and molecular docking processes between twenty nanomaterials (**N1–N20**) with DNA, it has been suggested that **N3**, **N10**, **N11**, **N9**, and **N2** compounds may be potential candidates for cancer diagnosis and therapy. This study will also form the basis of studies on new inorganic and organic nanomaterials.

Acknowledgment The authors thank Esin Akı Yalcin and the research group for their technical assistance.

References

1. Kaya SI, Ozcelikay G, Mollarasouli F, Bakirhan NK, Ozkan SA. Recent achievements and challenges on nanomaterial-based electrochemical biosensors for the detection of colon and lung cancer biomarkers. Sensors Actuators B Chem. 2022;351:130856. https://doi.org/10.1016/j.snb.2021.130856.
2. Siegel RL, Miller KD, Fuchs HE, Jemal A. Cancer statistics, 2021. CA Cancer J Clin. 2021;71:7–33. https://doi.org/10.3322/caac.21654.
3. Cui H, Huan ML, Ye WL, Liu DZ, Teng ZH, Mei QB, Zhou SY. Mitochondria and nucleus dual delivery system to overcome Dox resistance. Mol Pharm. 2017;14:746–56. https://doi.org/10.1021/acs.molpharmaceut.6b01016.
4. Xie X, Luo SY, Mukerabigwi JF, Mei J, Zhang YN, Wang SF, Xiao W, Huang XY, Cao Y. Targeted nanoparticles from xyloglucan–doxorubicin conjugate loaded with doxorubicin against drug resistance. RSC Adv. 2016;6:26137–46.
5. Lakshmi S, Balasubramanian D. Nanotechnology in dentistry-a review. Int J Dent Sci Res. 2013;2:40–4.

6. Subramani K, Ahmed W. Emerging nanotechnologies in dentistry. William Andrew is an imprint of Elsevier, Waltham, USA; Oxford, UK, 2012: 78–97, 322–89.
7. Mitra SB, Holmes BN. An application of nanotechnology in advanced dental materials. J Am Dent Assoc. 2003;134:1382–90.
8. Naderinezhad S, Amoabediny G, Haghiralsadat F. Co-delivery of hydrophilic and hydrophobic anticancer drugs using biocompatible pH-sensitive lipid-based nanocarriers for multidrug-resistant cancers. RSC Adv. 2017;7:30008.
9. Wasfy AF, Aly AA, Behalo MS, Mohamed NS. An efficient synthesis of some new 1, 4-disubstituted phthalazine derivatives and their anticancer activity. Der PharmaChemica. 2013;5:82–96.
10. Majd MH, Asgari D, Barar J, Valizadeh H, Kafil V, Abadpour A, Moumivand E, Mojarrad JS, Rashidi MR, Coukos G, Omidi Y. Tamoxifen loaded folic acid armed PEGylated magnetic nanoparticles for targeted imaging and therapy of cancer. Colloids Surf B: Biointerfaces. 2013;106:117–25.
11. Khalid K, Tan X, Zaid HFM, Tao Y, Chew CL, Chu DT. Advanced in developmental organic and inorganic nanomaterial: a review. Bioengineered. 2020;11:328–55.
12. Liang R, Wei M, Evans DG, Duan X. Inorganic nanomaterials for bioimaging, targeted drug delivery, and therapeutics. Chem Commun. 2014;50:14071–81.
13. Zhang X, Tian W, Cai X, Wang X, Dang W, Tang H, Cao H, Wang L, Chen T. Hydrazinocurcumin encapsuled nanoparticles "re-educate" tumor-associated macrophages and exhibit anti-tumor effects on breast cancer following STAT3 suppression. PLoS One. 2013;8(6):e65896. https://doi.org/10.1371/journal.pone.0065896.
14. Liu J, Cao Z, Lu Y. Functional nucleic acid sensors. Chem Rev. 2009;109:1948–98. https://doi.org/10.1021/cr030183i.
15. Breaker RR, Joyce GF. A DNA enzyme that cleaves RNA. Chem Biol. 1994;1:223–9. https://doi.org/10.1016/1074-5521(94)90014-0.
16. Silverman SK. Deoxyribozymes: selection design and serendipity in the development of DNA catalysts. Acc Chem Res. 2009;42:1521–31. https://doi.org/10.1021/ar900052y.
17. Liu M, Chang D, Li Y. Discovery and biosensing applications of diverse RNA-cleaving DNAzymes. Acc Chem Res. 2017;50:2273–83. https://doi.org/10.1021/acs.accounts.7b00262.
18. Lu L, Zhang X, Kong R, Yang B, Tan W. A ligation-triggered DNAzyme cascade for amplified fluorescence detection of biological small molecules with zero-background signal. J Am Chem Soc. 2011;133:11686–91. https://doi.org/10.1021/ja203693b.
19. Shen L, Chen Z, Li Y, He S, Xie S, Xu X, Liang Z, Meng X, Li Q, Zhu Z, Li M, Chris Le X, Shao Y. Electrochemical DNAzyme sensor for lead based on amplification of DNA− Au Bio-Bar codes. Anal Chem. 2008;80:6323–8. https://doi.org/10.1021/ac800601y.
20. Liu J, Lu Y. Stimuli-responsive disassembly of nanoparticle aggregates for light-up colorimetric sensing. J Am Chem Soc. 2005;127:12677–83. https://doi.org/10.1021/ja053567u.
21. Dass CR, Choong PF, Khachigian LM. DNAzyme technology and cancer therapy: cleave and let die. Mol Cancer Ther. 2008;7:243–51. https://doi.org/10.1158/1535-7163.MCT-07-0510.
22. Baum DA, Silverman SK. Deoxyribozymes: useful DNA catalysts in vitro and in vivo cell. Mol Life Sci. 2008;65:2156–74. https://doi.org/10.1007/s00018-008-8029-y.
23. Cairns MJ, Hopkins TM, Witherington C, Wang L, Sun LQ. Target site selection for an RNA-cleaving catalytic DNA. Nat Biotechnol. 1999;17(5):480–6. https://doi.org/10.1038/8658.
24. Fahmy RG, Waldman A, Zhang G, Mitchell A, Tedla N, Cai H, Geczy CR, Chesterman CN, Perry M, Khachigian LM. Suppression of vascular permeability and inflammation by targeting of the transcription factor c-Jun. Nat Biotechnol. 2006;24:856–62. https://doi.org/10.1038/nbt1225.
25. Feng J, Xu Z, Liu F, Zhao Y, Yu W, Pan M, Wang F, Liu X. Versatile catalytic deoxyribozyme vehicles for multimodal imaging-guided efficient gene regulation and photothermal therapy. ACS Nano. 2018;12:12888–901. https://doi.org/10.1021/acsnano.8b08101.
26. Elahy M, Dass CR. Dz13: c-Jun downregulation and tumour cell death. Chem Biol Drug Des. 2011;78:909–12. https://doi.org/10.1111/j.1747-0285.2011.01166.x.

27. Fahmy RG, Dass CR, Sun LQ, Chesterman CN, Khachigian LM. Transcription factor Egr-1 supports FGF-dependent angiogenesis during neovascularization and tumor growth. Nat Med. 2003;9:1026–32. https://doi.org/10.1038/nm905.
28. Fan H, Zhang X, Lu Y. Recent advances in DNAzyme-based gene silencing. Sci China Chem. 2017;60:591–601. https://doi.org/10.1007/s11426-016-0472-1.
29. Zhou W, Ding J, Liu J. Theranostic DNAzymes theranostics. 2017;7:1010–25. https://doi.org/10.7150/thno.17736.
30. Yuan Y, Gu Z, Yao C, Luo D, Yang D. Nucleic acid-based functional nanomaterials as advanced cancer therapeutics. Small. 2019;15:1900172.
31. Wang H, Luo D, Wang H, Wang F, Liu X. Construction of smart stimuli-responsive DNA nanostructures for biomedical applications. Chem Eur J. 2021;27:3929–43.
32. Dai Z, Leung HM, Lo PK. Stimuli-responsive self-assembled DNA nanomaterials for biomedical applications. Small. 2017;13:1602881.
33. Santoro SW, Joyce GF. A general purpose RNA-cleaving DNA enzyme. Proc Natl Acad Sci U S A. 1997;94:4262–6. https://doi.org/10.1073/pnas.94.9.4262.
34. Kato RB, Roy B, De Oliveira FS, Ferraz EP, De Oliveira PT, Kemper AG, Hassan MQ, Rosa AL, Beloti MM. Nanotopography directs mesenchymal stem cells to osteoblast lineage through regulation of microRNASMAD-BMP-2 circuit. J Cell Physiol. 2014;229(11):1690–6. https://doi.org/10.1002/jcp.24614.
35. Bobo D, Robinson KJ, Islam J, Thurecht KJ, Corrie SR. Nanoparticle-based medicines: a review of FDA-approved materials and clinical trials to date. Pharm Res. 2016;33(10):2373–87.
36. Ventola CL. Progress in nanomedicine: approved and investigational nanodrugs. P & T. 2017;42(12):742–55.
37. Lombardo D, Kiselev MA, Caccamo MT. Smart nanoparticles for drug delivery application: development of versatile nanocarrier platforms in biotechnology and nanomedicine. J Nanomater 2019;2019:3702518.
38. Chen X, Mangala LS, Rodriguez-Aguayo C, Kong X, Lopez-Berestein G, Sood AK. RNA interference-based therapy and its delivery systems. Cancer Metastasis Rev. 2018;37:107–24.
39. Takeshita F, Ochiya T. Therapeutic potential of RNA interference against cancer. Cancer Sci. 2006;97:689–96.
40. Makeyev EV, Maniatis T. Multilevel regulation of gene expression by microRNAs. Science. 2008;319:1789–90.
41. Yoon J, Shin M, Lee JY, Lee SN, Choi JH, Choi JW. RNA interference (RNAi)-based plasmonic nanomaterials for cancer diagnosis and therapy. J Control Release. 2022;342:228–40. https://doi.org/10.1016/j.jconrel.2022.01.012.
42. Sunoqrot S, Abujamous L. pH-sensitive polymeric nanoparticles of quercetin as a potential colon cancer targeted nanomedicine. J Drug Deliv Sci Technol. 2019;52:670–6.
43. LeGarrec D, Gori S, Luo L, Lessard D, Smith DC, Yessine MA, Ranger M, Leroux JC. Poly(N-vinylpyrrolidone)-block-poly(d,l-lactide) as a new polymeric solubilizer for hydrophobic anticancer drugs: in vitro and in vivo evaluation. J Control Release. 2004;99:83–101.
44. Zhu Z, Li Y, Li X, Li R, Jia Z, Liu B, Guo W, Wu W, Jiang X. Paclitaxel-loaded poly(N-vinylpyrrolidone)-b-poly(ε-caprolactone) nanoparticles: preparation and antitumor activity in vivo. J Control Release. 2010;142:438–46.
45. Bailly N, Thomas M, Klumperman B. Poly(N-vinylpyrrolidone)-block-poly(vinyl acetate) as a drug delivery vehicle for hydrophobic drugs. Biomacromolecules. 2012;13:4109–17.
46. Gavas S, Quazi S, Karpiński TM. Nanoparticles for cancer therapy: current progress and challenges. Nanoscale Res Lett. 2021;16:173. https://doi.org/10.1186/s11671-021-03628-6.
47. Dehkhodaei M, Sahihi M, Rudbari HA, Ariaeefar M, Gharaghani S, Azadbakht R, Taheri S, Kajani AA. Multi experimental and computational studies for DNA and HSA interaction of new nano-scale ultrasound-assisted synthesized Pd(II) complex as a potent anticancer drug. J Mol Liq. 2018;264:386–97. https://doi.org/10.1016/j.molliq.2018.05.077.
48. Dehkhodaei M, Sahihi M, Rudbari HA, Gharaghani S, Azadbakht R, Taheri S, Kajani AA. Studies of DNA- and HSA-binding properties of new nano-scale green synthesized Ni (II)

complex as anticancer agent using spectroscopic methods, viscosity measurement, molecular docking, MD simulation and QM/MM. J Mol Liq. 2017;248:24–35. https://doi.org/10.1016/j.molliq.2017.10.044.
49. Abdel-Rahman LH, Abu-Dief AM, El-Khatib RM, Abdel-Fatah SM. Sonochemical synthesis, DNA binding, antimicrobial evaluation and in vitro anticancer activity of three new nano-sized Cu(II), Co(II) and Ni(II) chelates based on tri-dentate NOO imine ligands as precursors for metal oxides. J Photochem Photobiol B Biol. 2016a;162:298–308. https://doi.org/10.1016/j.jphotobiol.2016.06.052.
50. Adwin Jose P, Sankarganesh M, Dhaveethu Raja J, Sakthivel A, Annaraj J, Jeyaveeramadhavi S, Girija A. Spectrophotometric and fluorometric detection of DNA/BSA interaction, antimicrobial, anticancer, antioxidant and catalytic activities of biologically active methoxy substituted pyrimidine-ligand capped copper nanoparticles. Spectrochim Acta A Mol Biomol Spectrosc. 2022;267(2):120454. https://doi.org/10.1016/j.saa.2021.120454.
51. Abdel-Rahman LH, Abu-Dief AM, El-Khatib RM, Abdel-Fatah SM. Some new nano-sized Fe(II), Cd(II) and Zn(II) Schiff base complexes as precursor for metal oxides: sonochemical synthesis, characterization, DNA interaction, in vitro antimicrobial and anticancer activities. Bioorg Chem. 2016b;69:140–52. https://doi.org/10.1016/j.bioorg.2016.10.009.
52. Yaghobi Z, Ranjbar ZR, Gharbi S. Synthesis and characterization of d10 transition metal complexes in bulk and nano scales: DNA binding, molecular docking and anticancer activity against MCF-7 cell line. Polyhedron. 2019;164:176–84. https://doi.org/10.1016/j.poly.2019.02.039.
53. Sankarganesh M, Adwin Jose P, Dhaveethu Raja J, Kesavan MP, Vadivel M, Rajesh J, Jeyamurugan R, Senthil Kumar R, Karthikeyan S. New pyrimidine based ligand capped gold and platinum nano particles: synthesis, characterization, antimicrobial, antioxidant, DNA interaction and in vitro anticancer activities. J Photochem Photobiol B Biol. 2017;176:44–53. https://doi.org/10.1016/j.jphotobiol.2017.09.013.
54. El-ghamry MA, Shebl M, Saleh AA, Khalil SME, Dawy M, Ali AAM. Spectroscopic characterization of Cu(II), Ni(II), Co(II) complexes, and nano copper complex bearing a new S, O, N-donor chelating ligand. 3D modeling studies, antimicrobial, antitumor, and catalytic activities. J Mol Struct. 2022;1249:131587. https://doi.org/10.1016/j.molstruc.2021.131587.
55. Marchand N, Lienard P, Siehl H, Izato H. Applications of molecular simulation software SCIGRESS in industry and university. Fujitsu Sci Tech J. 2014;50:46–51.
56. Lipinski CA, Lombardo F, Dominy BW, Feeney PJ. Experimental and computational approaches to estimate solubility and permeability in drug discovery and development settings. Adv Drug Deliv Rev. 2001;46:3–26.
57. Veber DF, Johnson SR, Cheng HY, Smith BR, Ward KW, Kopple KD. Molecular properties that influence the oral bioavailability of drug candidates. J Med Chem. 2002;45:2615–23.
58. Accelrys Software Inc. Discovery studio modeling environment, Release 3.5 Accelrys Software Inc, San Diego; 2013.
59. Morris GM, Huey R, Lindstrom W, Sanner MF, Belew RK, Goodsell DS, Olson AJ. AutoDock4 and AutoDockTools4: automated docking with selective receptor flexibility. J Comput Chem. 2009;30(16):2785–91. https://doi.org/10.1002/jcc.21256.
60. Drew HR, Wing RM, Takano T, Broka C, Tanaka S, Itakura K, Dickerson RE. Structure of a B-DNA dodecamer: conformation and dynamics. Proc Natl Acad Sci. 1981;78(4):2179.
61. Barani M, Hosseinikhah SM, Rahdar A, Farhoudi L, Arshad R, Cucchiarini M, Pandey S. Nanotechnology in bladder cancer: diagnosis and treatment. Cancer. 2021;13:2214. https://doi.org/10.3390/cancers13092214.
62. Lamprecht A. Nanotherapeutics: drug delivery concepts in nanoscience. Singapore: Pan Stanford; 2016.
63. Yavuz O, Marangoz Ö. Farmakoloji ve toksikolojide in siliko yöntemlerin kullanımı. In: Güvenç D, editor. İlaç Araştırma, Geliştirme ve Toksikolojik Çalışmalarda Kullanılan Alternatif Yöntemler. 1. Baskı. Ankara: Türkiye Klinikleri; 2018. p. 35–42.
64. Fard JK, Jafari S, Eghbal MA. A review of molecular mechanisms involved in toxicity of nanoparticles. Adv Pharm Bull. 2015;5(4):447–54.

65. Marangoz Ö. Nano ilaç ve nano ilaç taşıma sistemleri. Doktora Semineri, Ondokuz Mayıs Üniversitesi Sağlık Bilimleri Enstitüsü; 2018.
66. Sayıner Ö, Çomoğlu T. Nanotaşıyıcı sistemlerde hedeflendirme. Ankara Ecz Fak Derg. 2016;40(3):62–79.
67. Abud MB, Louzada RN, Isaac DLC, Souza LG, Dos Reis RG, Lima EM, de Ávila MP. In vivo and in vitro toxicity evaluation of liposome-encapsulated sirolimus. Intern J Retina Vitreous. 2019;5(1):35. https://doi.org/10.1186/s40942-019-0186-7.

Recent Progress in Detection of Breast Cancer Biomarkers by Clinical and Imprinting Polymer-Based Sensors

Nurgul K. Bakirhan and Cigdem Yucel

1 Introduction

1.1 Breast Cancer

Cancer is known to be the leading cause of death worldwide according to recent reports by the World Health Organization (WHO), 2020. Among all cancers, both sexes and all ages, breast cancer has the highest number of new cases, nearly 2.3 million (11.7%) in an estimated 19.3 million worldwide, and was fifth in several deaths (6.9%) according to the Global Cancer Observatory (GCO) [1, 2]. Among women, the most frequently seen cancer is breast cancer. The disease accounts for over 1/10 of newly diagnosed cancer annually. It is the second leading cause of mortality from cancer among women worldwide. At the end of the year 2020, 7.8 million women were diagnosed with this disease; hence, this disease's importance was increasing in recent years. The American Cancer Society (ACS) has given the breast cancer incidence report in women of different racial and ethnic groups as below [1]:

- Non-Hispanic white: 128.1/100,000
- African American: 124.3/100,000
- American Indian/Alaska Native: 91.9/100,000
- Hispanic/Latina: 91.0/100,000

N. K. Bakirhan (✉)
Department of Analytical Chemistry, Gulhane Faculty of Pharmacy, University of Health Sciences, Istanbul, Turkey

C. Yucel (✉)
Department of Biochemistry, Gulhane Faculty of Pharmacy, University of Health Sciences, Istanbul, Turkey

R. S. Chaughule et al. (eds.), *Nanomaterials for Cancer Detection Using Imaging Techniques and Their Clinical Applications*,
https://doi.org/10.1007/978-3-031-09636-5_11

- Asian American/Pacific Islander: 88.3/100,000

Certain factors increase the risk of breast cancer, which are:

1. Age: The incidence rate of breast cancer is increased by age, from 1.5/100,000 in women between 20 and 24 years of age to 421.3/100,000 in women 75–79 years of age; and 95% of new cases occur in women over 40 years. The median age of diagnosis with breast cancer is 61 years.
2. Gender: Female gender is the major and strongest risk factor for breast cancer. Only 0.5–1% of breast cancers occur in men [3].
3. Family history and genetic risk factors: In first-degree relatives of breast cancer patients, the risk of having breast cancer is increased by 2–3-fold. 5–10% of breast cancers are caused by genetic vulnerabilities, but they compromise 25% of breast cancer in women <30 years of age. Two major genes responsible for increased risk of breast cancer are *BRCA1* and *BRCA2*. When there is cancer in one breast, the risk of cancer is also increased in the other one.
4. Reproductive risk factors: Reproductive features related to exposure to estrogen over a lifetime increase the risk of breast cancer. These features can be listed as the onset of menarche <12 years of age, first childbirth >30 years of age, null parity, and menopause >55 years of age.
5. Hormone replacement therapy (HRT): Therapeutic or supplemental usage of steroid hormones like estrogen and progesterone which are taken basically for contraception in the premenopausal era and hormone replacement therapy in the postmenopausal era. Prolonged usage of HRT causes an increased risk of breast cancer [4–6].

Breast cancer is a heterogeneous complex of diseases, a spectrum of many subtypes with distinct biological features, and physiological and clinical presentations. The female breast is positioned in the front chest wall, and it has glands for milk production. It is stabilized in the chest by pectoralis major muscle and supporting ligaments. The fat tissue surrounding the lobes causes differences in size and shape. Lobules containing the glands in each lobe are responsible for milk production under hormonal stimuli.

In invasive, the overall structure deteriorates and cells are infiltrated into a variable amount of stroma in a hazardous way. Invasive ductal cancer (infiltrating ductal carcinoma) is the most frequent type of breast cancer and constitutes 50–70% of invasive breast cancers. 10% of breast cancers are invasive lobular types, and mixed ductal carcinoma and lobular carcinoma have also been recognized, though rare.

Breast cancer arises in the epithelia of the ducts (85%) and lobules (15%) in the glandular breast tissue. At first, cancer is restricted to the duct or lobule termed “in situ” carcinoma, where it is asymptomatic and has the minimal potential for metastasis. Widespread metastasis is the major cause of mortality in breast cancer.

Breast cancer can be caused by DNA damage genetically alterations. These can be triggered by estrogen exposure. In some cases, the presence of some inherited DNA defects and precancerous genes, namely, *BRCA1* and *BRCA2*, causes breast cancer. As a result family history of ovarian or previous breast cancer causes the risk of having breast cancer to be increased [7–11].

1.2 *Imprinting Polymers*

Molecularly imprinted polymers (MIPs) can mimic natural molecules such as antibodies and biological receptors [12, 13]. Chemical and biological molecules such as proteins, amino acids, drugs, foods, and hazardous materials can easily be detected with the help of MIP technology [14–17]. MIP is a complex structure between target and monomer parts. The recognition process occurs with intermolecular interactions like dipole-dipole, ionic interactions, and hydrogen bonds between the target and polymer matrix. A three-dimensional polymer network occurred with an excess of cross-linking agents [18]. After the successful polymerization process, the template is removed from the polymer network. The polymer can recognize target molecules selectively due to the formed template cavity (Fig. 1) [19].

The selectivity parameter is so important for the analysis of compounds and validation of developed sensors and methods. By the electrochemical techniques, many compounds could be sensitively analyzed, but selectivity parameters may be missing for them. Hence, MIPs are excellent structures at this point.

MIPs are used in the design of sensors, drug delivery systems, separation, sciences and purification, catalysis, and biological antigen-antibody systems [20–26]. They have cheap procedures, a long lifetime, excellent physical features, strength, resistance to elevated temperature, pressure, and stability in acids, bases, and organic solutions. Its high selectivity property is used in imprinting to detect proteins, nucleic acids, and drug compounds. The chapter aims to present MIP technology for the detection of breast cancer markers with electrochemical methods. The recent studies will be explained briefly.

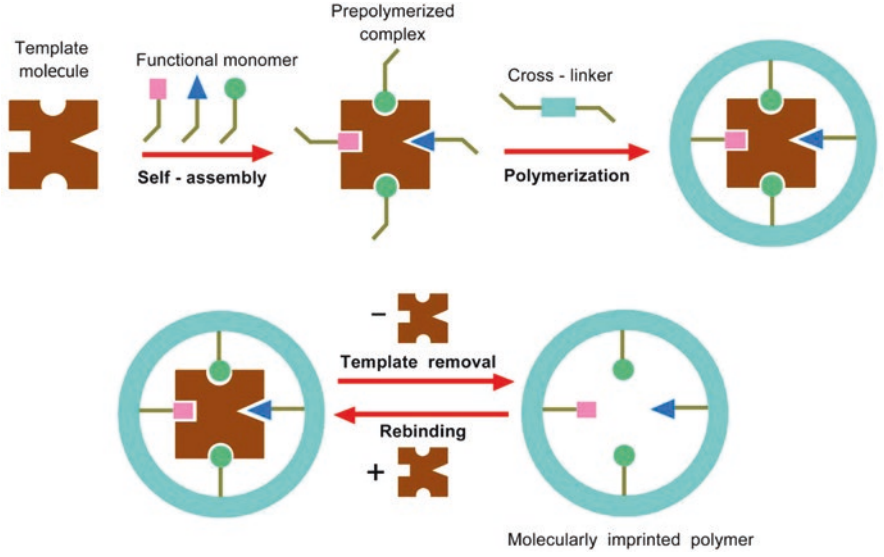

Fig. 1 Schematic representation of molecularly imprinted polymers [19]

1.3 Electrochemical Methods

Electrochemical biosensors have selective biochemical recognition of target molecules with high sensitivity [27]. Electrochemical methods have excellent properties such as responsibility, cheap, fast, small volumes of solutions, and simple and easy usage [28–31]. The small concentrations of breast cancer biomarkers from biological samples could be detected easily via electrochemical methods. Especially, invasive usage is so important for patients. Hence, these developed biosensors may have a chance to easy and fast usage. Polymers have been used to obtain the more sensitive and selective response of analytes. They have unique chemical, physical, and mechanical properties. MIPs have been preferred widely due to their low LOD values and good precision [32].

Polymers have been preferred for the fabrication of sensitive and selective sensors. A novel electrochemical immunosensor was fabricated for the detection of CEA with AuNPs-decorated Prussian blue-poly(3,4-ethylene dioxythiophene) (AuNPs/PB-PEDOT) (Fig. 2) [33]. This sensor structure is biocompatible and environment-friendly. PEDOT has good electron transfer and good stability. The electrochemical measurement was evaluated by DPV techniques within the 0.05 and 40 ng/mL working range and 0.01 ng/mL LOD values. The developed sensor could be applied in human serum samples with high recoveries. Results were compared with the ELISA method, and results showed a good correlation with electrochemical results.

MCF-7 is a breast cancer cell. It is determined by an aptasensor, polyadenine (polydA)-aptamer-modified gold electrode, and a polydA-apta-functionalized AuNPs/GO hybrid (Fig. 3) [34]. The developed sensor showed high selectivity against MCF-7 cells in the presence of other non-tumorigenic cells and other cancer

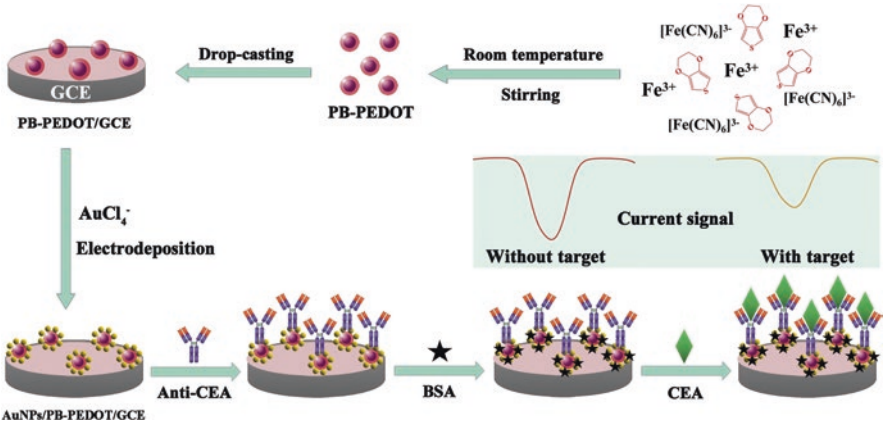

Fig. 2 The fabrication of label-free immunosensor for the CEA determination. (Reprinted from [33] with the permission of Elsevier)

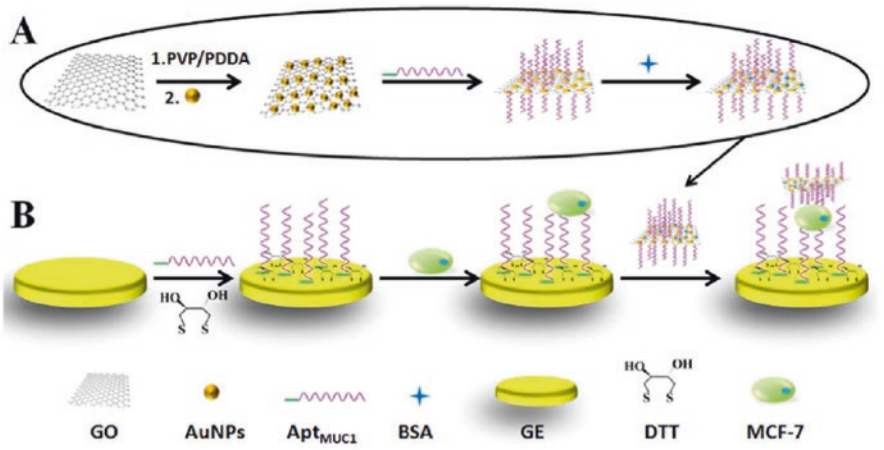

Fig. 3 Representation of aptasensor for MCF-7 quantification. (**a**) AuNPs/GO hybrid was prepared by self-assembly of AuNPs/GO (**b**) AptMUC1 was constructed on AuNPs/GO hybrid. (Reprinted from [34] with the permission of Elsevier)

cells. A wide linear range was observed between 10 and 10^5 cells/ml with a LOD of 8 MCF-7 cells/ml in spiked human serum samples.

In this chapter, we have focused MIP-based sensors for the detection of breast cancer biomarkers by electrochemical methods.

2 Clinical Diagnosis of Breast Cancer

Breast cancer is detected either with screening tests or some symptoms. Early-stage breast cancers are mostly asymptomatic and can be found by chance during screening. Screening of healthy women is important as it causes the detection of smaller tumors, which have a lower possibility to metastasize, are more easily removed by surgery, and will not require any further medical therapy [35].

2.1 Breast Examination

A breast exam is moderately sensitive but highly specific for breast cancer detection, and the degree of predictivity changes with age. Sensitivity is 57–83% between 50 and 59 years and around 70% between 40 and 49 years. Specificity on the other hand is higher, 88–96% between 50 and 59 years and 70–85% among women of age 40–49 years. It is more beneficial in younger women, as the use of mammography is not recommended in these women.

2.2 Mammography

Mammography is the gold standard method for screening and diagnosis of breast cancer and is also the only screening modality that is known to reduce mortality. Sensitivity is 46–80%, while specificity reaches up to 82–99%. The false negativity rate is among 10–15%, reaching up to 40% in patients with dense breasts. Almost 60% of false-positive results in women between 40 and 50 years of age can be seen, while the false positivity ratio decreases with increasing age. The average age for initial mammography scanning is suggested as 45 years, while other personal differences and physicians' recommendations are also to be kept in mind. A clinical abnormality on palpation should be considered in a normal mammogram, and further investigation with other methods like ultrasonography, needle aspiration, and conventional open biopsy is needed [36, 37].

2.3 Digital Mammography

In recent years, digital mammography has come to the front of diagnosis. The power of prediction of this method is not proven to be better than the analog type, but in the premenopausal era, and with women aged below 50 years having dense breasts, the diagnostic efficiency is superior when compared to conventional mammography. When digital breast tomosynthesis is combined with a full-field digital mammogram, it also reduces false positivity and enhances the detection rate. The only disadvantage of digital tomosynthesis combined with screening is that the radiation dose to which the patient is exposed is multiplied by two [38, 39].

2.4 Ultrasound

Ultrasonography is a non-ionizing, patient-friendly method; its predictive value is lower when compared to a mammogram. It may not catch low-level calcifications so it is less efficient alone for screening. It can be considered a supporting tool when a mammogram is not enough to clarify a diagnosis with asymmetry and dense breasts. Breast cancer in ultrasound images is seen as a solid irregular nodule, having imprecise margins and spikes with heterogeneous internal echoes [40].

2.5 Magnetic Resonance Imaging (MRI)

Magnetic resonance imaging is a new tool of diagnosis with increasing importance recently. It has greater sensitivity in breast cancer detection, but false-positive rates are still high with this technique. It is needed when the suspected lesion cannot be

identified by other imaging techniques, in patients having BRCA1 and BRCA2 mutations, and in monitoring response to neoadjuvant chemotherapy, to evaluate the integrity of the prosthetic breast after surgery and in diagnoses of masked breast cancer lesions [41, 42]. The use of MRI together with mammography has a superior sensitivity for malignant tissue (92.7%) than the use of ultrasound combined with mammography (52%). Especially for women with a lifetime risk of breast cancer >20%, breast MRI together with mammography is recommended by the ACS [43].

2.6 Biopsy

In clinical applications, suspected tissue is generally examined by fine needle or core needle biopsy, or by surgical removal. Fine needle biopsy (FNAB) is a simple, low-cost, and outpatient method. It is generally ultrasound-guided, but it does not give information about invasion or histological grade. The false-positive rate is under 2%. Core needle biopsy (CNB) is carried out with a bigger needle and automated equipment, and it has nearly 100% sensitivity and specificity. It is also an outpatient procedure carried out under local anesthesia. Mammotomy is also possible with CNB which rotates the cannula and cuts a piece of breast tissue. CNB and mammotomy allow the assessment of invasion, histological class, and immunohistochemical pattern. Also, a plan for therapy options before the operation becomes possible [44, 45].

2.7 Pathological Evaluation

Tissue specimens obtained by biopsy or mammotomy are subjected to immunohistochemical and molecular diagnostic tests for tissue characterization.

2.8 Prognosis

Immunohistochemistry (IHC) is used to classify and control breast cancer. The main prognostic factors for breast cancer include axillary lymph node status, tumor size, histological type and grade, hormone receptors, and human epidermal growth factor receptor 2 (HER2) (c-erbB2). Tissue-derived markers, such as the progesterone receptor (PR), expression of estrogen receptor (ER), and human epidermal growth factor receptor 2 (HER2), are crucial in tumor subtyping, prognostic evaluation, and systemic treatment selection. Immunohistochemical analysis is routinely carried out to detect estrogen receptor (ER), progesterone receptor (PR), and Her2/neu (HER2) status. These histological tumor markers show significant intratumoral variations. In situ hybridization can confirm HER2 amplification by IHC or as gene

sequencing. DNA microarrays and high-throughput RT-PCR assays for ER and PR-related genes are also important classifications and detection of tumor type [46–48].

2.9 Estrogen Receptor

Estrogen is the major steroid hormone in breast cancer proliferation and progression. It is the predominant hormone in the luminal epithelium, which is the masse-cuite of neoplastic transformation. The ER, in particular, is thought to be of great importance, predicting approximately 50–75% response rate to hormonal therapy. ER's usefulness as a biomarker stems from its dependence on binding to estrogenic ligands, such as 17β-estradiol used in the signaling pathway. The prognosis of ER+ breast cancer is better than ER-negative ones. Still, nearly 30% of patients are likely to have a relapse under chemo-adjuvant therapy [49–51].

2.10 Progesterone Receptor

PR expression is also a significant prognostic biomarker in breast cancer progression. PR is a gene target stimulated by ER and it is a regulator of the estrogen receptor. It is expressed in more than 50% of ER+ cancers. Low or no expression of PR in ER+ cancers is related to a more aggressive also highly proliferative disease, with a worse prognosis and worse clinical features. When PR agonists like progesterone and progestin are used, PR associates with ER and regulates ER chromatin binding in cancerous cellular nuclei, forming a gene expression pattern match that leads to better clinical outcomes [52, 53].

2.11 Human Epidermal Receptor 2 (HER2)

The human epidermal receptor 2 protein (HER2/c-ErbB2) belongs to the ErbB family, which involves plasma membrane-bound receptor tyrosine kinases. C-erbB2 is the growth factor receptor encoded by HER2 proto-oncogene, and it is overexpressed in breast cancer. HER2 dimers phosphotyrosine residues in the cytoplasm and triggers the signaling cascades of Ras/MAPK, PI3K/Akt, and STAT pathways, which as a result promotes cellular proliferation, migration, and adhesion and enhances the life span of cells. The detection of HER2 overexpression is both a prognostic and a predictive indicator. Nearly 15–20% of all breast cancers tests response are positive for the HER2 gene. Multivariate analyses also have shown a correlation between HER2 gene amplification and poor clinical outcome,

pinpointing ER2 as a prognostic factor. HER2 is also a predictive histological marker, as evaluation of HER2 status is a key component in the classification of patients into different therapy regimens [54, 55].

2.12 Ki67

Ki67 is a relatively new prognostic marker for breast cancer. It is a cell proliferation marker and is expressed in cellular nucleoli. Ki67 expression is related to tumor grade, mortality rate, disease-free survival, and distant metastasis. When there is a 20% increase in Ki67 expression after neoadjuvant therapy, the disease-free and overall survival rates will be lower when compared to patients with stable or decreasing Ki67 expression [56, 57].

2.13 Staging

Breast cancer staging was made by TNM system (**T**umor size, Lymph **N**ode status, **m**etastases) in the year 2018 [58]. Since then, tumor grade, estrogen receptor status, progesterone receptor status, and HER2 status have been added to the classification criteria. Table 1 is a general table showing the meaning of different stages. The basic and non-detailed staging of breast cancer is summarized in Table 2.

2.14 Grading

The histological grade is done according to tumor differentiation, nuclear grade, and several mitoses. A grade is attributed to every parameter, and the total score ascertains if the tumor is graded as I, II, and III. The 5-year survival rate of grade III cancers is around 35%.

Table 1 The clinical meaning of the cancer stages

Stage	Clinical meaning
Stage 0	Abnormal cells are present
Stage I, stage II, and stage III	Cancer is present
Cancer	Cancer has spread to distant parts of the body

Table 2 TNM cancer stages

Tumours	T0/Tis	T1	T2	T3	T4
Tumour size	T0: No primary tumour Tis: tumour only in breast ducts or lobules	≤2 cm	>2–≤5 cm	>5 cm	Tumour of any size with extension to chest wall/skin (ulceration or skin nodules)
Nodes	N0	N1	N2	N3	
	N0 lymph node metastases	Metastases in 1–3 axillary lymph nodes	Metastases in 4–9 axillary lymph nodes	Metastases in infra- or supraclavicular lymph nodes or in ≥10 axillary lymph nodes	
Metastasis	M0	M1			
	No evidence of cancer metastasis	Cancer found in other areas of body			

3 Clinical Treatment for Breast Cancer

3.1 Surgery

The first-choice treatment option for locoregional breast cancer is surgery. At the beginning of the 1900s, breast cancer was mostly treated by radical mastectomy together with removal of lymph nodes in the axilla and excision of both major pectoral muscles. This technique was then replaced by breast conservation surgery (BCS) when the survival after lumpectomy and radiation seemed to be equal to that of radical mastectomy. Also, it is now well understood that breast cancer is not a local disease as it spreads by micrometastases via the bloodstream, so lymphadenectomy would not increase survival and it can only be accepted as a prognostic factor. Advanced breast cancer screening resulted in the detection of non-palpable carcinomas, bringing together the settlement of a localization approach for surgery. Later, the development of various systemic interventions like chemotherapy and adjuvant and endocrine therapies led to the search for less aggressive and harmless techniques for controlling the localized disease. Rather than removing the axillary lymph nodes, sentinel lymph node biopsy (SLNB) introduced in 1994 by Giuliano is a great advance in breast cancer surgery as the procedure has >98% accuracy with negative results and no more dissection is carried out. Also, with positive SLNB results, complete axillary lymph node removal is of no use for enhanced locoregional control and overall survival. This procedure is more comfortable than complete axillary dissection as the risk of lymphedema is much lower [59–61].

3.2 Radiation

Radiation has an important part in local disease control. Radiation therapy is beneficial in large tumors above 5 cm or if the tumor has invaded the skin or chest muscle and lymph nodes are positive. Radiation is also a good palliative therapy option for tumors metastasized to the central nervous system (CNS) and bones [62, 63]. It is also effective in the treatment of stage 0 carcinoma (ductal carcinoma in situ). Radiation therapy can also control nodal disease in high-risk patients with advanced-stage cancer. Patients generally receive post-mastectomy radiation if they have ≥4 positive axillary lymph nodes, T3 tumor size, and positive surgical margins, also with locally advanced or inflammatory breast carcinoma. Radiation will be useful for patients with lymphovascular invasion, younger age, higher-grade tumors, or hormone receptor-negative (triple-negative breast cancer) [64–66].

3.3 Medical Oncology

Hormone receptor evaluation is routinely done to estimate prognosis and estimation of response to endocrine treatment. Estrogen and progesterone receptors and HER2/neu are analyzed by IHC. Breast carcinomas are divided into luminal (ER+ and/or PR+), triple-negative (ER−, PR−, and HER2−), and HER2+ types on a molecular basis. Luminal carcinomas have the best, while triple-negative carcinomas have the worst prognosis. Treatment and medication regimens are planned according to these analyses. Chemotherapy, hormone therapy, and targeted therapy are the applicable treatments for breast cancer [67].

3.4 Adjuvant Chemotherapy

Adjuvant chemotherapy following initial surgery is highly recommended for patients at risk of recurrence. Cyclosporine, taxanes (docetaxel and paclitaxel), and anthracyclines (epidoxorubicin and adriamycin) are mostly used in chemotherapy pharmaceuticals. There is a 25% reduction in relapse risk over 10–15 years of time with the use of first-generation chemotherapy drugs like cyclophosphamide, methotrexate, and 5-fluorouracil (CMF) for a 6-month cycle. The mortality caused by breast cancer is also decreased by 30% over 15 years [67, 68].

3.5 HER2-Directed Therapy

Trastuzumab increases the survival of patients (who have HER2+ breast cancer) if early-stage cancer occurs and is strongly recommended to be administered along with chemotherapy. The drug is a monoclonal antibody of HER2 which is useful in patients with overexpressed HER2 genes. In metastatic cancer, trastuzumab used together with taxanes is known to improve survival. Because of the cardiotoxic effects of anthracycline and trastuzumab-containing medications, non-anthracycline and taxane-containing drugs can be the drugs of choice. Together with any chemotherapy regimen, trastuzumab should be administered for 1 year, with cardiac testing every 3 months. Pertuzumab which is a monoclonal antibody targeting a different site of HER2 receptor can also be considered by physicians [69, 70].

3.6 Endocrine Therapy

Patients with ER+ or PR+ breast cancers should receive endocrine therapy. Aromatase inhibitors are the drugs of choice. If the risk of osteoporosis is high in the patient or aromatase inhibitors are not well tolerated, tamoxifen can be used. The treatment response is better when the tumor is both ER and PR positive. Treatment starts after chemotherapy is finished. The common regimen for endocrine therapy is tamoxifen at a dose of 20 mg/day administered orally for 5 years and can be prolonged to 10 years if necessary. Tamoxifen is a competitive estrogen receptor antagonist. It's contraindicated in patients who had a previous deep vein thrombosis (DVT). Recently, it is clarified that third-generation aromatase inhibitors are more beneficial for recurrence reduction in comparison with tamoxifen in the postmenopausal period. So, aromatase inhibitors are better included in endocrine therapy in postmenopausal women. After menopause, the main production pathway of estrogen is the peripheral conversion from androgens by aromatase, an enzyme located predominantly in adipose tissue. That's why aromatase inhibitors are more beneficial, as they seize the production of estrogen, while tamoxifen deactivates the already produced hormone [71–73].

3.7 Therapy for Metastatic Disease

The metastatic disease is accepted to be incurable, so the goal of therapy in metastatic patients is to extend life span and minimize symptoms and side effects. Patients with ER+ or PR+ and HER2 breast cancers generally have endocrine therapy several times before getting single-drug chemotherapy. Taxane together with trastuzumab or pertuzumab is needed to be given to patients with HER2+ metastatic breast cancer. Latest therapies mostly include trastuzumab-memantine, lapatinib, or

trastuzumab combined with single chemotherapy drugs. The single and efficient choice of treatment for patients with ER−, PR−, and HER2− (triple-negative) breast cancer remains to be chemotherapy [74–76].

4 Important Tumor Markers for Breast Cancer

A tumor marker is defined to be any substance found in blood, urine, or any other body fluids that are elevated by any type of cancer. The tumor itself can produce a tumor marker, or its level is raised as a host defense against a tumor. An ideal tumor marker will have high specificity and sensitivity to detect low tumor burden to be useful in early diagnosis and screening [77]. Tumor markers are most useful in monitoring disease progression after chemotherapy and radiotherapy cycles are completed to evaluate the efficacy of different treatment options. From a clinical perspective, both primary and recurring breast cancer are needed to be detected early, as treatment decisions can be made while the tumor burden is not high, and when patients are candidates to respond to adjuvant therapy. Recently, the serum tumor marker levels are used to determine tumor activity. Tumor markers are minimally invasive, low-cost tools, and they provide data priceless for disease follow-up, prognosis, and therapy options [78, 79].

The tumor markers with the highest clinical utilization and suggested for use in follow-up involve CA 15-3, CA 27-29, CEA, ER, PR, and HER2 [80].

Among these, HER2, ER, and PR are immunohistochemically detected markers that have mostly prognostic values as discussed above.

4.1 Serum Markers

CA 15-3, CA 27-29, and EA are serum markers that can be used in breast cancer. CEA is a glycoprotein cell surface receptor used as a common tumor marker for colorectal, gastrointestinal, lung, and breast cancers. CEA is helpful in diagnosis, staging, post-surgery recurrence, and treatment monitoring in patients undergoing chemotherapy/radiotherapy. CA 15-3 detects MUC1 protein which is the most widely used serum marker in breast cancer patients. Its detection is very important for the early detection of recurrent or metastatic disease [81]. The other serum marker is the CA 27–29 which has been approved by the US FDA for monitoring of breast cancer [82].

4.2 Diagnostic Markers of Breast Cancer

4.2.1 BRCA1/BRCA2 Mutations

Breast carcinoma has subtype types which vary in the site they appear and their potential for invasion. Most breast cancers are sporadic meaning that they do not have any family cancer histories or genetic vulnerabilities. However, approximately 15% of breast cancers are classified as familial in which a patient's first- or second-degree relatives are affected. Nearly 10% of breast cancer cases are caused by inherited germline mutations in proto-oncogenes. Today, over 25 tumor-suppressing genes are known to be related to hereditary breast cancer which takes part in genome-stabilizing pathways, especially in DNA repair. BRCA1 and BRCA2 are two well-defined and highly penetrant tumor suppressor genes. Mutated BRCA1 and BRCA2 genes are detected in nearly 25% of inherited breast cancer cases [83–87].

BRCA1 and BRCA2 are producing elements for the repair of double-stranded DNA breaks. BRCA1 mutation mostly causes the development of triple-negative breast cancer (TNBC) with a high proliferation rate. On the other hand, BRCA2 mutation carriers tend to develop ER + or PR+ breast cancers. In a recent study, it was proposed that patients with germline BRCA1/2mut ER+ genes had a higher risk of recurrence and cancer-caused mortality in comparison with noncarriers. BRCA gene mutations cause the chromosomes to be unstable, and chromosome breaks are accepted to be predictive biomarkers. BRCA1 and BRCA2 complex with various proteins which protect the genome through damage signal control and initiate maintenance by different effectors [88–90].

Extensively proliferated cancer needs higher oxygen use and, when combined with inadequate blood supply to the tumor, causes tissue hypoxia [91–93].

DNA extraction from peripheral blood samples and polymerase chain reaction (PCR) analysis is routinely carried out to detect BRCA1 and BRCA 2 mutations. Negative control DNA is extracted from a patient without any BRCA mutations. Oligonucleotide primers of known sequences are used and DNA is amplified. Positive control DNA is obtained from BRCA mutation carriers' blood. Both control DNAs are fragmented by restriction enzyme digestion and proofed by DNA sequencing. Negative control, positive control, and blank sample without any DNA (contamination check) are studied in each batch [94].

Direct genetic screening and PCR analysis are expensive procedures. As an alternative, immunohistochemistry (IHC) for *BRCA* is a less-complicated, easy to perform, and cheaper protocol that is applied in the most pathological laboratories [95, 96].

BRCA1 and BRCA2 mutation analysis can be done at the time of diagnosis, so BRCA mutation status has to be evaluated in treatment and determination of preventive precautions for carriers of this mutation. Women who are candidates for BRCA mutation-associated breast cancer are candidates for either breast-conserving surgery or double mastectomy [97].

MIP technology was applied for the first time for the detection of BRCA1 by You and coworkers with gold nanoparticle-reduced graphene oxide-modified glassy carbon electrode covered with the layer of MIP synthesized with rhodamine B as a template, methacrylic acid as the monomer, and nafion as additive (Fig. 4) [98]. DNA probes were constructed on SiO_2@AgNPs to form SiO_2@Ag/DNA. The hybridization process was performed with rhodamine B-labeled DNA and SiO_2@Ag/DNA. All conditions were optimized, and the developed biosensor showed linear behavior between 10 fM and 100 nM with a low detection limit of 2.53 fM. The application procedure was applied in serum samples, and results showed that the developed biosensor could be successfully applied in clinical diagnostics.

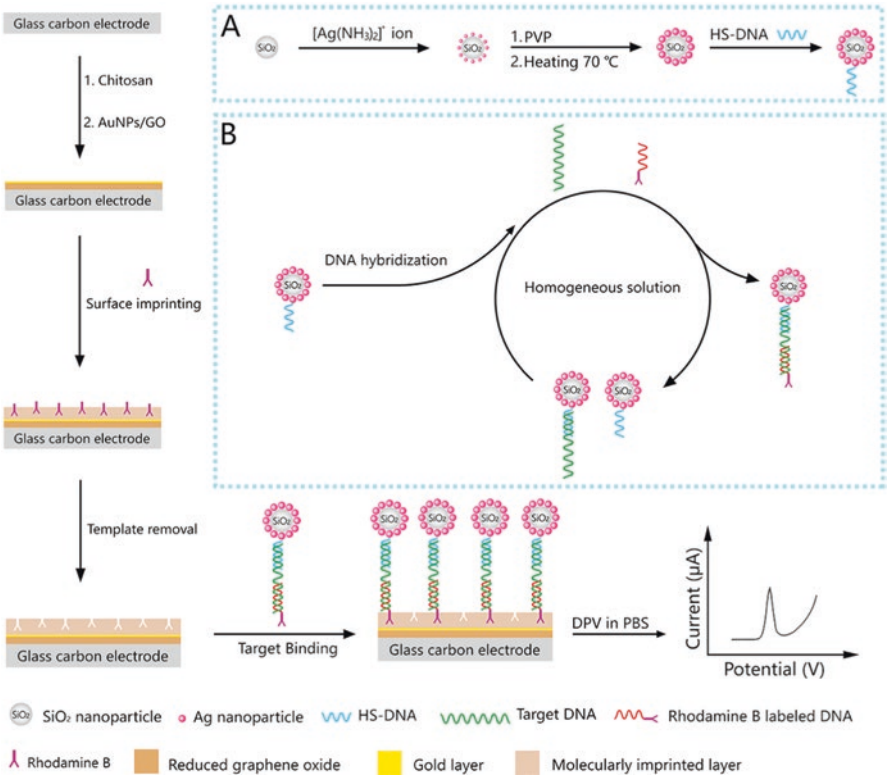

Fig. 4 The fabrication of MIP-based biosensor for the detection of BRCA1. Inset of (**a**) representation of SiO_2@Ag/DNA (**b**) the hybridization of DNA. *AuNPs-GO* gold nanoparticle-reduced graphene oxide, *PVP* polyvinylpyrrolidone, *HS-DNA* human serum DNA, *SiO_2* silicium dioxide, *PBS* phosphate buffer saline. (Reprinted from [98] with the permission of Elsevier)

4.2.2 Human Epidermal Receptor 2 (HER2)

The proto-oncogene HER2/neu (C-erbB2) has been localized to chromosome 17q and encodes a transmembrane tyrosine kinase growth factor receptor. It is well known that HER2-positive tumors are more aggressive and generally have a higher grade with a high proliferative rate. HER2 gene amplification and its receptor protein overexpression are known to be associated with poor prognosis [99, 100].

In current practice, HER2 is assessed by IHC to evaluate protein expression and/or by fluorescence in situ hybridization (FISH) method to evaluate gene amplification. Immunohistochemically staining is graded in a semiquantitative manner, with no (0) to incomplete, faint (1+) membrane staining being negative; incomplete and/or weak/moderate (2+) membrane staining being equivocal; and complete, intense (3+) membrane staining being positive [101]. When IHC 2+, it indicates there is indeterminacy in the Her2/neu protein expression; FISH, which is considered a gold standard, evaluates HER2 gene amplification at the DNA level. HER2 status confirmation has become a very important step in breast cancer as it is critical for both prognosis and defining therapy alternatives. Anti-HER2 treatments are effective in HER2-positive breast cancers, especially monoclonal antibodies like trastuzumab. These drugs have significantly improved the prognosis of patients with or without metastasis, as described above in the "treatment section." Therefore, correct detection of Her2/neu with high sensitivity and specificity is critical. The recent ASCO/CAP 2013 criteria are used in the detection of Her2/neu in the diagnosis, prognosis, treatment, and management of breast cancer [102].

The extracellular domain of the human epidermal growth factor receptor 2 (HER2-ECD) is a protein breast cancer biomarker, and its determination from peripheral blood is important for diagnosis. Pacheco and coworkers developed a HER2-ECD biosensor that is MIP-based gold screen-printed electrode (Fig. 5) [103]. Phenol was chosen as a monomer; electropolymerization was applied for the polymerization of the monomer. The characterization study of the sensor was applied with cyclic voltammetry and electrochemical impedance spectroscopy. The

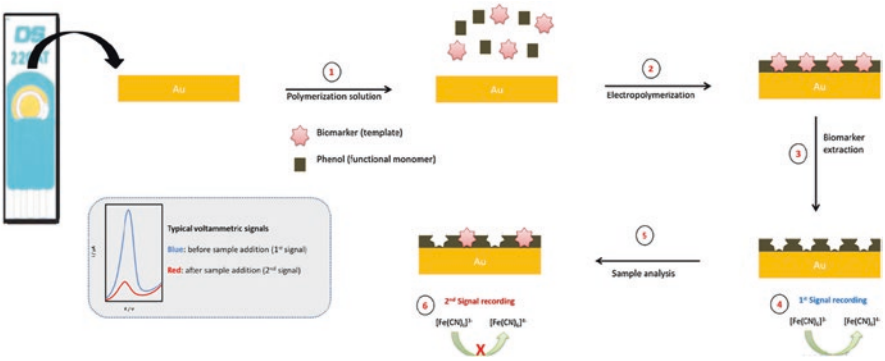

Fig. 5 Representation of MIP/AuSPE for the quantification of HER2-ECD. (Reprinted from [103] with the permission of Elsevier)

quantification of HER2-ECD was performed by differential pulse voltammetry using a ferri/ferro redox probe. The calibration study resulted in a 10–70 ng/ml linear range with a LOD of 1.6 ng/ml and LOQ of 5.2 ng/ml. The selectivity of the sensor was tested with selected molecules, and the proposed sensor was found as selective. The recovery was achieved with adequated values.

4.2.3 Serum Tumor Markers of Breast Cancer: Carcinoembryonic Antigen (CEA) and Cancer Antigen (CA) 15-3

Serum tumor biomarkers may have potentially useful applications in many clinical settings, such as tumor staging, and treatment monitoring recurrence detection during follow-up [104].

Breast cancer is the second most common type of cancer worldwide. The disease is heterogeneous, caused by various genetic and environmental factors and several risk factors. In recent years, serum tumor marker levels have been widely utilized to detect tumor activity. Tumor markers give the possibility of a minimally invasive low-cost source of data amenable for monitorization of disease, prognosis, and helpful treatment plans. Individual test specifications and limitations for each tumor marker should be well known for optimal use of these markers and a better understanding of results [79].

The tumor markers accepted for clinical utilization and recommended for use in the routine are CA 15-3, carcinoembryonic antigen (CEA), estrogen receptor (ER), progesterone receptor (PR), and human epidermal growth factor receptor 2 (HER2). ER, PR, and HER2 have been described in the above sections, and they are immunohistochemical markers. Among serum markers, CEA and CA 15-3 come to the front.

Electrochemical methods are sensitive and rapid, but selectivity may be a problem for some applications. MIPs are interesting materials for solving selectivity problems in systems. According to one study in 2018, 2-aminophenol was polymerized for MIP fabrication with CA 15-3 (Fig. 6) [105]. MIP was fabricated on AuSPE in two ways: firstly, CA 15-3 was absorbed on the bare electrode surface, AuSPE, and, secondly, there is electropolymerization of 2-aminophenol around the CA 15-3 on the surface of AuSPE. For the evaluation of the performance MIP-based developed sensor, an extraction step was applied, and the difference between the before and after template signal magnitudes was evaluated in ferri/ferro redox solution. The proposed sensor was investigated by the obtained responses of MIP and NIP via voltammetry and electrochemical impedance spectroscopy. The linearity behavior was observed between 5 and 50 U/mL with a detection limit of 1.5 U/mL. Selectivity of the developed sensor was checked with HER2 and cysteine (Cys), a biomarker of kidney function; as a result, HER2 had some interference. The developed sensor gave a response in a short time like 15 min. Hence, the sensor could be integrated into a small portable point of care device.

Poly(toluidine blue) is a conducting polymer; it was used for the MIP formation as a synthetic receptor for the detection of CA 15-3 on the AuSPE surface [106].

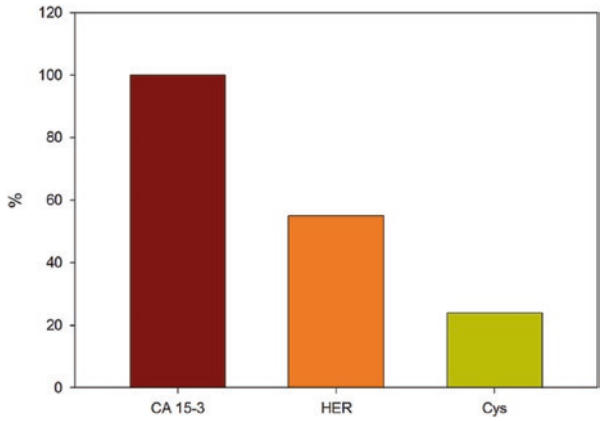

Fig. 6 Selectivity study of MIP/AuSPE. *HER* human epidermal growth factor receptor, *Cys* cysteine. (Reprinted from [105] with the permission of Elsevier)

The binding affinity of the MIP system against NIP was found as higher than 12-fold. Differential pulse voltammetry was applied, and the linear range was observed between 0.10 U/ml and 100 U/ml with 0.1 U/ml LOD in a neutral buffer solution. Serum samples were used for the application of the developed sensor. The rapid, sensitive, and selective sensor was obtained with satisfactory recovery results.

O-phenylenediamine is the most popular monomer; it is used in many studies for the selective determination of analytes. CA15-3 was detected by the electrochemical polymerization of o-phenylenediamine on the AuSPE surface [107]. The surface was characterized by Raman and atomic force microscopy. The developed device showed linearity between 0.25 U/mL and 10 U/mL with 0.05 U/mL LOD. The CA15-3 detection was successfully applied from PBS buffer and serum samples.

In another study, pyrrole was electropolymerized around the CA15-3 marker on a fluorine-doped tin oxide (FTO) conductive glass [108]. Ethanol was used for the removal of CA15-3 from the MIP cavity. The analysis procedure was performed in a 4-(2-hydroxyethyl)-1-piperazineethanesulfonic acid (HEPES) buffer, of pH 6.5. According to a calibration study, LOD was found as 1.07 U/mL for CA 15-3, with a linear response from 1.44 to 13.2 U/mL. The applicability of the developed sensor was tested in spiked serum samples with high accuracy.

4.2.4 Carcinoembryonic Antigen (CEA)

Carcinoembryonic antigen (CEA) is the most extensively utilized tumor marker in the clinical setting. CEA family in humans is well characterized. It consists of 29. 18 of these genes are expressed; 7 of them belong to the CEA subgroup and 11 of them are included in the pregnancy-specific glycoprotein subgroup. Members of the CEA subgroup are associated with the cell membrane, and they are selectively expressed in the epithelial cells. 45–50% of CEA is composed of carbohydrate moieties. It is a

single polypeptide chain that contains 641 amino acids, and the N-terminal position contains lysine amino acids. It is well known that invasion and metastasis of cancer cells are associated with adhesion mechanisms. CEA may play an important role in the alteration of cellular adhesion because of its epithelial properties [109, 110]. A continuous rise in CEA levels in breast cancer patients can be a sign of recurrence or poor response to treatment. For evaluation of recurring disease after treatment, 5 months for an increase in CEA levels will be beneficial. CEA levels are also higher in patients with end-stage or metastatic disease when compared to ones with local disease. For screening of the general asymptomatic population or initial cancer diagnosis in a high-risk group, CEA level determination will not be sufficient as it has relatively low sensitivity and specificity. CEA is better to be used to help with diagnosis, postoperative recurrence, clinical staging, and monitoring of the therapeutic response in patients receiving medical or radiation therapy [111].

In metastatic patients, CEA levels are elevated. Preoperative CEA levels are also well correlated with pathological stage and tumor burden. The size of the tumor (primary or metastatic) is also directly proportional to blood CEA levels. Lately, CEA is being replaced by more specific markers, such as CA 15-3. Single use of CEA is known to be nonspecific for breast cancer diagnosis. The combined usage of CEA and CA 15-3 together with clinic pathological parameters will be more accurate for the detection of metastasis in breast cancer patients [112].

4.2.5 Cancer Antigen (CA) 15-3

CA 15-3 is a carbohydrate-containing protein antigen called mucin (MUC). CA 15-3 belongs to the MUC1 family. Although the MUC1 gene is found in several tissues, its core protein is identical among tissues. Differences in the level of glycosylation (carbohydrate content) are used for the discrimination of the protein among different tissues. The carbohydrate content of breast tissues is quite high, nearly about 50%. Even though the physiological significance of MUC1 proteins is not well understood, they are considered to reduce cell-to-cell interaction and inhibit the lysis of tumorous cells. The CA 15-3 is so-called because of a combination of its molecular composition and the assays developed to detect it. The numbers 15-3 represent the antibodies utilized in immunoassay detection of the antigens.

There is an overexpression of the MUC1 gene in breast malignancies, which allows the use of gene product CA 15-3 as a tumor marker in this disease. CA 15-3 is accepted as a specific blood marker for breast cancer because of its higher specificity to breast tissue when compared with CEA. Still, it should be kept in mind that CA 15-3 levels also increase in other malignancies such as the cancers of the pancreas, lung, ovaries, colon, and liver. CA 15-3 levels were also found to be elevated in benign breast diseases which comprises a false positivity. Like CEA, CA 15-3 is also a more powerful marker in the determination of prognosis and monitorization of treatment efficiency in breast cancer. CA 15-3 serum levels also correlate with disease severity (stage) and/or with tumor size. It is also reported to be an independent prognostic factor in metastatic breast cancer patients [113, 114].

4.2.6 Detection of CEA and CA 15-3 in Serum

The reference range of CEA in the healthy population is accepted as <3.0 ng/mL for nonsmokers, 3.0–5.0 ng/mL for smokers, gray zone between 5.0 and 10 ng/mL, and >10 ng/mL for cancer. CA 15-3 is measured in units per milliliter (U/mL). A normal test should be less than or equal to 30 U/mL.

CEA and CA 15-3 determination are available on numerous automated analysis platforms. Due to the highly heterogeneous nature of polyclonal antibodies used for detection of these markers, it is suggested that the same assay will better be used for serial monitoring. The major principle is that immunoassays are based on detection by antigen-antibody binding. Generally, two-site immunoenzymatic sandwich assays are commonly used. The most commonly used techniques are chemiluminescent microparticle immunoassay (CMIA) and electrochemiluminescence immunoassay (ECLIA). The 95% level of confidence and measuring range for both assays are around 0.5–1500 ng/mL. Both assays have high sensitivity and specificity of over 90%, with diagnostic sensitivities greater than 95%, and they can be used in routine analysis of tumor markers in serum with different available autoanalyzer systems found in routine laboratories [115].

4.2.7 Co-evaluation of CEA and CA 15-3 Levels in Breast Cancer

Serum tumor markers have critical roles in disease screening, early detection of recurring disease, and monitorization of treatment in a variety of cancers when used together with traditional pathological factors like size and grade of tumors, lymph node status, and molecular biomarkers like hormone receptor status and HER2 expression. CEA and CA15-3 are the two most commonly used serum tumor markers of breast cancer in the clinical setting for over 30 years. Recently, the prognostic value of preoperative evaluation of the levels of these serum markers in breast malignancies has gained much attention. Studies have shown that combined evaluation of levels of these two markers before the operation will provide useful information for the diagnosis and treatment of patients. CEA and CA 15-3 are complementary to one another as CEA has superior sensitivity of around 75%, while CA 15-3 is more specific (around 97%) to breast cancer. The combined usage of these two markers has yielded the highest diagnostic accuracy. The European Group on Tumor Markers has suggested co-evaluation of CEA and CA15-3 levels for prognosis, early progression, and treatment monitorization in breast cancer. But, single utilization of both markers for screening and diagnosis of early breast cancers without metastasis is limited to an extent because of relatively low sensitivity and specificity [111, 116].

Serial measurements of these markers in combination are useful for detecting or monitoring treatment efficiency in metastatic breast cancer patients because there usually is an elevation of the levels of these markers above the normal range in this group. In addition to their value in diagnosis and monitorization, increased levels of CEA and CA 15-3 at the time of systemic breast cancer recurrence are known to be

correlated strongly with patient prognosis. Since serum biomarkers are relatively easy, minimally invasive, and low cost, serial measurement of these markers can provide useful information for earlier detection of recurring diseases [113].

4.2.8 Tumor Marker Velocity

The major applications of serum tumor markers are known to be monitoring prognosis and disease response to treatment. Clinicians accept that the serial measurement of tumor markers in the blood is a simple test that can help the detection of recurrence within 9 months. Among the serum tumor markers evaluated for breast cancer, CA 15-3 and CEA come to the front as the two most sensitive and widely used ones. In recent years, a term known as "tumor velocity," meaning the rate of the tumor marker increase in 1 year, is trying to be incorporated into clinical practice in detecting recurrence of breast cancer surveillance. Tumor marker velocity has been used for prostate cancer antigen (PSA) since 1992 for follow-up of the annual increase in PSA levels. Similar dynamics for tumor markers have not been defined for breast cancer yet. Evaluation of serum markers is a quick and relatively easy procedure with a high positive predictive value. That's why a routine detection of CEA and CA 15-3 could be useful in the early detection of recurring cancer. Also, an increase above the highest level of the reference range in either of the levels of these markers during surveillance will be a sign of locoregional or distant organ metastasis in breast cancer. Tracking of marker levels for surveillance will be appropriate in 3–4-month intervals to detect early subclinical recurring disease. The serial detection of tumor markers should better be done in every 3–4 months, at least for a year. With a total time of 18 months, follow up with serial tumor marker measurement, up to 60% detection rate of recurrence before any signs of clinical and/or radiological recurrence is found by elevation of the level of these markers. The optimal cutoff values for CA 15-3 and CEA velocity are 2.5 U/mL/year and 1.2 ng/mL/year, respectively. Patients with either CA 15-3 velocity over 2.5 U/mL/year or CEA velocity greater than 1.2 ng/mL/year can be accepted to be nearly 40 times more prone to have recurring cancer. Tumor marker velocity might be a helpful contribution to absolute tumor marker measurements in discriminating between clinically important elevations in the level of these markers from baseline values. This in turn might be helpful in refining the clinical utilization of serial measurements of CA 15-3 and CEA for follow-up of surveillance in breast cancer [113, 117–119].

5 Conclusion

This chapter has attempted to outline breast cancer biomarkers. Clinical and imprinting polymer technology applications are reported briefly. Clinical procedures take a long time and heavy workload, requirement of many personnel, and expensive

devices. The progress in the molecularly imprinting technology showed that the sensitive, fast, and selective detection of breast cancer markers has been achieved with electrochemical methods. Their cheap, stable, and long-life features make them preferred. In recent years, breast cancer biomarkers could be easily detected with developed electrochemical molecular imprinted polymers based on disposable small devices.

References

1. Cancer. https://www.who.int/health-topics/cancer#tab=tab_1. Accessed 3 Apr 2022.
2. Asia S, Asia S, Hdi H. Source: Globocan. 2020;419:1–2.
3. Ruddy KJ, Winer EP. Male breast cancer: risk factors, biology, diagnosis, treatment, and survivorship. Ann Oncol. 2013;24:1434–43. https://doi.org/10.1093/ANNONC/MDT025.
4. Parada H, Sun X, Tse CK, et al. Lifestyle patterns and survival following breast cancer in the Carolina breast cancer study. Epidemiology. 2019;30:83–92. https://doi.org/10.1097/EDE.0000000000000933.
5. Board PS and PE. Breast cancer screening (PDQ®). PDQ Cancer Inf Summ. 2021:22–4. https://www.cancer.gov/types/breast/hp/breast-screening-pdq.
6. Gucalp A, Traina TA, Eisner JR, et al. Male breast cancer: a disease distinct from female breast cancer. Breast Cancer Res Treat. 2019;173:37–48. https://doi.org/10.1007/S10549-018-4921-9.
7. Clark BZ, Onisko A, Assylbekova B, et al. Breast cancer global tumor biomarkers: a quality assurance study of intratumoral heterogeneity. Mod Pathol. 2019;32:354–66. https://doi.org/10.1038/S41379-018-0153-0.
8. Narod SA. Personalised medicine and population health: breast and ovarian cancer. Hum Genet. 2018;137:769–78. https://doi.org/10.1007/S00439-018-1944-6.
9. Mahvi DA, Liu R, Grinstaff MW, et al. Local cancer recurrence: the realities, challenges, and opportunities for new therapies. CA Cancer J Clin. 2018;68:488–505. https://doi.org/10.3322/CAAC.21498.
10. McCormack V, McKenzie F, Foerster M, et al. Breast cancer survival and survival gap apportionment in sub-Saharan Africa (ABC-DO): a prospective cohort study. Lancet Glob Health. 2020;8:e1203–12. https://doi.org/10.1016/S2214-109X(20)30261-8.
11. Wang F, Fang Q, Ge Z, et al. Common BRCA1 and BRCA2 mutations in breast cancer families: a meta-analysis from a systematic review. Mol Biol Rep. 2012;39:2109–18. https://doi.org/10.1007/S11033-011-0958-0.
12. Piletska EV, Guerreiro AR, Whitcombe MJ, Piletsky SA. Influence of the polymerization conditions on the performance of molecularly imprinted polymers. Macromolecules. 2009;42:4921–8. https://doi.org/10.1021/MA900432Z/ASSET/IMAGES/MA900432Z.SOCIAL.JPEG_V03.
13. Poma A, Turner APF, Piletsky SA. Advances in the manufacture of MIP nanoparticles. Trends Biotechnol. 2010;28:629–37. https://doi.org/10.1016/J.TIBTECH.2010.08.006.
14. Morelli I, Chiono V, Vozzi G, et al. Molecularly imprinted submicron spheres for applications in a novel model biosensor-film. Sensors Actuators B Chem. 2010;150:394–401. https://doi.org/10.1016/J.SNB.2010.06.046.
15. Scorrano S, Mergola L, del Sole R, Vasapollo G. Synthesis of molecularly imprinted polymers for amino acid derivates by using different functional monomers. Int J Mol Sci. 2011;12:1735. https://doi.org/10.3390/IJMS12031735.

16. Puoci F, Cirillo G, Curcio M, et al. Molecularly imprinted solid-phase extraction for the selective HPLC determination of alpha-tocopherol in bay leaves. Anal Chim Acta. 2007;593:164–70. https://doi.org/10.1016/J.ACA.2007.04.053.
17. Baggiani C, Anfossi L, Giovannoli C. Solid-phase extraction of food contaminants using molecularly imprinted polymers. Anal Chim Acta. 2007;591:29–39. https://doi.org/10.1016/J.ACA.2007.01.056.
18. Ramström O, Mosbach K. Synthesis and catalysis by molecularly imprinted materials. Curr Opin Chem Biol. 1999;3:759–64. https://doi.org/10.1016/S1367-5931(99)00037-X.
19. Suwanwong Y, Boonpangrak S. Molecularly imprinted polymers for the extraction and determination of water-soluble vitamins: a review from 2001 to 2020. Eur Polym J. 2021;161:110835. https://doi.org/10.1016/J.EURPOLYMJ.2021.110835.
20. Vasapollo G, Del SR, Mergola L, et al. Molecularly imprinted polymers: present and future prospective. OPEN ACCESS Int J Mol Sci. 2011;12:12. https://doi.org/10.3390/ijms12095908.
21. Pichon V, Chapuis-Hugon F. Role of molecularly imprinted polymers for selective determination of environmental pollutants–a review. Anal Chim Acta. 2008;622:48–61. https://doi.org/10.1016/J.ACA.2008.05.057.
22. Andersson LI. Molecular imprinting: developments and applications in the analytical chemistry field. J Chromatogr B Biomed Sci Appl. 2000;745:3–13. https://doi.org/10.1016/S0378-4347(00)00135-3.
23. Wei S, Mizaikoff B. Recent advances on noncovalent molecular imprints for affinity separations. J Sep Sci. 2007;30:1794–805. https://doi.org/10.1002/JSSC.200700166.
24. Tamayo FG, Turiel E, Martín-Esteban A. Molecularly imprinted polymers for solid-phase extraction and solid-phase microextraction: recent developments and future trends. J Chromatogr A. 2007;1152:32–40. https://doi.org/10.1016/J.CHROMA.2006.08.095.
25. Haginaka J. Monodispersed, molecularly imprinted polymers as affinity-based chromatography media. J Chromatogr B Anal Technol Biomed Life Sci. 2008;866:3–13. https://doi.org/10.1016/J.JCHROMB.2007.07.019.
26. Lasáková M, Jandera P. Molecularly imprinted polymers and their application in solid-phase extraction. J Sep Sci. 2009;32:799–812. https://doi.org/10.1002/JSSC.200800506.
27. Campuzano S, Pedrero M, Pingarrón JM. Non-invasive breast cancer diagnosis through electrochemical biosensing at different molecular levels. Sensors. 2017;17:1993. https://doi.org/10.3390/S17091993.
28. Miao P, Wang B, Yu Z, et al. Ultrasensitive electrochemical detection of microRNA with star trigon structure and endonuclease mediated signal amplification. Biosens Bioelectron. 2015;63:365–70. https://doi.org/10.1016/J.BIOS.2014.07.075.
29. Cardoso AR, Moreira FTC, Fernandes R, Sales MGF. Novel and simple electrochemical biosensor monitoring attomolar levels of miRNA-155 in breast cancer. Biosens Bioelectron. 2016;80:621–30. https://doi.org/10.1016/J.BIOS.2016.02.035.
30. Moscovici M, Bhimji A, Kelley SO. Rapid and specific electrochemical detection of prostate cancer cells using an aperture sensor array. Lab Chip. 2013;13:940–6. https://doi.org/10.1039/C2LC41049D.
31. Zhu Y, Chandra P, Shim Y-B. Ultrasensitive and selective electrochemical diagnosis of breast cancer based on a hydrazine–Au nanoparticle–aptamer bioconjugate. Anal Chem. 2013;85:1058–64. https://doi.org/10.1021/ac302923k.
32. Azimzadeh M, Rahaie M, Nasirizadeh N, et al. An electrochemical nanobiosensor for plasma miRNA-155, based on graphene oxide and gold nanorod, for early detection of breast cancer. Biosens Bioelectron. 2016;77:99–106. https://doi.org/10.1016/J.BIOS.2015.09.020.
33. Chen M, Wang Y, Su H, et al. Three-dimensional electrochemical DNA biosensor based on 3D graphene-Ag nanoparticles for sensitive detection of CYFRA21-1 in non-small cell lung cancer. Sensors Actuators B Chem. 2018;255:2910–8. https://doi.org/10.1016/j.snb.2017.09.111.

34. Wang K, He MQ, Zhai FH, et al. A novel electrochemical biosensor based on polyadenine modified aptamer for label-free and ultrasensitive detection of human breast cancer cells. Talanta. 2017;166:87–92. https://doi.org/10.1016/J.TALANTA.2017.01.052.
35. Fuller MS, Lee CI, Elmore JG. Breast cancer screening: an evidence-based update. Med Clin North Am. 2015;99:451–68. https://doi.org/10.1016/J.MCNA.2015.01.002.
36. Nazário ACP, Facina G, Filassi JR. Breast cancer: news in diagnosis and treatment. Rev Assoc Med Bras. 2015;61:543–52. https://doi.org/10.1590/1806-9282.61.06.543.
37. Pace LE, Keating NL. A systematic assessment of benefits and risks to guide breast cancer screening decisions. JAMA. 2014;311:1327–35. https://doi.org/10.1001/JAMA.2014.1398.
38. Friedewald SM, Rafferty EA, Rose SL, et al. Breast cancer screening using tomosynthesis in combination with digital mammography. JAMA. 2014;311:2499–507. https://doi.org/10.1001/JAMA.2014.6095.
39. Svahn TM, Houssami N, Sechopoulos I, Mattsson S. Review of radiation dose estimates in digital breast tomosynthesis relative to those in two-view full-field digital mammography. Breast. 2015;24:93–9. https://doi.org/10.1016/J.BREAST.2014.12.002.
40. Brem RF, Lenihan MJ, Lieberman J, Torrente J. Screening breast ultrasound: past, present, and future. AJR Am J Roentgenol. 2015;204:234–40. https://doi.org/10.2214/AJR.13.12072.
41. Lehman CD, Gatsonis C, Kuhl CK, et al. MRI evaluation of the contralateral breast in women with recently diagnosed breast cancer. N Engl J Med. 2007;356:1295–303. https://doi.org/10.1056/NEJMOA065447.
42. Houssami N, Turner R, Macaskill P, et al. An individual person data meta-analysis of preoperative magnetic resonance imaging and breast cancer recurrence. J Clin Oncol. 2014;32:392–401. https://doi.org/10.1200/JCO.2013.52.7515.
43. Berg WA, Blume JD, Cormack JB, et al. Combined screening with ultrasound and mammography vs mammography alone in women at elevated risk of breast cancer. JAMA. 2008;299:2151–63. https://doi.org/10.1001/JAMA.299.18.2151.
44. Liberman L. Centennial dissertation. Percutaneous imaging-guided core breast biopsy: state of the art at the millennium. AJR Am J Roentgenol. 2000;174:1191–9. https://doi.org/10.2214/AJR.174.5.1741191.
45. Villegas-Carlos F, Andino-Araque V, Valverde-Quintana M, et al. Predictive factors of invasion in ductal carcinoma in situ diagnosed by core-needle biopsy. Cir Cir. 2022;90:41–9. https://doi.org/10.24875/CIRU.21000136.
46. Bennett NC, Farah CS. Next-generation sequencing in clinical oncology: next steps towards clinical validation. Cancers (Basel). 2014;6:2296–312. https://doi.org/10.3390/CANCERS6042296.
47. Perou CM, Sørile T, Eisen MB, et al. Molecular portraits of human breast tumors. Nature. 2000;406:747–52. https://doi.org/10.1038/35021093.
48. Ross JS, Linette GP, Stec J, et al. Breast cancer biomarkers and molecular medicine. Expert Rev Mol Diagn. 2003;3:573–85. https://doi.org/10.1586/14737159.3.5.573.
49. Dowsett M, Dunbier AK. Emerging biomarkers and new understanding of traditional markers in personalized therapy for breast cancer. Clin Cancer Res. 2008;14:8019–26. https://doi.org/10.1158/1078-0432.CCR-08-0974.
50. Lim E, Metzger-Filho O, Winer EP. The natural history of hormone receptor-positive breast cancer. Oncology (Williston Park). 2012;26:688–95.
51. Pan H, Gray R, Braybrooke J, et al. 20-year risks of breast-cancer recurrence after stopping endocrine therapy at 5 years. N Engl J Med. 2017;377:1836–46. https://doi.org/10.1056/NEJMOA1701830.
52. Patani N, Martin LA, Dowsett M. Biomarkers for the clinical management of breast cancer: international perspective. Int J Cancer. 2013;133:1–13. https://doi.org/10.1002/IJC.27997.
53. Mohammed H, Russell IA, Stark R, et al. Progesterone receptor modulates ERα action in breast cancer. Nature. 2015;523:313–7. https://doi.org/10.1038/NATURE14583.
54. Rubin I, Yarden Y. The basic biology of HER2. Ann Oncol Off J Eur Soc Med Oncol. 2001;12 Suppl 1:S3–8. https://doi.org/10.1093/ANNONC/12.SUPPL_1.S3.

55. Ross JS, Slodkowska EA, Symmans WF, et al. The HER-2 receptor and breast cancer: ten years of targeted anti-HER-2 therapy and personalized medicine. Oncologist. 2009;14:320–68. https://doi.org/10.1634/THEONCOLOGIST.2008-0230.
56. Luporsi E, André F, Spyratos F, et al. Ki-67: level of evidence and methodological considerations for its role in the clinical management of breast cancer: analytical and critical review. Breast Cancer Res Treat. 2012;132:895–915. https://doi.org/10.1007/S10549-011-1837-Z.
57. Ding Y, Ding K, Qian H, et al. Impact on survival of estrogen receptor, progesterone receptor, and Ki-67 expression discordance pre- and post-neoadjuvant chemotherapy in breast cancer. PLoS One. 2020;15:e0231895. https://doi.org/10.1371/JOURNAL.PONE.0231895.
58. Huang SH, O'Sullivan B. Overview of the 8th edition TNM classification for head and neck cancer. Curr Treat Options in Oncol. 2017;18:1–13. https://doi.org/10.1007/S11864-017-0484-Y.
59. Fischer JP, Wes AM, Tuggle CT, et al. Mastectomy with or without immediate implant reconstruction has similar 30-day perioperative outcomes. J Plast Reconstr Aesthet Surg. 2014;67:1515–22. https://doi.org/10.1016/J.BJPS.2014.07.021.
60. Veronesi U, Saccozzi R, Del Vecchio M, et al. Comparing radical mastectomy with quadrantectomy, axillary dissection, and radiotherapy in patients with small cancers of the breast. N Engl J Med. 1981;305:6–11. https://doi.org/10.1056/NEJM198107023050102.
61. Giuliano AE, Kirgan DM, Guenther JM, Morton DL. Lymphatic mapping and sentinel lymphadenectomy for breast cancer. Ann Surg. 1994;220:391–401. https://doi.org/10.1097/00000658-199409000-00015.
62. Wang X, Xu L, Yin Z, et al. Locoregional recurrence-associated factors and risk-adapted postmastectomy radiotherapy for breast cancer staged in cT1-2N0-1 after neoadjuvant chemotherapy. Cancer Manag Res. 2018;10:4105–12. https://doi.org/10.2147/CMAR.S173628.
63. Tang L, Matsushita H, Jingu K. Controversial issues in radiotherapy after breast-conserving surgery for early breast cancer in older patients: a systematic review. J Radiat Res. 2018;59:789–93. https://doi.org/10.1093/JRR/RRY071.
64. Turaka A, Freedman GM, Li T, et al. Young age is not associated with increased local recurrence for DCIS treated by breast-conserving surgery and radiation. J Surg Oncol. 2009;100:25–31. https://doi.org/10.1002/JSO.21284.
65. Ng SP, David S, Alamgeer M, Ganju V. Impact of pretreatment combined (18) F-fluorodeoxyglucose positron emission tomography/computed tomography staging on radiation therapy treatment decisions in locally advanced breast cancer. Int J Radiat Oncol Biol Phys. 2015;93:111–7. https://doi.org/10.1016/J.IJROBP.2015.05.012.
66. Haviland JS, Owen JR, Dewar JA, et al. The UK Standardisation of Breast Radiotherapy (START) trials of radiotherapy hypofractionation for treatment of early breast cancer: 10-year follow-up results of two randomized controlled trials. Lancet Oncol. 2013;14:1086–94. https://doi.org/10.1016/S1470-2045(13)70386-3.
67. Paik S, Shak S, Tang G, et al. A multigene assay to predict recurrence of tamoxifen-treated, node-negative breast cancer. N Engl J Med. 2004;351:2817–26. https://doi.org/10.1056/NEJMOA041588.
68. Wu YT, Xu Z, Zhang K, et al. Efficacy and cardiac safety of the concurrent use of trastuzumab and anthracycline-based neoadjuvant chemotherapy for HER2-positive breast cancer: a systematic review and meta-analysis. Ther Clin Risk Manag. 2018;14:1789–97. https://doi.org/10.2147/TCRM.S176214.
69. Tolaney SM, Barry WT, Dang CT, et al. Adjuvant paclitaxel and trastuzumab for node-negative, HER2-positive breast cancer. N Engl J Med. 2015;372:134–41. https://doi.org/10.1056/NEJMOA1406281.
70. Mavroudis D, Saloustros E, Malamos N, et al. Six versus 12 months of adjuvant trastuzumab in combination with dose-dense chemotherapy for women with HER2-positive breast cancer: a multicenter randomized study by the Hellenic Oncology Research Group (HORG). Ann Oncol Off J Eur Soc Med Oncol. 2015;26:1333–40. https://doi.org/10.1093/ANNONC/MDV213.

71. Pagani O, Regan MM, Walley BA, et al. Adjuvant exemestane with ovarian suppression in premenopausal breast cancer. N Engl J Med. 2014;371:107–18. https://doi.org/10.1056/NEJMOA1404037.
72. Davies C, Pan H, Godwin J, et al. Long-term effects of continuing adjuvant tamoxifen to 10 years versus stopping at 5 years after diagnosis of estrogen receptor-positive breast cancer: ATLAS, a randomized trial. Lancet (London, England). 2013;381:805–16. https://doi.org/10.1016/S0140-6736(12)61963-1.
73. Leal F, Liutti VT, Antunes dos Santos VC, et al. Neoadjuvant endocrine therapy for resectable breast cancer: a systematic review and meta-analysis. Breast. 2015;24:406–12. https://doi.org/10.1016/J.BREAST.2015.03.004.
74. Finn RS, Crown JP, Lang I, et al. The cyclin-dependent kinase 4/6 inhibitor palbociclib in combination with letrozole versus letrozole alone as first-line treatment of estrogen receptor-positive, HER2-negative, advanced breast cancer (PALOMA-1/TRIO-18): a randomized phase 2 study. Lancet Oncol. 2015;16:25–35. https://doi.org/10.1016/S1470-2045(14)71159-3.
75. Turner NC, Ro J, André F, et al. Palbociclib in hormone-receptor-positive advanced breast cancer. N Engl J Med. 2015;373:209–19. https://doi.org/10.1056/NEJMOA1505270.
76. Swain SM, Baselga J, Kim S-B, et al. Pertuzumab, trastuzumab, and docetaxel in HER2-positive metastatic breast cancer. N Engl J Med. 2015;372:724–34. https://doi.org/10.1056/NEJMOA1413513.
77. Kilpatrick ES, Lind MJ. Appropriate requesting of serum tumor markers. BMJ. 2009;339:859. https://doi.org/10.1136/BMJ.B3111.
78. Shah R, Rosso K, David Nathanson S. Pathogenesis, prevention, diagnosis and treatment of breast cancer. World J Clin Oncol. 2014;5:283–98. https://doi.org/10.5306/WJCO.V5.I3.283.
79. Banegas MP, Bird Y, Moraros J, et al. Breast cancer knowledge, attitudes, and early detection practices in United States-Mexico border Latinas. J Women's Health (Larchmt). 2012;21:101–7. https://doi.org/10.1089/JWH.2010.2638.
80. Donepudi MS, Kondapalli K, Amos SJ, Venkanteshan P. Breast cancer statistics and markers. J Cancer Res Ther. 2014;10:506–11. https://doi.org/10.4103/0973-1482.137927.
81. Duffy MJ, Evoy D, McDermott EW. CA 15-3: uses and limitation as a biomarker for breast cancer. Clin Chim Acta. 2010;411:1869–74. https://doi.org/10.1016/J.CCA.2010.08.039.
82. Kurian S, Khan M, Grant M. CA 27-29 in patients with breast cancer with pulmonary fibrosis. Clin Breast Cancer. 2008;8:538–40. https://doi.org/10.3816/CBC.2008.N.067.
83. Zheng G, Yu H, Hemminki A, et al. Familial associations of female breast cancer with other cancers. Int J Cancer. 2017;141:2253–9. https://doi.org/10.1002/IJC.30927.
84. Couto E, Hemminki K. Estimates of heritable and environmental components of familial breast cancer using family history information. Br J Cancer. 2007;96:1740–2. https://doi.org/10.1038/SJ.BJC.6603753.
85. Claus EB, Schildkraut JM, Thompson WD, Risch NJ. The genetic attributable risk of breast and ovarian cancer. Cancer. 1996;77:2318–24. https://doi.org/10.1002/(sici)1097-0142(19960601)77:11<2318::aid-cncr21>3.0.co;2-z.
86. Apostolou P, Fostira F. Hereditary breast cancer: the era of new susceptibility genes. Biomed Res Int. 2013;2013:747318. https://doi.org/10.1155/2013/747318.
87. Nielsen FC, Van Overeem HT, Sørensen CS. Hereditary breast and ovarian cancer: new genes in confined pathways. Nat Rev Cancer. 2016;16:599–612. https://doi.org/10.1038/NRC.2016.72.
88. Mavaddat N, Barrowdale D, Andrulis IL, et al. Pathology of breast and ovarian cancers among BRCA1 and BRCA2 mutation carriers: results from the Consortium of Investigators of Modifiers of BRCA1/2 (CIMBA). Cancer Epidemiol Biomark Prev. 2012;21:134–47. https://doi.org/10.1158/1055-9965.EPI-11-0775.
89. Vocka M, Zimovjanova M, Bielcikova Z, et al. Estrogen receptor status oppositely modifies breast cancer prognosis in BRCA1/BRCA2 mutation carriers versus non-carriers. Cancers (Basel). 2019;11. https://doi.org/10.3390/CANCERS11060738.

90. Yadav S, Couch FJ. Germline genetic testing for breast cancer risk: the past, present, and future. Am Soc Clin Oncol Educ Book Am Soc Clin Oncol Annu Meet. 2019;39:61–74. https://doi.org/10.1200/EDBK_238987.
91. Gilkes DM, Semenza GL. Role of hypoxia-inducible factors in breast cancer metastasis. Future Oncol. 2013;9:1623–36. https://doi.org/10.2217/FON.13.92.
92. Salceda S, Caro J. Hypoxia-inducible factor 1alpha (HIF-1alpha) protein is rapidly degraded by the ubiquitin-proteasome system under normoxic conditions. Its stabilization by hypoxia depends on redox-induced changes. J Biol Chem. 1997;272:22642–7. https://doi.org/10.1074/JBC.272.36.22642.
93. Masoumi Moghaddam S, Amini A, Morris DL, Pourgholami MH. Significance of vascular endothelial growth factor in growth and peritoneal dissemination of ovarian cancer. Cancer Metastasis Rev. 2012;31:143–62. https://doi.org/10.1007/S10555-011-9337-5.
94. Zhang L, Kirchhoff T, Yee CJ, Offit K. A rapid and reliable test for BRCA1 and BRCA2 founder mutation analysis in paraffin tissue using pyrosequencing. J Mol Diagn. 2009;11:176–81. https://doi.org/10.2353/JMOLDX.2009.080137.
95. Meisel JL, Hyman DM, Garg K, et al. The performance of BRCA1 immunohistochemistry for detecting germline, somatic, and epigenetic BRCA1 loss in high-grade serous ovarian cancer. Ann Oncol Off J Eur Soc Med Oncol. 2014;25:2372–8. https://doi.org/10.1093/ANNONC/MDU461.
96. Garg K, Levine DA, Olvera N, et al. BRCA1 immunohistochemistry in a molecularly characterized cohort of ovarian high-grade serous carcinomas. Am J Surg Pathol. 2013;37:138–46. https://doi.org/10.1097/PAS.0B013E31826CABBD.
97. Smith KL, Isaacs C. BRCA mutation testing in determining breast cancer therapy. Cancer J. 2011;17:492–9. https://doi.org/10.1097/PPO.0B013E318238F579.
98. You M, Yang S, Tang W, et al. Molecularly imprinted polymers-based electrochemical DNA biosensor for the determination of BRCA-1 amplified by SiO 2@Ag. Biosens Bioelectron. 2018;112:72–8. https://doi.org/10.1016/J.BIOS.2018.04.038.
99. Ali IU, Campbell G, Lidereau R, Callahan R. Amplification of c-erbB-2 and aggressive human breast tumors? Science. 1988;240:1795–6. https://doi.org/10.1126/SCIENCE.3289120.
100. Garnock-Jones KP, Keating GM, Scott LJ. Trastuzumab: a review of its use as adjuvant treatment in human epidermal growth factor receptor 2 (HER2)-positive early breast cancer. Drugs. 2010;70:215–39. https://doi.org/10.2165/11203700-000000000-00000.
101. Wolff AC, Hammond MEH, Hicks DG, et al. Recommendations for human epidermal growth factor receptor 2 testing in breast cancer: American Society of Clinical Oncology/College of American Pathologists clinical practice guideline update. Arch Pathol Lab Med. 2014;138:241–56. https://doi.org/10.5858/ARPA.2013-0953-SA.
102. Wolff AC, Hammond MEH, Schwartz JN, et al. American Society of Clinical Oncology/College of American Pathologists guideline recommendations for human epidermal growth factor receptor 2 testing in breast cancer. Arch Pathol Lab Med. 2007;131:18–43. https://doi.org/10.5858/2007-131-18-ASOCCO.
103. Pacheco JG, Rebelo P, Freitas M, et al. Breast cancer biomarker (HER2-ECD) detection using a molecularly imprinted electrochemical sensor. Sensors Actuators B Chem. 2018;273:1008–14. https://doi.org/10.1016/J.SNB.2018.06.113.
104. Amayo AA, Kuria JG. Clinical application of tumor markers: a review. East Afr Med J. 2009;86. https://doi.org/10.4314/EAMJ.V86I12.62909.
105. Pacheco JG, Silva MSV, Freitas M, et al. Molecularly imprinted electrochemical sensor for the point-of-care detection of a breast cancer biomarker (CA 15-3). Sensors Actuators B Chem. 2018;256:905–12. https://doi.org/10.1016/J.SNB.2017.10.027.
106. Ribeiro JA, Pereira CM, Silva AF, Sales MGF. Disposable electrochemical detection of breast cancer tumour marker CA 15-3 using poly(Toluidine Blue) as imprinted polymer receptor. Biosens Bioelectron. 2018;109:246–54. https://doi.org/10.1016/J.BIOS.2018.03.011.

107. Gomes RS, Moreira FTC, Fernandes R, Goreti Sales MF. Sensing CA 15-3 in point-of-care by electropolymerizing O-phenylenediamine (oPDA) on Au-screen printed electrodes. PLoS One. 2018;13:e0196656. https://doi.org/10.1371/JOURNAL.PONE.0196656.
108. Santos ART, Moreira FTC, Helguero LA, Sales MGF. Antibody biomimetic material made of pyrrole for CA 15-3 and its application as sensing material in ion-selective electrodes for potentiometric detection. Biosensors. 2018;8:8. https://doi.org/10.3390/BIOS8010008.
109. Hammarström S. The carcinoembryonic antigen (CEA) family: structures, suggested functions, and expression in normal and malignant tissues. Semin Cancer Biol. 1999;9:67–81. https://doi.org/10.1006/SCBI.1998.0119.
110. Grunnet M, Sorensen JB. Carcinoembryonic antigen (CEA) as a tumor marker in lung cancer. Lung Cancer. 2012;76:138–43. https://doi.org/10.1016/J.LUNGCAN.2011.11.012.
111. Wu S g, He Z y, Zhou J, et al. Serum levels of CEA and CA15-3 in different molecular subtypes and prognostic value in Chinese breast cancer. Breast. 2014;23:88–93. https://doi.org/10.1016/J.BREAST.2013.11.003.
112. Park BW, Oh JW, Kim JH, et al. Preoperative CA 15-3 and CEA serum levels as predictor for breast cancer outcomes. Ann Oncol Off J Eur Soc Med Oncol. 2008;19:675–81. https://doi.org/10.1093/ANNONC/MDM538.
113. Shao Y, Sun X, He Y, et al. Elevated levels of serum tumor markers CEA and CA15-3 are prognostic parameters for different molecular subtypes of breast cancer. PLoS One. 2015;10:e0133830. https://doi.org/10.1371/JOURNAL.PONE.0133830.
114. Bahrami-Ahmadi A, Makarian F, Mortazavizadeh MR, et al. Symptomatic metastasis prediction with serial measurements of CA 15.3 in primary breast cancer patients. J Res Med Sci. 2012;17:850.
115. Asad-Ur-Rahman F, Saif MW. Elevated level of serum carcinoembryonic antigen (CEA) and search for a malignancy: a case report. Cureus. 2016;8:e648. https://doi.org/10.7759/CUREUS.648.
116. Lee JS, Park S, Park JM, et al. Elevated levels of preoperative CA 15-3 and CEA serum levels have independently poor prognostic significance in breast cancer. Ann Oncol Off J Eur Soc Med Oncol. 2013;24:1225–31. https://doi.org/10.1093/ANNONC/MDS604.
117. Puglisi F, Fontanella C, Numico G, et al. Follow-up of patients with early breast cancer: is it time to rewrite the story? Crit Rev Oncol Hematol. 2014;91:130–41. https://doi.org/10.1016/J.CRITREVONC.2014.03.001.
118. Li X, Dai D, Chen B, et al. Clinicopathological and prognostic significance of cancer antigen 15-3 and carcinoembryonic antigen in breast cancer: a meta-analysis including 12,993 patients. Dis Markers. 2018;2018:1–15. https://doi.org/10.1155/2018/9863092.
119. Hing JX, Mok CW, Tan PT, et al. Clinical utility of tumor marker velocity of cancer antigen 15-3 (CA 15-3) and carcinoembryonic antigen (CEA) in breast cancer surveillance. Breast. 2020;52:95–101. https://doi.org/10.1016/J.BREAST.2020.05.005.

Engineered Hybrid Nanoparticles for Multimodal Medical Imaging and Diagnosis

Aishwarya Shetty and Sudeshna Chandra

Abbreviations

17-AAG	17-allylamino-17-demethoxygeldanamycin
^{99m}Tc	Technetium-99 m
Ag	Silver
Ag	Silver
AuF	Gold nanoflower
AuNC	Gold nanocage
Bi	Bismuth
CD	Carbon dots
CPN	Conjugated polymer nanoparticle
Cr	Chromium
CS	Chitosan
CUR	Curcumin
DOX	Doxorubicin
Ga_2O_3	Gallium(III) oxide
GC	Glycol, chitosan
Gd_2O_3	Gadolinium(III) oxide
GE	Genistein
GNP/AuNP	Gold nanoparticle
GOD	Glucose oxidase
HMNP	Hollow mesoporous nanoparticle
HP	Hyaluronic acid and penetratin
HSA	Human serum albumin
HSP	Hyperbranched semiconducting polymer

A. Shetty
Sunandan Divatia School of Science, SVKM's NMIMS University, Mumbai, India

S. Chandra (✉)
Sunandan Divatia School of Science, SVKM's NMIMS University, Mumbai, India

Institute of Analytical Chemistry, University of Regensburg, Regensburg, Germany
e-mail: Chandra.Sudeshna@chemie.uni-regensburg.de

R. S. Chaughule et al. (eds.), *Nanomaterials for Cancer Detection Using Imaging Techniques and Their Clinical Applications*,
https://doi.org/10.1007/978-3-031-09636-5_12

IO	Iron oxide (γ-Fe_2O_3)
iTSL	Imaging thermosensitive liposome
JNP	Janus nanoparticle
Lips/LP	Liposome
LMWC	Low-molecular-weight chitosan
MDP	Muramyl dipeptide
MoO_2	Molybdenum oxide
MPI	Magnetic particle imaging
MPN	Metal phenolic nanoparticles
MSC	Mesenchymal stem cell
Nd	Neodymium
NGO	Nano graphene oxide
OA	Oleic acid
PAA	Poly acrylic acid
PCL	Polycaprolactone
PDA	Polydopamine
PFP	Perfluoropentane
PLI	Photoluminescence imaging
PMPC	Poly[(2-methacryloyloxy) ethyl phosphorylcholine]
PVP	Polyvinyl pyrrolidone
TM	Thermosensitive magnetoliposome
UCL	Upconversion luminescence
UCNP	Upconversion nanoparticles
USIONPs	Ultrasmall iron oxide nanoparticles
XFCT	X-ray fluorescence computed tomography

1 Introduction

Medical imaging is a technique that involves imaging of the interior body organs for clinical interventions and visual representation of physiological organs, thus comprising both molecular and anatomical imaging. Optical imaging, single-photon emission computed tomography (SPECT), and positron emission tomography (PET) are molecular imaging modalities wherein they are used to visualize processes at the molecular and cellular levels. Whereas structural or anatomical imaging techniques like ultrasound (US), X-ray computed tomography (CT), photoacoustic imaging (PAI), and magnetic resonance imaging (MRI) give information about anatomy [1–4]. Traditional imaging contrast agents like iohexol (iodine-based, used for CT), gadodiamide (gadolinium-based, used in MRI), and barium sulfate (barium-based, used in CT) are limited due to nonspecific distribution, low spatial resolution, and toxicity [2]. On the other hand, nanoparticles when used as imaging probes or contrast agents are found to improve imaging by providing better spatial resolution. Nanoparticles can also be functionalized by targeting moieties to enhance signal sensitivity at cellular and molecular levels [3]. The

ability to monitor biological processes and functional visualization are some additional advantages when nanoparticles are used as imaging agents, for example, the use of nanoparticles for molecular imaging of angiogenesis and noninvasive imaging of macrophages [4, 5].

Nanoparticles investigated for biomedical imaging applications can be broadly classified into organic and inorganic materials. Inherent molecular properties of inorganic nanoparticles allow them to create contrast upon imaging. An example of this intrinsic property is the high number of electrons moving freely between the conduction and valence bands of metallic nanoparticles [6]. Their application as contrast agents in different imaging modalities arises from the interactions of these free electrons. For example, the 3D shell of Fe^{+2} ion in superparamagnetic iron oxide nanoparticles (SPIONs) contains four unpaired electrons that give rise to superparamagnetism and therefore can be used as a contrast agent in MRI. Several SPION formulations such as Feridex®, Combidex®, and Resovist® have been used as MRI contrast agents in clinical settings. However, artifacts from magnetic susceptibility of the iron oxide core and toxicity limit the use of SPIONs in clinical settings [7–9]. Gadolinium (Gd)-based contrast agents have also been used for MRI; however, adverse effects such as nephrogenic systemic fibrosis have been associated with the release of free Gd ions from the agents [9]. Localized surface plasmon resonance (LSPR) of gold nanoparticles (Au NPs) has been used for optical imaging, PA, CT, and PET imaging [10]. Other inorganic nanoparticles used for bioimaging include upconversion nanoparticles (UCNPs), metallic nanoparticles composed of copper (Cu), silver (Ag), palladium (Pd), platinum (Pt), and carbon dots (C dots). These materials have also been used in conjunction with each other to achieve multiple imaging modalities for improved monitoring. For example, gold and copper sulfide (Au@CuS) core-shell nanoparticles were developed by Lv et al. for multimodal in vivo surface-enhanced Raman spectroscopy (SERS) and PA imaging. Enhancement in the photothermal performance and imaging properties was observed due to LSPR coupling of CuS semiconductor and plasmonic Au metal into a single unit [11]. In another study, UCNPs@Bi@SiO_2 nanoparticles were synthesized as a core-shell structure, which was designed to protect the bismuth (Bi) core from oxidation by forming a silica (SiO_2) shell around it. Applications of the nanoparticle involved upconversion luminescence (UCL) from UCNPs and CT imaging from the Bi core [12]. Additionally, inorganic nanoparticles commonly used in in vivo diagnostics are quantum dots (QDs) which are single crystals composed of semiconductor materials ranging a few nanometers in diameter. The presence of Fermi levels between the valence and conduction bands makes optical excitation of QDs strongly size-dependent [13]. Organic nanomaterials for imaging include dendrimers, fullerenes, and lipid-based nanoparticles (liposomes, micelles, and lipid nanoparticles). Dendrimers are highly branched three-dimensional structures with successive generations showing an increase in payload capacity. Conjugation of drugs, imaging agents, and ligands on dendrimers is feasible due to the presence of functional groups on the surface and internal voids [14]. Liposomes are composed of phospholipid and cholesterol, with a lipid bilayer encapsulating an aqueous core, whereas micelles consist of a closed monolayer of lipid with the

polarity of the surface depending on the nature of the fatty acids [15]. Biocompatibility, self-assembly, and high bioavailability make lipid-based nanoparticles the most repeatedly FDA-approved class of nanomedicines. Examples of such FDA-approved liposomal formulations include Doxil®, DaunoXome®, Onpattro$_{TM}$, Visudyne®, Marqibo®, Vyxeos®, etc. [16].

In comparison to inorganic nanoparticles, as organic nanoparticles often resemble the structure of the imaging subject, they may be unable to produce adequate contrast. On the other hand, despite the favorable intrinsic properties of inorganic nanoparticles, they show substantial toxicity in vivo. To overcome the limitations of individual nanomaterials, a new generation of hybrid nanoparticles composed of a mixture or combination of these components is being explored. The combinations may include (i) organic and inorganic, (ii) organic and organic, or even (iii) inorganic and inorganic components in a single platform which could lead to multiple imaging/therapeutic modalities. Components in these systems are judiciously chosen to enhance integrated functionalities leading to better therapeutics and theranostics.

2 Hybrid Nanoparticles in Optical Imaging

Optical imaging is a minimally invasive technique that makes use of nonionizing light to procure images at cellular and molecular levels. Depending on the composition of the tissue, when light travels through it, photons undergo absorption, reflection, or scattering. These interactions are then analyzed by optical imaging systems to yield distinctive spectral signatures observed as images. For example, inelastic scattering of light is analyzed by Raman spectroscopy, whereas emission of light after its absorption is used in fluorescence and phosphorescence. The high spatial resolution of optical imaging is limited by its poor depth of penetration as there is scattering and absorption of visible light by biological molecules such as water, hemoglobin, and fats resulting in signal attenuation. However, this can be overcome by using near-infrared (NIR) light which shows relatively low scattering in biological tissues [17]. Different types of optical imaging techniques include fluorescence, photoacoustic imaging, and Raman spectroscopy. Fluorescence imaging is the most widely used optical imaging technique due to its high specificity, sensitivity, and ability to image biomolecular interaction, cellular localization, and molecular and cellular movements [18]. Photoacoustic imaging is based on irradiation with a laser (usually NIR light) and the generation of a photoacoustic signal from tissues due to thermoelastic expansion upon absorption of incident radiation. The photoacoustic signals are then detected by a transducer to generate images [19]. Semiconductor and metallic nanoparticles that undergo radiative recombination of charge carriers exhibit fluorescence. Metallic nanoparticles show extraordinary optical properties due to surface plasmon resonance (noble metals) and *sp-d* band electronic transitions. The quantum confinement effect in semiconductor quantum dots enables tuning of emission color by varying the particle size. Semiconductor nanoparticles

doped with rare-earth metals that emit intense monochromatic light are also used as phosphors [20]. Combinations of these materials may be used to obtain multimodal imaging agents or enhance intrinsic properties in order to obtain better quantum efficiencies. Organic nanoparticles in optical imaging may be used to carry fluorophores or in combination with metallic nanoparticles to make systems more biocompatible.

3 Nanoparticles in Fluorescence Imaging

A major advantage of fluorescence imaging as compared to other imaging techniques is the high spatial resolution at microscopic levels. Apart from this, nanoparticles can be used to load higher quantities of fluorescent dyes and prevent photobleaching effects. Strategies for use of nanoparticles in fluorescence imaging involve the use of inherently fluorescing nanomaterials or encapsulation of hydrophilic/hydrophobic fluorescent dyes. Fluorescent molecules such as indocyanine green (ICG), cyanine dyes (e.g., Cy 5.5), doxorubicin (DOX), Nile red, etc. are commonly encapsulated in nanoparticle systems to enable fluorescence imaging. Encapsulation of such agents into a nanoparticle could lead to their targeted accumulation compared to when used freely, thus increasing their efficacy as well. For example, a hybrid organic nanoparticle system synthesized using porphyrin lipid nanoparticles was used for the encapsulation of DOX. This enabled fluorescence which allows real-time detection of therapeutic effects of a nanosystem [21]. In another study, Luo et al. in 2021 successfully co-encapsulated a fluorescent dye Nile red and magnetic SPIONs into a polymeric matrix composed of methyl methacrylate, styrene, and methacrylic acid to obtain P/Fe_3O_4/Nile red nanoparticles. Though close contact between the transition metal in Fe_3O_4 and the fluorescent dye led to some quenching, the nanoparticles exhibited bright orange-red fluorescence under UV irradiation [22]. Dong et al. in 2019 synthesized a composite hydrogel system based on CpG NPs (cytosine-phosphate-guanine nanoparticles) and IR820 hydrogel. The CpG NPs were synthesized using genipin as a cross-linker, whereas the IR820 copolymer hydrogel was synthesized by self-assembly of IR820-αcyclodextrin co-polymer and polyethylene glycol (PEG_{4000}). The resulting IR820 conjugated hydrogel loaded with self-cross-linked CpG NPs was capable of self-dual fluorescence and immuno-photothermal therapies. Genipin in the CpG NPs showed emission at 670 nm after excitation at 595 nm, and the IR820 copolymer showed emission at 840 nm after excitation at 735 nm. The authors successfully discriminated dual fluorescence by in vitro experiments demonstrating red and green fluorescence of CpG NPs and IR820 hydrogel, respectively, and a yellow fluorescence from the CpG NPs/IR820 hydrogel system (Fig. 1a). Quantitative estimation of fluorescence signal intensity enabled the authors to detect the rate of hydrogel degradation and CpG release from the hydrogel as depicted in Fig.1b, c. Thus, the composite hydrogel system enabled real-time tracking of therapy based

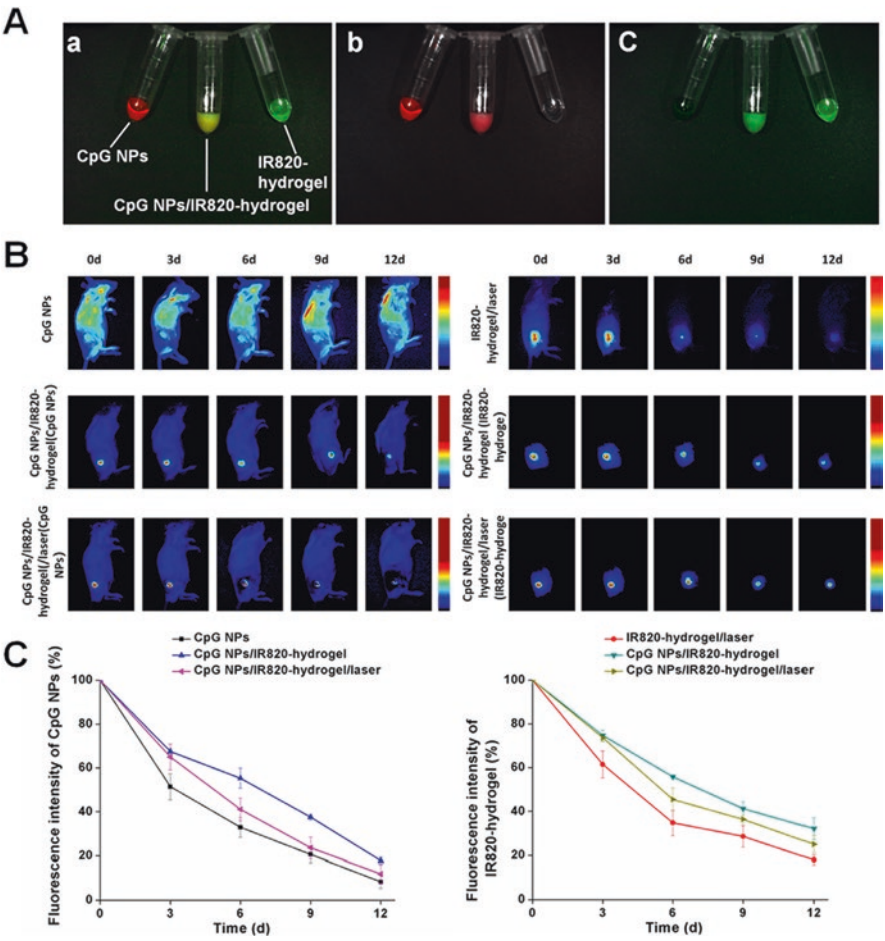

Fig. 1 Fluorescence images of CpG NPs/IR820 hydrogel. (**a**) In vitro imaging showing dual fluorescence of CpG NPs/IR820 hydrogel, (**b**) In vivo fluorescence imaging for respective nanoparticle formulations, (**c**) quantitative estimation of fluorescence signal intensity of different animal groups ($n = 3$). (Image adapted from Ref. [27])

on the optical properties of the individual components of the composite hydrogel system [23].

Jiang et al. 2019 synthesized afterglow luminescent nanoparticles (ALNPs) which showed long-lasting fluorescence even after excitation was discontinued. The afterglow luminescence of the ALNPs was based on the assembly of three components, namely, the afterglow initiator, substrate, and relay unit. The initiator, i.e., a photosensitizer (PS), served as an agent to absorb and convert energy from a source of light into ROS which would act as a substrate to form a chemiluminescent intermediate; the relay unit, i.e., a fluorescent agent would then release photons by absorbing energy from this intermediate by means of chemically initiated electron

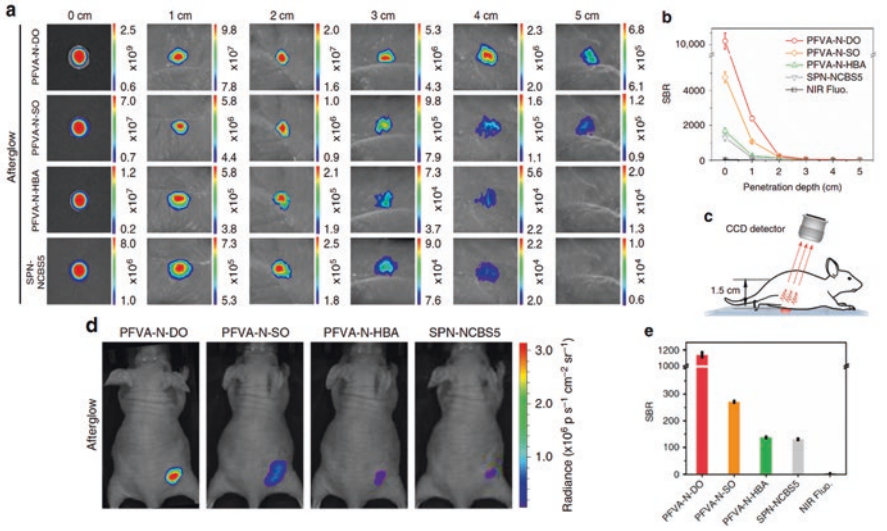

Fig. 2 Study of penetration depth of ALNPs. (**a**) Images representing afterglow of different ALNPs from various depths of breast tissues of chicken, (**b**) signal-to-background ratio of the afterglow of different ALNPs, (**c**) schematic representation of optical imaging in vivo, (**d**) images representing afterglow of different ALNPs in vivo, (**e**) quantitative estimation of the signal-to-background ratio of afterglow. (Image adapted from Ref. [28])

exchange luminescence. Authors tried different combinations of materials for each of the components and tested the nanosystems quantitatively for their afterglow intensities (Fig. 2). The selected system was based on the use of semiconducting amphiphilic copolymers as their relay unit. The copolymer-based nanoparticles showed superior afterglow luminescence, reduced signal-to-background ratio, and were able to image up to tissue depths of 5 cm [24].

A system based on Au nanoclusters (AuNC) loaded in albumin (BSA) nanoparticles was synthesized by Park et al. 2019 for fluorescence imaging and photothermal therapy [25]. The use of quantum dots for fluorescence or optical imaging was demonstrated by Kumawat et al. 2019. The authors synthesized graphene oxide sheets which were functionalized with graphene quantum dots (GQDs) using polyethyleneimine (PEI) linkers to yield GO-PEI-GQDs. The presence of a metal oxide surface in close proximity to a QD often results in quenching *via* photoinduced charge transfer. However, these effects were avoided with the use of PEI which prevented quenching effects and thus acted as a photoluminescence enhancer. Further, the authors showed that the emission of GO-PEI-GQDs was dependent on the excitation wavelength which varied with the pH of the medium (Fig. 3a). The red and green fluorescence exhibited by GO-PEI-GQDs is represented in Fig. 3b–d [26]. In another study by Liu et al. 2020, the authors used carbon nanosheets (CN) to embed graphitic carbon nitride quantum dots (g-C_3N_4). The authors employed g-C_3N_4 QDs as a means to introduce fluorescence imaging in the system due to their favorable properties such as high quantum yield and wide emission range. The

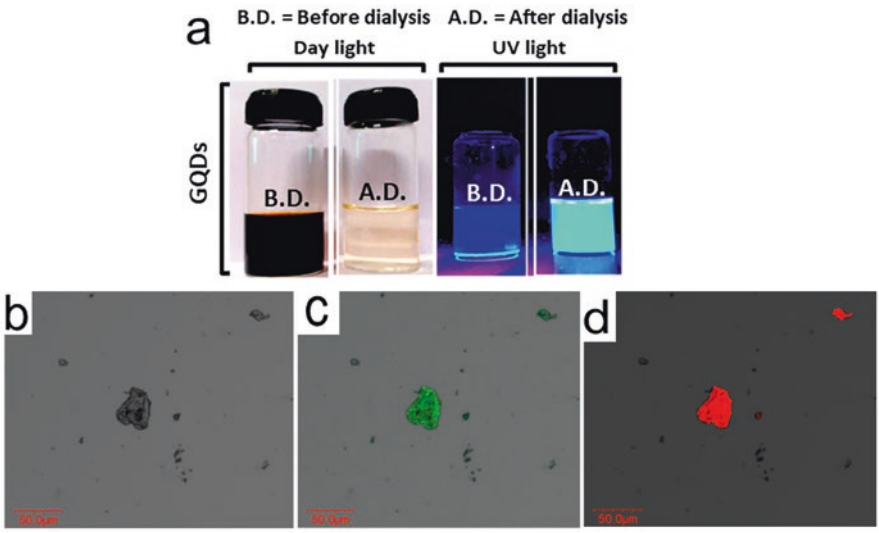

Fig. 3 (**a**) Optical images of GQDs under daylight and UV excitation at 375 nm, before and after dialysis, (**b**–**d**) green and red fluorescence of GO-PEI-GQDs as observed under a confocal microscope. (Image adapted from Ref. [30])

fabricated CNQD-CN nanoparticles showed emission at 363 nm (Fig. 4a) observed in the form of blue fluorescence after UV excitation. Figure 4b, c show the NIR imaging ability of CNQD-CN nanoparticles in vivo which shows bright fluorescence [27].

One of the strategies to avoid quenching as observed in rare-earth-doped nanoparticles is the fabrication of a core@shell structure that prevents the interaction of emitting ions with its surrounding. This strategy was employed by Ortgies et al. in 2018 wherein the synthesized $NaYF_4$: Yb, Nd@CaF_2 core@shell nanoparticles. The calcium fluoride (CaF_2) shell prevented the interaction of $NaYF_4$: Yb, Nd@CaF_2 core with the surrounding medium, thus reducing quenching. With tuning of rare-earth doping, the authors were also able to tune the luminescence lifetime of the core@shell nanoparticles [28].

4 Nanoparticles in Photoacoustic/Ultrasound Imaging

Photoacoustic imaging is an emerging modality that makes use of Au- and CuS-based nanostructures to generate contrast. Metal nanoparticles are often employed as a result of their intense PA signal. Plasmonic or AuNPs were among the first nanoparticles to be used as PAI contrast agents and are still studied today with respect to varied shapes and sizes. Some examples highlighting the use of hybrid nanoparticles for PAI are discussed in the following section. Kim and colleagues

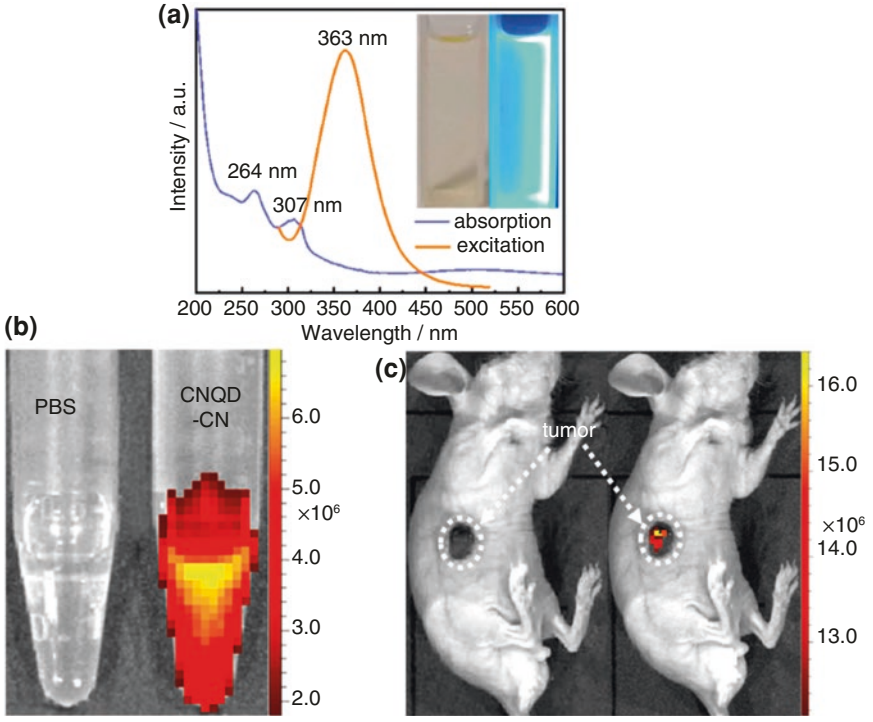

Fig. 4 (**a**) UV-vis spectrum of CNQD-CN with inset showing before and after irradiation with 365 nm laser, (**b**) NIR imaging of CNQD-CN in vitro, (**c**) representative images showing in vivo NIR imaging using CNQD-CN. (Image adapted from Ref. [31])

synthesized silver-coated gold nanorods (Ag-AuNR) to treat bacterial infections assisted by PAI. The fabricated Ag-AuNR nanoparticle showed loss or recovery of AuNR photoacoustic signal depending upon the presence or absence of the surrounding Ag shell. Decomposition or etching of the Ag shell was observed under mild oxidizing conditions resulting in the release of Ag^+ ions which also acted as antibacterial agents. Thus, depending on the status of the Ag shell on the AuNR, the PAI signal turned on or off and the resulting contrast provided real-time dosimetry of Ag^+ ions. As observed in Fig. 5a, PAI signal after addition of Ag shell was negligible which was recovered after etching of Ag shell resulting in a signal equivalent to that of bare AuNR. Figure 5b shows increasing PAI activity of etched Ag-AuNR in response to increasing concentrations of H_2O_2 and $ONOO^-$ (peroxynitrite) ions. Figure 5c, d represent in vivo PAI activity of Ag-AuNR in the presence and absence of Ag etching. As depicted in the figure, etching of Ag resulted in a significant increase in PAI contrast as compared to PAI signal in the presence of Ag shell [29].

Zhou et al. in 2020 synthesized self-assembled Au nanochains encapsulated in silica ($AuNC@SiO_2$) nanoparticles for tumor activatable PAI-guided PTT. In presence of excessive H_2O_2 which is often found in the tumor microenvironment, citrate ligands on the Au NPs would detach from them, resulting in the fusion of Au NPs

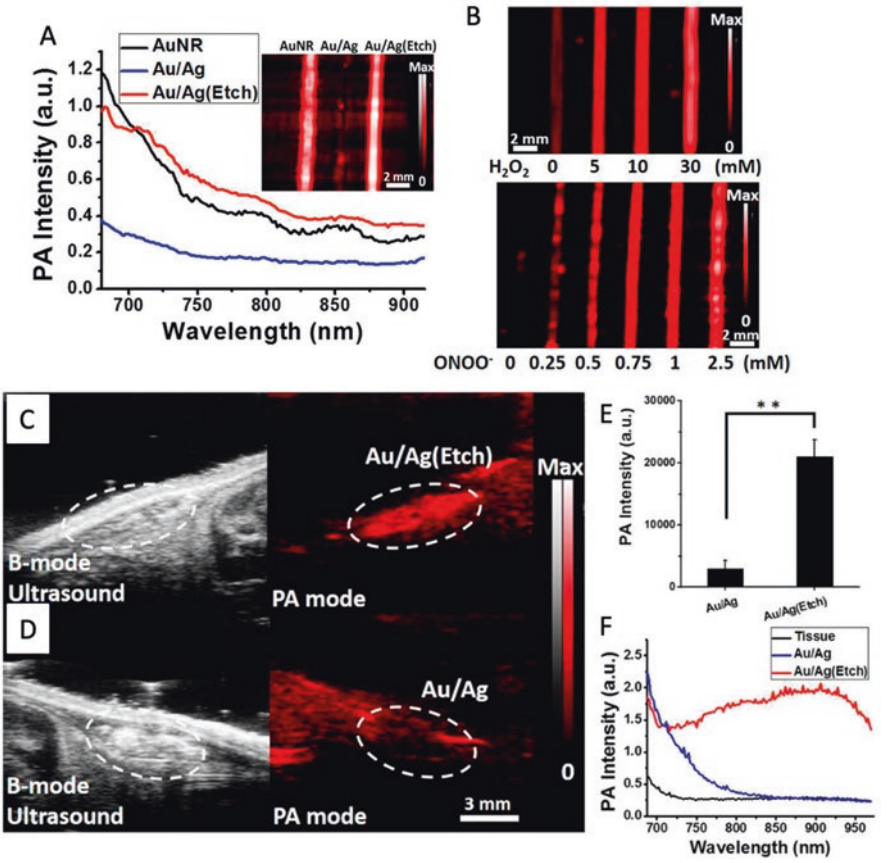

Fig. 5 (**a**) Quantitative estimation of in vitro PA activity of AuNR, Ag-AuNR, and Ag etched AuNR with inset showing PAI, (**b**) in vitro PAI activity of etched Ag-AuNR in the presence of $ONOO^-$ and H_2O_2 at various concentrations, (**c**) representative PAI of Ag etched AuNR and Ag-AuNR in vivo and (E,F) its quantitative estimation. (Image adapted from Ref. [33])

within the confined local spaces of AuNC@SiO_2. This generates a strong PA signal that can be used for tumor-specific diagnostics. AuNC@SiO_2 nanoparticles demonstrated PA signal intensity corresponding to the concentration of H_2O_2. In order to assess H_2O_2 responsive PAI activity in vivo, authors injected AuNC@SiO_2 nanoparticles intratumorally and intramuscularly. The concentration of H_2O_2 being high in tumors and negligible in normal tissue, nanoparticles generated a strong PA signal in the tumor as opposed to normal tissue. Further, to prove the relationship between the concentration of H_2O_2 and PA signal intensity in vivo, authors introduced H_2O_2 generating (β-phenylethyl isothiocyanate, i.e., PEITC) and scavenging (dimethylthiourea, i.e., DTMU) molecules into animals before treating them with the nanoparticles. The PA intensity in presence of PEITC was highest as compared to the control and DTMU-treated groups. From this experiment, the authors demonstrated that by

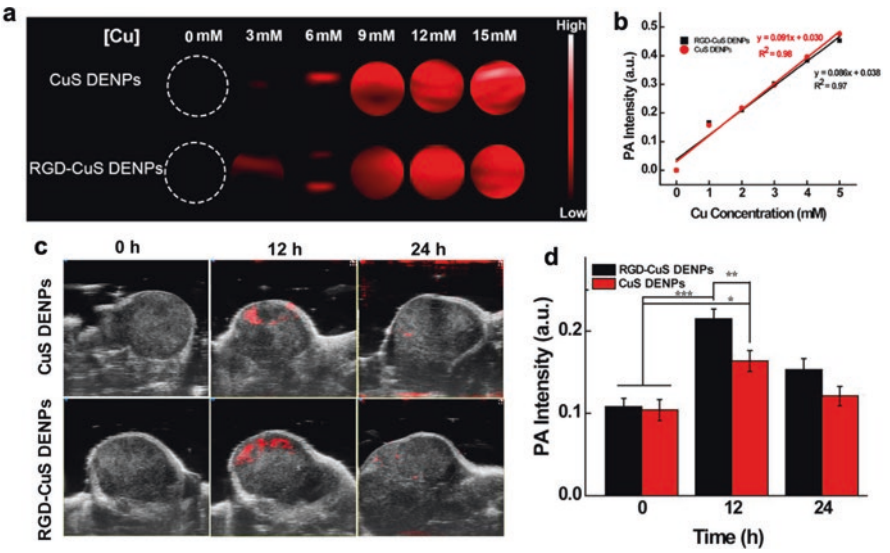

Fig. 6 (**a**) In vitro PAI of RGD-CuS DENPs and (**b**) quantitative estimation of PA signal, (**c**) representative images of PAI in vivo, and (**d**) quantitative estimation of PA signal. (Image adapted from Ref. [35])

mediating different concentrations of H_2O_2, the PA signal intensity of AuNC@SiO_2 also varied thus proving their H_2O_2-responsive PAI ability [30].

Ouyang et al. 2021 synthesized poly(amidoamine) dendrimer-entrapped CuS nanoparticles functionalized with RGD peptide (RGD-CuS DENPs) for PAI-guided PTT/gene therapy. Figure 6 demonstrates the PAI ability of RGD-CuS DENPs. Figure 6a, b are representative images for in vitro PAI activity that was found to depend on the concentration of Cu in the formulation. As observed in Fig. 6d, the PAI signal of RGD-CuS DENPs was higher than non-targeted nanoparticles, which peaked 12 hours postinjection. A decrease in PAI intensity over a period was due to the elimination of the nanoparticles [31].

5 Hybrid Nanoparticles in Ultrasound Imaging

Ultrasound imaging makes use of acoustic signals of frequencies above 20 kHz and is based on the reflection or scattering of the signals. Images from ultrasound can be obtained in real time as a result of which it is often used to view the movement of internal organs. High spatial resolution, noninvasiveness, portability, real-time imaging, and low cost have made US imaging one of the most commonly used imaging techniques. Traditional US imaging agents consisted of shell encapsulated air- or gas-filled bubbles whose size often ranged in micrometers (microbubbles). The stability and durability of a microbubble depend on its shell, whereas the

acoustic and imaging properties are determined by the gas core. Depending on the material used, the shell could either be hard (polymeric- and protein-shelled microbubbles) or soft (phospholipid- and surfactant-stabilized microbubbles). The gas core in US imaging contrast agents consists of air, nitrogen, or a high-molecular-weight inert gas (e.g., perfluorochemicals, sulfur hexafluoride). To overcome the limitations of microbubbles, a similar strategy of shell encapsulating gas has been adapted at the nanoscale. As opposed to microbubbles, nanobubbles can extravasate into small spaces and can also be easily functionalized to improve their targeting with prolonged circulation. Nanoparticles employed as US contrast agents generally consist of a shell of organic or inorganic nanomaterial encapsulating materials like perfluorochemicals, sodium bicarbonate ($NaHCO_3$), or hydrogen peroxide (H_2O_2). These can be classified into three types, namely, gas-generating or gas-filled echogenic bubbles and bubbles with perfluorochemicals [32, 33].

Jiang et al. in 2020 fabricated stretchable DMA-co-MAA hydrogel composed of N, N-dimethyl acrylamide (DMA), and methacrylic acid (MAA) with zinc oxide (ZnO) nanoparticles encapsulated in the polymer matrix. Authors developed "ZnO-gel" for use as a stretchable strain-sensing device for implantation. The stretchable gel when attached to a target organ would enable US imaging of changes or deformations in the hydrogel under applied mechanical strains. The ultrasound contrast in the gel resulted from the back-scattered signal arising from the incident ultrasound wave colliding against ZnO nanoparticles dispersed in the hydrogel. An increase in US contrast signal was observed with increasing ZnO concentration up to 10% w/w, after which there was no significant increase (Fig. 7a–e). To mimic in vivo conditions of implantation into abdominal organs, the authors also assessed US contrast by placing the gel under 10-mm-thick porcine skin (Fig. 7f, g) [34].

In another study, Wu et al. 2021 synthesized a self-assembled nanogel in which hydrogelation of small molecules (Fmoc-Tyr (H_2Po_3)-OH) and their self-assembly was triggered using acid phosphatase (AP)-modified magnetic nanoparticle as the core template. Dual enzymes catalase (CAT) and lactate oxidase (LOD) were co-immobilized on the supramolecular nanogel (NG) to yield LCNG. The authors hypothesized that in the acidic and hypoxic tumor microenvironment, the dual enzymes would work on the decomposition of lactic acid and H_2O_2 to yield oxygen which in turn would act as microbubbles and significantly contribute to US contrast. Figure 8a, b represents in vitro assessment of US imaging of LCNG in PBS (phosphate-buffered saline), H_2O_2, lactate (Lac), and a combination of H_2O_2 and Lac. As observed in the figure, the presence of H_2O_2 and Lac led to the significant generation of O_2 bubbles, which increased in proportion to Lac and generated significant US contrast. As observed in Fig. 8b, control groups containing only H_2O_2 or PBS showed no significant US contrast. The US generating ability of LCNG was also reflected in vivo. Figure 8d depicts representative images of in vivo US contrast generated by LCNG upon intravenous administration at different time points. As observed in the figure, significant US contrast was observed 30 min posttreatment with mean grayscale six times higher than that of pretreatment [35].

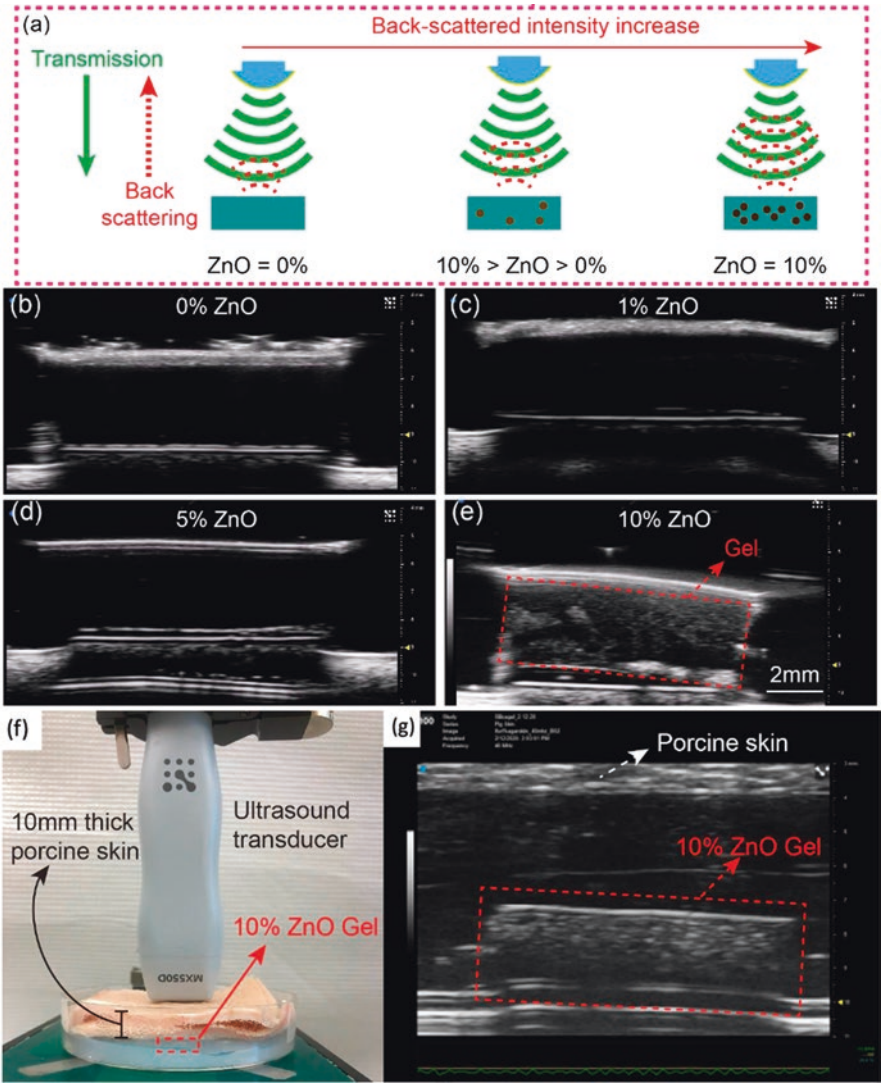

Fig. 7 (**a–e**) US imaging ability of the hydrogel with different concentrations of ZnO nanoparticles, (F–G) Ex vivo US imaging of ZnO-gel when placed under porcine skin. (Image adapted from Ref. [38])

6 Hybrid Nanoparticles in Computed Tomography Imaging

Computed tomography imaging makes use of the penetrating power of X-rays to produce signals which are then analyzed by a computer to generate cross-sectional images. Generated CT contrast is dependent on the mass attenuation coefficient or the photoelectric effect which in turn is proportional to the atomic number of the

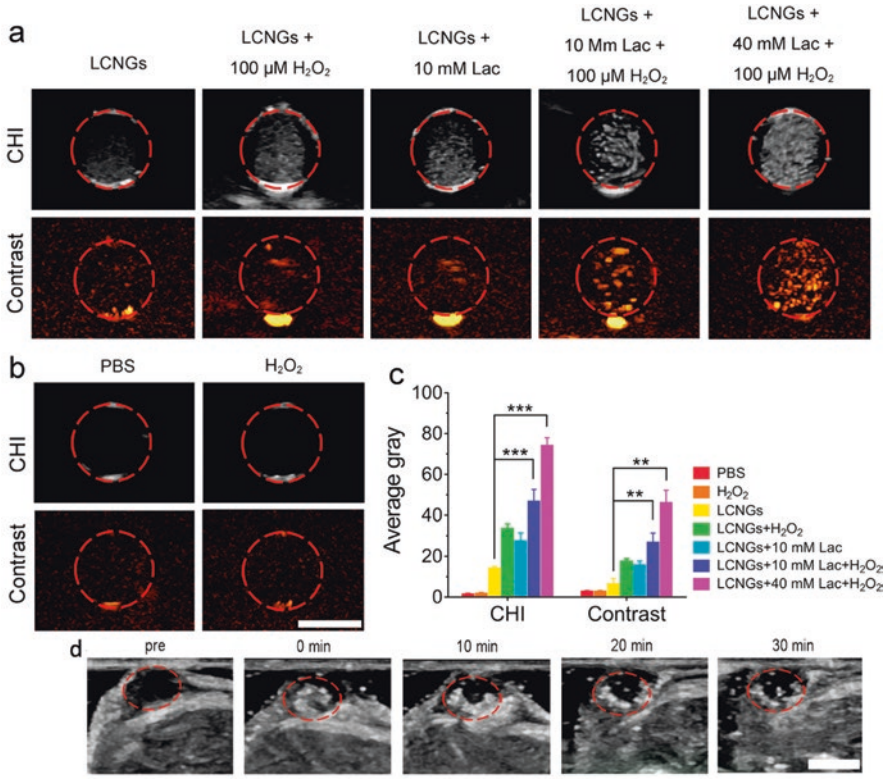

Fig. 8 (**a**) In vitro US images indicating ROI, (**b**) in vitro US images of H_2O_2 and PBS controls, (**c**) graph depicting corresponding mean gray values indicating ROI, (**d**) representative images of in vivo US after LCNGs were injected intratumorally at different time points. (Image adapted from Ref. [39])

material used. To produce good CT contrast, nanoparticles employed are generally composed of inorganic materials having high atomic numbers like tantalum (Ta), gold (Au), and bismuth (Bi). High Z nanoparticles also show advantages like reduction in radiation exposure to patients as a result of the low concentration required to generate significant CT contrast, as compared to traditionally used iodine-based CT contrast agents. Generally, Au is the preferred choice of material due to its biocompatibility and physiological stability. However, a combination of materials including Au may also be used to improve imaging contrast [36].

Sanzhakov et al. 2021 synthesized composite Ph-GNPs by encapsulating Au NPs (GNPs) in phospholipid (Ph) bilayers to increase the stability and decrease the cytotoxicity of Au NPs. Synthesized Ph-GNPs were then functionalized with targeting fragments in the phospholipid bilayer and assessed for their targeting effects via CT imaging in vivo. Figure 9 depicts in vivo CT images obtained after Ph-GNPs were injected intravenously with targeted and non-targeted nanoparticles. The authors concluded that targeted nanoparticles showed greater accumulation in tumors

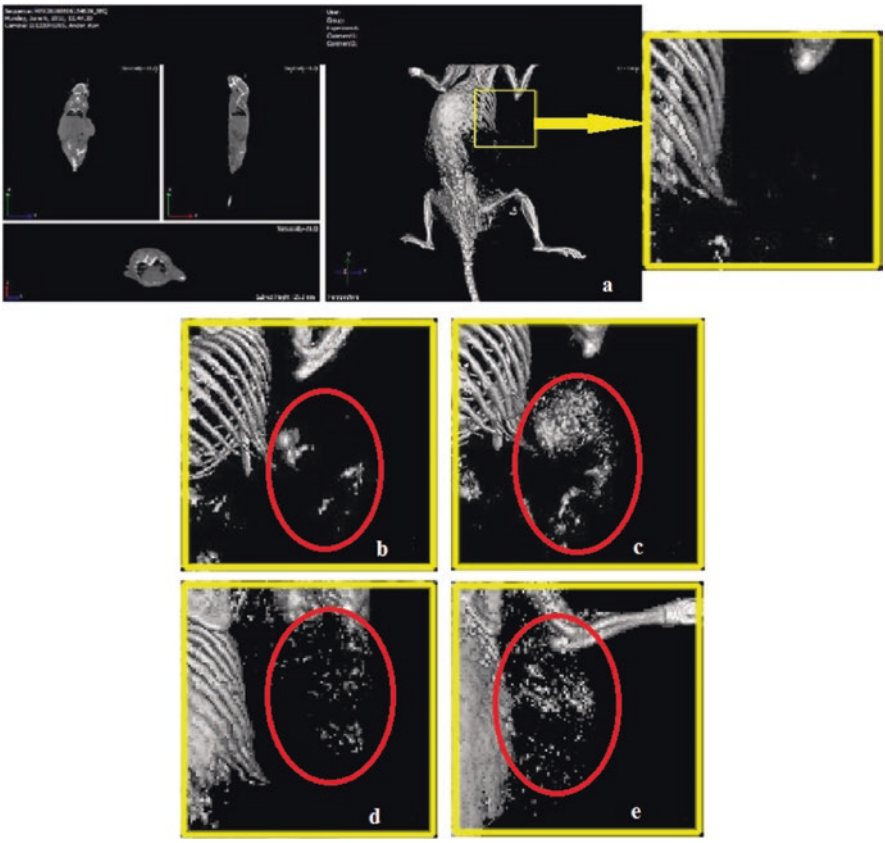

Fig. 9 Representative CT images of mice treated with Ph-GNP (**a**) before injection, (**b**) 1.5 h and (**c**) 2.5 h after treatment with targeted Ph-GNP, (D) 1.5 h and (E) 2.5 h after treatment with non-targeted Ph-GNP. (Image adapted from Ref. [41])

(Fig. 9b, c) as compared to non-targeted Ph-GNP (Fig. 9d, e) and could thus serve as suitable CT contrast agents for imaging of tumors [37]. In another study, Keshavraj et al. in 2018 fabricated alginate hydrogel for loading chemotherapeutic drug cisplatin and Au NPs (ACA nanoparticles) for CT imaging-guided chemotherapy. The nanoparticles showed increasing CT values corresponding to an increase in Au content [38].

He et al. in 2021 synthesized ultrasmall bimetallic nanoparticles composed of gold and bismuth in a 1:1 ratio, capped with captopril (Au_1Bi_1-SR NPs). The introduction of bismuth into Au-SR nanoparticles resulted in the increase of CT value from 20.96 HU for Au-SR NPs to 24.13 HU for Au_1Bi_1-SR NPs. As observed in Fig. 10a, posttreatment with Au_1Bi_1-SR NPs, there is a significant improvement in CT contrast. Figure 10b shows in vivo CT images after intravenous injection of Au_1Bi_1-SR NPs. At 30 min postinjection, CT contrast was clearly observed at the tumor site and the liver. These signals remained significantly visible up to 1 and

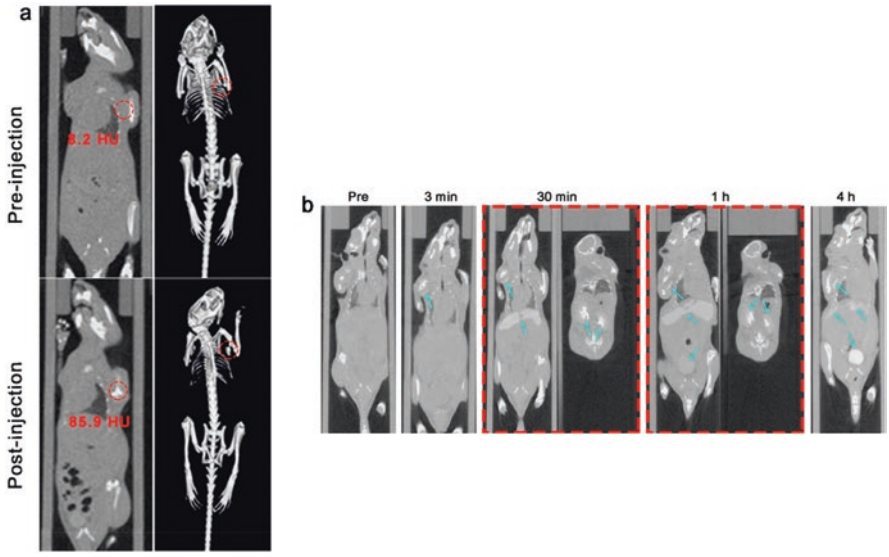

Fig. 10 Representative images of in vivo CT images (**a**) pre- and posttreatment with Au_1Bi_1-SR NPs injected intratumorally (**b**) pre- and posttreatment with Au_1Bi_1-SR NPs at different time intervals. (Image adapted from Ref. [43])

4 hours after treatment indicating the accumulation property of Au_1Bi_1-SR NPs. CT signals were also detected in the kidneys at 30 min and 1 hour posttreatment. Authors claimed metabolization of the nanoparticles through urine as a significant CT signal was also detected in the urinary bladder 1 hour after treatment with Au_1Bi_1-SR NPs [39].

7 Hybrid Nanoparticles in Positron Emission Tomography (PET) and Single-Photon Emission Computed Tomography (SPECT) Imaging

PET/SPECT imaging are nuclear imaging techniques based on the use of radiopharmaceuticals. In both imaging techniques, radiotracers are injected into a subject; however, they differ in their detection mechanism. While SPECT is based on the detection of γ-rays emitted from the radiotracer, in PET imaging radioactive decay of the tracer produces positrons which are then detected by a scanning device. PET is more advantageous than SPECT due to higher spatial and temporal resolution, superior quantitative ability, and higher sensitivity. Nanoparticles used as PET/SPECT tracers are generally nuclides with a long half-life. Commonly used radionuclides for PET include copper-64, indium-111, and zirconium-89, whereas technetium-99 m is commonly used for SPECT [40].

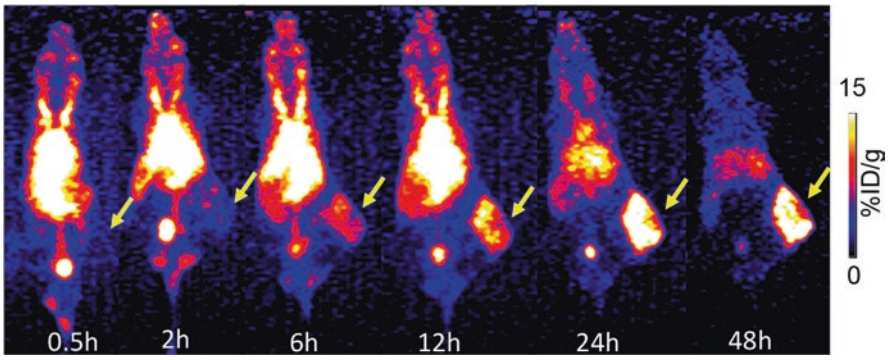

Fig. 11 Representative images of PET imaging in mice treated with ^{86}Y-DOTA-UPSN. (Image adapted from Ref. [45])

Ferreira et al. 2021 utilized ultrasmall porous silica nanoparticle (UPSN) to carry Yttrium-based theranostic pair of radiopharmaceuticals ($^{86/90}$Y) which enabled PET-guided radiotherapy. Figure 11 shows representative PET images taken at different time intervals posttreatment with ^{86}Y-DOTA-UPSN. As observed in the figure, a significant PET signal of ^{86}Y-DOTA-UPSN was observed in blood exhibiting a prolonged circulation time which slowly decreased over time. In the initial time points, PET signal was also observed in the bladder which the authors attributed to renal excretion of nanoparticles with sizes <10 nm. At 48 hours, a significant decrease of PET signal was observed from RES organs, i.e., the liver and spleen which was ascribed to hepatobiliary clearance of ^{86}Y-DOTA-UPSN [41].

Meanwhile, Tian and colleagues modified PEGylated calcium bisphosphonate nanoparticles with radioisotopes ^{99m}Tc (technetium) and ^{32}P (phosphorous) for SPECT-based radioisotope therapy. Fabricated CaBP(^{99m}Tc)-PEG nanoparticles were injected intravenously, and images were captured at various time points post-treatment to determine SPECT imaging ability of the nanoparticles. As observed in Fig. 12c, post-intravenous injection of CaBP(^{99m}Tc)-PEG nanoparticles, gradual time-dependent increase in the tumor, and a decrease in blood circulation in SPECT signal were observed [42].

8 Bimodal or Multimodal Imaging

Advances in materials science and engineering have led to the development of systems that combine different materials into a single system. In terms of imaging, different materials are chosen to give rise to combinations of imaging modalities in a single system which can significantly improve diagnostics as compared to individual counterparts. More recent nanoparticles used for imaging functionalities are often composed of materials that fuse functional and anatomical imaging techniques. The resulting nanoparticle capable of multimodal imaging applications can

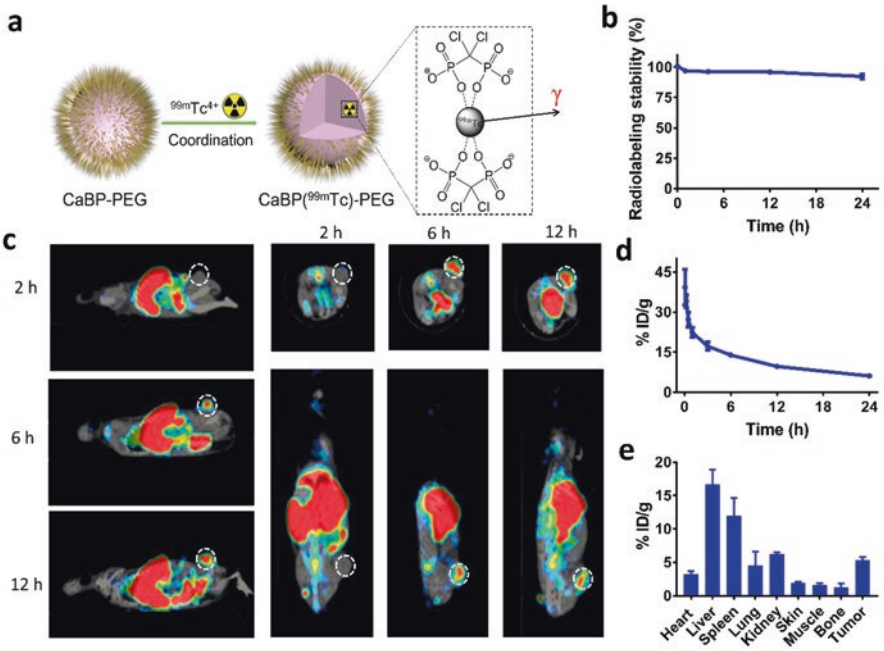

Fig. 12 (**a**) Scheme showing radiolabeling of CaBP-PEG nanoparticles, (**b**) radiolabeling stability of CaBP(^{99m}Tc)-PEG nanoparticles, (**c**) representative in vivo SPECT images of tumor-bearing mice injected with CaBP(^{99m}Tc)-PEG nanoparticles at different time points, (**d**) circulation profile of CaBP(^{99m}Tc)-PEG nanoparticle, (**e**) biodistribution profile of CaBP(^{99m}Tc)-PEG nanoparticles 24 h posttreatment. (Image adapted from Ref. [46])

relay images with higher sensitivity and sometimes can be activated based on a stimulus. Such combinations can also overcome the limitations of individual imaging techniques. In addition to multimodal imaging, combinations of nanomaterials into a single system may also result in increased sensitivity for a particular imaging technique resulting in improved contrast [43]. Examples listing such hybrid nanoparticles capable of multimodal imaging have been discussed below.

SPIONs are most often combined with other imaging moieties or imaging nanoparticles as a result of their favorable properties. The superparamagnetic property of SPIONs enables them to be controlled externally by applying magnetic fields and directing them to the site of interest and simultaneously be used as contrast for MRI. For example, Rodriguez et al. 2019 synthesized multifunctional graphene oxide/iron oxide nanoconjugates (GO-Fe_3O_4) to magnetically control the delivery of graphene oxide (GO) and dual MRI/fluorescence imaging. Toxicity-related issues observed with commercially available Gd^{+3}-based imaging agents such as accumulation in the kidneys and brain were avoided with the use of GO. The authors reported a higher r_2/r_1 ratio of 10.7 as compared to individual Fe_3O_4-based systems, which was attributed to the partial obstruction of Fe_3O_4 by GO reducing its interaction with water molecules. In terms of fluorescence imaging, nanoconjugates

showed peaks in the visible and IR regions, respectively. These peaks showed shifts in alkaline pH indicating their pH-responsive emission behavior as is the case with fluorescence in GO. As the nanoconjugates exhibited green fluorescence, the emission intensity of the GO-Fe_3O_4 system was higher than background autofluorescence [44]. On the other hand, Song et al. in 2017 synthesized Janus nanoparticles consisting of SPIONs embedded in a semiconducting fluorescent polymer that enabled optical imaging upon excitation at 540 nm. SPIONs in the nanosystem were utilized for magnetic particle imaging (MPI) and MRI contrast. The fabricated Fe_3O_4-PFODBT-COOH Janus nanoparticles showed seven times improved MRI contrast as compared to Feraheme with the same iron concentration and three times improved performance than the commercial MPI agent Vivotrax [45]. In another study, Zhang et al. 2017 synthesized Au/Fe_3O_4@C Janus nanoparticles for CT and magnetic resonance-based dual imaging. The controlled synthesis included encapsulation of Fe_3O_4 in carbon (C), while the Au part remained exposed. The exposed Au domain in the nanoparticle was further modified with PEG containing amine and thiol groups and folic acid [46].

Yang et al. 2019 developed a hybrid system for MR/fluorescence imaging by modifying silk fibroin (SF) nanoparticles. Crystallization of manganese oxide (MnO_2) on SF nanoparticles enabled MRI and encapsulation of ICG enabled fluorescence imaging and PTT-PDT [47]. In another study by Hu and colleagues, MnO_2, chlorin e6 (Ce6), and DOX were loaded into a polymeric nanoparticle system (CDM NPs) for theranostic applications. The polymeric nanoparticle system consisted of poly (ε-caprolactone-co-lactide)-b-poly (ethylene glycol)-b-poly (ε-caprolactone-co-lactide), i.e., PCLA-PEG-PCLA amphiphilic block copolymer. The presence of Mn^{+2} enabled T_1-weighted MRI, whereas Ce6 was exploited for PA and fluorescence imaging (Fig. 13). The polymeric matrix acted as a suitable carrier for the hydrophobic and hydrophilic moieties in a single system [48].

There are several such examples of inorganic and organic hybrid nanoparticles wherein the inorganic moiety imparts imaging functionality and the organic moiety

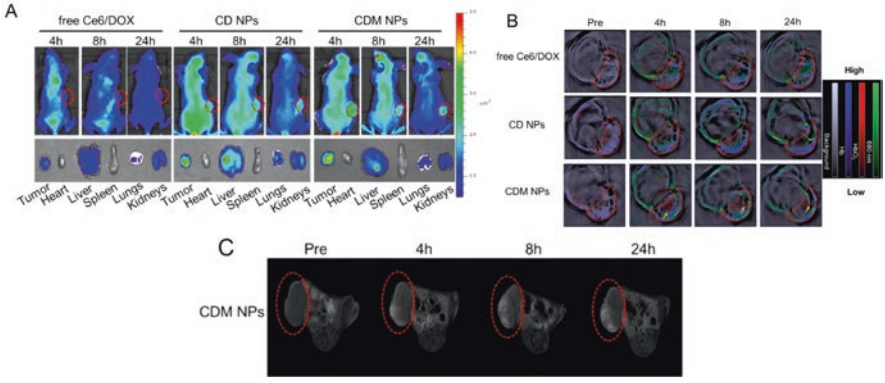

Fig. 13 (**a**) Fluorescence images, (**b**) PA images, and (C) T_1-weighted MRI images of tumor-bearing mice treated with CDM NPs. (Image adapted from Ref. 52)

is used for encapsulating additional imaging molecules. For example, Shen et al. in 2019 reported SPIONs coated with PEGylated phospholipid coating for MR/fluorescence imaging modalities. The SPION enabled MRI, whereas the phospholipid coating was used to encapsulate ICG which in turn was used for fluorescence imaging [49]. In another example, doping with manganese (Mn) was employed to enhance the imaging properties and impart multimodal imaging functionalities to the nanoparticle. Zhou et al. 2018 synthesized a distinctly fluorescent/MR dual imaging nanoparticle system using mesoporous silica nanoparticles with Mn-doped zinc selenide (ZnSe) quantum dots loaded into its pores. High fluorescence and MRI contrast were obtained by preventing agglomeration of the QDs and enrichment of Mn^{+2} concentration. Mn doping increased the fluorescence signal intensity 143-fold and r_1 value by 4 times [50]. Shi et al. in 2019 synthesized nanoparticles capable of MR/fluorescence bimodal imaging by doping Gd^{+3} into CuS nanodisks, which were then coated with PEGylated phospholipid polymer ($DSPE\text{-}PEG_{2000}$) to improve biocompatibility, aqueous solubility, and blood circulation. The nanoparticle assembly was used to carry the fluorophore dye Cy5.5 and matrix metalloproteinase 2 (MMP-2)-cleavable peptide labeled with a quencher, i.e., QSY21. As a result of this, in the presence of MMP-2, the peptide labeled with QSY21 would get cleaved from the nanodisks resulting in a fluorescence signal of Cy5.5. The nanoparticle assembly thus enabled MRI contrast with deep tissue penetration in addition to real-time monitoring of accumulation in vivo noninvasively [51]. In another study, Rich et al. 2020 reported the use of manganese dioxide (MnO_2)-coated ultrasmall $NaYF_4:Nd^{3+}/NaGdF_4$ nanocrystals to modulate hypoxia in head and neck squamous cell carcinoma *via* PAI and MRI. The authors exploited the catalytic property of MnO_2 to convert H_2O_2 (aq) found in the tumor microenvironment into H_2O and O_2 which also enabled PAI. Mn^{+2} generated upon decomposition of MnO_2 in the acidic tumor microenvironment in addition to the Gd ($NaGdF_4$) present in the nanocrystal provided significant contrast for MRI. The resulting usNP-MnO_2 led to an increase in O_2 levels significantly upon the addition of H_2O_2 as observed in Fig. 14a. Figure 14b shows the MRI ability of different concentrations of usNP-MnO_2 in response to treatment with H_2O_2. As observed in the figure, decomposition of the MnO_2 coating into Mn^{2+} ions led to increasing in R_1 in a concentration-dependent manner. Intratumorally injected usNP-MnO_2 also showed significant MRI contrast, whereas PAI of the injected region showed an increase in O_2 levels [52].

Sun et al. 2021 synthesized a hybrid multifunctional nanoparticle consisting of melanin (MNP) coated with Au NR (GNR) and labeled with $^{64}Cu^{2+}$ and Gd^{3+} to yield GNR@MNPs-Gd-^{64}Cu for PAI/MRI/PET-guided PTT of laryngeal cancer. The addition of GNR improved the PAI/PTT ability of the nanoparticle compared to MNP alone, whereas $^{64}Cu^{2+}$ and Gd^{3+} enabled PET and MRI, respectively. The authors assessed in vivo multimodal imaging ability of GNR@MNPs-Gd-^{64}Cu by injecting the nanoparticles in mice bearing Hep-2 tumor and imaging at different time intervals. As observed in Fig. 15a, c, e, signal intensity for each of the imaging techniques peaked at 12 hours postinjection which is in accordance with Fig. 15b showing GNR@MNPs-Gd-^{64}Cu uptake peaked at 12 hours postinjection [53].

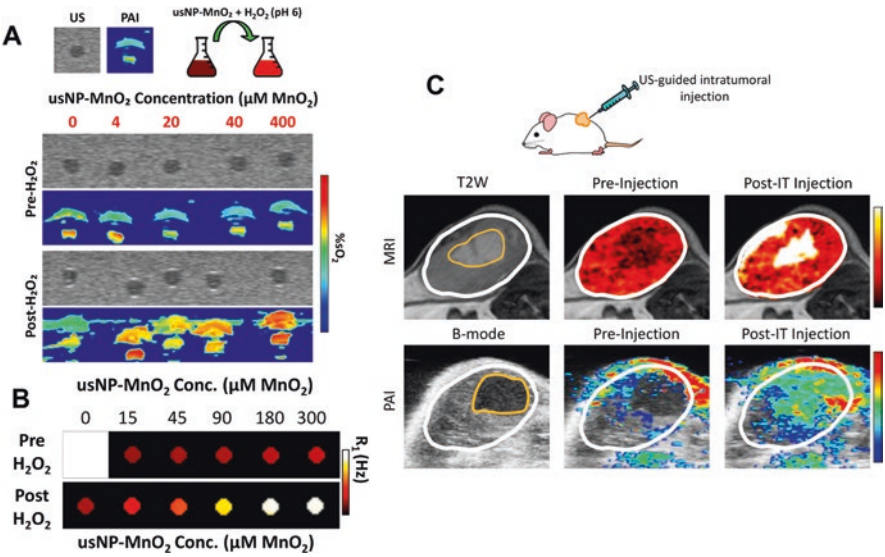

Fig. 14 (**a**) In vitro MR and PA images of usNP-MnO_2 before and after exposure to H_2O_2 in blood, (**b**) T_1 pseudocolorized maps of varying concentrations of usNP-MnO_2 upon exposure to H_2O_2 in water, (**c**) representative MR and PA images of usNP-MnO_2-treated mice before and after treatment. (Image adapted from Ref. 56)

Zhang et al. in 2020 developed a hybrid nanoparticle system capable of triple modal imaging abilities because of its therapeutic effects. The nanoparticle system termed "R-NCNP" consisted of a core@shell nitrogen-doped graphene quantum dot@hollow mesoporous silica nanosphere (N) coated with a layer of mesoporous carbon nitride (C) finally functionalized with PEGylated RGD peptide (R) (Fig. 16a). Nitrogen-doped graphene quantum dots or N-GQDs and carbon nitride or C_3N_4 upon UV-visible irradiation generated significant oxygen radicals that translated into PTT-PDT. N-GQDs also acted as water-splitting agents resulting in the formation of oxygen bubbles. Generated ROS and oxygen bubbles led to mismatched tissue impedance giving rise to echogenicity signals which could be detected by US transducers. Apart from US imaging, R-NCNPs were also able to impart infrared thermal imaging because of PTT activity and fluorescence imaging (Fig. 16b–h) [54]. Table 1 presents striking examples of hybrid nanoparticles that have been used as a multimodal platform for imaging.

9 Conclusions and Perspective

Research on hybrid nanomaterials is currently being undertaken by various biologists, chemists, material scientists, and physicists to integrate and develop novel systems that can be used for clinical purposes. Unique optical properties of hybrid

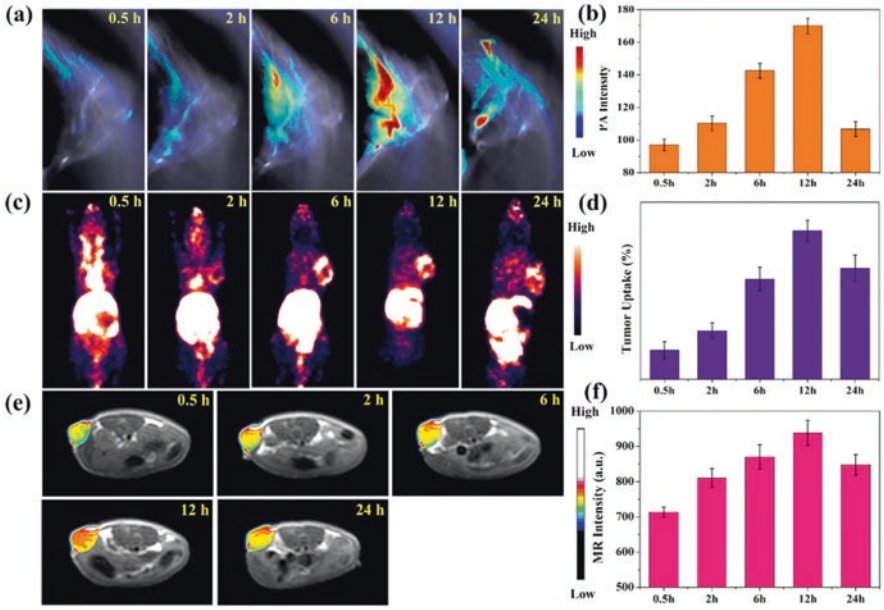

Fig. 15 Representative images of in vivo (**a**) PAI and (**b**) its quantitative estimation, (**c**) PET imaging, (**d**) tumor uptake of GNR@MNPs-Gd-^{64}Cu, (**e**) MRI, and (**f**) its quantitative estimation. (Image adapted from Ref. [57])

nanomaterials can open avenues to be used in clinical imaging modalities. Hybrid nanomaterials can synergize the properties of individual components to get an optimized platform for a specific application. However, it is essential to consider the physicochemical properties of the hybrid nanomaterials especially the size, shape, and surface chemistry of the hybrid nanoparticles for enhancing imaging efficacy and minimizing side effects. Hybrid nanomaterials for on-demand diagnostics and therapeutics have become a hot topic in nanomedicine.

Every imaging technique has certain disadvantages, e.g., limited tissue penetration of optical imaging, poor resolution, sensitivity of radioisotope imaging, and low sensitivity of MRI. It is also thought that combining multiple imaging techniques could complement one another, and, therefore, the development of a multimodal imaging system is envisaged which could be achieved by hybrid nanoparticles. Although significant improvement in the performance of imaging has been demonstrated by hybrid nanomaterials in vitro and in vivo, there are stipulations in their clinical and long-term applications. Usage of nanomaterials is often restricted due to their rapid clearance, poor pharmacokinetic properties, efficacy, and risks associated with the inorganic/organic molecules.

Innovations in precise and fast medical imaging have transformed healthcare science right from diagnosis, monitoring, treating, and even predicting illness.

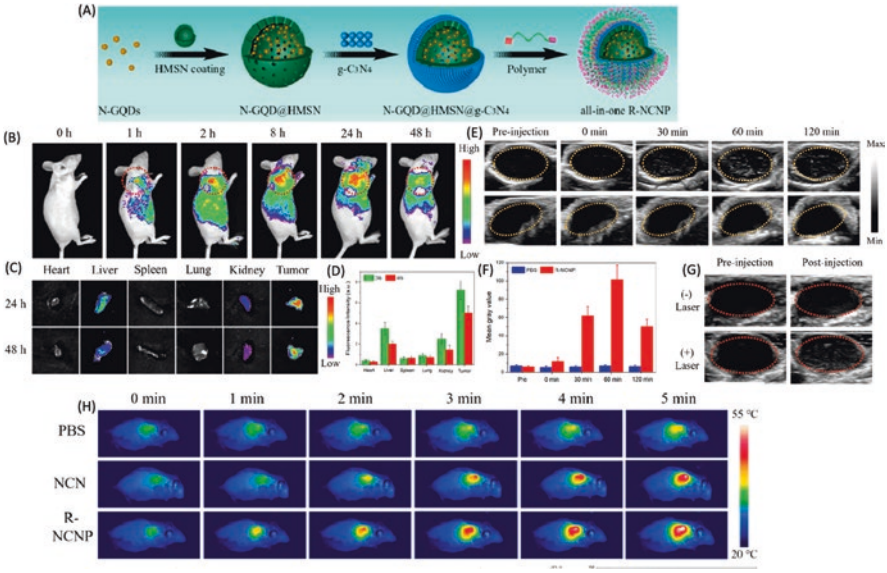

Fig. 16 (**a**) Scheme illustrating the development of R-NCNP, representative images of (**b**) fluorescence imaging in vivo at different time points after treatment with R-NCNP, (**c**) ex vivo fluorescence of different organs at 24 and 48 hours after treatment and (**d**) their quantitative estimation, (**e**) in vivo US imaging of tumor regions before and after treatment with R-NCNP and (**f**) their corresponding mean gray value, (**g**) in vivo US imaging pre-and postinjection of R-NCNP without and with laser irradiation, (**h**) in vivo infrared thermal imaging after 980 nm laser exposure post-treatment with PBS, NCN, and R-NCNP. (Image adapted from Ref. [58])

Nanotechnology has promoted the transformation of medical research to medical practice in the current scenario. We envision that use of hybrid nanomaterials as mentioned in various sections of the chapter will open new avenues for clinical diagnosis and therapy. The use of noninvasive, nonionized, multidimensional imaging modalities can significantly improve clinical diagnosis and boost translational research. Nanotechnology-based on nanohybrids can realize long-term and real-time monitoring of clinical interventions while also comprehending early and accurate diagnosis. In the future, personalized treatment plans can be possible with in-depth research on hybrid nanomaterials.

Hybrid materials chemistry is an upcoming scientific domain that has tremendous potential to impact medical demands. It is an interdisciplinary field of research that encompasses a variety of materials like colloids and nanomaterials of organic and inorganic origin, polymers, interfaces and surfaces, multidimensional nanocomposites, and so on and so forth.

Table 1 Hybrid nanoparticles for singular or multimodal imaging applications

Hybrid nanoparticle system	Imaging modalities	Comments	Disease	Reference
Au@$Cu_{2-x}Se$	PA: Au PTI: Au	NIR-II laser responsive nanoparticles for PA/PT imaging-guided cancer therapy	Cancer	[55]
GNR@PDA	PAI: Au	PDA-coated ultrasmall GNR showed improved PAI contrast as compared to GNR alone	Cancer	[56]
Bi@mSiO_2@MnO_2/DOX	CT: Bi MRI: MnO_2	H_2O_2-triggered MRI contrast observed, CT value (6.865 HU mM^{-1}) higher than that of commercial CT agent iohexol	Cancer	[57]
CUR/CD liposomes	Fluorescence: CD	Liposomes loaded with CD in the aqueous layer and CUR in hydrophobic layer functionalized with anti-CD44 antibodies for fluorescence imaging	Cancer	[58]
GNP-labeled exosomes	CT: Au	MSC-derived exosomes were labeled using glucose-modified GNPs. CT signals were detected in the myocardium, liver, spleen, and kidney	Myocardial infarction	[59]
^{99m}Tc-HSP-PEG	SPECT/CT: ^{99m}Tc	Nanoparticles showed strong radioactive signals depending on the inflammatory state of joints and paws with significant radioactivity observed 1 hour after injection	Rheumatoid arthritis	[60]
Nps@lips	Fluorescence: UCNP	Rare-earth nanoparticles coated with liposomes (Nps: $NaYF_4$:Yb30, Er6@$NaYbF_4$@$NaYF_4$: Nd40)	Brown adipose tissue imaging, vascular and lymph node imaging	[61]
Fe_3O_4@Au@PAA	MRI: Fe_3O_4 CT: Au	Hybrid nanoparticles showed 3X improve T_2-weighted MRI contrast with a CT value of 133.5 HU in vivo 30 min postinjection	–	[62]
CuS@GOD@Gd-MSN	MRI: Gd	GOD, CuS, and Gd loaded MSN for MRI-guided cancer therapy	Cancer	[63]

(continued)

Table 1 (continued)

Hybrid nanoparticle system	Imaging modalities	Comments	Disease	Reference
GC-AuNPs	PAI/US: Au	Nanoparticles injected on right side of tongue. PAI signals detected in primary lymph node 10 min posttreatment followed by signals from secondary lymph node 1 hour posttreatment	Lymph node imaging	[64]
LP@$MnAs_x$	MRI: Mn	Liposomes encapsulating arsenic-manganese complex for MRI-guided therapy. Mn^{+2} released in the acidic environment acts as MRI contrast thus giving pH-responsive MRI contrast agent	Carcinoma	[65]
IO/HSA	MRI: IO Fluorescence: Cy7 CT: Iohexol	Core/shell structure with IO at the core surrounded by different layers of HSA. The different layers were used to entrap cy7 and substitute with iohexol	–	[66]
Ag-UCNPs@SiO_2 (UCNP: $NaYF_4$:Yb^{3+}/Er^{3+})	Fluorescence: Ag-UCNP Micro-CT: Ag-UCNP	The presence of Ag increased fluorescence intensity of UCNPs whereas, the presence of Er in UCNP-enabled micro-CT imaging	Cancer	[67]
MSN@AuNC	CT: Au Fluorescence: MSN@au	BSA-capped AuNCs were loaded into amine-functionalized MSN. The mesoporous structure of MSN resulted in improved CT contrast (2X) and fluorescence. MSN: Enriching contrast medium	–	[68]
MoO_2-SiO_2-Cy5.5	XFCT: MoO_2, Cy5.5	Nanoparticles capable of optical and X-ray fluorescent imaging capabilities	–	[69]
OA-UCNP/ PDA-AuF JNPs	Fluorescence: UCNP CT: AuF MRI: AuF, PDA	Nanoparticles capable of bimodal CT and MR imaging abilities show CT value: 16.2575 HU mM^{-1} and r_2 value: 10.4 s^{-1} mM^{-1}, respectively	Cancer	[70]

(continued)

Table 1 (continued)

Hybrid nanoparticle system	Imaging modalities	Comments	Disease	Reference
UCNPs@bi@SiO_2@ GE HP-lips	UCL: UCNP	Bi was grown on synthesized UCNPs followed by deposition of a layer of SiO_2. GE, and UCNPs@bi@SiO_2 were loaded in the hydrophobic and hydrophilic layers of liposomes. Formulated nanoparticles showed green UCL	Ocular diseases	[71]
CD90@DiR/TMs	Fluorescence: DiR MRI: SPION	Thermosensitive magnetoliposomes encapsulating NIR dye DiR and functionalized with anti-CD90. Imaging signals increased with an increase in time posttreatment followed by a decline after 72 hours	Cancer	[72]
^{68}Ga/DOX/ Si-pc-loaded HMNPs (HMNP: Doped with $Ga_2O_3:Cr^{3+}$, Nd^{3+}, Gd_2O_3)	MRI: Gd_2O_3 PLI: $Ga_2O_3:Cr^{3+}$, Nd^{3+} PET: ^{68}Ga	The combination of gallium and gadolinium oxides and neodymium enabled NIR-responsive PLI, whereas the presence of Gd enabled MRI. Doping was performed on MSN	Cancer	[73]
Bi-Ag@PVP NPs	CT: Bi PA: Ag	Nanoparticles showed higher CT contrast compared to iohexol (CT value: 52.39 HU) in addition to good PA contrast	Bacterial infections in cancer	[74]
SPION/NGO@ PCL-LMWC	MRI: SPION	PCL and chitosan-coated iron oxide/nanographene nanoparticles were synthesized for MRI-guided thermo-chemotherapy	Cancer	[75]
^{64}Cu-DAPTA comb	PET: ^{64}Cu CT: ^{64}Cu	CCR5 targeting DAPTA peptide comb nanoparticles conjugated to ^{64}Cu which showed 40% sensitivity in the detection of atherosclerosis plaques	Atherosclerosis	[76]

(continued)

Table 1 (continued)

Hybrid nanoparticle system	Imaging modalities	Comments	Disease	Reference
iTSL-DOX	Fluorescence: Gd	Thermosensitive liposomes encapsulating Gd-linked lipid in hydrophobic layer and DOX in the hydrophilic layer	Triple-negative breast cancer	[77]
IONP-doped CPN	MRI: IONP Fluorescence: CPN	CPN containing IONP core for MRI and fluorescence-guided cancer therapy	Cancer	[78]
^{99m}Tc-USIONPs	MRI: SPION SPECT/CT: ^{99m}Tc	Nanoparticles showed r_2/r_1 ratio of 4.4 appropriate for T_1 MRI, zwitterionic form prevented RES uptake resulting in higher tumor accumulation and higher contrast	Cancer	[79]
MPN	SPECT/CT: ^{111}In PET/CT: ^{64}Cu	Two formulations: In-MPN-FA and Cu-MPN-PEG. MPN was prepared by mixing respective metal with imidazole and catechol and coating with PEG, followed by functionalization with FA	Cancer	[80]
AuNC-Fe_3O_4/MDP/PFP	PA: Au US: PFP MRI: Fe_3O_4	Mesoporous structure of AuNC in addition to PFP resulted in enhanced low-intensity focused ultrasound, whereas the combined presence of Au and Fe enhanced PA	Retinoblastoma	[81]
Au@CS-PMPC	Fluorescence: Au	Size distribution of nanoparticles ranged from 133–153 nm and showed red fluorescence	–	[82]
Magnetoliposomes	MPI: SPION	Iron oxide nanoparticles loaded into liposomes	–	[83]
$FeWO_x$-PEG-RGD	MRI: Fe CT: W	Ternary oxide material (Fe incorporated in tungsten oxide), nanoparticles showed T_2/T_1 switchable MRI imaging responsive to pH and CT value increased in response to increasing concentrations of W	Cancer	[84]

References

1. Rosenkrans ZT, Ferreira CA, Ni D, Cai W. Internally responsive nanomaterials for activable multimodal imaging of cancer. Adv Healthc Mater. 2020;10(5):2000690–708. https://doi.org/10.1002/adhm.202000690.
2. Shang W, Zeng C, Du Y, Hui H, Liang X, Chi C, Wang K, Wang Z, Tian J. Core-shell gold nanorod@metal-organic framework nanoprobes for multimodality diagnosis of glioma. Adv Mater. 2017;29:1604381–90. https://doi.org/10.1002/adma.201604381.
3. Gindy ME, Prud'homme R. K. "Multifunctional nanoparticles for imaging, delivery and targeting in cancer therapy", expert opinion. Drug Deliv. 2009;6(8):865–78. https://doi.org/10.1517/17425240902932908.
4. Su T, Wang YB, Han D, Wang J, Qi S, Gao L, Shao YH, Qiao HY, Chen JW, Liang SH, Nie YZ, Li JY, Cao F. Multimodality imaging of angiogenesis in a rabbit atherosclerotic model by GEBP11 peptide targeted nanoparticles. Theranostics. 2017;7(19):4791–804. https://doi.org/10.7150/thno.20767.
5. Weissleder R, Nahrendorf M, Pittet MJ. Imaging macrophages with nanoparticles. Nat Mater. 2014;13(2):125–38. https://doi.org/10.1038/nmat3780.
6. Zhang XF, Liu ZG, Shen W, Gurunathan S. Silver nanoparticles: synthesis, characterization, properties, applications, and therapeutic approaches. Int J Mol Sci. 2016;17:1534–68. https://doi.org/10.3390/ijms17091534.
7. Palanisamy S, Wang YM. Superparamagnetic iron oxide nanoparticulate system: synthesis, targeting, drug delivery and therapy in cancer. Dalton Trans. 2019;48(26):9391–834. https://doi.org/10.1039/c9dt00459a.
8. Fu H, Miao C, Rui Y, Hu F, Shen M, Xu H, Zhang C, Dong Y, Wang W, Gu H, Duan Y. Strategy to prevent cardiac toxicity induced by polyacrylic acid decorated iron MRI contrast agent and investigation of its mechanism. Biomaterials. 2019;222:119442–57. https://doi.org/10.1016/j.biomaterials.2019.119442.
9. Guo S, Xiao X, Wang X, Luo Q, Zhu H, Zhang H, Li H, Gong Q, Luo K. Reductive microenvironment responsive gadolinium-based polymers as potential safe MRI contrast agents. Biomater Sci. 2019;7:1919–32. https://doi.org/10.1039/C8BM01103F.
10. Yang X, Yang M, Pang B, Vara M, Xia Y. Gold nanomaterials at work in biomedicine. Chem Rev. 2015;115(19):10410–88. https://doi.org/10.1021/acs.chemrev.5b00193.
11. Lv Q, Min H, Duan DB, Fang W, Pan GM, Shen AG, Wang QQ, Nie G, Hu JM. Total aqueous synthesis of Au@Cu_2-xS core-shell nanoparticles for *in vitro* and *in vivo* SERS/PA imaging-guided photothermal cancer therapy. Adv Healthc Mater. 2018;8(2):1801257–68. https://doi.org/10.1002/adhm.201801257.
12. Zhao S, Tian R, Shao B, Feng Y, Yuan S, Dong L, Zhang L, Liu K, Wang Z, You H. Designing of UCNPs@bi@SiO_2 hybrid theranostic nanoplatforms for simultaneous multimodal imaging and photothermal therapy. ACS Appl Mater Interfaces. 2019;11:394–402. https://doi.org/10.1021/acsami.8b19304.
13. Shimizu T, Ding W, Kameta N. Soft-matter nanotubes: a platform for diverse, functions and applications. Chem Rev. 2020;120(4):2347–407. https://doi.org/10.1021/acs.chemrev.9b00509.
14. Svenson S. The dendrimer paradox – high medical expectations but poor clinical translation. Chem Soc Rev. 2015;44(12):4131–44. https://doi.org/10.1039/c5cs00288e.
15. Bozzuto G, Molinari A. Liposomes as nanomedical devices. Int J Nanomedicine. 2015;10:975–99. https://doi.org/10.2147/IJN.S68861.
16. Mitchell MJ, Billingsley MM, Haley RM, Wechsler ME, Peppas NA, Langer R. Engineering precision nanoparticles for drug delivery. Nat Rev Drug Discov. 2021;20:101–24. https://doi.org/10.1038/s41573-020-0090-8.
17. Gallagher FA, Thakor AS, Serrao EM, Goh V. Functional and molecular imaging for personalised medicine in oncology. In: Adam A, Dixon AK, Gillard JH, Schaefer-Prokop CM,

editors. Grainger and Allison's diagnostic radiology: a textbook for medical imaging. Elsevier Inc; 2021. p. 1755–70.
18. Li C, Wang Q. Opportunities for intravital near-infrared fluorescence imaging technology in the second transparent window. ACS Nano. 2018;12(10):9654–9. https://doi.org/10.1021/acsnano.8b07536.
19. Stender AS, Marchuk K, Liu C, Sander S, Meyer MW, Smith EA, Neupane B, Wang G, Li J, Cheng JX, Huang B, Fang N. Single cell optical imaging and spectroscopy. Chem Rev. 2013;113(4):2469–527. https://doi.org/10.1021/cr300336e.
20. Chawla S. Nanoparticles and fluorescence. In: Aliofkhazraei M, editor. Handbook of nanoparticles. Springer; 2016. p. 961–83. https://doi.org/10.1007/978-3-319-15338-4_43.
21. Hameed S, Bhattarai P, Liang X, Zhang N, Xu Y, Chen M, Dai Z. Self-assembly of porphyrin-grafted lipid into nanoparticles encapsulating doxorubicin for synergistic chemo-photodynamic therapy and fluorescence imaging. Theranostics. 2018;8(19):5501–18. https://doi.org/10.7150/thno.27721.
22. Luo C, Yu B, Qi Q, Mi Y, Cao Z, Cui Q, Mi Y, Cao Z, Cui Q, Zhao Z. Construction of magnetic-fluorescent bifunctional nanoparticles *via* miniemulsion polymerization for cell imaging. Colloids Surf A Physicochem Eng Asp. 2021;613:1–8. https://doi.org/10.1016/j.colsurfa.2020.126062.
23. Dong X, Liang J, Yang A, Qian Z, Kong D, Lv F. Fluorescence imaging guided CpG nanoparticles-loaded IR820-hydrogel for synergistic photothermal immunotherapy. Biomaterials. 2019;209:111–25. https://doi.org/10.1016/j.biomaterials.2019.04.024.
24. Jiang Y, Huang J, Zhen X, Zeng Z, Li J, Xie C, Miao Q, Chen J, Chen P, Pu K. A generic approach towards afterglow luminescent nanoparticles for ultrasensitive *in vivo* imaging. Nature Commun. 10:1–10. https://doi.org/10.1038/s41467-019-10119-x.
25. Park S, Kim H, Lim SC, Lim K, Lee SE, Oh KT, Choi HG, Youn YS. Gold nanocluster-loaded hybrid albumin nanoparticles with fluorescence-based optical visualization and photothermal conversion for tumor detection/ablation. J Control Release. 2019;304:7–18. https://doi.org/10.1016/j.jconrel.2019.04.036.
26. Kumawat MK, Thakur M, Bahadur R, Kaku T, Prabhuraj RS, Ninawe A, Srivastava R. Preparation of graphene oxide-graphene quantum dots hybrid and its applications in cancer theranostics. Mater Sci Eng C. 2019;103:1–11. https://doi.org/10.1016/j.msec.2019.109774.
27. Liu H, Lv X, Qian J, Li H, Qian Y, Wang X, Meng X, Lin W, Wang H. Graphitic carbon nitride quantum dots embedded in carbon nanosheets for near-infrared imaging-guided combined photo-chemotherapy. ACS Nano. 2020;14(10):13304–15. https://doi.org/10.1021/acsnano.0c05143.
28. Ortgies DH, Tan M, Ximendes EC, del Rosal B, Hu J, Xu L, Wang X, Rodriguez EM, Jacinto C, Fernandez N, Chen G, Jaque D. Lifetime-encoded infrared-emitting nanoparticles for *in vivo* multiplexed imaging. ACS Nano. 2018;12(5):4362–8. https://doi.org/10.1021/acsnano.7b09189.
29. Kim T, Zhang Q, Li J, Zhang L, Jokerst J. A gold/silver hybrid nanoparticle for treatment and photoacoustic imaging of bacterial infection. ACS Nano. 2018;12(6):5615–25. https://doi.org/10.1021/acsnano.8b01362.
30. Zhou C, Zhang L, Sun T, Zhang Y, Liu Y, Gong M, Xu Z, Du M, Liu Y, Liu G, Zhang D. Activatable NIR-II plasmonic nanotheranostics for efficient photoacoustic imaging and photothermal cancer therapy. Adv Mater. 2020;33(3):1–11. https://doi.org/10.1002/adma.202006532.
31. Ouyang Z, Li D, Xiong Z, Song C, Gao Y, Liu R, Shen M, Shi X. Antifouling dendrimer-entrapped copper sulfide nanoparticles enable photoacoustic imaging-guided targeted combination therapy of tumors and tumor metastasis. ACS Appl Mater Interfaces. 2021;13(5):6069–80. https://doi.org/10.1021/acsami.0c21620.
32. Li L, Guan Y, Xiong H, Deng T, Ji Q, Xu Z, Kang Y, Pang J. Fundamentals and applications of nanoparticles for ultrasound-based imaging and therapy. Nano Select. 2020;1(3):263–84. https://doi.org/10.1002/nano.202000035.

33. Zeng F, Du M, Chen Z. Nanosized contrast agents in ultrasound molecular imaging. Front Bioeng Biotechnol. 2021;9:1–7. https://doi.org/10.3389/fbioe.2021.758084.
34. Jiang H, Carter N, Zareei A, Nejati S, Waimin J, Chittiboyina S, Niedert E, Soleimani T, Lelievre S, Goergen C, Rahimi R. A wireless implantable strain sensing scheme using ultrasound imaging of highly stretchable zinc oxide/poly dimethylacrylamide nanocomposite hydrogel. ACS Appl Bio Mater. 2020;3(7):4012–24. https://doi.org/10.1021/acsabm.9b01032.
35. Wu Q, Zhang Q, Yu T, Wang X, Jia C, Zhao Z, Zhao J. Self-assembled hybrid nanogel as a multifunctional theranostic probe for enzyme-regulated ultrasound imaging and tumor therapy. ACS Appl Bio Mater. 2021;4(5):4244–53. https://doi.org/10.1021/acsabm.1c00079.
36. Shilo M, Reuveni T, Motiei M, Popovtzer R. Nanoparticles as computed tomography contrast agents: current status and future prospects. Fut Nanomed. 2012;7(2):257–69. https://doi.org/10.2217/nnm.11.190.
37. Sanzakhov M, Kudinov V, Baskaev K, Morozevich G, Stepanova D, Torkhovskaya T, Tereshkina Y, Korotkevich E, Tikhonova E. Composite phospholipid-gold nanoparticles with targeted fragment for tumor imaging. Biomed Pharmacother. 2021;142:1–8. https://doi.org/10.1016/j.biopha.2021.111985.
38. Keshavraj M, Moloudi K, Paydar R, Abed Z, Beik J, Ghaznavi H, Shakeri-Zadeh A. Alginate hydrogel co-loaded with cisplatin and gold nanoparticles for computed tomography image-guided chemotherapy. J Biomater Appl. 2018;33(2):161–9. https://doi.org/10.1177/0885328218782355.
39. He F, Ji H, Feng L, Wang Z, Sun Q, Zhong C, Yang D, Gai S, Yang P, Lin J. Construction of thiol-capped ultrasmall Au-Bi bimetallic nanoparticles for X-ray CT imaging and enhanced antitumor therapy efficacy. Biomaterials. 2021;264:1–13. https://doi.org/10.1016/j.biomaterials.2020.120453.
40. Livieratos L. Basic principles of SPECT and CT imaging. In: Fogelman I, Gnanasegaran G, van der Wall H, editors. Radionuclide and hybrid bone imaging. Springer; 2012. p. 1–16. https://doi.org/10.1007/978-3-642-02400-9_12.
41. Ferreira C, Goel S, Ehlerding E, Rosenkras Z, Jiang D, Sun T, Aluicio-Sarduy E, Engle J, Ni D, Cai W. Ultrasmall porous silica nanoparticles with enhanced pharmacokinetics for cancer theranostics. Nano Lett. 2021;21(11):4692–9. https://doi.org/10.1021/acs.nanolett.1c00895.
42. Tian L, Yi X, Dong Z, Xu J, Liang C, Chao Y, Wang Y, Yang K, Liu Z. Calcium bisphosphonate nanoparticles with chelator-free radiolabeling to deplete tumor-associated macrophages for enhanced cancer radioisotope therapy. ACS Nano. 2018;12(11):11541–51. https://doi.org/10.1021/acsnano.8b06699.
43. Han X, Xu K, Taratula O, Farsad K. Applications of nanoparticles in biomedical imaging. Nanoscale. 2019;11(3):799–819. https://doi.org/10.1039/c8nr07769j.
44. Gonzalez-Rodriguez R, Campbell E, Naumov A. Multifunctional graphene oxide/iron oxide nanoparticles for magnetic targeted drug delivery dual magnetic resonance/fluorescence imaging and cancer sensing. PLoS One. 2019:1–18. https://doi.org/10.1371/journal.pone.0217072.
45. Song G, Chen M, Zhang Y, Cui L, Qu H, Zheng X, Wintermark M, Liu Z, Rao J. Janus iron oxide @ semiconducting polymer nanoparticle tracer for cell tracking by magnetic particle imaging. Nano Lett. 2017;18(1):182–9. https://doi.org/10.1021/acs.nanolett.7b03829.
46. Zhang Q, Zhang L, Li S, Chen X, Zhang M, Wang T, Li L, Wang C. Designed synthesis of au/Fe_3O_4@C Janus nanoparticles for dual-modal imaging and actively targeted chemo-photothermal synergistic therapy of cancer cells. Nanomedicine. 2017;23(18):17242–8. https://doi.org/10.1002/chem.201703498.
47. Yang R, Hou M, Gao Y, Zhang L, Xu Z, Li CM, Kang Y, Xue P. Biomineralization-inspired crystallization of manganese oxide on silk fibroin nanoparticles for *in vivo* MR/fluorescence imaging-assisted tri-modal therapy of cancer. Theranostics. 2019;9(21):6314–33. https://doi.org/10.7150/thno.36252.
48. Hu DR, Chen LJ, Qu Y, Peng JR, Chu BY, Shi K, Hao Y, Zhong L, Wang MY, Qian ZY. Oxygen-generating hybrid polymeric nanoparticles with encapsulated doxorubicin and

chlorin e6 for trimodal imaging-guided combined chemo-photodynamic therapy. Theranostics. 2018;8(6):1558–74. https://doi.org/10.7150/thno.22989.
49. Shen C, Wang X, Zheng Z, Gao C, Chen X, Zhao S, Dai Z. Doxorubicin and indocyanine green loaded superparamagnetic iron oxide nanoparticles with PEGylated phospholipid coating for magnetic resonance with fluorescence imaging and chemotherapy of glioma. Intl J Med. 2019;14:101–17. https://doi.org/10.2147/IJN.S173954.
50. Zhou R, Sun SK, Li C, Wu L, Hou X, Wu P. Enriching Mn-doped ZnSe quantum dots onto mesoporous silica nanoparticles for enhanced fluorescence/MRI dual-modal bio-imaging. ACS Appl Mater Interfaces. 2018;10(40):34060–7. https://doi.org/10.1021/acsami.8b14554.
51. Shi H, Sun Y, Yan R, Liu S, Zhu L, Liu S, Feng Y, Wang P, He J, Zhou Z, Ye D. Magnetic semiconductor Gd-doping CuS nanoparticles as activatable nanoprobes for bimodal imaging and targeted photothermal therapy of gastric tumors. Nano Lett. 2019;19(2):937–47. https://doi.org/10.1021/acs.nanolett.8b04179.
52. Rich L, Damasco J, Bulmahn J, Lutscher H, Prasad P, Sheshadri M. Photoacoustic and magnetic resonance imaging of hybrid manganese dioxide-coated ultra-small NaGdF4 nanoparticles for spatiotemporal modulation of hypoxia in head and neck cancer. Cancers. 2020;12(11):1. https://doi.org/10.3390/cancers12113294.
53. Sun J, Li L, Cai W, Chen A, Zhang R. Multifunctional hybrid nanoprobe for photoacoustic/PET/MR imaging-guided photothermal therapy of laryngeal cancer. ACS Appl Bio Mater. 2021;4(6):5312–23. https://doi.org/10.1021/acsabm.1c00423.
54. Zhang X, Machuki JO, Pan W, Cai W, Xi Z, Shen F, Zhang L, Yang Y, Gao F, Guan M. Carbon nitride hollow theranostic nanoegulators executing laser-activatable water splitting for enhanced ultrasound/fluorescence imaging and cooperative phototherapy. ACS Nano. 2020;14(4):4045–60. https://doi.org/10.1021/acsnano.9b08737.
55. Shan B, Liu H, Li L, Lu Y, Li M. Near-Infrared II Plasmonic phototheranostics with glutathione depletion for multimodal imaging-guided hypoxia-tolerant chemodynamic-photocatalytic-photothermal cancer therapy triggered by a single laser. Small. 18(4):1–10. https://doi.org/10.1002/smll.202105638.
56. Yim W, Borum R, Zhou J, Mantri Y, Wu Z, Wu Z, Zhou J, Jin Z, Creyer M, Jokerst J. Ultrasmall gold-nanorod-polydopamine hybrids for enhanced photoacoustic imaging and photothermal therapy in second near-infrared window. Nano. 2022;6(1):79–90. https://doi.org/10.7150/ntno.63634.
57. Zhao H, Wang J, Li X, Li Y, Li C, Wang X, Wang J, Guan S, Xu Y, Deng G, Chen Y, Lu J, Liu X. A biocompatible theranostic agent based on stable bismuth nanoparticles for X-ray computed tomography/magnetic resonance imaging-guided enhanced chemo/photothermal/chemodynamic therapy for tumours. J Colloid Interface Sci. 2021;604:80–90. https://doi.org/10.1016/j.jcis.2021.06.174.
58. Demir B, Moulahoum H, Ghorbanizamani F, Barlas F, Yesiltepe O, Gumus Z, Meral K, Demirkol D, Timur S. Carbon dots and curcumin-loaded CD-44 targeting liposomes for imaging and tracking cancer chemotherapy: a multi-purpose tool for theranostics. J Drug Del Sci Technol. 2021;62:1–9. https://doi.org/10.1016/j.jddst.2021.102363.
59. Gong L, Weng Y, Zhou W, Zhang K, Li W, Jiang J, Zhu J. *In vivo* CT imaging of gold nanoparticle-labeled exosomes in a myocardial infarction mouse model. Annals Transl Med. 2021;9(6):1–10. https://doi.org/10.21037/atm-21-981.
60. Zhang Q, Li D, Zhong J, Wu Y, Shi Y, Yang H, Zhao L, Yang K, Lin J. SPECT imaging and highly efficient therapy of rheumatoid arthritis based on hyperbranched semiconducting polymer nanoparticles. Biomater Sci. 2021;9(5):1845–54. https://doi.org/10.1039/d0bm02037k.
61. Yang J, He S, Hu Z, Zhang Z, Cao C, Cheng Z, Fang C, Tian J. *In vivo* multifunctional fluorescence imaging using liposome-coated lanthanide nanoparticles in near-infrared-II/IIa/IIb windows. Nano Today. 2021;38:1–11. https://doi.org/10.1016/j.nantod.2021.101120.
62. Nguyen H, Le T, Nguyen T, Phan T, Ho D, Pham H, Nguyen T, Le T, Tran L. Molecular imaging contrast properties for dual-mode MR/CT imaging applications. Chem Select. 2021;6(35):9389–98. https://doi.org/10.1002/slct.202102791.

63. Ye Y, Huang X, Luo B, Wang X, Cai X. Multiparametric magnetic resonance imaging to monitor the early antitumor effect of CuS@GOD nanoparticles in a 4T1 breast cancer xenograft model. J Magn Reson Imaging. 2021;55(1):301–10. https://doi.org/10.1002/jmri.27867.
64. Sun I, Jo S, Dumani D, Yun W, Yoon H, Lim D, Ahn C, Emelianov S, Kim K. Theranostic glycol chitosan-conjugated gold nanoparticles for photoacoustic imaging f regional lymph nodes and delivering tumor antigen to lymph nodes. Nano. 2021;11(7):1–13. https://doi.org/10.3390/nano11071700.
65. Jin Z, Yi X, Yang J, Zhou M, Wu P, Yan G. Liposome-coated arsenic-manganese complex for magnetic resonance imaging-guided synergistic therapy against carcinoma. Int J Nanomedicine. 2021;16:3775–88. https://doi.org/10.2147/IJN.S31962.
66. Ganguly S, Neelam G, Margel S. Layer by layer controlled synthesis at room temperature of tri-modal (MRI, fluorescence and CT) core/shell superparamagnetic IO/human serum albumin nanoparticles for diagnostic applications. Polym Adv Technol. 2021;32(10):3909–21. https://doi.org/10.1002/pat.5344.
67. Zhang W, Lu Y, Zang Y, Han J, Xiong Q, Xiong J. SiO_2 coated up-conversion nanomaterial doped with Ag nanoparticles for micro-CT imaging. Nano. 2021;11(12):1–12. https://doi.org/10.3390/nano11123395.
68. Yuan Y, Zhou R, Li T, Qu S, Bai H, Liang J, Cai X, Guo B. Enriched Au nanoclusters with mesoporous silica nanoparticles for improved fluorescence/computed tomography dual-modal imaging. Cell Prolif. 2021;54(4):1–11. https://doi.org/10.1111/cpr.13008.
69. Saladino G, Vogt C, Li Y, Shaker K, Brodin B, Svenda M, Hertz H, Toprak M. Optical and X-ray fluorescent nanoparticles for dual mode bioimaging. ACS Nano. 2021;15(3):5077–85. https://doi.org/10.1021/acsnano.0c10127.
70. Chen X, Zhang X, Zhang L, Gao Y, Wang C, Hong W, Zhao G, Li L, Liu R, Wang C. Amphiphilic Janus nanoparticles for imaging-guided synergistic chemo-photothermal hepatocellular carcinoma therapy in the second near-infrared window. Nanoscale. 13(7):3974–82. https://doi.org/10.1039/d0nr09017d.
71. Yu Y, Huang Y, Feng W, Yang M, Shao B, Li J, Ye F. NIR-triggered upconversion nanoparticles@thermo-sensitive liposome hybrid theranostic nanoplatform for controlled drug delivery. RSC Adv. 2021;11:29065–72. https://doi.org/10.1039/D1RA044314A.
72. An Y, Yang R, Wang X, Han Y, Jia G, Hu C, Zhang Z, Liu D, Tang Q. Facile assembly of thermosensitive liposomes for active targeting imaging and synergetic chemo−/magnetic hyperthermia therapy. Front Bioeng Biotechnol. 202;9:1–12. https://doi.org/10.3389/fbioe.2021.691091.
73. Zou R, Gao Y, Zhang Y, Jiao J, Wong K, Wang J. 68Ga-labeled magnetic-NIR persistent luminescent hybrid mesoporous nanoparticles for multimodal imaging-guided chemotherapy and photodynamic therapy. ACS Appl Mater Interfaces. 2021;13(8):9667–80. https://doi.org/10.1021/acsami.0c21623.
74. Zhou Z, Xie J, Ma S, Luo X, Liu J, Wang S, Chen Y, Yan J, Luo F. Construction of smart nanotheranostic platform Bi-Ag@PVP: multimodal CT/PA imaging-guided PDT/PTT for cancer therapy. ACS Omega. 2021;6(16):10723–34. https://doi.org/10.1021/acsomea/1c00225.
75. Kiamohammadi L, Asadi L, Shirvalilou S, Khoei S, Khoee S, Soleymani M, Minaei S. Physical and biological properties of 5-fluorouracil polymer-coated magnetite nanographene oxide as a new thermosensitizer for alternative magnetic hyperthermia and a magnetic resonance imaging contrast agent: *in vitro* and *in vivo* study. ACS Omega. 2021;6(31):20192–204. https://doi.org/10.1021/acsomega/1c01763.
76. Detering L, Abdilla A, Luehmann H, Williams J, Huang L, Sultan D, Elvington A, Heo G, Woodard P, Gropler R, Randolph G, Hawker C, Liu Y. CC chemokine receptor 5 targeted nanoparticles imaging the progression and regression of atherosclerosis using positron emission tomography/computed tomography. Mol Pharm. 2021;18(3):1386–96. https://doi.org/10.1021/acs.molpharmaceut.0c01183.
77. Amrahli M, Centelles M, Cressey P, Prusevicius M, Gedroyc W, Xu X, So P, Wright M, Thanou M. MR-labelled liposomes and focused ultrasound for spatiotemporally controlled

drug release in triple negative breast cancers in mice. Nano. 2021;5(2):125–42. https://doi.org/10.7150/ntno.52168.
78. Arias-Ramos N, Ibarra L, Serrano-Torres M, Yagüe B, Caverzán M, Chesta C, Palacios R, López-Larraubia P. Iron oxide incorporated conjugated polymer nanoparticles for simultaneous use in magnetic resonance and fluorescent imaging of brain tumors. Pharmaceutics. 2021;13(8):1–21. https://doi.org/10.3390/pharmaceutics13081258.
79. Wang P, Sun W, Guo J, Zhang K, Liu Y, Jiang Q, Su D, Sun X. One pot synthesis of zwitterionic 99mTc doped ultrasmall iron oxide nanoparticles for SPECT/T1-weighted MR dual-modality tumor imaging. Colloids Surf B: Biointerfaces. 2021;197:1–7. https://doi.org/10.1016/j.colsurfb.2020.111403.
80. Suárez-García S, Esposito T, Neufeld-Peters J, Bergamo M, Yang H, Saatchi K, Schaffer P, Häfeli U, Ruiz-Molina D, Rodríguez C, Novio F. Hybrid metal-phenol nanoparticles with polydopamine-like coating for PET/SPECT/CT imaging. ACS Appl Mater Interfaces. 2021;13(9):10705–8. https://doi.org/10.1021/acsami.0c20612.
81. Wang M, Yang Q, Li M, Zou H, Wang Z, Ran H, Zheng Y, Jian J, Zhou Y, Luo Y, Ran Y, Jiang S, Zhou X. Multifunctional nanoparticles for multimodal imaging-guided low-intensity focused ultrasound/immunosynergistic retinoblastoma therapy. ACS Appl Mater Interfaces. 2020;12(5):5642–57. https://doi.org/10.1021/acsami.9b22072.
82. Ma K, Cheng Y, Wei X, Chen D, Zhao X, Jia P. Gold embedded chitosan nanoparticles with cell mimetic polymer coating for pH-sensitive controlled drug release and cellular fluorescence imaging. J Biomater Appl. 2020;35(7):857–68. https://doi.org/10.1177/0885328220952594.
83. Rost N, Sen K, Savliwala S, Singh I, Liu S, Unni M, Raniero L, Rinaldi C. Magnetic particle imaging performance of liposomes encapsulating iron oxide nanoparticles. J Magn Magn Mater. 2020;504:1–7. https://doi.org/10.1016/j.jmmm.2020.166675.
84. Cheng Y, Lu H, Yang F, Zhang Y, Dong H. Biodegradable $FeWO_x$ nanoparticles for CT/MR imaging-guided synergistic photothermal, photo-dynamic, and chemodynamic therapy. Nanoscale. 2021;13:3049–60. https://doi.org/10.1039/d0nr07215j.

Hybrid Nanoparticles in Biomedical Applications

Navjeet Kaur Lotey, Suhas Pednekar, and Ramesh Chaughule

Abbreviations

API	Active Pharmaceutical Ingredient
BBB	Blood-Brain Barrier
CNT	Carbon Nanotubes
DOX	Doxorubicin
ECM	Extra Cellular Matrix
EPR	Enhanced Permeability and Retention
FDA	Food and Drugs Association
FRET	Fluorescence Resonance Energy Transfer
GRAS	Generally Recognized as Safe
HPV	Human Papilloma Virus
MNPs	Magnetic Nanoparticles
MRI	Magnetic Resonance Imaging
NIR	Near Infrared
NLC	Nanostructured Lipid Carriers
NPs	Nanoparticles
PAE	Polyamideamine-epichlorohydrin
PAMAM	Polyamidoamine
PAMAMOS	Polyamidoamine Organosilicon

N. K. Lotey (✉)
National Center for Nanoscience and Nanotechnology, University of Mumbai, Mumbai, India

Ramnarain Ruia Autonomous College, Mumbai, India
e-mail: navjeet.kaur@nano.mu.ac.in

S. Pednekar
University of Mumbai, Mumbai, India

R. Chaughule
Ramnarain Ruia Autonomous College, Mumbai, India

R. S. Chaughule et al. (eds.), *Nanomaterials for Cancer Detection Using Imaging Techniques and Their Clinical Applications*,
https://doi.org/10.1007/978-3-031-09636-5_13

PCL	Polycaprolactone
PCT	Paclitaxel
PDT	Photo Dynamic Therapy
PEG	Polyethylene Glycol
PEI	Polyethyleneimine
PGA	Polyglycolic Acid
PLA	Poly (L-Lactic) Acid
PLA	Polylactic Acid
PLGA	Polylactic-co-Glycolic Acid
PPI	Polypropylene Ether Imine
PTT	Photo Thermal Therapy
PVA	Polyvinyl Alcohol
PVP	Polyvinylpyrrolidone
RES	Reticuloendothelial System
SEM	Scanning Electron Microscope
SLN	Solid Lipid Nanoparticle
SPIONs	Superparamagnetic Iron Oxide Nanoparticles
TEM	Tunnelling Electron Microscope
VEGF	Vascular Endothelial Growth Factor

1 Introduction

In the past two decades, nanotechnology has introduced many transformational inventions and dramatic possibilities in the field of nanomedicine. Nanoparticles in general are identified as entities with unique physical and chemical properties compared to conventional materials. Nanoparticles can be designed out of single materials or can also be hybridized with two or more materials. The properties of such nanosystems can be tuneable by manipulating factors such as size, shape, and surface chemistry.

Many areas of medicine have benefited from the applications of hybrid nanomaterials. These hybrid systems have been beneficial in increasing the bioavailability of many drugs and therapeutics which have poor solubility or stability. They behave as appropriate carriers to ensure the protection and passage of sensitive compounds through biological barriers as well as enabling targeted and sustained release as required. Cancer targeting has been the most dominant application as it can dramatically transform the disease prognosis and outcome. Alongside, many researchers are also working on drug delivery applications related to inflammation, gene therapy, and brain-related disorders [1, 2]. Many combinations of functionalized nanomaterials are being increasingly explored for this purpose and many of them are presently in preclinical and clinical trials. Nanomaterials have significantly improvised the specificity, sensitivity, and rapid detection of diagnostic tools based on biosensors, lab-on-chip, and nanofluidic devices. In the case of imaging, nanoparticles have enabled higher-resolution output and improved contrast in many

techniques based on microscopy, tomography, and MRI [3, 4]. Nanoparticles are also being studied for their application in tissue regeneration and wound healing because of their excellent penetration efficiency, low toxicity, and biocompatibility [5]. Additionally, certain nanoparticles have intrinsic potentials wherein they are being used as antimicrobial agents or therapeutic compounds themselves. The overall efficiency of existing diagnostic and therapeutic applications has been elevated by the use of nanosystems.

Despite the several superior characteristics of nanosystems, the use of single material may have some limitations. The interaction of nanoparticles with biological systems is an intricate and complicated process. There are several barriers in living organisms that protect the body from "foreign" particles. Various approaches have been explored to address this wide range of problems which contribute majorly to the overall effectiveness of the therapy. The barriers in physical form such as the dermal layers or mucus block the free passage of materials by maintaining unfavorable physicochemical barriers, pH variations, protective fluids over the cornea and tympanum, mucus lining of varying thickness, and more. All therapeutic molecules must be able to surpass these primary barriers of defense and then also overcome cellular level barriers which range from general to highly specific recognition and response patterns. Figure 1 represents some of the commonly encountered nanoparticle-cell surface interactions. These receptors and markers will vary from one individual to another with heterogeneity under a diseased state. Encountering these barriers depends greatly on the mode of administration of the payload agent. For example, a drug that has been orally ingested would have to retain stability and functionality after overcoming the first pass effect of metabolism in the gastrointestinal (GI) tract. The same drug if administered intravenously would directly enter the circulatory system avoiding the barriers of the GI tract. However, selecting the material and design of delivery vehicles depends on many critical parameters such as ease of administration, site of action, onset and duration of action, the quantity of

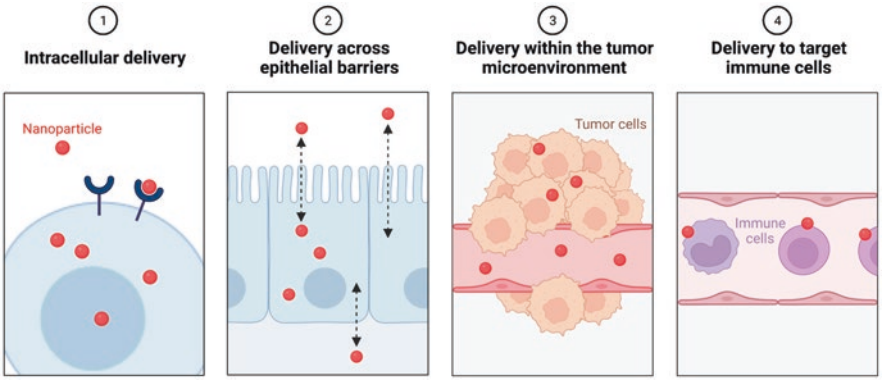

Fig. 1 Modes of the interaction of nanoparticles with different types of cells and tissues. As illustrated, in figure (*1*), intracellular delivery of the payload can be achieved only after successfully interacting with the cell surface receptors of the target tissue

the drug, metabolism by the liver, excretion by the kidney, and the fate of by-products and toxicity profile.

Thus, choosing materials suitable to meet such complicated and interlinked properties involves careful crafting developed through elaborate and structured scientific studies. Some key factors such as safety, solubility, and stability of the payload, pharmacokinetic properties, microenvironment of the target tissue, degree of vascularization, frequency of dosage, and economic considerations will help in selecting the optimal combination suitable for "tailor-made" medicine [6].

Nanomaterials such as polymers improve their blood circulation and retention time preventing premature leakage, evading macrophage clearance, attaining better specificity, and enhancing the drug release kinetics. These hybrid nanoparticles can also be designed specifically for personalized tailor-made medicine to suit the needs on a case-to-case basis. This approach not only helps in alleviating problems associated with toxicity but also improves performance synergistically. The properties of hybrid nanostructures have been appreciated by several researchers. A variety of organic and inorganic materials have been explored for this purpose. In this chapter, we have focused on hybrid nanomaterials as the majority of applications in the nanomedicine or biomedical sector. We have added a special focus on dendrimers which possess unique architectural properties and are an emerging trend in nanomedicine [7].

2 Design and Architecture

In the purview of biomedical applications, hybrid nanostructures are one of the most sought-after designs. Combining properties from different materials can be directed toward synergistic action for overcoming these biological barriers. To begin with the choice of nanomaterial, one can filter the properties of interest to be incorporated in the desired carrier vehicle. Organic materials, in general, have a lower refractive index, lower conductivity, lower density, and lower thermal stability, but generally flexible and soft owing to elastic properties. Inorganic materials, on the other hand, have a higher refractive index, higher conductivity, higher density, and higher thermal stability giving better strength and hardness. But inorganic materials are not easily biocompatible, may lead to toxicity, and may have poor retention and clearance properties in a living system. Researchers continue to explore several combinations of these hybrid structures to optimize their performance in a given application. Customizing these properties to suit the desired end product can be made possible by hybridizing these nanomaterials [8]. Figure 2 illustrates a generic hybrid nanoparticle composed of a core and a polymeric branched coating which has been further decorated with moieties such as therapeutic drugs, markers, targeting ligands, and imaging agents. This system can be controlled by means of external or internal stimuli which, upon trigger, would enable the release of the payload.

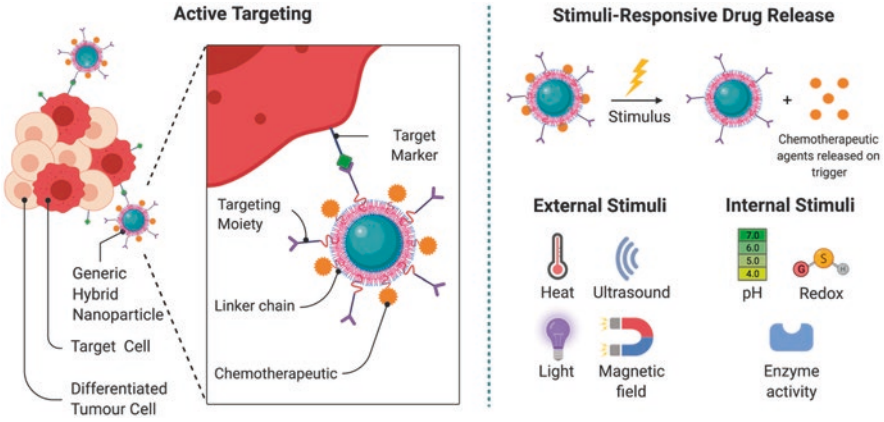

Fig. 2 Delivery mechanism of a hybrid nanoparticle conjugated with multifunctional ligands

The design and architecture of nanoparticles will be pivotal in determining their multifunctional behavior across biological barriers with a variety of ligands. The design of these particles would also enable the possibilities and flexibility of stimulus-based control for delivery or activation of the therapeutic agents. Different materials have their own advantages and limitations. Hybridization is, thus, a careful intricate trade-off between these properties to achieve an overall superior hybrid composition as compared to its individual components. For example, iron oxide nanoparticles are the most widely inorganic materials due to their magnetic properties and biocompatibility. However, size-, shape-, and concentration-dependent cytotoxicity and bioavailability issues have also been reported in many cases. They may also face issues associated with agglomeration, rapid systemic clearance, and attack by the natural defense mechanism. On the other hand, materials like lipids and polymers have excellent biocompatibility and can easily surpass biological barriers. For example, by combining magnetic nanoparticles with organic polymers, synergistic action is achieved which is overall superior in performance as compared to the individual properties of these materials. A polymer-coated magnetic nanoparticle is able to achieve magnetic targeting, magnetofection, magnetic response-dependent phototherapy, magnetic imaging contrast agent, or even a theranostic particle [7, 9, 10]. Individually, neither the magnetic particles nor the polymers are capable of performing such combined actions in a single dose of application.

There are several designs that are used to hybridize such materials. In general, a core material such as a metal that is conjugated polymeric branches emerging like corona-like spherical from the core is referred to as *core brush hybrids*. *Hybrid nanogels* are made by embedding or encapsulating core nanoparticles inside a gel-like matrix of polymeric chains. Figure 3 illustrates the most widely explored designs, viz., core brush, nanogel, and a core shell. A core brush structure is usually composed of a solid inorganic core conjugated with a network of polymeric branches. A nanogel is composed of solid inorganic NPs entrapped within a cross-linked gel formed out of polymeric monomers. A core shell represents a type of

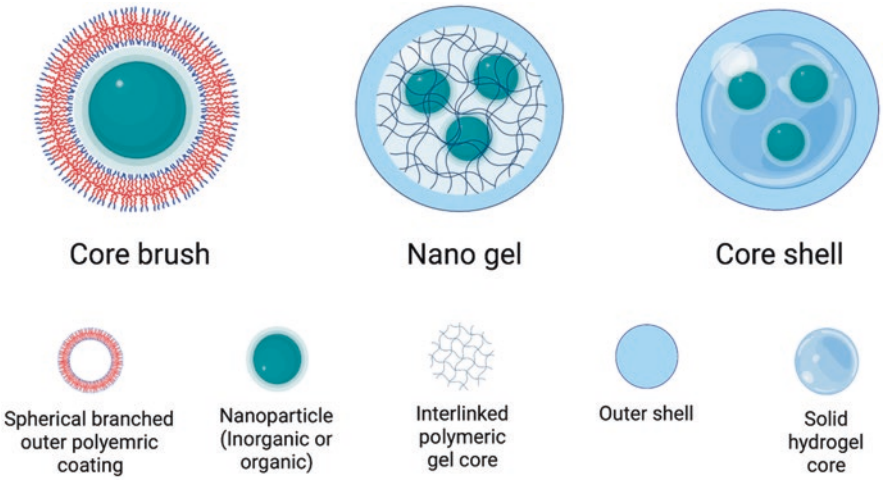

Fig. 3 Different structural combinations of hybrid nanoparticles

design made up of a compact defined matrix to encapsulate the core nanoparticle by interacting closely with its surface [11]. It should be noted that these schematics are an oversimplified representation of the copious possibilities of hybrid structures that can be generated by manipulating the physical and chemical properties of individual components.

A synergistic model is advantageous as it encompasses improved properties of interacting and actively performing in dynamic biological environments. Ismail et al. have reported one such simple hybrid nanomaterial composed of inorganic ZnO nanoparticles and organic polymer Carbopol (shown in Figs. 4 and 5) to achieve a synergistic effect with enhanced antibacterial properties [8].

Hybrid nanoparticles encompass a wide variety of possible combinations of materials. While several innovative methods continue to emerge, there are a few generalized techniques used to achieve hybridization. Depending upon materials, a wide range of interactions can be involved such as covalent bonds, ionic complexion, self-assembly, intermolecular interactions, electrostatic interactions, dispersion interactions, H-bonds, weak bonds, and microstructuring [12, 13].

The most common approaches are physical adsorption and covalent interactions. Physical adsorption is a widely used, simple-to-perform technique, wherein inorganic components such as metallic NPs are surface-treated to adsorb organic materials like polymers [14]. Although this method is simpler to perform and involves fewer steps, it has limited control over stimuli triggers and may also have limitations with respect to functionalization. The covalent interactions approach is comparatively laborious and time-consuming, but it offers precise control over targeting, functionalization, and controlling the release or activation of agents upon a defined stimulus. This method makes use of covalent bonding between the hybridizing materials and can be further divided into the following strategies which have also been represented in Fig. 6.

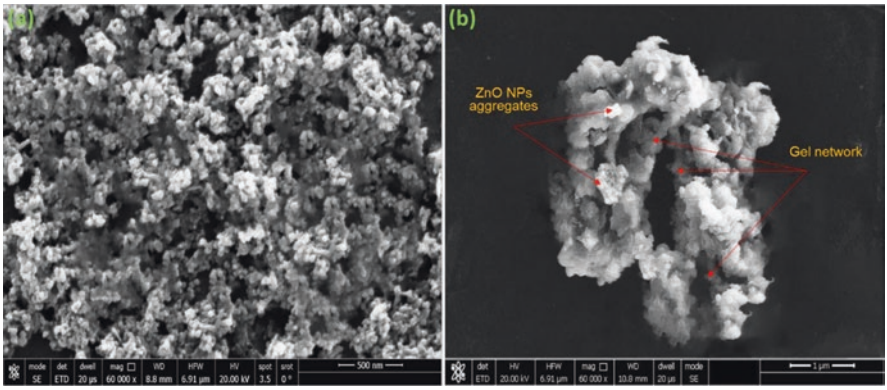

Fig. 4 Field-emission SEM image of (**a**) ZnO NPs and (**b**) Carbopol/ZnO hybrid nanoparticles gel. (Image adapted from open access article by Ismail et al. (2021) [8])

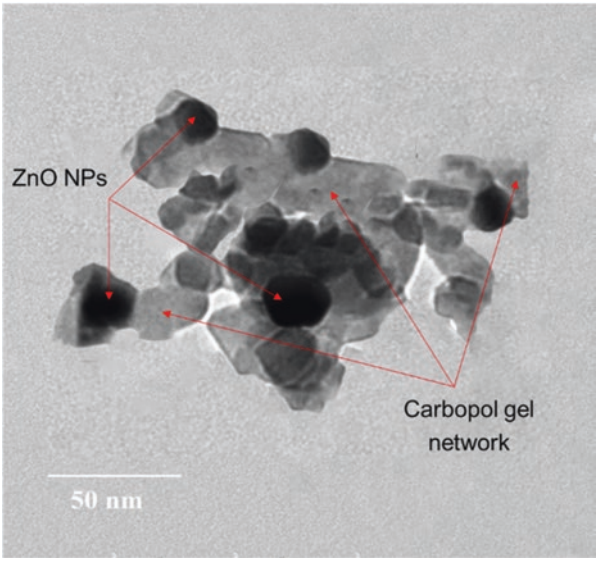

Fig. 5 HR-TEM image of ZnO-Carbopol hybrid NPs representing the Carbopol gel network with ZnO NPs embedded in it. (Image adapted from open access article by Ismail et al. (2021) [8])

(a) *Grafting to:* The materials of interest are synthesized individually and are later conjugated by means of a linker or some other agent if required [7] (Fig. 6a).
(b) *Grafting from*: The surface of a core nanoparticle is decorated with "initiator" molecules which are used to initiate the growth of polymeric chains [9],[15] (Fig. 6b).
(c) *Grafting through*: The inorganic nanoparticle is incorporated inside the polymer chains which have been cross-linked through the groups attached on the surface of NPs [14], [7] (Fig. 6c).

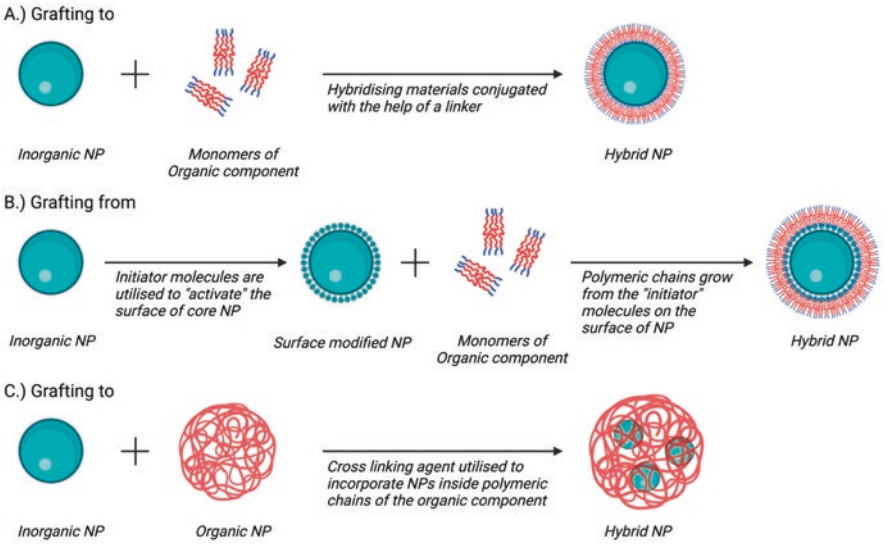

Fig. 6 Synthesis strategies for generating hybrid nanoparticles – Hybridisation with the help of a linker (**a**), Polymeric chains growing onto the modified surface of a particle (**b**) and cross linking the particles indside a chain or mesh like polymeric structure (**c**) have been represented schematically

3 Nanomaterials Used in Hybrid Compositions

Hybrid nanomaterials are generally defined as unique chemical conjugates of organic and/or inorganic materials [16]. They could either comprise two or more organic, inorganic, or a mixture of both types of material. Based on composition, they can be classified into the following categories, viz., polymeric, inorganic, and lipid-based as represented in Fig. 7.

Over the past two decades, nanomedicine has seen a consistent uprise in innovative hybrid material products. Some of the materials appealing to the desired properties of products to be used in biological systems have been discussed in this section. The purview of products that have been successfully commercialized or are currently undergoing clinical trials is majorly composed of biocompatible lipids, liposomes, polymeric NPs, albumin NPs, and selected inorganic NPs.

3.1 Organic

Organic materials have been a popular choice of nanomaterials for drug delivery and other biomedical applications owing to higher biocompatibility with living systems. Some of the most commonly used organic-based nanomaterials used in hybridization have been discussed below.

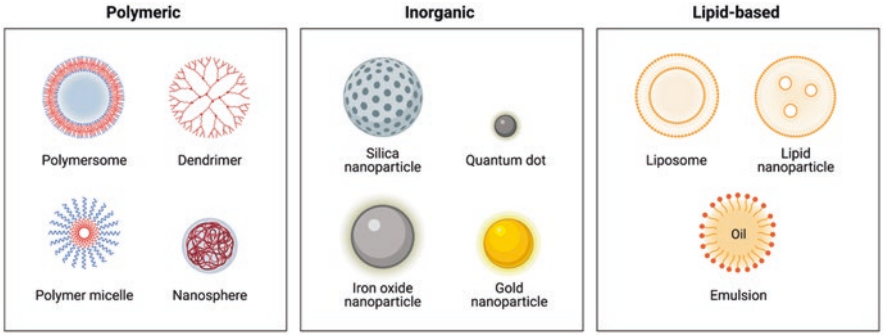

Fig. 7 Major categories of nanoparticles used in the nanomedicine sector based on the material composition

3.1.1 Lipids and Liposomes

Lipids are found both in nature and can be synthesized easily. Liposomes are amphipathic lipid vesicles with one or more bilayers. Liposomes can be synthesized artificially and can readily be surface-modified to enhance their properties. Many liposomal-based drug combinations have been approved by the FDA, and the recent ones seem to be significantly better-performing than their individual counterparts. Owing to the amphiphilic properties, lipids and liposomes are attributed as thermodynamically stable structures. Some common phospholipids used in lipid-based vesicles or liposomal structures are listed below:

- *Phosphatidylcholine.*
- *Phosphatidylethanolamine.*
- *Phosphatidylserine.*
- *Phosphatidylglycerol.*

Lipids and liposomes have been recommended for the vehiculation of many drugs to reduce their toxicity and increase their targeting and bioavailability. They are categorized as compounds that are "generally recognized as safe" (GRAS) owing to the natural origin of raw compounds [17]. Lipid-based materials are often hybridized with several nanoparticles which have limitations such as enzymatic degradation, cellular uptake, rapid systemic clearance, and pharmacokinetic properties. They are readily functionalized stable structures that can protect the conjugated nanoparticle and/or payload from biological barriers such as harsh GI tract conditions [18]. Owing to the amphiphilic nature of lipid-based nanoparticles, they can co-deliver both hydrophobic and hydrophilic drugs efficiently thus enabling higher possibilities of synergistic multidrug therapies [19]. An interesting geometry of scalable, biocompatible, and high drug loading capacity is found in solid lipid nanoparticles (SLN) and nanostructured lipid carriers (NLC). SLNs are composed of solid lipids with melting points above 40 °C which offer controlled release. Alongside, they offer more chemical versatility and production scalability as compared to liposomes and emulsions. NLCs are compounds made with a mixture of

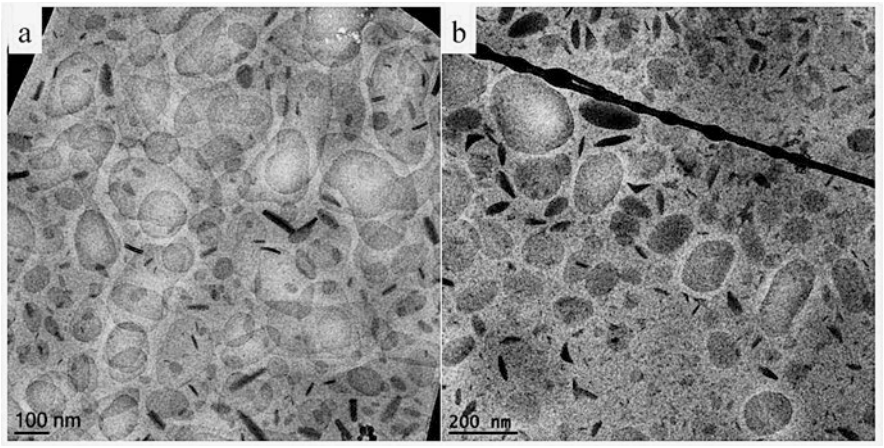

Fig. 8 TEM micrograph of SLN AND NLC based structures. (Image adapted from open access article by Hallan SS (2021) [18])

solid and liquid lipids (oils) which are blended to remain solid at body temperatures but may have lower melting points as compared to SLNs. The advantage of using oils enhances the lipophilic drug-carrying capacity and avoids recrystallization of the solid lipid layer over prolonged storage conditions. SLNs and NLCs have been highly appreciated for the flexibility they offer to enable a wide range of lipophilic compounds [17]. Figure 8 represents a TEM image of SLN and NLCs.

Although lipids and liposomes offer several advantages as delivery vehicles, they have certain disadvantages such as high polydispersity, rapid burst release, nontarget interactions, etc. which reduce their specificity and sensitivity for personalized medicine [20]. The overall advantage of hybridizing materials for nanomedicine-based applications is to increase solubility and circulation time, improvise stability and specificity, and decrease toxicity during systemic distribution. The limitations of lipid-based vesicles have been mitigated several folds by hybridizing with polymers leading to a new generation of nanosystems named lipid-polymer hybrid nanoparticles (LPHNPs) [21]. Such systems combine several advantages of both the materials such as enhanced biocompatibility, higher carrying capacity, better control over drug release profile, and pharmacokinetics. In general, LPHNPs are made up of a polymeric core conjugated with the payload which is encapsulated in a lipid liposomal bilayer. They are mainly classified into the following major categories based on their structure:

- *Monolithic hybrid nanosystems.*
- *Core-shell nanosystems.*
- *Hallow core-shell nanoparticles.*
- *Biomimetic lipid-polymer hybrid nanosystems.*
- *Polymer-caged liposomes.*

Several combinations of polymers have been explored as a component of LPHNPs. The next section describes a few of them. LPHNPs have been studied widely, and several reports confirm greater vehicular stability with minimal losses of the payload [22]. The outmost lipid shell of LPHNPs enables functionalization and conjugation of ligands which contribute to properties enhancing targeting and receptor-mediated internalization and thereby reducing undesired side effects of the drugs for non-diseased tissues [23]. Hybridized lipid-polymeric structures have been reported to perform superior as compared to mono-component structures in terms of drug loading capacity, target cell internalization, and controlled sustained drug release. LPHNPs have also been employed for the co-administration of drugs along with radioisotopes, nucleotide sequences, proteins, and diagnostic agents [24]. Some of the recent developments of LPHNPs have been summarized in Table 1 located at the end of the chapter.

3.1.2 Polymers

Biodegradable and bioabsorbable polymers have enabled the formulation and delivery of several drugs which were otherwise limited by solubility, bioavailability, systemic clearance, and toxicity issues. Several polymers have been studied as hybridizing components of nanosystems. Polymeric NPs can also be artificially synthesized and are readily functionalized. They are mostly used in "core-shell" types of construct hybrids. Some of the most commonly used polymers in biomedical applications are:

- *Polyethylene glycol (PEG).*
- *Polycaprolactone (PCL).*
- *Polyglycolic acid (PGA).*
- *Polylactic acid (PLA).*
- *Polyethyleneimine (PEI).*
- *Poly β-amino ester (PAE).*
- *Polyvinyl alcohol (PVA).*
- *Chitosan.*
- *Cyclodextrin.*
- *Polysaccharides.*
- *Alginate.*
- *Hyaluronic acid*

Polymers possess characteristics such as high mechanical strength and stability. This helps in improvising kinetics during systemic circulation and long-term storage. Bioabsorbable and biodegradable hydrogels like PLA, PGA, and their derivatives have been extensively used to deliver therapeutic agents in deeper tissues of the body [25]. PEG is a water-soluble building block that is used to construct micelles. They are highly biocompatible and biodegradable enabling better retention and clearance properties. For example, PEG-coated lipid particles have been known to have better circulation time in vivo by evading the immune system

Table 1 Examples of hybrid nanomaterials used for drug delivery and other biomedical applications

Core material	Hybridized material	Hybrid conjugation strategy	API conjugate	Drug release mechanism	Target action/ application	Ref.
Exosomes	Liposomes	Incubation resulting in similar lipid membranes fusion	CRISPR/Cas9	Transfection	Gene therapy-based tool. Allows crossing of stringent membranes like the blood-brain barrier or placental barrier while evading rapid phagocytosis	[5]
Polysiloxane matrix	Gadolinium	Chelation	Custom	Tumor EPR	Antitumor activity, exploiting ultrasmall size (< 5 nm) particles for overcoming stringent biological barriers; ultrasmall size of NPs crosses blood-brain barrier, high retention time	[6]
1,2-dioleoyl-3-trimethylammonium-propane	PLGA	Ultrasonic emulsification	17AAG	Receptor-mediated endocytosis	Colon cancer HSP90 inhibitor; greater efficiency in tumor cell apoptosis and better antitumor results	[7]
Hollow mesoporous silica nanoparticles	Acetylated carboxymethyl cellulose	Carbodiimide linkage	Doxorubicin, AS1411 aptamer	Receptor-mediated endocytosis	Antitumor agent, nucleolin receptor on MCF-7 and C26 cell lines; enhanced targeting in overexpressed nucleolin receptor on cancer cell lines	[8]
GITR antibody decorated PLGA	PLG and PLH	Electrostatic interactions	Imatinib and IR-780 dye	Receptor-mediated endocytosis, pH-sensitive	Photothermal, photodynamic therapy, and anticancer effect; multifunctional hybrid nanoparticle carrier complex enhances receptor-mediated internalization of the drug, delivers dyes for photothermal and photodynamic therapy, and alongside improvises T cell-based functions	[9]

Chitosan	Liposomes	Carbodiimide linkage	Moxifloxacin hydrochloride	Receptor-mediated endocytosis	Targeting intraocular inflammation, antibacterial activity; improved drug retention time, enhanced corneal permeability, improved bioavailability of a hydrophobic drug	[10]
Zien	Lecithin	Phase separation	Panax notoginseng saponins	Receptor-mediated endocytosis	Targeting cardiovascular and cerebrovascular disease, penetrating intestinal epithelium; greater penetration into mucus layers, higher drug loading capacity, enhanced oral bioavailability	[11]
PCL chain triglyceride (MCT) hybrid core	Octadecylamine and poloxamer 188	Ultrasonic emulsification	Cabazitaxel	pH-sensitive	Overcoming GI barrier to deliver anticancer therapeutics; improved solubility of the drug, increased penetration in mucus membranes, increased oral bioavailability	[8]
Poly (lactide-co-glycoside)	Phospholipid	Solvent diffusion	Nitric oxide (shell) and doxorubicin (core)	Diffusion	Antitumor activity targeted through photoactivation; precise regulation of drug release with light-activated components enhanced intracellular drug concentration	[12]
DSPE-MPEG5000 and ISL	PLGA	Nano-precipitation	Paclitaxel and triptolide	Diffusion	Non-small cell lung cancer, synergistic antitumor effect; improved multidrug resistance, reduced tumor growth compared to free drug, reduced systemic toxicity	[13]

(continued)

Table 1 (continued)

Core material	Hybridized material	Hybrid conjugation strategy	API conjugate	Drug release mechanism	Target action/ application	Ref.
DSPE-PEG2K-MAL	PLGA-COOH	Nano-precipitation	Plumbagin	Transferrin receptor-mediated endocytosis, EPR	B-16, F-12 melanoma antitumor activity; significant reduction/ disappearance of melanoma induced tumor with negligible distress or side effect in model organisms	[14]
DSPE-PEG-2000	PLGA	Nano-precipitation	Beta-sitosterol	Microcirculation through size control	Hepato-protective agent, CYP2E1 enzyme inhibition; increased bioavailability, potentially scalable method	[7]
Chitosan	Lecithin	Ionic gelation	Curcumin and tamoxifen	pH-sensitive	Antitumor activity, arrest of go/G1 phase, controlled release; efficient multidrug carrier system, synergistic effect of drugs controlled tumor growth more aggressively than solo therapy	[15]
L soybean L-α-phosphatidyl-ethanolamine and L-α-phosphatidylcholine	Magnesium hydroxide	Microfluidic double emulsion	VEGF	pH-sensitive	Significant improvement in stability and bioactivity of VEGF	[16]
Lecithin	PLGA	Nano-precipitation	Doxorubicin	Controlled release diffusion	Breast cancer, enhanced antitumor activity in biocompatible formulations	[17]
Myristic acid	Polyoxyethylene (40) stearate and polyoxyethylene (100) stearate	Ultrasonic emulsification	Doxorubicin	pH-sensitive	Targeting breast cancer, enhanced intra-tumoral penetration and retention of doxorubicin	[18]

PLGA-PEG	L-α-phosphatidylcholine from soybean	Carbodiimide linkage	A10–3.2 aptamer; curcumin and cabazitaxel	Controlled release diffusion	Targets prostate cancer, aptamer functionalized; improved tumor cell inhibition efficiency due to synergistic effect	[19]
Stearic acid	PEG	Carbodiimide linkage	Docetaxel and resveratrol	EPR, active targeting	Overexpressed EGFR receptor targeting in NSCLC; significant synergistic effect on tumor tissue, low systemic toxicity	[20]
Chitosan	Glyceryl monooleate	Self-assembly	Paclitaxel D-α-tocopherol PEG 1000 succinate, pluronic P123, CYP450 inhibitor- BC0	Controlled release diffusion	Increased oral and intestinal absorption of BCS IV drugs; enhanced oral absorption, muco-adhesion and stability, improved absorption in intestines due to addition of P-gp and BC0 inhibitors	[21]
Chitosan	Lipoid S75	Ionic gelation	Cisplatin	Sustained released	Targeting testicular and ovarian cancer, higher cellular internalization leads to a higher cytotoxic effect; a suitable, low immunogenic platform for poorly water-soluble drugs like cisplatin	[22]
Iron oxide nanoparticles	Graphene oxide	One-pot hydrothermal method	Curcumin	Receptor-dependent	Cancer, bacterial infections, autoimmune diseases, human serum albumin targeted; increased bioavailability and enhanced targeting effects	[23]
Silver nanoparticles	P[(2-((2-((camptothecin)-oxy) ethyl) disulfanyl) ethylmethacrylate)-co-(2-(D-galactose) methylmethacrylate)] (P(MACPTS-co-MAGP))	Nanoparticle surface energy transfer (NSET) effect	Camptothecin	Redox-responsive disulfide bonds	Drug delivery and fluorescence imaging. Monitoring real-time drug release response in tumor tissues	[39]

(continued)

Table 1 (continued)

Core material	Hybridized material	Hybrid conjugation strategy	API conjugate	Drug release mechanism	Target action/ application	Ref.
Alginate polymer	Cellulose nanocrystals	Ionic gelation	Rifampicin	pH-sensitive	Tuberculosis antibiotic with improved stability, durability, and diffusion rate of hybrid carrierdrug protected from gastric conditions	[40]
Nanocurcumin	Virosome	Encapsulation	N/A	Receptor-mediated and pH-sensitive	Targets influenza A H1/N1, enhanced targeting, reduced cytotoxicity, nanocurcumin had better physical and chemical stability	[41]
Biodegradable polymer PCL – PEG-PCL	1,2-dioleoyl-3-trimethylammonium-propane	Thin-film hydration and ultrasonic dispersion	Antigen and dual TLR agonists	Receptor-mediated and pH-sensitive	Antitumor agent, targeting dendritic cells through mannose targeting. Enhanced antigen uptake and processing, elevated internalization by dendritic cells	[42]
Stearic acid	Eudragit RS100 and sodium lauryl sulfate	Ultrasonic emulsification	Norfloxacin	Burst release, pH-sensitive	Antibacterial activity, inhibiting enzyme bacterial DNA gyrase; higher entrapment efficiency leading to enhanced bioavailability; improved drug stability at body temperature	[67]
Amorphous calcium carbonate	DSPE-PEG	Solvent diffusion	Doxorubicin, folic acid receptor	Receptor-mediated endocytosis	Antitumor activity; greatly enhanced stability of the drug, enhanced tumor penetration leading to greater antitumor activity	[68]
Amorphous calcium carbonate	DSPE-PEG	Solvent diffusion	Mitoxantrone, folic acid receptor	Receptor-mediated and pH-sensitive	Antitumor activity; longer circulation times prevents premature excretion	[69]

PLGA	Sophorolipid	Nano-precipitation	Silibinin and curcumin	The rapid release followed by slow release	Targeting breast cancer, overcoming GI barrier to deliver anticancer therapeutics; increased antimetastatic capacity due to mucus-penetrating delivery systems	[70]
PLGA-PEG	PLA	Ultrasonic emulsification	siRNA for silencing IGF-1R	Cell surface interactions	Targeting breast cancer, IGFR-1R silencing leading to arrest in cell proliferation; easy drug loading strategies, remarkable downregulation of IGFR-1R gene leading to cancer cell apoptosis	[71]
G5 PPI dendrimers cystamine core	Gold NPs	Surface grafting	Doxorubicin	pH-sensitive	Higher drug loading capacity of antitumor therapeutic agents. Higher generations of biocompatible dendrimers	[72]
G3 PAMAM dendrimer	Magnetite	Solution casting method for nanocomposite	Silver NPs	Diffusion	Antimicrobial action by surface destabilization of bacterial cell membrane. Carrageenan and carrageenan-based nanocomposite films as packaging materials. The nanocomposite exhibits excellent antimicrobial action on food-borne pathogenic bacteria	[73]
Sulfonic acid-terminated G1 PAMAM dendrimer	Lignin-silica hybrid nanoparticles	Precipitation method and sulfonation	N/A	N/A	Can be used for various applications such as chemical sensing, drug delivery, gene therapy, nanoparticle synthesis, catalysis, electronics, fuel cells, water treatment, etc.	[74]

(continued)

Table 1 (continued)

Core material	Hybridized material	Hybrid conjugation strategy	API conjugate	Drug release mechanism	Target action/ application	Ref.
PEGylated G5 PAMAM dendrimer	Gold NPs	Carbodiimide linkage	Curcumin	Diffusion	Antitumor activity, anti-inflammatory. Cancer therapeutic agent. Increased solubility, reduced cardiotoxicity as compared to other drugs	[75]
PAMAM dendrimer	Carbon dots, micelles, viral capsules, and other NPs	Covalent bonding and sandwich method	APIs with limitations to cross the BBB	Diffusion	Targets glioblastoma, efficient system to carry therapeutic agents such as miRNAs, siRNAs, and other biomolecules across the BBB while being biocompatible, nontoxic, and biodegradable	[76]
PAMAM	mPEG	Encapsulation	DNA, siRNA molecules	Diffusion and pH-sensitive	Cancer therapeutic agent. Can overcome multidrug resistance, increases solubility and bioavailability of many drugs	[77]
PAMAM (various)	Gold NPs	Various	Various	Diffusion and stimuli-sensitive	Cancer therapeutic agent. Surface-modified dendrimers act as excellent anticancer drug delivery systems possessing remarkable ability as theranostic agents	[78]
G1 poly ester amine dendrimer	Methoxypoly-(ethylene glycol)-b-poly(ε-caprolactone) (mPEG-b-PCL)	Self-assembly	Vancomycin	Diffusion	Antibiotic activity. Both in vitro and in vivo tests exhibited remarkably enhanced antibiotic activity in comparison to free drug treatment; this system represents great potential for poorly water-soluble drugs with low bioavailability problems	[79]

Amphiphilic dendrimer	PEG-PLA	Solvent evaporation	siRNA and paclitaxel	Diffusion	Cancer therapeutic agent, co-delivering of hydrophobic and hydrophilic therapeutic agents for synergistic action. Demonstrates prolonged and stronger effect resulting in faster antitumor actions and reducing toxicity arising from conventional high-dose chemotherapeutic drugs	[80]
G4 PAMAM	Coumarin	Self-assembly	Doxorubicin	pH-sensitive	Antitumor activity by the pH-sensitive and photoactivated release of drug. Precise control over drug release can be achieved by irradiating the treated area with 254 nm of UV light in the case of coumarin. Similarly, other photoactivated drugs can also be incorporated in such systems giving precise control on drug release conditions	[81]
Citric acid-modified G3	Graphene oxide	CA core, divergent synthesis	Doxorubicin	Diffusion and pH-sensitive	Antitumor activity, theranostic agent. The dendrimer encapsulated graphene oxide prevents restacking of GO sheets and also passivates the GO surface to revitalize its fluorescence properties. It has been proposed as an efficacious pH-sensitive drug delivery system	[82]

[26–28]. Studies have reported that PLGA-coated drugs and vehicles demonstrated protection from enzymatic degradation and sustained release of the payload thereby reducing nontarget tissue toxicity. PGA, PLA, and their derivatives have been useful in enabling a range of reactions such as esterification, reduction, oxidation, and more. They are also used as coatings over several inorganic NPs to enable them as biocompatible entities and also protect them from the reticuloendothelial system (RES). Bioabsorbable and biodegradable polymers such as PGA, PLA, PCL, and several classes of polyesters and polyanhydrides have been widely explored and applied in drug delivery systems. Cyclodextrin derivatives, hyaluronic acid, and other naturally occurring polymers are nontoxic and biocompatible materials that have been used in gene delivery, cell and tissue regeneration, and controlled delivery applications [29, 30]. Synthetic hydrogels and polymers such as poly (N-isopropyl acrylamide), PEI, and PAE have been developed with unique characteristics such as unique physical and chemical properties such as resistance coating materials, thermo-responsive polymers, intrinsic chemotherapeutic properties, and unique docking sites [31–33]. Chitosan is a water-soluble cationic polysaccharide which makes it an ideal choice for delivering polyanion conjugates [34]. However, a strong cationic surface charge may induce undesirable conditions as well such as nanoparticle aggregation, protein adsorption, and early clearance from blood circulation. These issues can be mitigated by using appropriate hybridization strategies such as with anionic polymers like PAA, PVA, and polysaccharides. Polysaccharides are long chains of carbohydrate molecules that can be composed of monosaccharides such as glucose, fructose, and glyceraldehyde. They have been broadly used as drug carriers, profiting from their natural composition, biocompatibility, gelation conditions, and mucoadhesive features [35]. Owing to their natural biomolecular composition, they've also been explored as drug delivery systems including the blood-brain barrier [25]. Their long-term stability, storage conditions, and mechanical properties for controlled drug delivery can be improvised by hybridizing with other suitable polymers and inorganic NPs.

In general, upon hybridization, polymers enhance the mechanical properties of the system increasing its stability and systemic tolerance. Synthetic polymers are constructed with characteristic features and high durability. However, they may also elicit unfavorable immunogenic responses. Hybridization of such materials with biocompatible candidates enhances their spectra of applications. Several polymers used as hybridizing agents have been described in Table 1 located at the end of the chapter.

3.1.3 Dendrimers

Among the variety of nanomaterials being explored for biomedical applications, dendrimers have emerged as interesting architectural moieties with unique physicochemical and structural properties. They are three-dimensional, hyperbranched, biocompatible, highly water-soluble, and polyvalent entities. There mainly exist three traditional macromolecular architectural classes which are used to generate

polydisperse structures of varied molecular weights, viz., linear, cross-linked, and branched. Dendrimers are available in a wide variety specialized for specific applications. Variations in the core can direct different branching patterns giving rise to three-dimensional spatial structures with large loading capacities. Some of the well-studied types of dendrimers are listed below:

- *Polyamido amine (PAMAM) dendrimers*.
- *Polypropylene ether imine (PPI) dendrimers*.
- *Fréchet-type dendrimers*.
- *Peptide-based dendrimers*.
- *Triazine dendrimers*.
- *Glycodendrimers.*
- *Tecto dendrimers*.
- *Chiral dendrimers*.

Dendrimers may also have intrinsic therapeutic properties and have been studied as anti-inflammatory, antimicrobial, and antiviral agents [36]. These unique properties distinguish them from other nanomaterials and make them lucrative candidates for biomedical applications such as drug and gene delivery. The hybridization of dendrimers has thus naturally been explored to cater to a variety of needs and customized needs in the field of drug delivery, diagnostics, and theranostics. Hybridization with different targeting moieties and biocompatible polymers like PEG has proven to stabilize and improve the bioavailability of dendrimer-based drug delivery vehicles and imaging agents. Hybridized dendrimers have been used to improve the solubility of poorly water-soluble drugs. Owing to their multiple functional groups, dendrimers make it possible to conjugate multiple moieties in a single entity. Surface-modified hybridized dendrimers have been reported to improve transdermal delivery, enhance cellular uptake, and facilitate controlled sustained delivery. Dendrimers have also been reported as one of the few candidates with the potential of gene transfection agents [37, 38].

3.2 Inorganic

As discussed in the section above, organic materials have several advantages over inorganic materials with respect to biocompatibility, bioavailability, and low toxicity concerns. However, they do have limitations such as structural disintegration over time, burst leakage, corona formation during systemic circulation, and agglomeration [39]. On the other hand, inorganic materials are rich in mechanical and physical properties which offer great control over the system design. They possess excellent stability and optical, electromagnetic, and catalytic properties. They offer vast variations and modifications of shapes, sizes, and surface properties. Figure 9 represents a variety of morphologies attainable with inorganic materials enabling enormous possibilities for vehicular designs spheres, rods, cubes, and others [40, 41]. These modalities can then be further modified by appropriate hybridization to

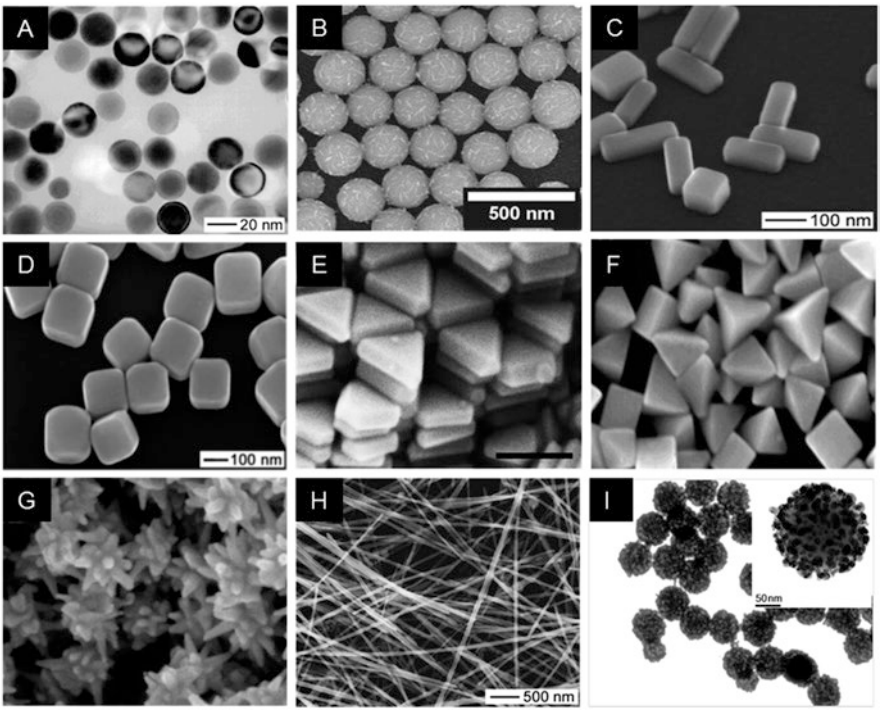

Fig. 9 SEM micrographs of Ag nanostructures, demonstrating that diverse sizes and morphologies are made possible by controlling the reaction chemistry. (**a**) Nanosphere, (**b**) necklaces, (**c**) nanobars, (**d**) nanocubes, (**e**) nanoprism, (**f**) bipyramids, (**g**) nanostar, (**h**) nanowires, (**i**) nanoparticle embedded silica particle hybrid. (Image adapted from open access article by Sang Lee (2019) [40]

create unique delivery vehicles suiting therapeutic and diagnostic requirements with a wide range of parameters. This section covers a few major types of inorganic nanomaterials which can be exploited in hybridized nanomaterials to obtain better control over the morphology and functionality of delivery vehicles used for diagnostic and therapeutic purposes.

3.2.1 Iron Oxide

Among inorganic NPs, iron oxide nanoparticles (IONPs) have been prevalent since the 1960s for diagnostic and therapeutic purposes. IONPs have several types and phases out of which magnetite (Fe_3O_4) has been most widely used. Magnetite is known for its low cytotoxicity making it more biocompatible than certain other inorganic counterparts. Its properties are easily tunable with respect to its size variations and surface modifications. It is categorized as superparamagnetic iron oxide nanoparticles (SPIONs) due to its excellent magnetic responsiveness and has been

approved by FDA as an MRI contrast agent. The responsiveness to external magnets is a highly sought-after property as it offers precision control and targeting of diseased tumor tissues [42]. Drug-loaded IONPs can be navigated to the target site under the influence of an external magnetic field thereby reducing undesired side effects of the excess drug in the systemic circulation. Hybridizing magnetic IONPs with suitable ligands, markers, and coating agents can enhance their functionality such as aiding stimuli-based drugs released by triggers such as pH, temperature, or enzymatic reactions. Furthermore, biocompatibility and cellular internalization can be improvised by coating them with lipids, polymers such as PEG, PLGA, and the like [43]. In comparison to unbound moieties or mono-material vehicles; several reports have demonstrated the advantage of using hybridized IONPs to diversify the loading of a variety of hydrophobic and lipophilic moieties, enable cell-specific binding, increase payload effectiveness, facilitate stimuli triggered drug release, and prolong the retention time by using external magnets [44, 45]. Multifunctional dendrimer-coated SPIONs have also been explored for carrying higher drug load and increasing cellular uptake in targeted tissues. The same vehicle can also be conjugated with fluorescence molecules to attain imaging-based monitoring and diagnosis. But, more importantly, dendrimer-coated SPIONs act as excellent contrast agents for MRI which makes them highly sought-after candidates for theranostic applications [46–48]. Apart from these applications, hybrid IONPs have also been evaluated for their use in photothermal (PTT) and photodynamic therapies (PDT) which have been discussed in Chap. 6. There are several possibilities and applications to look forward to depending upon the materials and the synergistic advantage arising from their hybridization. Table 1 (located at the end of the chapter) enlists some recent examples of hybrid IONPs and their biomedical applications.

3.2.2 Gold NPs

Gold colloids and particles are perhaps the most ancient inorganic materials to be applied for biomedical purposes. Gold NPs are almost inert, highly biocompatible, easily tunable, and excellent drug carriers. Since the evolution of nanomedicine, gold NPs have been studied as carriers for various APIs, genes, therapeutic proteins, and more [49].

They exhibit almost non-immunogenicity while also displaying features like high cellular uptake. To retain their stability in nanoform during systemic circulation and storage conditions, gold NPs are often hybridized with suitable polymers like PEG [50]. Gold NPs have also been explored in the fabrication of biosensors used to detect heavy metals, nucleic acids, and other biomolecules [51]. Upon appropriate coupling with another material, they can also be used as theranostic particles. Many researchers have proposed the conjugation of Au and Fe NP hybrids to provide controlled delivery drugs alongside imaging possibilities. PEG-gold hybrid NPs which have higher cellular uptake have been suggested for this

application [41]. Dendrimer-coated NPs are used for multimodal imaging, multi-drug loading, and attaining multifunctionality owing to the properties of the hybridized dendrimers. Hybrid AuNPs possess excellent X-ray attenuation ability and high photothermal transduction efficiency as well. Thus, like IONPs, gold NPs have also suitable candidates for application in PDT and PTT [50]. Hybridizing nontoxic, stable materials like AuNPs enhances the potential of the biocompatibility quotient of the other nanoparticle. Reciprocally, the unique physical or chemical features of other materials such as attaining multifunctionality through polymers and dendrimers or the magnetic properties of IONPs generate the potential of theranostic vehicles in the future of nanomedicine [52–54].

Similar to IONPs and AuNPs, many other inorganic materials have also been highlighted by researchers globally. Each of these NPs has its own unique features which can be optimized to suit the end application. For example, mesoporous silica nanoparticles (MSNPs) have unique structural features due to their nanopores which can be used to encapsulate and deliver both hydrophobic and hydrophilic drugs. They can also be modified to enable stimuli-responsive drug release systems. Another widely explored material is calcium phosphate for its unique bioactivity used for bone and tissue repairs [55, 56]. Ca phosphate NPs have been hybridized with hyaluronic acid to resemble the natural composition of bone tissue (refer to Sect. 4.4 for more details) [57]. Many more such hybrid materials have shown remarkable capabilities to be used as multifunctional systems for drug delivery, imaging, and theranostics.

4 Biomedical Applications of Hybrid Nanoparticles

Hybrid nanostructures are designed with an intention to overcome or improvise on the limitations or disadvantages of singular materials. A core material may be chosen to perform tissue targeting, transfection, transport, or stimulus-responsive behavior, while the hybridized material would be chosen to either mitigate cytotoxicity issues of core material or complement its performance by improvising its drug loading capacity, systemic stability, circulation time, thermostability, bioavailability, and escape from other biological barriers. Some hybrid nanomaterials may even possess intrinsic therapeutic properties such as antimicrobial action, wound healing, anti-inflammation, and such related actions. Not only does hybridization improvise individually diagnostic or drug delivery-based applications, but it can also enable the use of materials to combine properties of both applications resulting in theranostic particles. Some of the recent advances in various hybrid nanoparticles in biomedical applications of nanomaterials have been summarized in Table 1 located at the end of the chapter. In this section, we will focus on some of the major biomedical applications of hybrid nanoparticles.

4.1 Drug Delivery

Drug delivery systems focus on increasing the concentration of active drugs in localized regions of interest. This ensures enhanced therapeutic outcomes while lowering the side effects by reducing nontarget systemic circulation of drugs. Various nanosystems are already being used as successful drug delivery vehicles. However, these systems can further be optimized to overcome rapid clearance, protection against cellular barriers, and controlled release of the payloads. Polymers, lipids, and liposomes have been widely explored as hybridizing agents to enhance the efficacy of nano-based drug delivery systems. Cancer-targeting ligands and chemotherapeutic agents such as doxorubicin (DOX) and paclitaxel (PTX) have been most widely reported for drug delivery applications [9]. Successful attempts have been made to develop stimuli-responsive systems maximizing drug effectiveness while minimizing side effects. "Magnetoliposomes" are a class of drug delivery systems made out of superparamagnetic iron oxide NPs (SPIONs) encapsulated in liposomes. The magnetic properties of SPIONs enable drug targeting by application of an external magnetic field, while liposomal membranes enhance biocompatibility and cellular internalization thereby achieving a synergistic effect of increased concentration of drug local localization [10, 11]. Magnetoliposomes have been used to deliver several diverse drugs including curcumin, DOX, PTX, cisplatin, cuphen, and others [8, 12–14]. Many other core materials such as platinum-, silica-, calcium-, and zinc-based NPs have been hybridized with materials like chitosan, polyvinylpyrrolidone (PVP), polypeptides, membranes, and other polymeric compounds to study the delivery of a wide variety of drugs [7]–[16]. Many of these compounds are intrinsically therapeutic with antibacterial, antiviral, anti-inflammatory, or antitumor-type properties. Some new age synthetic polymers such as dendrimers have peculiar and interesting architectural motifs which allow multifunctionalization in a single entity. However, many dendrimers exhibit generation and dose-dependent cytotoxicity. This can be mitigated by hybridizing with appropriate surface coating with biocompatible materials such as chitosan or PRG. Combining the "best-fit" choices for a given application helps in developing the next-generation drug delivery systems.

4.2 Gene Delivery

Gene delivery is an important segment in the next-generation therapeutics of clinical significance. However, its success rates depend on the efficiency of gene delivery through various biological barriers. Present methods used to facilitate gene delivery make use of viral as well as engineered nonviral vectors. Some challenges faced by these systems include trade-offs between payload carrying capacity, transfection efficiency, and side effects such as inflammation [2]. Hybridizing such systems with materials such as liposomes may help overcome challenges by improving properties such as cellular internalization owing to their positive surface charge and

lipid shell structure. One study reports the use of AuNP-liposome composition for delivering siRNA actively targeted for ovarian cancer while avoiding lysosomal degradation [3–5]. The application of hybrid metal NPs for gene editing with stimuli-responsive control using laser or radiation or photo-responsive in in vivo models has also been well reported [6, 7]. Hybridized inorganic components such as magnetic NPs have proven to be a superior choice for targeted gene delivery over nonmagnetic counterparts [8]. Such combinations are being explored continually based on target tissues and end applications thereby paving the way to increase the success rates and breakthroughs in the field of gene delivery.

4.3 Phototherapy

Phototherapy refers to the usage of external radiation for therapeutic purposes. Wavelengths between NIR-I region (700–1000 nm) are known to penetrate deep inside layers of biological tissues [17]. Phototherapy is mainly split into two main branches:

(i) *Photothermal therapy (PTT):* PTT harnesses the energy radiations which are used to increase the temperature in the localized target tissue with the help of photo-absorbing NPs. An increased temperature is directly associated with the ablation of tumorous cells.
(ii) *Photodynamic therapy (PDT):* PDT utilizes this energy to activate photosensitive nanotherapeutics to generate reactive oxygen species which is a fatal condition for abnormal tumor cells.

Hybrid nanoparticles are being increasingly explored to suit the application of phototherapy.

Metals such as gold and iron have been explored for their photothermal applications. The internalization of core materials has been improvised by hybridizing with highly biocompatible encapsulating agents such as liposomes and polymers. Apart from the enhanced permeability and retention (EPR) effect, hybrid materials can be functionalized to improve tissue targeting and localization [18–20]. Combination photochemotherapy is an emerging field of next-generation cancer treatment. Several reports suggest the application of photo-responsive or thermo-responsive hybrid metallic NPs coupled with chemotherapeutic drugs can act as delivery agents. In this manner, apart from delivering the drug, the NPs can also respond to phototherapy [21–23]. Simultaneously, some researchers have also exploited the use of other radiations such as X-rays to trigger the release of chemotherapeutic drugs conjugated with photosensitizing materials such as verteporfin [24]. Hybridization of nanomaterials provides opportunities to develop highly effective, synergistic, stimuli-controlled targeted therapeutic approaches. One such example has been recently reported by Beatriz et al. (2022) wherein they've described a liposomal magnetic hybrid nanoparticle system. The reported hybrid has the potential to be used as a dual antitumor drug carrier while possessing pH and thermosensitive

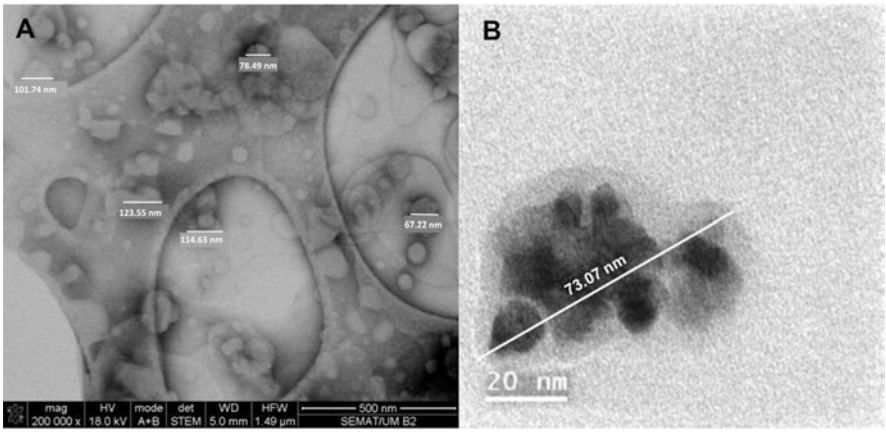

Fig. 10 (**a**) SEM image of magnetoliposomes showing spherical structures around 100 nm size. (**b**) TEM image of a magnetoliposome. (Image adapted from open access article by Ribeiro et al. (2022) [55])

properties. Alongside, it can also be for PDT and PTT by inducing magnetic hyperthermia activated by external electromagnets. Figure 10 shows an SEM and TEM micrograph of this magnetoliposome [55]. For more details on PDT and PTT, refer to the chapter by Danny Jian Hang Tng et al. in this book.

4.4 Tissue Engineering and Regeneration

Hybrid nanosystems have demonstrated tissue regeneration and wound healing abilities. Hybrid metallic NPs such as those obtained from silver have shown remarkable improvement in conventional wound healing. Cytotoxic effects of only metal-based NPs have been successfully mitigated by hybridizing with biopolymers such as chitosan and collagen [4, 25]. Gold, silver, and zinc NPs have been reported to possess antioxidant, antimicrobial, anti-inflammatory, and plasmonic properties which can act synergistically to aid the healing tissue in a shorter span of time [26, 27]. Copper NPs also contribute to a critical parameter of tissue regeneration by inducing angiogenesis through enhanced release of vascular endothelial growth factor (VEGF), upregulation of factors such as integrin, and also balancing the extracellular matrix (ECM) [28]. Polymer matrix-embedded zinc oxide and silica-based NPs have been associated with increased reepithelialization, tissue granulation, keratinocyte migration, fibroblast migration, hemostasis, as well as collagen deposition. This enables improved grafting properties in otherwise difficult-to-heal wounds such as those caused by burns or in diabetic patients [29, 30]. Hybrid NPs have already been commercially established in this domain and the studies continue to evolve to improvise and optimize these combinations.

4.4.1 Bone and Cartilage Tissue

Nanophase hybrid ceramics have received natural attention in the field of bone and cartilage implants as they resemble the natural composition of the bone matrix. Nanophase calcium phosphate NPs have shown increased osteoblastic activity which is one of the key parameters in tissue engineering and regeneration. Nanoscale hydroxyapatite (nHA), calcium phosphate, and titania-based hybrids have been explored to enable adequate osteoblast activity and calcium and collagen deposition ability [31, 32]. Integration of these hybrid matrices with growth-promoting peptides and proteins has been reported to enhance osteoblastic activity and increase in differentiation of mesenchymal stem cells and ECM thereby improving the overall growth and health of the regenerating bone tissue [33, 34]. Other combinations of hybrid nanosystems for bone and cartilage tissue regeneration include the integration of gold-, silver-, and zinc-based NPs [35–38].

4.4.2 Vascular Tissue

Owing to lifestyle issues, vascular grafts and organ replacements continue to remain in high demand. In this context, attempts have been made to make use of nanofibrous scaffolds based on matrices consisting of collagen, elastin, or poly (L-lactic acid) (PLLA). The major concern in this graft is related to "gain of function" in the implant tissue. Certain biocompatible materials such as gelatin-based nanosilicates have been studied in this regard wherein they have demonstrated the ability to form connective tissue in the lumen of blood vessels [39, 40]. A study reports the use of CNT hybrids has shown electrical-impulse transmission ability similar to the native myocardium cells, while another study reports the use of CNTs to deliver enhanced synchronous beating rate [41]. While most of these studies are limited to an experimental level, they open avenues to explore complex hybrid systems to attain maximum response rate in these artificial sensitive implant grafts.

4.4.3 Neural Tissue

Hybrid nanosystems are probably one of few select choices when it comes to treating conditions related to the nervous system. Nanomaterials with superior mechanical and electrical properties have been studied in this regard. Nanofibers derived from PLLA and PCL have been proposed for peripheral never repair, while iron oxide- and melatonin-based NPs have been proposed for nerve regeneration [38, 42]. Manipulation of the surface change, which is a crucial property of nerve conductivity, has been reported with the use of CNTs and metallic nanoparticles like gold [43, 44]. Hybridization of these functional particles in graft matrices may collectively result in successful implants of such tissues.

4.5 Antimicrobials

Silver and copper nanoparticles have been most widely explored in this domain due to their well-known antimicrobial activities. However, there are concerns related to the cytotoxicity and environmental impact of these NPs involving processes during production and post-disposal. Hybridization of these NPs hence plays an important role in ways that can either enhance their microbicidal effects and/or reduce the cytotoxic impact of these highly potent particles. Conjugation with magnetic iron oxide NPs has also shown enhanced penetration into bacterial films [45]. Another study suggests the conjugation of hybrid NPs with magnetic responsive, photosensitive, or thermosensitive agents for antibacterial activity in a sustained release pattern [46]. Hybridizing two or more of these antibacterial components has been reported to have shown rapid, enhanced, and targeted antimicrobial activity in comparison to singular individual components [47–49]. Hybrid NPs are powerful entities that can be multifunctionalized and customized to meet the needs of desired applications. With the rising concern of antibiotic resistance and multidrug resistance, hybrid NPs may be able to play a significant role in controlling these conditions.

4.6 Diagnostics

Early detection of a diseased condition is pivotal in determining the overall outcome of its treatment. Several diagnostics tools are developed and are also continually improvised to enhance selectivity and sensitivity. Recently, many hybrid nanomaterials have been reported for various diagnostic and routine monitoring applications. Gold-, silver-, and carbon-based hybrid systems have been dominantly used owing to their biocompatibility and physical properties [54, 55]. Hybrid metallic nanomaterial-based detection kits have been developed for routine monitoring of glucose levels and detecting tumors. A combination of functionalized NPs made of quantum dots, metals, and polymers has been reported to detect viruses like HPV and influenza. Fluorescence resonance energy transfer (FRET) detection based on hybridized metallic NPs has been reported for viral detection [56]. Additionally, some highly sensitive polymer-coated carbon NPs and some metal-based NPs systems have been reported to detect trace quantities of small molecules such as drugs and antibiotics [57, 58]. Non-hybrid nanomaterials have their limitations with respect to the constrained physical properties of a given material. Hybrid nanomaterials are able to overcome this limitation by allowing changes in the physical parameters of the overall system.

4.7 Imaging

Tumor detection and imaging techniques usually make use of contrast agents to improve the output of the scanned image. These contrast agents are typically made out of biocompatible and bioavailable materials which respond to external radiation or magnetism for detection. MRI is a widely used imaging technique wherein NPs based on gadolinium and iron oxide are used as contrast agents to improve image clarity. Some organic nanomaterials like PAMAM dendrimers have also been reported to exhibit contrast generating properties in MRI. Hybridized materials like PAMAM-coated SPIONs could be used as biocompatible theranostic vehicles. Researchers have reported pH-responsive functionalized hybrid NPs based on metals and metal oxides of magnesium, iron, silica, gold, and silver with superior properties as compared to their non-hybrid counterparts [4], [50–53]. Hybrid nanosystems have also been reported for detection techniques involving fluorescence and photoacoustic imaging [54]. For more details on imaging techniques, refer to the chapter by Shetty and Chandra in this book.

4.8 Theranostics

In recent years, theranostics has gained increasing importance owing to the possibility of developing combined therapeutic and diagnostic tools. Liposome-encapsulated AuNPs and quantum dots have been explored for delivering chemotherapeutic drugs while also responding photo sensitively to X-ray computed tomography for tumor detection [59]. Similarly, a gold- and ammonium bicarbonate-based liposome hybrid system has been developed which has demonstrated increased uptake of the system for delivering drugs while also enhancing bubble formation for ultrasound imaging [60]. Magnetoliposomes which have been mentioned earlier in the chapter are also used for enhancing ultrasound imaging. Magnetoliposomes and iron oxide-based NPs also act as excellent contrast agents that aid in the reduction of T1 and improve MRI imaging [61–64]. Simultaneously they can also be functionalized to deliver chemotherapeutics at targeted locations and can also be controlled by external magnets. Similar properties have also been reported using hybrid gadolinium-based NPs. These materials can also be conjugated with photo, thermo, and magneto-responsive agents to attain controlled sustained release of therapeutics. Many polymer or dendrimer hybridized inorganic NPs are drug-loaded and also sued to enhance imaging or fluorescence signals and act as useful theranostic vehicles [65]. Hybrid nanosystems made from gold, silver, palladium, carbon, and other conjugates have been used for controlled drug release and photoacoustic imaging simultaneously [66]. Poly(allylamine), PLGA, PLA, and such polymers have been used to enable functionality, targeting, and bioavailability of these systems to them multifunctional modalities in theranostics. This domain allows a wide range of creative and functional architecture to be explored by utilizing synergistic properties of different materials.

5 Conclusion

The past two decades have witnessed remarkable innovations arising from the use of nanomaterials. Nano-sized materials have significantly contributed to the improvement of therapeutics and imaging. They are easy to reproduce and can be scaled up to desired quantities of production. Despite several advantages, the singular systems have certain limitations with respect to their biocompatibility, bioavailability, and cytotoxicity which vary with respect to changes in shape, size, dosage, and surface properties. Naturally, hybridization comes as a viable approach to overcome these obstacles. Hybrid nanoparticles have shown significant improvisations over single-component therapies as discussed in this chapter. With hybrid nanosystems, one can add multifunctionality to a single design. The future of medicine belongs to fast-acting, minimal dosage, personalized, and precision therapies. Hybrid nanoparticles are capable of encompassing all these properties and thus enable diagnostics and treatments which were otherwise difficult to implement. Several potential drugs struggling with bioavailability issues can be used for therapies by conjugating them with appropriate nanohybrid systems. Biocompatible and customizable delivery vehicles can be developed using hybrid nanosystems to cater to the obscurity while dealing with antibiotic resistance, superbugs, and cases with failure of first line of treatments. Alongside, hybrid nanosystems have also significantly contributed to the diagnostic sector as well. Several combinations of hybrid nanosystems have contributed toward improvising existing tools as well as emerging with novel ones. Upcoming fields in medicine aim to develop theranostic tools which minimize procedures and maximize outcomes by combining therapy and diagnosis and/or monitoring in a single entity. Hybrid nanosystems are ideal candidates to develop these sophisticated tools in the new age of nanomedicine.

As of today, several hybrid nanosystems are undergoing clinical trials, and many more are already in pipeline. There has been a steady increase in the publication trends in the application of hybrid nanosystems in biomedical fields, especially in areas related to cancer drug delivery, drug development, diagnostics, and imaging. While the studies related to these materials continue to evolve by the day, it is also important to highlight the significance of toxicological and environmental concerns arising from production and waste disposal related to these materials. Most countries struggle with the legislature related to drafting safety laws in this sector mostly due to lack of information. It hence relies on the learned scientific fraternity to conceptualize the production, usage, and disposal of these materials through detailed studies. Nevertheless, by following sustainable practices, hybrid nanosystems seem to be the next revolution in medicine.

Acknowledgments All illustrative Figures/diagrams have been created using biorender.com.

References

1. Abdel-Mageed HM, AbuelEzz NZ, Radwan RA, Mohamed SA. Nanoparticles in nanomedicine: a comprehensive updated review on current status, challenges and emerging opportunities. J Microencapsul. 2021;38:414–36.
2. Weinstein JS, Varallyay CG, Dosa E, Gahramanov S, Hamilton B, Rooney WD, Muldoon LL, Neuwelt EA. Superparamagnetic iron oxide nanoparticles: diagnostic magnetic resonance imaging and potential therapeutic applications in neurooncology and central nervous system inflammatory pathologies, a review. J Cereb Blood Flow Metab. 2010;30:15–35.
3. Na H bin, Song IC, Hyeon T (2009) Inorganic nanoparticles for MRI contrast agents. Adv Mater 21:2133–2148.
4. Kim D, Kwon SJ, Wu X, Sauve J, Lee I, Nam J, Kim J, Dordick JS. Selective killing of pathogenic bacteria by antimicrobial silver nanoparticle – cell wall binding domain conjugates. ACS Appl Mater Interfaces. 2018;10:13317–24.
5. Khalid A, Ullah H, Ul-Islam M, Khan R, Khan S, Ahmad F, Khan T, Wahid F. Bacterial cellulose-TiO_2 nanocomposites promote healing and tissue regeneration in burn mice model. RSC Adv. 2017;7:47662–8.
6. Macchione MA, Biglione C, Strumia M. Design, synthesis and architectures of hybrid nanomaterials for therapy and diagnosis applications. Polymers (Basel). 2018; https://doi.org/10.3390/polym10050527.
7. Yang R, Wei T, Goldberg H, Wang W, Cullion K, Kohane DS. Getting drugs across biological barriers. Adv Mater. 2017; https://doi.org/10.1002/adma.201606596.
8. Ismail SH, Hamdy A, Ismail TA, Mahboub HH, Mahmoud WH, Daoush WM. Synthesis and characterization of antibacterial carbopol/ZnO hybrid nanoparticles gel. Crystals (Basel). 2021; https://doi.org/10.3390/cryst11091092.
9. Vargas-Bernal R. Introductory chapter: hybrid nanomaterials. Hybrid Nanomater Flexible Electron Mater. 2020; https://doi.org/10.5772/intechopen.92012.
10. Abbasi E, Aval SF, Akbarzadeh A, Milani M, Nasrabadi HT, Joo SW, Hanifehpour Y, Nejati-Koshki K, Pashaei-Asl R. Dendrimers: synthesis, applications, and properties. Nanoscale Res Lett. 2014;9:1–10.
11. Wu L, Glebe U, Böker A. Surface-initiated controlled radical polymerizations from silica nanoparticles, gold nanocrystals, and bionanoparticles. Polym Chem. 2015;6:5143–84.
12. Saveleva MS, Eftekhari K, Abalymov A, Douglas TEL, Volodkin D, Parakhonskiy B v., Skirtach AG (2019) Hierarchy of hybrid materials-the place of inorganics-in-organics in it, their composition and applications. Front Chem https://doi.org/10.3389/fchem.2019.00179.
13. Ananikov VP (2019) Organic–Inorganic Hybrid Nanomaterials. Nanomaterials 9:1197.
14. Micaela AM, Catalina B, Strumia M. Design, synthesis and architectures of hybrid nanomaterials for therapy and diagnosis applications. Polymers (Basel). 2018;10:527.
15. Functionalization of iron oxide magnetic nanoparticles with poly(methyl methacrylate) brushes via grafting-from atom transfer radical polymerization | Enhanced Reader.
16. Ajayan PM (Pulickel M), Schadler LS (Linda S), Braun PV (Paul V). Nanocomposite science and technology. Wiley-VCH. 2003.
17. Souto EB, Baldim I, Oliveira WP, Rao R, Yadav N, Gama FM, Mahant S. SLN and NLC for topical, dermal, and transdermal drug delivery. Expert Opin Drug Deliv. 2020;17:357–77.
18. Hallan SS, Sguizzato M, Esposito E, Cortesi R. Challenges in the physical characterization of lipid nanoparticles. Pharmaceutics. 2021; https://doi.org/10.3390/pharmaceutics13040549.
19. Zacheo A, Bizzarro L, Blasi L, Piccirillo C, Cardone A, Gigli G, Ragusa A, Quarta A. Lipid-based Nanovesicles for simultaneous intracellular delivery of hydrophobic, hydrophilic, and amphiphilic species. Front Bioeng Biotechnol. 2020; https://doi.org/10.3389/fbioe.2020.00690.
20. Mitchell MJ, Billingsley MM, Haley RM, Wechsler ME, Peppas NA, Langer R. Engineering precision nanoparticles for drug delivery. Nat Rev Drug Discov. 2021;20:101–24.

21. Rao S, Prestidge CA. Polymer-lipid hybrid systems: merging the benefits of polymeric and lipid-based nanocarriers to improve oral drug delivery. Expert Opin Drug Deliv. 2016;13:691–707.
22. Tahir N, Madni A, Correia A. Erratum: lipid-polymer hybrid nanoparticles for controlled delivery of hydrophilic and lipophilic doxorubicin for breast cancer therapy (Int J Nanomed. 2019;14:4961–4974), https://doi.org/10.2147/IJN.S209325). Intl J Nanomed. 2020;15:839.
23. Mohanty A, Uthaman S, Park IK. Utilization of polymer-lipid hybrid nanoparticles for targeted anti-cancer therapy. Molecules. 2020; https://doi.org/10.3390/molecules25194377.
24. Jiang T, Mo R, Bellotti A, Zhou J, Gu Z. Gel-liposome-mediated co-delivery of anticancer membrane-associated proteins and small-molecule drugs for enhanced therapeutic efficacy. Adv Funct Mater. 2014;24:2295–304.
25. Sung YK, Kim SW. Recent advances in polymeric drug delivery systems. Biomater Res. 2020; https://doi.org/10.1186/s40824-020-00190-7.
26. Yeh M-K, Chang W-K, Tai Y-J, Chiang C-H, Hu C, Hong P-d. The comparison of protein-entrapped liposomes and lipoparticles: preparation, characterization, and efficacy of cellular uptake. Int J Nanomedicine. 2011;2403
27. Wang AZ, Yuet K, Zhang L, Gu FX, Huynh-Le M, Radovic-Moreno AF, Kantoff PW, Bander NH, Langer R, Farokhzad OC. ChemoRad nanoparticles: a novel multifunctional nanoparticle platform for targeted delivery of concurrent chemoradiation. Nanomedicine. 2010;5:361–8.
28. Hatziantonioy S, Demetzos C. Lipids of membranes: chemistry, biological role and applications as drug carriers. Stud Nat Prod Chem. 2008;34:173–202.
29. Yoo J, Park C, Yi G, Lee D, Koo H. Active targeting strategies using biological ligands for nanoparticle drug delivery systems. Cancers (Basel). 2019; https://doi.org/10.3390/cancers11050640.
30. Pourasghar M, Koenneke A, Meiers P, Schneider M. Development of a fast and precise method for simultaneous quantification of the PLGA monomers lactic and glycolic acid by HPLC. J Pharmaceut Anal. 2019;9:100–7.
31. Gavard J, Hanini S, Kacem C, Ammar GJ. Evaluation of iron oxide nanoparticle biocompatibility. Int J Nanomedicine. 2011;787
32. Fukushima D, Sk UH, Sakamoto Y, Nakase I, Kojima C. Dual stimuli-sensitive dendrimers: Photothermogenic gold nanoparticle-loaded thermo-responsive elastin-mimetic dendrimers. Colloids Surf B: Biointerfaces. 2015;132:155–60.
33. Pan H, Yang J, Kopečková P, Kopeček J. Backbone degradable multiblock N-(2-hydroxypropyl) methacrylamide copolymer conjugates via reversible addition-fragmentation chain transfer polymerization and thiol-ene coupling reaction. Biomacromolecules. 2011;12:247–52.
34. Xu P, Bajaj G, Shugg T, van Alstine WG, Yeo Y. Zwitterionic chitosan derivatives for pH-sensitive stealth coating. Biomacromolecules. 2010;11:2352–8.
35. Deng S, Gigliobianco MR, Censi R, di Martino P. Polymeric nanocapsules as nanotechnological alternative for drug delivery system: current status, challenges and opportunities. Nano. 2020; https://doi.org/10.3390/nano10050847.
36. Santos A, Veiga F, Figueiras A. Dendrimers as pharmaceutical excipients: synthesis, properties, toxicity and biomedical applications. Materials. 2020;13:65.
37. Hsu HJ, Bugno J, Lee SR, Hong S. Dendrimer-based nanocarriers: a versatile platform for drug delivery. Wiley Interdiscip Rev Nanomed Nanobiotechnol. 2017; https://doi.org/10.1002/wnan.1409.
38. Li J, Liang H, Liu J, Wang Z. Poly (amidoamine) (PAMAM) dendrimer mediated delivery of drug and pDNA/siRNA for cancer therapy. Int J Pharm. 2018;546:215–25.
39. Mukherjee A, Waters AK, Kalyan P, Achrol AS, Kesari S, Yenugonda VM. Lipid-polymer hybrid nanoparticles as a nextgeneration drug delivery platform: state of the art, emerging technologies, and perspectives. Int J Nanomedicine. 2019;14:1937–52.
40. Lee SH, Jun BH. Silver nanoparticles: synthesis and application for nanomedicine. Int J Mol Sci. 2019; https://doi.org/10.3390/ijms20040865.
41. Persano F, Gigli G, Leporatti S. Lipid-polymer hybrid nanoparticles in cancer therapy: current overview and future directions. Nano Express. 2021;2:012006.

42. Kumar P, Agnihotri S, Roy I. Preparation and characterization of superparamagnetic iron oxide nanoparticles for magnetically guided drug delivery. Int J Nanomedicine. 2018;13:43–6.
43. Zhu N, Ji H, Yu P, Niu J, Farooq MU, Akram MW, Udego IO, Li H, Niu X. Surface modification of magnetic iron oxide nanoparticles. Nano. 2018; https://doi.org/10.3390/nano8100810.
44. Shabatina TI, Vernaya OI, Shabatin VP, Melnikov MY. Magnetic nanoparticles for biomedical purposes: modern trends and prospects. Magnetochemistry. 2020;6:1–18.
45. Akbarzadeh A, Samiei M, Davaran S. Magnetic nanoparticles: preparation, physical properties, and applications in biomedicine. Nanoscale Res Lett. 2012; https://doi.org/10.1186/1556-276X-7-144.
46. Khanh Luong D, Khanh D (2016) Dendrimer-coated iron oxide Theranostic nanoparticles for cancer imaging and therapy.
47. Khodadust R, Unsoy G, Yalcın S, Gunduz G, Gunduz U. PAMAM dendrimer-coated iron oxide nanoparticles: synthesis and characterization of different generations. J Nanopart Res. 2013; https://doi.org/10.1007/s11051-013-1488-6.
48. Sosnovik DE, Weissleder R. Emerging concepts in molecular MRI. Curr Opin Biotechnol. 2007;18:4–10.
49. Sengani M, Grumezescu AM, Rajeswari VD. Recent trends and methodologies in gold nanoparticle synthesis – a prospective review on drug delivery aspect. OpenNano. 2017;2:37–46.
50. Ding X, Li D, Jiang J. Gold-based inorganic nanohybrids for nanomedicine applications. Theranostics. 2020;10:8061–79.
51. Paul W, Sharma CP. Inorganic nanoparticles for targeted drug delivery. In: Biointegration of medical implant materials. Elsevier; 2019. p. 333–73.
52. Guillaume B, Francois L, Sandrine D, Yannick C, Camille V, Olivier T. EPR mediated tumor targeting using ultrasmall-hybrid nanoparticles: from animal to human with theranostic AGulX nanoparticles. Theranostics. 2020;10:1319–31.
53. Efremova MV, Naumenko VA, Spasova M, et al. Magnetite-gold nanohybrids as ideal all-in-one platforms for theranostics. Sci Rep. 2018;8:11295.
54. Bardhan R, Lal S, Joshi A, Halas NJ. Theranostic nanoshells: from probe design to imaging and treatment of cancer. Acc Chem Res. 2011;44:936–46.
55. Ribeiro BC, Alvarez CAR, Alves BC, et al. Development of thermo- and pH-sensitive liposomal magnetic carriers for new potential antitumor thienopyridine derivatives. Materials. 2022;15:1737.
56. Pulvirenti L, Monforte F, lo Presti F, Li Volti G, Carota G, Sinatra F, Bongiorno C, Mannino G, Cambria MT, Condorelli GG (2022) Synthesis of MIL-modified Fe3O4 magnetic nanoparticles for enhancing uptake and efficiency of Temozolomide in glioblastoma treatment. Int J Mol Sci 23:2874.
57. Degli Esposti L, Carella F, Adamiano A, Tampieri A, Iafisco M. Calcium phosphate-based nanosystems for advanced targeted nanomedicine. Drug Dev Ind Pharm. 2018;44:1223–38.
58. Zhang N, Chen H, Liu AY, Shen JJ, Shah V, Zhang C, Hong J, Ding Y. Gold conjugate-based liposomes with hybrid cluster bomb structure for liver cancer therapy. Biomaterials. 2016;74:280–91.
59. Ye H, Tong J, Liu J, Lin W, Zhang C, Chen K, Zhao J, Zhu W. Combination of gemcitabine-containing magnetoliposome and oxaliplatin-containing magnetoliposome in breast cancer treatment: a possible mechanisms with potential for clinical application. Oncotarget. 2016;7(28):43762.
60. Aadinath W, Bhushani A, Anandharamakrishnan C. Synergistic radical scavenging potency of curcumin-in-β-cyclodextrin-in-nanomagnetoliposomes. Mater Sci Eng C. 2016;64:293–302.
61. Saber MM, Bahrainian S, Dinarvand R, Atyabi F. Targeted drug delivery of Sunitinib malate to tumor blood vessels by cRGD-chitosan-gold nanoparticles. Int J Pharm. 2017;517:269–78.
62. Ramalingam V, Varunkumar K, Ravikumar V, Rajaram R. Target delivery of doxorubicin tethered with PVP stabilized gold nanoparticles for effective treatment of lung cancer. Sci Rep. 2018; https://doi.org/10.1038/s41598-018-22172-5.

63. Maney V, Singh M. The synergism of platinum-gold bimetallic nanoconjugates enhances 5-fluorouracil delivery in vitro. Pharmaceutics. 2019; https://doi.org/10.3390/pharmaceutics11090439.
64. Jones CH, Chen CK, Ravikrishnan A, Rane S, Pfeifer BA. Overcoming nonviral gene delivery barriers: perspective and future. Mol Pharm. 2013;10:4082–98.
65. Xu F, Bandara A, Akiyama H, Eshaghi B, Stelter D, Keyes T, Straub JE, Gummuluru S, Reinhard BM. Membrane-wrapped nanoparticles probe divergent roles of GM3 and phosphatidylserine in lipid-mediated viral entry pathways. Proc Natl Acad Sci U S A. 2018;115:E9041–50.
66. Du B, Gu X, Han X, Ding G, Wang Y, Li D, Wang E, Wang J. Lipid-coated gold nanoparticles functionalized by folic acid as gene vectors for targeted gene delivery in vitro and in vivo. ChemMedChem. 2017;12:1768–75.
67. Muhammad AK, Shahzeb K, Mohsin K, Sultan MA, Muhammad S, Shafi UK, Zahid H, Muhammad S. Norfloxacin loaded lipid polymer hybrid nanoparticles for oral administration: fabrication, characterization, in silico modelling and toxicity evaluation. Pharmaceutics. 2021;13:1632.
68. Wang C, Liu X, Chen S, Hu F, Sun J, Yuan H. Facile preparation of phospholipid-amorphous calcium carbonate hybrid nanoparticles: toward controllable burst drug release and enhanced tumor penetration. Chem Commun. 2018;54:13080–3.
69. Cheng W, Min H, Xuerong L, Shaoqing C, Fuqiang H, Jihong S, Hong Y. Mitoxantrone-preloaded water-responsive phospholipid-amorphous calcium carbonate hybrid nanoparticles for targeted and effective cancer therapy. Int J Nanomedicine. 2019;12:1503–17.
70. Liu Y, Shen J, Shi J, et al. Functional polymeric core–shell hybrid nanoparticles overcome intestinal barriers and inhibit breast cancer metastasis. Chem Eng J. 2022; https://doi.org/10.1016/j.cej.2021.131742.
71. Monirinasab H, Asadi H, Rostamizadeh K, Esmaeilzadeh A, Khodaei M, Fathi M. Novel lipid-polymer hybrid nanoparticles for siRNA delivery and IGF-1R gene silencing in breast cancer cells. J Drug Deliv Sci Technol. 2018;48:96–105.
72. Najafi F, Salami-Kalajahi M, Roghani-Mamaqani H, Kahaie-Khosrowshahi A. Effect of grafting ratio of poly(propylene imine) dendrimer onto gold nanoparticles on the properties of colloidal hybrids, their DOX loading and release behavior and cytotoxicity. Colloids Surf B: Biointerfaces. 2019;178:500–7.
73. Saedi S, Rhim JW. Synthesis of Fe_3O_4@SiO_2@PAMAM dendrimer@AgNP hybrid nanoparticles for the preparation of carrageenan-based functional nanocomposite film. Food Packag Shelf Life. 2020; https://doi.org/10.1016/j.fpsl.2020.100473.
74. Ahmadi H, Abdollahi M. Synthesis and structural characterization of lignin/silica hybrid nanoparticles functionalized with sulfonic acid-terminated polyamidoamine. Wood Sci Technol. 2020;54:249–68.
75. Alibolandi M, Hoseini F, Mohammadi M, Ramezani P, Einafshar E, Taghdisi SM, Ramezani M, Abnous K. Curcumin-entrapped MUC-1 aptamer targeted dendrimer-gold hybrid nanostructure as a theranostic system for colon adenocarcinoma. Int J Pharm. 2018;549:67–75.
76. Guo Y, Shen M, Shi X. Construction of poly(amidoamine) dendrimer/carbon dot Nanohybrids for biomedical applications. Macromol Biosci. 2021; https://doi.org/10.1002/mabi.202100007.
77. Kececiler-Emir C, Ilhan-Ayisigi E, Celen-Erden C, Nalbantsoy A, Yesil-Celiktas O. Synthesis of resveratrol loaded hybrid silica-PAMAM dendrimer nanoparticles with emphases on inducible nitric oxide synthase and cytotoxicity. Plant Foods Hum Nutr. 2021;76:219–25.
78. Maji R, Omolo CA, Agrawal N, Maduray K, Hassan D, Mokhtar C, Mackhraj I, Govender T. PH-responsive lipid-dendrimer hybrid nanoparticles: an approach to target and eliminate intracellular pathogens. Mol Pharm. 2019;16:4594–609.
79. Mignani S, Shi X, Ceña V, Rodrigues J, Tomas H, Majoral JP. Engineered non-invasive functionalized dendrimer/dendron-entrapped/complexed gold nanoparticles as a novel class of theranostic (radio)pharmaceuticals in cancer therapy. J Control Release. 2021;332:346–66.

80. Li X, Sun AN, Liu YJ, Zhang WJ, Pang N, Cheng SX, Qi XR. Amphiphilic dendrimer engineered nanocarrier systems for co-delivery of siRNA and paclitaxel to matrix metalloproteinase-rich tumors for synergistic therapy. NPG Asia Mater. 2018;10:238–54.
81. Pashaei-Sarnaghi R, Najafi F, Taghavi-Kahagh A, Salami-Kalajahi M, Roghani-Mamaqani H. Synthesis, photocrosslinking, and self-assembly of coumarin-anchored poly(amidoamine) dendrimer for smart drug delivery system. Eur Polym J. 2021; https://doi.org/10.1016/j.eurpolymj.2021.110686.
82. Hashemi H, Namazi H. Understanding the pH dependent fluorescence and doxorubicin release from graphene oxide functionalized citric acid dendrimer as a highly efficient drug delivery system. Mater Today Commun. 2021; https://doi.org/10.1016/j.mtcomm.2021.102593.

A Voyage on Biomedical Applications of Multicomponent Nanoparticles in Medical Imaging

A. Lenin Fred, S. N. Kumar, L. R. Jonisha Miriam, H. Ajay Kumar, Christina Jane, Parasuraman Padmanabhan, and Balázs Gulyás

1 Introduction

Nanoparticles play a vital role in the health-care sector and the classification of Nanoparticles based on their chemical composition is depicted in Fig. 1. The liposome nanoparticles are spherical vesicles enclosed in a membrane comprising of a lipid bilayer, an aqueous substance. The active compounds can be hydrophilic or hydrophobic and are widely used for chemotherapy drug delivery in cancer treatment. Apart from the health-care sector, it has immense applications in the food and cosmetics industry because of its biodegradability and biocompatibility. Table 1 represents the characteristics of medical imaging with nanomaterials deployed.

Nanomaterials have amazing capabilities that aren't present in bulk materials, yet multifunctionality on a single material is still a challenge. The silica nanoparticles gain prominence in multifunctional nanodevices. The benefits of silica nanoparticles as a medium for multifunctional nanodevices are as follows: biocompatibility, degradability, changeable shape, and simplicity of modification; it is widely used in drug delivery. The silica nanoparticles when mixed with other materials improve the property. Furthermore, silica nanoparticles can be combined with other materials to gain additional properties and provide theranostic and multimodal imaging capabilities. The properties of silica nanoparticles for bio-applications are compared to other well-known nanomaterials, and standard techniques to synthesize and

A. L. Fred · L. R. J. Miriam · H. A. Kumar · C. Jane
Mar Ephraem College of Engineering and Technology, Elavuvilai, Tamil Nadu, India

S. N. Kumar (✉)
Amal Jyothi College of Engineering, Koovappally, Kerala, India

P. Padmanabhan · B. Gulyás
Lee Kong Chian School of Medicine, Nanyang Technological University, Singapore, Singapore

R. S. Chaughule et al. (eds.), *Nanomaterials for Cancer Detection Using Imaging Techniques and Their Clinical Applications*,
https://doi.org/10.1007/978-3-031-09636-5_14

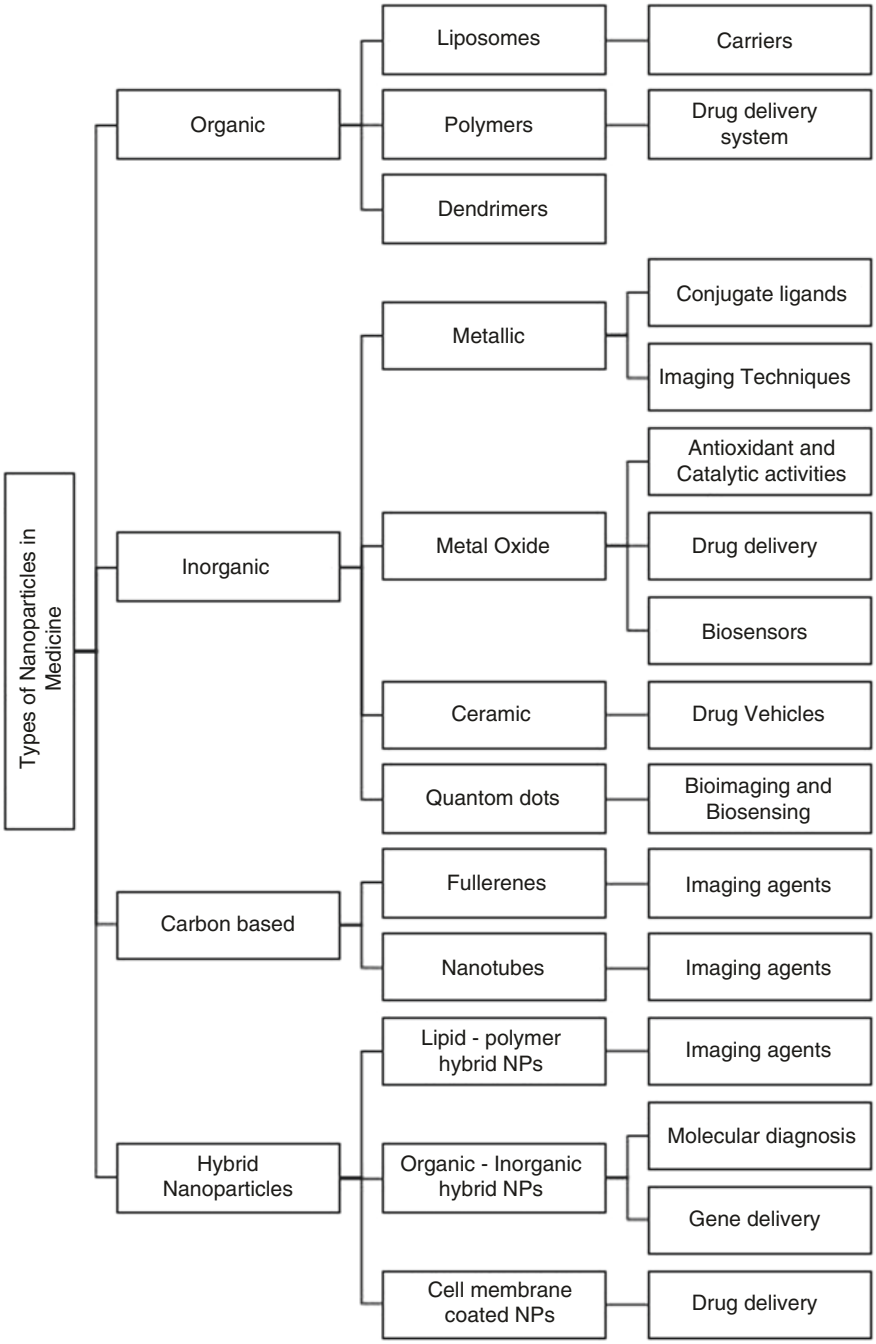

Fig. 1 Flow diagram representing the types of nanoparticles in the medical field

Table 1 Characteristics of medical imaging with nanomaterials deployed

Modality	Spatial resolution	Penetration depth	Sensitivity	Cost	Nanomaterials used
MRI [1]	25–100μm	Limitless	*Low* ($10^{-3} - 10^{-5}$ *moles*)	High	Paramagnetic liposome, USPIO nanoparticles, gadolinium, carbon, manganese, silicon, peptide
PET [1]	1–2 mm	Limitless	*High* ($10^{-11} - 10^{-12}$ *moles*)	Very high	Gold nanoparticles, copper, polymer, quantum dots
CT [2]	50–200 μm	Limitless	*Low* ($10^{-1} - 10^{-4}$ *moles*)	Very low	Gold nanoparticle, USPIO nanoparticle, iodine, bismuth
US [1]	50–500 μm	Mm–cm	Medium ($10^{-9} - 10^{-12}$ *moles*)	Low	Nano bubbles, chitosan NBs
SPECT [2]	8–10 mm	Limitless	*High* ($10^{-8} - 10^{-10}$ *moles*)	High	Gold nanoparticles, technetium ($^{99m}T_c$)
Optical imaging [2]	2–5 mm	Cm	*High* ($10^{-9} - 10^{-17}$ *moles*)	Low	Fluorescence, quantum dots, gold nanoparticles, persistent luminescence NPs

incorporate silica nanoparticles are described [3]. Inorganic nanoparticles play a vital role in biological imaging; however, before application, toxic nature has to be verified. The origin of inorganic nanomaterials and their properties are discussed in detail. The toxicology of inorganic nanoparticles is investigated, and knowledge for designing safer inorganic nanomaterials for clinical uses is presented in ref. [4]. Figure 1 depicts the different nanomaterials with their applications in the healthcare sector. In [5], radiolabeled nanomaterials gain prominence in nuclear imaging. The radionuclides have nuclear emissions and have therapeutic applications; choosing the most appropriate radiolabeling approach and understanding its limits are important when using it for functional imaging. The radiolabeling procedure relies on the type of material. The various radiolabeling strategies are discussed, together with a critical assessment of their benefits, and drawbacks are discussed in [3].

The different types of nanoparticles that have their role in the biomedical sector are highlighted in [4]; specific focus was given to gold nanoparticles (Au NPs). The unique optical and electrical sensing and biological capabilities of Au NPs make them the most fascinating nanomaterial among the nanomaterials. In the early identification, diagnosis, and treatment of illnesses, Au NPs might be used for medical imaging, medication administration, and tumor therapy. The recent and advanced applications of Au NPs in drug delivery and administration and the molecular nanoprobes are also discussed in [6]. The precision medicine applications of nanoscience were discussed in this work; "next-generation sequencing" signifies the gene that is responsible for cancer. This novel technique is different from all other cancer treatments, concentrating on identifying the anatomical organ malignancies detection. A

recently developed "microRNA replacement treatment," which uses nanocarriers to control the driving oncogene, is used to treat tumors at the molecular level. Furthermore, the genetically defined, patient-derived xenograft models must be used to precisely assess the effect of nanomediated oncogenic regulation [7]. The recent applications of nanomaterials in the health-care sector focusing on oncology therapy are discussed in [8]. The role of nanomaterials in vivo imaging was discussed in [9]. This study focuses on current breakthroughs in nanomaterials that are essential in medical research, as well as nanomaterials that might be possibilities for usage in the health-care sector. The nanomaterial's most important features, functional activities, benefits, and downsides are also explored. The biosensor is gaining prominence in many applications, and the importance of nanomaterials in the design of biosensors is also discussed in this work [10]. The role of nanomaterials in stem cell imaging is gaining prominence for treating a variety of traumas and neurodegenerative disorders. The features and challenges of regenerative medicine are discussed in this work [11]. The cellular therapy and drug delivery using nanomaterials are highlighted in [12]. The four types of radiolabeling techniques for PET imaging are discussed in [11]. The stability of radiolabeled nanoparticles is analyzed in this work with its role in multimodal molecular imaging which is also put forward in this work [13]. A historical perspective on the role of nanomaterials in circulating tumor cell isolation and analysis is discussed in [14].

Engineered nanoparticles can suppress or augment immune responses, as well as prevent the immune system from detecting them. Alteration in immune system function may cause some harm in addition to the advantages. As a result, a thorough evaluation of new nanomaterials appears to be required before they may be used in therapy. However, little is known about the toxicological and biological impacts of nanomaterials, particularly about possible methods of interacting and managing nanoparticles in the body, as well as the body's response to these substances. To date, accessing nanomaterials' toxicological impacts has been made considerably more challenging due to their wide variety and diverse features. The goal of this study is to get a better understanding of the possible advantages and hazards of employing nanomaterials on the immune system so that these substances may be designed and used safely in therapeutic applications [15]. Section 2 describes the features of multicomponent nanoparticles. The nanoparticles utilized in CT, MR, and PET imaging are highlighted in Sects. 3, 4, and 5.

2 Features of Multicomponent Nanoparticles

Multicomponent nanostructures, which are made by combining different metals into a single nanoparticle, are becoming a popular type of functional nanoscale architecture with applications spanning from catalysis to plasmonics to biological imaging [16, 17]. Diverse metal components are bonded together in an alloyed or phase-separated form in these complex nanoparticle designs, resulting in many heterogeneous surfaces at the atomic or nanometer scale. Unique synergistic coupling

effects are facilitated by the formed interfaces between distinct components, resulting in chemical and physical qualities that are superior to pure components. As a result, much work has gone into producing collections of multimetallic nanoparticles with more than three metal components, with some breakthrough discoveries. Organic microparticles and nanoparticles consisting of numerous conjugated molecules have attracted a lot of interest in comparison to inorganic analogs because of their promising performance in photonics and electronics applications.

2.1 Synthesis of Multicomponent Nanoparticles

The alloy multicomponent nanoparticles (MCNP) were synthesized using a combination approach that included controlled precipitation and hydrothermal techniques. Controlling the precipitation of iron (III) chloride hexahydrate, nickel (II) chloride, and copper (II) chloride dihydrate in distilled water at an alkaline condition in a nitrogen environment yielded magnetic multicomponent nanoparticles. First, distilled water was used to dissolve a particular amount of iron (III) chloride hexahydrate ($FeCl_3$, $6H_2O$), copper (II) chloride dihydrate ($CuCl_2$ $2H_2O$), and nickel (II) chloride ($NiCl_2$). Three distinct forms of magnetic multicomponent nanoparticles (Cu_x Ni_{1-x} Fe_2O_4) were manufactured using the reaction: $Cu^{+2} + Ni^{+2} + 2Fe^{+3} + 8OH^-$ gives $Cu_xNi_{1-x}Fe_2O_4$, where x1 40.0, 0.6, and 1.0. The mixture was then agitated for 15 minutes at 1000 rpm using a magnetic stirrer. Meanwhile, an oil bath was heated to 80 °C, and the mixture was heated in the same oil bath in a nitrogen environment with steady stirring at 500 rpm for 30 minutes until it reached the temperature of 80 °C. Following this, 1.2 M sodium hydroxide solution was added drop by drop while under nitrogen gas. The mixture was then moved to a Teflon-lined autoclave and held at 250 °C for 12 h until the procedure was completed. It was then allowed to cool to room temperature naturally. The items were rinsed multiple times with distilled water before being dried in a vacuum oven at 80–85 °C for 15 h. Annealing at 800 1C for 2 h yielded magnetic multicomponent nanoparticles. The classification of nanoparticles with typical examples utilized in medical imaging modalities is depicted in Fig. 2.

The structure and particle sizes were determined using X-ray powder diffraction (XRD). Cu K radiation was used in a Rigaku SmartLab diffractometer at 40 kV and 35 mA. Scanning electron microscopy (SEM) at 15 kV was used to determine the size and shape of the MNPs. The Malvern Instruments Zeta Sizer Nano-ZS device was also used to measure the nanoparticle sizes. A Quantum Design vibrating sample magnetometer was used to conduct the magnetic investigations (QD-VSM). Under 50 Oe, measurements of zero-field cooling (ZFC) and field cooling (FC) were made from 10 to 300 K. These readings were then used to calculate blocking temperatures. At 10, 50, 100, 200, and 300 K, hysteresis curves were recorded between 715 kOe. From the observed hysteresis loops, saturation magnetization (Ms), remanent magnetization (Mr), and coercivity field (Hc) were calculated. The role of multicomponent nanoparticles in biomedical imaging was depicted in Fig. 3.

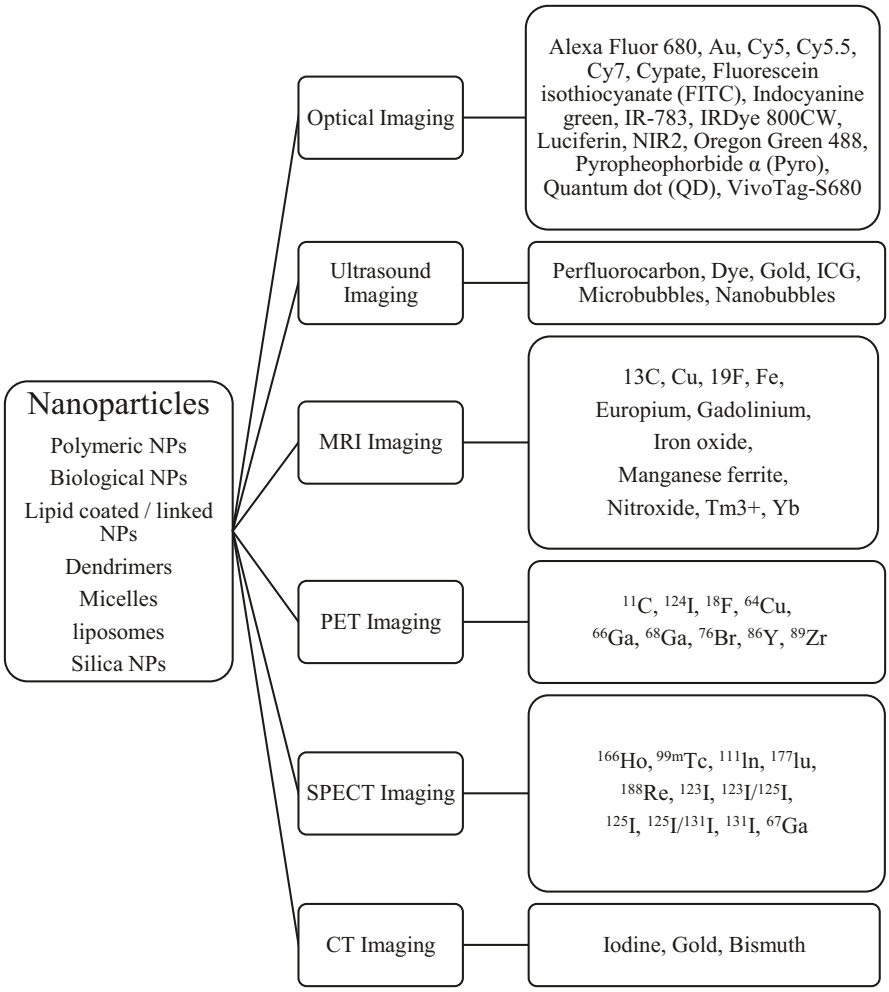

Fig. 2 Nanoparticles utilized in medical imaging modalities

Multifunctional nanoparticles can carry one or more therapeutic agents, to offer the biomolecular targeting through one or more conjugated antibodies or other recognition agents to give imaging signal amplification, by way of co-encapsulated contrast agents. Bioconjugation offers exquisite chemo- and regioselective control for the efficient functionalization of nanoparticles with a variety of biological substrates. These nanoparticles, through nanocrystalline synthesis, advanced polymer processing, and coating and functionalization strategies, have the potential to integrate various functionalities, simultaneously providing (a) contrast for different imaging modalities, (b) targeted delivery of drug/gene, and (c) thermal therapies.

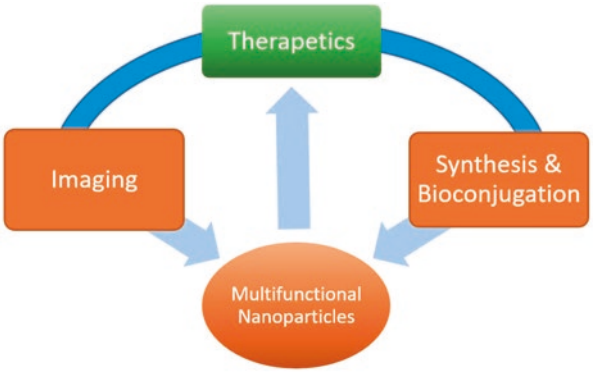

Fig. 3 Role of multifunctional nanoparticles in biomedical imaging

Nano-sized inorganic particles, whether simple or complex, have unique physical and chemical characteristics and are becoming a more significant material in the creation of new nanodevices for a variety of physical, biological, medicinal, and pharmacological applications. Nano-sized inorganic particles, whether simple or complex, have unique physical and chemical characteristics and are becoming a more significant material in the creation of new nanodevices for a variety of physical, biological, medicinal, and pharmacological applications.

3 Multicomponent Nanoparticles Used in Computed Tomography

The nanoparticles used in computed tomography (CT) play an important role in the diagnosis for early detection and therapy of various disease and response assessments. These nanoparticles help in the detection of the lesion at an early stage and also visualize the functional and anatomical information very accurately. The nanoparticles are used for medical imaging as contrast agents for the abnormality detection and functionality of the organs. Biomedical imaging has improved with nanomaterials due to active and passive properties and the targeted reactive properties. The size of the nanomaterials as contrast agents greatly plays in the tumor imaging as it exhibits enhanced permeability and retention (EPR) with tumor cells [18].

The nano-sized contrast agents are used to distinguish the tissues with similar attenuation coefficients. As of now most of the CT contrast agents are iodine-based, and also the other CT contrast agents are gold nanoparticles and bismuth nanomaterials [19]. These nano-sized CT contrast agents have different capabilities like cellular uptake, CT attenuation, and targeted delivery of drugs (Table 2).

Table 2 Nanoparticles with their utilization in CT imaging with gold, bismuth, and iodine as a contrast agent

Contrast agent	Abbreviated name of nanoparticles	Target category	Inferences	Reference details
Gold	AuNPs	Nontargeted	Contrast enhancement of CT in the circulatory and respiratory organs, kidneys, and tumor in mice	[20]
Gold	PEG-AuNPs	Phagocytosis, blood pool retention	Cancer CT imaging and photothermal agents	[21]
Bismuth	BPNPs	Phagocytosis, endocytosis	Contrast enhancement CT for the heart lungs, liver, and lymph nodes in mice	[22]
Iodine	DHOG	Nonspecific blood circulation and hepatic uptake pathway of chylomicron remnants	Contrast enhancement CT for bloodstream imaging and contrast enhancement of micro-CT in the liver in small animal	[23]
Iodine	Iobitridol	Nontargeted throughout blood vessels and organs	Contrast enhancement in the drug delivery route along with the blood flow, and the concentration of the iodine in the target region.	[24]
Iodine	N1177	Macrophages, phagocytosis	During the development of atherosclerotic plaques, macrophages detect.	[25]
Iodine	IX-C particles	Phagocytosis	IX-C particles are degraded inside the phagocytic cells for the contrast enhancement of the liver.	[26]
Iodine	LPNCs	Nonspecific filling of blood vessels and tissues, phagocytosis by the RES	Used as a contrast agent for lymphography and hysterosalpingography	[27]
Iodine	Ioversol	Nonspecific filling of blood vessels and tissues	Used as nonionic contrast agents in the blood vessels, heart, kidneys, brain, and whole body	[28]
Iodine	Iopentol	Nonspecific filling of blood vessels and tissues	Used for arteriography, urography, phlebography and computed tomography enhancement, arthrography, endoscopic retrograde cholangiopancreatography, hysterosalpingography, and gastrointestinal studies	[29]

(continued)

Table 2 (continued)

Contrast agent	Abbreviated name of nanoparticles	Target category	Inferences	Reference details
Iodine	Ioxilan	Nonspecific filling of blood vessels and tissues	CT contrast-enhanced with ioxilan for imaging of the head and body	[30]
Iodine	Tyropanoate sodium	Hepatic uptake and biliary excretion after oral absorption	Contrast agent for the gallbladder and the biliary tree imaging	[31]

Table 3 Nanoparticles with their utilization in MR imaging with 13C as the contrast agent

Contrast	Abbreviated name of nanoparticles	Target category	Inferences	References
13C	[1,4-$^{13}C_2$]fumarate	Enzymes	Used to detect the early response of tumors and treatment detection	[34]
13C	[1-^{13}C]DHA	Enzyme	React rapidly and beneficial results for the brain, liver, kidney, and TRAMP tumor	[35]
13C	HP[^{13}C]HEPP	Other – Metabolism	Suitable for pharmacokinetic tracing	[36]
13C	Hyperpolarized$H^{13}CO_3^-$	Enzymes	Used for imaging of blood vessels and tissue perfusion	[34]
13C	HP[^{13}C]Pyr	Other – metabolism	Used for the detection of primary tumors and lymph node metastases	[37]
13C	[1-^{13}C]KIC	Enzymes	Metabolism reports in vivo in small animals by BCATs	[38]

4 Multicomponent Nanoparticles Used in Magnetic Resonance Imaging

The MRI contrast agents are used to detect the normal and abnormal tissues and also for the therapeutic treatment of diseases. The nanoparticle contrast agents used in MRI greatly depend on the T1 and T2 relaxation times [32]. The mostly used MRI contrast agents are iron oxide-based and gadolinium-based, and the other contrast agents are based on 13C, 19F, Cu, europium, Fe, manganese ferrite, nitroxide, Tm3+, and Yb. The contrast agents are categorized into T1-weighted contrast agents, T2-weighted contrast agents, and dual-weighted contrast agents [33]. The nano-sized contrast agents are used in the gene, proteins, cells, and organs (Tables 3, 4, 5 and 6).

Table 4 Nanoparticles with its utilization in MR imaging with Eu as the contrast agent

Contrast agents	Abbreviated name of nanoparticles	Target category	Inferences	References
Eu	4GdPeptide	Acceptor	4GdPeptide can penetrate through thrombi to bind fibrin in depth via passive diffusion and distinguish between occlusive and nonocclusive arterial thrombi or between thrombi of different sizes and ages	[39]
Eu	C3d-SA-GdAF	Adhesion molecule	Contrast enhancements in the liver (85%), kidneys (30%), and muscle (3%) after 5 h, showing the Gd complex persisted in the apoferritin cavity	[40]
Eu	MGd	Other	Radiation sensitizer for brain metastases with whole-brain radiation therapy	[41]
Eu	Anti-c-Met-Gd-albumin	Binding	A contrast agent was present in the glioma tissue for the next 3 h	[42]
Eu	Gd-DTPA-anti-ICAM-1 antibody	Antibody-ligand binding	For studying inflammation with MRI	[43]
Eu	MDA2 micelles	Antigen	Atherosclerotic lesions were detected in mice models	[44]
Eu	Anti-VEGF PLA-PEG-PLL-DTPA-Gd NPs, anti-VEGF PLA-PEG-PLL-Gd NPs	Protein	High signal intensity in the tumor for 2 h	[45]
Eu	Avidin-Gd	Protein-protein binding	The NT-5 tumors hold the contrast for 8–24 h after MRI treatment	[46]
Eu	Biotin-BSA-GdDTPA	Tumor-associated stroma	Contrast agent-treated cells indicating the cells migrated to the stroma and facilitated the analysis concerning the spread of cancer	[47]
Eu	P866	Folate receptor	MRI contrast agent for folate receptor expression in nude mice bearing human cancer xenografts and in rats with arthritis	[48]
Eu	EB-DTPA-Gd	Nonspecific binding to proteins	The detection of atherosclerotic lesions by MRI	[49]

(continued)

Table 4 (continued)

Contrast agents	Abbreviated name of nanoparticles	Target category	Inferences	References
Eu	P1133	Receptor	In vivo MRI of breast cancer in mice using folate-conjugated PEG-USPIO nanoparticles	[50]
Eu	Gd-BOPTA	Blood-brain barrier breakdown	Gd-BOPTA provided better diagnostic information in intracranial lesions	[51]
Eu	Gd-DO3A-butrol	Nontargeted, blood pool, extracellular fluid space	A nonionic, paramagnetic contrast agent enhanced contrast in tissue with MRI	[52]
Eu	Gd-DOTA-cFlFlFK	Receptor	Gd-DOTA-cFlFlFK with MRI imaging of neutrophils at the sites of inflammation	[53]
Eu	Gd-DOTAMA-C6-Gln	Transporter	The Gln transportation rate for tumors like hepatoma is 10–20 times faster than that for healthy hepatocytes. The Gln used to distinguish between tumors and tissues via contrast agent-enhanced MRI	[54]
Eu	Gd-DTPA-PLGA	Nontargeted	In vivo imaging of the liver in rabbits, exhibiting enhanced MRI and ultrasound signals	[55]
Eu	Gd-DOTA-R832	Receptor	As a noninvasive MRI contrast agent for detection of atherosclerosis in endothelial cells of the heart	[56]
Eu	$Gd_3N@C_{80}[DiPEG_{5000}(OH)_x]$	Retention	It increases the T_1 relaxivity as much as 30 times more than that of Gd-DOTA	[57]

5 Multicomponent Nanoparticles Used in PET Imaging

Positron emission tomography (PET) is widely used for the diagnosis of anomalies at the molecular or cellular level. The radiopharmaceutical activity is employed in PET imaging to generate better quality images than other modalities, the sensitivity is high, and, however, the cost limits its use in clinical diagnosis.

The magnetic iron oxide nanoparticles play a prominent role in biomedical applications like drug delivery and medical imaging [82–84]. Superparamagnetic nanoparticles are employed as contrast agents to distinguish the healthy and affected tissues in molecular and cell imaging [85, 86]. The MRI has low sensitivity for molecular imaging; however, the bimodal imaging such as MRI/PET yields

Table 5 Nanoparticles with its utilization in MR imaging with iron oxide as the contrast agent

Contrast agents	Nanoparticles	Abbreviated name	Target category	Inferences	References
Superparamagnetic iron oxide	Amine-modified silica-coated polyhedral superparamagnetic iron oxide nanoparticle-labeled rabbit bone marrow-derived mesenchymal stem cells	SPIO@ SiO_2-NH_2-labeled MSCs	Nontargeted	For MRI real-time cell tracking of implanted MSCs	[58]
Microparticle iron oxide	Anti-vascular cell adhesion molecule antibody M/K 2.7-conjugated microparticles of iron oxide	VCAM-MPIO	Antigen	Inflammation stage detection in atherosclerosis and renal ischemia	[59]
Superparamagnetic iron oxide	Citrate-coated (184th variant) very small superparamagnetic iron oxide particles	VSOP-C184	Phagocytosis	MRI studies on 20 rabbits for contrast agent and dose bearing on liver tumors with 1.5 T	[60]
Superparamagnetic iron oxide	Doxorubicin-loaded poly(ethylene oxide)-trimellitic anhydride chloride-folate superparamagnetic iron oxide nanoparticles	YCC-DOX	Receptor	Nanoparticles, which are conjugated to target-seeking molecules, bind only to cells that produce the appropriate biomarker, are used as MRI contrast agents and serve as multifunctional drug delivery and imaging agents	[61]
Fe_3O_4	FluidMAG iron nanoparticle-labeled mesenchymal stem cells for tracking cell homing to tumors	FluidMAG iron nanoparticle-labeled MSCs	Nontargeted	MSCs labeled with fluidMAG iron nanoparticles to track tumors in MRI	[62]

(continued)

Table 5 (continued)

Contrast agents	Nanoparticles	Abbreviated name	Target category	Inferences	References
Fe_3O_4	Glycol chitosan/ heparin-immobilized gold-deposited iron oxide nanoparticles	Composite NPs	Adhesion molecules	Composite NPs have been shown to selectively distribute in tumors in an animal model of murine squamous cell carcinoma (SCC).	[63]
Cross-linked iron oxide nanoparticles (CLIO)	H18/7 $F(ab')_2$ E-selectin monoclonal antibody conjugated to cross-linked iron oxide nanoparticles	CLIO-H18/7 $F(ab')_2$	Receptor	A noninvasive MRI, the CLIO nanoparticles conjugated for of E-selectin expression in endothelial cell	[64]
Fe_3O_4	Iron oxide nanoparticles-poly-L-lysine complex	SPIO-PLL	Other	Used to find the liver lesion	[65]
Superparamagnetic iron oxide nanoparticles	Lactoferrin-conjugated superparamagnetic iron oxide nanoparticles	Lf-SPIONs	Receptors	Lf-SPIONs were able to effectively enhance the glioma contrast	[66]
Ultrasmall superparamagnetic iron oxide (USPIO)	MES-1 F(ab')2 E-selectin monoclonal antibody conjugated to ultrasmall superparamagnetic iron oxide nanoparticle	MES-1-USPIO	Antigen	For noninvasive MR imaging, USPIO nanoparticles target the E-selectin expression in inflammation	[67]

proficient results. The work [82] highlights the novel magnetic nanoparticles for the PET/MRI imaging technology. Superparamagnetic iron nanoparticles were utilized in this work for the bimodal imaging of the liver and kidney. The nanoparticles are synthesized under hydrothermal conditions and highlight the activity of anatomical organs in a better manner.

In PET imaging, a radioactive isotope called the tracer is utilized, and it has the highest sensitivity when compared with the other medical imaging modalities; however, the spatial resolution is poor. PET imaging is usually accompanied by CT imaging, and it reflects the biochemical activity also. In cancer therapy, fluorodeoxyglucose (FDG)-positron emission tomography (PET) (or FDG–PET/CT) is used for tumor prognosis and radiotherapy. Apart from ^{18}F, other materials used are ^{64}Cu

Table 6 Nanoparticles with its utilization in MR imaging with different contrast agents

Contrast	Abbreviated name	Target category	Examples	References
19F	6-FPOL	Protonation and deprotonation of the 3-phenolic OH in diverse pH environments	The transmembrane pH gradient of tumors could be measured	[68]
19F	CS-1000	Cell tracking	Used for quantitative cell tracking	[69]
19F	PFPE-DCs	Inflamed tissue	Dendritic cells are labeled with PFPE (PFPE-DCs) for ^{19}F magnetic resonance imaging (MRI)	[70]
19F	PFPE-BTCs	Inflamed tissue	The fluorescence-labeled PFPE appeared to bind to the cell membrane	[70]
19F	VCAM-1-targeted nanoparticles	Receptor	VHPKQHRGGSKGC was synthesized and conjugated to liquid perfluorocarbon (PFC) nanoparticles to form VCAM-1-targeted nanoparticles	[71]
Cu	Au_3Cu_1-NPs	Blood pool retention	Au3Cu1 nanoparticles as bimetallic MRI contrast agents with enhancing effects in T1- and T2-weighted imaging	
Eu	Eu-DOTA-OBZ_2-Gly_2, Eu-DOTAM-OBZ_2-Gly_2	Nontargeted	Detects the accumulation of a PARACEST agent, Eu-DOTA-OBZ_2-Gly_2, in the liver tissue.	[72]
Fe	BM3h-8C8	Neurotransmitter	High affinity for dopamine, and low affinity for arachidonic acid	[73]
Gd	EGadMe	Enzyme	Used to distinguish the nontransfected one by MRI and their descendants as well	[74]
Manganese ferrite	MDA2-Mn micelles	Antigen	In $apoE^{-/-}$ mice, MDA2-Mn micelles exhibited sensitivity and robustness in vivo to the finding of atherosclerotic lesions using MRI	[75]
Manganese ferrite	Mn-DOTA-G3-CLT1	Acceptor	Mn-DOTA-G3-CLT1 as an MRI tumor contrast agent in nude mice bearing MDA-MB-231 human breast carcinoma xenografts	[76]

(continued)

Table 6 (continued)

Contrast	Abbreviated name	Target category	Examples	References
Manganese ferrite	$VEGF_{121}$/ rGel-MNPs	Receptors	VEGF121/rGel-MNPs when delivered to intratumoral vessels as target and was tested with immunofluorescence staining of the gelonin and endothelial cells	[77]
Nitroxide	[^{15}N] TEMPONE	Reactive oxygen species (ROS)	^{14}N- and ^{15}N-labeled nitroxides can be tracked concurrently in same the anatomic image with co-registration	[78]
Nitroxide	3CxP	Reactive oxygen species (ROS)	In vivo pharmacokinetics of 3CxP in tumors is studied in MR imaging	[79]
Nitroxide	$H_2{}^{17}O$	Nontargeted	Cerebral blood flow (CBF) in cats with MRI using $H_2{}^{17}O$	[80]
Tm3+	Tm-DOTA-Gly	Nontargeted	Tm-DOTA-Gly, accumulated in tumor tissue of a mouse model of MCF-7 human mammary carcinoma is detected in MRI	[72]
Yb	Yb-DO3A-oAA	Nontargeted	Yb-DO3A-oAA, the PARACEST agent accumulated within the tumor tissue of mice bearing human mammary carcinoma *MDA-MB-231* cell tumors, is detected in CEST-FISP MRI protocol	[81]

and 99mTc. The radiolabeled nanoparticles gain prominence in cancer therapy and multimodal imaging. The nanoparticles used in PET/SPECT imaging are labeled with positron emitters. Radionuclides are classified into short-lived and long-lived ones, as the name itself states that short-lived radionuclides are used for the short frame measurement, whereas the long-lived ones are utilized for long frame measurement. The half-life period of ^{18}F is 109.8 min and is widely used in many applications.

Quantum dots are semiconductor nanocrystals formulated from heavy metal alloys and have excellent optical properties. The toxic nature of the metals limits their usage in many applications. Upconversion nanoparticles rely on the phenomena of upconversion luminance. The upconversion luminescence is a process in which a high-energy photon is liberated when rare-earth ions absorb two or more low-energy photons. It is a bioluminescence marker; low toxicity and chemical stability make it superior when compared with the quantum dots. The characteristics of the upconverting nanoparticles (UCNP's) are as follows:

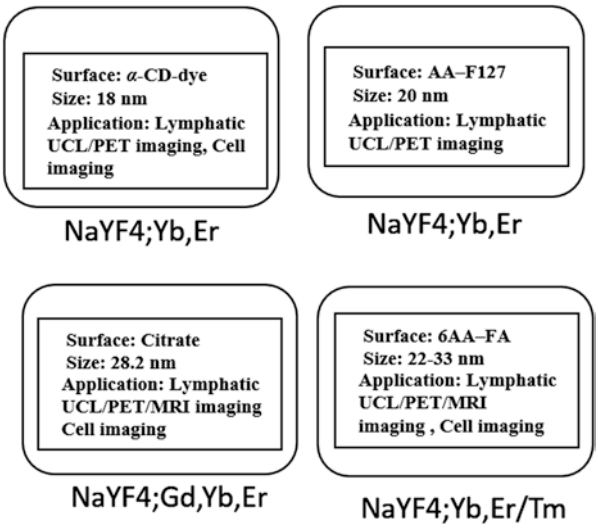

Fig. 4 Biological applications of typical upconversion nanoparticles

(i) They are soluble in water.
(ii) Proton-emitting efficiency is high.
(iii) Easy to control because of the smaller size.
(iv) Active group on the surface.

The biological applications of typical UCNP's are depicted in Fig. 4.

The UCNPs are also utilized in image-guided cancer therapy and drug delivery systems. The mesoporous silica nanoparticles (MSNs) also gain prominence in medical imaging. The CdSe/CdZnS DSPE-PEG2000-NH2 $_{\text{nano}}$particle is discussed in [86] with its size greater than or equal to 20 nm, and the reaction time is 145 min. The NaYF4 (co-doped with Yb, Er, Tm, Gd) nanoparticle is discussed in [87] with its size in the range of 10–20 nm, and the reaction time is 10 minutes. The gold/CLPFFD (peptide) nanoparticle is discussed in [88] with its size of 23 nm, and the reaction time is 60 minutes.

6 Conclusion

Medical images are utilized in the health-care sector for disease diagnosis and surgical preplanning. This chapter proposes a detailed study on the role of nanomaterials in medical imaging. The generic classification of nanomaterial that finds its role health-care sector is initially discussed in this chapter. The synthesis and characteristics of multicomponent nanoparticles are then highlighted followed by the typical nanoparticles utilized in CT, MRI, and PET imaging. The outcome of this chapter

paves a way for the researchers in the choice of nanoparticles with contrast agents for respective imaging modalities in the disease diagnosis.

References

1. Jang H-Y, Kim H-R, Kang M-S, Kim M-H, Zhang B-T. The demand for quantitative techniques in biomedical image informatics. Biomed Eng Lett. 2014 Dec;4(4):319–27.
2. Kalimuthu S, Jeong JH, Oh JM, Ahn B-C. Drug discovery by molecular imaging and monitoring therapy response in lymphoma. Int J Mol Sci. 2017 Jul;18(8):1639.
3. Chen F, Hableel G, Zhao ER, Jokerst JV. Multifunctional nanomedicine with silica: role of silica in nanoparticles for theranostic, imaging, and drug monitoring. J Colloid Interface Sci. 2018;521:261–79.
4. Li J, Chang X, Chen X, Gu Z, Zhao F, Chai Z, et al. Toxicity of inorganic nanomaterials in biomedical imaging. Biotechnol Adv. 2014;32(4):727–43.
5. Pellico J, Gawne PJ, de RTM R. Radiolabelling of nanomaterials for medical imaging and therapy. Chem Soc Rev. 2021;50:3355–423.
6. Kong F-Y, Zhang J-W, Li R-F, Wang Z-X, Wang W-J, Wang W. Unique roles of gold nanoparticles in drug delivery, targeting and imaging applications. Molecules. 2017;22(9):1445.
7. Wang Y, Sun S, Zhang Z, Shi D. Nanomaterials for cancer precision medicine. Adv Mater. 2018;30(17):1705660.
8. Siddique S, Chow JCL. Application of nanomaterials in biomedical imaging and cancer therapy. Nano. 2020;10(9):1700.
9. Smith BR, Gambhir SS. Nanomaterials for in vivo imaging. Chem Rev. 2017;117(3):901–86.
10. Bhuiyan MTH, Chowdhury MN, Parvin MS. Potential nanomaterials and their applications in modern medicine: an overview. ARC J Cancer Sci. 2016;2(2):25–33.
11. Solanki A, Kim JD, Lee KB. Nanotechnology for regenerative medicine: nanomaterials for stem cell imaging. Nanomedicine. 2008;3(4):567–78.
12. Lavik E, von Recum H. The role of nanomaterials in translational medicine. ACS Nano. 2011;5(5):3419–24.
13. Sun X, Cai W, Chen X. Positron emission tomography imaging using radiolabeled inorganic nanomaterials. Acc Chem Res. 2015;48(2):286–94.
14. Yoon HJ, Kozminsky M, Nagrath S. Emerging role of nanomaterials in circulating tumor cell isolation and analysis. ACS Nano. 2014;8(3):1995–2017.
15. Rezaei R, Safaei M, Mozaffari HR, Moradpoor H, Karami S, Golshah A, et al. The role of nanomaterials in the treatment of diseases and their effects on the immune system. Open Access Maced J Med Sci. 2019;7(11):1884.
16. Choi J, Wang NS. Nanoparticles in biomedical applications and their safety concerns. Biomed Eng from theory to Appl. 2011;29:486.
17. Bystrzejewski Michałand Cudziło S, Huczko A, Lange H, Soucy G, Cota-Sanchez G, Kaszuwara W. Carbon encapsulated magnetic nanoparticles for biomedical applications: thermal stability studies. Biomol Eng. 2007;24(5):555–8.
18. Nakamura Y, Mochida A, Choyke PL, Kobayashi H. Nanodrug delivery: is the enhanced permeability and retention effect sufficient for curing cancer? Bioconjug Chem. 2016;27(10):2225–38.
19. Kim D, Park S, Lee JH, Jeong YY, Jon S. Antibiofouling polymer-coated gold nanoparticles as a contrast agent for in vivo X-ray computed tomography imaging. J Am Chem Soc. 2007;129(24):7661–5.
20. Hainfeld JF, Slatkin DN, Focella TM, Smilowitz HM. Gold nanoparticles: a new X-ray contrast agent. Br J Radiol. 2006;79(939):248–53.

21. Cai Q-Y, Kim SH, Choi KS, Kim SY, Byun SJ, Kim KW, et al. Colloidal gold nanoparticles as a blood-pool contrast agent for X-ray computed tomography in mice. Investig Radiol. 2007;42(12):797–806.
22. Rabin O, Perez JM, Grimm J, Wojtkiewicz G, Weissleder R. An X-ray computed tomography imaging agent based on long-circulating bismuth sulphide nanoparticles. Nat Mater. 2006;5(2):118–22.
23. O'Donoghue J. Visualization of experimental lung and bone metastases in live nude mice by X-ray micro-computed tomography. Technol Cancer Res Treat. 2006;5(2).
24. Fournier PJ, Steinbrich W, Freitag P, Voegeli E. Evaluation of the clinical safety and efficacy of iobitridol (Xenetix) in intravenous urography. Eur J Radiol. 1996;23(3):185–9.
25. Weissleder R, Nahrendorf M, Pittet MJ. Imaging macrophages with nanoparticles. Nat Mater. 2014;13(2):125–38.
26. Li C, Kan Z, Yang DJ, Kuang L-R, Liu CW, Wright KC, et al. Preparation, characterization, and evaluation of ioxilan carbonate particles for computed tomography contrast enhancement of liver. Investig Radiol. 1994;29(11):1006–13.
27. Swanson DP, Alpern MB. Contrast media for computed tomography: intravascular, intracavitary, xenon, reticuloendothelial. In: Swanson DP, Thrall HMCJH, editors. Pharmaceutical medical imaging. New York: Macmillan Publishing Company; 1990. p. 99–124.
28. Floriani I, Ciceri M, Torri V, Tinazzi A, Jahn H, Noseda A. Clinical profile of ioversol: a meta-analysis of 57 randomized. Double-Blind Clinical Trials Invest Radiol. 1996;31(8):479–91.
29. Aakhus T, Stokke O, Stormorken H, Berg KJ, Dahlström K. Pharmacologic effects of iopentol after intravenous injection in healthy volunteers. Preliminary report. Acta Radiol Suppl. 1987;370:109–12.
30. Callantine MR, Sovak M, Lu H-P. Ioxilan initial clinical observations. Investig Radiol. 1990;25:S107–8.
31. Amberg JR, Thompson WM, Golberger L, Williamson S, Alexander R, Bates M. Factors in the intestinal absorption of oral cholecystopaques. Investig Radiol. 1980;15(6 Suppl):S136–41.
32. Issa B, Obaidat IM. Magnetic nanoparticles as MRI contrast agents. Magn Reson Imaging. 2019;378:40.
33. Mosleh-Shirazi S, Abbasi M, Shafiee M, Kasaee SR, Amani AM. Renal clearable nanoparticles: an expanding horizon for improving biomedical imaging and cancer therapy. Mater Today Commun. 2021;26:102064.
34. Gallagher FA, Kettunen MI, Hu D-E, Jensen PR, Karlsson M, Gisselsson A, et al. Production of hyperpolarized [1, 4-13C2] malate from [1, 4-13C2] fumarate is a marker of cell necrosis and treatment response in tumors. Proc Natl Acad Sci. 2009;106(47):19801–6.
35. Keshari KR, Kurhanewicz J, Bok R, Larson PEZ, Vigneron DB, Wilson DM. Hyperpolarized 13C dehydroascorbate as an endogenous redox sensor for in vivo metabolic imaging. Proc Natl Acad Sci. 2011;108(46):18606–11.
36. Olsson LE, Chai C-M, Axelsson O, Karlsson M, Golman K, Petersson JS. MR coronary angiography in pigs with intraarterial injections of a hyperpolarized 13C substance. Magn Reson Med Off J Int Soc Magn Reson Med. 2006;55(4):731–7.
37. Chen AP, Albers MJ, Cunningham CH, Kohler SJ, Yen Y-F, Hurd RE, et al. Hyperpolarized C-13 spectroscopic imaging of the TRAMP mouse at 3T—initial experience. Magn Reson Med Off J Int Soc Magn Reson Med. 2007;58(6):1099–106.
38. Karlsson M, Jensen PR, in't Zandt R, Gisselsson A, Hansson G, Duus Jens Øand Meier S, et al. Imaging of branched chain amino acid metabolism in tumors with hyperpolarized 13C ketoisocaproate. Int J Cancer 2010;127(3):729–736.
39. Sirol M, Fuster V, Badimon JJ, Fallon JT, Toussaint J-F, Fayad ZA. Chronic thrombus detection with in vivo magnetic resonance imaging and a fibrin-targeted contrast agent. Circulation. 2005;112(11):1594–600.
40. Crich SG, Bussolati B, Tei L, Grange C, Esposito G, Lanzardo S, et al. Magnetic resonance visualization of tumor angiogenesis by targeting neural cell adhesion molecules with the highly sensitive gadolinium-loaded apoferritin probe. Cancer Res. 2006;66(18):9196–201.

41. Richards GM, Mehta MP. Motexafin gadolinium in the treatment of brain metastases. Expert Opin Pharmacother. 2007;8(3):351–9.
42. Towner RA, Smith N, Doblas S, Tesiram Y, Garteiser P, Saunders D, et al. In vivo detection of c-Met expression in a rat C6 glioma model. J Cell Mol Med. 2008;12(1):174–86.
43. Choi K-S, Kim S-H, Cai Q-Y, Kim S-Y, Kim H-O, Lee H-J, et al. Inflammation-specific T1 imaging using anti-intercellular adhesion molecule 1 antibody-conjugated gadolinium diethylenetriaminepentaacetic acid. Mol Imaging. 2007;6(2):2007–7290.
44. Briley-Saebo KC, Shaw PX, Mulder WJM, Choi S-H, Vucic E, Aguinaldo JGS, et al. Targeted molecular probes for imaging atherosclerotic lesions with magnetic resonance using antibodies that recognize oxidation-specific epitopes. Circulation. 2008;117(25):3206–15.
45. Liu Y, Chen Z, Liu C, Yu D, Lu Z, Zhang N. Gadolinium-loaded polymeric nanoparticles modified with anti-VEGF as multifunctional MRI contrast agents for the diagnosis of liver cancer. Biomaterials. 2011;32(22):5167–76.
46. Artemov D, Mori N, Okollie B, Bhujwalla ZM. MR molecular imaging of the Her-2/neu receptor in breast cancer cells using targeted iron oxide nanoparticles. Magn Reson Med Off J Int Soc Magn Reson Med. 2003;49(3):403–8.
47. Granot D, Kunz-Schughart LA, Neeman M. Labeling fibroblasts with biotin-BSA-GdDTPA-FAM for tracking of tumor-associated stroma by fluorescence and MR imaging. Magn Reson Med Off J Int Soc Magn Reson Med. 2005;54(4):789–97.
48. Wang ZJ, Boddington S, Wendland M, Meier R, Corot C, Daldrup-Link H. MR imaging of ovarian tumors using folate-receptor-targeted contrast agents. Pediatr Radiol. 2008;38(5):529–37.
49. Yasuda S, Ikuta K, Uwatoku T, Oi K, Abe K, Hyodo F, et al. In vivo magnetic resonance imaging of atherosclerotic lesions with a newly developed Evans blue-DTPA-gadolinium contrast medium in apolipoprotein-E-deficient mice. J Vasc Res. 2008;45(2):123–8.
50. Meier R, Henning TD, Boddington S, Tavri S, Arora S, Piontek G, et al. Breast cancers: MR imaging of folate-receptor expression with the folate-specific nanoparticle P1133. Radiology. 2010;255(2):527–35.
51. Spinazzi A, Lorusso V, Pirovano G, Kirchin M. Safety, tolerance, biodistribution, and MR imaging enhancement of the liver with gadobenate dimeglumine: results of clinical pharmacologic and pilot imaging studies in nonpatient and patient volunteers. Acad Radiol. 1999;6(5):282–91.
52. Pediconi F, Catalano C, Occhiato R, Venditti F, Fraioli F, Napoli A, et al. Breast lesion detection and characterization at contrast-enhanced MR mammography: gadobenate dimeglumine versus gadopentetate dimeglumine. Radiology. 2005;237(1):45–56.
53. Stasiuk GJ, Smith H, Wylezinska-Arridge M, Tremoleda JL, Trigg W, Luthra SK, et al. Gd 3+ cFLFLFK conjugate for MRI: a targeted contrast agent for FPR1 in inflammation. Chem Commun. 2013;49(6):564–6.
54. Crich G, Cabella C, Barge A, Belfiore S, Ghirelli C, Lattuada L, et al. In vitro and in vivo magnetic resonance detection of tumor cells by targeting glutamine transporters with Gd-based probes. J Med Chem. 2006;49(16):4926–36.
55. Ao M, Wang Z, Ran H, Guo D, Yu J, Li A, et al. Gd-DTPA-loaded PLGA microbubbles as both ultrasound contrast agent and MRI contrast agent—a feasibility research. J Biomed Mater Res Part B Appl Biomater. 2010;93(2):551–6.
56. Burtea C, Laurent S, Port M, Lancelot E, Ballet S, Rousseaux O, et al. Magnetic resonance molecular imaging of vascular cell adhesion molecule-1 expression in inflammatory lesions using a peptide-vectorized paramagnetic imaging probe. J Med Chem. 2009;52(15):4725–42.
57. Fatouros PP, Corwin FD, Chen Z-J, Broaddus WC, Tatum JL, Kettenmann B, et al. In vitro and in vivo imaging studies of a new endohedral metallofullerene nanoparticle. Radiology. 2006;240(3):756–64.
58. Wang H-H, Wang Y-X, Leung KC-F, Au DWT, Xuan S, Chak C-P, et al. Durable mesenchymal stem cell labelling by using polyhedral superparamagnetic iron oxide nanoparticles. Chem Eur J. 2009;15(45):12417.

59. Akhtar AM, Schneider JE, Chapman SJ, Jefferson A, Digby JE, Mankia K, et al. In vivo quantification of VCAM-1 expression in renal ischemia reperfusion injury using non-invasive magnetic resonance molecular imaging. PLoS One. 2010;5(9):e12800.
60. Schnorr J, Wagner S, Abramjuk C, Drees R, Schink T, Schellenberger EA, et al. Focal liver lesions: SPIO-, gadolinium-, and ferucarbotran-enhanced dynamic T1-weighted and delayed T2-weighted MR imaging in rabbits. Radiology. 2006;240(1):90–100.
61. Islam T, Josephson L. Current state and future applications of active targeting in malignancies using superparamagnetic iron oxide nanoparticles. Cancer Biomark. 2009;5(2):99–107.
62. Loebinger MR, Kyrtatos PG, Turmaine M, Price AN, Pankhurst Q, Lythgoe MF, et al. Magnetic resonance imaging of mesenchymal stem cells homing to pulmonary metastases using biocompatible magnetic nanoparticles. Cancer Res. 2009;69(23):8862–7.
63. Yuk SH, Oh KS, Cho SH, Lee BS, Kim SY, Kwak B-K, et al. Glycol chitosan/heparin immobilized iron oxide nanoparticles with a tumor-targeting characteristic for magnetic resonance imaging. Biomacromolecules. 2011;12(6):2335–43.
64. Kang HW, Josephson L, Petrovsky A, Weissleder R, Bogdanov A. Magnetic resonance imaging of inducible E-selectin expression in human endothelial cell culture. Bioconjug Chem. 2002;13(1):122–7.
65. Bulte JWM, Arbab AS, Douglas T, Frank JA. Preparation of magnetically labeled cells for cell tracking by magnetic resonance imaging. Methods Enzymol. 2004;386:275–99.
66. Xie H, Zhu Y, Jiang W, Zhou Q, Yang H, Gu N, et al. Lactoferrin-conjugated superparamagnetic iron oxide nanoparticles as a specific MRI contrast agent for detection of brain glioma in vivo. Biomaterials. 2011;32(2):495–502.
67. Reynolds PR, Larkman DJ, Haskard DO, Hajnal JV, Kennea NL, George AJT, et al. Detection of vascular expression of E-selectin in vivo with MR imaging. Radiology. 2006;241(2):469–76.
68. Mason RP. Transmembrane pH gradients in vivo: measurements using fluorinated vitamin B6 derivatives. Curr Med Chem. 1999;6(6):481–500.
69. Bonetto F, Srinivas M, Heerschap A, Mailliard R, Ahrens ET, Figdor CG, et al. A novel 19F agent for detection and quantification of human dendritic cells using magnetic resonance imaging. Int J Cancer. 2011;129(2):365–73.
70. Ahrens ET, Flores R, Xu H, Morel PA. In vivo imaging platform for tracking immunotherapeutic cells. Nat Biotechnol. 2005;23(8):983–7.
71. Southworth R, Kaneda M, Chen J, Zhang L, Zhang H, Yang X, et al. Renal vascular inflammation induced by Western diet in ApoE-null mice quantified by 19F NMR of VCAM-1 targeted nanobeacons. Nanomed Nanotechnol Biol Med. 2009;5(3):359–67.
72. Liu G, Ali MM, Yoo B, Griswold MA, Tkach JA, Pagel MD. PARACEST MRI with improved temporal resolution. Magn Reson Med Off J Int Soc Magn Reson Med. 2009;61(2):399–408.
73. Shapiro MG, Westmeyer GG, Romero PA, Szablowski JO, Küster B, Shah A, et al. Directed evolution of a magnetic resonance imaging contrast agent for noninvasive imaging of dopamine. Nat Biotechnol. 2010;28(3):264–70.
74. Louie AY, Hüber MM, Ahrens ET, Rothbächer U, Moats R, Jacobs RE, et al. In vivo visualization of gene expression using magnetic resonance imaging. Nat Biotechnol. 2000;18(3):321–5.
75. Briley-Saebo KC, Nguyen TH, Saeboe AM, Cho Y-S, Ryu SK, Volkava E, et al. In vivo detection of oxidation-specific epitopes in atherosclerotic lesions using biocompatible manganese molecular magnetic imaging probes. J Am Coll Cardiol. 2012;59(6):616–26.
76. Tan M, Wu X, Jeong E-K, Chen Q, Parker DL, Lu Z-R. An effective targeted nanoglobular manganese (II) chelate conjugate for magnetic resonance molecular imaging of tumor extracellular matrix. Mol Pharm. 2010;7(4):936–43.
77. Cho E-J, Yang J, Mohamedali KA, Lim E-K, Kim E-J, Farhangfar CJ, et al. Sensitive angiogenesis imaging of orthotopic bladder tumors in mice using a selective magnetic resonance imaging contrast agent containing VEGF121/rGel. Investig Radiol. 2011;46(7):441–9.
78. Utsumi H, Yamada K, Ichikawa K, Sakai K, Kinoshita Y, Matsumoto S, et al. Simultaneous molecular imaging of redox reactions monitored by Overhauser-enhanced MRI with 14N-and 15N-labeled nitroxyl radicals. Proc Natl Acad Sci. 2006;103(5):1463–8.

79. Hyodo F, Yasukawa K, Yamada K, Utsumi H. Spatially resolved time-course studies of free radical reactions with an EPRI/MRI fusion technique. Magn Reson Med Off J Int Soc Magn Reson Med. 2006;56(4):938–43.
80. Arai T, Nakao S, Morikawa S, Inubushi T, Yokoi T, Shimizu K, et al. Measurement of local cerebral blood flow by magnetic resonance imaging: in vivo autoradiographic strategy using 17O-labeled water. Brain Res Bull. 1998;45(5):451–6.
81. Sheth VR, Li Y, Chen LQ, Howison CM, Flask CA, Pagel MD. Measuring in vivo tumor pHe with CEST-FISP MRI. Magn Reson Med. 2012;67(3):760–8.
82. Stegh AH. Toward personalized cancer nanomedicine--past, present, and future. Integr Biol. 2013;5(1):48–65.
83. Etzioni R, Urban N, Ramsey S, McIntosh M, Schwartz S, Reid B, et al. The case for early detection. Nat Rev Cancer. 2003;3(4):243–52.
84. Weissleder R, Pittet MJ. Imaging in the era of molecular oncology. Nature. 2008;452(7187):580–9.
85. Davis ME, Chen Z, Shin DM. Nanoparticle therapeutics: an emerging treatment modality for cancer. Nanosci Technol A Collect Rev Nat J. 2010:239–50.
86. Ducongé F, Pons T, Pestourie C, Hérin L, Thézé B, Gombert K, et al. Fluorine-18-labeled phospholipid quantum dot micelles for in vivo multimodal imaging from whole body to cellular scales. Bioconjug Chem. 2008;19(9):1921–6.
87. Liu Q, Sun Y, Li C, Zhou J, Li C, Yang T, et al. 18F-labeled magnetic-upconversion nanophosphors via rare-earth cation-assisted ligand assembly. ACS Nano. 2011;5(4):3146–57.
88. Guerrero S, Herance JR, Rojas S, Mena JF, Gispert JD, Acosta GA, et al. Synthesis and in vivo evaluation of the biodistribution of a 18F-labeled conjugate gold-nanoparticle-peptide with potential biomedical application. Bioconjug Chem. 2012;23(3):399–408.

Nanotheranostic: A Versatile Approach for Eye Cancer Diagnosis and Treatment

Fahima Dilnawaz and Sanjeeb Kumar Sahoo

1 Introduction

Eye health renders maximized vision, the functional ability that is having profound implications in many aspects of life. In all stages of life, eye conditions can be affected irrespective of age. The diseases of the eye directly affect human vision and quality of life. By 2050, ocular health will be affected by an estimated 895 million people [1]. Ocular diseases include both anterior and posterior segments of the eye. The eye possesses unique anatomy and physiology mechanism, effective drug delivery for the treatment of eye in terms of eye drops, injections, and implants, etc. The current treatment modality can seldom restore vision loss or detect severity at an early stage as therapeutics suffers from low bioavailability and lack of specificity [2, 3]. Therefore, for ocular diseases, there is a need for improved diagnostics and therapeutics, which are receiving intense attention. Recently, the use of a nanotechnology-based approach has experienced exponential growth for the diagnosis and treatment of tumors and eye disorders. In the past couple of decades, there have been remarkable advances in the field of drug delivery and material sciences which has led to the development of numerous nanomaterials [4]. To accommodate drug delivery toward the anterior and posterior segment of the eye, various nanosystems are designed that are either based on natural or synthetic or metallic elements. These nanocarriers offer controlled release and improved drug bioavailability for ocular disease therapy [2, 3]. Moreover, nanoparticles are being used in diagnostics for enhancement of sensitivity and selectivity compared to conventional diagnostic agents. Nanotheranostics events are carried out with specially designed

F. Dilnawaz · S. K. Sahoo (✉)
Laboratory of Nanomedicine, Institute of Life Sciences, Chandrasekharpur, Odisha, India

R. S. Chaughule et al. (eds.), *Nanomaterials for Cancer Detection Using Imaging Techniques and Their Clinical Applications*,
https://doi.org/10.1007/978-3-031-09636-5_15

nanoparticles that can deliver real-time information regarding drug biodistribution and release, in vivo [5, 6]. Nanotechnology-based ocular delivery mostly deals with different types of nanocarriers such as nanoparticles, micelles, liposomes, hydrogels, nanocages, nanocapsules, dendrimers, etc. which provides several advantages over routine diagnostics/therapies [7].

2 Ocular Barriers for Drug Delivery Systems

The human eye is a bulbous structured organ having a size of about 24 mm, consisting of two principal segments: the anterior and posterior [8] (Fig. 1). Both anterior and posterior parts possess various biological barriers, which provide protection to the eye from foreign substances. The corneal, iris, lens, and aqueous humor are the components of the anterior portion of the eyes, whereas the vitreous body, retina, choroid, and back of the sclera are the components of the posterior portion of the eye**.** The cornea is the transparent part of the eye that allows the light to enter inside, and it covers the iris and the pupil. The cornea has five layers: epithelium, Bowman's membrane, stroma, Descemet's membrane, and endothelium [9, 10]. The corneal epithelium is a vital part of the corneal barrier as it consists of multilayers of corneal epithelial cells that are interconnected by tight junctions. The presence of a tight junction severely curtails the penetration of hydrophilic drug molecules. Moreover, the corneal stroma hinders the passage of hydrophobic molecules because of its highly organized hydrophilic collagen. Various efflux transporters on epithelial cells prevent the entry of various antiviral and antiglaucoma drugs [11, 12]. Further, the intraocular environment comprises two main barriers: blood-aqueous and blood-retinal barriers. The blood-aqueous barrier consists of the nonpigmented epithelium

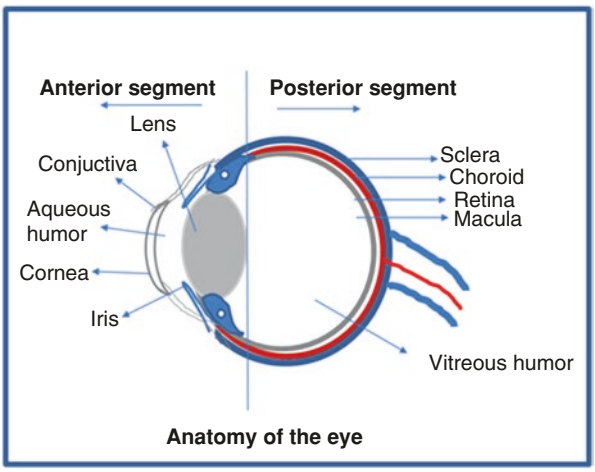

Fig. 1 Anatomy of eye illustrating the segments of anterior and posterior portions

of the ciliary body that includes epithelium, iris vessel endothelium with tight junction, and Schlemm's canal endothelium. The active and paracellular transport of materials is controlled by tight junctions of cells [13, 14]. The blood-retinal barrier is divided into the inner retinal barrier (composed of retinal vascular endothelium with tight junctions) and outer blood-retinal barriers (which consists of a monolayer of retinal pigment epithelium (RPE) with tight junctions) [13, 14]. These two components prohibit the entry of essential components to the intraocular chamber, and as a result, the insufficient drug reaches the intraocular tissues.

3 Ocular Delivery Routes and Their Limitations

There are three primary modes of drug administration to the eye, such as topical, local ocular (i.e., subconjunctival, intravitreal, retrobulbar, intracameral), and systemic. The feasible route administration mostly depends on the area of the eye that needs to be treated. Systemic administration methods for ocular drug delivery are intravenous injection and oral dosing. The outer blood-retinal barrier of RPE cells governs the entry of the drug from the choroid into the retina, the tight junction of the RPE hinders the entrance of the drug, and only 1–2% of the drug can gain access to the retina and retina body [14]. For the conjunctiva, cornea, anterior chamber, and iris, the topical administration is well responded. The eyelids can be treated with topical therapy but more frequently require systemic therapy. Systemic therapy is essentially required by the posterior segment because most topical medications do not penetrate to the posterior segment. Further, the retrobulbar and orbital tissues are treated systemically. The eye drop is the most favorable mode of drug administration due to its better patient compliance and economic reflection. The eye drops are mainly absorbed by two routes: the corneal route (cornea, aqueous humor, intraocular tissue) and the conjunctiva route (conjunctiva, sclera, choroid, retina, vitreous body). Post-administration less than 5% of totally administered drugs can reach the aqueous humor [15]. For the treatment of corneal diseases, iris diseases, and glaucoma, eye drops are beneficial. However, for treating posterior eye diseases, like intraocular cancers and retina diseases, they are not suitable, even after following frequent dosage regimens [16]. Posterior eye diseases are treated through intravitreal injections that are beneficial, as they can deliver high local drug concentrations in the vitreous body and retina [17]. However, being an invasive method, the requirement of repeated injection results sequence of side effects like cataracts, iritis, endophthalmitis, uveitis, retinal detachment, and intraocular hemorrhage. To overcome these drawbacks of systemic administration, periocular injection is followed that is less invasive than intravitreous injection as it is administered via a route of retrobulbar, peribulbar, sub-tenon, and subconjunctival. Through periocular delivery routes, administered drugs can reach the posterior segment of the eye either through penetration of the corneal choroid or sclera [18, 19]. However, all these routes of administration suffer inefficiency in prolonging the drug retention time.

4 Nanoparticle Route of Delivery to the Retina

Different modes of administration routes were taken into account for retinal drug delivery. In the retina, the route of administration ranges from systemic to intravitreal injections [4]. (i) Intravitreal route is the most common method that is practiced for the administration of macromolecules, whereas 27- or 30-gauge needles are steadily utilized for incorporating various drugs into the vitreous body. On this route, there is passive diffusion of drugs in all directions. (ii) Periocular route refers to the space surrounding the eyeball within the orbit. Through this route minimally invasive drug administration is done, in which the sclera is not punctured and displays good patient compliance and safety. In periocular pathways various sub-routes such as the subconjunctival, retrobulbar, peribulbar, and sub-tenon routes are present. Commonly subconjunctival route is explored among various periocular routes for injection of drug-loaded nanoparticles [20, 21]. (iii) Subretinal route is explored for the subretinal cavity space present between RPE cells and photoreceptors. It is more invasive, and the injected material comes in direct contact with the RPE cells. Higher concentrated therapeutics reach with minimal dilution [22, 23]. (iv) Systemic route is considered as impracticable for ocular drug delivery as less than ~2% of administered drugs could reach the vitreous. BRB prohibits entry into the posterior segment of the eye as the direction of drug penetration is opposite to the intraocular liquid concentration [24]. However, still, the systemic route is an attractive strategy, despite its lower efficacy, as it is convenient and does not involve penetration into ocular tissues.

5 Nanoparticles for Theranostics

Various types of nanocarriers are engaged for theranostic activities (Fig. 2). For ocular therapy study, several imaging approaches (OCT, fundus photography, fluorescein angiography, positron emission tomography (PET), magnetic resonance imaging (MRI), ultrasonography, and confocal microscopy) are employed for ocular disease diagnosis, and they have displayed significance toward monitoring of disease diagnosis and recovery. These imaging faculties are limited in action due to poor imaging sensitivity which displays inadequacy for disease diagnosis. As an example, PET displays high sensitivity with fractional spatial resolution, while MRI has better spatial resolution but feeble sensitivity [25]. Gd-perfluorocarbon nanoparticulate emulsion linked with a biotinylated anti-αvβ3 monoclonal integrin antibody DM101 was used for site-directed contrast enhancement study of angiogenic vessels in a rabbit corneal neovasculature mode. Post-administration 25% average signal intensity of MRI was enhanced in vivo [26]. Gold nanoparticles are considered as attractive contrast agents for OCT. Its optical resonance wavelengths can be precisely tuned with controlled sizes and shapes [27]. Cang et al. used gold nanocages (35 nm edge length) which can display cross-section absorption about five

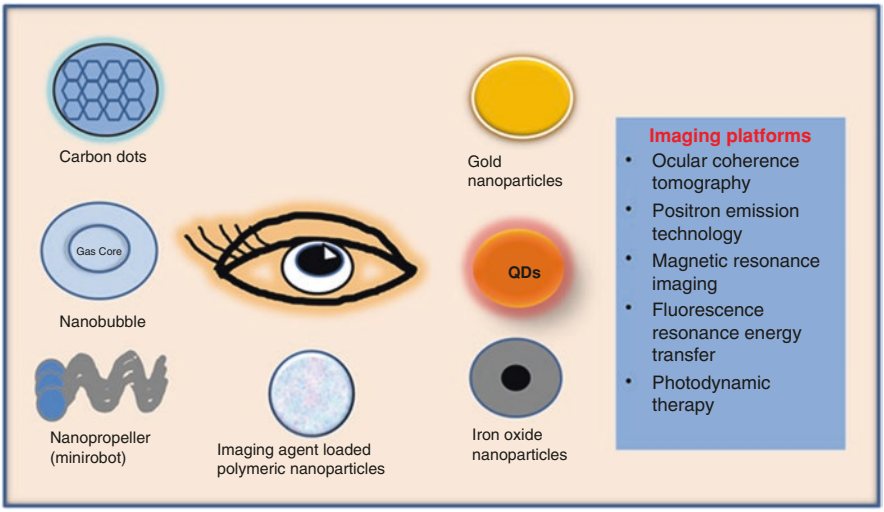

Fig. 2 Variuos types of nanovehicles used for ocular theranostic activity

orders of magnitude than that of conventional indocyanine green in the near-infrared spectral region [28]. Strategies used for other disease diagnoses can also be used for guiding the diagnosis and treatment of ocular disease. A hydrogel nanosystem can be used for tumor targeting; triggered drug delivery enabling photo-to-heat conversion can be utilized for multimodal imaging as well as controlled release of therapeutics in human tumor xenografts [29].

In medical imaging, the application of robot modalities would assist surgery while providing accurate positioning inside the body. In this regard, robotic systems are valuable tools for navigating deep tissue regions that are unreachable through blood vessel absorption. These magnetic-powered microrobots illustrate superior control ability and biocompatibility that can be navigated inside the eye. Its biocompatibility was enhanced with polypyrrole coating, to minimize biofouling interactions [30]. A study conducted by Ullrich et al. demonstrated microrobot's mobility and controllability inside the living rabbit eye. Through a surgical opening of the eye, the micro−/nanorobots were injected into the vitreous cavity and externally controlled by a magnetic coil system for navigating toward the posterior segment of a rabbit eye [31]. In another study, a nanorobot was constructed that can overcome the vitreous body by actively swimming to the retina. Wu et al. have developed a mini robot for the first time that can specifically pass through the solid tissue of the vitreous body into the back of the eye. The nanopropeller structure was conceptualized from helical flagella of the coli bacterium, and it moves like a corkscrew. For their easy movement through the vitreous body, they were coated with nonstick coating, which is composed of two biocompatible layers, a solid layer (made of silane molecules, which would dock to the robot surface) and a liquid one (liquid layer coats the nanopropellers and minimizes adhesion to the surrounding tissue). A weak magnetic field is applied for its movement to reach its desired destination [32].

6 Metal and Oxide Nanoparticles

In the treatment of ocular diseases, different types of metals and metal oxide are used which possess attractive biomedical properties. Gold, silver, and titanium oxide (TiO_2) illustrated the promising potential of antiangiogenic effects in choroidal and retinal neovascularization, including AMD, DR, and RP [33, 34]. Gold nanoparticles (AuNPs) have been extensively studied for both diagnosis and therapy tools [34, 35]. Mitra et al. developed EpCAM-conjugated PEI-capped AuNPs to knock down EpCAM gene in retinoblastoma (RB) cells. Y79 cells showed better significant internalization with downregulation of the EpCAM expression levels, demonstrating the potentiality for targeted therapy. Basuki et al. designed polymer-coated bevacizumab-loaded gold nanoparticles (AuNPs) inside an agarose hydrogel for photothermal therapy. AuNP-agarose matrix released the drug bevacizumab with the upsurge of localized temperature under light exposure [36]. AuNPs have their plasmon band which can be readily modulated via controlling Au size and shape. Some AuNPs can demonstrate absorbance of NIR energy, which can be utilized as contrast agents in OCT for diagnosis [37, 38]. With AuNPs the performance of OCT can be enhanced for providing better images as well as distinguishing diverse ocular tissues for early detection of multiple ocular diseases. In an antibacterial study, the effect of antibody-targeted gold nanoparticles combined with pulsed laser irradiation was evaluated in *S. aureus*. The laser-activated nanoparticles significantly lower the percentage of viable organisms illustrating new treatment modality when used either alone or aiding to the existing conventional antibiotic therapy. The most common complication after cataract surgery that mostly occurs is posterior capsule opacification (PCO) often referred to as "secondary cataract." For which silica-coated Au nanorods ($Au@SiO_2$) are used for decorating the commercially available IOLs (C-IOLs) toward the prevention of PCO [39]. To restore visual function in the blind human retina, enabling near-infrared light sensitivity may supplement or restore visual function in patients with regional retinal degeneration. In a study, Nelidova et al. developed Au nanorods with temperature-sensitive engineered transient receptor potential (TRP) channels for empowering NIR light sensitivity. The NIR stimulation can activate the cortical visual circuits of photoreceptors in mice retina, enabling a learned light-responsive behavior. This type of NIR sensor in ex vivo human retinas will allow NIR-evoked postmortem activation of human retinal cell types, demonstrating a great promise in supplementing light sensitivity or restoring the visual function of a blind human retina [40].

The AuNP's intrinsic therapeutic activities such as antiangiogenic and anti-inflammatory properties can have used to detect the pathological disorder. In the posterior segment of the eye, the retinal and CNV are pathological disorders that are highly associated with the overexpression of VEGF. AuNPs can significantly inhibit endothelial/fibroblast cell proliferation in vitro and VEGF-induced penetrability as well as angiogenesis in vivo by specifically binding to vascular permeability factor/vascular endothelial growth factor (VPF/VEGF)-165 and basic fibroblast growth factor [41]. In another study, Jo et al. developed AuNPs loaded with corona proteins

for the improvement of in vivo performance while preventing them from nonspecific protein attachment, by retaining its antiangiogenic effect [5]. In stereotactic radiosurgery, AuNPs are applied for improvement of therapeutic efficiency for the treatment of AMD, while attributing the enhancement of radiation dose toward a specific segment of the eye. This type of treatment is helpful for patients with AMD to preserve vision reducing at the same time they need for anti-VEGF injections every few years [42]. AuNPs could be used along with brachytherapy by 103Pd and 125I for improvement of the therapeutic efficiency in choroidal melanoma [43]. Pereira studied the efficacy of AuNPs in the LPS-induced eye inflammatory response, where topical AuNPs administration decreases intraocular inflammation and oxidative damage by interfering in the TLR4-NF-κB pathway [44]. The most common malignant intraocular tumor is retinoblastoma (RB). Wang et al. developed multifunctional-multimodal imaging-guided low-intensity focused ultrasound (LIFU)/immune synergistic RB therapy. Gold nanocages (AuNCs) are conjugated with iron oxide nanoparticles (AuNCs−Fe_3O_4), muramyl dipeptide (MDP), and encapsulated with perfluoropentane (PFP). Post-administration these multifunctional drug-loaded nanoparticles are accumulated in tumors through a magnetic field. Under LIFU irradiation the nanoparticles underwent phase transition and MDP was released. The therapeutic effects were significantly enhanced with AuNCs-Fe_3O_4/MDP/PF leading to direct apoptosis/necrosis of tumors facilitating the cancer theranostic platforms [45].

Cerium oxide nanoparticles (nanoceria) possess remarkable radical scavenging activities. In ocular disease, in several diseases, the intracellular reactive oxygen species are mostly involved in diabetic retinopathy, aged macular degeneration, and retinal degeneration [46]. In a study, Chen et al. revealed that nanoceria has prevented ROS-induced cell apoptosis while maintaining the normal function of photoreceptor cells [47]. Nanoceria offered sustained protection against photoreceptor degeneration after intravitreal injection by upregulating the genes related to antioxidant defense as well as photoreceptor-specific genes [48]. In other studies, nanoceria showed promising suppressing activity in the neovascularization model via downregulating the ASK1-P38/JNK-NF-κB pathways [49], as well as the slowdown of dysfunction of photoreceptor cells in an autosomal dominant retinitis pigmentosa rat model [50]. The metallic oxide (titanium dioxide) that is extensively used in cosmetic products shows a therapeutic role such as suppression of pathologic angiogenesis, in vivo retinal neovascularization, without demonstrating any kind of toxicity at the cellular viability and apoptotic activity in C57BL/6 mice model [51]. Zhang et al. used vancomycin (Van)-modified fluorescent silicon nanoparticles (SiNPs-Van) theranostic nanoagents for rapid and noninvasive diagnosis and treatment of Gram-positive bacteria-induced keratitis. The nanoagent SiNPs-Van has the ability of imaging bacteria in a short time both in vitro (5 min) and in vivo (10 min), for the detection of bacterial keratitis. At a particular concentration (0.5 μg/mL), SiNPs-Van illustrated superior efficacy of 92.5% in against *Staphylococcus aureus* (*S. aureus*) compared to native vancomycin is 23.3%. The therapeutic efficiency on the treatment of *S. aureus*-induced keratitis can be achieved by SiNPs-Van eye drops [52].

7 Quantum Dots as Drug Delivery and Imaging

In an ophthalmology study, use of visible light may cause autofluorescence from ocular structures; therefore it's necessary to reduce the contrast of ocular fluorophores [53]. Without interfering with autofluorescence, QDs can offer both visible and NIR emissions of the electromagnetic spectrum [54]. The most common QDs used in eyes for diagnostic and therapeutic purposes are the cadmium selenium QDs with zinc sulfide core (CdSe/ZnS-QDs) [55]. QDs are effectively used for the labeling and bioimaging applications in ophthalmology, for clarity in the pathophysiological events occurring in ocular structures and diseases. The most common adult primary tumor of the eye is uveal melanoma. For early detection, the aid of nanoparticle-based early detection and diagnosis has illustrated great potential in terms of noninvasive biomarkers [56]. Nanoparticles invented by Tari et al. can differentiate between the early and late stages of retinal vascular diseases. Smaller particle sizes could travel from the circulation in the early stages of the disease, and by labeling, with color dye, the tracing, tracking, and monitoring of the disease status can be done [57]. In ocular vascular imaging, ophthalmoscopy as well as optical coherence tomography can take the advantage of optical imaging modalities. In one of the studies, anti-GFAP-QDs are utilized for imaging intermediate filaments in astrocyte and Muller glial cells in rat neural sensory retina [58]. Yamamoto developed aqueous colloidal QD (ACQD) for the detection of vitreous lesions and guidance for vitrectomy surgery [59]. QDs can also be used for the early detection of the spontaneous CNV of age-related macular degeneration (AMD). The study conducted by Takeda et al. showed that early detection and diagnosis are possible in AMD to protect patient's vision. CCR3-targeting quantum dots can locate and reduce the vision loss by therapeutic angioinhibition [60]. QDs are applied into the ocular lymphatic pathway for monitoring the glaucoma eye pressure [61]. Antibody-conjugated QDs are used for the detection of melanoma by a high-throughput screening system. QDs were constructed to recognize the melanoma cells from the co-culture cells of melanoma-melanocyte co-culture model [62]. In OCT and other imaging approaches, gold nanocages and nanoshells are used [63]. Iron oxide nanoparticles are used for intravitreal injection to detect cells by magnetic resonance imaging [64]. Manganese oxide nanoparticles were developed as a T1 contrast agent for the detection and integrity of retinal vessel structure. Iron oxide particles are used as a contrast agent for MRI for detecting uveal melanoma in rabbit models [65]. The administered contrast agent increased the ratio of the T_1 to T_2 signal intensity in all of the ocular tissue. To evaluate the potential of tracking endothelial progenitor cells EPCs in ocular angiogenesis, a critical pathologic feature of several blinding conditions of eye. Multispectral quantum dot nanocrystals (QD) to acetyl low-density lipoprotein (acLDL) to track CD34 (+) EPCs in a rat model of laser-induced choroidal neovascularization (LCNV) [66]. QDs have been used to track the transplantation of bone marrow stem cells in CNV. The therapeutic potential of the bone marrow-derived stem cells (BMSCs) was evaluated for laser-induced visual impairment due to retina degeneration. Intravitreal transplantation of BMSCs effectively repaired the retinal lesions by differentiating into retinal cells [67].

Ocular lymphatic contributes to aqueous humor outflow. For the treatment of glaucoma, latanoprost, a prostaglandin F2 alpha analog, is commonly used to lower the intraocular pressure (IOP), by increasing the lymphatic drainage from the eye thereby preventing blindness from glaucoma. Latanoprost stimulates ocular lymphatic drainage, and it was illustrated by multiple administrations of QDs and the signal intensity in the latanoprost-treated group compared with controls [68]. The traditional standard approach of surgical eye removal, plaque radiotherapy, has been used to control the primary uveal melanoma, but these procedures lead to cosmetic defects and eventual loss of vision. Chemotherapy treatments are provided for treating liver metastases of uveal melanoma, but could not prolong the survival rate of the patient. Further blood-retinal barrier and aqueous and corneal barrier restrict the access of drugs in the eyes [69, 70].

8 Carbon Nanomaterials and Imaging

Carbon-based nanoparticles are made only of carbonaceous nanomaterials. Carbon dots (CDs) are new type of nanoparticles appropriate for the applications of drug and gene delivery, imaging, as well as biosensing. CDS are spherically shaped nanocarriers with a diameter of <10 nm [71]. Different functional groups (e.g., -OH, -COOH, -NH2) are present on the surface of carbon core which are endowed with better biological activity, good water solubility, and formation of stable conjugates with organic and inorganic substances and display low cytotoxicity, high degree of oxidation, and good water retention ability [72]. Various types of CDs like carbon quantum dots (CQDs), carbonized polymer dots (CPDs), carbon nanodots (CNDs), and graphene quantum dots (GQDs) can be outlined depending by taking into the account of the structure of the carbon core, surface groups, and properties [73, 74]. CDs have photoluminescence (PL) properties that are size-dependent, and it yields different fluorescence colors which makes them an imperative material for biomedical applications [75]. The application of CDs has been used for ocular gene delivery. Carbon quantum dots are synthesized from biogenic polyamines and are used as a promising antibacterial agent for the treatment of microbial infection (keratitis) [76]. For disease diagnosis and therapy as well as bioimaging, folic acid (FA), hyaluronic acid (HA), and RGD peptide have been conjugated with CDs. In a study Liu et al. constructed PEI-CDs for gene delivery to the cells. The PEI-CDs showed higher gene expression of plasmid DNA, illustrating the capability of CD-PEI concerning gene delivery and bioimaging [77]. Fluorescein angiography (FA) was done with selenium and nitrogen co-doped CDs having a high green fluorescence. The co-doped CDs were administered to C57BL/6 J mice, which produced a clear FA image of the retinal vasculature as well as details of the capillary bed, illustrating its efficacy as a high-performance fluorescent imaging platform for angiography [78]. Karakoçak et al. developed red-emissive nitrogen-doped CDs for enhanced bioimaging which demonstrated highly effective diffusion and distribution in porcine eyes after intravitreal injection of CDs in ex vivo results [79]. VEGF aptamers functionalized CDs were used to reduce angiogenesis in an in vitro model of CNV. It

was found that the antiangiogenic effect of the anti-VEGF-CDs was similar to commercially available (bevacizumab and aflibercept) anti-VEGF agents [80]. Another carbon-based nanomaterial, nanodiamond (ND), is recently used which is competent in carrying biomolecules such as protein, DNA, and small drug molecules. ND-based CRISPR-Cas 9 delivery tools are used as vectors, and that was functionalized with carboxyl (-COOH) and covalently conjugated with fluorescent 6His-tagged mCherry reporter protein for creating in vitro and in vivo disease models X-linked retinoschisis (XLRS). These nanocarriers were internalized by human-induced pluripotent stem cells (iPSCs) and mouse retinas via the endosome pathway. In NDs with the addition of bovine serum albumin, the mCherry protein remains stables in the retina for up to 2 weeks [81].

9 Upconversion Nanoparticles

Upconversion nanoparticles (UCNPs) are built on rare-earth-based lanthanide- or actinide-doped transition metals that are able to emit high-energy photons by sequentially absorbing low-energy photons. UCNP are able to absorb NIR energy and can emit light in visible or ultraviolet regions. This behavior is advantageous in biomedical applications for exercising deep penetration depth with negligible damage to cells or tissues. These inimitable features of UCNP platforms are effectively applied in photochemical reactions, bioimaging, and biosensing [82]. In a study Ma et al. constructed smart ocular injectable photoreceptor-binding upconversion nanoparticles by using sodium yttrium fluoride NaYF4 and ytterbium (YB)/erbium (Er) for enabling NIR light sensation and pattern vision. The Yb/Er@NaYF4 nanoparticle was conjugated with a protein concanavalin A (Con A) with polyacrylic acid coating. These water-soluble nanoparticles are anchored to the retinal photoreceptors to create NIR light image vision with negligible side effects. The unique feature of UCNPs is the generation of green light under light illumination at 980 nm, the administered nanoplatforms into subretina permitted the mice to achieve NIR image vision as the green light. The UCNPs could be effectively used for the study of light-related behaviors of mammals and will have the potential to treat vision disorders in the future [83].

10 Ultrasound-Responsive Nanobubbles

Ultrasound-mediated generation of nanometer size bubbles is known as nanobubbles. These nanobubbles were designed to get efficient drug delivery systems with minimal invasiveness, rendering longer residence time. Their small sizes allocate extravasation from blood vessels into surrounding tissues with the ultrasound-targeted site-specific release [84]. Nanocarriers such as drug-loaded polymeric hydrogels or nanobubbles, after administration, are exposed to ultrasound waves forming

cavitation with high temperatures at the site, causing the rupture of the polymeric chains of the nanobubble [85, 86]. Ultrasound-responsive systems-mediated drug delivery to the specific site prevents the side effects which can be seen with systemic administration of certain drugs. Combination of nanobubbles and ultrasound has the capacity that may improve the consequences of intravitreally administered drugs by influencing the directionality of drug-containing particle migration. Thakur et al. evaluated the impact of trans-scleral or corneal distribution of intravitreally injected rhodamine-tagged gas-entrapped nanobubbles injected into ex vivo bovine and porcine eyes. The particles are able to move in a directional manner away through the intervention of an ultrasound wave source indicating effective control of the rate and path of nanobubble migration toward prompt therapeutic intervention [87]. By the use of ultrasound-responsive systems, drugs were delivered at a rate that is controlled from an external source which is useful for cancer treatment. Bhandari et al. used oxygen nanobubbles for the delivery of mitocin-C to lower the tumor progression rate with a 50% lower drug concentration [88].

11 Nanoparticles for Phototherapy

The quantification of tumor development was studied with green fluorescent protein (GFP). Glioblastoma is an aggressive tumor with a greater rate of recurrence [89]. It rapidly grows and spreads into nearby brain tissue affecting visual capabilities and spreading to the optic nerve [90]. Goswami et al. in a study developed an ocular xenograft model in which green fluorescent protein (GFP)-expressed human glioblastoma cells that were implanted into the subretinal space of immunodeficient mice. For xenograft model was visualized and imaged noninvasively using combined fluorescence scanning laser ophthalmoscopy (SLO) and volumetric OCT. The tumors were treated intravenously with nanodox (doxorubicin-containing porphyrin and cholic acid-based nanoparticles). Fluorescence resonance energy transfer (FRET) emission (doxorubicin → porphyrin) was used to localize nanodox in the xenografts, and it was activated with light exposure of 690 nm. After exposure, there was a reduction in tumor volume. Through "nanodox" light-activated breakdown of the nanocarrier and release of doxorubicin and imaging enable to focus the laser beam directly to tumor for a period of 15 to 30 mins for better photodynamic and photothermal therapy, without irradiating nontumor tissue [91].

12 Challenges in the Clinical Translation

Nanomedicine has to get through several for its validation of use in the clinical trials. Various obstacles are being encountered while transiting from nanomedicine to nanopharmaceutical design include large-scale production to Good Manufacturing Practice standards and quality control, i.e., (formulation to commercialization

(production scale) (Fig. 3). The choice of optimum technique would influence, support and speed up the scalability process. Further, quality control testing should ensure the safety and efficacy of the pharmaceutical product during the process and support the batch-to-batch variability [92].

13 Conclusion and Future Perspective

Early detection of cancer is undoubtedly a very important step toward effective cancer treatment. However, the early stage determination of cancer diagnosis remains as a formidable challenge. The emergence of nanoformulations has played a very vital role in the therapeutic strategy of ocular disease. It has also aimed at the management of the ocular disease because of its bioadhesives, sustained release, and targeted delivery. Further, several multifunctional nanosystems have been developed that are specifically aimed at real-time visualization of tumor cells and their adjacent tumor microenvironment behavior that could provide valuable information on cancer progression. Different approaches such as OCT, fundus photography, fluorescein angiography, PET, MRI, US, confocal microscopy, etc. are employed in the ocular diagnosis and recovery process. But these approaches have some advantages when compared to one another for disease diagnosis. To overcome these drawbacks, nanotheranostics options open up a new window that provides multiple therapeutic options. Theranostic nanomedicine is the means for potential applications of a multidisciplinary approach to cancer diagnosis and treatment. The development of nanorobots (and nanodevices) will aid to study the dual function of tissue diagnosis and repair with a full external control mechanism. Recently nanorobots are developed, a slippery coating that can efficiently swim in the vitreous body of the eye. These nanorobots will be the future drug transporter into the eye. In ophthalmic studies, the future plan would be toward the development of noninvasive delivery routes that can be catered to ocular diseases in both segments. As a result

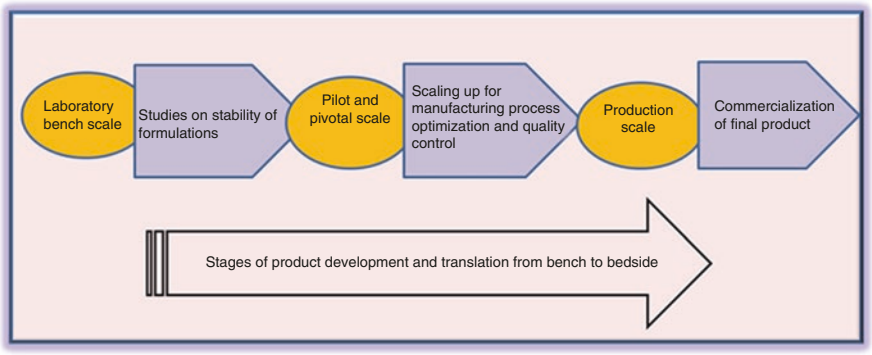

Fig. 3 Diagrammatic depiction of steps towards product development from bench to bedside

of which, a combination package, the diagnostic and therapeutic functions, may be introduced to enable visual tracking during the treatment of ocular disease.

Acknowledgments FD gratefully acknowledges the Department of Science and Technology, Government of India, for the financial support (SR/WOS-A/LS-448/2017) in the form of Women Scientist-A fellowship.

References

1. Burton MJ, Ramke J, Marques AP, Bourne RRA, Congdon N, Jones I, et al. The lancet Global Health Commission on global eye health: vision beyond 2020. Lancet Glob Health. 2021;9:e489–551.
2. Sahoo SK, Dilnawaz F, Krishnakumar S. Nanotechnology in ocular drug delivery. Drug Discov Today. 2008;13(3–4):144–51.
3. Weng Y, Liu J, Jin S, Guo W, Liang X, Hu Z. Nanotechnology-based strategies for treatment of ocular disease. Acta PharmSin B. 2017;7:281–91.
4. Jiang S, Franco YL, Zhou Y, Chen J. Nanotechnology in retinal drug delivery. Int J Ophthalmol. 2018;11(6):1038–44.
5. Jo DH, Kim JH, Son JG, Dan KS, Song SH, Lee TG, et al. Nanoparticle-protein complexes mimicking corona formation in ocular environment. Biomaterials. 2016;109:23–31.
6. Wong XY, Sena-Torralba A, Alvarez-Diduk R, Muthoosamy K, Merkoçi A. Nanomaterials for nanotheranostics: tuning their properties according to disease needs. ACS Nano. 2020;14:2585–627.
7. Das SS, Bharadwaj P, Bilal M, Barani M, Rahdar A, Taboada P, Bungau S, Kyzas G.Z. . Stimuli-responsive polymeric nanocarriers for drug delivery, imaging, and theragnosis. Polymers 2020;12:1397.
8. Todd TW, Beecher H, Williams GH, Todd AW. The weight and growth of the human eye ball. Hum Biol. 1940;12:1–20.
9. Dingeldein SA, Klyce SD. The topography of normal corneas. Arch Ophthalmol. 1989;107:512–518.
10. Klyce SD, Beuerman RW. Structure and function of the cornea. In: Kaufman HE, Barron BA, McDonald MB, Waltman SR, editors, The cornea NewYork: Churchill Livingstone Inc. 1988. p. 3–54.
11. Prausnitz M, Noonan JS. Permeability of cornea, sclera, and conjunctiva: a literature analysis for drug delivery to the eye. J Pharm Sci. 1998;87:1479–88.
12. Yi X, Wang Y. Yu FS corneal epithelial tight junctions and their response to lipopolysaccharide challenge. Invest Ophthalmol Vis Sci. 2000;41:4093–100.
13. Furuichi MC, ChibaT AK, Kogure S, Iijima H, Tsukahara S, et al. Cystoid macular edema associated with topical latanoprost in glaucomatous eyes with a normally functioning blood–ocular barrier. J Glaucoma. 2001;10:233–6.
14. Cunha-Vaz JG. The blood–ocular barriers: past, present, and future. Doc Ophthalmol. 1997;93:149–57.
15. Weijtens O, Schoemaker RC, Romijn FP, Cohen AF, Lentjes EG, van Meurs JC. Intraocular penetration and systemic absorption after topical application of dexamethasone disodium phosphate. Ophthalmology. 2002;109:1887–91.
16. Baudouin C, Labbé A, Liang H, Pauly A, Brignole-Baudouin F. Preservatives in eye drops: the good, the bad and the ugly. Prog Retin Eye Res. 2010;29:312–34.
17. Ward AH, Siegwart JT Jr, Frost MR, Norton TT. The effect of intravitreal injection of vehicle solutions on form deprivation myopia in tree shrews. Exp Eye Res. 2016;145:289–96.
18. Ghate D, Edelhauser HF. Ocular drug delivery. Expert Opin Drug Deliv. 2006;3:275–87.

19. Raghava S, Hammond M, Kompella UB. Periocular routes for retinal drug delivery. Expert Opin Drug Deliv. 2004;1:99–114.
20. Rajala A, Wang Y, Zhu Y, Ranjo-Bishop M, Ma J-X, Mao C, Rajala RVS. Nanoparticle-assisted targeted delivery of eye-specific genes to eyes significantly improves the vision of blind mice in vivo. Nano Lett. 2014;14(9):5257–63.
21. Shen H-H, Chan EC, Lee JH, Bee YS, Lin T-W, Dusting GJ, Liu G-S. Nanocarriers for treatment of ocular neovascularization in the back of the eye: new vehicles for ophthalmic drug delivery. Nanomedicine (Lond). 2015;10(13):2093–107.
22. Gaudana R, Ananthula HK, Parenky A, Mitra AK. Ocular drug delivery. AAPS J. 2010;12(3):348–60.
23. Regnier A, Schneider M, Concordet D, Toutain PL. Intraocular pharmacokinetics of intravenously administered marbofloxacin in rabbits with experimentally induced acute endophthalmitis. Am J Vet Res. 2008;69(3):410–5.
24. Varela-Fernández R, Díaz-Tomé V, Luaces-Rodríguez A, Conde-Penedo A, García-Otero X, Luzardo-Álvarez A, Fernández-Ferreiro A, Otero-Espinar FJ. Drug delivery to the posterior segment of the eye: biopharmaceutic and pharmacokinetic considerations. Pharmaceutics. 2020;12(3):269.
25. Finger PT, Kurli M, Reddy S, Tena LB, Pavlick AC. Whole body PET/CT for initial staging of choroidal melanoma. Brit J Ophthalmol. 2005;89:1270–4.
26. Anderson SA, Rader RK, Westlin WF, Null C, Jackson D, Lanza GM, et al. Magnetic resonance contrast enhancement of neovasculature with αvβ3-targetednanoparticles. Magn Reson Med. 2000;44:433–9.
27. Zagaynova EV, Shirmanova MV, Kirillin MY, Khlebtsov BN, Orlova AG, Balalaeva IV et al. Contrasting properties of gold nanoparticles for optical coherence tomography: phantom, in vivo studies and Monte Carlo simulation. Phys Med Biol 2008;53:4995–5009.
28. Cang H, Sun T, Li ZY, Chen J, Wiley BJ, Xia Y, et al. Gold nanocages as contrast agents for spectro scopic optical coherence tomography. Opt Lett. 2005;30:3048–50.
29. Hosoya H, Dobroff AS, Driessen WH, et al. Integrated nanotechnology platform for tumor-targeted multimodal imaging and therapeutic cargo release. Proc Natl Acad Sci U S A. 2016;113(7):1877–82.
30. Pokki J, Ergeneman O, Chatzipirpiridis G, Lühmann T, Sort J, Pellicer E, Pot SA, Spiess BM, Pané S, Nelson BJ. Protective coatings for intraocular wirelessly controlled microrobots for implantation: corrosion, cell culture, and in vivo animal tests. J Biomed Mater ResPart B. 2017;105(4):836–45.
31. Ullrich F, Bergeles C, Pokki J, Ergeneman O, Erni S, Chatzipirpiridis G, et al. Mobility experiments with microrobots for minimally invasive intraocular surgery. Invest Ophthalmol Vis Sci. 2013;54:2853–63.
32. Wu Z, Troll J, Jeong H-H, Wei Q, Stang M, Ziemssen F, et al. A swarm of slippery micropropellers penetrates the vitreous body of the eye. Sci Adv. 2018;4(11):eaat4388.
33. Kong L, Alves CS, Hou W, Qiu J, Möhwald H, Tomás H, Shi X. RGD peptide-modified dendrimer-entrapped gold nanoparticles enable highly efficient and specific gene delivery to stem cells. ACS Appl Mater Interfaces. 2015;7(8):4833–43.
34. Masse F, Ouellette M, Lamoureux G, Boisselier E. Gold nanoparticles in ophthalmology. Med Res Rev. 2019;39(1):302–27.
35. Daraee H, Eatemadi A, Abbasi E, Fekri Aval S, Kouhi M, Akbarzadeh A. Application of gold nanoparticles in biomedical and drug delivery. Artif Cells Nanomed Biotechnol. 2016;44(1):410–22.
36. Basuki JS, Qie F, Mulet X, Suryadinata R, Vashi AV, Peng YY, et al. Photo-modulated therapeutic protein release from a hydrogel depot using visible light. Angew Chem Int Ed Engl. 2017;56(4):966–71.
37. Adler DC, Huang SW, Huber R, Fujimoto JG. Photothermal detection of gold nanoparticles using phase-sensitive optical coherence tomography. Optic Express. 2008;16(7):4376–93.

38. Goldmann C, Lazzari R, Paquez X, Boissière C, Ribot F, Sanchez C, et al. Charge transfer at hybrid interfaces: plasmonics of aromatic thiol-capped gold nanoparticles. ACS Nano. 2015;9(7):7572–82.
39. Lin YX, Hu XF, Zhao Y, Gao YJ, Yang C, Qiao SL, et al. Photothermal ring integrated intraocular lens for high-efficient eye disease treatment. Adv Mater. 2017;29(34):1701617.
40. Nelidova D, Morikawa RK, Cowan CS, Raics Z, Goldblum D, Scholl HPN, et al. Restoring light sensitivity using tunable near-infrared sensors. Sci Adv. 2020;368(6495):1108–13.
41. Mukherjee P, Bhattacharya R, Wang P, Wang L, Basu S, Nagy JA, et al. Antiangiogenic properties of gold nanoparticles. Clin Canc Res. 2005;11(9):3530–4.
42. Brivio D, Zygmanski P, Arnoldussen M, Hanlon J, Chell E, Sajo E et al. Kilovoltage radiosurgery with gold nanoparticles for neovascular age-related macular degeneration (AMD): a Monte Carlo evaluation. Phys Med Biol 2015;60(24): 9203–13.
43. Rezaei H, Zabihzadeh M, Ghorbani M, Goli Ahmadabad F, Mostaghimi H. Evaluation of dose enhancement in presence of gold nanoparticles in eye brachytherapy by (103)Pd source. Australas Phys Eng Sci Med. 2017;40(3):545–53.
44. Pereira DV, Petronilho F, Pereira HR, Vuolo F, Mina F, Possato JC, et al. Effects of gold nanoparticles on endotoxin-induced uveitis in rats. Invest Ophthalmol Vis Sci. 2012;53(13):8036–41.
45. Wang M, Yang Q, Li M, Zou H, Wang Z, Ran H, et al. Multifunctional nanoparticles for multimodal imaging-guided low-intensity focused ultrasound/Immunosynergistic retinoblastoma therapy. ACS Appl Mater Interfaces. 2020;12(5):5642–57.
46. Barnham KJ, Masters CL, Bush AI. Neurodegenerative diseases and oxidative stress. Nat Rev Drug Discov. 2004;3(3):205–14.
47. Chen J, Patil S, Seal S, McGinnis JF. Rare earth nanoparticles prevent retinal degeneration induced by intracellular peroxides. Nat Nanotechnol. 2006;1(2):142–50.
48. Cai X, Sezate SA, Seal S, McGinnis JF. Sustained protection against photoreceptor degeneration in tubby mice by intravitreal injection of nanoceria. Biomaterials. 2012;33(34):8771–81.
49. Cai X, Seal S, McGinnis JF. Sustained inhibition of neovascularization in vldlr−/− mice following intravitreal injection of cerium oxide nanoparticles and the role of the ASK1-P38/JNK-NF-κB pathway. Biomaterials. 2014;35(1):249–58.
50. Wong LL, Pye QN, Chen L, Seal S, McGinnis JF. Defining the catalytic activity of nanoceria in the P23H-1 rat, a photoreceptor degeneration model. PLoS One. 2015;10(3):e0121977.
51. Jo DH, Kim JH, Son JG, Song NW, Kim Y-I, Yu YS, et al. Anti-angiogenic effect of bare titanium dioxide nanoparticles on pathologic neovascularization without unbearable toxicity. Nanomed Nanotechnol Biol Med. 2014;10(5):e1109–17.
52. Zhang L, Ji X, Su Y, Zhai X, Xu H, Song B, et al. Fluorescent silicon nanoparticles-based nanotheranostic agents for rapid diagnosis and treatment of bacteria-induced keratitis. Nano Res. 2021;14(1):52–8.
53. Krebs I, Lois N, Forrester JV. Fundus autofluorescence. Graefes Arch Clin Exp Ophthalmol. 2011;249(2):309.
54. Matea CT, Mocan T, Tabaran F, Pop T, Mosteanu O, Puia C, Iancu C, Mocan L. Quantum dots in imaging, drug delivery and sensor applications. Int J Nanomedicine. 2017;12:5421–31.
55. Zarbin MA, Montemagno C, Leary JF, Ritch R. Nanotechnology in ophthalmology. Can J Ophthalmol. 2010;45(5):457–76.
56. Cormode DP, Skajaa GO, Delshad A, Parker N, Jarzyna PA, Calcagno C, et al. A versatile and tunable coating strategy allows control of nanocrystal delivery to cell types in the liver. Bioconjug Chem. 2011;22(3):353–61.
57. Tari SR, Barile GR, Kompella UB. Polychromatic, diversely-sized particles for angiography. In: Office USP, editor, United States: The Trustees of Columbia University in the City of New York Board or Reagents of the University of Nebraska Varner Hall 2009:19.
58. Pathak S, Tolentino R, Nguyen K, D'Amico L, Barron E, Cheng L, et al. Quantum dot labeling and imaging of glial fibrillary acidic protein intermediate filaments and gliosis in the rat neural retina and dissociated astrocytes. J Nanosci Nanotechnol. 2009;9(8):5047–54.

59. Yamamoto S, Manabe N, Fujioka K, Hoshino A, Yamamoto K. Visualizing vitreous using quantum dots as imaging agents. IEEE Trans Nanobioscience. 2007;6(1):94–8.
60. Takeda A, Baffi JZ, Kleinman ME. CCR3 is a target for age-related macular degeneration diagnosis and therapy. Nature. 2009;460(7252):225–30.
61. Tam AL, Gupta N, Zhang Z, Yucel YH. Quantum dots trace lymphatic drainage from the mouse eye. Nanotechnology. 2011;22(42):425101.
62. Jayagopal A, Russ PK, Haselton FR. Surface engineering of quantum dots for in vivo vascular imaging. Bioconjug Chem. 2007;18(5):1424–33.
63. Prabhu P, Patravale V. The upcoming field of theranostic nanomedicine: an overview. J Biomed Nanotech. 2012;8(6):859–82.
64. Raju HB, Hu Y, Padgett KR, Rodriguez JE, Goldberg JL. Investigation of nanoparticles using magnetic resonance imaging after intravitreal injection. Clin Experiment Opthalmol. 2012;40(1):100–7.
65. Krause M, Kwong KK, Xiong J, Gragoudas ES, Young LH. MRI of blood volume and cellular uptake of superparamagnetic iron in an animal model of choroidal melanoma. Opthalmic Res. 2002;34(4):241–50.
66. Barnett JM, Penn JS, Jayagopal A. Imaging of endothelial progenitor cell subpopulations in angiogenesis using quantum dot nanocrystals. In: Rosenthal SJ, Wright DW, editors. NanoBiotechnology protocols. Totowa: Humana Press; 2013. p. 45–56.
67. Wang HC, Brown J, Alayon H, Stuck BE. Transplantation of quantum dot-labelled bone marrow-derived stem cells into the vitreous of mice with laser-induced retinal injury: survival, integration and differentiation. Vis Res. 2010;50(7):665–73.
68. Tam ALC, Gupta N, Zhang Z, Yücel YH. Latanoprost stimulates ocular lymphatic drainage: an in vivo Nanotracer study. Transl Vis Sci Technol. 2013;2(5):3–3.
69. Kompella UB, Amrite AC, Pacha Ravi R, Durazo SA. Nanomedicines for back of the eye drug delivery, gene delivery, and imaging. Prog Retin Eye Res. 2013;36:172–98.
70. Rowe-Rendleman CL, Durazo SA, Kompella UB, Rittenhouse KD, Di Polo A, Weiner AL, et al. Drug and gene delivery to the back of the eye: from bench to bedside. Invest Ophthalmol Vis Sci Nature. 2014;55(4):2714–30.
71. Mishra V, Patil A, Thankur S, Prashant K. Carbon dots: emerging theranostic nanoarchitectures. Drug Discov Today. 2018;23:1219–32.
72. Hu S-L, Niu K-Y, Sun J, Yang J, Zhao N-Q, Du XW. One-step synthesis of fluorescent carbon nanoparticles by laser irradiation. J Mater Chem. 2009;19:484–8.
73. Tabish TA, Zhang S. Graphene quantum dots: synthesis, properties, and biological applications. Compr Nanosci Nanotechnol. 2016;3:171–92.
74. Xia C, Zhu S, Feng T, Yang M, Yang, B. Evolution and synthesis of carbon dots: from carbon dots to carbonized polymer dots. Adv Sci (Weinh). 2019;6:1901316.
75. Sharma A, Das J. Small molecules derived carbon dots: synthesis and applications in sensing, catalysis, imaging, and biomedicine. J Nanobiotechnol. 2019;17:1–24.
76. Jian H-J, Wu R-S, Lin T-Y, Li Y-J, Lin H-J, Harroun SG, et al. Super-cationic carbon quantum dots synthesized from spermidine as an eye drop formulation for topical treatment of bacterial keratitis. ACS Nano. 2017;11(7):6703–16.
77. Liu C, Zhang P, Zhai X, Tian F, Li W, Yang J, et al. Nano-carrier for gene delivery and bioimaging based on carbon dots with PEI-passivation enhanced fluorescence. Biomaterials. 2012;33:3604–13.
78. Qu D, Miao X, Wang X, Nie C, Li Y, Luo L, et al. Se & N co-doped carbon dots for high-performance fluorescence imaging agent of angiography. J Mater Chem B 5. 2017;4988–92.
79. Karakoçak B, Liang J, Kavadiya S, Berezin MY, Biswas P, Ravi N. Optimizing the synthesis of red-emissive nitrogen-doped carbon dots for use in bioimaging. ACS Appl Nano Mater. 2018;1:3682–92.
80. Shoval A, Markus A, Zhou Z., Liu X., Cazelles R., Willner I. Anti-VEGF-aptamer modified c-dots-a hybrid nanocomposite for topical treatment of ocular vascular disorders. Small. 2019;15:e1902776.

81. Yang TC, Chang CY, Yarmishyn AA, Mao YS, Yang YP, Wang ML, et al. . Carboxylated nanodiamond-mediated CRISPR-Cas9 delivery of human retinoschisis mutation into human iPSCs and mouse retina. Acta Biomater 2020;101:484–494.
82. Zhu X, Zhang J, Liu J, Zhang Y. Recent progress of rare-earth doped upconversion nanoparticles: synthesis, optimization, and applications. Adv Sci (Weinh). 2019;6(22):1901358.
83. Ma Y, Bao J, Zhang Y, Li Z, Zhou X, Wan C, Huang L, Zhao Y, Han G, Xue T. Mammalian near-infrared image vision through injectable and self-powered retinal nanoantennae. Cell. 2019;177(2):243–55.
84. Cavalli R Soster M, Argenziano M. Nanobubbles: a promising efficient tool for therapeutic delivery. Ther Deliv. 2016;7(2):117–138.
85. Mahlumba P, Choonara YE, Kumar P, du Toit LC, Pillay V. Stimuli-responsive polymeric systems for controlled protein and peptide delivery: future implications for ocular delivery. Molecules 2016;21:1002.
86. Mura S, Nicolas J, Couvreur P. Stimuli-responsive nanocarriers for drug delivery. Nat Mater. 2013;12:991–1003.
87. Thakur SS, Chen Y-S, Houston ZH, Fletcher N, Barnett NL, Thurecht KJ, et al. Ultrasound-responsive nanobubbles for enhanced intravitreal drug migration: an ex vivo evaluation. Eur J Pharm Biopharm. 2019;136:102–7.
88. Bhandari P, Novikova G, Goergen CJ, Irudayaraj J. Ultrasound beam steering of oxygen nanobubbles for enhanced bladder cancer therapy. Sci RepB. 2018;8(3112).
89. Chiu TI, Wang MJ, Su CC. The treatment of glioblastoma multiforme through activation of microglia and TRAIL induced by rAAV2-mediated IL-12 in a syngeneic rat model. J Biomed Sci. 2012;19(1):45.
90. Meleis AM, Mahtabfar A, Danish S, Foty RA. Dexamethasone-mediated inhibition of Glioblastoma neurosphere dispersal in an ex vivo organotypic neural assay. PLoS One. 2017;12(10):e0186483.
91. Goswami M, Wang X, Zhang P, Xiao W, Karlen SJ, Li Y, et al. Novel window for cancer nanotheranostics: non-invasive ocular assessments of tumor growth and nanotherapeutic treatment efficacy in vivo. Biomed Opt Express. 2019;10(1):151–66.
92. Souto EB, Silva GF, Dias-Ferreira J, Zielinska A, Ventura F, Durazzo A, Lucarini M, Novellino E, Santini A. Nanopharmaceutics: Part I-clinical trials legislation and good manufacturing practices (GMP) of nanotherapeutics in the EU. Pharmaceutics. 2020;12(2).146.

Protein and Peptide-Based Therapeutics for Cancer Imaging

Suhaas Rayudu Aluri

1 Introduction

In 2021, it was estimated that about 1,900,000 Americans were diagnosed with cancer and about a third of them succumbed to the illness [1]. Hence, early detection of cancer is essential to ensure timely intervention and treatment. Many clinicians resort to biopsies for an informed histopathological diagnosis [2, 3]. Biopsies require an invasive procedure for tissue collection and qualified pathologists for accurate tissue assessment [2, 3]. Though cost-effective, biopsies can be inaccurate leading to misdiagnosis and repeat sampling through multiple invasive procedures [2]. Hence, progress made in imaging instrumentation, protein sciences, and molecular biology has allowed researchers and clinicians to implement cancer imaging tools that are more effective and robust [4]. These imaging tools are noninvasive and are used to visualize and diagnose tumors at all stages. These tools not only provide clinicians with the ability to detect neoplasms but also provide them with valuable information on tumor growth, metabolism, and metastasis [4, 5].

The six (6) major imaging modalities employed in the clinic are (1) X-ray/computer tomography (CT), (2) ultrasound, (3) magnetic resonance imaging (MRI), (4) single-photon emission computed tomography (SPECT), (5) positron emission tomography (PET), and (6) optical imaging [5]. However, these techniques are used with systemically administered contrast agents/imaging agents to improve the signal-to-noise ratio (SNR) of interested tumors against surrounding tissues [5]. These agents localize in the tumor using both targeted and untargeted (passive) approaches thereby enhancing the tumor's SNR for imaging [5–8]. To date, there have been more than ten clinically approved contrast/imaging agents for cancer (Tables 1 and 2) and several others currently in various stages of clinical development.

S. R. Aluri (✉)
Seagen, Bothell, WA, USA

R. S. Chaughule et al. (eds.), *Nanomaterials for Cancer Detection Using Imaging Techniques and Their Clinical Applications*,
https://doi.org/10.1007/978-3-031-09636-5_16

Table 1 FDA-approved tumor imaging agents exploiting untargeted (passive) mechanisms

Product	Imaging modality	Description	Manufacturer
Axumin®	PET	Fluorine F-18-labeled synthetic amino acid analog Fluciclovine	Blue Earth Diagnostics [23]
Fludeoxyglucose F-18 injection	PET	Fluorine F-18-labeled glucose (Fludeoxyglucose, FDG)	The Feinstein Institute for Medical Research [24]
Megatope®	SPECT	Iodinated (Iodine I-131) Albumin	Iso-Tex Diagnostics Inc. [25]
Gadavist®	MRI	Gadobutrol (Gadolinium (Gd^{3+}) chelate)	Bayer Healthcare [26]
ProHance®	MRI	Gadoteridol (Gadolinium (Gd^{3+}) chelate)	Bracco Diagnostics [27]
IC-GREEN™	NIR fluorescence	Indocyanine green	Akorn Inc. [28]

Table 2 FDA-approved imaging agents exploiting active targeting mechanisms

Product	Imaging modality	Description	Manufacturer
Bexxar®[a]	SPECT	Tositumomab and Iodine I-131 Tositumomab	GlaxoSmithKline [34]
Gallium Ga-68 PSMA-11 injection	PET	Gallium Ga-68 chelated to HBED-CC and PSMA-11 peptidomimetic conjugate	University of California, Los Angeles [35]
Lymphoseek®[b]	SPECT	Technetium Tc-99 m chelated to DTPA and tilmanocept conjugate	Cardinal Health [36]
Netspot™	PET	Gallium Ga-68 dotatate (Gallium-68 chelated to DOTA conjugated Octreotate)	Gipharma/Advanced Accelerator Applications [37]
Octreoscan™	SPECT	Indium In-111 chelated to DTPA and Somatostatin peptide analogue conjugate	Curium [38]
Protascint®	SPECT	Indium In-111 chelated to DTPA and anti-PSMA Murine IgG1 conjugate	EUSA Pharma [39]
Verluma®[a]	SPECT	Technetium Tc-99 m chelated to merpentan and anti MS4A1 murine Fab conjugate	Boehringer Ingelheim [40]
Zevalin®	SPECT	Indium In-111/Yttrium Y-90 chelated to tiuxetan and ibritumomab conjugate	Spectrum Pharmaceuticals [41]

[a]The manufacturing of Bexxar® and Verluma® has been discontinued by their respective manufacturers

[b]A technetium Tc-99 m chelated version of Lymphoseek® is available as Tektrotyd®

This chapter aims to provide the reader with a holistic review of protein- and peptide-based contrast/imaging agents used in various imaging modalities. It also summarizes the key targeting approaches exploited by these contrast/imaging agents for accurate tumor recognition and imaging.

2 Targeting Approaches Used for Tumor Imaging

The combination of protein engineering and recombinant technologies has led to the approval of several proteins and peptide therapies against multiple tumor types [7, 9]. Protein- and peptide-based therapies specifically bind tumor markers, thereby inducing an antitumor effect [7, 9]. Due to their target specificity, proteins and peptides are heavily used as targeting agents for drug delivery applications [10, 11]. Concurrently, imaging modalities have significantly improved in precision and reliability by adapting proteins and peptides based targeting approaches in both clinical and translational imaging [5, 12–16]. Targeting approaches utilized in imaging overlap extensively with those developed for cancer drug delivery. Hence, these approaches can similarly be classified into (1) "passive" and (2) "active" targeting [7].

Note: The phrases "contrast agents," "imaging agents," and "tracers" will be used interchangeably throughout the text depending on the imaging modality used.

2.1 "Passive" Targeting of the Tumor via the Enhanced Permeability and Retention (EPR) Effect

Tumors require a large amount of energy, nutrients, and oxygen to support their metabolic needs. This forces tumors to rapidly develop their own vasculature through angiogenesis and connects the tumor masses with existing functional vasculature for constant nourishment [17]. The rapid and chaotic vascular development produces semi-porous blood vessels which are inefficient and haphazardly arranged. These semi-porous blood vessels possess pores with diameters of around 400–600 nm [18], which allows easy diffusion and accumulation of constructs with diameters of $\leq$100 nm into the tumor microenvironment [18]. The accumulation at the tumor site is further enhanced by the lack of a lymphatic system which allows for increased retention of imaging agents at the tumor site [8, 19]. The combination of these two mechanisms is generally referred to as the enhanced permeability and retention (EPR) effect (Fig. 1). Table 1 lists FDA-approved imaging agents which passively diffuse into tumors and exploit the EPR effect.

In spite of its simplicity, passive EPR-based targeting is impacted by (1) elevated interstitial pressure due to lack of lymphatic drainage [6, 20, 21], (2) vascularity of the tumor [21, 22], and (3) inconsistent cellular density in tumors [20, 22]. All these factors combined lead to the variable tumor accumulation and in some cases

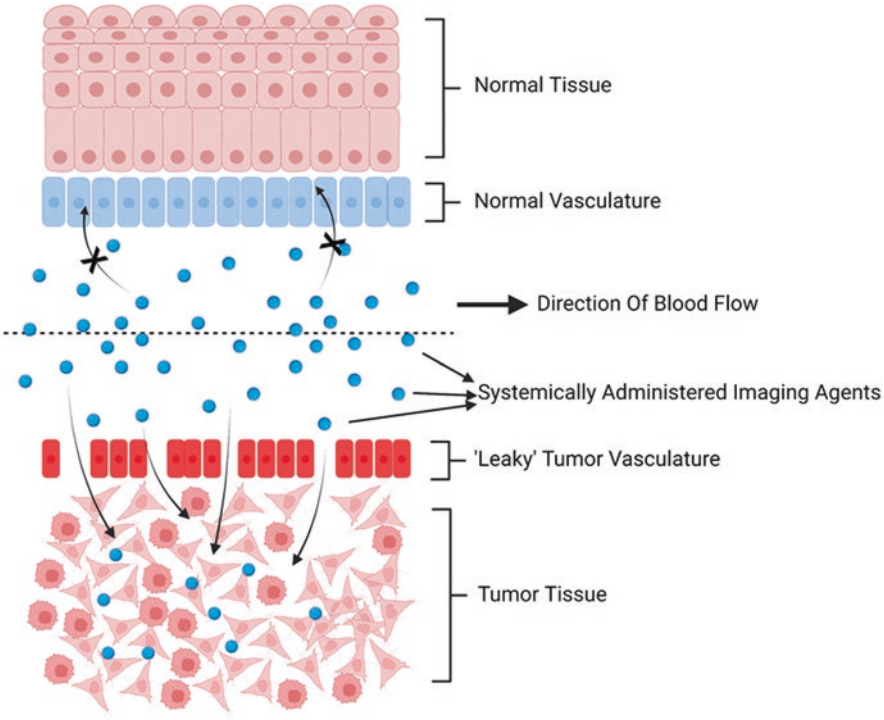

Fig. 1 Description of the EPR effect: The haphazard development of tumor blood vessels leads to a "leaky" vascular system which promotes "passive" extravasation of imaging agents into the tumor microenvironment compared to an intact normal vascular system

"washout" of retained imaging agents [21, 22] (Fig. 2). Although these tumoral characteristics can be modified to boost accumulation, only a modest increase is observed [20]. Hence, passive targeting approaches need to be augmented to ensure accuracy and specificity.

2.2 Active Targeting of Tumors Using Proteins and Peptides

Active targeting of tumor can be achieved by conjugation of imaging agents to tumor-specific ligands or molecules. Following passive EPR-driven tumor accumulation, active targeting allows the imaging agents to engage tumor-specific surface markers [7]. Engagement of these surface markers increases the number of accumulated imaging agents and boosts retention [29]. A vast number of cell surface receptors are upregulated in tumor cells and serve as ideal markers for tumor targeting. Examples of such tumor markers include epidermal growth factor receptors (EGFR), vascular endothelial growth factor receptors (VEGFR), CD20, prostate-specific membrane antigen (PSMA), transferrin receptor (TF), folate receptors (FR),

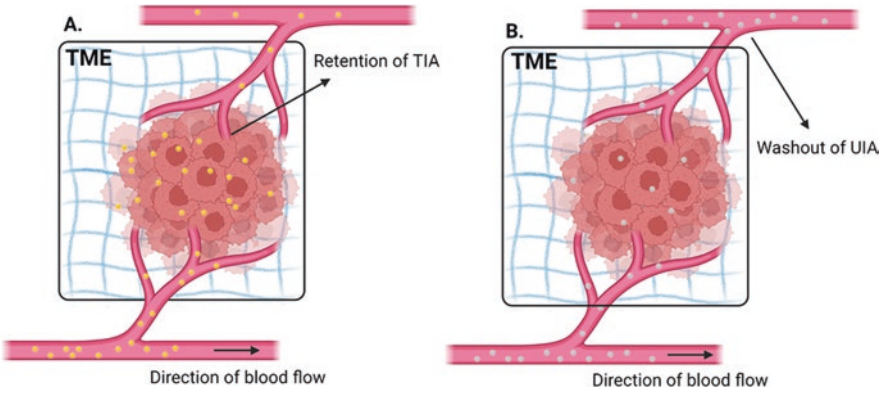

Fig. 2 Impact of active targeting on tumoral retention of imaging agents: Tumoral retention of imaging agents is driven by a combination of passive and active targeting mechanisms. (**a**) Targeted imaging agents (TIA) passively diffuse into the tumor microenvironment through the EPR effect and actively engage tumor-specific targets leading to improved tumor penetration and retention. (**b**) Untargeted imaging agents (UIA) passively diffuse into the tumor microenvironment through the EPR effect. However, UIAs fail to engage tumor-specific targets leading to poor tumor retention and penetration. The poor retention combined with the high interstitial pressure washes the UIAs which reduces the efficiency of the imaging agent. Abbreviations: *TIA* targeted imaging agent, *TME* tumor microenvironment, *UIA* untargeted imaging agent

E-selectin, and somatostatin receptors (SR). All the listed targets play a crucial role in tumorigenesis, tumor progression, and tumor metastasis.

Despite the obvious benefits of active targeting, this approach is limited by (1) expression levels of tumor surface markers [30], (2) inconsistent tumor penetration due to variable tumor densities [18, 20, 31], and (3) immunogenicity of the conjugated protein or peptide ligand [32]. A combination of these factors could lead to rapid clearance of the imaging agent, thereby reducing imaging efficiency [32]. Hence, imaging agents have to be developed to exploit the combined effect of both passive and active approaches [29, 33]. This would allow high tumoral retention with minimal "washout" of the imaging agent (Fig. 2) [21, 29]. The retention of the imaging agent improves the signal-to-noise ratio (SNR), leading to higher contrast images for accurate diagnosis/prognosis of cancer [5]. This approach also decreases the off-target localization of imaging agents which lowers the diagnostic efficiency of the imaging agent [30]. Table 2 lists FDA-approved targeted imaging agents.

3 Tumor Imaging Approaches Using Proteins and Peptides

Protein and peptides have attracted a lot of interest in tumor imaging and targeting. They provide perfect development platform due to their (1) high target specificity (many receptor ligands are typically proteins and peptide), (2) ease of modification, and (3) ease of conjugation [42, 43]. Protein engineering and screening technologies have yielded a huge library of highly selective tumor-targeting agents like

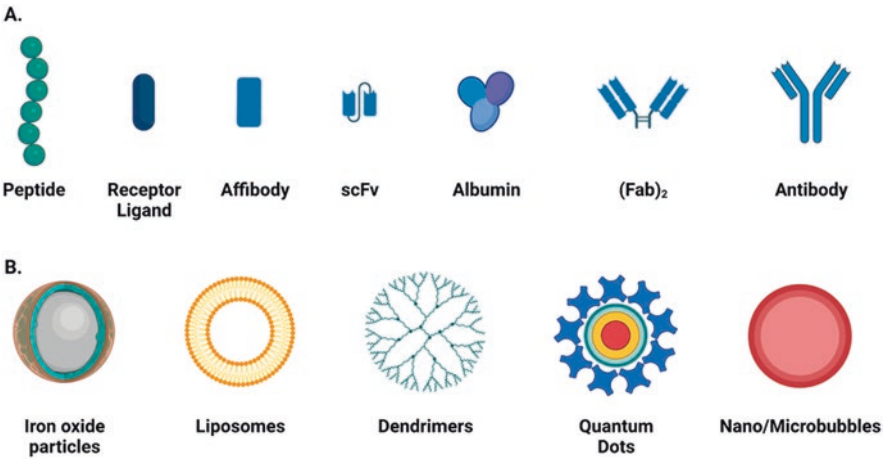

Fig. 3 Targeting motifs and carriers used in tumor imaging: (**a**) Examples of protein and peptide motifs typically used in tumor targeting. (**b**) Examples of contrast/imaging agent carriers used in various tumor imaging modalities. Abbreviations: *Fab* fragment antigen binding, *scFv* single-chain variable fragment

peptides, protein ligands, affibodies, antibodies, and antibody fragments (single-chain variable fragment (scFv) and fragment antigen binding (Fabs)) (Fig. 3a), for various tumor-targeting purposes. These agents can also be used to functionalize imaging particles (Fig. 3b) to enhance their capabilities. Some of these approaches have shown promise as therapeutic agents and have been approved for the treatment of cancers. A list of tumor markers, functions, and approved products is summarized in Table 3.

As imaging agents, proteins and peptides have found use as both carriers and targeting ligands [76]. As carriers, they do not possess the encapsulation efficiency of micelles or liposomes. However, they serve as carriers themselves via conjugation of imaging agents through both covalent and non-covalent approaches. Examples of proteins or peptide-based carriers include RGD peptides [77–81], ligands [82], antibodies [83–85], albumin [86, 87], ProCA1 [88, 89], and polylysine [90]. The application of each will be elaborated on in relevant sections.

Protein and peptides also serve as targeting ligands and are used in functionalizing nonspecific imaging agent carriers (Fig. 3b) against tumor targets [76]. Due to the huge repertoire of targeting ligands and imaging agents, researchers have the ability to develop "plug and play" approaches, where imaging agents and ligands are chosen based on the imaging modality and tumor type, respectively [14, 91–94]. For example, an MRI imaging approach using an anti-HER2 targeted contrast agent can easily be adapted for PET imaging by simply swapping out the contrast agent.

Table 3 Summary of tumor targets, functions, and clinically approved targeted therapies

Tumor marker	Function	Approved products	References
Cathepsins (B, L, and S)	Lysosomal proteases which play a significant role in tumor metastasis. They are upregulated in tumors, causing degradation of the extracellular matrix leading to metastatic spreading	None available	[44–46]
CD20	A B-cell surface receptor with no natural ligand. The function of CD20 receptor is unclear but targeting CD20 has translated to several approved cancer therapies	Rituximab (Rituxan®) Ocrelizumab (Ocrevus®) Ofatumumab (Kesimpta®)	[47–49]
Endoglin (CD105)	A transmembrane cell surface receptor is highly expressed on a variety of tumor vasculatures. Plays a role in tumor angiogenesis and progression	None available	[50, 51]
EGF/EGFR (EGF/ epithelial growth factor receptors)	EGF and EGFRs are highly upregulated on cancerous cells and are known to promote tumorigenesis. Targeting EGF/ EGFR has translated to several approved cancer therapies. These targets include the HER2 receptor as well	Cetuximab (Erbitux®) Trastuzumab (Herceptin®), panitumumab (Vectibix®) Necitumumab (Portrazza®)	[52–54]
EpCAM (epithelial cell adhesion molecule)[a]	A transmembrane protein is highly expressed on tumor cells. Plays a crucial role in tumor progression by promoting cell proliferation. Targeting EpCAM has translated to several approved cancer therapies	Edrecolomab (Panorex®) Catumaxomab (Removab®)	[53, 55, 56]
E-selectin	Selectins are adhesion molecules that are highly upregulated on tumor cells. They promote the interaction of tumor cells with epithelial cells promoting tumor metastasis	None available	[57, 58]
Fibrin-fibronectin	The fibrin-fibronectin system plays a crucial role in clotting but also promotes tumor stroma formation. They promote angiogenesis and are abundantly present in the tumor extracellular matrix (ECM)	None available	[59, 60]
Glucose transporters (GLUT)	Glucose transporter is upregulated in tumor cells for glucose supply due to their high energy demand. GLUT targeting had been utilized in approved tumor imaging products	None available	[61–63]

(continued)

Table 3 (continued)

Tumor marker	Function	Approved products	References
Integrins[b]	Integrins are a group of heterodimeric transmembrane receptors which play a crucial role in tumor metastasis and progression	Abciximab (Reopro®) Natalizumab (Tysabri®)	[64, 65]
p32	A mitochondrial protein which bind various intracellular and extracellular proteins. Shown to be highly upregulated in tumors, especially in hypoxic regions on the tumor	None available	[66]
P-selectin	Selectins are adhesion molecules which are highly upregulated on tumor cells. They promote interaction of tumor cells with platelets and leukocytes promoting tumor metastasis	None available	[67, 68]
PSMA (prostate-specific membrane antigen)	PSMA is a membrane protein with enzymatic properties. It is highly upregulated in prostate cancer and correlates well with the aggressiveness of the disease	None available	[69]
Transferrin receptor	Transferrin receptors are iron transporters that are upregulated in tumor cells for iron supply due to their high metabolic demand	None available	[70, 71]
VCAM (vascular cell adhesion molecules)	VACMs are adhesion molecules expressed that mediate the attachment of lymphocytes to epithelia. It is suggested that upregulated VCAMs (VCAM-1) expression in tumors may promote tumor immune evasion by promoting T-cell migration	None available	[72, 73]
VEGF/VEGFR (vascular endothelial growth factor / vascular endothelial growth factor receptor)	VEGF and VEGFRs are upregulated in tumors and play a crucial role in tumor angiogenesis. Targeting VEGF/VEGFR has translated to several approved cancer therapies	Aflibercept (Eylea®) Bevacizumab (Avastin®)	[74, 75]

[a]Approved antibodies against EpCAM have been withdrawn from the market
[b]Approved antibodies against various integrins have not been indicated for use in cancer applications

3.1 X-Ray/Computer Tomography (CT)

X-ray-based imaging is the oldest noninvasive imaging technique in use today [95]. This technique utilizes the absorption of the high-intensity electromagnetic waves by the body's organs generating a single plain view of the patient's anatomy [96]. CT utilizes a rotating beam of X-rays to capture absorption signals. These signals

are converted to images and are collated to form a 3D image of the organ/tissue of interest [96]. To generate sufficient contrast in the tissue of interest, a contrast agent is typically used. Products like iohexol (Omnipaque™) and iopromide (Ultravist™) are approved iodine-based contrast agents. Due to their small size, they are rapidly cleared through the kidney and significantly reduce their application as tumor contrast agents [97]. To improve the application of these contrast agents to tumor imaging, carriers have to be developed to ensure sufficient tumor localization to generate sufficient contrast when compared to tissue background [97]. However, none of these approaches have been approved by the FDA for tumor imaging. Hence, this section aims to summarize work performed by various researchers utilizing proteins and peptides to develop novel tumor-targeting contrast agents for x-ray imaging.

Proteins and peptides do not possess the required opacity to be used as contrast agents. However, several groups have exploited their target specificity to functionalize commonly used contrast agents like gold and iodine-containing nanoparticles to improve tumor contrast. Gaikwad et al. and Tsvirkun et al. developed contrast agents targeting cathepsins which are upregulated in metastatic tumors [46]. Both the groups utilized a novel peptide-based broad cathepsin enzyme inhibitor, GB111 [94, 98]. The peptide based cathepsin inhibitor, GB111, was covalently conjugated to iodine-tagged dendrimers (Gaikwad et al.) and gold nanoparticles (Tsvirkun et al.) respectively. Gaikwad et al. demonstrated that the cathepsin-targeted dendrimers not only inhibited tumoral cathepsins but also showed their applicability for tumor imaging in vivo. A 2.1-fold increase in signal was observed compared to the untargeted dendrimer control in the evaluated mouse tumor model [94]. Likewise, Tsvirkun et al. generated gold nanoparticles of various sizes (10 nm–100 nm in diameter) and compared their tumor uptake to similarly sized GB111-tagged nanoparticles in a mouse tumor model. The gold particles demonstrated a size-dependent uptake with the smallest GB111-tagged gold nanoparticles (10 nm) showing the highest accumulation in vivo. These particles showed a significantly high accumulation of up to 12% of tumor volume in the evaluated subcutaneous tumor model [98].

Angiogenic marker Integrin (αvβ3) is widely studied for various tumor-targeting approaches [99]. The αvβ3 integrin is targeted efficiently using cyclic arginine-glycine-aspartic acid (RGD) tripeptide motif [78]. Yu et al. generated cyclic RGD-functionalized chitosan-graft-poly(l-lysine) (CPL)-based gold particles[90]. In mice, these particles produced visibly superior tumor images when compared to Omnipaque®, an orally administered contrast agent. The RGD-functionalized particles also improved tumor delivery of shRNA thereby improving the tumor-killing efficacy of CPL particles [90].

Several tumor surface markers like p32 [100], transferrin receptor [101], and E-selectin [102] have been used as targets for CT-based imaging. Using Lyp-1, a p32 receptor-targeting peptide (sequence "CGNKRTRGC"), Kinsella et al. successfully demonstrated tumor accumulation of p32-targeted Bi_2S_3 nanoparticles in a mouse-human breast cancer xenograft model. The p32-targeted Bi_2S_3 nanoparticles showed a 260% higher tumor accumulation than untargeted nanoparticles and also improved tumor visualization [100]. Similarly, Miayata et al. and Wyss et al.

functionalized liposomes against transferrin receptor and E-selectin, respectively. Miayata et al. functionalized iodine-containing contrast liposomes with transferrin, a transferrin receptor ligand, and successfully tracked them in rat F98 glioma cells [101]. They reported stable imaging of implanted tumors for up to 72 h postinjection with the transferrin-tagged liposomes, while the control liposomes showed tissue wash out within 24 h [101]. Wyss et al. functionalized iodine-containing contrast liposomes with E-selectin-binding peptide (ESBP). The ESBP was identified through screening of a recombinant peptide library and has the sequence "BCDSDSDITW-DQLWDLMK," where B is beta-alanine. Using micro-CT, the group demonstrated selective tumor accumulation of the targeted liposomes in HT-29 tumor-bearing mice. They reported an increase of – 8 Hounsfield units (HU) in the tumor due to accumulation of targeted liposomes. Thereby, validating the use of E-selectin targeted contrast agents for tumor imaging [102].

Several antibodies have also been used to functionalized CT contrast agents to further enhance tumor contrast. Popovtzer et al. conjugated anti α6β4 (A9 antigen) antibodies to polyacrylic acid functionalized gold nanoparticles and demonstrated fivefold higher tumor accumulation than non-targeted control in a squamous cell carcinoma xenograft model. They also demonstrated a three to fourfold increase in signal when compared to non-targeted tissues [103]. Hainfeld et al. used trastuzumab (Herceptin®), a monoclonal antibody against HER2, to enhance tumor uptake of gold nanoparticles. The targeted carriers showed a 1.6-fold increase in HER2 + ve tumors when compared to HER2-ve tumors. CT images taken of the HER2+ve tumor show particle accumulation in the tumor periphery. The particles also showed 22-fold higher tumor accumulation compared to surrounding tissue allowing for distinct recognition of tumors during imaging [84]. Similarly, Ashton et al. used cetuximab (marketed as Erbitux®), a monoclonal antibody against EGFR. Cetuximab-conjugated gold nanoparticles showed a significantly higher accumulation in the tumor when compared to experimental controls. The images obtained were qualitatively superior to the controls. The total amount of gold nanoparticles accumulated in the tumor is twofold higher than the experimental controls [104].

3.2 Ultrasound Imaging

Ultrasound is a routine noninvasive technique used for imaging various tissues and has found applicability in tumors. This technique detects high-frequency sound waves (1–20 kHz) [91, 96] reflected by high-density organ/tissue to generate a computer image of the organ/tissue. The sound waves are generated by piezoelectric crystals which are the main component of the ultrasound transducer. The transducer is the source and receiver of the reflected sound waves [96]. To enhance contrast of tumors versus surrounding tissue, contrasting agents with significantly different compressibility and reflectivity compared to the surrounding tissues are

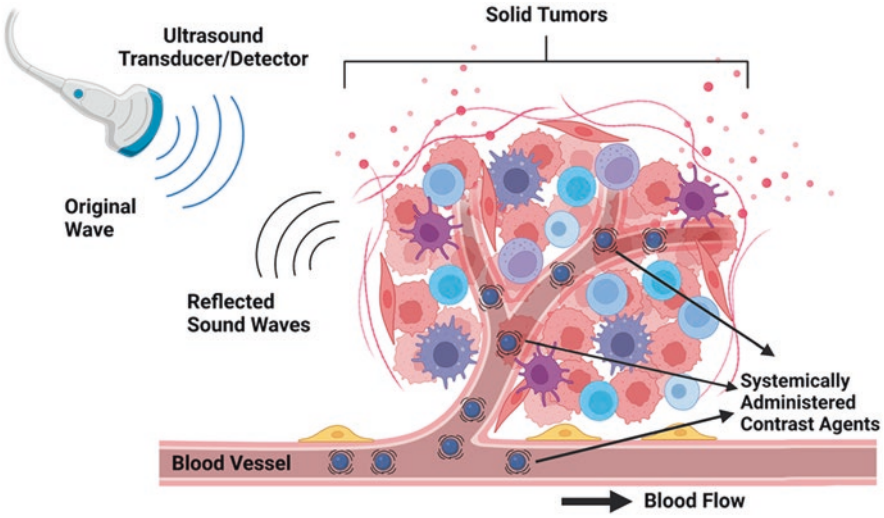

Fig. 4 Principle behind ultrasound contrast agents: The ultrasound transducer generates sound waves which propagate and scatter throughout the imaging area. The sounds waves induce nonlinear oscillations in the MBs/NBs generating backscatter waves which are sent back to the transducer to be processed. The signal generated by MBs/NBs tends to be more distorted than surrounding tissue allowing for quick identification and interpretation

recommended [105]. Hence, particles like microbubbles (MB)/nanobubbles (NB) make good contrast agents due to their compressibility in a sonic field (Fig. 4) [106]. MBs are made of a gaseous core stabilized in a hard shell usually made from lipids, proteins, or polymers [105–107]. SonoVue® and Lumson® are examples of MB-based contrast agents approved for ultrasound imaging. MBs usually range from 1–10 μm in size and largely circulate in the blood pool, limiting their applicability for tumor imaging due to poor extravasation into the tumor microenvironment [107]. However, the lack of tumor diffusion allows MBs to be used for tumor vasculature characterization. Nanobubbles (NB) on the other hand are much smaller than MBs and ideal for both passive and active targeting approaches [108]. Hence, functionalizing of MB/NBs with tumor-specific targets allows for both characterization of tumors and their vasculature [16]. The various protein and peptide-based approaches utilized for ultrasound contrast agents are summarized in this section. However, none have been approved by the FDA.

Similar to X-ray-based imaging, proteins and peptides by themselves cannot be used as ultrasound contrasting agents but can be employed as targeting moieties. In order to generate integrin-targeted MBs, Otani et al. modified a commercially available MB preparation, Sonazoid® (Daiichi Sankyo, Japan), with lactadherin [109]. Lactadherin binds both αvβ3 and αvβ5 through an epidermal growth factor (EGF)-like domain displaying the RGD motif [110, 111]. By incorporating the lactadherin protein, there is a significant increase in tumor accumulation of the αvβ3 targeted Sonazoid® particles in a SKOV-3 ovarian adenocarcinoma xenograft model.

Similarly, integrin αvβ3 can also be targeted using the simple RGD motif as demonstrated by Hu et al. [77]. The work was performed to demonstrate a tumor size-dependent accumulation of MBs in a human tumor. Hu et al. demonstrated significantly higher update in small tumors than large tumors, concluding that higher tumor necrosis observed in large tumor reduces tumor accumulation, hence, demonstrating the application of MBs in monitoring tumor angiogenesis during tumor growth [77].

Commonly investigated tumor targets like HER2, VEGFR-2, and endoglin (CD105) were also evaluated as targets for contrast agents. Yang et al. [112] successfully targeted HER2 using NBs coated with an anti-Erb2 affibody. The affibody-coated NBs demonstrated a statistically significant increase in ultrasound signal and image contrast when compared to the unlabeled NBs and SonoVue® controls. Yang et al. also demonstrated increased tumoral residence times for targeted NBs which lead to significant enhancements in tumoral signal when compared to experimental controls [112]. Endoglin (CD105), an important angiogenesis biomarker [113, 114], was successfully targeted by Shan et al. using MBs functionalized with anti-CD105 antibodies, to detect tumor-specific vasculature in a hepatoblastoma xenograft model [114]. A threefold increase in intensity was observed over the experimental control group, making this approach a viable option for the diagnosis of liver carcinomas.

To enhance synergy between various targets, multi-specific MBs have also been evaluated. Yuan et al. utilized a dual-targeting approach with VEGFR-2 and αvβ3 integrin-specific MBs. The individual and dual-targeted MBs showed >90% contrast enhancement compared to untargeted particles when evaluated in an MHCC-97H human liver carcinoma xenograft model [115]. Similar to the previous dual-targeting approach, Warram et al. [116] designed triple-targeted MB-based contrast agent against VEGFR-2, P-selectin, and αvβ3. When evaluated in vivo using an MDA-MB-231 tumor xenograft mouse model, the triple-targeted MBs showed a 40% increase in image intensity over both the single- and dual-targeted MBs. Hence, multipronged approaches improve the apparent avidity of the contrast agent, thereby increasing the likelihood of efficient tumor recognition and thereby improving image contrast.

All of this research culminated in the first targeted MB-based contrast agent being introduced into clinical trials. In 2010, the first Phase 1 trial using vascular endothelial growth factor receptor-2 (VEGFR-2)-targeted microbubbles, called BR55, was initiated for breast and ovarian cancer imaging [117]. The BR55 MBs were functionalized with a lipopeptide that specifically binds VEGFR-2. In the clinical study, VEGFR-2 expression on tumors matched well with ultrasound imaging signal in 93% of breast and 85% of ovarian malignant lesions. BR55 was also shown to be well tolerated by all dosed patients [118]. Information on product progress and commercialization is currently unavailable. However, this is still very promising development for targeted ultrasound contrast agents and a validation of targeting technologies overall.

3.3 *Magnetic Resonance Imaging (MRI)*

MRI is an imaging technique which utilizes signals emitted by the hydrogen atom when disturbed by energy induced by radio waves under a constant magnetic field [13]. It allows for both deep-tissue and whole-body imaging and has gained popularity as a valuable diagnostic tool in cancer imaging [119, 120]. To further enhance the contrast between normal tissues and tumor tissues, biocompatible MRI contrasting agents are administered systemically to study changes to the longitudinal and transverse (i.e., T1 and T2) relaxation times of hydrogen at the tumor site[121]. The principle behind MRI imaging is illustrated in Fig. 5. The T1 contrast agents for MRI usually include transitional metal ions like Gd^{3+} or Mn^{2+} [121]. They are usually administered in chelated form to reduce serious side effects [121]. The T2 contrast agents for MRI include superparamagnetic iron oxide particles coated with dextran [121]. Both types of contrast agents are currently approved for various tumor imaging applications, but a majority of clinically used contrast agents are

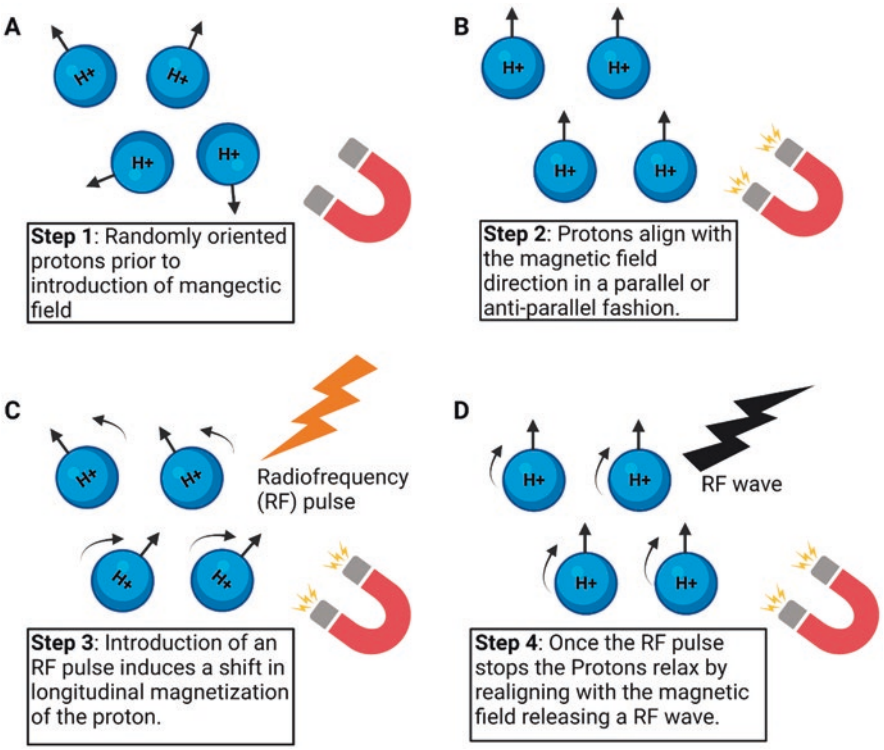

Fig. 5 Principle behind MRI contrast agents: The figure outlines the MRI imaging process. Briefly, a magnetic field is induced to align randomly oriented protons found in tissue of interest. The aligned protons are then perturbed using a RF pulse. The perturbed protons return to their original aligned state by releasing a RF signal which is deconvoluted to produce the MRI signal [92]

Gd^{3+}-based chelates [121]. However, tumor-targeted MRI agents are yet to be approved by the FDA. A summary of protein and peptide application in both imaging techniques is summarized in this section.

3.3.1 T1 Contrasting Agents

Gd^{3+} chelates are inherently small molecules with very low circulation half-lives which are of the order of 1–2 h [122]. To improve circulation and tumoral delivery of Gd^{3+} chelates, proteins and peptide like albumin, polylysine, and ProCAs are used as both covalent and non-covalent carriers. Approved Gd^{3+} chelates like Multihance® (Gd-BOPTA), Eovist® (Gd (EOB-DTPA)) and Ablavar® (MS-325) (Fig. 6) nonspecifically bind albumin, which increases their circulation time and passive diffusion into tumors by exploiting the EPR effect [121]. Covalent complexes of albumin and chelators were evaluated as imaging agents as early as 1987. Schmiedl et al. conjugated complexed Gd^{3+}-DTPA chelator to free amines on albumin and demonstrated enhanced circulation and slow clearance [87]. Due to the enhanced circulation of these albumin complexes, they have found use as imaging agents for tumor microvessel characterization [123]. Polylysine polymers are FDA-approved, biocompatible, and non-immunogenic making them ideal nano-delivery systems [124]. Liu et al. targeted polylysine polymers to VEGFR using anti-VEGF antibodies using the biotin-avidin conjugation system. The VEGFR-targeted polymers showed a significant enhancement in signal when compared to untargeted polymers and also a commercially available contrast agent, Magnevist®. Furthermore, targeting VEGFR improved the diagnostic time from <1 h to 2.5 h [125]. The final MRI agent carriers are a novel class of protein-based chelators called ProCAs. ProCAs do not need the use of small-molecule chelators since they themselves serve as chelators through amino acid side chain interactions [126]. ProCAs are easily modified by getting ligands using recombinant technology [127]. Qiao et al. demonstrated this approach by generating ProCA-HER2 affibody constructs, which efficiently targeted HER2 positive tumors in a mouse xenograft model. The ProCA-HER2 affibody construct exhibited strong contrast enhancement even after 24 h postinjection [127].

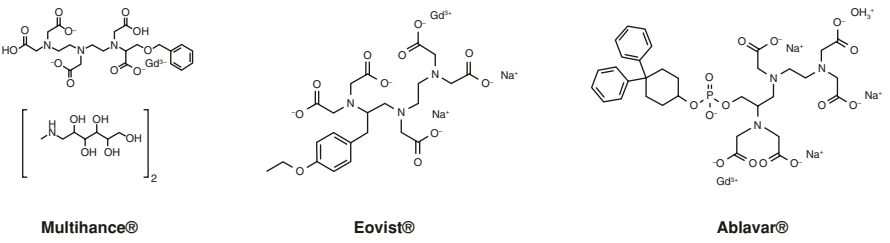

Fig. 6 Chemical structures of FDA-approved MRI agents: Multihance®, Eovist®, and Ablavar® are all linear gadolinium-based contrast agents (GBCAs)

Peptide motifs targeting integrins and the fibrin-fibronectin systems like RGD, CGLIIQKNEC (CLT1) and CREKA have successfully been conjugated to Gd^{3+} chelates to enable tumor targeting. Chelates of Gd-DOTA were efficiently targeted to αvβ3 integrins via conjugation to the RGD motif. These targeted chelates show improved hepatocellular carcinoma contrast by 45% when compared to the untargeted chelate in a transgenic mouse model [80]. Fibrin, is ubiquitously present in the tumor ECM and is targeted using CLT1 [128] and CREKA [129] peptide sequences. These peptides were identified by phage display and specifically bind tumor fibrin-fibronectin complexes [128, 129]. The CLT1-(Gd-DTPA) chelate constructed by Ye et al. efficiently detected HT-29 human colon carcinoma xenografts in a mouse tumor model. The tumor signal increased over time with the highest observed 60 min postinjection. The signal obtained was appreciably higher than the untargeted and quenched controls [130]. Similarly, the CREKA-Tris-Gd (DOTA) chelate made by Zhuo et al. using click chemistry produced a significantly higher SNR when compared Prohance™, a commercially approved contrast agent in a 4 T1 breast tumor model in mice. The SNR for CREKA-Tris-Gd (DOTA) was shown to be approximately sevenfold higher when compared to experimental controls [131].

Artemov et al. evaluated a pretargeting approach for HER2+ve tumors. The method combined biotinylated anti-HER2 antibody, trastuzumab (Herceptin®), with avidin labeled Gd-DTPA chelates. Mice bearing both HER2 + ve and HER2-ve tumors were first administered with biotinylated HER2 antibodies followed by avidin-(Gd-DTPA) chelates. The data showed great retention and contrast at 24 h in the HER2+ve tumor, whereas HER2-ve tumor showed a marked decrease in contrast. Although novel, this technique suffers due to the short circulation time of the avidin-Gd-DTPA chelate [132]. Also in vivo applications of the avidin label can be hampered by its immunogenicity [133].

3.3.2 T2 Contrasting Agents

Unlike T1 contrast agents, T2 contrast agents are larger in size and typically range between 60 and 150 nm in size [134]. Ferumoxide® and Ferrixan/Ferucarbotran® are examples of commercially approved T2 contrast agents and are typically made of superparamagenetic iron oxide particles (SPIO) [134]. In order to improve their applicability to a variety of tumors, the coating on SPIOs can be modified to allow for labeling by ligands using simple click chemistry. T2 contrast agents modified with motifs against integrin αvβ3 [79], vascular cell adhesion molecule-1 (VCAM-1) [135], and transferrin [136] have shown promise. Unfortunately, their uptake by the reticuloendothelial (RES) system in the liver reduces their application in tumor imaging [137]. However, due to their proclivity for accumulation in the liver and lymph nodes, T2 contrast agents have found use in the detection of liver and splenic tumors [137].

3.4 Single-Photon Emission Computed Tomography (SPECT) and Positron Emission Tomography (PET)

SPECT and PET are imaging techniques which utilize systemically administered radionuclides as imaging agents. SPECT tracers agents decay by releasing photons via gamma rays. PET tracers decay by positron emission which further undergoes an annihilation event with electrons, yielding photons emitted in opposite directions [138]. SPECT instruments detects emitted photons screened through a lead collimator, leading to lower picture resolution. PET instruments on the other hand use coincidence detection which allows for simultaneous detection of two photons which are 180° apart in trajectory [96]. This difference makes PET a more sensitive imaging technique than SPECT (Fig. 7) [138]. However, SPECT imaging is widely adopted over PET due to relatively wider clinical acceptance and cheaper instrumentation. Both techniques use a wide array of radioisotopes with varying half-lives. Examples of radioisotopes used in SPECT imaging are technetium Tc-99 m, indium In-111, iodine I-123, and iodine I-131 [138]. Examples of radioisotopes used in PET imaging include fluorine F-18, copper Cu-64, and iodine I-124 [138]. The radionuclides are chosen based on imaging application and the length of study. However, due to the ionizing nature of the radionuclides, agents with relatively short half-lives are preferred for imaging purposes [139].

Due to vast clinical adoption of SPECT and PET imaging and an equally exhaustive list of available literature, this section will focus on highlighting approved and clinically relevant SPECT and PET imaging products using proteins and peptides.

3.4.1 SPECT Imaging Agents

SPECT tracers are small chelated molecules with poor circulation times and non-specific tissue accumulation [140]. To improve circulation and tumoral accumulation, SPECT imaging agents are directly conjugated to proteins and peptides, which serve as both carriers and targeting agents. These approaches have yielded a wide range of commercially approved targeted SPECT tracers [138]. Proteins like albumin have been approved as carriers for SPECT imaging. Nanocoll™ is technetium Tc-99 m-labeled colloid human serum albumin (HSA) developed to detect sentinel node localization in breast cancers [141]. The sentinel node is hypothesized to be the primary site for lymphatic metastasis and making Nanocoll™ an invaluable tool for clinicians [142]. Nanocoll™ is prepared by addition of sodium pertechnetate (technetium Tc-99 m) to lyophilized albumin particles which are <80 nm in size. The radiolabeled albumin complex can be administered intravenously or subcutaneously [142]. Megatope® is another HSA preparation where the HSA is iodinated (iodine I-131). Although used manly as blood pool imaging agent, it is indicated for use in the detection and characterization of cerebral neoplasms [86].

Similar to HSA, peptide- and antibody-based SPECT imaging agents have been approved for clinical use. An FDA approved peptide-based SPECT imaging agent is

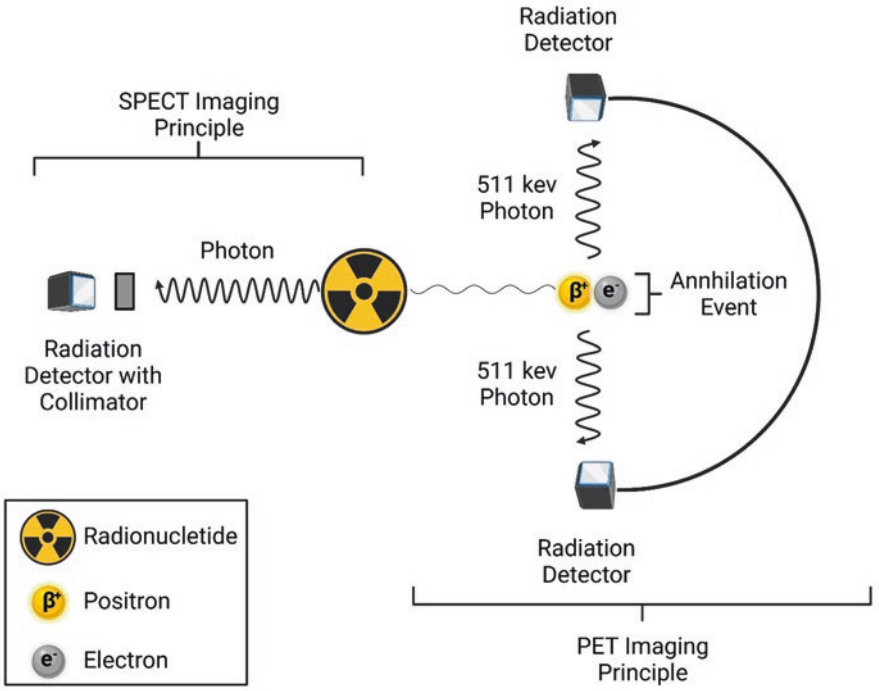

Fig. 7 Differences between SPECT and PET imaging: The mechanism on the left depicts a SPECT tracers decaying by emitting a photon as gamma rays. The gamma rays are filtered through the lead collimator to reach the radiation detector. The mechanism on the right depicts a PET tracer decaying by emitting a positron. The positron undergoes an annihilation event by colliding with electrons present in tissue of interest to release two photons. The released photos are in trajectories which are 180° apart. All PET agents produce photons with an energy of 511 KeV

Octreoscan™. Octreoscan™ is DTPA labeled octreotide, a synthetic somatostatin analog, which is chelated to indium In-111 before systemic administration into patients [143]. Octreotide specifically targets primary and metastatic neuroendocrine tumors bearing somatostatin receptors [143]. Zevalin®, ibritumomab tiuxetan, is the first approved radiotherapy drug for NHL. Ibritumomab is a mouse IgG1 antibody that targets CD20 receptor on B cells. The antibody is conjugated to tiuxetan which serves as a radionuclide chelator. The radionuclide used in Zevalin® is switched between indium In-111 and yttrium Y-90 depending on its clinical application. Indium In-111 is used for imaging purposes, whereas yttrium Y-90 is used for radiation therapy [144]. Protascint®, capromab pendetide, is another imaging approved for imaging of prostate tumors. Capromab is a mouse IgG1 antibody against PSMA which is highly expressed in prostate cancers. The antibody is conjugated to pendetide which is the chelator for indium In-111 [145]. However, the application of Protascint® and Zevalin® as imaging agents is vastly reduced due to formation of human anti-mouse antibodies which causing rapid clearance of these agents when administered clinically [146]. Hence, a lot of clinically approved human/

humanized antibody treatments are also being adapted for use in SPECT imaging. Anti-HER2 antibodies like trastuzumab (Herceptin®) and pertuzumab (Perjeta®) are being investigated clinically as imaging agents using a variety of chelators and radionuclides [147]. Similarly, different targeting modalities like peptides [148, 149], affibodies [150], and Fabs [151, 152] are also being evaluated against the HER2 receptor. Similarly, PD1/PD-L1 antibodies like nivolumab (Opdivo®) and atezolizumab (Tecentriq®) have been applied for monitor changes in colorectal carcinomas [153] and studying metastasis [154]. Imaging agents have also been designed to bind validated tumor targets like integrins [155–157] and VEGFR [158, 159].

3.4.2 PET Imaging Agents

PET imaging agents are also small molecules and encounter the same pitfalls as SPECT imaging agents. The mostly widely used PET imaging agent is 18F-fluoro-2-deoxy-D-glucose (FDG) [62], which is selectively taken up by rapidly dividing cancer cells. However, tumoral uptake of FDG is dependent on cell-specific expression of GLUT receptors which is further impacted by several tumorigenic factors [63]. Furthermore, the small tracer size leads to short circulation times and fast clearance [160].

Compared to SPECT imaging agents, there are fewer clinically approved PET agents which use proteins or peptides. There have been only two approved targeted PET imaging agents, with both targeting PSMA. Gallium Ga-68-PSMA-11 is the first targeted PET agent indicated for imaging of prostate cancer [161]. It is designed to target PSMA surface receptors on prostate cancer cells [161]. The Ga-68 is chelated to the HBED chelator conjugated to the PSMA-targeting peptidomimetic, PSMA-11 [161]. Similarly, piflufolastat fluorine F-18 (Pylarify®) was developed to target PSMA using a similar peptidomimetic moiety to PSMA-11. But, piflufolastat fluorine F-18 does not contain a chelator since fluorine F-18 is chemically conjugated to the unlabeled piflufolastat precursor [162].

Similar to SPECT imaging, several approved antibodies are being tested as carriers for several PET imaging agents. Copper Cu-64-labeled trastuzumab (Herceptin®), an anti-HER2 antibody, has shown promise in detecting HER2 + ve tumors in breast cancer patients. The antibody conjugate showed low off-target accumulation and high tumor contrast at 48 h postinjection, which is an improvement over the zirconium Zr-89 labeled trastuzumab time of 5 days [85, 163]. Similarly, different targeting motifs like affibodies [164] and ADAPTs [165] are being evaluated for PET imaging against the HER2 receptor. Similarly, zirconium-labeled atezolizumab (Tecentriq®), an anti PD-L1 antibody, can potentially be used to predict response prior to treatment by accurately quantifying PD-L1 expression levels [166].

3.5 Optical Imaging

Optical imaging detects emitted light from systemically administered fluorescent probes. It is a safe technique due to the use of nonionizing radiation [30]. It is also an affordable technique due to the use of inexpensive equipment [96]. The fluorescent probes used are easy to handle and possess a safe toxicological profile [30]. This technique mainly uses the near infrared (NIR) spectral range from 650 to 900 nm, which has good tissue penetration and reduced absorption [30]. In spite of NIR's favorable imaging properties, the sensitivity of this technique is reduced for deep-seated tumors, due to increased scattering of light and tissue absorption [167].

Due to the huge library of fluorescent labels, optical imaging can be performed over a wide spectral range. Fluorescein isothiocyanate (FITC), 5-aminolevulinic acid (5-ALA), and indocyanine green (ICG, IC-GREEN®) are nonspecific fluorescent probes currently approved by the FDA for optical imaging. The use of FITC and 5-ALA is limited due to photobleaching, high background from blood and tissues, and nonspecific tissue uptake [30]. However, ICG nonspecifically binds albumin upon systemic administration, leading to passive diffusion into tumors through the EPR effect. This has led to ICG being used as a surgical guide in cancer surgery [30]. Another advantage of ICG is that its peak emission wavelength is near 800 nm, which helps overcome hemoglobin absorption and tissue interference [30].

In optical imaging, proteins and peptides are used as targeted carriers as well as target recognition motifs. Many fluorescent labels are covalently linked to the protein/peptide carrier using simple chemistry. This approach has widely been used to target validated tumor markers like EGFR, HER2, and VEGF through various targeting motifs like antibodies and natural ligands. For example, EGFR was targeted using antibodies and the EGF ligand. Fluorescently (IRDye800CW) labeled cetuximab (Erbitux®), an anti-EGFR antibody, has shown promise in several tumor xenograft models and is now being evaluated as an imaging agent in several clinical trials [168–170]. Nitin et al. utilized Alexa Fluor® 647-labeled EGF to image epithelial tumors with overexpressed EGFR in patients [171]. However, using a natural ligand for imaging must be performed with care due to the receptor activation causing downstream signaling [82]. Similarly, HER2 and VEGF were targeted using fluorescently labeled trastuzumab (Herceptin®) [172] and bevacizumab (Avastin®) [173]. Fluorescent probes have also been chemically conjugated to peptide sequences like RGD [81] and SNFYMPL [174] to target integrin αvβ3 and OE33 adenocarcinoma cells, respectively.

Apart from small-molecule fluorescent probes, proteins and peptides have been used as targeting motifs for fluorescent nanocarriers like quantum dots (QD) and fluorophore-encapsulated liposomes. QDs are nanoparticles with unique optical properties which can be used as alternatives to existing small-molecule fluorophores [175]. Their optical properties can be tailored to generate spectra in the NIR range [175]. QDs by themselves passively diffuse into tumor by the EPR effect and can easily be surface functionalized with target motifs [175]. These unique probes have already been applied to imaging approaches where the QDs improved and enhanced

tumor contrast via anti-PSMA antibody [176] and RGD peptide [177] targeting approaches. Similarly, RGD [178] and anti-endoglin scFv [179] tagged fluorescent liposomes demonstrated tumor-specificity in vitro and in vivo.

4 Conclusion

In summary, proteins and peptides offer clinicians and researchers a "plug and play" format which allows easy adaptation of targeting approaches to a variety of imaging modalities. They demonstrate tremendous versatility as both carriers and targeting agents. Products like Bexxar®, Verluma®, Zevalin® and Protascint®, have been widely used in the clinic for various tumor imaging purposes. With advances in recombinant technology and sequence humanization, many non-immunogenic proteins and peptides are currently being explored to develop the next generation of imaging agents. However, it must be highlighted that the applicability of protein and peptide as targeting motifs can be limited by heterogeneity in target expression as well as heterogeneity in the tumor microenvironment. These issues can be overcome by developing multifunctional imaging agents which can be tracked and imaged using two independent imaging modalities.

Acknowledgments The author would like to thank Dr. Ramesh Chaughule for the opportunity. The author would also like to thank A. Uma Devi and A. Chandra Sekar Rao for their support and constructive feedback. All images were designed using www.biorender.com.

References

1. American Cancer Society. Cancer facts & figures 2021. Atlanta; 2021.
2. Meek RD, Mills MK, Hanrahan CJ, Beckett BR, Leake RL, Allen H, et al. Pearls and pitfalls for soft-tissue and bone biopsies: a cross-institutional review. RadioGraphics [Internet]. Radiological Society of North America; 2020; 40:266–90. Available from: https://doi.org/10.1148/rg.2020190089.
3. Ziv E, Durack JC, Solomon SB. The importance of biopsy in the era of molecular medicine. Cancer J [Internet]. 2016;22:418–22. Available from: https://pubmed.ncbi.nlm.nih.gov/27870685
4. Fass L. Imaging and cancer: a review. Mol Oncol [Internet]. 2008/05/10. Wiley. 2008; 2:115–52. Available from: https://pubmed.ncbi.nlm.nih.gov/19383333
5. Frangioni JV. New technologies for human cancer imaging. J Clin Oncol [Internet]. Am Soc Clin Oncol. 2008; 26:4012–21. Available from: https://pubmed.ncbi.nlm.nih.gov/18711192
6. Heldin C-H, Rubin K, Pietras K, Östman A. High interstitial fluid pressure – an obstacle in cancer therapy. Nat Rev Cancer [Internet]. 2004;4:806–13. Available from: https://doi.org/10.1038/nrc1456.
7. Aluri S, Janib SM, Mackay JA. Environmentally responsive peptides as anticancer drug carriers. Adv Drug Deliv Rev [Internet]. 2009/07/20. 2009;61:940–52. Available from: https://pubmed.ncbi.nlm.nih.gov/19628014

8. Maeda H, Wu J, Sawa T, Matsumura Y, Hori K. Tumor vascular permeability and the EPR effect in macromolecular therapeutics: a review. J Control Rel [Internet]. 2000;65:271–84. Available from: https://www.sciencedirect.com/science/article/pii/S0168365999002485
9. Padma VV. An overview of targeted cancer therapy. Biomedicine (Taipei) [Internet]. 2015/11/28. China Medical University; 2015; 5:19. Available from: https://pubmed.ncbi.nlm.nih.gov/26613930
10. Jeong W, Bu J, Kubiatowicz LJ, Chen SS, Kim Y, Hong S. Peptide–nanoparticle conjugates: a next generation of diagnostic and therapeutic platforms? Nano Convergence [Internet]. 2018; 5:38. Available from: https://doi.org/10.1186/s40580-018-0170-1.
11. Vargason AM, Anselmo AC, Mitragotri S. The evolution of commercial drug delivery technologies. Nature Biomed Eng [Internet]. 2021; 5:951–67. Available from: https://doi.org/10.1038/s41551-021-00698-w.
12. Lento PH, Primack S. Advances and utility of diagnostic ultrasound in musculoskeletal medicine. Curr Rev Musculoskelet Med [Internet] Humana Press Inc. 2008;1:24–31. Available from: https://pubmed.ncbi.nlm.nih.gov/19468895
13. Berger A. Magnetic resonance imaging. BMJ [Internet]. 2002;324:35. Available from: https://pubmed.ncbi.nlm.nih.gov/11777806
14. Israel O, Pellet O, Biassoni L, de Palma D, Estrada-Lobato E, Gnanasegaran G, et al. Two decades of SPECT/CT – the coming of age of a technology: an updated review of literature evidence. Eur J Nucl Med Mol Imaging [Internet]. 2019/07/04. Springer, Berlin Heidelberg. 2019;46:1990–2012. Available from: https://pubmed.ncbi.nlm.nih.gov/31273437
15. Hadjipanayis CG, Jiang H, Roberts DW, Yang L. Current and future clinical applications for optical imaging of cancer: from intraoperative surgical guidance to cancer screening. Semin Oncol [Internet]. 2011;38:109–18. Available from: https://pubmed.ncbi.nlm.nih.gov/21362519
16. Kaur S, Venktaraman G, Jain M, Senapati S, Garg PK, Batra SK. Recent trends in antibody-based oncologic imaging. Cancer Lett [Internet]. 2011/10/20. 2012; 315:97–111. Available from: https://pubmed.ncbi.nlm.nih.gov/22104729
17. Carmeliet P, Jain RK. Angiogenesis in cancer and other diseases. Nature [Internet]. 2000; 407:249–57. Available from: https://doi.org/10.1038/35025220.
18. Yuan F, Dellian M, Fukumura D, Leunig M, Berk DA, Torchilin VP, et al. Vascular permeability in a human tumor xenograft: molecular size dependence and cutoff size. Cancer Res. 1995;55:3752–6.
19. Yuan F, Leunig M, Huang SK, Berk DA, Papahadjopoulos D, Jain RK. Mirovascular permeability and interstitial penetration of sterically stabilized (stealth) liposomes in a human tumor xenograft. Cancer Res. 1994;54:3352–6.
20. Kobayashi H, Watanabe R, Choyke PL. Improving conventional enhanced permeability and retention (EPR) effects; what is the appropriate target? Theranostics [Internet] Ivyspring International Publisher. 2013;4:81–9. Available from: https://pubmed.ncbi.nlm.nih.gov/24396516
21. Nakamura Y, Mochida A, Choyke PL, Kobayashi H. Nanodrug Delivery: Is the Enhanced Permeability and Retention Effect Sufficient for Curing Cancer? Bioconjug Chem [Internet]. 2016/09/02. 2016; 27:2225–38. Available from: https://pubmed.ncbi.nlm.nih.gov/27547843
22. Wadih A, Renata P, Erkki R. Cancer treatment by targeted drug delivery to tumor vasculature in a mouse model. Science (1979) [Internet]. American Association for the Advancement of Science; 1998; 279:377–80. Available from: https://doi.org/10.1126/science.279.5349.377.
23. Blue Earth Diagnostics Ltd. Axumin. Package Insert. 2021.
24. The Feinstein Institute for Medical Research. Fludeoxyglucose F-18 Injection. Package Insert. 2010.
25. Iso-Tex Diagnostics Inc. Megatope. Package Insert. 2020.
26. Bayer Healthcare. Gadavist. Package Insert. 2011.
27. Bracco Diagnostics Inc. ProHance. Package Insert. 2013.
28. Akorn Inc. IC-GREEN. Package Insert. 2015.

29. Rosenblum D, Joshi N, Tao W, Karp JM, Peer D. Progress and challenges towards targeted delivery of cancer therapeutics. Nat Commun [Internet]. 2018; 9:1410. Available from: https://doi.org/10.1038/s41467-018-03705-y.
30. Joshi BP, Wang TD. Targeted optical imaging agents in cancer: focus on clinical applications. Contrast Media Mol Imaging [Internet]. Hindawi; 2018; 2018:2015237. Available from: https://pubmed.ncbi.nlm.nih.gov/30224903
31. Subhan MA, Yalamarty SSK, Filipczak N, Parveen F, Torchilin VP. Recent advances in tumor targeting via EPR effect for cancer treatment. J Pers Med [Internet]. MDPI; 2021; 11:571. Available from: https://pubmed.ncbi.nlm.nih.gov/34207137
32. Davda J, Declerck P, Hu-Lieskovan S, Hickling TP, Jacobs IA, Chou J, et al. Immunogenicity of immunomodulatory, antibody-based, oncology therapeutics. J Immuno Therapy Cancer [Internet]. 2019; 7:105. Available from: https://doi.org/10.1186/s40425-019-0586-0.
33. Li R, Zheng K, Yuan C, Chen Z, Huang M. Be active or not: the relative contribution of active and passive tumor targeting of nanomaterials. Nanotheranostics [Internet] Ivyspring International Publisher. 2017;1:346–57. Available from: https://pubmed.ncbi.nlm.nih.gov/29071198
34. GlaxoSmithKline. Bexxar. Package Insert. 2012.
35. University of California LA. Gallium Ga-68 PSMA-11 Injection. Package Insert. 2020.
36. Cardinal Health. Lymphoseek. Package Insert. 2021;
37. Gipharma S.r.l/Advanced Accelerator Applications. Netspot. Package Insert. 2016.
38. Curium US LLC. Octreoscan. Package Insert. 2022.
39. EUSA Pharma. ProtaScint. Package Insert. 2012.
40. Boehringer Ingelheim. Verluma. Package Insert 1996.
41. Spectrum Pharmaceuticals. Zevalin. Package Insert. 2018.
42. Scodeller P, Asciutto EK. Targeting tumors using peptides. Molecules [Internet]. MDPI; 2020; 25:808. Available from: https://pubmed.ncbi.nlm.nih.gov/32069856
43. Attarwala H. Role of antibodies in cancer targeting. J Nat Sci Biol Med [Internet]. Medknow Publications Pvt Ltd; 2010; 1:53–56. Available from: https://pubmed.ncbi.nlm.nih.gov/22096337
44. Sudhan DR, Siemann DW. Cathepsin L targeting in cancer treatment. Pharmacology & Therapeutics [Internet]. 2015;155:105–16. Available from: https://www.sciencedirect.com/science/article/pii/S0163725815001655
45. Ruan H, Hao S, Young P, Zhang H. Targeting Cathepsin B for cancer therapies. Horiz Cancer Res [Internet]. 2015;56:23–40. Available from: https://pubmed.ncbi.nlm.nih.gov/26623174
46. Tan G-J, Peng Z-K, Lu J-P, Tang F-Q. Cathepsins mediate tumor metastasis. World J Biol Chem [Internet]. Baishideng Publishing Group Co Limited. 2013;4:91–101. Available from: https://pubmed.ncbi.nlm.nih.gov/24340132
47. Pavlasova G, Mraz M. The regulation and function of CD20: an "enigma" of B-cell biology and targeted therapy. Haematologica [Internet]. 2020; 105:1494–506. Available from: https://haematologica.org/article/view/9425
48. Marshall MJE, Stopforth RJ, Cragg MS. Therapeutic antibodies: what have we learnt from targeting CD20 and where are we going? Front Immunol [Internet]. 2017;8. Available from: https://www.frontiersin.org/article/10.3389/fimmu.2017.01245
49. Cragg MS, Walshe CA, Ivanov AO, Glennie MJ. The biology of CD20 and its potential as a target for mAb therapy. Curr Direct Autoimmun [Internet]. 2005. p. 140–74. Available from: https://www.karger.com/DOI/10.1159/000082102
50. Nassiri F, Cusimano MD, Scheithauer BW, Rotondo F, Fazio A, Yousef GM, et al. Endoglin (CD105): a review of its role in angiogenesis and tumor diagnosis, progression and therapy. Anticancer Res [Internet]. 2011;31:2283. Available from: http://ar.iiarjournals.org/content/31/6/2283.abstract
51. González Muñoz T, Amaral AT, Puerto-Camacho P, Peinado H, de Álava E. Endoglin in the Spotlight to Treat Cancer. Int J Mol Sci [Internet]. MDPI; 2021; 22:3186. Available from: https://pubmed.ncbi.nlm.nih.gov/33804796

52. Sasaki T, Hiroki K, Yamashita Y. The role of epidermal growth factor receptor in cancer metastasis and microenvironment. In Vigetti D, editors. BioMed Research International [Internet]. Hindawi Publishing Corporation; 2013; 2013:546318. Available from: https://doi.org/10.1155/2013/546318.
53. Cai W-Q, Zeng L-S, Wang L-F, Wang Y-Y, Cheng J-T, Zhang Y, et al. The latest battles between EGFR monoclonal antibodies and resistant tumor cells. Front Oncol [Internet]. 2020;10. Available from: https://www.frontiersin.org/article/10.3389/fonc.2020.01249
54. Sigismund S, Avanzato D, Lanzetti L. Emerging functions of the EGFR in cancer. Mol Oncol [Internet]. 2017/11/27. John Wiley and Sons Inc.; 2018; 12:3–20. Available from: https://pubmed.ncbi.nlm.nih.gov/29124875
55. Imrich S, Hachmeister M, Gires O. EpCAM and its potential role in tumor-initiating cells. Cell Adh Migr [Internet] Landes Bioscience. 2012;6:30–8. Available from: https://pubmed.ncbi.nlm.nih.gov/22647938
56. Sasaki T, Hiroki K, Yamashita Y. The Role of Epidermal Growth Factor Receptor in Cancer Metastasis and Microenvironment. Vigetti D, editor. BioMed Research International [Internet]. Hindawi Publishing Corporation; 2013; 2013:546318. Available from: https://doi.org/10.1155/2013/546318.
57. Harjes U. E-selectin fills two needs for metastasis. Nat Rev Cancer [Internet]. 2019; 19:301. Available from: https://doi.org/10.1038/s41568-019-0151-7.
58. Burdick M, Henson K, Delgadillo L, Choi YE, Goetz D, Tees D, et al. Expression of E-selectin ligands on circulating tumor cells: cross-regulation with cancer stem cell regulatory pathways? Front Oncol [Internet]. 2012;2. Available from: https://www.frontiersin.org/article/10.3389/fonc.2012.00103
59. Simpson-Haidaris PJ, Rybarczyk B. Tumors and fibrinogen. Ann N Y Acad Sci [Internet]. John Wiley & Sons, Ltd; 2001;936:406–25. Available from: https://doi.org/10.1111/j.1749-6632.2001.tb03525.x.
60. Palumbo JS, Kombrinck KW, Drew AF, Grimes TS, Kiser JH, Degen JL, et al. Fibrinogen is an important determinant of the metastatic potential of circulating tumor cells. Blood [Internet]. 2000; 96:3302–9. Available from: https://doi.org/10.1182/blood.V96.10.3302.
61. Adekola K, Rosen ST, Shanmugam M. Glucose transporters in cancer metabolism. Curr Opin Oncol [Internet]. 2012;24:650–4. Available from: https://pubmed.ncbi.nlm.nih.gov/22913968
62. Anan N, Zainon R, Tamal M. A review on advances in 18F-FDG PET/CT radiomics standardisation and application in lung disease management. Insights Imag [Internet]. 2022; 13:22. Available from: https://doi.org/10.1186/s13244-021-01153-9.
63. Mochizuki T, Tsukamoto E, Kuge Y, Kanegae K, Zhao S, Hikosaka K, et al. FDG uptake and glucose transporter subtype expressions in experimental tumor and inflammation models. J Nuclear Med [Internet]. 2001;42:1551. Available from: http://jnm.snmjournals.org/content/42/10/1551.abstract
64. Bergonzini C, Kroese K, Zweemer AJM, Danen EHJ. Targeting integrins for cancer therapy – disappointments and opportunities. Front Cell Develop Biol [Internet]. 2022;10. Available from: https://www.frontiersin.org/article/10.3389/fcell.2022.863850
65. Millard M, Odde S, Neamati N. Integrin targeted therapeutics. Theranostics [Internet], Ivyspring International Publisher; 2011; 1:154–188. Available from: https://pubmed.ncbi.nlm.nih.gov/21547158
66. Fogal V, Zhang L, Krajewski S, Ruoslahti E. Mitochondrial/cell-surface protein p32/gC1qR as a molecular target in tumor cells and tumor stroma. Cancer Res [Internet]. 2008;68:7210–8. Available from: https://pubmed.ncbi.nlm.nih.gov/18757437
67. Fabricius H-Å, Starzonek S, Lange T. The role of platelet cell surface P-selectin for the direct platelet-tumor cell contact during metastasis formation in human tumors. Front Oncol [Internet]. 2021;11. Available from: https://www.frontiersin.org/article/10.3389/fonc.2021.642761
68. Chen M, Geng J-G. P-selectin mediates adhesion of leukocytes, platelets, and cancer cells in inflammation, thrombosis, and cancer growth and metastasis. Archivum Immunologiae

et Therapiae Experimentalis [Internet]. 2006; 54:75–84. Available from: https://doi.org/10.1007/s00005-006-0010-6.
69. Chang SS. Overview of prostate-specific membrane antigen. Rev Urol [Internet]. MedReviews, LLC; 2004;6 Suppl 10: S13–8. Available from: https://pubmed.ncbi.nlm.nih.gov/16985927
70. Xiao C, Fu X, Wang Y, Liu H, Jiang Y, Zhao Z, et al. Transferrin receptor regulates malignancies and the stemness of hepatocellular carcinoma-derived cancer stem-like cells by affecting iron accumulation. PLOS ONE [Internet]. Public Library of Science; 2020;15:e0243812-. Available from: https://doi.org/10.1371/journal.pone.0243812.
71. Shen Y, Li X, Dong D, Zhang B, Xue Y, Shang P. Transferrin receptor 1 in cancer: a new sight for cancer therapy. Am J Cancer Res [Internet]. e-Century Publishing Corporation; 2018;8:916–31. Available from: https://pubmed.ncbi.nlm.nih.gov/30034931
72. Wu T-C. The role of vascular cell adhesion molecule-1 in tumor immune evasion. Cancer Res [Internet]. 2007;67:6003–6. Available from: https://pubmed.ncbi.nlm.nih.gov/17616653
73. Chen Q, Massagué J. Molecular pathways: VCAM-1 as a potential therapeutic target in metastasis. Clin Cancer Res [Internet]. 2012/08/09. 2012;18:5520–5. Available from: https://pubmed.ncbi.nlm.nih.gov/22879387
74. Meadows KL, Hurwitz HI. Anti-VEGF therapies in the clinic. Cold Spring Harb Perspect Med [Internet]. Cold Spring Harbor Laboratory Press; 2012;2: a006577. Available from: https://pubmed.ncbi.nlm.nih.gov/23028128
75. Escalante CP, Zalpour A. Vascular endothelial growth factor inhibitor-induced hypertension: basics for primary care providers. Cardiol Res Pract [Internet]. 2011/05/10. SAGE-Hindawi Access Res; 2011; 2011:816897. Available from: https://pubmed.ncbi.nlm.nih.gov/21629798
76. Chen X. Protein and peptide probes for molecular imaging. Amino Acids [Internet]. 2011;41:1009–12. Available from: https://pubmed.ncbi.nlm.nih.gov/21643775
77. Hu Q, Wang X-Y, Kang L-K, Wei H-M, Xu C-M, Wang T, et al. RGD-targeted ultrasound contrast agent for longitudinal assessment of Hep-2 tumor Angiogenesis in vivo. PLOS ONE [Internet]. Public Library of Science; 2016;11:e0149075. Available from: https://doi.org/10.1371/journal.pone.0149075.
78. Garrigues HJ, Rubinchikova YE, Dipersio CM, Rose TM. Integrin alphaVbeta3 Binds to the RGD motif of glycoprotein B of Kaposi's sarcoma-associated herpesvirus and functions as an RGD-dependent entry receptor. J Virol [Internet]. 2007/11/28. American Society for Microbiology (ASM); 2008; 82:1570–80. Available from: https://pubmed.ncbi.nlm.nih.gov/18045938
79. Lin R-Y, Dayananda K, Chen T-J, Chen C-Y, Liu G-C, Lin K-L, et al. Targeted RGD nanoparticles for highly sensitive in vivo integrin receptor imaging. Contr Media Mol Imaging [Internet]. John Wiley & Sons, Ltd; 2012;7:7–18. Available from: https://doi.org/10.1002/cmmi.457.
80. Park J-A, Lee J-J, Jung J-C, Yu D-Y, Oh C, Ha S, et al. Gd-DOTA conjugate of RGD as a potential tumor-targeting MRI contrast agent. ChemBioChem [Internet]. John Wiley & Sons, Ltd; 2008;9:2811–3. Available from: https://doi.org/10.1002/cbic.200800529.
81. Cheng Z, Wu Y, Xiong Z, Gambhir SS, Chen X. Near-infrared fluorescent RGD peptides for optical imaging of integrin alphavbeta3 expression in living mice. Bioconjug Chem [Internet]. 2005; 16:1433–41. Available from: https://pubmed.ncbi.nlm.nih.gov/16287239
82. Adams KE, Ke S, Kwon S, Liang F, Fan Z, Lu Y, et al. Comparison of visible and near-infrared wavelength-excitable fluorescent dyes for molecular imaging of cancer. J Biomed Optics [Internet]. 2007; 12:1–9. Available from: https://doi.org/10.1117/1.2717137.
83. Dayton PA, Pearson D, Clark J, Simon S, Schumann PA, Zutshi R, et al. Ultrasonic analysis of peptide- and antibody-targeted microbubble contrast agents for molecular imaging of alphavbeta3-expressing cells. Mol Imaging [Internet]. 2004; 3:125–34. Available from: https://pubmed.ncbi.nlm.nih.gov/15296677
84. Hainfeld JF, O'Connor MJ, Dilmanian FA, Slatkin DN, Adams DJ, Smilowitz HM. Micro-CT enables microlocalisation and quantification of Her2-targeted gold nanoparticles within

tumour regions. Br J Radiol [Internet]. 2010/11/16. The British Institute of Radiology.; 2011;84:526–33. Available from: https://pubmed.ncbi.nlm.nih.gov/21081567
85. Dijkers EC, Oude Munnink TH, Kosterink JG, Brouwers AH, Jager PL, de Jong JR, et al. Biodistribution of 89Zr-trastuzumab and PET Imaging of HER2-positive lesions in patients with metastatic breast cancer. Clin Pharmacol Therap [Internet]. John Wiley & Sons, Ltd; 2010;87:586–92. Available from: https://doi.org/10.1038/clpt.2010.12.
86. An F-F, Zhang X-H. Strategies for preparing albumin-based nanoparticles for multifunctional bioimaging and drug delivery. Theranostics [Internet]. Ivyspring International Publisher; 2017; 7:3667–3689. Available from: https://www.thno.org/v07p3667.htm
87. Schmiedl U, Ogan M, Paajanen H, Marotti M, Crooks LE, Brito AC, et al. Albumin labeled with Gd-DTPA as an intravascular, blood pool-enhancing agent for MR imaging: biodistribution and imaging studies. Radiology [Internet]. Radiological Society of North America; 1987; 162:205–10. Available from: https://doi.org/10.1148/radiology.162.1.3786763.
88. Pu F, Qiao J, Xue S, Yang H, Patel A, Wei L, et al. GRPR-targeted protein contrast agents for molecular imaging of receptor expression in cancers by MRI. Scientific Reports [Internet]. 2015; 5:16214. Available from: https://doi.org/10.1038/srep16214.
89. Li S, Jiang J, Zou J, Qiao J, Xue S, Wei L, et al. PEGylation of protein-based MRI contrast agents improves relaxivities and biocompatibilities. J Inorg Biochem [Internet]. 2011/11/19. 2012; 107:111–8. Available from: https://pubmed.ncbi.nlm.nih.gov/22178673
90. Yu S, Wen R, Wang H, Zha Y, Qiu L, Li B, et al. Chitosan-graft-Poly(l-lysine) dendron-assisted facile self-assembly of Au nanoclusters for enhanced X-ray computer tomography imaging and precise MMP-9 plasmid shRNA delivery. Chem Mater [Internet]. American Chemical Society; 2019; 31:3992–4007. Available from: https://doi.org/10.1021/acs.chemmater.9b00507.
91. Cootney RW. Ultrasound imaging: principles and applications in rodent research. ILAR J [Internet]. 2001; 42:233–47. Available from: https://doi.org/10.1093/ilar.42.3.233.
92. Grover VPB, Tognarelli JM, Crossey MME, Cox IJ, Taylor-Robinson SD, McPhail MJW. Magnetic resonance imaging: principles and techniques: lessons for clinicians.. J Clin Exp Hepatol [Internet]. 2015/08/20 Elsevier; 2015; 5:246–255. Available from: https://pubmed.ncbi.nlm.nih.gov/26628842
93. Cormode DP, Naha PC, Fayad ZA. Nanoparticle contrast agents for computed tomography: a focus on micelles. Contrast Media Mol Imaging [Internet]. 2014; 9:37–52. Available from: https://pubmed.ncbi.nlm.nih.gov/24470293
94. Gaikwad HK, Tsvirkun D, Ben-Nun Y, Merquiol E, Popovtzer R, Blum G. Molecular imaging of cancer using X-ray computed tomography with protease targeted iodinated activity-based probes. Nano Letters [Internet]. American Chemical Society; 2018; 18:1582–91. Available from: https://doi.org/10.1021/acs.nanolett.7b03813.
95. Howell JD. Early clinical use of the X-ray. Trans Am Clin Climatol Assoc [Internet]. American Clinical and Climatological Association; 2016; 127:341–349. Available from: https://pubmed.ncbi.nlm.nih.gov/28066069
96. Beyer T, Bidaut L, Dickson J, Kachelriess M, Kiessling F, Leitgeb R, et al. What scans we will read: imaging instrumentation trends in clinical oncology. Cancer Imaging [Internet]. 2020; 20:38. Available from: https://doi.org/10.1186/s40644-020-00312-3.
97. Hainfeld JF, Ridwan SM, Stanishevskiy Y, Smilowitz NR, Davis J, Smilowitz HM. Small, long blood half-life iodine nanoparticle for vascular and tumor imaging. Sci Rep [Internet]. Nature Publishing Group UK; 2018; 8:13803. Available from: https://pubmed.ncbi.nlm.nih.gov/30218059
98. Tsvirkun D, Ben-Nun Y, Merquiol E, Zlotver I, Meir K, Weiss-Sadan T, et al. CT imaging of enzymatic activity in cancer using covalent probes reveal a size-dependent pattern. J Am Chem Soc [Internet]. American Chemical Society; 2018; 140:12010–20. Available from: https://doi.org/10.1021/jacs.8b05817.

99. Hamidi H, Ivaska J. Every step of the way: integrins in cancer progression and metastasis. Nat Rev Cancer [Internet]. 2018;18:533–48. Available from: https://pubmed.ncbi.nlm.nih.gov/30002479
100. Kinsella JM, Jimenez RE, Karmali PP, Rush AM, Kotamraju VR, Gianneschi NC, et al. X-ray computed tomography imaging of breast cancer by using targeted peptide-labeled bismuth sulfide nanoparticles. Angew Chem Int Ed Engl [Internet]. 2011/10/26. 2011; 50:12308–11. Available from: https://pubmed.ncbi.nlm.nih.gov/22028313
101. Miyata S, Kawabata S, Hiramatsu R, Doi A, Ikeda N, Yamashita T, et al. Computed tomography imaging of transferrin targeting liposomes encapsulating both boron and iodine contrast agents by convection-enhanced delivery to F98 Rat Glioma for boron neutron capture therapy. Neurosurgery [Internet]. 2011; 68:1380–7. Available from: https://doi.org/10.1227/NEU.0b013e31820b52aa.
102. Wyss C, Schaefer SC, Juillerat-Jeanneret L, Lagopoulos L, Lehr H-A, Becker CD, et al. Molecular imaging by micro-CT: specific E-selectin imaging. Eur Radiol [Internet]. 2009; 19:2487–94. Available from: https://doi.org/10.1007/s00330-009-1434-2.
103. Popovtzer R, Agrawal A, Kotov NA, Popovtzer A, Balter J, Carey TE, et al. Targeted gold nanoparticles enable molecular CT imaging of cancer. Nano Lett [Internet]. 2008; 8:4593–6. Available from: https://pubmed.ncbi.nlm.nih.gov/19367807
104. Ashton JR, Gottlin EB, Patz Jr EF, West JL, Badea CT. A comparative analysis of EGFR-targeting antibodies for gold nanoparticle CT imaging of lung cancer. PLoS One [Internet]. Public Library of Science; 2018;13:e0206950–e0206950. Available from: https://pubmed.ncbi.nlm.nih.gov/30408128
105. Gessner R, Dayton PA. Advances in molecular imaging with ultrasound. Mol Imaging [Internet]. 2010;9:117–27. Available from: https://pubmed.ncbi.nlm.nih.gov/20487678
106. Unnikrishnan S, Klibanov AL. Microbubbles as ultrasound contrast agents for molecular imaging: preparation and application. Am J Roentgenol [Internet]. American Roentgen Ray Society; 2012; 199:292–9. Available from: https://doi.org/10.2214/AJR.12.8826.
107. van Rooij T, Daeichin V, Skachkov I, de Jong N, Kooiman K. Targeted ultrasound contrast agents for ultrasound molecular imaging and therapy. Interl J Hyperthermia [Internet]. Taylor & Francis; 2015; 31:90–106. Available from: https://doi.org/10.3109/02656736.2014.997809.
108. Yin T, Wang P, Zheng R, Zheng B, Cheng D, Zhang X, et al. Nanobubbles for enhanced ultrasound imaging of tumors. Int J Nanomed [Internet]. 2012/02/22 Dove Medical Press. 2012;7:895–904. Available from: https://pubmed.ncbi.nlm.nih.gov/22393289
109. Otani K, Nishimura H, Kamiya A, Harada-Shiba M. Simplified preparation of αvβ3 integrin-targeted microbubbles based on a clinically available ultrasound contrast agent: validation in a tumor-bearing mouse model. Ultras Med Biol [Internet]. 2018;44:1063–73. Available from: https://www.sciencedirect.com/science/article/pii/S0301562918300413
110. Taylor MR, Couto JR, Scallan CD, Ceriani RL, Peterson JA. Lactadherin (formerly BA46), a membrane-associated glycoprotein expressed in human milk and breast carcinomas, promotes Arg-Gly-Asp (RGD)-dependent cell adhesion. DNA and Cell Biol [Internet]. Mary Ann Liebert, Inc., publishers; 1997;16:861–9. Available from: https://doi.org/10.1089/dna.1997.16.861.
111. Bu H-F, Zuo X-L, Wang X, Ensslin MA, Koti V, Hsueh W, et al. Milk fat globule–EGF factor 8/lactadherin plays a crucial role in maintenance and repair of murine intestinal epithelium. J Clin Investig [Internet]. The American Society for Clinical Investigation; 2007; 117:3673–83. Available from: https://doi.org/10.1172/JCI31841.
112. Yang H, Cai W, Xu L, Lv X, Qiao Y, Li P, et al. Nanobubble–affibody: novel ultrasound contrast agents for targeted molecular ultrasound imaging of tumor. Biomaterials [Internet]. 2015; 37:279–88. Available from: https://www.sciencedirect.com/science/article/pii/S0142961214010606
113. Nair A, Ingram N, Verghese ET, Wijetunga I, Markham AF, Wyatt J, et al. CD105 is a prognostic marker and valid endothelial target for microbubble platforms in cholangiocarcinoma.

Cell Oncol (Dordr) [Internet]. 2020/05/28. Springer Netherlands; 2020; 43:835–845. Available from: https://pubmed.ncbi.nlm.nih.gov/32468445
114. Shan R, Wang B, Wang A, Sun Z, Dong F, Liu J, et al. Endoglin-targeted contrast-enhanced ultrasound imaging in hepatoblastoma xenografts. Oncol Lett [Internet]. 2018/07/04. D.A. Spandidos; 2018; 16:3784–3790. Available from: https://pubmed.ncbi.nlm.nih.gov/30127989
115. Yuan H, Wang W, Wen J, Lin L, Exner AA, Guan P, et al. Dual-targeted microbubbles specific to integrin αVβ3 and vascular endothelial growth factor receptor 2 for ultrasonography evaluation of tumor angiogenesis. Ultras Med Biol [Internet]. Elsevier; 2018; 44:1460–7. Available from: https://doi.org/10.1016/j.ultrasmedbio.2018.03.022.
116. Warram JM, Sorace AG, Saini R, Umphrey HR, Zinn KR, Hoyt K. A triple-targeted ultrasound contrast agent provides improved localization to tumor vasculature. J Ultrasound Med [Internet]. 2011; 30:921–31. Available from: https://pubmed.ncbi.nlm.nih.gov/21705725
117. Pochon S, Tardy I, Bussat P, Bettinger T, Brochot J, von Wronski M, et al. BR55: A lipopeptide-based VEGFR2-targeted ultrasound contrast agent for molecular imaging of angiogenesis. Investig Radiol [Internet]. 2010;45. Available from: https://journals.lww.com/investigativeradiology/Fulltext/2010/02000/BR55__A_Lipopeptide_Based_VEGFR2_Targeted.6.aspx
118. Willmann JK, Bonomo L, Testa AC, Rinaldi P, Rindi G, Valluru KS, et al. Ultrasound molecular imaging with BR55 in patients with breast and ovarian lesions: first-in-human results. J Clin Oncol [Internet]. 2017/03/14. American Society of Clinical Oncology; 2017; 35:2133–40. Available from: https://pubmed.ncbi.nlm.nih.gov/28291391
119. Haris M, Yadav SK, Rizwan A, Singh A, Wang E, Hariharan H, et al. Molecular magnetic resonance imaging in cancer. J Transl Med [Internet]. 2015; 13:313. Available from: https://doi.org/10.1186/s12967-015-0659-x.
120. Lu Z-R. Magnetic resonance molecular imaging for non-invasive precision cancer diagnosis. Curr Opin Biomed Eng [Internet]. 2017/11/16. 2017; 3:67–73. Available from: https://pubmed.ncbi.nlm.nih.gov/30272041
121. Wahsner J, Gale EM, Rodríguez-Rodríguez A, Caravan P. Chemistry of MRI contrast agents: current challenges and new frontiers. Chem Rev [Internet]. 2018/10/16. 2019; 119:957–1057. Available from: https://pubmed.ncbi.nlm.nih.gov/30350585
122. Aryal S, Stigliano C, Key J, Ramirez M, Anderson J, Karmonik C, et al. Paramagnetic Gd3+ labeled red blood cells for magnetic resonance angiography. Biomaterials [Internet]. 2016; 98:163–70. Available from: https://www.sciencedirect.com/science/article/pii/S0142961216301636
123. Barrett T, Kobayashi H, Brechbiel M, Choyke PL. Macromolecular MRI contrast agents for imaging tumor angiogenesis. Eur J Radiol [Internet]. Elsevier; 2006; 60:353–66. Available from: https://doi.org/10.1016/j.ejrad.2006.06.025.
124. Shukla SC, Singh A, Pandey AK, Mishra A. Review on production and medical applications of ε-polylysine. Biochem Eng J [Internet] 2012; 65:70–81. Available from: https://www.sciencedirect.com/science/article/pii/S1369703X1200085X
125. Liu Y, Wu X, Sun X, Wang D, Zhong Y, Jiang D, et al. Design, synthesis, and evaluation of VEGFR-targeted macromolecular MRI contrast agent based on biotin–avidin-specific binding. International Journal of Nanomedicine. Dove Press; 2017; 12:5039.
126. Xue S, Qiao J, Pu F, Cameron M, Yang JJ. Design of a novel class of protein-based magnetic resonance imaging contrast agents for the molecular imaging of cancer biomarkers. Wiley Interdiscip Rev Nanomed Nanobiotechnol [Internet]. 2013/01/17. 2013; 5:163–79. Available from: https://pubmed.ncbi.nlm.nih.gov/23335551
127. Qiao J, Li S, Wei L, Jiang J, Long R, Mao H, et al. HER2 targeted molecular MR imaging using a De Novo designed protein contrast agent. PLOS ONE [Internet]. Public library of science; 2011;6:e18103. Available from: https://doi.org/10.1371/journal.pone.0018103.
128. Pilch J, Brown DM, Komatsu M, Järvinen TAH, Yang M, Peters D, et al. Peptides selected for binding to clotted plasma accumulate in tumor stroma and wounds. Proc Natl Acad Sci U

S A [Internet]. 2006/02/13. National Academy of Sciences; 2006; 103:2800–2804. Available from: https://pubmed.ncbi.nlm.nih.gov/16476999
129. Newman MR, Benoit DSW. In vivo translation of peptide-targeted drug delivery systems discovered by phage display. Bioconjug Chem [Internet]. 2018/06/29. 2018; 29:2161–9. Available from: https://pubmed.ncbi.nlm.nih.gov/29889510
130. Ye F, Jeong E-K, Jia Z, Yang T, Parker D, Lu Z-R. A peptide targeted contrast agent specific to fibrin-fibronectin complexes for cancer molecular imaging with MRI. Bioconjugate Chem [Internet]. American Chemical Society; 2008; 19:2300–3. Available from: https://doi.org/10.1021/bc800211r.
131. Zhou Z, Wu X, Kresak A, Griswold M, Lu Z-R. Peptide targeted tripod macrocyclic Gd(III) chelates for cancer molecular MRI. Biomaterials [Internet]. 2013/07/14. 2013; 34:7683–93. Available from: https://pubmed.ncbi.nlm.nih.gov/23863450
132. Artemov D, Mori N, Okollie B, Bhujwalla Z. MR molecular imaging of the Her-2/neu receptor in breast cancer cells using targeted iron oxide nanoparticles. Magnet Resonan Med. 2003;49:403–8.
133. Chinol M, Casalini P, Maggiolo M, Canevari S, Omodeo ES, Caliceti P, et al. Biochemical modifications of avidin improve pharmacokinetics and biodistribution, and reduce immunogenicity. Br J Cancer [Internet]. 1998;78:189–97. Available from. https://doi.org/10.1038/bjc.1998.463.
134. Cheng W, Ping Y, Zhang Y, Chuang K-H, Liu Y. Magnetic resonance imaging (MRI) contrast agents for tumor diagnosis. J Healthcare Eng [Internet]. Multi Science Publishing; 2013; 4:143865. Available from: https://doi.org/10.1260/2040-2295.4.1.23.
135. Tsourkas A, Shinde-Patil VR, Kelly KA, Patel P, Wolley A, Allport JR, et al. In vivo imaging of activated endothelium using an anti-VCAM-1 magnetooptical probe. Bioconjugate Chem [Internet]. American Chemical Society; 2005; 16:576–81. Available from: https://doi.org/10.1021/bc050002e.
136. Kresse M, Wagner S, Pfefferer D, Lawaczeck R, Elste V, Semmler W. Targeting of ultrasmall superparamagnetic iron oxide (USPIO) particles to tumor cells in vivo by using transferrin receptor pathways. Magnet Reson Med [Internet]. John Wiley & Sons, Ltd; 1998;40:236–42. Available from: https://doi.org/10.1002/mrm.1910400209.
137. Wang Y-XJ, Xuan S, Port M, Idee J-M. Recent advances in superparamagnetic iron oxide nanoparticles for cellular imaging and targeted therapy research. Curr Pharm Des [Internet]. Bentham Science Publishers; 2013; 19:6575–6593. Available from: https://pubmed.ncbi.nlm.nih.gov/23621536
138. van Dort ME, Rehemtulla A, Ross BD. PET and SPECT Imaging of Tumor Biology: New Approaches towards Oncology Drug Discovery and Development. Curr Comput Aided Drug Des [Internet]. 2008; 4:46–53. Available from: https://pubmed.ncbi.nlm.nih.gov/19809593
139. Liu Y, Liu G, Hnatowich DJ. A brief review of chelators for radiolabeling oligomers. Materials [Internet]. MDPI; 2010; 3:3204–3217. Available from: https://www.ncbi.nlm.nih.gov/pmc/articles/PMC5445922/
140. Forte E, Fiorenza D, Torino E, Costagliola di Polidoro A, Cavaliere C, Netti PA, et al. Radiolabeled PET/MRI nanoparticles for tumor imaging. J Clin Med [Internet]. MDPI; 2019; 9:89. Available from: https://pubmed.ncbi.nlm.nih.gov/31905769
141. Hornok V. Serum albumin nanoparticles: problems and prospects. Polymers (Basel) [Internet]. MDPI; 2021; 13:3759. Available from: https://pubmed.ncbi.nlm.nih.gov/34771316
142. Gommans GMM, Gommans E, van der Zant FM, Teule GJJ, van der Schors TG, de Waard JWD. 99mTc Nanocoll: a radiopharmaceutical for sentinel node localisation in breast cancer—In vitro and in vivo results. Appl Radiat Isotopes [Internet]. 2009; 67:1550–8. Available from: https://www.sciencedirect.com/science/article/pii/S0969804309002012
143. Maxwell JE, Howe JR. Imaging in neuroendocrine tumors: an update for the clinician. Int J Endocr Oncol [Internet]. 2015;2:159–68. Available from: https://pubmed.ncbi.nlm.nih.gov/26257863

144. Rizzieri D. Zevalin® (ibritumomab tiuxetan): after more than a decade of treatment experience, what have we learned? Critic Rev Oncol/Hematol [Internet]. 2016;105:5–17. Available from: https://www.sciencedirect.com/science/article/pii/S1040842816301640
145. Taneja SS. ProstaScint(R) scan: contemporary use in clinical practice. Rev Urol [Internet]. MedReviews, LLC; 2004;6 Suppl 10:S19–28. Available from: https://pubmed.ncbi.nlm.nih.gov/16985928
146. Mukherjee S, Ayanambakkam A, Ibrahimi S, Schmidt S, Charkrabarty JH, Khawandanah M. Ibritumomab tiuxetan (Zevalin) and elevated serum human anti-murine antibody (HAMA). Hematol/Oncol Stem Cell Therapy [Internet]. 2018; 11:187–8. Available from: https://www.sciencedirect.com/science/article/pii/S1658387618300050
147. Massicano AVF, Marquez-Nostra BV, Lapi SE. Targeting HER2 in nuclear medicine for imaging and therapy. Mol Imaging [Internet]. SAGE Publications; 2018; 17:1536012117745386. Available from: https://pubmed.ncbi.nlm.nih.gov/29357745
148. Du S, Luo C, Yang G, Gao H, Wang Y, Li X, et al. Developing PEGylated reversed D-peptide as a novel HER2-targeted SPECT imaging probe for breast cancer detection. Bioconjugate Chem [Internet]. American Chemical Society; 2020; 31:1971–80. Available from: https://doi.org/10.1021/acs.bioconjchem.0c00334.
149. Li L, Wu Y, Wang Z, Jia B, Hu Z, Dong C, et al. SPECT/CT imaging of the novel HER2-targeted peptide probe, 99mTc-HYNIC-H6F in breast cancer mouse models. J Nuclear Med [Internet]. 2017; 58:821. Available from: http://jnm.snmjournals.org/content/58/5/821.abstract
150. Sörensen J, Sandberg D, Sandström M, Wennborg A, Feldwisch J, Tolmachev V, et al. First-in-human molecular imaging of HER2 expression in breast cancer metastases using the 111In-ABY-025 affibody molecule. J Nucl Med [Internet]. 2014; 55:730. Available from: http://jnm.snmjournals.org/content/55/5/730.abstract
151. Razumienko EJ, Scollard DA, Reilly RM. Small-animal SPECT/CT of HER2 and HER3 expression in tumor xenografts in athymic mice using trastuzumab Fab–Heregulin bispecific radioimmunoconjugates. J Nuclear Med [Internet]. 2012; 53:1943. Available from: http://jnm.snmjournals.org/content/53/12/1943.abstract
152. Facca VJ, Al-saden N, Ku A, Reilly RM. Imaging of HER2-positive tumors in NOD/SCID mice with Pertuzumab Fab-hexahistidine peptide immunoconjugates labeled with [99mTc]-(I)-Tricarbonyl complex. Mol Imaging Biol [Internet]. 2021; 23:495–504. Available from: https://doi.org/10.1007/s11307-020-01571-z.
153. Li D, Li X, Yang J, Shi Z, Zhang L, Li R, et al. Nivolumab-DTPA-based PD-1 imaging reveals structural and pathological changes in colorectal carcinoma. Front Bioeng Biotechnol [Internet]. 2022;10. Available from: https://www.frontiersin.org/article/10.3389/fbioe.2022.839756
154. Chatterjee S, Lesniak W, Nimmagadda S. Noninvasive imaging of immune checkpoint ligand PD-L1 in tumors and metastases for guiding immunotherapy. Mol Imaging. 2017;16:153601211771845.
155. Jin X, Liang N, Wang M, Meng Y, Jia B, Shi X, et al. Integrin imaging with 99mTc-3PRGD2 SPECT/CT shows high specificity in the diagnosis of lymph node metastasis from non–small cell lung cancer. Radiology [Internet]. Radiological Society of North America; 2016; 281:958–66. Available from: https://doi.org/10.1148/radiol.2016150813.
156. Zhao H, Gao H, Luo C, Yang G, Zhao X, Gao S, et al. An Integrin-αvβ6/α5β1-bitargeted probe for the SPECT imaging of pancreatic adenocarcinoma in preclinical and primary clinical studies. Bioconjugate Chem [Internet]. American Chemical Society; 2021; 32:1298–305. Available from: https://doi.org/10.1021/acs.bioconjchem.1c00296.
157. John AE, Luckett JC, Tatler AL, Awais RO, Desai A, Habgood A, et al. Preclinical SPECT/CT Imaging of αvβ6 integrins for molecular stratification of idiopathic pulmonary fibrosis. J Nuclear Med [Internet]. 2013; 54:2146. Available from: http://jnm.snmjournals.org/content/54/12/2146.abstract

158. Dijkgraaf I, Boerman OC. Molecular imaging of angiogenesis with SPECT. Eur J Nucl Med Mol Imaging [Internet]. Springer-Verlag; 2010;37 Suppl 1:S104–13. Available from: https://pubmed.ncbi.nlm.nih.gov/20617435
159. Rainer E, Wang H, Traub-Weidinger T, Widhalm G, Fueger B, Chang J, et al. The prognostic value of [123I]-vascular endothelial growth factor ([123I]-VEGF) in glioma. Eur J Nuclear Med Mol Imaging [Internet]. 2018; 45:2396–403. Available from: https://doi.org/10.1007/s00259-018-4088-y.
160. Paquette M, Phoenix S, Lawson C, Guérin B, Lecomte R, Tai L-H, et al. A preclinical PET dual-tracer imaging protocol for ER and HER2 phenotyping in breast cancer xenografts. EJNMMI Res [Internet]. 2020; 10:69. Available from: https://doi.org/10.1186/s13550-020-00656-8.
161. Bois F, Noirot C, Dietemann S, Mainta IC, Zilli T, Garibotto V, et al. [(68)Ga]Ga-PSMA-11 in prostate cancer: a comprehensive review. Am J Nucl Med Mol Imaging [Internet]. e-Century Publishing Corporation; 2020; 10:349–74. Available from: https://pubmed.ncbi.nlm.nih.gov/33329937
162. Keam SJ. Piflufolastat F 18: diagnostic first approval. Mol Diag Therapy [Internet]. 2021; 25:647–56. Available from: https://doi.org/10.1007/s40291-021-00548-0.
163. Tamura K, Kurihara H, Yonemori K, Tsuda H, Suzuki J, Kono Y, et al. ^{64}Cu-DOTA-trastuzumab PET imaging in patients with HER2-positive breast cancer. J Nucl Med [Internet]. 2013; 54:1869. Available from: http://jnm.snmjournals.org/content/54/11/1869.abstract
164. Xu Y, Wang L, Pan D, Yu C, Mi B, Huang Q, et al. PET imaging of a (68)Ga labeled modified HER2 affibody in breast cancers: from xenografts to patients. Br J Radiol [Internet]. 2019/10/08. The British Institute of Radiology.; 2019;92:20190425. Available from: https://pubmed.ncbi.nlm.nih.gov/31593482
165. Garousi J, Lindbo S, Nilvebrant J, Åstrand M, Buijs J, Sandström M, et al. ADAPT, a novel scaffold protein-based probe for radionuclide imaging of molecular targets that are expressed in disseminated cancers. Cancer Res [Internet]. 2015; 75:4364–71. Available from: https://doi.org/10.1158/0008-5472.CAN-14-3497.
166. Bensch F, van der Veen EL, Lub-de Hooge MN, Jorritsma-Smit A, Boellaard R, Kok IC, et al. 89Zr-atezolizumab imaging as a non-invasive approach to assess clinical response to PD-L1 blockade in cancer. Nature Med [Internet]. 2018; 24:1852–8. Available from: https://doi.org/10.1038/s41591-018-0255-8.
167. Hellebust A, Richards-Kortum R. Advances in molecular imaging: targeted optical contrast agents for cancer diagnostics. Nanomedicine (Lond) [Internet]. 2012;7:429–45. Available from: https://pubmed.ncbi.nlm.nih.gov/22385200
168. Rosenthal EL, Warram JM, de Boer E, Chung TK, Korb ML, Brandwein-Gensler M, et al. Safety and tumor specificity of cetuximab-IRDye800 for surgical navigation in head and neck cancer. Clin Cancer Res [Internet]. 2015; 21:3658–66. Available from: https://doi.org/10.1158/1078-0432.CCR-14-3284.
169. Amini A, Safdari Y, Tash Shamsabadi F. Near-infrared fluorescence imaging of EGFR-overexpressing tumors in the mouse xenograft model using scFv-IRDye800CW and Cetuximab-IRDye800CW. In Azhdarinia A, editor. Molecular Imaging [Internet]. Hindawi; 2022; 2022:9589820. Available from: https://doi.org/10.1155/2022/9589820.
170. Feroldi F, Verlaan M, Knaus H, Davidoiu V, Vugts DJ, van Dongen GAMS, et al. High resolution combined molecular and structural optical imaging of colorectal cancer in a xenograft mouse model. Biomed Opt Express [Internet]. Optical Society of America; 2018; 9:6186–6204. Available from: https://pubmed.ncbi.nlm.nih.gov/31065422
171. Nitin N, Rosbach KJ, El-Naggar A, Williams M, Gillenwater A, Richards-Kortum RR. Optical molecular imaging of epidermal growth factor receptor expression to improve detection of oral neoplasia. Neoplasia [Internet]. Neoplasia Press Inc.; 2009; 11:542–51. Available from: https://pubmed.ncbi.nlm.nih.gov/19484143
172. Sampath L, Kwon S, Hall MA, Price RE, Sevick-Muraca EM. Detection of cancer metastases with a dual-labeled near-infrared/positron emission tomography imaging agent. Transl Oncol

[Internet]. Neoplasia Press Inc.; 2010; 3:217–307. Available from: https://pubmed.ncbi.nlm.nih.gov/20885893
173. Lamberts LE, Koch M, de Jong JS, Adams ALL, Glatz J, Kranendonk MEG, et al. Tumor-specific uptake of fluorescent Bevacizumab–IRDye800CW microdosing in patients with primary breast cancer: a phase I feasibility study. Clin Cancer Res [Internet]. 2017; 23:2730–41. Available from: https://doi.org/10.1158/1078-0432.CCR-16-0437.
174. Li M, Anastassiades CP, Joshi B, Komarck CM, Piraka C, Elmunzer BJ, et al. Affinity peptide for targeted detection of dysplasia in Barrett's esophagus. Gastroenterology [Internet]. 2010/07/14. 2010; 139:1472–80. Available from: https://pubmed.ncbi.nlm.nih.gov/20637198
175. McHugh KJ, Jing L, Behrens AM, Jayawardena S, Tang W, Gao M, et al. Biocompatible semiconductor quantum dots as cancer imaging agents. Adv Mat [Internet]. John Wiley & Sons, Ltd; 2018;30:1706356. Available from. https://doi.org/10.1002/adma.201706356.
176. Gao X, Cui Y, Levenson R, Chung L, Nie S. In vivo cancer targeting and imaging with semiconductor quantum dots. Nat Biotechnol. 2004;22:969–76.
177. Cai W, Chen K, Li Z-B, Gambhir SS, Chen X. Dual-function probe for PET and near-infrared fluorescence imaging of tumor vasculature. J Nucl Med [Internet]. 2007; 48:1862. Available from: http://jnm.snmjournals.org/content/48/11/1862.abstract
178. Srinivasan R, Marchant RE, Sen Gupta A. In vitro and in vivo platelet targeting by cyclic RGD-modified liposomes. J Biomed Mater Res A [Internet]. 2010; 93:1004–15. Available from: https://pubmed.ncbi.nlm.nih.gov/19743511
179. Tansi FL, Rüger R, Kollmeier AM, Rabenhold M, Steiniger F, Kontermann RE, et al. Endoglin based in vivo near-infrared fluorescence imaging of tumor models in mice using activatable liposomes. Biochimica et Biophysica Acta (BBA) General Subjects [Internet]. 2018; 1862:1389–400. Available from: https://www.sciencedirect.com/science/article/pii/S0304416518300746

Therapeutic Uses of TheraCour™ Polymeric Nanomicelles Against Cancer, Infectious Diseases, and More

Anil Diwan, Jayant Tatake, and Ashok Chakraborty

1 Introduction

Recent advances in nanotechnology and biotechnology have contributed to the development of engineered nanoscale materials as innovative prototypes to be used for biomedical applications and optimized therapy. Due to their unique features, including a large surface area, structural properties, and a long circulation time in blood compared with small molecules, a plethora of nanomaterials has been developed, with the potential to revolutionize the diagnosis and treatment of several diseases, in particular, by improving the sensitivity and recognition ability of imaging contrast agents and/or by selectively directing bioactive agents to biological targets.

Typically, cancer therapies involve the systemic or oral administration of drugs into the body, both of which routes can damage healthy tissues by significant off-target accumulation and thereby generate serious side effects. Further, the off-target accumulation limits the dosage that can be administered. To overcome these limitations, various targeting strategies are being investigated.

A. Diwan
AllExcel, Inc, Shelton, CT, USA

NanoViricides, Inc, Shelton, CT, USA

Karveer Medi-tech, Pvt. Ltd, Kolhapur, Maharashtra, India
e-mail: anil.diwan@allexcel.com; adiwan@nanoviricides.com

J. Tatake
AllExcel, Inc, Shelton, CT, USA

NanoViricides, Inc, Shelton, CT, USA

A. Chakraborty (✉)
AllExcel, Inc, Shelton, CT, USA
e-mail: ashok.chakraborty@allexcel.com

R. S. Chaughule et al. (eds.), *Nanomaterials for Cancer Detection Using Imaging Techniques and Their Clinical Applications*,
https://doi.org/10.1007/978-3-031-09636-5_17

An extensively investigated polymer is poly(lactic-co-glycolic acid) (PLGA), a synthetic thermoplastic aliphatic biocompatible polyester. There are specific formulations based on PLGA and its related homopolymers, poly(lactic acid) (PLA) and poly(glycolic acid) (PGA), which are considered safe, and a few biodegradable polymer products have been approved by the US Food and Drug Administration (FDA) as well as by the European Medicines Agency (EMA) for pharmaceutical application [1]. Generally, PLA, PGA, or PLGA polymers in different forms and shapes are used for creating "nanocapsules" of chemotherapeutics (i.e., essentially solid-form drug depots at nanoscale) which is akin to using hand grenades (nanocapsules) in place of bullets (the small chemical drug as is). While they provide protection from stomach acid, enabling drug delivery further downstream in the gastrointestinal tract, they generally lack the specificity of receptor targeting, and if not properly formulated, can even increase the risk of localized side effects (just as hand grenades cause stronger collateral damage compared to bullets) [2].

2 Addressed Targeting

Targeting of specific overexpressed receptors by an enveloping nanostructure for the purpose of delivering a cargo of chemotherapeutics into cancer cells can reduce the risk of off-target effects. Nanostructures most used for accomplishing this effect have been liposomes, lipid nanoparticles, and their pegylated versions, dendrimers, and others, although certain classes of polymeric micelles may offer unique advantages as discussed further below. This is referred to as address-based targeting to distinguish it from specific enzyme inhibitors that have been generally described as targeted therapy in the cancer field (e.g., kinase inhibitors, PARP inhibitors, DNA methylation and histone acetylation modifiers, etc.).

Addressed targeting can be accomplished using antibodies, natural ligands, natural ligand mimetics, specific peptides, as well as small chemical ligands often derived from structure-based drug design.

2.1 Addressed Targeting by Monoclonal Antibodies

- Monoclonal antibodies have for several years been the preferred class of targeting ligands, primarily because of the ease of obtaining and optimizing them using medium- to high-throughput screening. Once an effective antibody is found, molecularly engineered monoclonal antibodies can be derived, preferably those capable of evading the clearance immune system, and have been widely used in the development of targeted nanoparticles.
- PEGylation (covalent attachment of PEG chains, typically methoxy-PEG, mPEG) has been used to minimize reticuloendothelial clearance extending the half-life as well as minimizing immunogenicity and allergenicity. It has been

found that antibodies to mPEG can be generated in patients, limiting usefulness. It was also found that native PEG or hydroxyl-PEG is not immunogenic or substantially less immunogenic than mPEG [3]. The current development of monoclonal antibodies has led to chimeric and humanized derivatives to enable modulation of their immunogenicity. Specific sequence engineering has become possible with advances in molecular bioengineering technology.

- Specifically, a change in the Fc region that enables superior adsorption onto Fc-R-bearing cells has been found to increase the half-life of antibodies substantially, enabling infrequent dosing (monthly or even less) in some diseases such as for modulating human immune response [4]. As an example, sotrovimab, an antibody against the S-antigen of the SARS-CoV-2 virus, was engineered using this modification to enable a long half-life [5].

The ability of engineered monoclonal antibodies to target and interfere with cellular processes has been demonstrated by the success of several monoclonal antibody therapeutics [6, 7]. For example, antibodies such as rituximab or trastuzumab conjugated to PLA nanoparticles show a significant increase in the rate of particle uptake compared with their non-targeted counterparts [8].

However, despite the intense efforts undertaken for their development, monoclonal antibodies still have a number of limitations. Their large size puts limits on the maximum amount of cargo and minimum amount of the nanostructure, except in the case of radio-isotopically tagged antibodies. The overall structure imposes difficulty in managing nanoparticle scale-up and manufacturing. Their potentially immunogenic characteristics, resulting in rapid nanoparticle clearance, require extensive optimization through molecular engineering technologies. Due to these problems in using monoclonal antibodies, there is increasing interest in engineering and using antibody fragments as targeting molecules to retain the high antigen-binding specificity of the parent antibodies, but with reduced immunogenicity and a smaller size improving molecular targeting. These approaches include the Fab fragments, single-chain variable fragments (scFv), mini bodies, diabodies, and nanobodies [9, 10].

2.2 Addressed Targeting by Aptamers and Dendrimers

Aptamers are small, single-stranded RNA or DNA sequences of oligonucleotides that can be designed as ligands capable of binding to targets with high sensitivity and specificity [11, 12]. They are small in size (usually approximately 15 kDa), and have less immunogenicity with respect to monoclonal antibodies or other macromolecules, leading to better stability and biodistribution [13, 14].

Such biomolecules fold by intramolecular interactions into unique three-dimensional conformations and topologies, thereby presenting the ligand-binding characteristics needed for efficient target (receptor/antigen) affinity. Selective aptamers, with binding affinity toward a specific target, are currently being

identified by an in vitro chemical process known as "systemic evolution of ligands by exponential enrichment" (SELEX) [15]. In this process, which is proposed to be scalable at a relatively low cost, a library of ten random oligonucleotides is enriched in order to identify the prototype with the highest affinity and specificity.

Using this technology, Langer and Farokhzad designed and developed customized controlled-release nanoparticles loaded with docetaxel and having tumor-targeting capability toward prostate-specific membrane antigen (PSMA) [16–20]. Targeted nanoparticles have been obtained by decorating their shell surface with RNA A10-aptamer to bind PSMA [21–23], a clinically validated tumor marker that is not only overexpressed on the surface of prostate cancers but also on the neovasculature of many solid tumors. This approach constituted the proof of principle for the development of the first targeted polymeric nanoformulation, BIND-014, which had a PLGA hydrophobic core nanocapsule holding docetaxel, with mPEG hydrophilic surface tails, and a dipeptide targeting PSMA instead of the aptamer. It failed in clinical trials, after showing some success in early clinical trials. Other similarly designed drugs, called "Accurins," by BIND Therapeutics also did not meet anticipated milestones. These failures led to a bankruptcy filing by BIND and its subsequent acquisition by Pfizer in 2016. It would be important to learn from such failures, as what was the root cause, whether specificity, immunogenicity, insufficient drug content, manufacturing difficulties, clinical trial designs, other issues, or a combination of issues resulted in the failure of the hypothesis. However, we have not been able to find such an analysis.

Dendrimers are another class of polymers that have been applied to nanomedicine. They are versatile and biocompatible macromolecules that are characterized by a three-dimensional branch structure [24, 25]. Their multiple functional groups on the surface enhance the capability of loading and delivering therapeutic agents. Starpharma has developed some dendrimer-based antiviral drugs that are in use in condoms for the prevention of HIV transmission [26]. In general, dendrimers, while reasonably simple and scalable for manufacturing, have not resulted in many approved drug products. This can be traced to their inherent immunogenicity. Several approaches have been tried for reducing their immunogenicity, generally involving imitation of the secondary amines, but the tertiary amines and potentially some quaternary amines as well as entrapped surfactants resulting from the chemistry and manufacture remain problematic leading to rapid clearance and immunogenicity issues.

2.3 Addressed Targeting by Proteins and Peptide-Based Targeting Molecules

Several endogenous proteins capable of selectively binding to specific receptors on membrane cells can be used for targeting purposes via receptor-mediated endocytosis [27]. For example, transferrin, an iron-transporting protein that binds specifically

to transferrin receptors (TfR) located on the cell surface and overexpressed in many cancers, has been used to transport nanoparticles into different types of cells [27, 28]. However, their effectiveness for targeting purposes may be limited by their immunogenicity and susceptibility to early clearance.

- The target receptors for these proteins are also commonly expressed on various types of non-targeted cells, which can lead to unwanted off-target effects.
- Peptide-based ligands are emerging as attractive alternative targeting molecules due to their small size, engineered high stability, and relatively low immunogenicity as compared with corresponding proteins.
- Identification of specific targeting peptide ligands has usually derived from previously or newly focused peptide phage/bacterial/plasmid peptide display libraries, as well as the use of newer and easier screening technologies [29].

2.4 Addressed Targeting by Small Molecules

Like monoclonal antibodies and aptamers, peptides can be designed to bind specifically to several molecular targets with a high degree of affinity, and provide ease of manufacture by covalent conjugation to polymers, lipids, and various nanoparticle surfaces [30, 31].

Small molecules, usually defined as low molecular weight organic molecules with a molecular weight of 200–800 Da, constitute a promising class of targeting molecules because of their small size, high stability, chemical management, and low production cost [32–34].

Some further advantages of small molecules as targeting ligands include:

- Availability of suitable facile coupling chemical methods for their conjugation
- The possibility to modulate ligand densities and charge on nanoparticle surfaces, since these parameters can affect stability, size, and morphology, as well as targeting efficiency
- Availability of a wide range of targeting ligands with variable physicochemical properties and a variety of functional groups
- Fewer immunogenic effects in vivo
- Reproducibility, scalability, and economical manufacturing

Among the large number of small molecules identified as potential targeting ligands, folic acid has been one of the most extensively studied and used ligands in targeted drug delivery [34, 35]. Due to its high affinity for folate receptors, which are overexpressed in many types of tumor cells, the vitamin folate has also been used to deliver drug conjugates and many drug delivery systems (i.e., liposomes, polymeric nanoparticles, dendrimers) to selectively accumulate drugs into cancer cells via folate receptor-mediated endocytosis [36].

Pomper et al. have previously identified small hydrophilic molecules from a series of urea-based PSMA inhibitors as novel diagnostic agents capable of

targeting the PSMA receptor in prostate cancer cells with affinity and specificity similar to that of antibodies and aptamers [37–39].

Interestingly, a small molecule belonging to this class of molecules, i.e., the pseudomimetic dipeptide 2-{[(5-amino-1-carboxypentyl)carbamoyl]amino}pentanedioic acid [32], already used by Sechi et al. for development of (−)-epigallocatechin-3-gallate-loaded PSMA-targeted nanoparticles [40] and by Chandran et al. for preparation of docetaxel-PLA/PCL-based targeted nanoparticles was also used as a targeting ligand in the development of BIND-014 discussed earlier [41, 42].

Concerning other small molecules that could be used as targeting ligands, carbohydrates, i.e., sugar-based compounds, have also gained attention due to their low molecular weight, high availability and biocompatibility, and ease of production due to advances in carbohydrate chemistry. Several of these carbohydrate ligands target membrane carbohydrate-binding proteins (membrane lectins) that are differentially expressed on the cellular and intracellular membranes, and some carbohydrates, such as mannose, glucose, galactose, and their derivatives, have been considered as potential ligands for carriers in cell-selective drug delivery [43, 44]. The efforts toward clinical translation of the above-described technologies have ushered in a new era in the development of innovative therapeutic nanoparticles that are capable of targeting and controlled release, also considering the possibility of co-delivery of multiple active agents.

3 Clinical Development of Nanovehicles for Address-Targeted Therapies

To date, only three address-targeted liposomes and four targeted polymeric nanoparticles appear to have progressed in clinical development. The prototype that reach clinical trials was MCC-465, a new generation of liposome-encapsulated doxorubicin with a surface covered by both PEG and antigen-binding fragments [F(ab')2] to confer immune shielding and targeting, respectively, which is used in the treatment of human stomach cancer [45].

Another site-directed liposome is SGT53-01, a TfR-functionalized nanoformulation containing a chain antibody fragment (TfRscFv) as the targeting ligand. It has been designed to carry the p53 tumor suppressor gene to cancer cells and is currently undergoing Phase I clinical trials in combination with doxorubicin for the treatment of solid tumors [46, 47].

3.1 Liposomes and Polymeric Drug-Releasing Nanoformulations in Clinical Development

Despite the progress made in the clinical development of liposome-based nanocarriers, there are several issues that limit their wider consideration as a main drug delivery platform, including the difficulty in modulating their drug release in vivo, the limited amount of drug that can be loaded, possible oxidation of liposomal phospholipids, and the inherent instability of liposomes.

In contrast, polymeric nanocarriers demonstrate superior stability in vivo as compared to liposomes, provide a high drug-loading capacity, and enable both controlled and triggered release of drugs. Therefore, polymer-based nanomaterials have the potential to provide solutions for a range of problems in nanomedicine [32, 33, 48–50]. The way forward for the clinical translation of controlled-release polymeric nanoparticles was paved by the seminal work of Langer and Folkman in 1976 [51], which demonstrated the controlled release of macromolecules from biodegradable polymers in a temporal manner. Moreover, a landmark paper by Langer et al. in 1994 provided further evidence that di-block copolymers of biocompatible polymers with PEG can dramatically increase the controlled release and circulation half-life of polymeric nanoparticles [52].

In the field of breast and prostate cancer, the application of liposomes has been increasingly common [53–55]. Multiple paclitaxel liposomes have been demonstrated to have higher antitumor efficiency and improved bioavailability compared to free paclitaxel [56]. Liposomal doxorubicin has been proven to reduce cardiotoxicity and has comparable efficacy in breast cancer [57, 58]. Doxil, a pegylated form of liposomal doxorubicin, was the first such drug approved for cancer treatment, leading to an explosion of research and development in this field. Furthermore, liposome-based nanosystems have also offered an option for delivering drug combinations, which can enhance the therapeutic effect [59, 60], and even reverse the drug resistance [61]. Nowadays, many liposome-based drugs have entered into clinical use for cancer treatment [62].

Polymer-based nanoparticles (NPs) are another type of NP with specific structural arrangements for drug delivery formed by different monomers [63]. All polymeric nanopharmaceuticals benefit from the “enhanced permeability and retention (EPR)” effect. Briefly, as tumors grow, new blood vessels are formed to provide oxygen and nutrients to the growing tumor (neo-angiogenesis) that are more porous than normal blood vessels and allow cross-passage by large polymeric nanopharmaceuticals from the blood into the tumor space. The polymeric nanoparticles can be designed to be small enough to enter the cancer cell, but are too large to then be shuttled out by the tumor cell’s transport pumps. They can then disintegrate over time while dynamically releasing the active drug payload within the tumor cell.

Research on nanotechnology and paclitaxel (PTX) nanoformulations has enhanced the medical outcome of chemotherapy and cancer [64]. Paclitaxel is a highly effective anti-tubulin chemotherapeutic agent, which is widely employed for the treatment of numerous malignancies. Nanomedicine forms of PTX have been

developed both by compounding PTX into polymers and by conjugation to polymers. The objective is to improve bioavailability and reduce the incidence of adverse effects. Many natural and synthetic polymers have been used for PTX nanoencapsulation, including PLGA NPs, PLA NPs, chitosan NPs, and polymeric micelles [64]. The in vivo tumor inhibitory activity of paclitaxel-loaded PLGA nanoparticles was markedly better in transplanted liver tumors [65]. In the live small animals, laser confocal scanning microscopy and fluorescence imaging showed the location of the fluorescence-labeled paclitaxel-A10-3.2-PLGA and nanobubbles.

Opaxio (Paclitaxel polyglumex, Xyotax, CT-2103, Cell Therapeutics) is a covalent conjugate of PTX to poly-L-glutamic acid that has gone through multiple clinical trials for the treatment of a variety of cancers including prostate, breast, ovarian, colorectal, and lung cancers [66]. The drug was shown to concentrate at tumor sites due to the EPR effect. In clinical trials, it failed to meet the primary endpoint of improved survival, although side effects were significantly reduced compared to the standard control arm therapy models. Its development appears to have been stopped.

Focusing on one of the first clinically tested targeted nanomedicines, a major effort went into the development of BIND-014 [42], a new docetaxel formulation developed by a team led by Langer and Farokhzad at the Massachusetts Institute of Technology, Harvard Medical School, and BIND Therapeutics, as a programmable nanomedicine that entered Phase II clinical testing for the treatment of patients with solid tumors (approved for breast cancer, head and neck cancer, and gastric cancer).

With regard to targeted polymeric nanoformulations, CALAA-01 was the first nanotherapeutic to reach clinical development for siRNA delivery in 2008 [67]. This nanosystem consists of TfR-targeted cyclodextrin-based PEGylated nanoparticles containing siRNA, and is capable of reducing the expression of the M2 subunit of ribonucleotide reductase. The safety of CALAA-01 was evaluated in Phase I clinical trial by intravenous administration to adults with solid tumors refractory to standard of care therapies [68].

Several systems to provide address-targeted therapy of this type have been designed and have undergone testing. Micelles and liposomes offer another option for the delivery of chemotherapeutic agents. Micelles, in particular, provide an important tool to make aqueous-insoluble drugs soluble due to their hydrophobic core and hydrophilic shell. If the micelle's surface is further PEGylated, it increases the ability of the nanocarriers to get through the fenestrated vasculature of tumors and inflamed tissue through passive transport, thus resulting in higher drug concentration in tumors. As of now, several polymeric micelles containing anticancer drugs, NK012, NK105, NK911, NC-6004, and SP1049C are in clinical trials [69], and one such system, Genexol-PM (paclitaxel), is approved for breast cancer patients [70].

3.2 Preclinical and Clinical Investigations of Nanoparticles

- *Taxanes*, paclitaxel, and docetaxel are cornerstones in the treatment of breast cancer and several other solid tumors [71–74]. They are highly potent anticancer drugs [75], but because of their low aqueous solubility, they require special formulations to enable parenteral administration.
- *Abraxane (ABI-007)* is a cremophor-free nanoparticulate albumin-bound paclitaxel (nab-paclitaxel), which was developed by VivoRx-Abraxis Bioscience, later acquired by Celgene, using Celgene's proprietary nanoparticle albumin-bound (nab) technology platform. Abraxane combines paclitaxel with a naturally occurring human albumin protein and exploits endogenous albumin transport pathways, resulting in enhanced transport across endothelial cells. The transcytosis of nab-paclitaxel is facilitated by its binding to the gp60 receptor and caveolar transport. In the interstitium, nab-paclitaxel binds to the secreted protein acidic and rich in cysteine (SPARC), which is overexpressed in the majority of solid tumors, thus achieving enhanced drug targeting and penetration in tumors.

Abraxane delivers 49% more paclitaxel to tumors as compared to solvent-based paclitaxel formulations (Taxol, Cremophore™-Ethanol formulation of Paclitaxel, Bristol-Myers-Squibb) and eliminates solvent-mediated toxicities, such as hypersensitivity reactions [76]. Abraxane has been approved in 41 countries, including the USA, Canada, the European Union, and Japan as a first-line treatment for metastatic breast cancer.

- *BIND-014* is a PEGylated polylactic acid nanoparticle-containing docetaxel conjugated with a small-molecule targeting prostate-specific membrane antigen (PSMA) for prostate cancer. This preparation allows the gradual release of docetaxel upon degradation of the polylactic acid, and the presence of surface PEG enables its escape from the host's immune response, while the PSMA ligand restricts the cytotoxic effect to PSMA-expressing cells [21, 77]. Preclinical studies showed pharmacokinetic properties of BIND-014 that were markedly different from those of standard solvent-based docetaxel. It exhibited a higher peak concentration (Cmax), a greater area under the curve (AUC), and a lower volume of distribution and clearance, indicating that BIND-014 is retained in the plasma compartment and releases docetaxel at a slow and controlled rate [78]. Administration of BIND-014 to animals bearing tumor xenografts was found to result in higher intra-tumoral docetaxel concentrations and increased antitumor activity as compared to free docetaxel [78]. In Phase I clinical studies, BIND-014 was reported to be well-tolerated as compared to conventional docetaxel (Von Hoff et al., 2016), which led to a Phase II study called iNSITE 1 (investigation of Sacroiliac Fusion Treatment) in patients with metastatic castration-resistant prostate cancer [79]. In this Phase II study, BIND-014 demonstrated a 52.5% 6-week disease control rate for the intention-to-treat population and 70% in the per-protocol population, which marginally exceeded the trial target rate of 65% [80].

However, a second study (iNSITE 2) in patients with cervical and head and neck cancers reported poor performance of BIND-014 in reaching study goals. Based on these results and the lack of resources to develop and further test this technology, clinical trials were aborted and BIND Therapeutics filed for bankruptcy in 2016.

- *Livatag®* is a nanoparticulate doxorubicin formulation developed by Onxeo (Paris, France). The drug is encapsulated within 100–200 nm nanoparticles composed of polyalkylcyanoacrylate, cyclodextrin, and poloxamer (doxorubicin Transdrug), and these were presented as ultra-dispersed colloidal systems for the treatment of primary liver cancer. The success of Livatag depended on its efficacy to treat cancer cells that had become resistant to chemotherapy, with an assumption that the nanoparticle formulation would prevent the rejection of doxorubicin out of the cell. Although doxorubicin is commonly used for the intrahepatic arterial delivery of chemotherapy for hepatocellular carcinoma [81], free doxorubicin is associated with high morbidity, and its efficacy in tumor regression and overall survival is poor [82]. Initial studies with Livatag showed that it generated a 12-fold increase in drug exposure within the hepatic tumor tissue as compared to free doxorubicin, without increasing the drug's exposure in the heart or other vital organs [83]. Nanoparticles were taken up by the liver after only a few minutes, and this approach appeared to avoid the drug resistance mediated by the rapid efflux of free drug [83]. However, Livatag's clinical trial showed frequent and severe adverse pulmonary events; at the same time, its efficacy was in the same range as that achieved by other existing drugs. Moreover, the trial found no dose-dependent differences between the two Livatag arms, and it failed to meet the primary endpoint in a Phase III trial in adult patients with unresectable hepatocellular carcinoma. Based on these observations, further development of Livatag was stopped [84].

Cerulean acquired the intellectual property assets of Insert Therapeutics, which had developed a unique nano-drug delivery platform that can deliver drugs that target tumors by taking advantage of the abnormally large pores associated with tumor blood vessels (the EPR effect). Cerulean's lead product candidate was CRLX101 (formerly known as IT-101). IT-101 is a linear polymer of a monomer unit comprising cyclodextrin pendants attached to PEG, with the cancer drug payload camptothecin covalently attached to the polymer. Cerulean also had another drug candidate, in which docetaxel was the anticancer payload in the same nanocarrier system. Cerulean also developed an RNA delivery program that has produced a variety of RNA-containing nanopharmaceuticals that have shown strong potential in addressing some of the challenges associated with RNA administration. CRLX101 failed to meet the primary endpoint in multiple anticancer clinical trials and performed worse than the standard of care control arms. Its development was stopped, with Cerulean serving as a shell vehicle for Dare Bio to become a publicly traded company. Companies such as RNAi drug developer [Dicerna Pharmaceuticals] have developed their own nanoparticle delivery systems.

There have been a consistently far greater number of failures than successes in anticancer drug development based on various hypotheses for designing

nanomedicine systems. The reasons for this are many. Firstly, cancer is a heterogeneous disease with multiple causes, multiple effectors, and multiple presentations that enables generating a large number of therapeutic hypotheses from a scientific perspective. Secondly, animal models of cancer are extremely limited in their utility for predicting human clinical results. Thirdly, the plethora of design options presented by nanomedicine approaches does not by itself enable optimal choice of design options. Further, the manufacturing and characterization of such complex nanomedicine systems is a daunting challenge. Finally, clinical trial design in the cancer space to obtain meaningful results is as yet an art rather than science, no matter how scientifically we attempt to speak of it.

Thus, the development of effective nanomedicines and fulfillment of the promise of nanomedicines is going to require efforts in many dimensions that are just being peeked into at present. With abundant failures and few successes, it would be helpful if a comparative study of multiple approaches along with a number of dimensions – design, manufacture, quality control, hypothesis validity, preclinical development, safety/toxicology, PK/PD, clinical trials designs, and finally clinical vs. preclinical results – can be made. However, consistent datasets for performing such reviews are currently not feasible. Part of the reason is that publication is generally made of successful results; failures go into press releases but are not critically dissected in scientific literature. Another part is that often clinical failure leads to the failure of the sponsor company, leaving no competent scientists to do such "post-mortem" work for presenting the results. An important part is that confidentiality of such information becomes critical from legal and intellectual property perspectives. Thus, there are many barriers to learning from both failures and successes of nanomedicines.

We took a different track and approached the nanomedicine design problem not from the perspective of what material is available but what material needs to be there for successful design, manufacture, quality control, safety/toxicology, and PK/PD considerations, resulting in the development of the TheraCour™ polymeric materials.

4 TheraCour Polymeric Micelle Approach for Anticancer Regimen

TheraCour platform polymer is a self-assembling, uniform, tailorable linear homopolymer that comprises polyethylene glycol (PEG) within its monomer unit which is heterochemically functionalized with a specially designed linker unit so that covalently connected aliphatic chains are suspended from it and separately site-targeting ligands are also covalently attached to it [85–87] (Fig. 1).

This simple scheme results in a polymer that is like a half-biological membrane. In aqueous systems, it self-assembles into micelles with hydrophobic, flexible core

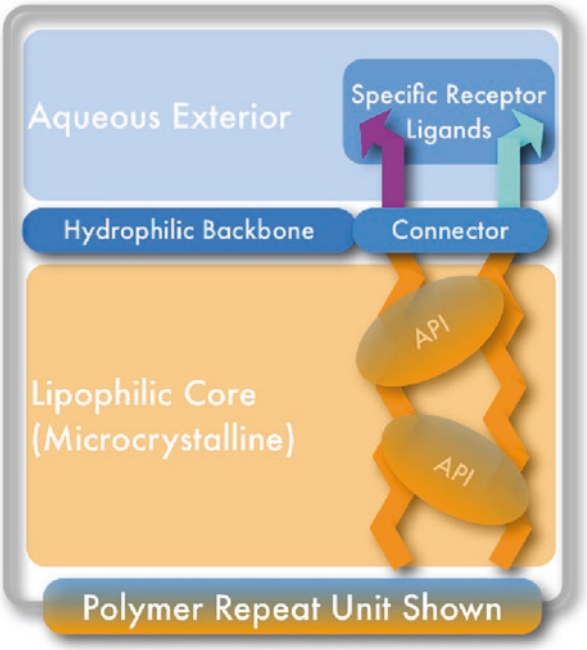

Fig. 1 Schematic design of TheraCour biopolymer

region made of the lipid chains, hydrophilic ligands directing outward into the aqueous milieu ready to seek their partners, connected together by the corona of PEG.

Upon binding of the TheraCour polymeric micelle to a cellular receptor sought out by the ligand, multiple interactions with cellular receptors can take place resulting in increased avidity, due to the regular presentation of ligand at each monomer unit. This forces the corona close to the cell membrane and may initiate lipid-mixing of the flexible pendant interior lipid chains of the micelle with the flexible lipids of the cell membrane, leading to passive fusion. Alternatively, receptor-mediated endocytosis can take place at properly chosen receptors. These processes would result in site-specified or address-targeted delivery of the encapsulated drug payload content of the micelle. As encapsulated rather than covalently immobilized, the drug payload can immediately go to work and does not have the latency of the need to be released from the polymer backbone in a covalent system.

The TheraCour approach solves important problems in the entire drug use chain (Table 1) and has superior features by design to most other nanomedicine technologies (Table 2).

The graphical model of anticancer mechanism of TheraCour platform technology is shown in Fig. 2.

This polymer can effectively encapsulate many types of chemotherapeutic APIs, target the cancer cell based on the selected ligand, and thereby result in effective anticancer activity

Table 1 TheraCour approaches solves problems in the entire drug use chain

Vehicle	Administer	Blood Stream	Specific Targeting	Cell Membrane
TheraCour	Injection	Encapsulated	"Nano Velcro Snaking"	Take API Across
Liposomes	Infusion	Unstable	Not Much Success	Partial Effect
Cremophore	Infusion	Unstable	None	Some Effect?
Cydex	Infusion	Fall Apart	None	None
PEGylation	Infusion	Stable	None	None
Polydrug	Injection	Stable	None	Depends
Polypeptides	Infusion/Injection	Stable	None	None
Dendrimers	Infusion/Injection	Toxic	Hard Sphere Few Points	May Take API Across

Table 2 TheraCour approach presents unique beneficial features by design compared to other nanomedicine approaches

Vehicle	TheraCour	Dendrimer	PLA/PLGA	Virus-Based	Nano-shells, Mettalics
Nano-Scale Velcro Effect with Wrap-On	Yes	No	No	No	No
Technology Complexity	Simple	Complex	Medium	Complex	Complex
Safety	Safe	No	Medium	No	Medium
Specific Targeting	Yes: Flexible Wrap-On	Yes: Limited by Hard Bal	No	No	May be
Detection	Yes	Yes	No	No	May be
Extended Release	Yes	May be	Yes	Yes	Accumulate
Controlled Release	Yes	May be	Yes	No	No
Efficacy Improvements	Yes, Very Large	Yes	No (Slow Release Only)	Yes but infectious	May be

Figure 3 shows the cell proliferation data of two lung cancer cell lines (A549 and H441), and two breast cancer cell lines (SKBR3 and BT474), in the presence of an untargeted TheraCour polymer (i.e., no ligand), a targeted TheraCour polymer (in this case, folate), with or without encapsulated API (camptothecin, CPT).

The enhancement in effectiveness of folate-targeted TheraCour-encapsulated delivery of camptothecin over that of CPT by itself in these cell culture studies is significant, enabling 75–90% inhibition at nontoxic concentrations of the drug, wherein CPT alone reached less than 20% inhibition, in three of the cancer cell lines; such high levels of inhibition are hardly ever reached with no cytotoxicity

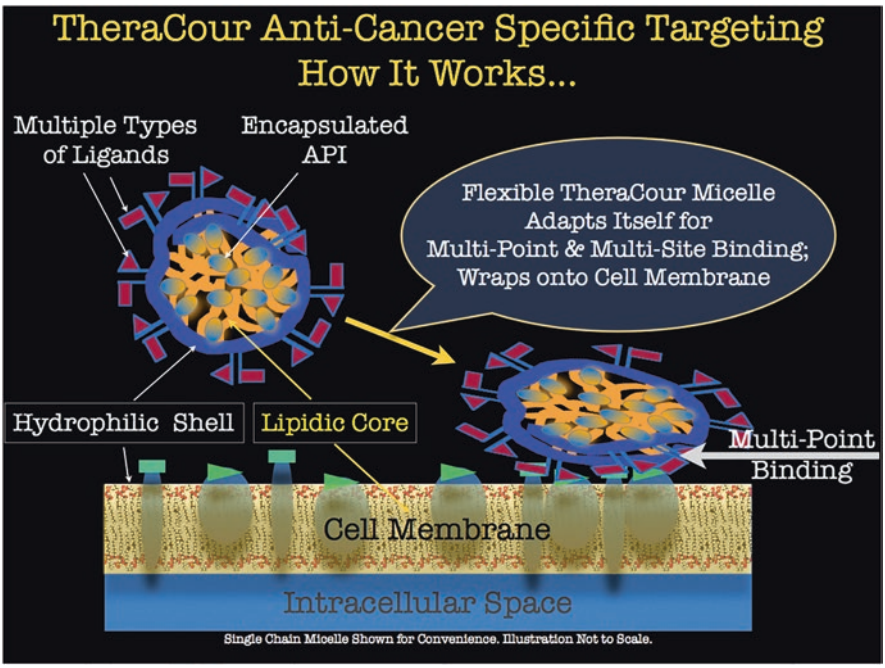

Fig. 2 Graphical representation of TheraCour anticancer mechanisms of specific targeting

without the nanomedicine construct. The exception was that the folate-TheraCour-CPT drug showed 20% inhibition in multidrug-resistant breast cancer cell line BT474, which was still 10X greater than that from CPT alone. These highly promising results need to be taken further into animal model studies and, if confirmed, then into full-fledged drug development.

The TheraCour platform provides an extremely wide range of tolerability: (A) Of course, different ligands can be chosen to attack correspondingly different targets. (B) The hydrophobic/hydrophilic balance can be beneficially and systematically altered by choosing appropriate lipid length, and balancing PEG-monomer chain length. Increasing the lipid chain length can result in a more hydrophobic polymer that would form more stable and larger micelles, and would be more suitable for dermal topical delivery as a cream or as an ointment formulation. In contrast, very short lipid chains would make a water-soluble yet micelle-forming polymer wherein the targeting ligand itself behaves as a polymer-conjugated drug, and the short lipid chains merely assist in conformational stability and adherence to cell membrane once attachment takes place, albeit with diminished encapsulated API cargo capacity. A medium between these illustrations would be well suited for drug delivery as an injectable drug. Thus, the final usage (route of administration) informs the design itself. (C) The connector can be modified to tailor the rate of release of the API by controlling the rate of depolymerization advantageously using natural enzymes such as esterases in the bloodstream, proteases, caspases, and

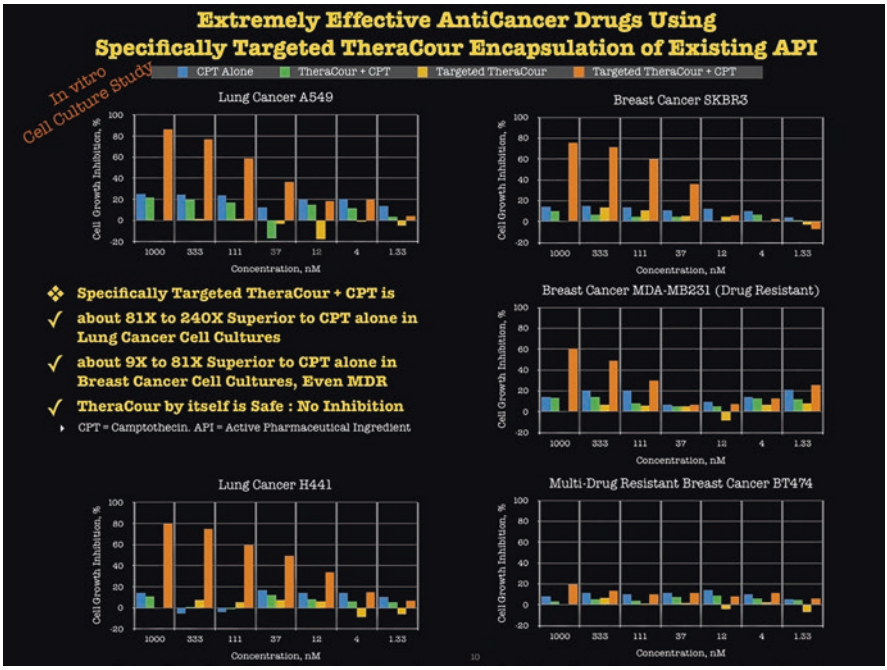

Fig. 3 Cell proliferation of cancer cell lines is most inhibited by a folate-targeted TheraCour polymer delivering camptothecin

others in the tumor vicinity. (D) The connector can be modified to present a suitable net electrical charge state. A net negative electroosmotic potential on the micelles is beneficial for keeping the drug solution stable and keeping it from agglomerating. A strong negative zeta potential would result in a reduction in nonspecific binding to cells, thus minimizing off-target effects. Adding spatially designed positive charges within the milieu of net negative zeta potential can lead to interesting effects such as concentration into extracellular matrices and thus proximity to the tumor. (E) The polymerization can be controlled, within the limits of the Flory equation, to provide desirable clearance characteristics. Thus, an overall molecular weight (including encapsulated API contribution) greater than about 10KDa is generally expected to minimize renal clearance until after polymer degradation, thereby limiting renal injury, a key issue in several chemotherapeutics. At very large molecular weights, the drug would only circulate or deposit in the bloodstream and only slow introduction into extravascular space upon polymer chain degradation would be expected. The optimal molecular weight lies somewhere between these extremes, to minimize renal clearance and simultaneously enable EPR-based concentration in extravascular tumor space. (F) More than one different APIs can be encapsulated, enabling combination drug therapy within single delivery, albeit in a fixed-dose ratio mode. (G) More than one different ligand targeted to different receptors can be attached. Choosing two different ligands targeted at the same receptor but at different

locations can help select the stereo-pose of the receptor (e.g., activated vs. native, or open vs. bound to natural ligand or inhibiting or enhancing dimerization possibility of the receptor) to achieve specificity. Choosing multiples of the same ligand at each connector can lead to receptor multimerization, kicking off intracellular pathways. Choosing two different ligands directed at two different receptors can significantly enhance tumor selectivity, and further, can also enable heterodimer formation to kick off intracellular pathways. (H) Limited cross-linking can be introduced into the linear polymer chain if depot-type controlled-release properties are desired. (I) Signal-based (or triggered) release of contents can be tailored by using appropriate connector chemistry, typically pH sensing, or esterase or protease-specific functions can be incorporated for this purpose.

We have generally chosen small chemicals, small peptides (such as fragments modified from natural ligands), or small peptidomimetics as the targeting ligands, as their sizes are in proportion with the polymer size constraints discussed already. Antibodies tend to be very large and are only suitable when high-affinity antibodies are attached at one or both chain ends of the polymer.

In working with the TheraCour platform and its applications, its similarity to how viruses infect cells is noticeable. Enveloped viruses carry a lipidic membrane derived from the host cell membrane where they came out. Thus, choosing a virus-directed ligand can potentially enable the TheraCour machinery to attack viruses. Even more, interestingly, an active API is not required in this scenario if the ligand is properly chosen. This is because, once the virus is attacked by the micelle-carrying ligands, lipid-lipid mixing essentially pulls the lipid membrane of the virus to the site of the attack, as the micellar-polymer fuses with it and spreads onto it. The glycoproteins that the virus uses to concentrate at (attachment), as well as specifically bind to (binding), and internalize using (fusion), are all suspended in this lipid membrane of the virus, and they get uprooted and dispersed, which can result in a naked virus capsid that cannot infect cells.

4.1 TheraCour Platform for Antiviral Nanomedicines

We have applied the TheraCour platform to develop antiviral nanomedicines, called "nanoviricides®" [85, 88, 89]. In this model, specifically designed chemicals that bind to the glycoprotein of the virus at the same site that the virus uses for binding to its cognate cell surface receptor are used as ligands covalently attached to the TheraCour polymer [88, 89]. The resulting self-assembling nanoviricide micelle is predicted to bind to the virus particle at numerous sites, spread onto the virus surface, thereupon fuse with the viral membrane by lipid-lipid mixing, and simultaneously uproot the glycoproteins the virus requires for gaining entry into cells (Fig. 4) [86, 87].

This is often expected to end in complete neutralization of the virus, without help from the host's immune and clearance systems. In contrast, antibodies only bind to

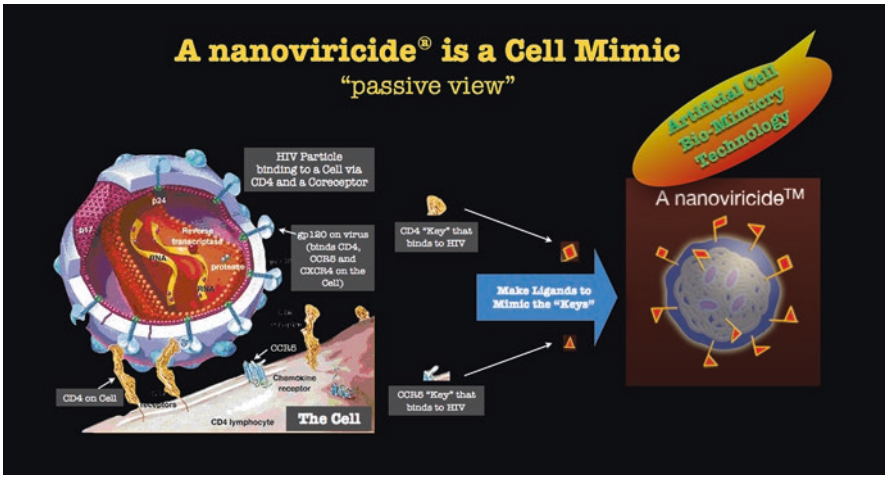

Fig. 4 Novel platform technology: nanoviricide is a cell mimic. A nanoviricide "looks like" a human cell to the virus. The nanoviricide micelle is large enough for a virus particle to latch onto it, but yet small enough to circulate readily in the body. Rather than the virus particle entering into a nanoviricide, a nanoviricide micelle wraps around the virus particle and encapsulates it. Viral resistance to the nanoviricide drug is unlikely because even as the virus mutates, it still binds to the same cell surface receptors, in the same fashion.

the virus with two sites and need the host system for clearance and processing of the resulting antibody-virus complex.

Drug resistance developing in viruses is a major problem facing antiviral drug development. Antibodies are used as antiviral medications and they can be generated readily against viral antigens. However, antibodies are highly specific. Viruses change rapidly due to multiple effects including replication errors (mutations, insertions, deletions), acquisition of attributes by homologous recombinations, or exchanges of segments with other viruses usually of the same type (reassortments). Because of their high propensity to tolerate genomic changes, viruses readily escape antibodies as well as small chemical drugs especially when allowed to expand under such antagonistic evolutionary pressure. For the same reason, vaccine-escapist or vaccine-resistant viruses evolve in the field, particularly in the scenario of vaccination levels insufficient to result in herd immunity of a population.

However, no matter how much a virus changes, it uses the same entry receptor on the human cells, and the site on the viral glycoprotein that binds to the entry receptor binds in the same fashion. Thus, an appropriate ligand designed to mimic the site on the entry receptor which has the binding site to the virus, when attached to the nanoviricide, would result in a surface that has the cell-binding features on the nanoviricide micelle to which the virus binds no matter how much it mutates. In other words, this approach of mimicking the cellular receptor's essentially invariant binding site for the virus would result in a nanoviricide that the virus cannot escape from, unlike antibodies and vaccines. Escape from such a nanoviricide would require drastic changes that result in generation of a new and different virus that, if

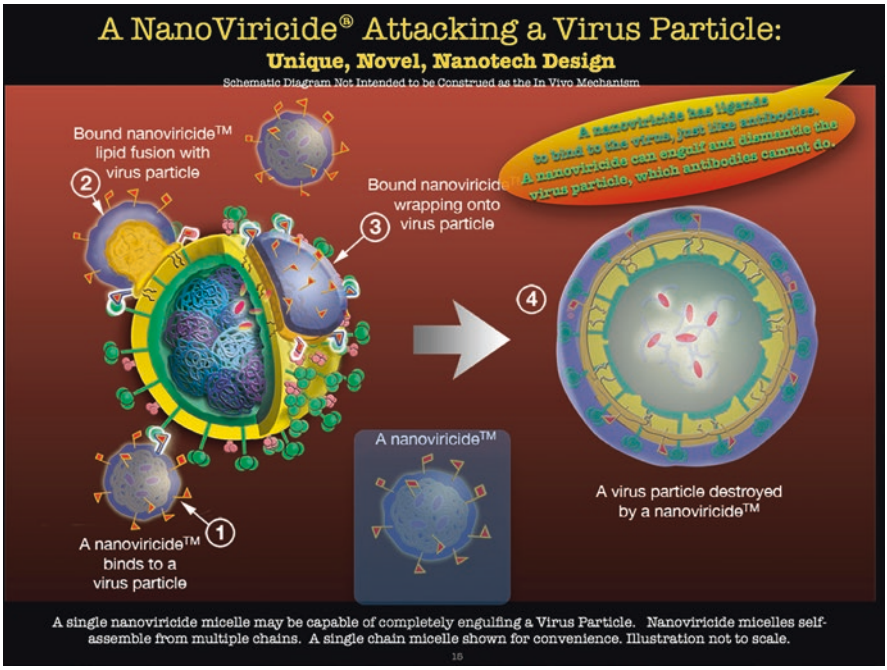

Fig. 5 Graphical representation of the mechanism of action of *nanoviricide* binding and inactivation of viruses. **Step 1:** A *nanoviricide™* binds to virus particle. **Step 2:** Bound *nanoviricide™* lipid fusion with virus particles. **Step 3:** Bound *nanoviricide™* wrapping onto virus particles. **Step 4:** A virus particle destroyed by a *nanoviricide™*

infectious, would be using a different pathway of cellular entry. Thus, this approach promises an elegant biomimetic solution to overcoming the problem of drug resistance evolution in viruses.

A graphical representation of the proposed mechanism of *nanoviricide* is shown in Fig. 5.

4.2 Nanoviricide Polymeric Micelle Drug Development Against SARS-CoV-2

SARS-CoV-2, a recent threat to human life, belongs to the beta family of human respiratory coronavirus and causes the severe lower tract communicable disease termed COVID-19 [90]. Throughout the global pandemic that began circa November 2019, the virus has continuously evolved in both continuous and stepwise fashion. The stepwise generated variants have caused repeated waves of the pandemic throughout the world. Newer variants that take over from the prior ones have possessed greater transmissibility, defined by the "baseline reproduction factor," R0

(pronounced R-naught) which is the average number of humans a person sick with the virus is transmitting the virus to. As of April 2022, the Omicron BA.2 and its subvariants have reached R0 of about 12, which brings it into the range of one of the most infectious viruses known to humans, the measles virus R0 of about 15 to 18 [91]. While at the same time, the receptor-binding site (RBS) on the Spike or S-protein of the virus has changed under immune pressure, the antibody drugs designed against the original Wuhan strain are no longer effective. The efficacy of vaccines in preventing infection has dropped to very low levels, while vaccinated persons are still less likely to have severe disease or die from SARS-CoV-2 infection than unvaccinated persons. The newer variants are thought to cause milder disease, and a reduced rate of deep lung infections, which may be related to the changes in the RBS promoting more binding in the upper respiratory tract or the general buildup of immunity from prior infections or vaccinations, although the possibility of a stepwise evolving newer variant with high pathogenicity cannot be ignored.

A major threat that cannot be ignored, particularly because vaccination cannot reach herd immunity for the global population in the current circumstances, is the generation of a novel virus variant that causes antibody-dependent enhancement of disease (the "ADE effect"). The related SARS-CoV-1 and MERS-CoV are known to be capable of causing ADE, although neither of these viruses has resulted in a widespread pandemic [92]. In ADE, a virus variant that is sufficiently different from the prior virus such that it is not neutralized by the host's antibodies (generated either due to vaccination or prior infection, or given in a therapeutic protocol) still binds to such antibodies, and the antibodies in turn bind to Fc-receptor-rich human cells (such as dendritic cells, macrophages, neutrophils, eosinophils, basophils, mast cells, and NK cells) [93], and thereafter upon internalization, the virus infects the cells and propagates more adventitiously than in absence of such antibodies, causing a substantially more severe disease as a reverse effect of having antibodies.

The currently available drugs, remdesivir (Gilead), molnupiravir (Merck), and Paxlovid™ (Pfizer), have significant limitations and limited effectiveness. Molnupiravir is mutagenic and has very poor efficacy. Paxlovid is virostatic and the virus rebounds upon the end of the therapy course. Remdesivir is highly effective in cell cultures, but in vivo, its efficacy is very limited primarily due to body metabolism and toxicity. Thus, novel drug development targeted at SARS-CoV-2 of drugs that the virus would not escape is badly needed.

We began SARS-CoV-2 drug development around January 2020 and successfully developed drug candidates worthy of further development already as of May 2020. The GLP Safety/Tolerability studies of the chosen drug candidate, NV-387, were substantially completed as of February 2021. Process scale-up and formulations development has been completed as of this writing and we are preparing for human clinical trials. Our drug development work could have been substantially accelerated if the scientific community had understood the power of this novel antiviral nanomedicine approach and supported the development in a manner similar to how mRNA vaccine development as well as other small chemical development was accelerated.

Our objective was to develop a broad-spectrum, pan-coronavirus drug. In addition to SARS-CoV-2, SARS-CoV-1 and MERS-CoV are known major threats with high fatality rates. Further, there are at least four commonly circulating coronaviruses that cause common colds, and in particular, one of these, h-CoV-NL63, binds to the same ACE2 receptor as SARS-CoV-1 and SARS-CoV-2, and results in the same but less severe lung pathology and morbidity with significantly lower fatality rates. We developed an animal model based on hCoV-NL63 lethal lung infection that mimicked the SARS-CoV-2 lung pathology in humans to test the effectiveness of our drug candidates during the screening process.

We designed several ligands using molecular modeling using the SARS-CoV-1 S-protein, generated nanoviricide drugs from them by covalently conjugating them to the TheraCour polymer backbone, and tested them in cell culture assays first against distinctly different coronaviruses. The successful candidates were then promoted to animal studies for efficacy as well as for safety. Eventually, we settled on NV-387 as the drug candidate for further development based on several considerations including safety, efficacy, as well as scalability and complexity of manufacture. NV-387 is the code name for the active pharmaceutical ingredient, and the corresponding formulated drug product is called NV-CoV-2. In this paper, both designations NV-387 and NV-CoV-2 are generally used interchangeably.

NV-387 was highly effective in cell cultures against coronavirus hCoV-NL63 which binds to ACE2 as the cellular receptor, as well as against coronavirus hCoV-229E which binds to a distinctly different cellular receptor, aminopeptidase N (APN), indicating a broad-spectrum anti-coronavirus effectiveness [94–98]. The broad-spectrum activity of NV-CoV-2 against both hCoV-NL63 and hCoV-229E together indicates that it should still stay active against a variety of coronaviruses, even after they mutate [87, 94, 96–98].

4.3 Encapsulation of the Virus Leads to Disintegration

NV-CoV-2 is designed to bind to the free virion particles at different places through viral-glycoprotein receptor-ligand interactions and potentially encapsulate the virus particle that disables it from infecting the cells. Similarly, to "nano-velcro-tape," these multiple binding interactions may lead to a lipid-lipid fusion of the alkyl chains in the nanoviricide micelle with the lipid envelope of the virus. This dismantles the virus into the capsid form that does not require any involvement from the host immune system. This putative mechanism is orthogonal to almost all other anti-coronavirus agents in development enabling potential supplementation with additive or synergistic effects in combination [85].

The support of this mechanism is shown in the electron photomicrographs in Fig. 6. In this study, the murine cytomegalovirus (MCMV) was incubated with a nanoviricide displaying sialic acid as a ligand. MCMV encloses multiple virus capsids within a single lipid membrane that hosts the viral glycoproteins, making it an ideal candidate for studying attack by a nanoviricide. The light area at the top right

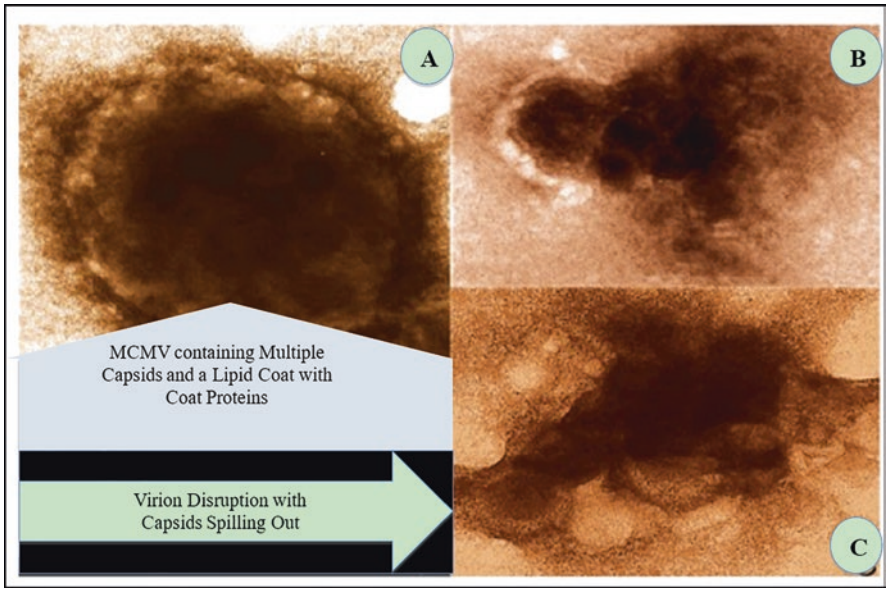

Fig. 6 Effects of two different nanoviricides binding to murine cytomegalovirus (MCMV). (**a**) Control-treated virion: MCMV containing multiple capsids and a lipid coat with coat proteins. (**b**, **c**) MCMV virions treated with two different nanoviricides. Virion disruption with capsids spilling out

corner in Fig. 6b indicates that the lipid coat was pulled together, suggesting a nanoviricide micelle binding event in this area. The loss of the viral envelope is seen to result in the multiple enclosed capsids spilling out of this attacked virus particle. The virus capsids lack viral glycoproteins required for cellular entry and infection and are noninfectious. Figure 6c shows that only virion capsids remain as a result of the attack. The proposed mechanism of action for the nanoviricides is not expected to interfere with the intracellular replication of the virus to any appreciable extent [96, 85]. Therefore, it may be possible to achieve a stronger antiviral effect by combining NV-CoV-2 therapy with other anti-coronavirus therapies in the future.

The proposed mechanism of action for the nanoviricides is not expected to interfere with the intracellular replication of the virus to any appreciable extent [85, 96]. Therefore, it may be possible to achieve a stronger antiviral effect by combining NV-CoV-2 therapy with other anti-coronavirus therapies in the future. We have demonstrated strong success in animal models for our drug candidate NV-CoV-2 which encapsulates remdesivir into the NV-CoV-2 polymeric micelle.

4.4 Protection by Encapsulation for Delivery of Other Small Antiviral Drugs

NV-CoV-2 polymeric micelle can encapsulate a number of hydrophobic drugs effectively. We postulate that it would deliver any encapsulated cargo with a strong preference for infected cells over healthy cells. In fact, it's only the infected cells that display the viral antigen S-protein (or S1 and S2 proteins), on either budding virion or on exposed cell membrane structures that NV-CoV-2 preferentially binds to as per design.

Further, encapsulation of another drug within NV-CoV-2 can protect the encapsulated drug from bodily metabolism until entry into cells, improving its pharmacokinetic and pharmacodynamics properties.

Remdesivir (RDV), the only drug with full or normal approval for use in hospitalized patients, and recently in pediatric patients, is extremely effective in cell culture studies. EC50 of remdesivir in SARS-CoV-2-infected primary human airway epithelial (HAE) cells and Vero cells has been found at 9.9 nM and 750 nM, respectively, at 48 h post-treatment [99]. Further, it is also extremely safe, with a therapeutic index of greater than 10 in cell culture studies. It was approved based on a clinical trial that demonstrated that remdesivir infusion treatment for 9 days resulted in an average reduction in hospitalization stay of SARS-CoV-2 patients by about 7–8 days. (ClinicalTrials.gov number, NCT04280705) [100]. However, follow-on clinical trials did not show such effectiveness unambiguously. A recently completed multicenter multinational clinical trial resulted in suggesting that remdesivir treatment was not statistically different from the standard of care arm (ClinicalTrials.gov Identifier: NCT04365725) [101]. The stark contrast between its cell culture and in vivo effectiveness is traced to the rapid bodily metabolism that turns it into the des-phosphate derivative, GS441524, which is significantly less effective than RDV itself [102].

We hypothesized that NV-CoV-2 encapsulation of RDV may provide substantial synergistic antiviral effects in vivo, by virtue of (1) the inhibition of the reinfection cycle afforded by NV-CoV-2, (ii) the inhibition of the replication cycle afforded by RDV, and (iii) increased effective circulating of RDV at higher concentration and potentially higher intracellular RDV concentration due to encapsulation of RDV affording protection from bodily metabolism, when compared to standard remdesivir therapy. This could result in rapid recoveries of the patients, providing essentially a cure in most cases. When RDV was encapsulated within NV-CoV-2, the antiviral efficacy of the resulting drug, NV-CoV-2, was substantially increased over that of either NV-CoV-2 or RDV in lethal lung infection model rat studies [103–105].

In this study, the untreated rats and the vehicle-treated rats infected with the CoV-NL63 virus directly into lungs only survived for 5 days. The group of rats treated daily with a dose of RDV at 10 mg/kg (NV376, formulated remdesivir as per standard SBECD Veklury® formulation, double dose on the first day, mimicking standard Veklury protocol) survived up to 7.5 days. The group of rats treated with NV-CoV-2, 320 mg/kg (high, given on alternate days for five doses), survived until

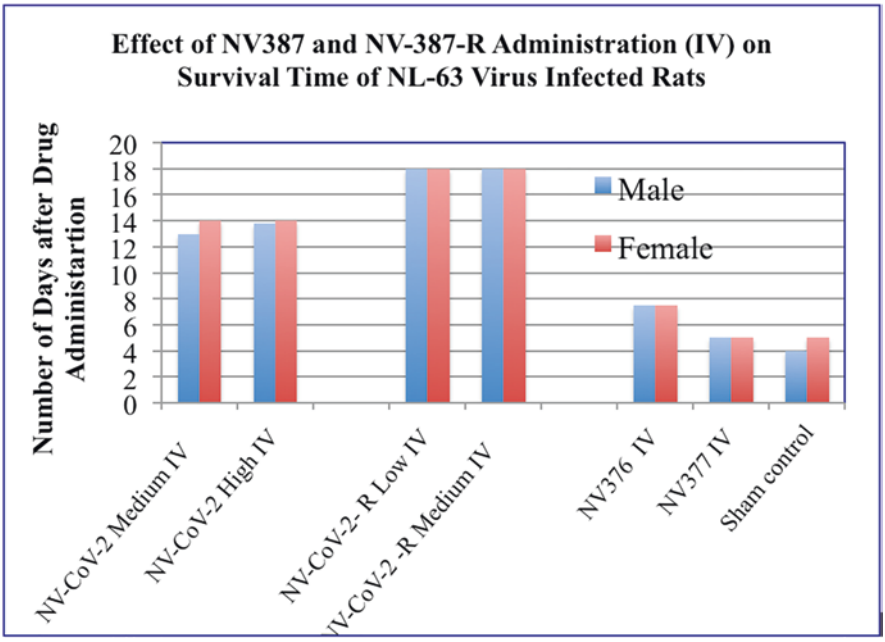

Fig. 7 Survival of rats from NL63 infection after administration of NV-CoV-2-R for varying number of days beginning with day 0

day 14. The survival rate of the rats administered with NV-CoV-2-R (comprising 160mg/kg NV-CoV-2/med, 16mg/kg RDV/low, given on alternate days for five doses) increased to 18 days. The total RDV dose was matched in the RDV and NV-CoV-2-R groups enabling a simple comparison of the effect on survival [106] (Fig. 7).

5 Pharmacokinetics of Remdesivir-SBECD and Remdesivir Encapsulated in NV-CoV-2 (i.e., NV-CoV-2-R) in the Presence of Plasma In Vitro and In Vivo (Figs. 8 and 9)

Figure 8 demonstrates that NV-387-polymer encapsulation protects RDV in vitro from plasma-mediated catabolism, with only 25% loss in 4 h, and substantial stability even after overnight incubation, whereas Gilead formulation of RDV in SBECD (S-beta-ethyl-cyclodextrin) does not do as well, with 50% loss in 4 h, and limited stability in overnight incubation. Therefore, it is expected that in vivo our polymer encapsulation can provide RDV for longer periods of time improving its antiviral activity [107].

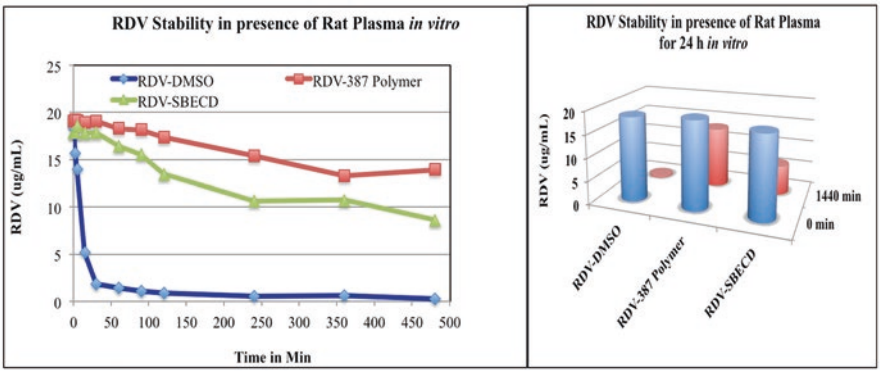

Fig. 8 Comparison of stability of RDV in DMSO, in polymer 387 encapsulated, and in SBECD in vitro in the presence of rat plasma. Stability in RPL: The samples, RDV, RDV-encapsulated in NV-387 polymer, and RDV in SBECD (Gilead formulation), were tested for their stability in the presence of rat plasma in vitro. Methodologies of incubation in the reaction mixture, and extractions, are the same as we did for standard curve determinations of RDV/GS. The results show that RDV by itself has a very short life in the presence of plasma, RDV in SBECD is somewhat better than RDV alone, but encapsulation in NV-387 polymer substantially improved RDV stability even after overnight incubation. GS-441524 metabolite formations are representative of RDV breakdown and supportive of the RDV stability data

We tested the in vivo stability of NV-CoV-2 polymer-encapsulated RDV in a pharmacokinetic study in rats (uninfected). NV-CoV-2-R, RDV-SBECD, NV-CoV-2 polymer alone, and vehicle were introduced by slow-push tail-vein injection at two different strengths into female rats. The RDV-SBECD followed standard Veklury protocol, double dose on day 1 followed by daily dose until day 9. NV-CoV-2 and NV-CoV-2-R followed a simplified protocol of five doses at 48-h intervals, i.e., days 1, 3, 5, 7, and 9. After the first and fifth injections (day 1 and day 9), blood samples were collected at different time points for 24 h, and the amount of remdesivir was quantitated using a specially designed LC-MS protocol [108].

Figure 9 shows a comparative analysis of RDV levels in female rat plasma after the first and fifth injections of the drugs. Accumulation of RDV in the system was better after the fifth injection of NV-CoV-2-Med than the first injection. For all the doses of NV-CoV-2-R, RDV was detected in rat plasma producing an initial increase that peaked between 4 and 8 h and was followed by a slow decrease between 24 and 48 h. Although the pattern of pharmacokinetics with 376-R (remdesivir-sulfobutylether-beta-cyclodextrin, SBECD) formulation mimicking Gilead Veklury®) was similar to that of NV-CoV-2-R, the half-life of RDV when NV-COV-2 encapsulated was more than 24 h, whereas in the standard RDV-SBECD formulation, it was only around 8 h (Fig. 9).

The nanoviricide polymer, NV-387, is thus found to be an encapsulator capable of protecting the encapsulated small-molecule drug from degradation in vivo. RDV has a low water solubility of 0.339 mg/mL which is still appreciable in the context of plasma levels, and is expected to have resulted in continued loss of encapsulated

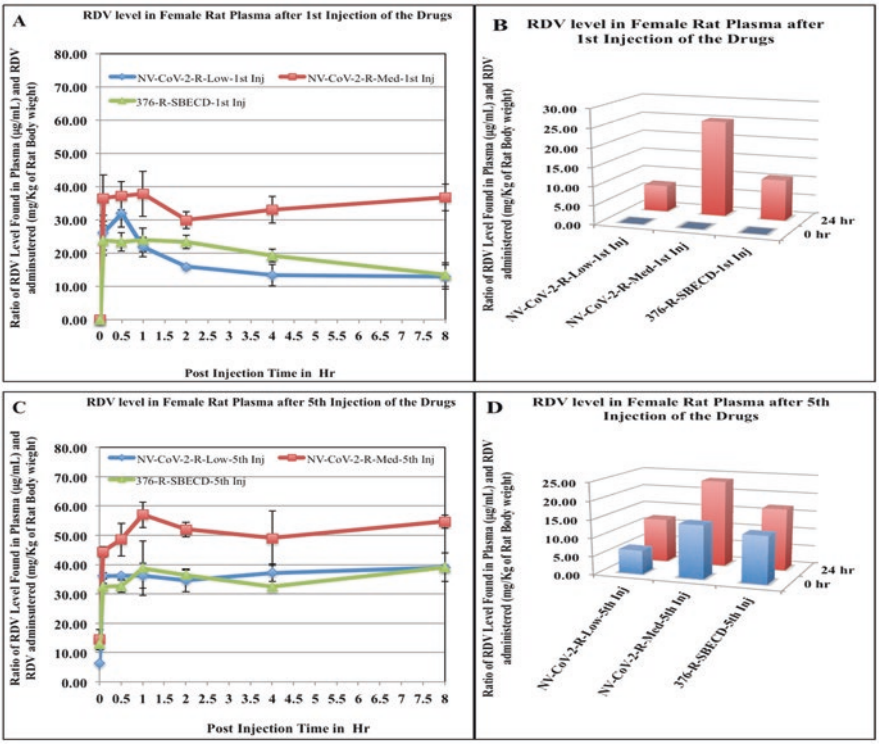

Fig. 9 RDV concentrations in female rat plasma after the first injection (panel, A, B) and fifth injection (panel, C, D) of the drugs. The blood samples collected at different time points after drug administration i.v. to the animals were collected and measured for RDV level by a specially designed LC-MS quantitation protocol with isotopic remdesivir standards. The values obtained as mg/mL were normalized by dividing with the RDV amount administered (mg/Kg of rat body weight). Each data point is the mean (±SD) of three values and the experiment was repeated three times with similar results

RDV to dilution into the bodily fluids. In spite of this, substantial metabolic protection and sustained level of RDV were seen.

These PK characteristics of the TheraCour polymeric micelle platform enable longer-term, sustained delivery of drugs, which is very important for cancer therapeutics. The PK characteristics of drugs that are less water-soluble than RDV are expected to be improved even more than what we saw with RDV. Further, as discussed earlier, attaching appropriate site-directing ligands to NV-387 (or other TheraCour® family polymers) enables address-directed delivery into selected cell types, identified by the ligand(s).

Thus, the TheraCour platform polymeric micelles are capable of meeting the holy grail demands of cancer therapy: (a) sustained high concentrations of the encapsulated drug and (b) address-based site-specific selective delivery into cancer cells.

6 Safety Studies of Drug Substance, NV-387, and Drug Product NV-CoV-2

Of the TheraCour platform polymers, NV-387 is most advanced toward translation into the clinic. NV-387 is a drug substance (API) that, when formulated as a drug product, bears the designation NV-CoV-2. For the purposes of this review, the terms NV-387 and NV-CoV-2 are used interchangeably, although there are regulatory and compositional subtleties that distinguish a drug product from a drug substance.

NanoViricides has conducted safety pharmacology studies on NV-387 that included core battery tests as defined in the ICH S7A guidelines conducted on the respiratory and central nervous systems in the standardized conscious rat model, and the cardiovascular system in a nonhuman primate model (cynomolgus monkeys – *Macaca fascicularis)* upon intravenous administration of NV-CoV-2. No significant adverse effects on respiratory function or in neurobehavioral effects were observed at 1 h post-dose time point in all dose groups of rats. Body temperature in rats was not affected by the intravenous administration of NV-CoV-2.

The intravenous administration of NV-CoV-2 in conscious telemetered cynomolgus monkeys did not induce any significant, biologically relevant effects on heart rate, arterial blood pressure, cardiac rhythm, and ECG parameters. All monkeys maintained sinus rhythm throughout the study.

Additionally, NV-387 was found to be non-immunogenic in a rat model. NV-387 was nonallergenic in several animal models given as injection as well as given orally. NV-387 was found to be non-mutagenic in the standardized bacterial reverse mutation test (Ames test), and non-genotoxic in the standardized micronucleus test. The micronucleus test is a genotoxicity test to detect the chromosome damaging potential after exposure to a test chemical in human TK6 cells in vitro.

The TheraCour platform polymers have a similar general chemical structure as NV-387 and similar characteristics. The polymer molecular weight is expected to influence PK/PD and especially the PK/PD of encapsulated guest molecules. The hydrophobicity, or more specifically, the hydrophilic/hydrophobic balance in the polymer, is expected to affect its aggregation properties as well as interactions with proteins and cell membranes. Nevertheless, the design principles that we used, of incorporating PEG in the backbone to enable "stealth mode," and pendant alkyl chains to enable mimicking cellular membranes and enabling self-assembly that presents an unstructured hydrophilic PEG surface for the micelle, are expected to enable similar non-mutagenic, non-immunogenic, nonallergenic, and non-genotoxic characteristics to the TheraCour polymer platform.

7 Discussion

Traditional cancer chemotherapy is cytotoxic to cells, and therefore, it can damage healthy cells as well as cancer cells, whereas site-directed address-specific cancer cell-selective therapy would affect only cancer cells sparing the normal, healthy cells, to the extent of the selectivity. While antibodies, antibody-radio-conjugates, or antibody-drug conjugates are substantially site-directed, such therapies have presented many challenges. The radio-immunoconjugates in particular cause substantial collateral damage in nearby cells and the tissue. The drug loading capability of antibodies is limited without losing their specificity. Liposomal drug delivery with selective ligands derived from antibodies or small chemicals has been attempted with some success. However, liposomes are not stable upon the dilution that occurs in the bloodstream, and rather small fractions of the encapsulated API are delivered as encapsulated to the cancer tissue, with a large fraction entering the bloodstream naked. Liposomes also have presented issues of immunogenicity, allergenicity, immune activation, or inflammatory responses, among others. Liposomes have manufacturing challenges as well due to their complex compositions and narrow phase stability diagrams with respect to phase ratios as well as with respect to temperature. Off-the-shelf polymers such as PLA, PGA, PLGA, PMMA/PAA, etc. have also resulted in substantial challenges.

Thus, the design of appropriate polymers for site-directed, address-selective cancer therapeutics has become very important. Recent advances in nanotechnology and biotechnology have contributed to the advent of engineered nanoscale materials as innovative prototypes to be used for biomedical applications and optimized therapy. However, several obstacles, including difficulty in achieving the optimal combination of physicochemical parameters for tumor targeting, evading particle clearance mechanisms, and controlling drug release, have limited the translation of nanomedicines into therapy. Recent efforts are focused on developing functionalized nanoparticles for delivery of therapeutic agents to specific molecular targets overexpressed on different cancer cells. Particularly, the mixture of targeted and controlled-release polymer nanotechnologies has resulted in a new programmable nanotherapeutic formulation of docetaxel, which recently entered clinical testing for patients with solid tumors.

Nanotechnologies are having a significant impact on drug delivery, and over recent years, several first-generation therapeutic nanoproducts are moving ahead toward clinical development. Particularly, targeted polymeric nanoparticles, capable of increased cell uptake and enhanced accumulation in the target tissue, are often successfully obtained by attaching specific binding entities onto the surface of the nanoparticles. Such active targeting, together with the passive EPR effect and other targeting-based approaches, is envisaged to be an efficient strategy, and a number of other ligand-targeted nanotherapeutics are either approved or under clinical evaluation, resulting in second-generation nanomedicines.

A polymeric drug delivery nanovehicle containing the chemotherapeutic agent docetaxel is approved to be used for the treatment of several common cancers,

including breast, lung, and prostate. To date, other complex targeted nanosystems addressed to varied cancers, also combining diagnostic and therapeutic agents, or that may trigger drug release at the target site when exposed to external stimuli, are currently in clinical development.

We have presented a novel TheraCour polymeric micelle-forming self-assembling platform technology here that is capable of solving a number of the problems facing successful nanomedicine development for cancer treatment. Interestingly, our insight into the mechanism of this polymeric platform is leading to the development of antiviral nanomedicines at a quicker pace than that of anticancer nanomedicines.

Acknowledgment We acknowledge all our colleagues and secretaries for their help during the preparation of the manuscript by providing all the relevant information. Thanks to Ms. Bethany Pond for her editorial assistance.

Conflict of Interest Authors, Anil Diwan and Jayant Tatake, are employed by the company NanoViricides, Inc. The authors declare that there are no conflicts of interest between the companies, AllExcel, Inc., TheraCour Pharma, Inc., and NanoViricides, Inc., consistent with existing contractual and licensing relationships between them. The authors declare that the research was conducted in the absence of any commercial or financial relationships that could be construed as a potential conflict of interest.

Source of Funding NanoViricides, Inc., a publicly traded company listed on NYSE American, stock symbol NNVC, has financed the development of nanoviricides platform and antiviral drugs based on it, under several license agreements with TheraCour Pharma, Inc., the holder of the TheraCour intellectual property. All other developments of the TheraCour platform are conducted by AllExcel, Inc., and are financed independently by NanoViricides, Inc.

Certificate We certify that all the figures and schematic designs that are presented in this manuscript are our own.

References

1. Pandey A, Jain DS, Chakraborty S. Poly Lactic-Co-Glycolic Acid (PLGA) copolymer and its pharmaceutical application. Handb Polym Pharm Technol. 2015;2:151–72. https://doi.org/10.1002/9781119041412.ch6.
2. Patra JK, Das G, Fraceto LF. et al. Nano based drug delivery systems: recent developments and future prospects. J Nanobiotechnol vol. 16, pp. 71-104, 2018. 10.1186/s12951-018-0392-8.
3. Shiraishi K, Yokoyama M. Toxicity and immunogenicity concerns related to PEGylated-micelle carrier systems: a review. Sci Technol Adv Mater. 2019;20(1):324–36. https://doi.org/10.1080/14686996.2019.1590126.
4. Liu R, Oldham RJ, Teal E, Beers SA, Cragg MS. Fc-engineering for modulated effector functions-improving antibodies for cancer treatment. Antibodies (Basel). 2020;9(4):64–72. https://doi.org/10.3390/antib9040064.
5. Klasse PJ, Moore JP. Antibodies to SARS-CoV-2 and their potential for therapeutic passive immunization. eLife. 2020;9:e57877. https://doi.org/10.7554/eLife.57877.
6. Schrama D, Reisfeld RA, Becker JC. Antibody targeted drugs as cancer therapeutics. Nat Rev Drug Discov. 2006;5(2):147–59.

7. Chames P, Van Regenmortel M, Weiss E, Baty D. Therapeutic antibodies: successes, limitations and hopes for the future. Br J Pharmacol. 2009;157(2):220–33.
8. Nobs L, Buchegger F, Gurny R, Allemann E. Biodegradable nanoparticles for direct or two-step tumor immunotargeting. Bioconjug Chem. 2006;17(1):139–45.
9. Peer D, Karp JM, Hong S, Farokhzad OC, Margalit R, Langer R. Nanocarriers as an emerging platform for cancer therapy. Nat Nanotechnol. 2007;2(12):751–60.
10. Weiner LM, Adams GP. New approaches to antibody therapy. Oncogene. 2000;19(53):6144–51.
11. Ellington AD, Szostak JW. In vitro selection of RNA molecules that bind specific ligands. Nature. 1990;346(6287):818–22.
12. Tuerk C, Gold L. Systematic evolution of ligands by exponential enrichment: RNA ligands to bacteriophage T4 DNA polymerase. Science. 1990;249(4968):505–10.
13. Keefe AD, Pai S, Ellington A. Aptamers as therapeutics. Nat Rev Drug Discov. 2010;9(7):537–50.
14. Xiao Z, Farokhzad OC. Aptamer-functionalized nanoparticles for medical applications: challenges and opportunities. ACS Nano. 2012;6(5):3670–6.
15. Daniels DA, Chen H, Hicke BJ, Swiderek KM, Gold L. A tenascin-C aptamer identified by tumor cell SELEX: systematic evolution of ligands by exponential enrichment. Proc Natl Acad Sci U S A. 2003;100(26):15416–21.
16. Shi J, Xiao Z, Kamaly N, Farokhzad OC. Self-assembled targeted nanoparticles: evolution of technologies and bench to bedside translation. Acc Chem Res. 2011;44(10):1123–34.
17. Farokhzad OC, Cheng J, Teply BA, et al. Targeted nanoparticle- aptamer bioconjugates for cancer chemotherapy in vivo. Proc Natl Acad Sci U S A. 2006;103(16):6315–20.
18. Gu F, Zhang L, Teply BA, et al. Precise engineering of targeted nanoparticles by using self-assembled biointegrated block copolymers. Proc Natl Acad Sci U S A. 2008;105(7):2586–91.
19. Farokhzad OC, Jon S, Khademhosseini A, Tran TN, Lavan DA, Langer R. Nanoparticle-aptamer bioconjugates: a new approach for targeting prostate cancer cells. Cancer Res. 2004;64(21):7668–72.
20. Cheng J, Teply BA, Sherifi I, et al. Formulation of functionalized PLGA-PEG nanoparticles for in vivo targeted drug delivery. Biomaterials. vol. 28, no. 5, pp. 869–876, 2007.
21. Chang SS, O'Keefe DS, Bacich DJ, Reuter VE, Heston WD, Gaudin PB. Prostate-specific membrane antigen is produced in tumor-associated neovasculature. Clin Cancer Res. 1999;5(10):2674–81.
22. Ghosh A, Heston WD. Tumor target prostate specific membrane antigen (PSMA) and its regulation in prostate cancer. J Cell Biochem. 2004;91(3):528–39.
23. Schulke N, Varlamova OA, Donovan GP, et al. The homodimer of prostate-specific membrane antigen is a functional target for cancer therapy. Proc Natl Acad Sci U S A. 2003;100(22):12590–5.
24. Nanjwade BK, Bechra HM, Derkar GK, Manvi FV, Nanjwade VK. Dendrimers: emerging polymers for drug-delivery systems. Eur. J. Pharm. Sci. 2009;38(3):185–96. https://doi.org/10.1016/j.ejps.2009.07.008.
25. Sherje AP, Jadhav M, Dravyakar BR, Kadam D. Dendrimers: A versatile nanocarrier for drug delivery and targeting. Intl J Pharm. 2018;548(1):707–20. https://doi.org/10.1016/j.ijpharm.2018.07.030.
26. Gajbhiye V, Palanirajan VK, Tekade RK, Jain NK. Dendrimers as therapeutic agents: a systematic review. J Pharm Pharmacol. 2009;61:989–1003.
27. Chou LY, Ming K, Chan WC. Strategies for the intracellular delivery of nanoparticles. Chem Soc Rev. 2011;40(1):233–45.
28. Choi CH, Alabi CA, Webster P, Davis ME. Mechanism of active targeting in solid tumors with transferrin-containing gold nanoparticles. Proc Natl Acad Sci U S A. 2010;107(3):1235–40. https://doi.org/10.1073/pnas.0914140107.
29. Brissette R, Prendergast JK, Goldstein NI. Identification of cancer targets and therapeutics using phage display. Curr Opin Drug Discov Devel. 2006;9(3):363–9.

30. Sugahara KN, Teesalu T, Karmali PP, et al. Coadministration of a tumor-penetrating peptide enhances the efficacy of cancer drugs. Science. 2010;328(5981):1031–5.
31. Chan JM, Zhang L, Tong R, et al. Spatiotemporal controlled delivery of nanoparticles to injured vasculature. Proc Natl Acad Sci U S A. 2010;107(5):2213–8.
32. Nicolas J, Mura S, Brambilla D, Mackiewicz N, Couvreur P. Design, functionalization strategies and biomedical applications of targeted biodegradable/biocompatible polymer-based nanocarriers for drug delivery. Chem Soc Rev. 2013;42(3):1147–235.
33. Kamaly N, Xiao Z, Valencia PM, Radovic-Moreno AF, Farokhzad OC. Targeted polymeric therapeutic nanoparticles: design, development and clinical translation. Chem Soc Rev. 2012;41(7):2971–3010.
34. Talekar M, Kendall J, Denny W, Garg S. Targeting of nanoparticles in cancer: drug delivery and diagnostics. Anticancer Drugs. 2011;22(10):949–62.
35. Lu Y, Low PS. Folate-mediated delivery of macromolecular anticancer therapeutic agents. Adv Drug Deliv Rev. 2002;54(5):675–93.
36. Liang C, Yang Y, Ling Y, Huang Y, Li T, Li X. Improved therapeutic effect of folate-decorated PLGA-PEG nanoparticles for endometrial carcinoma. Bioorg Med Chem. 2011;19(13):4057–66.
37. Maresca KP, Hillier SM, Femia FJ, et al. A series of halogenated heterodimeric inhibitors of prostate specific membrane antigen (PSMA) as radiolabeled probes for targeting prostate cancer. J Med Chem. vol. 52, no. 2, pp. 347–357, 2009.
38. Byun Y, Mease RC, Lupold SE, Pomper MG. Recent development of diagnostic and therapeutic agents targeting glutamate carboxypeptidase II (GCPII). In: Supuran CT, Winum JY, editors. Drug design of zinc-enzyme inhibitors: functional, structural, and disease applications. New York, NY: Binghe Wang Wiley Series in Drug Discovery and Development; 2009.
39. Zhou J, Neale JH, Pomper MG, Kozikowski AP. NAAG peptidase inhibitors and their potential for diagnosis and therapy. Nat Rev Drug Discov. 2005;4(12):1015–26.
40. Sanna V, Pintus G, Roggio AM, et al. Targeted biocompatible nanoparticles for the delivery of (−)-epigallocatechin 3-gallate to prostate cancer cells. J Med Chem. 2011;54(5):1321–32.
41. Chandran SS, Banerjee SR, Mease RC, Pomper MG, Denmeade SR. Characterization of a targeted nanoparticle functionalized with a urea-based inhibitor of prostate-specific membrane antigen (PSMA). Cancer Biol Ther. 2008;7(6):974–82.
42. Hrkach J, Von Hoff D, Mukkaram Ali M, et al. Preclinical development and clinical translation of a PSMA-targeted docetaxel nanoparticle with a differentiated pharmacological profile. Sci Transl Med. 2012;4(128):128–39.
43. Wijagkanalan W, Kawakami S, Hashida M. Glycosylated carriers for cell-selective and nuclear delivery of nucleic acids. Front Biosci (Landmark Ed). 2011;16:2970–87.
44. Hashida M, Nishikawa M, Yamashita F, Takakura Y. Cell-specific delivery of genes with glycosylated carriers. Adv Drug Deliv Rev. 2001;52(3):187–96.
45. Matsumura Y, Gotoh M, Muro K, et al. Phase I and pharmacokinetic study of MCC-465, a doxorubicin (DXR) encapsulated in PEG immunoliposome, in patients with metastatic stomach cancer. Ann Oncol. 2004;15(3):517–25.
46. ClinicalTrials.gov. Safety study of infusion of SGT-53 to treat solid tumors. Available from: http://clinicaltrials.gov/show/NCT00470613. Accessed 5 Nov 2013.
47. Sankhala KK, Mita AC, Adinin R, et al. A phase I pharmacokinetic (PK) study of MBP-426, a novel liposome encapsulated oxaliplatin. J Clin Oncol. vol. 2009;27:S2535–9.
48. Saneja A, Kumar R, Mintoo MJ, Dubey RD, Sangwan PL, Mondhe DM, et. al. Gemcitabine and betulinic acid co-encapsulated PLGA-PEG polymer nanoparticles for improved efficacy of cancer chemotherapy. Mater Sci Eng C Mater Biol Appl 98, pp. 764–771, 2019. doi: https://doi.org/10.1016/j.msec.2019.01.026.
49. Makadia HK, Siegel SJ. Poly lactic-co-glycolic acid (PLGA) as biodegradable controlled drug delivery carrier. Polymers (Basel). 2011;3(3):1377–97.
50. Elsabahy M, Wooley KL. Design of polymeric nanoparticles for biomedical delivery applications. Chem Soc Rev. 2012;41(7):2545–61.

51. Langer R, Folkman J. Polymers for the sustained release of proteins and other macromolecules. Nature. 1976;263(5580):797–800.
52. Gref R, Minamitake Y, Peracchia MT, Trubetskoy V, Torchilin V, Langer R. Biodegradable long-circulating polymeric nanospheres. Science. 1994;263(5153):1600–3.
53. Yari H, Nkepang G, Awasthi V. Surface modification of liposomes by a lipopolymer targeting prostate specific membrane antigen for theranostic delivery in prostate cancer. Materials. 2019;12:756–60. https://doi.org/10.3390/ma12050756.
54. Satsangi A, Roy SS, Satsangi RK, Tolcher AW, Vadlamudi RK, Goins B, et al. Synthesis of a novel, sequentially active-targeted drug delivery nanoplatform for breast cancer therapy. Biomaterials. 2015;59:88–101. https://doi.org/10.1016/j.biomaterials.2015.03.039.
55. Tang X, Li A, Xie C, Zhang Y, Liu X, Xie Y, et al. The PI3K/mTOR dual inhibitor BEZ235 nanoparticles improve radiosensitization of hepatoma cells through apoptosis and regulation DNA repair pathway. Nanoscale Res Lett. 2020;15:63–9. https://doi.org/10.1186/s11671-020-3289-z.
56. Han B, Yang Y, Chen J, Tang H, Sun Y, Zhang Z, et al. Preparation, Characterization, and Pharmacokinetic Study of a Novel Long-Acting Targeted Paclitaxel Liposome with Antitumor Activity. Int J Nanomed. 2020;15:553–71. https://doi.org/10.2147/ijn.s228715.
57. O'Brien ME, Wigler N, Inbar M, Rosso R, Grischke E, Santoro A, et al. Reduced cardiotoxicity and comparable efficacy in a phase III trial of pegylated liposomal doxorubicin HCl (CAELYX/Doxil) versus conventional doxorubicin for first-line treatment of metastatic breast cancer. Ann Oncol. 2004;15:440–9. https://doi.org/10.1093/annonc/mdh097.
58. Geisberg CA, Sawyer DB. Mechanisms of anthracycline cardiotoxicity and strategies to decrease cardiac damage. Curr Hypertens Rep. 2010;12:404–10. https://doi.org/10.1007/s11906-010-0146-y.
59. Eloy JO, Petrilli R, Topan JF, Antonio HM, Barcellos JPA, Chesca D, et al. Co-loaded paclitaxel/rapamycin liposomes: development, characterization and in vitro and in vivo evaluation for breast cancer therapy. Colloids Surf B Biointerf. 2016;141:74–82. https://doi.org/10.1016/j.colsurfb.2016.01.032.
60. Chen X, Zhang Y, Tang C, Tian C, Sun Q, Su Z, et al. Co-delivery of paclitaxel and anti-survivin siRNA via redox-sensitive oligopeptide liposomes for the synergistic treatment of breast cancer and metastasis. Int J Pharm. 2017;529:102–15. https://doi.org/10.1016/j.ijpharm.2017.06.071.
61. Meng J, Guo F, Xu H, Liang W, Wang C, Yang XD. Combination therapy using co-encapsulated resveratrol and paclitaxel in liposomes for drug resistance reversal in breast cancer cells in vivo. Sci Rep. 2016;6:22390–298. https://doi.org/10.1038/srep22390.
62. Misra R, Acharya S, Sahoo SK. Cancer nanotechnology: application of nanotechnology in cancer therapy. Drug Discov Today. 2010;15:842–50. https://doi.org/10.1016/j.drudis.2010.08.006.
63. Amreddy N, Babu A, Muralidharan R, Panneerselvam J, Srivastava A, Ahmed R, et al. Recent advances in nanoparticle-based cancer drug and gene delivery. Adv Cancer Res. 2018;137:115–70. https://doi.org/10.1016/bs.acr.2017.11.003.
64. Raza F, Zafar H, Khan MW, Ullah A, Khan AU, Baseer A, Fareed R, Sohail M. Mater Adv. 2022;3:2268–78. https://doi.org/10.1039/d1ma00961c.
65. Jin C, Bai L, Wu H, Song W, Guo G, Dou K. Cytotoxicity of paclitaxel incorporated in PLGA nanoparticles on hypoxic human tumor cells. Pharm Res. 2009;26:1776–84.
66. Larson N, Ghandehari H. Polymeric conjugates for drug delivery. Chem Mater. 2012 Mar 13;24(5):840–53. https://doi.org/10.1021/cm2031569.
67. ClinicalTrials.gov. http://clinicaltrials.gov/show/NCT00689065.
68. Davis ME. The first targeted delivery of siRNA in humans via a self- assembling, cyclodextrin polymer-based nanoparticle: from concept to clinic. Mol Pharm. 2009;6(3):659–68.
69. Oerlemans C, Bult W, et. al. Polymeric micelles in anticancer therapy: targeting, imaging and triggered release. Pharm Res 27, pp. 2569–2589, 2010.

70. Zhang X, Huang Y, et al. Nanomicellar carriers for targeted delivery of anticancer agents. Ther Deliv. 2014;5(1):53–68.
71. Nicoletti MI, Lucchini V, Massazza G, Abbott BJ, D'Incalci M, Giavazzi R. Antitumor activity of taxol (NSC-125973) in human ovarian carcinomas growing in the peritoneal cavity of nude mice. Ann Oncol Off J Eur Soc Med Oncol. 1993;4:151–5. https://doi.org/10.1093/oxfordjournals.annonc.a058419.
72. Geller JI, Wall D, Perentesis J, Blaney SM, Bernstein M. Phase I study of paclitaxel with standard dose ifosfamide in children with refractory solid tumors: a Pediatric Oncology Group study (POG 9376). Pediatr Blood Canc. 2009;52:346–50. https://doi.org/10.1002/pbc.21820.
73. Haigentz M, Moore PC, Ratner L, Henry DH, Rubinstein PG, Ramos JC, et al. Tolerability of paclitaxel/carboplatin (PCb) in solid tumor patients (pts) infected with HIV. J Clin Oncol. 2017;35:e14077. https://doi.org/10.1200/JCO.2017.35.15_suppl.e14077.
74. Zhu L, Chen L. Progress in research on paclitaxel and tumor immunotherapy. Cell Mol Biol Lett. 2019;24:40–7. https://doi.org/10.1186/s11658-019-0164-y.
75. Wani MC, Taylor HL, Wall ME, Coggon P, McPhail AT. Plant antitumor agents. VI. The isolation and structure of taxol, a novel antileukemic and antitumor agent from Taxus brevifolia. J Am Chem Soc. 1971;93:2325–7. https://doi.org/10.1021/ja00738a045.
76. Gradishar WJ, Tjulandin S, Davidson N, Shaw H, Desai N, Bhar P, et al. Phase III trial of nanoparticle albumin-bound paclitaxel compared with polyethylated castor oil–based paclitaxel in women with breast cancer. J Clin Oncol. 2005;23:7794–803.
77. Rajasekaran AK, Anilkumar G, Christiansen JJ. Is prostate- specific membrane antigen a multifunctional protein? Am J Physiol Cell Physiol. 2005;288:C975–81. https://doi.org/10.1152/ajpcell.00506.2004.
78. Von Hoff DD, Mita MM, Ramanathan RK, Weiss GJ, Mita AC, LoRusso PM, et al. Phase I study of PSMA-targeted docetaxel-containing nanoparticle BIND-014 in patients with advanced solid tumors. Clin Cancer Res. 2016;22(13):3157–63. https://doi.org/10.1158/1078-0432.CCR-15-2548.
79. Autio KA, Garcia JA, Alva AS, Hart LL, Milowsky MI, Posadas EM, et al. A phase 2 study of BIND-014 (PSMA-targeted docetaxel nanoparticle) administered to patients with chemotherapy-naïve metastatic castration-resistant prostate cancer (mCRPC). J Clin Oncol. 2016;4:1344–51. https://doi.org/10.1001/jamaoncol.2018.2168.
80. Autio KA, Dreicer R, Anderson J, Garcia JA, Alva A, Hart LL, et al. Safety and efficacy of BIND-014, a docetaxel nanoparticle targeting prostate-specific membrane antigen for patients with metastatic castration- resistant prostate cancer: a phase 2 clinical trial. JAMA Oncol. 2018;4:1344–51. https://doi.org/10.1001/jamaoncol.2018.2168.
81. Llovet JM, Real MI, Montaña X, Planas R, Coll S, Aponte J, et al. Arterial embolisation or chemoembolisation versus symptomatic treatment in patients with unresectable hepatocellular carcinoma: a randomised controlled trial. Lancet (London, England). 2002;359:1734–9. https://doi.org/10.1016/S0140-6736(02)08649-X.
82. Lai CL, Wu PC, Chan GC, Lok AS, Lin HJ. Doxorubicin versus no antitumor therapy in inoperable hepatocellular carcinoma. A prospective randomized trial. Cancer. 1988;62:479–83. https://doi.org/10.1002/1097-0142.
83. Bennis S, Chapey C, Robert J, Couvreur P. Enhanced cytotoxicity of doxorubicin encapsulated in polyisohexylcyanoacrylate nanospheres against multidrug-resistant tumour cells in culture. Eur J Canc. 1994;30:89–93. https://doi.org/10.1016/S0959-8049(05)80025-5.
84. Merle P, Camus P, Abergel A, Pageaux GP, Masliah C, Bronowicki JP, et al. Safety and efficacy of intra-arterial hepatic chemotherapy with doxorubicin-loaded nanoparticles in hepatocellular carcinoma. ESMO Open. 2017;2:e000238. https://doi.org/10.1136/esmoopen-2017-000238.
85. NanoViricides, Inc. Pan-coronavirus COVID-19 drug candidates are highly effective in pre-clinical animal studies in support of FDA Pre IND Application. March 9, 2021, 6:45 AM EST. https://www.bloomberg.com/press-releases/2021-03-09/nanoviricides-inc-pan-coronavirus-covid-19-drug-candidates-are-highly-effective-in-pre-clinical-animal-studies-i.

86. Barton RW, Tatake JG, Diwan AR. Nanoviricides – a novel approach to antiviral therapeutics. Bionanotechnology II. David E. Reisner. CRC Press/Taylor and Francis Group, Boca Raton (www.crcpress.com). p. 141–54, 2011.
87. Barton RW, Tatake JG, Diwan AR. Nanoviricides: targeted anti-viral nanomaterials handbook of clinical nanomedicine, nanoparticles, imaging, therapy, and clinical applications. In: Bawa R, Audette GF, editors. Israel Rubinstein. ISBN 9789814669207. Published February 24, 2016 by Jenny Stanford Publishing, pp:1039–1046.
88. NanoViricides is Developing Drugs Against SARS-CoV-2 with an Integrated Approach to Combat COVID-19, as Reported at The LD 500 Virtual Conference. Friday, September 4, 2020 6:50 AM. https://www.accesswire.com/604794/NanoViricides-is-Developing-Drugs-Against-SARS-CoV-2-with-an-Integrated-Approach-to-Combat-COVID-19-as-Reported-at-The-LD-500-Virtual-Conference.
89. DGAP-News: NanoViricides, Inc.: Broad-spectrum direct antiviral nanomedicine should remain effective against COVID-19 virus. January 27, 2021, 6:15 AM EST https://www.bloomberg.com/press-releases/2021-01-27/dgap-news-nanoviricides-inc-broad-spectrum-direct-antiviral-nanomedicine-should-remain-effective-against-covid-19-virus
90. Feng Y, Ling Y, Bai T, Xie Y, Huang J, Li J, et. al. "COVID-19 with different severities: a multicenter study of clinical features." Am J Respir Crit Care Med vol. 201, no. 11, pp 1380-1388, 2020, doi: https://doi.org/10.1164/rccm.202002-0445O.
91. Spencer Kimbal. HEALTH AND SCIENCE. More contagious omicron BA.2 subvariant now dominant in the U.S., CDC says. PUBLISHED TUE, MAR 29 20221:38 PM EDTUPDATED TUE, MAR 29 20226:24 PM EDT. https://www.cnbc.com/2022/03/29/more-contagious-omicron-bapoint2-covid-subvariant-dominant-in-the-us-cdc-says.html.
92. Ricke DO. Two Different Antibody-Dependent Enhancement (ADE) Risks for SARS-CoV-2 Antibodies. Front Immunol. 2021;12:640093. https://doi.org/10.3389/fimmu.2021.640093.
93. Qiu WQ, de Bruin D, Brownstein BH, Pearse R, Ravetch JV. Organization of the human and mouse low-affinity Fc gamma R genes: duplication and recombination. Science. 1990;248:732–5.
94. Belouzard S, Millet JK, Licitra BN, Whittaker GR. Mechanisms of coronavirus cell entry mediated by the viral spike protein. Viruses. 2012;4(6):1011–33. https://doi.org/10.3390/v4061011.
95. Li W, Sui J, Huang IC, Kuhn JH, Radoshitzky, Marasco, et. al. "The S proteins of human coronavirus NL63 and severe acute respiratory syndrome coronavirus bind overlapping regions of ACE2". Virology. vol. 367, no. 2, pp. 367-374, 2017. doi:https://doi.org/10.1016/j.virol.2007.04.035.
96. Chakraborty A, Diwan A. NL-63: a better surrogate virus for studying SARS-CoV-2. Integr Mol Med. 7, pp. 1-9, 2020. https://doi.org/10.15761/IMM.1000408.
97. Hofmann H, Pyrc K, van der Hoek L, Geier M, Berkhout B, Pöhlmann S. Human coronavirus NL63 employs the severe acute respiratory syndrome coronavirus receptor for cellular entry. Proc Natl Acad Sci USA. 2005;102:7988–93.
98. Liu DX, Liang JQ, Fung TS. Human coronavirus-229E, -OC43, NL63, and HKU1 (Coronaviridae). Encyclopedia of Virology. 2021. p. 428–40. https://doi.org/10.1016/B978-0-12-809633-8.21501-X.
99. https://hospitals.vchca.org/images/medical_staff/Remdesivir_Fact_Sheet_Health_Care_Providers_6-15-20.pdf
100. Beigel JM, Tomashek KM, Dodd LE, Mehta AE, Zingman BS, Kalil AC, et. al. Remdesivir for the treatment of Covid-19 – final report. N Engl J Med vol. 383, pp. 1813-1826, 2020. DOI: https://doi.org/10.1056/NEJMoa2007764.
101. ClinicalTrials.gov. Multicenter, retrospective study of the effects of remdesivir in the treatment of severe Covid-19 infections. Last Update Posted : April 19, 2021. https://clinicaltrials.gov/ct2/show/NCT04365725
102. Zhang L, Gu FX, Chan JM, Wang AZ, Langer RS, Farokhzad OC. Nanoparticles in medicine: therapeutic applications and developments. Clin Pharmacol Ther. 2008;83(5):761–9.

103. Ferrari M. Cancer nanotechnology: opportunities and challenges. Nat Rev Cancer. 2005;5(3):161–71.
104. Davis ME, Chen ZG, Shin DM. Nanoparticle therapeutics: an emerging treatment modality for cancer. Nat Rev Drug Discov. 2008;7(9):771–82.
105. Lammers T, Kiessling F, Hennink WE, Storm G. Drug targeting to tumors: principles, pitfalls and (pre-) clinical progress. J Control Release. 2012;161(2):175–87.
106. Chakraborty A, Diwan A, Arora V, Thakur Y, Chiniga V, Tatake J, et. al. Encapsulation of remdesivir in nanoviricide's platform technology based NV-CoV-2 polymer protects the drug and improves its pharmacokinetics. EC Pharmacol Toxicol vol. 10 no. 2, pp. 108-118, 2022.
107. Chakraborty A, Diwan A, Arora V, Thakur Y, Holkar P, Chiniga V. *Nanoviricides* platform technology based NV-387 polymer protects remdesivir from plasma-mediated catabolism *In vitro*: importance of its increased lifetime for *In vivo* action. Recent Adv Clin Trials. 2022;1(1):1–8.
108. Chakraborty A, Diwan A, Arora V, Thakur Y, Holkar P, and Chiniga V, et. al. Encapsulation of remdesivir in nanoviricide's platform technology based NV-CoV-2 polymer protects the drug and improves its pharmacokinetics. EC Pharmacol Toxicol. 2022; 10(2):108–118.

Nanomaterials for Cancer Theranostics: Clinical Trial Process, Market Statistics, and Factors to Increase Success Rate from Lab to Clinic

Anita J. Chavan

1 Introduction

Cancer is a significant cause of disease burden globally. It is forecasted that despite current developments in cancer biology research and diagnostic space, it will continue to grow over the next two decades. According to a Global Disease Burden study in 2019, there were approximately 23.6 million new cancer cases and ten million cancer deaths globally [1]. Cancer is the second leading cause of death worldwide despite recent advances in its diagnostic and treatment space. Hence, better diagnostic and treatment tools are urgently needed to detect and treat cancer early and effectively reduce its morbidity [2]. Cancer is a highly complex disease characterized by uncontrolled cell growth and is treated using a combination of chemotherapeutics, surgery, radiation, and hormonal therapy. However, these treatment options cannot fully eradicate cancer and face issues such as drug resistance causing reoccurrence, severe toxic side effects, and damage to the surrounding normal healthy tissue.

These complexities led to an unrealistic roadmap in cancer eradication, e.g., in 1971, former US president Nixon targeted to eradicate cancer in the brief duration of 5 years. On the other hand, the current Biden administration now takes a careful approach with a measurable 25 years goal of cancer death reduction by 50% to be achieved by the previously launched *Cancer Moonshot program* [3]. The Cancer Moonshot initiative was established in 2016 with total funding of US$ 1.8 billion. In addition, US National Cancer Institute (NCI) also targeted 240 projects to treat different types of cancers. Hence, the topic of cancer nanotheranostics (CNTN) will become more important for research, development, and innovation (RDI).

A. J. Chavan (✉)
Singapore, Singapore

R. S. Chaughule et al. (eds.), *Nanomaterials for Cancer Detection Using Imaging Techniques and Their Clinical Applications*,
https://doi.org/10.1007/978-3-031-09636-5_18

The main bottleneck, specifically for CNTN, is the translation of performed lab-level RDI activities to clinical trials and clinical trials to affordable therapies for clinics and homes. Some of the important aspects of this challenge were discussed in different review articles and reports.

Wang et al. [4] reviewed inorganic nanomaterials for biomedical applications and their clearance pathways. They pointed out that toxicity and bioaccumulation of nanoparticles must be addressed before starting their clinical trial process. They emphasized the importance of design understanding and metabolic pathways of inorganic nanomaterials in determining their toxicity and rapid clearance from the body. This in-depth understanding is essential for efficient biodegradable and rapidly clearable nanoparticle development required for a smooth clinical trial. They elaborated on different clearance pathways, viz., renal, hepatic, mucociliary, gastrointestinal, and reticuloendothelial system (RES) clearance and their role during the in vivo trials. Determination of nanomaterial's degradation and clearance pathway is a crucial challenge. Hence, imaging capabilities along with therapeutic effects are vital for clinical translation [4]. Siafaka [5] et al. investigated smart nanotheranostics (NTN), integrating bioactive specific tissue targeting with diagnosis modalities. They mainly focused on radiolabeled CNTN tools, including multifunctional nanomaterials of silica, silver, gold, polymers, carbon, and liposomes. They also elaborated on using these CNTN systems to reduce overdosing or underdosing, which is crucial in determining the success of clinical trials. They emphasized careful modification of CNTN systems to prevent RES clearance resulting in increased targeted delivery. The modifications include optimized particle size and tuned surface functionalities by aptamers, antibodies, polymers, lipids, and dendrites to prevent intrinsic recognition by the immune system.

Johnson et al. [6], in their recently published excellent review article, examined the in vivo status of specific CNTN materials and preclinical challenges for their successful translation to market. The investigated materials include 2D, hybrid, organic, and inorganic CNTN materials. They concluded the increased performance of these materials with (i) superior imaging intensity and contrast of cancer tumors, (ii) increased diagnostic and circulation time duration, (iv) controlled drug release and localization at the tumor site, and (v) superior anticancer performance, viz., inhibiting tumor growth at higher rates, suppressing metastasis completely, enhanced survival rate, and a massive reduction in recurrence. In addition, specific clinical challenges described in their article are elaborated on in the relevant sections of this chapter.

Chang et al. [7] reviewed the clinical performance of a range of stimuli-responsive polymeric nanomaterials (SRPNs) containing loadings of chemical, nucleic drugs, and imaging moieties for CNTN. They described SRPN's different triggering mechanisms governing their nanotheranostics performance: passive/internal stimuli (pH, enzyme, redox agents, and hypoxia) and active/external stimuli (light, temperature, magnetic field, and ultrasound). Their table of comparison [7] provided the status of ongoing clinical trials of SRPNs with Genexol-PM® in phase 4 and NK105, Doxorubicin Transdrug (Livatag) in phase 3 trials.

Wong et al. [8] investigated CNTN materials engineered for specific diseases. They described nanomaterial's penetrability and retention inside the body and the employed therapeutic and imaging mode as critical aspects of their clinical effectiveness, hence, their lab to clinic translation. They pointed out that understanding nanomaterial's interaction with different bio-barriers of the human body such as macrophages, serum proteins, and intra-tumoral delivery is crucial for their engineered response to target specific tumors resulting in their success in the labs and clinics. Singh et al. [9] briefly described translation challenges CNTN from lab to clinics. They discussed critical translation challenges which must be addressed urgently, such as nano-biointeraction leading to a range of side effects and commercially viable controllable-reproducible high-yield synthesis within tight margins of quality control. One of the approaches to resolve these challenges is developing a hybrid methodology, which was elaborated by Shetty et al. [10] in their review article on inorganic hybrid CNTN materials. They emphasized unique intrinsic properties of inorganic nanomaterials suitable and favorable for the development of CNTN, e.g., magnetic and hyperthermia of gold-coated magnetite nanoparticles. Their review article also analyzed patents and ongoing clinical trials of various CNTN materials to determine the missing link in bench-to-bed translation, transforming RDI activities into commercially viable and affordable nanotheranostics therapies for cancer patients. In addition, Dhupal et al. [11] reviewed the phytochemical CNTN approach and elaborated on their clinical trials translating to clinical utilization for effective cancer theranostics. Superior biocompatibility of phytochemicals resolves important hurdles of clinical trials, viz., resistance, cytotoxicity, and physiochemical dynamic response leading to high specificity toward cancer cells. They mainly described phytochemicals nanomedicines approved by the FDA or at different stages of clinical trials with a very high chance of FDA approval.

Fogel [12] reviewed the last 30 years' data and provided suggestions to increase the probability of clinical trials' success. Their survey identified common patterns in successful clinical trials, viz., study site, participated patients, the effect of trials on patients, and coordinators or investigators and their role as well as specific scenarios for AI-ML integration to improve and accelerate the drug trial process. This investigation determined vital factors which led to failed clinical trials, such as the following:

1. Unable to demonstrate efficacy or safety.
2. Lack of funding or long-term financial support; $\approx$ 22% of clinical trials failed due to this factor.
3. Failed to precisely determine eligibility criteria of patients, e.g., missed comorbidities, inefficient exclusion-inclusion criteria, age-group effects.
4. Patients' enrolment for clinical trials; if the number is insufficient due to lack of trust, motivation, ignored patients' concerns, or any other problems, it will indefinitely prolong the trial process and increase the cost.
5. Poor execution of trials, lack of efficient management, poor choices in enrolling patients, site selection, and dropouts of patients are repeated patterns creating huge hurdles in clinical trials. (vi) Lack of quantitative measurements, automatic reporting, and incorrect judgments lead to poor trials outcomes.

6. Patients' investment of time and money.

In addition to the technical and materials efficacy described earlier, the author described key factors summarized in a single sentence as minimizing the burden on patients and maximizing patient appreciation.

Bayda et al. [13] described lab to clinic translation of inorganic CNTN materials in their detailed review. They concluded that for successful bench-to-bed translation of inorganic CNTN materials, it requires superior synthesis methodology following an ecofriendly, simple, cost-effective, safe mode, better biosafety, and in-depth understanding of nano-biointeractions, pharmacokinetics, and biodistributions, with particular emphasis to solve carcinogenesis, long-term toxicity, tissue damage, inflammation, and immunogenicity. Tran et al. [14] reviewed successful CNTN approaches of different nanomaterials and described biological barriers. For the eradication of cancer, they highlighted the urgent need for superior CNTN materials to enhance chances of clinical trials and strong collaborations between pharmaceutical industries, academic labs, research institutes, and regulatory agencies. They discussed the case study of the FDA approval of Onivyde®: a nanomedicine for cancer treatment.

Evidently, the problem of nano-biointeractions and resulting toxicity is highly complex; one must consider theoretical descriptors, specific quantitative nanoscale measurements of materials properties, understanding of bio-clearance pathways, and experimental conditions of drug trials. In addition, one can also include cost and manufacturing challenges in the analysis, which will make the problem of superior CNTN complex enough for AI-ML-based approaches to predict adverse effects of the cancer drug as well as to form proactive risk analysis for safe, cost-effective drug design with a high probability of bench-to-bed translation success. Furxhi et al. [15] provide a highly comprehensive review of this modern AI-ML approach, specifically focusing on the toxicity aspect, which is one of the key hurdles for bench-to-bed translation. In addition, Damasco et al. [16], in their review, provide an experimental safe-by-design approach to address the challenge of drug toxicity of CNTN materials covering preclinical and clinical CNTN materials employed for imaging and therapy of cancer. The special emphasis of this review is to provide rational engineered materials design eliminating toxicity of inorganic nanoparticles for translatable CNTN materials from lab to clinics.

The author of this chapter provides her experience in the field of medical writing for the elaboration of the clinical trial process and how to accelerate it without compromising safety and clinical outcomes in the following sections.

In addition, some other helpful reading materials are also provided here, elaborating innovative approaches [17–19], precision nanomedicine for cancer treatment [20–22], in vitro-in vivo correlation [23], enrolment issues [24, 25], novel preclinical testing platform [26] as well as relevant topics on clinical development [27], nanotheranostics [28], radionanomedicine [29], costs and barriers of clinical trials [30], engineering nanoparticle constructs for efficient delivery [31], protocol amendments [32], regulatory issues [33], bottleneck in brain drug development [34], and effect of physicochemical properties of nanomaterials on toxicity [35].

2 Cancer Nanotheranostics

Nanotheranostic is creating a significant transformation in the personalized medicine space. It is a branch of modern medicine that combines therapy and diagnostics as a single-shot regimen based on nanomaterials. Thus, it provides the opportunity to bridge the current cancer treatment landscape gap. The main limitations of the currently available treatment options are that they are tedious, are invasive, and cause severe cytotoxic side effects. Nanotheranostics has created a significant revolution in the medical field with increased efficacy by combining nanotechnology and nanoparticles. However, the area is still in its early phase as it is challenging because each cancer type is unique and has its own environment.

Recent cell and molecular biology advancements caused significant development in theranostics efficacy and sensitivity. Many therapeutic phenomena that occur at the nanoscale are possible only due to nanoparticles, including photothermal and photodynamic therapy, targeted drug delivery, and other novel treatments [2]. In 2018, the Food and Drug Administration (FDA) approved its first theranostic product, lutetium Lu 177 dotatate injection [36] (Lutathera; Advanced Accelerator Applications), to treat somatostatin receptor-positive gastroenteropancreatic neuroendocrine tumors (GEP-NETs) [37]. The Lutathera treatment consists of a radiolabeled somatostatin analog, which resulted in improved progression-free survival (PFS) in patients suffering from GEP-NETS. The FDA had reviewed this application on a priority basis and later granted it an orphan drug designation. The second theranostic drug approved by the FDA is 177Lu-PSMA-617 which is targeted toward prostate-specific membrane antigen (PSMA), commonly found in cancerous prostate cells, and is for medical therapy use in patients with metastatic castration-resistant prostate cancer (mCRPC). Notably, the FDA had granted 177Lu-PSMA-617 both as a breakthrough therapy and a priority review designation [38]. The 177Lu-PSMA-617 plus standard of care (SOC) resulted in a statistically significant increase in PFS vs. SOC treatment alone. Although theranostic has been deployed to treat only cancers of the thyroid, prostate, and neuroendocrine origins, it can theoretically be used against all kinds provided unique targets are identified on cancer cells.

While results from preclinical studies appear promising for the rapid and efficient clinical use of such formulations, there are critical safety and ethical issues around the theranostics, which are significant hurdles to their clinical translation. This book chapter discusses these issues and possible solutions to proceed with their clinical translation.

3 Clinical Trial Process and Factors Driving Its Success

After years of medical research and investigation in a laboratory and successfully proving its safety and efficacy in animals, a drug moves into the clinical trial process, where it is studied in human subjects for the first time. Cancer clinical trials aim to find novel treatments, diagnose the disease early, discover new medicines,

and manage side effects associated with standard therapy. Typically, a drug moves through four clinical trial phases before reaching its patients. The initial phase 1 to 2 studies involve a smaller sample size and mainly focus on determining safety, serious side effects, pharmacokinetics, pharmacodynamics, and effective drug dose. Once this information is acquired, the drug moves into later phases 3 to 4 of its development. Finally, it is tested on a larger population (hundreds to thousands of people) to study its long-term safety, pharmacovigilance, and efficacy compared to standard treatment care.

Several factors determine the clinical trial outcome: study design, eligibility criteria, patient recruitment, funding, clinical site, investigator, and site staff. Cancer trial involves cancer patients who are already immunocompromised and thus at a greater risk of developing serious adverse events than healthy subjects. Therefore, investigators must make sure the site is equipped to perform necessary medical procedures in such circumstances. In addition, most of the time, cancer trials involve a specific cancer patient population at a particular stage of the disease affecting the patient recruitment. Hence meticulous evaluation of eligibility criteria is of paramount importance in recruiting enough patients and obtaining study-specific endpoints. The Tufts Center for the Study of Drug Development examined 3400 clinical trial protocols under various development phases. It revealed that around 40% of the protocols had to be amended before dosing their first subject. One-third of these amendments could have been avoided with thoughtful planning of study design and eligibility criteria [32]. Protocol amendments cost a significant amount of time and money to the study sponsor and affect the efficiency of the trial.

A primary reason most clinical trials fail is their failure to demonstrate efficacy. For example, an assessment of 640 phase 3 trials showed that almost 57% failed due to being less effective and 17% based on safety [27]. Although safety is studied at every clinical trial phase, safety concerns may be more visible in phase 3 or phase 4 (post-approval). For example, the increased risk of rare blood clots after COVID-19 vaccination became apparent when millions of people were vaccinated [39].

There is a vast amount of money needed to complete each phase of a clinical trial, and thus the availability of funding is another factor that decides the trial outcome. For example, about 22% of phase 3 trials were not completed due to a lack of funding.

Many oncology clinical trials face the long-term problem of recruiting enough patients, with only about 2–5% of cancer patients participating in the study. However, several start-up companies have recently addressed patient enrollment issues using AI-based methods. Especially in a lung cancer trial [40], the AI-based approach increased enrollment by 58.4%.

4 Market Statistics of Cancer Drug Development

As of 2018, there are 1120 drugs under development (DUD) to treat different cancers in the United States. In addition, the number of cancer DUD increased by almost 1.3 times from those in 2015 (No. of DUD = 836) and nearly 2.8 times from

those in 2005 (No. of DUD = 399) [41]. This data suggests that researchers, clinicians, and pharmaceutical industry partners aggressively seek better cancer treatment options. The interest is also reflected in the projected market growth [42] from 45.5 billion US dollars in 2016 to 310 billion US dollars in 2030, with a 14.1% compound annual growth rate from 2020 to 2021.

However, targeting cancers and developing drugs for treatment come at a very high cost, increasing from each drug trial phase. For cancer drug development in 2014, the average per clinical trial study cost [30] was 4.5 million US dollars for phase 1 to 38.9 million US dollars for phase 4 drug trials. For active pharmaceutical substances, the probability of success (PoS) for translation to the market was 91% after their first submission, which reduces to only 17% for the first patient dose and 7% for the first human dose. Only 5% make it to the first toxicity dose [43]. An estimated data of 108 k data points for 24 k unique drug developments performed from the year 2000 to 2018 provides interesting statistics [44, 45]: (i) three cancers with maximum DUD, viz., lung (1501), breast (1373), and colorectal (1351) cancers; (ii) three with minimum DUD hematological (141), testicular (123), and basal cell (123) cancers; (iii) for oncology PoS for DUD, ~ 3.3% and varies with cancer type, with breast cancer providing maximum PoS of 10.1%; and (iv) PoS of drug approval can be increased to 13.3% for all cancer types by careful selection of specific biomarkers in a patient.

Hence, in addition to the challenges of nanoparticle systems for cancer theranostics, targeting specific cancer also determines the outcome of the clinical trials. Moreover, some cancer types are physiologically difficult for theranostics and, hence, offer an unexplored area for research and future market.

5 Preclinical Theranostics: The Missing Link to Clinical Theranostic Translation

Preclinical animal studies in multiple models and validation of their results are critical in initiating a clinical trial for nanotheranostic formulations. Mostly mice models have played a key role in elucidating the complex disease mechanisms underlying cancer formation, metastasis, and a variety of tumor-specific biomarkers and studying their therapeutic [46]. Furthermore, the data generated about drug safety and toxicity during preclinical development provides a base to design dosing schedules in human clinical trials. Thus, rigorous evaluation of theranostic formulations surrounding their safety and cytotoxic effects can warrant successful clinical translation and minimize failure rates in clinical trials. Furthermore, it is vital to formulate these formulations that do not significantly alter their physiological properties once they are in the human body [23]. Thus, systematic studies assessing interactions of nanotheranostic at the nano-biolevel are a crucial determinant of their success in clinical trials.

The enhanced permeability and retention (EPR) effect plays a significant role in nanoparticles' release from blood circulation to the tumor site and determines their effectiveness. Although there is a greater understanding regarding cancer vasculature, the EPR effect varies across cancer patients, tumor types, and different tumor sites in the same patient [47]. Generally, preclinical studies employ the xenograft model to study the EPR effect, which often reports a high EPR effect and may be misleading. Thus, a deeper understating of the EPR effect is warranted at preclinical and clinical levels for an effective nanotheranostic translation [6].

6 Key Challenges of Cancer Nanotheranostics and Regulatory Process

Though theranostics combines diagnosis and therapy in a single system, it is tough to translate nanotheranostic from the lab to the clinic as multiple stages are involved before reaching patients. The main challenges in translating these nanotheranostics are biological barriers, theranostic composition, significant scale-up for industrial use, and regulatory processes [14].

6.1 Biological Barriers

The first and foremost hurdle is posed by the phagocytic cells. They may recognize nanoparticles as foreign entities and could lead to faster clearance from the blood via cytokine release. Other macromolecules could also potentially bind to nanoparticles resulting in changes in their biophysical properties, which might cause serious side effects on the human body. The kidney filtrates the blood to remove waste material; hence size, shape, and charge of nanoparticles are the most crucial parameters for them to pass through these barriers. It was shown that spherical nanoparticles of less than 6 nm diameter had greater renal clearance than those with >8 nm diameter. Therefore, it is also important to consider patients with kidney diseases.

The blood-brain barrier (BBB) poses another major challenge for brain cancer treatment. BBB is highly selective toward specific proteins, ions, and leukocytes [34]. One study demonstrated that nanoparticles with diameters of 20–70 nm are preferred for BBB transport [48]. In a study of rat brains, in situ perfusions and neutral and anionic nanoparticles were less neurotoxic than cationic ones [49]. Microglial cells play a crucial role in coordinating the inflammatory response in the brain; they can be negatively impacted due to nanoparticle accumulation at the tumor site. Hence, strategies to mitigate this negative effect are crucial in designing nanotheranostics [20]. Thus, it is of paramount importance to unveil biophysiochemical interactions of nanotheranostics at the nano-biolevel and elucidate such mechanisms.

These biological barriers are also responsible for the nonspecific accumulation and distribution of nanoparticles in organs such as the liver and spleen, thus preventing them from providing therapeutic effect at the tumor site.

6.2 Commercialization Challenges

Before nanotheranostic can be upscaled for industrial use, it is essential to critically evaluate the efficacy and cost-effectiveness of theranostic formulation against currently available cancer therapies. Theranostic medicine possesses crucial challenges of the tedious and complex manufacturing process, which leads to variable size and shape, irreproducibility, and low yield; these factors limit its upscaling. Since theranostic medicine involves biology, chemistry, and physics, a powerful collaboration across these disciplines and pharmaceutical industry partners and health authorities can pave the way toward the clinic's successful translation of theranostic formulations.

6.3 Regulatory Process

A rapid and successful clinical translation of nanotheranostic demands clear guidelines from regulatory authorities regarding safety standards, quality control, and the manufacturing process of theranostic medicine to enable their smooth and rapid clinical translation [33]. Researchers must rigorously address issues of theranostic regarding their safety in human patients and their effectiveness compared to available treatment options. For successful clinical translation of theranostic product, it is imperative to initiate early interaction with health authorities while designing the clinical trial with data supporting the selection of patient group, study endpoints, and assessment of safety and efficacy. Careful planning of clinical trials will ensure a higher success rate in obtaining approvals and bringing these life-saving medicines to the patients faster.

7 Key Strategies to Enhance Biocompatibility of Cancer Nanotheranostic

Among various technical difficulties, the fundamental problem that needs to be addressed urgently is their toxicity to human subjects. Generally, physical and chemical methods deployed to synthesize nanomaterials involve harsh conditions and chemicals leading to severe toxic products. Synthesizing nanomaterials using biological agents and tuning their physiochemical properties could make them more

biocompatible and thus reduce associated toxicity [50]. However, although biological synthesis offers a sustainable alternative, it is also possible to produce severe toxic by-products. For example, using bacteria as biological agents to synthesize nanoparticles could lead to endotoxin contamination.

7.1 Biophysicochemical Properties

The biophysiochemical properties of nanoparticles are fundamental in determining their toxicity and safety in preclinical studies [35, 51]. For sufficient in vivo evidence of a nanoparticle's effectiveness, one needs to design nanoparticles' size, shape, charge, coatings, and associated agents.

7.2 Toxicity

Successful clinical translation of nanotheranostics demands long-term toxicity studies detailing their uptake, clearance, and negative impact on humans upon prolonged accumulation. In recent years artificial intelligence methods have been used to predict toxicity without animal models [15]. At the cellular level, nanoparticles induce reactive oxygen species (ROS), leading to oxidative stress, DNA damage, and cell apoptosis [52]. At the systemic level, nanoparticles cause toxicity related to the gastrointestinal, reproductive, respiratory, cardiovascular, and immune systems [16]. Thus, integrating computational methods while studying toxicity in animal models can provide insights into nanoparticle toxicity quickly and cost-effectively.

The FDA, National Cancer Institute, and National Institute of Standards and Technology have jointly established the Nanotechnology Characterization Laboratory (NCL) to assist researchers in determining the toxicity and preclinical efficacy of their nanomaterials to enable researchers fast-track their research findings into helpful therapy.

7.3 Nanomaterial Composition

Multiple therapeutic and diagnostic treatments lead to combinatorial dual therapy, which utilizes individual agents' diagnostic and therapeutic properties in one system. However, this therapy must be performed at the right balance of these two agents to avoid undesirable effects of overdosing, underdosing, toxicity, compromised efficacy, irreproducible results, or a combination leading to a lengthy clinical trial process. It may also lead to failure in drug approval [53].

8 Conclusion

Nanotheranostics holds a great promise to change current cancer diagnosis and treatment methods and allow real-time monitoring of drug release, distribution, and treatment response in patients. However, to make this medical revolution a reality, much work is demanded to prove its safety and efficacy in human patients. Rigorous, long-term toxicity studies, thorough analysis of risk-benefit profile, and cost of theranostics are crucial for their successful use in the clinic. Artificial intelligence computational methods will prove pivotal in driving successful clinical trials by enabling patient selection and enrollment and rapidly processing massive patient data. A multidisciplinary collaboration between researchers across medical science (cell and molecular biology etc.), physical sciences (chemistry, physics, etc.), computational science, health administrations (FDA authorities, medical boards, etc.), and strong support of industrial partners would lead to more nanotheranostics reach its market potential and help millions of patients who have cancer.

References

1. Collaboration, G.B.o.D.C. Cancer incidence, mortality, years of life lost, years lived with disability, and disability-adjusted life years for 29 cancer groups from 2010 to 2019: a systematic analysis for the global burden of disease study 2019. JAMA Oncol. 2022;8:420–44. https://doi.org/10.1001/jamaoncol.2021.6987.
2. Ehlerding EB, Grodzinski P, Cai W, Liu CH. Big potential from small agents: nanoparticles for imaging-based companion diagnostics. ACS Nano. 2018;12:2106–21. https://doi.org/10.1021/acsnano.7b07252.
3. Ledford H. Cancer 'moonshot' has lofty new goal: halve deaths in 25 years. Nature Publishing Group; 2022.
4. Wang X, Zhong X, Li J, Liu Z, Cheng L. Inorganic nanomaterials with rapid clearance for biomedical applications. Chem Soc Rev. 2021;50:8669–742. https://doi.org/10.1039/d0cs00461h.
5. Siafaka PI, Okur NU, Karantas ID, Okur ME, Gundogdu EA. Current update on nanoplatforms as therapeutic and diagnostic tools: a review for the materials used as nanotheranostics and imaging modalities. Asian J Pharm Sci. 2021;16:24–46. https://doi.org/10.1016/j.ajps.2020.03.003.
6. Johnson KK, Koshy P, Yang JL, Sorrell CC. Preclinical cancer theranostics—from nanomaterials to clinic: the missing link. Adv Funct Mater. 2021;31(40):2104199. https://doi.org/10.1002/adfm.202104199.
7. Chang D, Ma Y, Xu X, Xie J, Ju S. Stimuli-responsive polymeric nanoplatforms for cancer therapy. Front Bioeng Biotechnol. 2021;9(707319):707319. https://doi.org/10.3389/fbioe.2021.707319.
8. Wong XY, Sena-Torralba A, Alvarez-Diduk R, Muthoosamy K, Merkoci A. Nanomaterials for nanotheranostics: tuning their properties according to disease needs. ACS Nano. 2020;14:2585–627. https://doi.org/10.1021/acsnano.9b08133.
9. Singh D, Dilnawaz F, Sahoo SK. Challenges of moving theranostic nanomedicine into the clinic. Nanomedicine (Lond). 2020;15:111–4. https://doi.org/10.2217/nnm-2019-0401.
10. Shetty A, Chandra S. Inorganic hybrid nanoparticles in cancer theranostics: understanding their combinations for better clinical translation. Mater Today Chem. 2020;18(15):100381. https://doi.org/10.1016/j.mtchem.2020.100381.

11. Dhupal M, Chowdhury D. Phytochemical-based nanomedicine for advanced cancer theranostics: perspectives on clinical trials to clinical use. Int J Nanomedicine. 2020;15:9125–57. https://doi.org/10.2147/IJN.S259628.
12. Fogel DB. Factors associated with clinical trials that fail and opportunities for improving the likelihood of success: a review. Contemp Clin Trials Commun. 2018;11:156–64. https://doi.org/10.1016/j.conctc.2018.08.001.
13. Bayda S, Hadla M, Palazzolo S, Riello P, Corona G, Toffoli G, Rizzolio F. Inorganic nanoparticles for cancer therapy: a transition from lab to clinic. Curr Med Chem. 2018;25:4269–303. https://doi.org/10.2174/0929867325666171229141156.
14. Tran S, DeGiovanni PJ, Piel B, Rai P. Cancer nanomedicine: a review of recent success in drug delivery. Clin Transl Med. 2017;6(44):44. https://doi.org/10.1186/s40169-017-0175-0.
15. Furxhi I, Murphy F, Mullins M, Arvanitis A, Poland CA. Practices and trends of machine learning application in nanotoxicology. Nano. 2020;10:116.
16. Damasco JA, Ravi S, Perez JD, Hagaman DE, Melancon MP. Understanding nanoparticle toxicity to direct a safe-by-design approach in cancer nanomedicine. Nanomaterials (Basel). 2020;10:2186. https://doi.org/10.3390/nano10112186.
17. Pucci C, Martinelli C, Ciofani G. Innovative approaches for cancer treatment: current perspectives and new challenges. Ecancermedicalscience. 2019;13:961. https://doi.org/10.3332/ecancer.2019.961.
18. Indoria S, Singh V, Hsieh MF. Recent advances in theranostic polymeric nanoparticles for cancer treatment: A review. Int J Pharm. 2020;582(119314):119314. https://doi.org/10.1016/j.ijpharm.2020.119314.
19. Kundu P, Singh D, Singh A, Sahoo SK. Cancer nanotheranostics: a nanomedicinal approach for cancer therapy and diagnosis. Anti Cancer Agents Med Chem. 2020;20:1288–99. https://doi.org/10.2174/1871520619666190820145930.
20. von Roemeling C, Jiang W, Chan CK, Weissman IL, Kim BYS. Breaking down the barriers to precision cancer nanomedicine. Trends Biotechnol. 2017;35:159–71. https://doi.org/10.1016/j.tibtech.2016.07.006.
21. Blau R, Krivitsky A, Epshtein Y, Satchi-Fainaro R. Are nanotheranostics and nanodiagnostics-guided drug delivery stepping stones towards precision medicine? Drug Resist Updat. 2016;27:39–58. https://doi.org/10.1016/j.drup.2016.06.003.
22. Lammers T, Rizzo LY, Storm G, Kiessling F. Personalized nanomedicine. Clin Cancer Res. 2012;18:4889–94. https://doi.org/10.1158/1078-0432.CCR-12-1414.
23. Jain P, Pawar RS, Pandey RS, Madan J, Pawar S, Lakshmi PK, Sudheesh MS. In-vitro in-vivo correlation (IVIVC) in nanomedicine: is protein corona the missing link? Biotechnol Adv. 2017;35:889–904. https://doi.org/10.1016/j.biotechadv.2017.08.003.
24. Feller, S.. One in four cancer trials fails to enroll enough participants. 2015: https://www.upi.com/Health_News/2015/12/30/One-in-four-cancer-trialsfails-to-enroll-enough-participants/2611451485504.
25. Fouad MN, Lee JY, Catalano PJ, Vogt TM, Zafar SY, West DW, Simon C, Klabunde CN, Kahn KL, Weeks JC. Enrollment of patients with lung and colorectal cancers onto clinical trials. J Oncol Pract. 2013;9:e40–7.
26. Rodrigues RO, Sousa PC, Gaspar J, Banobre-Lopez M, Lima R, Minas G. Organ-on-a-Chip: a preclinical microfluidic platform for the Progress of nanomedicine. Small. 2020;16(e2003517):2003517. https://doi.org/10.1002/smll.202003517.
27. Hwang TJ, Carpenter D, Lauffenburger JC, Wang B, Franklin JM, Kesselheim AS. Failure of investigational drugs in late-stage clinical development and publication of trial results. JAMA Intern Med. 2016;176:1826–33. https://doi.org/10.1001/jamainternmed.2016.6008.
28. Muthu MS, Leong DT, Mei L, Feng SS. Nanotheranostics – application and further development of nanomedicine strategies for advanced theranostics. Theranostics. 2014;4:660–77. https://doi.org/10.7150/thno.8698.
29. Choi H, Lee Y-S, Hwang DW, Lee DS. Translational radionanomedicine: a clinical perspective. Eur J Nanomed. 2016;8:71–84. https://doi.org/10.1515/ejnm-2015-0052.

30. Wong, H.-H., Jessup, A., Sertkaya, A., Birkenbach, A., Berlind, A., and Eyraud, J. (2014). Examination of clinical trial costs and barriers for drug development final.
31. Ryan SM, Brayden DJ. Progress in the delivery of nanoparticle constructs: towards clinical translation. Curr Opin Pharmacol. 2014;18:120–8. https://doi.org/10.1016/j.coph.2014.09.019.
32. Getz KA, Zuckerman R, Cropp AB, Hindle AL, Krauss R, Kaitin KI. Measuring the incidence, causes, and repercussions of protocol amendments. Drug Inform J DIJ Drug Inform Assoc. 2011;45:265–75. https://doi.org/10.1177/009286151104500307.
33. Gaspar R. Regulatory issues surrounding nanomedicines: setting the scene for the next generation of nanopharmaceuticals. Nanomedicine (Lond). 2007;2:143–7. https://doi.org/10.2217/17435889.2.2.143.
34. Pardridge WM. The blood-brain barrier: bottleneck in brain drug development. NeuroRx. 2005;2:3–14. https://doi.org/10.1602/neurorx.2.1.3.
35. Shin SW, Song IH, Um SH. Role of physicochemical properties in nanoparticle toxicity. Nanomaterials (Basel). 2015;5:1351–65. https://doi.org/10.3390/nano5031351.
36. Sartor O, de Bono J, Chi KN, Fizazi K, Herrmann K, Rahbar K, Tagawa ST, Nordquist LT, Vaishampayan N, El-Haddad G, et al. Lutetium-177-PSMA-617 for metastatic castration-resistant prostate cancer. N Engl J Med. 2021;385:1091–103. https://doi.org/10.1056/NEJMoa2107322.
37. FDA approves new treatment for certain digestive tract cancers. 2020. https://www.fda.gov/news-events/press-announcements/fda-approves-new-treatment-certain-digestive-tract-cancers#:~:text=The%20U.S.%20Food%20and%20Drug,tumors%20(GEP%2DNETs
38. Treskow AV. Novartis Pluvicto™ approved by FDA as first targeted radioligand therapy for treatment of progressive, PSMA positive metastatic castration-resistant prostate cancer. Novartis Media Relations. 2022.
39. Hippisley-Cox J, Patone M, Mei XW, Saatci D, Dixon S, Khunti K, Zaccardi F, Watkinson P, Shankar-Hari M, Doidge J, et al. Risk of thrombocytopenia and thromboembolism after covid-19 vaccination and SARS-CoV-2 positive testing: self-controlled case series study. BMJ. 2021;374:n1931. https://doi.org/10.1136/bmj.n1931.
40. Leventakos K, Helgeson J, Mansfield A, Deering E, Schwecke A, Adjei A, Molina J, Hocum C, Parikh K, Halfdanarson T, et al. P1.16-14 effects of an artificial intelligence (AI) system on clinical trial enrollment in lung cancer. J Thorac Oncol. 2019;14:S592. https://doi.org/10.1016/j.jtho.2019.08.1240.
41. Cancer drugs in development U.S. number 2005–2018. 2022. https://www.statista.com/statistics/268805/number-of-cancer-drugs-in-development-since-2005/.
42. Cancer Immunotherapy Market Size, Industry Analysis Report 2030. 2022. https://www.allied-marketresearch.com/cancer-immunotherapy-market#:~:text=The%20global%20cancer%20immunotherapy%20market,14.1%25%20from%202021%20to%202030.
43. Success probability to market for active substances 2015. 2022. https://www.statista.com/statistics/324959/probability-of-success-to-market-for-active-substances/.
44. Wong CH, Siah KW, Lo AW. Estimation of clinical trial success rates and related parameters. Biostatistics. 2019;20:273–86.
45. Wong, C.H., Siah, K.W., and Lo, A.W. (2022). What are the chances of getting a cancer drug approved?. https://alo.mit.edu/wp-content/uploads/2020/04/DIAGlobalForum20190501_OncologyPoS_Full.pdf.
46. Cheon DJ, Orsulic S. Mouse models of cancer. Annu Rev Pathol. 2011;6:95–119. https://doi.org/10.1146/annurev.pathol.3.121806.154244.
47. Hansen AE, Petersen AL, Henriksen JR, Boerresen B, Rasmussen P, Elema DR, Af Rosenschold PM, Kristensen AT, Kjaer A, Andresen TL. Positron emission tomography based elucidation of the enhanced permeability and retention effect in dogs with cancer using Copper-64 liposomes. ACS Nano. 2015;9:6985–95. https://doi.org/10.1021/acsnano.5b01324.

48. Shilo M, Sharon A, Baranes K, Motiei M, Lellouche JP, Popovtzer R. The effect of nanoparticle size on the probability to cross the blood-brain barrier: an in-vitro endothelial cell model. J Nanobiotechnol. 2015;13:19. https://doi.org/10.1186/s12951-015-0075-7.
49. Lockman PR, Koziara JM, Mumper RJ, Allen DD. Nanoparticle surface charges alter blood-brain barrier integrity and permeability. J Drug Target. 2004;12:635–41. https://doi.org/10.1080/10611860400015936.
50. Singh P, Kim YJ, Zhang D, Yang DC. Biological synthesis of nanoparticles from plants and microorganisms. Trends Biotechnol. 2016;34:588–99. https://doi.org/10.1016/j.tibtech.2016.02.006.
51. Gatoo MA, Naseem S, Arfat MY, Dar AM, Qasim K, Zubair S. Physicochemical properties of nanomaterials: implication in associated toxic manifestations. Biomed Res Int. 2014;2014:498420. https://doi.org/10.1155/2014/498420.
52. Khanna P, Ong C, Bay BH, Baeg GH. Nanotoxicity: an interplay of oxidative stress, inflammation and cell death. Nanomaterials (Basel). 2015;5:1163–80. https://doi.org/10.3390/nano5031163.
53. Wang YX, Idee JM, Corot C. Scientific and industrial challenges of developing nanoparticle-based theranostics and multiple-modality contrast agents for clinical application. Nanoscale. 2015;7:16146–50. https://doi.org/10.1039/c5nr03887a.

Index

R. S. Chaughule et al. (eds.), *Nanomaterials for Cancer Detection Using Imaging Techniques and Their Clinical Applications*,
https://doi.org/10.1007/978-3-031-09636-5